THE HYDRODYNAMICS OF SUPERCRITICAL PACKED COUNTERCURRENT COLUMNS

by

Hendrik Hermanus Franken

Dissertation presented for the Degree

of

DOCTOR OF PHILOSOPHY
(CHEMICAL ENGINEERING)

in the Faculty of Engineering
at Stellenbosch University

The financial assistance of the National Research Foundation (NRF) towards this research is hereby acknowledged. Opinions expressed and conclusions arrived at, are those of the author and are not necessarily to be attributed to the NRF.

Supervisor
C.E. Schwarz

Co-Supervisor
J.H. Knoetze

March 2020

Declaration

By submitting this dissertation electronically, I declare that the entirety of the work contained therein is my own, original work, that I am the sole author thereof (save to the extent explicitly otherwise stated), that reproduction and publication thereof by Stellenbosch University will not infringe any third party rights and that I have not previously in its entirety, or in part submitted it for obtaining any qualification.

This dissertation includes three original papers published in peer-reviewed journals or books and one unpublished publication. The development and writing of the papers (published and unpublished) were the principal responsibility of myself and, for each of the cases where this is not the case, a declaration is included in the dissertation indicating the nature and extent of the contributions of co-authors.

March 2020

Declaration with signature in possession of candidate and supervisor

Plagiarism Declaration

1. Plagiarism is the use of ideas, material and other intellectual property of another's work and to present it as my own.
2. I agree that plagiarism is a punishable offence because it constitutes theft.
3. I also understand that direct translations are plagiarism.
4. Accordingly, all quotations and contributions from any source whatsoever (including the internet) have been cited fully. I understand that the reproduction of text without quotation marks (even when the source is cited) is plagiarism.
5. I declare that the work contained in this assignment, except where otherwise stated, is my original work and that I have not previously (in its entirety or in part) submitted it for grading in this module/assignment or another module/assignment.

Initials and surname:	H.H. Franken
Signature:	*Declaration with signature in possession of candidate and supervisor*
Date:	20 January 2020

Abstract

Supercritical fluids are enjoying ever-increasing popularity as a solvent medium for extraction, stripping, absorption and fractionation processes. Although the potential of supercritical fluids as solvents have been known for more than a century, there are still several areas of uncertainty, one being the hydrodynamics of fractionation columns operating under supercritical conditions. Supercritical fractionation columns are readily tuneable and able to achieve sharp, highly efficient separations, presenting an attractive alternative to traditional solvents in specific niche applications.

Robust hydrodynamic models are key to the design of supercritical fractionation processes, but no such models are available in the open literature. To create models, investigations into fundamental hydrodynamics are required. Two aspects are of particular concern when investigating hydrodynamics. Firstly, the fluid properties of the respective phases involved must be known. Secondly, mass transfer should be minimised or quantified. No study found in the literature presents hydrodynamics under supercritical conditions with measured, not estimated, saturated fluid properties taken into consideration.

This study had the overarching aim to *Investigate hydrodynamics in countercurrent columns operating under supercritical conditions while laying groundwork for the eventual development of accurate predictive models and design methods.* This aim was broken down into five objectives to remove obstacles and generate the needed data to achieve the aim.

To address the lack of fluid property data, the first objective was to develop new equipment capable of concurrently measuring the required fluid properties of density and dynamic viscosity. The equipment setup (P_{max} 35 MPa; T_{max} 393 K) included a variable volume view cell to determine bubble/dew points and density, with a quartz-crystal resonator to measure dynamic viscosity. The equipment was validated, firstly using pure component fluid property measurements with n-dodecane and benzene at 0.1 - 30 MPa and 313 - 353 K and, secondly, using CO_2 + ethyl tetradecanoate (ET) for binary phase equilibrium measurement. New data were presented on the dynamic viscosity and density of both saturated CO_2 and ET phases.

Using the developed equipment, it was possible to evaluate binary systems implicitly for use in supercritical hydrodynamics, addressing the second objective of the study. Two Poly[dimethylsiloxane] (PDMS) fluids graded at 100 cSt and 200 cSt were selected. Saturation pressure was determined for 1 – 70 wt% PDMS in CO_2 at 313 – 353 K. The density (~900 – 800 kg.m^{-3}) and dynamic viscosity (~0.7 – 7 mPa.s) were measured at saturation. The

selected systems exhibited low mutual solubility and fluid properties in the ranges desired for further work.

The third objective, to conduct hydrodynamic pilot plant studies, could be planned and executed using the measured fluid property and phase data. The equipment was operated at 14 MPa and 333 - 323 K to investigate the hydrodynamic operability for a 38 mm diameter column packed with ¼ " Dixon rings. The temperature/pressure combination was selected to investigate a wide array of fluid properties while presenting the opportunity to differentiate between the influence of viscosity and density. The pressure drop, liquid hold-up, mass flow and massfractions were measured. Importantly, it was found that liquid hold-up and pressure drop are not reliable indicators of operability in supercritical systems. Three distinct types of inoperability were identified, namely liquid layer flooding, bubble column flooding and entrainment. The influence of the density and dynamic viscosity on hydrodynamics was found to be complex, yet significant. Further, no observable loading operating regime was observed, with the column only operating in the pre-loading or inoperable (flooded/entrained) regimes.

The fourth objective was to evaluate three hydrodynamic models for their ability to predict experimental and literature data. The Stichlmair et al. model was able to predict the liquid hold-up after a modification was made to take supercritical fluid properties into account, and the empirical constants were recalculated. The model could, however, not predict the experimental pressure drop or operability limits regardless of any modification. Maćkowiak's SBD model failed to predict any hydrodynamic properties. The model by Woerlee provided an order of magnitude estimation of liquid hold-up and pressure drop for specific conditions using very little empiricism. The model could not predict flooding at all. None of the models could present an accurate view of the hydrodynamics of the system regardless of attempted adjustments and modifications, with the models displaying different qualitative trends than the gathered experimental data.

The final objective tested the literature hypothesis that supercritical hydrodynamics are fundamentally similar to 'classical' hydrodynamics. Three conclusions made during this study cast doubt on the fundamental similarity. Firstly, the lack of a detectable loading zone was in contradiction with classical hydrodynamics where the loading zone plays a significant role. Secondly, pressure drop and liquid hold-up were found to be unreliable predictors of operability in the supercritical systems investigated, in contrast to classical systems. Thirdly, the investigated hydrodynamic models cannot predict pressure drop, flooding, or hydrodynamic capacity for the supercritical systems investigated.

The thesis presents the following novel contributions:

a) Equipment, presenting a novel combination of measurement techniques for concurrent determination of phase equilibria, density and viscosity at fluid saturation, as published in *J. Supercrit. Fluids*, 133 (2018) 444-454. The publication also contains novel data on benzene viscosity, phase equilibria, and saturated phase density and dynamic viscosity for CO_2 + ethyl tetradecanoate. It further presents the first measurement of saturated fluid properties of the supercritical phase found by the author in the literature.

b) New data on two PDMS + CO_2 systems, 100 cSt and 200 cSt, including phase equilibria, and saturated phase density and viscosity for both phases, as published in *J. Supercritical Fluids*, 139 (2018) 1-7. Given the lack of saturated fluid properties under supercritical conditions and the complexity of measurement, this represents a valuable contribution, especially being the only measurement of saturated supercritical fluid phase properties found in the literature.

c) New data on supercritical hydrodynamics allows various observations and conclusions. Observations include the identification of three different inoperability modes, the lack of an observable loading zone, as well as describing the influence of fluid properties on the hydrodynamic behaviour. Published in part in *Chem. Eng. Trans.*, 69 (2018), with a second publication planned.

d) The full evaluation of the Stichlmair et al. model, Maćkowiak's SBD model and Woerlee's model against the gathered data showcases the inability of the investigated classical hydrodynamic models to predict supercritical hydrodynamics. This finding, along with other findings mentioned above, highlight the possibility of a fundamental difference between classical and supercritical systems. However, there is insufficient information to make a definite statement.

Opsomming

Superkritiese vloeistowwe geniet toenemende populariteit as ’n oplosmiddel in ekstraksie-, stroping-, absorpsie- en fraksioneringsprosesse. Alhoewel die potensiaal van superkritiese vloeistowwe as oplosmiddels al vir meer as ’n eeu bekend is, is daar steeds verskeie areas van onsekerheid in die literatuur. Een so ‘n area is die hidrodinamika van fraksioneringskolomme wat onder superkritiese toestande werk. Superkritiese fraksioneringskolomme is maklik verstelbaar en in staat daartoe om skerp, doeltreffende skeidings te bewerkstellig wat ’n aantreklike alternatief tot tradisionele oplosmiddels in spesifieke nistoepassings bied.

Robuuste hidrodinamiese modelle is belangrik vir die ontwerp van superkritiese fraksioneringsprosesse, maar geen sulke modelle is in die oop literatuur beskikbaar nie. Om modelle te skep, is ondersoek tot die fundamentele hidrodinamika benodig. Twee aspekte is van besondere belang wanneer hidrodinamika ondersoek word. Eerstens, moet die vloeistofeienskappe van die betrokke fases bekend wees. Tweedens, moet massa-oordrag tot ‘n minimum beperk word, of gekwantifiseer word. Geen studie in die literatuur bevat hidrodinamika onder superkritiese kondisies met die gemete, nie geskatte, versadigde vloeistofeienskappe wat in ag geneem is nie. Hierdie studie het die oorkoepelende doelwit gehad om *hidrodinamika in superkritiese teenstroomkolomme te ondersoek en ‘n grondslag lê vir die uiteindelike ontwikkeling van akkurate modelle en ontwerpsmetodes.* Hierdie doelwit is opgedeel in vyf doelstellings om struikelblokke te verwyder en die nodige data te genereer.

Om die gebrek aan vloeistofeienskapdata aan te spreek, was die eerste doelstelling om nuwe toerusting te ontwikkel wat die vermoë het om die nodige vloeistofeienskappe, digtheid en dinamiese viskositeit, gelyktydig te meet. Die toerusting (P_{max} 35 MPa; T_{max} 393 K) bestaan uit ’n veranderlikevolume-sel met ‘n sigglas om borrel-/doupunte en digtheid te bepaal, asook ’n kwarts-kristalresonator om dinamiese viskositeit te meet. Die toerusting is gevalideer, eerstens, met behulp van suiwer-komponent vloeistofeienskapsmetings met n-dodekaan en benseen by 0.1 – 30 MPa en 313 – 353 K en, tweedens, met behulp van CO_2 + etieltetradekanoaat (ET) vir die meting van binêre fase-ewewig. Nuwe data is voorgelê vir die dinamiese viskositeit en digtheid van albei die versadigde CO_2- en ET-fases.

Met behulp van die ontwikkelde toerusting was dit moontlik om binêre sisteme te evalueer vir die implisiete doel om superkritiese hidrodinamika te meet, wat die tweede doelstelling van die studie aanspreek. Twee poli[dimetielsiloksaan] (PDMS) vloeistowwe, gegradeer as 100 cSt en 200 cSt, is gekies. Versadigingsdruk is bepaal vir 1-70 wt% PDMS in CO_2 by 313–353 K. Die digtheid (~900 - 800 kg.m^{-3}) en dinamiese viskositeit (~0.7 - 7 mPa.s) is by versadiging gemeet.

Die gekose stelsels het lae wedersydse oplosbaarheid, asook vloeistofeienskappe in die gewenste bereik, getoon.

Die derde doelstelling, om hidrodinamiese loodsaanlegstudies uit te voer, kon beplan en uitgevoer word met behulp van die gemete vloeistofeienskap- en fase-data. Die toerusting is bedryf by 14 MPa en 333 - 323 K om die hidrodinamiese bedryfsgrense van 'n 38 mm-deursnee kolom gepak met ¼''-Dixon ringe, te ondersoek. Die temperatuur/druk kombinasie is gekies om 'n wye verskeidenheid vloeistofeienskappe te ondersoek, asook om 'n geleentheid skep om die tussen invloed van viskositeit en digtheid te kan onderskei. Die drukval, vloeistof-oponthoud, massavloei en massafraksie is gemeet. Van belang is die bevinding dat vloeistof-oponthoud en drukval nie betroubare aanduiders van beryfbaarheid in superkritiese sisteme is nie. Drie afsonderlike bedryfsgrens-oorgange is geïdentifiseer, naamlik vloeistoflaagvloeding, borrelkolomvloeding en meesleuring. Die invloed van die digtheid en dinamiese viskositeit op hidrodinamika is gevind om kompleks te wees, dog beduidend. Verder is daar geen waarneembare ladingsbedryfregime gevind nie, met die kolom wat slegs in die voorladings- of onbedryfbare-(gevloede/meegesleurde) regimes werk.

Die vierde doelstelling was om drie hidrodinamiese modelle te evalueer vir hul vermoë om eksperimentele- en literatuurdata te voorspel. Die Stichlmair-et-al.-model kon die vloeistof-oponthoud voorspel nadat 'n modifikasie aangebring is om superkritiese vloeistofeienskappe in ag te neem, en die empiriese konstantes herbereken is. Die model kon egter nie die eksperimentele drukval of bedryfsgrense voorspel nie, ongeag enige modifikasies. Maćkowiak se SBD model kon geen hidrodinamiese eienskappe voorspel nie. Die model deur Woerlee was in staat tot 'n ordegrootte skatting van die gemete vloeistof-oponthoud en drukval vir van die stelsels met baie min empiriese invloed. Hierdie model kon glad nie die bedryfsgrense voorspel nie. Nie een van die modelle kon 'n akkurate oorsig van die hidrodinamika van die stelsel bied nie, ongeag pogings tot aanpassings en modifikasies, met die modelle wat anderse kwalitatiewe tendense as die eksperimentele data toon.

Die finale doelstelling het die literatuurhipotese getoets dat superkritiese hidrodinamika, in wese, dieselfde is as 'klassieke' hidrodinamika. Drie gevolgtrekkings is tydens die studie gemaak wat die fundamentele ooreenkoms in twyfel trek. Eerstens, is die gebrek aan 'n waarneembare ladingsbedryfregime in teenstelling met klassieke hidrodinamika waar die ladingsbedryfregime 'n belangrike rol speel. Tweedens, is daar gevind dat drukval en vloeistof-oponthoud onbetroubare voorspellers van die bedryfsgrense in die superkritiese sisteme is, in teenstelling met klassieke hidrodinamiese stelsels. Derdens, kan die ondersoekte hidrodinamiese modelle nie die drukval, vloeding, of hidrodinamiese kapasiteit voorspel vir die superkritiese sisteme wat ondersoek was nie.

Die proefskrif bied die volgende nuwe bydraes aan:

a) Toerusting wat ’n nuwe kombinasie van metingstegnieke vir die gelyktydige bepaling van fase-ewewig, digtheid en viskositeit by vloeistof versadiging, voorstel, soos gepubliseer in *J. Supercrit. Fluids*, 133 (2018) 444–454. Die publikasie bevat ook nuwe benseen-viskositeitsdata, asook fase-ewewig, en versadigde fase digtheids- en dinamiese viskositeitsdata vir CO_2 + etieltetradekanoaat. Dit stel verder ten toon die eerste meting van versadigde vloeistofeienskappe van die superkritiese fase wat deur die outeur in die literatuur gevind is.

b) Nuwe data op twee PDMS + CO_2-stelsels, 100 cSt en 200 cSt, wat insluit fase-ewewig, en versadigde fase digtheids- en viskositeitsdata vir beide fases, soos gepubliseer in *J. Supercritical Fluids*, 139 (2018) 1–7. Gegewe die gebrek aan versadigde vloeistofeienskappe onder superkritiese kondisies en die kompleksiteit van meting, verteenwoordig hierdie ’n waardevolle bydrae, veral omdat dit die enigste mate van versadigde superkritiese vloeistof fase-eienskappe is wat in die literatuur voorkom.

c) Nuwe data op superkritiese hidrodinamika laat verskeie waarnemings en gevolgtrekkings toe. Waarnemings sluit in die identifisering van drie verskillende bedryfsgrens-oorgange, die gebrek aan ’n waarneembare ladingsbedryfregime, asook die beskrywing van die invloed van vloeistofeienskappe op die hidrodinamiese gedrag. Die bevindings is gedeeltelik gepubliseer in *Chem. Eng. Trans.* 69 (2018), met ’n tweede publikasie wat beplan word.

d) Die volle evaluering van die Stichlmair-et-al.-model, Maćkowiak se SBD-model, en Woerlee se model teen die versamelde data wys die onvermoë van hierdie klassieke hidrodinamiese modelle om superkritiese hidrodinamika te voorspel. Hierdie bevinding, tesame met ander bevindings hierbo genoem, beklemtoon die moontlikheid van ’n fundamentele verskil tussen klassieke en superkritiese stelsels. Daar is egter onvoldoende inligting om ’n definitiewe standpunt te maak.

Acknowledgements

To the creator, for a world that will never, ever get boring even if I tried to make it so.

A multitude of people have contributed in small and big ways to the journey that has led here. Thank you to each of you – you matter, even if it might slip my mind to mention you here.

The first laurels go to my supervisors – Prof Cara Schwarz and Prof Knoetze. I sincerely appreciate your understanding and guidance throughout this road. To Prof Schwarz for her support, patience and admirable hunger to always improve on any work. Thank you for the many years of dealing with an often hard-headed student. To Prof Knoetze for his gentle way, deep knowledge and insight. If it wasn't for your example the road to this dissertation would have been much rockier.

To the workshop crew – Oom Jannie Barnard, Oom Anton Cordier, Oom Jos Weerdenburg. Thank you for all the technical support, words of life-wisdom and fantastic workmanship in all you made. My journey would not have been possible without you.

To the technical staff, Alvin Pieterson, Linda Mzayifani, Oliver Jooste. Thank you for a helping hand, a friendly laugh and always having a good word for a tough day.

To the admin staff, and in particular, Ms Juliana Steyl. Thank you for all the "behind the scenes" work to make things run smoothly.

To my friends, thank you can never cover your camaraderie, helping hands and minds, and many hours of laughs, debates, games and banter. This work is in some ways as much yours as mine, as without you I would not be the person who created this work. In particular, my humble thank you to the Chemical Engineering Crew: Jandre Lamprecht, Jamie Cripwell and Heinrich Bock.

To Laura Vizule, who through all this has been as patient as three stones, as understanding as a wise owl and a supporting pillar. Thank you for being an amazing person and letting me 'abandon' you during the many hours of "I need to work on the PhD".

To my mother, Hester Franken. Thank you for being you. It is a privelage to call myself your son and I only hope to one day have your strength, yet amazing compassion with the world.

And lastly, this work is dedicated to my father, Hennie Franken. We don't know what we have until it is lost. Thank you Dad for always being supportive, no matter what. I wish I had time for one more talk with you.

"It doesn't stop being magic just because you know how it works"

– Terry Pratchett

Academic Contributions

Abstracts and posters for conference contributions are presented in Appendix A.

Journal publications:

1. H.H. Franken, J.H. Knoetze, C.E Schwarz; *Concurrent Measurement of High-Pressure Binary Phase Equilibrium, Density and Dynamic Viscosity*; The Journal of Supercritical Fluids 133 (2018) 444–454.
2. H.H. Franken, J.H. Knoetze, C.E Schwarz; *High-pressure binary phase equilibria, density and dynamic viscosity of 100 & 200 cSt polydimethylsiloxane (PDMS) with supercritical* CO_2; The Journal of Supercritical Fluids 139 (2018) 1–7.
3. H.H. Franken, J.H. Knoetze, C.E Schwarz; *Hydrodynamics of a Packed Column Operated under Supercritical Conditions*; Chemical Engineering Transactions 69 (2018) 13-18. [The contents of this publication were presented at a conference, noted in point 6 below.]

Journal publication to be submitted:

4. H.H. Franken, J.H. Knoetze, C.E Schwarz; *Influence of Fluid Properties on Hydrodynamics, and the Dependant Operability of a Packed, Countercurrent Column Operated under Supercritical Conditions*; To be submitted to: Chemical Engineering Research and Design.

Conference presentations

5. H.H. Franken, J.H. Knoetze, C.E Schwarz; *Equipment for the Simultaneous Measurement of Supercritical Binary Phase Equilibrium, Density and Viscosity*; 15th European Meeting on Supercritical Fluids (EMSF), 6 - 14 May 2016.
6. H.H. Franken, J.H. Knoetze, C.E Schwarz; *Hydrodynamics of a Packed Column Operated Under Supercritical Conditions*; 11th International Conference on Distillation & Absorption (DA), 16 - 19 September 2018. [Published as in 3 above.]

Conference posters:

7. H.H. Franken, J.H. Knoetze, C.E Schwarz; *Concurrent Measurement of High Pressure Phase Equilibria, Density and Viscosity of PDMS in Supercritical* CO_2; 10th World Congress of Chemical Engineering (WCCE), 1 - 5 October 2017.
8. H.H. Franken, J.H. Knoetze, C.E Schwarz; *Concurrent Measurement of High Pressure Phase Equilibria, Density and Viscosity of PDMS in Supercritical* CO_2; 30th European Symposium on Applied Thermodynamics (ESAT), 10 – 13 June 2017.

Table of Contents

Abstract i

Opsomming iv

Acknowledgements vii

Academic Contributions viii

Nomenclature xviii

1. Introduction 1

1.1 Countercurrent Column Hydrodynamics 1

1.2 Supercritical Fluid as Extractive Solvent. 2

1.3 The Supercritical Countercurrent Separation Process 4

1.4 Study Context, Aim, Objectives and Structure 6

References 10

2. Background Literature 15

2.1 Supercritical Fluids 15

2.1.1 Temperature and Pressure Dependence 16

2.1.2 Typical Properties 18

2.1.3 Advantages and Disadvantages of Supercritical Fluid Solvents 18

2.2 Overview of Two-Phase Countercurrent Column Hydrodynamics 20

2.2.1 Packed Column Internals 20

2.2.2 Falling Films 21

2.2.2.1. Falling Films under Supercritical Conditions. 22

2.2.3 Pressure Drop 23

2.2.3.1. Dry and Wet Pressure Drop 24

2.2.3.2. Pressure Drop in Random vs Structured Packings 25

2.2.4 Liquid Hold-up 25

2.2.4.1. Static and Dynamic Liquid Hold-up 26

2.2.4.2. Droplet Entrainment 28

2.2.5 Liquid-Liquid Extractions. 28

2.3 Hydrodynamics under Supercritical Conditions 29

2.3.1 History of Hydrodynamics under Supercritical Conditions 29

2.3.2 Trends Expected 33

2.3.3 Computational Fluid Dynamic Studies on Supercritical Hydrodynamics 34

2.3.4 The Effect of Mass-Transfer 34

2.4 Semi-Empirical Correlations for Hydrodynamics under Supercritical Conditions .. 35

2.4.1 Model Structure Simplifications 35

2.4.2 Modified Stichlmair et al. Equations 36

2.4.2.1. Dry Pressure Drop 36
2.4.2.2. Liquid Hold-up below the Loading Point 37
2.4.2.3. Wet Pressure Drop and Liquid Hold-up above the Loading Point 39
2.4.2.4. Flooding 40
2.4.2.5. Range of Model 41

2.4.3 Maćkowiak Equations 42

2.4.3.1. Flooding Liquid Hold-up and -Gas Velocity 42
2.4.3.2. Liquid Hold-up 43
2.4.3.3. Pressure Drop 44
2.4.3.4. Range of Model 45

2.4.4 Woerlee Equations 45

2.4.4.1. Dry Pressure Drop and Channel Angle of Inclination 46
2.4.4.2. Liquid Hold-up 47
2.4.4.3. Wet Pressure Drop 47

2.4.5 Model Comparison 48

2.4.5.1. Liquid Hold-up 48
2.4.5.2. Wet Pressure Drop 50

2.5 Fluid Properties under Supercritical Conditions 53

2.6 Literature Shortcomings and Summary 54

2.7 Literature Conclusion 55

References 57

3. Publication 1 67

Preface 69

Abstract 69

3.1 Introduction 70

3.1.1 Phase Equilibria 71
3.1.2 Viscosity 71
3.1.3 Density 73
3.2 Materials and Methods 73
3.2.1 Experimental Set-up 73
3.2.2 Phase Equilibria Method 76
3.2.3 Dynamic Viscosity Theory and Method 76
3.2.4 Density Method 78
3.2.5 Uncertainty 79
3.2.6 Verification 80
3.2.7 Materials Used 81
3.3 Results and Discussion 82
3.3.1 n-Dodecane 82
3.3.2 Benzene 85
3.3.3 CO_2 + Ethyl tetradecanoate 87
3.4 Conclusions 92
Acknowledgements 92
Data Tables 93
References 96
4. Publication 2 101
Preface 103
Abstract 103
4.1 Introduction 104
4.2 Materials and Methods 106
4.2.1 Experimental Equipment and Procedure 106
4.2.1.1. Phase Equilibria 106
4.2.1.2. Density 107
4.2.1.3. Dynamic Viscosity 107
4.2.1.4. Uncertainty 108
4.2.2 Materials Used 109

4.3 Results and Discussion 110
  4.3.1 Phase Equilibria 110
  4.3.2 Density 112
  4.3.3 Dynamic Viscosity 116
4.4 Conclusions 119
Acknowledgements 119
Data Tables 120
References 122
5. Publication 3 125
Preface 127
Abstract 127
5.1 Introduction 128
5.2 Materials and Methods 130
  5.2.1 Experimental Equipment 130
  5.2.2 Materials Used 131
  5.2.3 Experimental Considerations and Procedure 131
    5.2.3.1. Pressure and Temperature Considerations 131
    5.2.3.2. Dry pressure drop 132
    5.2.3.3. Wet pressure drop and liquid hold-up 132
5.3 Results and Discussion: 132
  5.3.1 Dry Pressure Drop 133
  5.3.2 Flooding Determination 133
5.4 Conclusions 136
Acknowledgements 136
References 137
6. Manuscript 4 139
Preface 141
Abstract 141
6.1 Introduction 142
6.2 Materials and Methods 144

6.2.1 Experimental Equipment 144
6.2.2 Dry Pressure Drop Measurement 144
6.2.3 Wet Pressure Drop and Liquid Hold-up Measurement 144
6.2.4 Hydrodynamic Inoperability and Flooding/Entrainment 146
6.2.5 Pressure and Temperature Considerations 147
6.2.6 Column Wall Effects 148
6.2.7 Measurement and Uncertainty 149
6.2.7.1. Temperature 150
6.2.7.2. Pressure 150
6.2.7.3. Pressure drop 151
6.2.7.4. SF and Liquid Flow Rates. 151
6.2.7.5. Other 151
6.2.8 Materials Used 151
6.3 Results and Discussion 152
6.3.1 Dry Pressure Drop 152
6.3.2 100 cSt PDMS + CO_2 153
6.3.3 200 cSt PDMS + CO_2 161
6.3.4 Influence of Fluid Properties on Hydrodynamics 165
6.4 Conclusions 168
Nomenclature: 169
Funding 169
References 170
7. Hydrodynamic Model Evaluation vs Experimental Data 173
7.1 Liquid Hold-up 173
7.1.1 Maćkowiak Model Prediction 173
7.1.2 Stichlmair et al. Model Prediction 175
7.1.3 Woerlee Model Prediction 178
7.1.4 Hold-up Model Comparison 181
7.2 Pressure Drop 181
7.2.1 Stichlmair et al. Model Adjustments 182

7.2.2 Stichlmair et al. Model Prediction 183

7.2.3 Woerlee Model Prediction 185

7.2.4 Pressure Drop Model Comparison 188

7.3 Supercritical Hydrodynamics vs Atmospheric Hydrodynamics 188

References 191

8. Conclusions 193

8.1 Conclusions from Literature - Chapter 2: 193

8.2 Objective 1 - Chapter 3 194

8.3 Objective 2 - Chapter 4 195

8.4 Objective 3 - Chapters 5 and 6 196

8.5 Objective 4 - Chapter 7.1 and 7.2 198

8.6 Objective 5 - Chapter 7.3 200

8.7 Conclusions in Summary 201

9. Recommendations 203

10. Consolidated Reference List 205

Appendix A : Conference Presentations and Posters 211

A.1 Presentation - 15th European Meeting on Supercritical Fluids (EMSF 2016) 212

A 1.1 EMSF 2016 Abstract 212

A 1.2 EMSF 2016 Presentation 213

A.2 Poster - 10th World Congress of Chemical Engineering (WCCE 2017) 216

A 2.1 WCCE 2017 Abstract 216

A 2.2 WCCE 2017 Poster 217

A.3 Poster - 30th European Symposium on Applied Thermodynamics (ESAT 2017) 218

A 3.1 ESAT 2017 Abstract 218

A 3.2 ESAT 2017 Poster 219

A.4 Presentation - 11th International Conference on Distillation & Absorption (DA 2018) 220

A 4.1 DA 2018 Abstract 220

A 4.1 DA 2018 Presentation 221

Appendix B : Safe Working Procedures and Task Risk Assessment 225

B.1 High-pressure Gas Bomb Handling Procedure – CO_2 226

B.1.1 SWP - High-pressure Gas Bomb 226

B.1.2 TRA - High-pressure Gas Bomb 228

B.2 High-Pressure Viscosity Measurement View Cell 229

B.2.1 SWP – High-Pressure Viscosity View Cell – Loading Procedure 229

B.2.2 TRA - High-Pressure Viscosity Measurement View Cell – Loading Procedure . 232

B.2.3 SWP - High-Pressure Viscosity View Cell - Experimental 233

B.2.4 TRA - High-Pressure Viscosity View Cell - Experimental 235

B.2.5 SWP - High-Pressure Viscosity View Cell – Unloading/Cleaning 236

B.2.6 TRA - High-Pressure Viscosity View Cell - Unloading/Cleaning 239

B.3 Large Supercritical Pilot Plant 241

B.3.1 For First-time Users 241

B.3.2 SWP - Large Supercritical Pilot Plant - Start-up 242

B.3.3 TRA - Large Supercritical Pilot Plant - Start-up 247

B.3.4 SWP - Large Supercritical Pilot Plant - Experimental 248

B.3.5 TRA - Large Supercritical Pilot Plant - Experimental 252

B.3.6 SWP - Large Supercritical Pilot Plant - Shutdown/Clean-up 253

B.3.7 TRA - Large Supercritical Pilot Plant - Shutdown/Clean-up 256

Appendix C : Safety and Certification Forms 259

C.1 MSDS for CO_2 260

C.2 MSDS for Benzene 262

C.3 MSDS for n-Dodecane 264

C.4 MSDS for Ethyl Tetradecanoate 266

C.5 MSDS for PDMS 100 cSt / PDMS 200 cSt 268

C.6 MSDS for Methanol 270

C.7 MSDS for Xylene 272

C.8 MSDS for Isopropanol 274

Appendix D : High-Pressure Viscosity Measurement View Cell Design 277

D.1 Background ... 278

D.2 Equipment Description ... 278

D.3 Operating Principles ... 280

  D.3.1 General Operation ... 280

  D.3.2 Phase Equilibria Method ... 280

  D.3.3 Viscosity Measurement Method ... 280

D.4 Safety Considerations ... 281

  D.4.1 High Pressure ... 281

    D.4.1.1 Safety During Design ... 281
    D.4.1.2 Safety During Operation ... 282

  D.4.2 High Temperature ... 282

    D.4.2.1 Safety During Design ... 282
    D.4.2.2 Safety During Operation ... 282

  D.4.3 Flammability and Explosion ... 282

  D.4.4 Viscosity Measurement Equipment ... 283

    D.4.4.1 Safety During Design ... 283
    D.4.4.2 Safety During Operation ... 283

D.5 Technical Data ... 284

  D.5.1 Low-Pressure and Atmospheric Chamber and Piston Assembly ... 285

    D.5.1.1 Design Drawings ... 286

  D.5.2 High-Pressure Chamber ... 299

    D.5.2.1 Design Drawings ... 300
    D.5.2.2 High-Pressure Barrel Material Certificate ... 305

  D.5.3 Design Calculations and Drawing Review ... 306

    D.5.3.1 In-house Pressure Vessel Calculations ... 307
    D.5.3.2 Design and Drawing Review ... 313
    D.5.3.3 Low-Pressure Chamber Design Calculation Report ... 316
    D.5.3.4 High-Pressure Chamber Design Calculation Report ... 323

  D.5.4 RITC Certification ... 328

  D.5.5 Quartz Crystal and Crystal Holder ... 329

    D.5.5.1 Crystal Holder Design Drawings ... 330

  D.5.6 Cell Stand Design Drawings ... 338

D.5.6.1 Top Cell Height Block 339

D.5.6.2 Bottom Cell Height Block 340

D.5.6.3 Bearing Collar 341

D.5.6.4 Cell Flange 342

D.5.6.5 Cell Rod 343

D.5.6.6 Assembled Stand 344

D.5.6.7 Assembled Stand and Cell 345

D.5.7 Temperature Control 346

D.5.8 Measurement and Calibration Data 347

D.5.8.1 Temperature Calibrations 348

D.5.8.2 Pressure Calibration 355

D.5.8.3 Mass Calibration 362

D.5.8.4 Volume Calibration 364

D.5.8.5 Crystal Calibration 367

D.5.9 HD Camera Setup 369

D.5.10 Magnetic Stirrer 370

D.5.10.1 Magnet Holder Components 371

D.5.10.2 Magnet Holder 3D Representation 372

D.5.10.3 Controller Details and Code 373

D.5.11 Viscosity Measurement Equipment and Method 378

D.5.11.1 Software Screenshots and Instructions 379

D.5.11.2 Software Python Code 381

Appendix E : Pilot Plant Supplementary discussions 389

E.1 Steady state determination 390

E.2 Liquid hold-up measurement 391

Appendix F : Pilot Plant Experimental Data Tables 393

Nomenclature

Symbol	Description	Units
a	Packing surface area per unit volume	m^2/m^3
C_1	Empirical Constant	–
C_{FL}	Flooding point factor	–
d / D	Column diameter	m
d_h	Hydraulic bed diameter	m
d_p	Particle/Sphere diameter	m
d_{int}	Reduced Hydraulic bed diameter	m
d_T	Liquid droplet diameter	m
$\in$	Fractional void volume	m^3/m^3
F_G	Gas capacity factor/Vapor flow factor	$(m/s).(kg/m^3)^{0.5}$
$F_{G,FL}$	Gas capacity factor at flooding	$(m/s).(kg/m^3)^{0.5}$
g	Gravitational acceleration	m/s^2
G	Gaseous phase superficial mass flow rate	$kg/m^2.s$
H	Total packed height	m
$\mathrm{h}_{L,FL}$	Liquid hold-up at flooding	m^3/m
h_L	Total liquid hold-up	m^3/m^3
h_{Ld}	Dynamic liquid hold-up	m^3/m^3
$h_{Ld,0}$	Dynamic liquid hold-up below the loading point	m^3/m^3
h_{Ls}	Static liquid hold-up	m^3/m^3
K_x	Equation constant of number x	–
L	Liquid phase superficial mass flow rate	$kg/m^2.s$
n_t/H	Separation Efficiency/Number of theoretical stages per 1 m packing height	m^{-1}
$Ø_I$	Internal Diameter	mm
ΔP	Total measured pressure drop	Pa
$\Delta P/H$	Pressure drop per 1 m of irrigated or wet packing	Pa/m
$\Delta P_0/H$	Pressure drop per 1 m of dry packing	Pa/m
$\Delta P_\psi/H$	Frictional pressure drop per 1 m of dry packing	Pa/m
$\Delta P_G/H$	Geometric pressure drop per 1 m of dry packing	Pa/m
P	Pressure	Pa, bar
u_{int}	Interfacial velocity	m/s
u_L	Liquid phase superficial velocity	m/s
u_G	Gaseous phase superficial velocity	m/s
$u_{G,FL}$	Gaseous phase superficial velocity at flooding	m/s

Greek Symbols	**Description**	**Units**
α	Effective angle of Inclination	Degrees
α_0	Effective angle of inclination at an infinite column diameter	Degrees
δ	Liquid film thickness	mm
μ_L	Dynamic liquid phase viscosity	Pa.s
μ_G	Dynamic gaseous phase viscosity	Pa.s
$\Delta\rho$	Density difference (liquid minus gaseous)	kg/m^3
ρ_G	Gaseous density	kg/m^3
ρ_L	Liquid density	kg/m^3
σ	Liquid surface tension	mN/m
Dimensionless Numbers	**Description**	
B_L	Dimensionless liquid load	
Bo	Bond Number	
Fr_L	Froude Number of liquid	
K	Wall factor	
Re_G	Reynolds number of the gaseous phase	
Re_L	Reynolds number of the liquid phase	
θ	Dimensionless interface radius	
λ_0	Phase flow ratio at flooding	
μ_P	Irrigated packing form factor	
Φ	Flow parameter	
φ_p	Packing form factor	
ψ	Ergun friction factor	
ψ_{FL}	Resistance coefficient for single-phase flow of gas phase at flooding	
ψ_{VL}	Total resistance coefficient	
ψ_W	Wet packing friction factor	

Abbreviations and Acronyms	Description
ASME	American Society of Mechanical Engineers
ATM	Atmospheric
BHT	Butylated Hydroxytoluene
CFD	Computational Fluid Dynamics
DOE	Design of Experiments
EOS	Equation Of State
ET	Ethyl Tetradecanoate
GPDC	Generalized Pressure Drop Correlation
HMI	Human Machine Interface
LCST	Lower Critical Solution Temperature
LVDT	Linear Variable Differential Transformer
NIST	National Institute of Standards and Technology
PDMS	Poly(Dimethylsiloxane)
PEEK	Polyether Ether Ketone
PLC	Programmable Logic Controller
PPE	Personal Protective Equipment
SANAS	South African National Accreditation System
SEC	Size Exclusion Chromatography
SBD	Suspended Bed of Droplets
SRD	Standard Reference Data
SWP	Safe Work Procedure
SF	Supercritical Fluid
SynVisVar	Synthetic, Visual, Variable Volume Method
THF	Tetrahydrofuran
TRA	Task Risk Assessment
UCST	Upper Critical Solution Temperature

1. Introduction

Although the potential use of supercritical fluids as solvents have been known for more than a century, supercritical fluids have seen little industrial application until relatively recently. This neglect could be ascribed to a historical abundance of inexpensive energy and raw materials that negated the need for what was, at the time, perceived to be an expensive and dangerous process [1]. Hence, supercritical extraction was 'put on the shelf' for many years.

With increased competition for energy and raw materials, this situation has recently started to reverse. Firstly, supercritical fluid technology is reviving due to the ever-present drive to refine industrial processes, caused by an industry demand for ever sharper separation processes and higher efficiencies [2]. Secondly, the development of material sciences and globalisation have made supercritical fluid technology more accessible, with materials able to withstand high pressure becoming cheaper and more easily attainable. Thirdly, supercritical fluids have a few inherent advantages over traditional solvents [1]: typically being much less intrinsically harmful than traditional organic solvents and, importantly, able to effect difficult separations that are virtually impossible by traditional means [3].

However, a few elements, such as the lack of well-established design and costing methods, hamper the broader application of the technology. A lack of predictive models is especially evident for one of the workhorses of fractionation technology: the countercurrent extraction/fractionation column.

1.1 Countercurrent Column Hydrodynamics

Hydrodynamics in countercurrent columns entail the study of the behaviour of two discrete phases flowing countercurrently over column internals. A denser phase is added at the top (or middle) of the column, from where it flows over the surface of the column internals with the help of gravity. A second, less dense phase is actively pumped into the bottom of the column and flows upwards through the spaces between the internals. The phases interact, typically effecting mass transfer and a desired separation while flowing through the column in opposite directions. A range of different phase combinations are possible, such as a vapour-liquid system for fractionation (distillation), or a liquid-liquid system for liquid-liquid extraction.

The importance of hydrodynamics comes to light when sizing and designing new columns or retrofitting columns. The limits of operation and optimal efficiency of the column is determined by hydrodynamic capacity [4]. The hydrodynamic capacity is defined as the vapour- and liquid flow rate combinations at which the column becomes hydrodynamically inoperable or where performance, typically mass transfer performance, becomes unacceptable [5, 6]. This capacity depends directly on the physical aspects that limit flow in the column: the column internal's properties; the diameter of the column; the fluid flow rates; as well as the properties of the two co-existing phases [7]. The primary fluid properties that affect hydrodynamics are the density and dynamic viscosity. The interaction between the phases and the column internals causes retention or 'hold-up' of the denser phase in the column as well as a pressure drop over the column internals with respect to the less dense phase. These two phenomena, the liquid hold-up and the pressure drop over the column, are central to the study of column hydrodynamics [4].

Atmospheric column hydrodynamics are well developed, using proven, semi-empirical correlations and dimensionless numbers to predict the interaction between phases, liquid hold-up and pressure drop [4]. In contrast to this, very little work has been done on hydrodynamics under supercritical conditions. The lack of predictive models lead to uncertainties in column design and could lead to unnecessary expense (overdesign) or failure to meet required specifications. Modified subcritical hydrodynamic correlations have been used with some success to approximate supercritical column design [8]; however, they do not successfully compensate for the higher density, viscosity and surface tension of a supercritical fluid.

1.2 Supercritical Fluid as Extractive Solvent.

Supercritical fluids can provide an attractive alternative solvent in industrial separations, fractionations and extractions [1]. This attractiveness is due to several attributes stemming from its fundamental phase properties, providing a flexible, selective and efficient solvent.

Supercritical fluid properties are neither gas-like, nor liquid-like, but rather a set of properties describing an intermediate phase of matter. This phase has attributes somewhere between that of a liquid and a gas, for example being able to diffuse through solids like a gas and dissolve materials like a liquid.

A supercritical fluid is any substance at a temperature and pressure above its critical point, where distinct liquid and gas phases do not exist. An attempt will be made to present a definition derived from basic principles, after which a brief mention of supercritical fluid fundamental behaviour and its effect on the fluid as solvent is made [9]. The critical pressure of a substance is defined as being equal to its vapour pressure at its critical temperature [10]. In turn, the vapour pressure of a substance is defined as the pressure exerted by a vapour in thermodynamic equilibrium with its respective condensed phase in a closed system. It can be deduced that in any state above the critical point, the force exerted by the implied vapour pressure is higher than the liquid's physical limits. That is, the pressure exerted by the 'vapour' exceeds the cohesive forces in the liquid, and the clear interface between the phases break down [9]. This means beyond the critical point the specific volume can be changed on a continuum, eliminating any phase change behaviour. Explaining this from a liquid point of view, it can be inferred that the repellent forces between molecules in the liquid start exceeding the attractive forces due to the high pressure forcing molecules together. This means that the individual molecules have, on average, a larger kinetic energy than the existing attractive forces on the molecule.

This behaviour of supercritical fluids at the molecular scale gives rise to one of its fundamental features, being a localised clustering of molecules [9]. Clustering in the supercritical phase is caused by weak intermolecular forces, such as Van der Waals forces, and is much more dynamic than the stronger bonds found between molecules in liquids. Domination by this weaker intermolecular force influences the solution structure, which in turn influences the transport properties of the fluid, producing the attributes that make supercritical fluids such effective solvents [11, 12]. This clustering amplifies quadrupole interactions, allowing the non-polar CO_2 to dissolve polar and non-polar molecules in the SF phase [13]. Clustering dominates close to the critical point, becoming less significant at higher temperatures or pressures. Further away from the critical point this diminishes and eventually becomes immaterial.

Supercritical fluids also lend themselves to rapid changes in fluid properties such as density and viscosity. Indeed, close to the critical point, small changes in either temperature or pressure can transition the fluid from gas-like to liquid-like behaviour. The combination of the tuneable fluid properties and molecular behaviour, allowing both polar and non-polar interactions, creates a solvent that can 'selectively' dissolve molecules and even differentiate by functional group [1].

As a separations process involves a mixture of multiple components, the consideration of a supercritical fluid with a second component is imperative. Figure 1-1 shows the different recommended extraction methods for two pure components. It can be seen that the supercritical fluid processing regime (D) falls between the liquid-liquid (B) and distillation (C) regimes. The majority of available literature compares supercritical column processes to distillation, however, comparison with liquid-liquid processes will be valid at conditions where the supercritical fluid is more liquid-like, typically at low temperatures and high pressures. The 'in-between' nature of supercritical fluids makes it challenging to model supercritical fluid systems, as there are no models that span both liquid-liquid and gas-liquid operations.

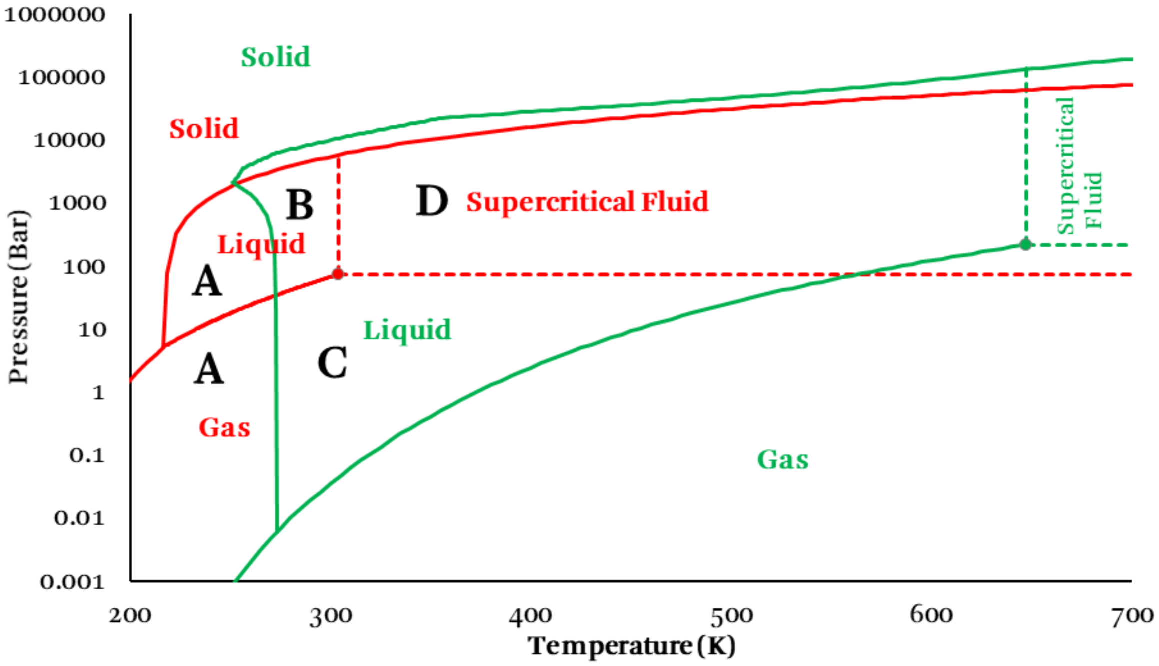

Figure 1-1: Phase diagram of CO_2 (Green) and water (Red). Letters denote different recommended separation techniques. A) Crystallization, B) Liquid-liquid extraction, C) Distillation and D) Supercritical fluid processing. [14, 15]

1.3 The Supercritical Countercurrent Separation Process

The principles behind supercritical fluids have been known since the early 1800s [16], with its properties and advantages as a solvent demonstrated abundantly since. An example of a countercurrent supercritical fractionation plant process flow is seen in Figure 1-2. A supercritical fractionation pilot plant typically consists of four sections: being the solvent-, feed-, fractionation- and separator sections. Many other technologies and configurations are possible, and the below serves as a typical example of the technology.

The feed section consists of a feed tank (V-1) and a positive displacement pump (P-1). From the feed tank, the liquid feed is pumped by a positive displacement pump to the column section.

The solvent section consists of a solvent feed source, a solvent buffer tank (V-2) and positive displacement pump (P-2). Initially, fresh solvent is loaded into the system from the solvent source, after which the solvent recirculates and is topped up as needed. The recirculated, gas-phase solvent is cooled to a liquid phase by refrigeration coils or chilled heat exchangers (HX-1). The liquefied solvent is stored in the solvent buffer tank, from where it is pressurised and pumped onwards by a positive displacement pump. The solvent is pumped through a heat exchanger (HX-2) where it is heated into the supercritical phase and to the appropriate operating temperature before it enters the column. A solvent bypass line is typically present to facilitate column isolation and system startup.

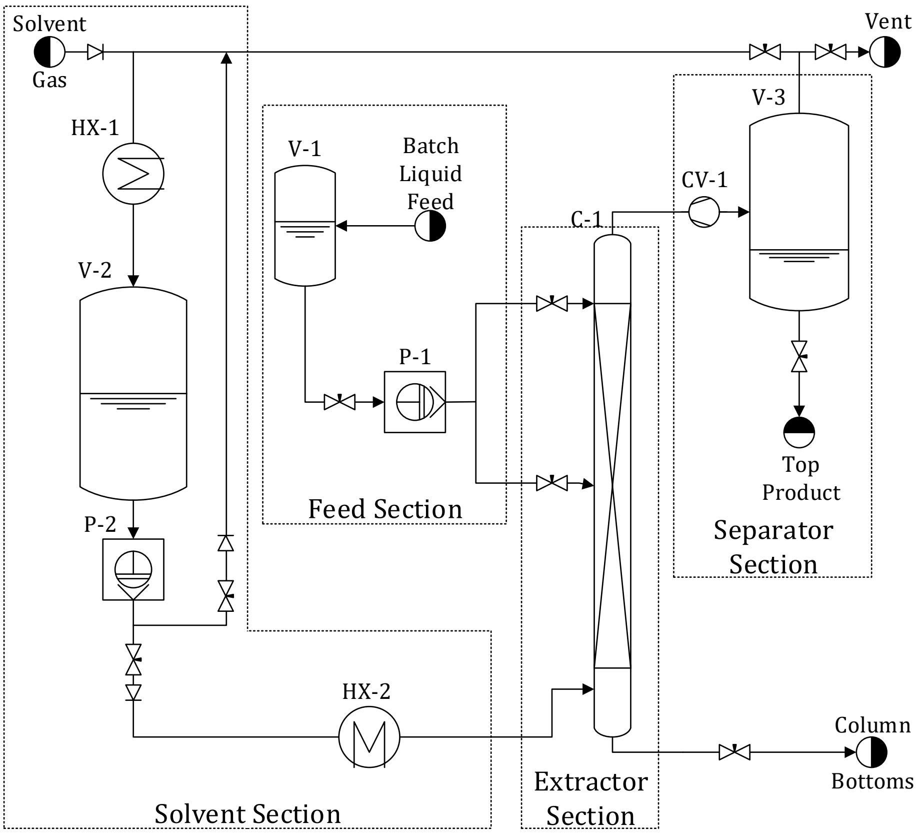

FIGURE LEGEND

V-1	Liquid feed tank	HX-2	Solvent heater
P-1	Liquid feed pump	C-1	Fractionation column(s)
V-2	Liquid solvent buffer tank	CV-1	Pressure control valve
P-2	Solvent feed pump	V-3	Separator(s)
HX-1	Solvent condenser		

Figure 1-2: Process flow diagram for a typical supercritical countercurrent process with a packed fractionation column and solvent recovery.

The fractionation section consists of one or more columns in series or parallel (C1). Columns can be packed with structured or random packing. Depending on the separation requirements, columns can have middle and/or top liquid feed ports. The optimum location of the liquid feed to the column depends on the composition and properties of the liquid, and the degree of separation required [8]. In the column, the liquid and solvent interact to effect mass transfer. The solvent from the solvent section is typically pumped in at at the bottom of the fractionation column and leaves the column at the top rich with solutes. The 'loaded' solvent leaving the column is fed to the separator section. The liquid bottoms product is typically decanted or fed to a downstream process.

The separator section contains a pressure control valve (CV-1) and one or more separator vessels (V-3). The solute rich solvent from the column is expanded through the control valve into the separator vessel to a pressure below the critical point. The solvent reverts to a gas phase, and the solutes are precipitated out with a liquid or solid product allowed to settle by gravity.

The gaseous solvent then passes through a filter and fed back into the solvent section where it is condensed and then recycled. The liquid column bottoms is typically decanted in a batch-wise fashion.

1.4 Study Context, Aim, Objectives and Structure

This study follows a Master's study, during which a supercritical pilot plant was constructed [10]. The pilot plant was designed with the measurement of supercritical hydrodynamics in mind and can measure a range of fluid flows at pressures up to 30 MPa and 473 K.

This study further complements previous and ongoing research into supercritical fractionation using countercurrent columns, and supercritical phase equilibria and mass transfer at Stellenbosch University. To date, the research has involved high-pressure bubble and dew point measurements [17-27], piloting [28-31], column hydrodynamic studies [10], low-pressure VLE and VLLE measurements and theoretical modelling [32-35].

The dissertation is preambled by a literature review (Chapter 2). It was found that no systems in the literature present the full complement of data required for a comprehensive hydrodynamic study, and no comprehensive hydrodynamic studies were found. Essential data required when investigating hydrodynamics are the phase equilibria and fluid property data (in particular density and viscosity) at saturation, for both phases. Finally, no robust hydrodynamic models exist for columns operating with supercritical fluids.

This aim of this study is to investigate hydrodynamics in countercurrent columns operating under supercritical conditions, laying groundwork for the eventual development of accurate predictive models and design methods.

To achieve this aim, the study is separated into five objectives, each discussed separately below, were defined. The objectives follow the sequence depicted in Figure 1-3, in short to:

1) Develop equipment for the measurement of fluid properties;
2) Binary system selection and fluid property measurement;
3) Hydrodynamic experiments, operability, fluid property influence and results analysis;
4) Model evaluation vs gathered data;
5) Hypothesis test: fundamental similarity with classical hydrodynamics.

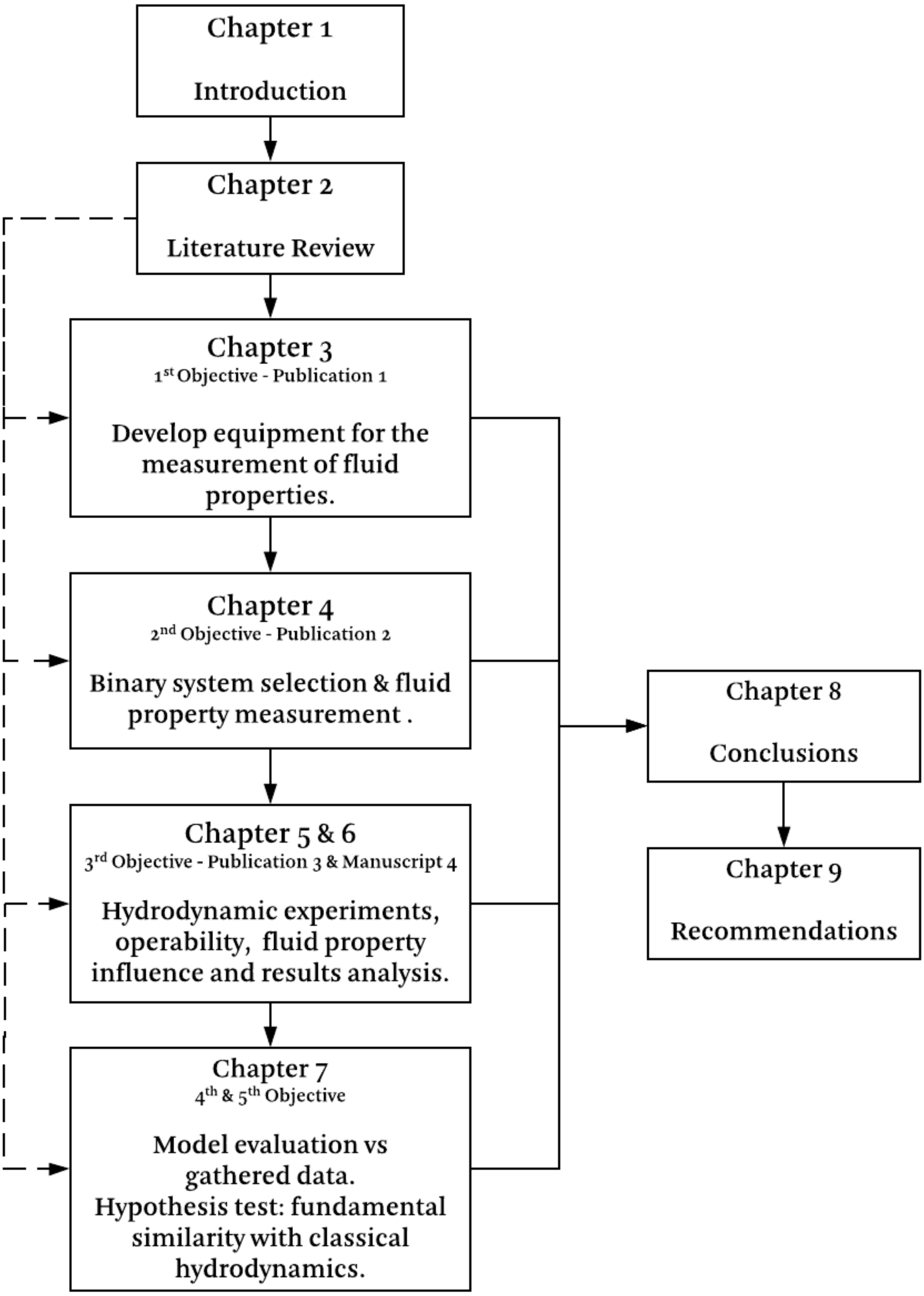

Figure 1-3: Thesis layout illustrating the relationship between different chapters and, where applicable, a short comment on the chapter content.

The detailed objectives and how they were addressed can be found below.

This dissertation is presented towards obtaining a PhD through publication, as allowed by the Stellenbosch University. PhD through publication implies that a large part of the work in this document has either already been published, or has been submitted for publication, on peer-reviewed platforms. Chapters 3-5 address specific aims and are published journal articles and are presented as published, with comments in footnotes where needed. Chapter 4 has been submitted for publication at the time of the submission of the dissertation. Additional research outputs in the form of conference presentations and posters can be found in Appendix A.

The first and second objectives were identified to address the gap in the literature with regards to phase equilibria and physical property data:

1. To design, construct, commission, and verify equipment capable of simultaneously measuring the phase equilibria and fluid properties of density and dynamic viscosity at saturation under supercritical conditions.
2. Use the constructed equipment to measure binary phase equilibria and property data with a supercritical fluid as one of the components. Use the measured data to identify experimental systems exhibiting low mutual solubility (reducing the effect of mass transfer), with fluid properties similar to that of industrially relevant processes.

The first objective is addressed in Publication 1: *Concurrent Measurement of High-Pressure Binary Phase Equilibrium, Density and Dynamic Viscosity* [36] (Chapter 3). In this paper, new equipment was presented that was designed, constructed and commissioned. The equipment offered a novel method of concurrently determining the binary phase equilibria as well as the density and dynamic viscosity of the saturated fluid. The equipment and method was validated for single-component fluids as well as a binary supercritical system using n-dodecane, benzene and CO_2 + ethyl tetradecanoate. New data for benzene is presented as well as new saturated phase properties for the binary system.

The first publication presents the equipment needed to achieve the second objective. The validated equipment is used to gather fluid property data needed for hydrodynamic studies.

The second objective is addressed in Publication 2: *High-pressure Binary Phase Equilibria, Density and Dynamic Viscosity of 100 & 200 cSt Polydimethylsiloxane (PDMS) with Supercritical* CO_2 [37] (Chapter 4). This paper first presents a discussion on the selection of an appropriate experimental system for hydrodynamic study. Two PDMS + CO_2 systems, PDMS 100 cSt and PDMS 200 cSt, are identified as suitable; promising low mutual solubility and appropriate fluid properties. New phase equilibria and saturated fluid properties were then measured for the systems exhibiting the required characteristics.

The data gathered and published in the second publication provide a basis from which to plan hydrodynamic experiments that can isolate the influence of fluid properties on hydrodynamics while minimising the effect of mass transfer.

The gathered data allows progression to the third, fourth and final objectives to address the lack of hydrodynamic data:

3. To measure hydrodynamic data, namely liquid hold-up and pressure drop, for the selected system(s). The hydrodynamics can then be used to determine A) the operability limits of the system and B) the influence of the fluid properties of viscosity and density on hydrodynamics.
4. To compare the gathered hydrodynamic data to available models to determine their accuracy in predicting supercritical hydrodynamics.
5. To test the literature hypothesis that supercritical hydrodynamics are fundamentally similar to atmospheric systems.

The third objective is addressed in Publication 3: *Hydrodynamics of a Packed Column Operated under Supercritical Conditions* [38] (Chapter 5) and Manuscript 4: *Influence of Fluid Properties on Hydrodynamics, and the Dependant Operability of a Countercurrent Column Operated under Supercritical Conditions* (Chapter 6), to be submitted for publication. Publication 3 is a conference publication provides a brief snapshot of flooding in particular in the PDMS 100 cSt + CO_2 system and presents preliminary hydrodynamic results. Manuscript 4 expands on Publication 3, presenting a full complement of hydrodynamic data for both fluid systems used, being 100 cSt and 200 cSt PDMS with supercritical CO_2. The column operability limits and modes of reaching inoperability are discussed. The section is concluded by investigating the influence of the fluid properties on the hydrodynamics

The fourth objective is addressed in Chapter 7: *Comparison with Hydrodynamic Models and Literature*. The experimental results are compared to the available hydrodynamic models (to be discussed in Chapter 2.4). The liquid hold-up and pressure drop are modelled, and adjustments to the models are suggested to provide better predictions of the data.

The fifth and final objective is addressed in Chapter 7.3: *Supercritical Hydrodynamics vs Atmospheric Hydrodynamics*.

The work is concluded with a conclusions chapter, where the results are reviewed and summarised, and recommendations for future work.

References

[1] Schwarz, C.E. and Knoetze, J.H., *Design of Supercritical Fluid Processes for High Molecular Mass Petrochemicals*, 'Supercritical Fluids', M. Belinsky (ed). Nova Science Publishers Inc., 2009.

[2] Nieuwoudt, I., *The Fractionation of High Molecular Weight Alkane Mixtures with Supercritical Fluids*; PhD Dissertation, Stellenbosch University, Department of Process Engineering, 1994.

[3] Seibert, A.F. and Moosberg, D.G., *Performance of Spray, Sieve Tray, and Packed Contactors for High Pressure Extraction*, Sep. Sci. Tech., 23 (1988) 2049-2063.

[4] Maćkowiak, J., *Fluid Dynamics of Packed Columns*, Springer, Berlin, Germany, 2010.

[5] Lamprecht, S.M., *Establishing a Facility to Measure Packed Column Hydrodynamics*; Masters Dissertation, Stellenbosch University, Department of Process Engineering, 2010.

[6] Sherwood, T.K., Shipley, G.H. and Holloway, F.A.L., *Flooding Velocities in Packed Columns*, Ind. Eng. Chem., 30 (1938) 765-769.

[7] Eckert, J.S., *How tower packings behave*, Chem. Eng., 2 (1975) 70-76.

[8] Brunner, G., *Counter-current separations*, J. Supercrit. Fluids, 47 (2009) 574 - 582.

[9] Arai, Y., Sako, T. and Takebayashi, Y., *Supercritical fluids - Molecular interactions, Physical Properties and New Applications*, Springer: London, England, 2002.

[10] Franken, H.H., *Establishment of a Supercritical Pilot Plant and the Hydrodynamics of Supercritical Countercurrent Columns*; Masters Dissertation, Stellenbosch University, Department of Process Engineering, 2014.

[11] Saito, S., *Research activities on supercritical fluid science and technology in Japan—A review*, J. Supercrit. Fluids, 8 (1995) 177-204.

[12] Bright, F.V. and McNally, M.E., *Supercritical Fluid Technology- Theoretical and Applied Approaches to Analytical Chemistry*; ACS Symposium Series, Vol. 488, Washington DC, United States of America, 1992.

[13] Raveendran, P., Ikushima, Y. and Wallen, S.L., *Polar Attributes of Supercritical Carbon Dioxide*, Acc. Chem. Res., 38 (2005) 478-485.

[14] Wagner, W., Saul, A and Pruss, A., *International Equations for the Pressure along the Melting and along the Sublimation Curve for Ordinary Water Substance*, J. Phys. Chem. Ref. Data, Vol 23, No 3, 1994

[15] Span, R. and Wagner, W., *A New Equation of State for Carbon Dioxide Covering the Fluid Region from the Triple-Point Temperature to 1100 K at Pressures up to 800 MPa*, J. Phys. Chem. Ref. Data, 25 (1996) 1509-1596.

[16] Berche, B., Henkel, M. and Kenna, R., *Critical phenomena: 150 years since Cagniard de la Tour*, J. Phys. Stud, 13 (2009) 1-4.

[17] Schwarz, C.E., Nieuwoudt, I. and Knoetze, J.H., *Phase equilibria of long chain n-alkanes in supercritical ethane: Review, measurements and prediction*, J Supercrit. Fluids, 46 (2008) 226-232.

[18] Schwarz, C.E., Nieuwoudt, I. and Knoetze, J.H., *Phase equilibrium of propane and alkanes Part III: Beyond hexacontane*, J. Supercrit. Fluids, 41 (2007) 327-334.

[19] Nieuwoudt, I., and Du Rand, M., *Measurement of phase equilibria of supercritical carbon dioxide and paraffins*, J. Supercrit. Fluids, 22 (2002) 185-199.

[20] Du Rand, M. and Nieuwoudt, I., *Measurement of phase equilibria of supercritical ethane and paraffins*, J. Supercrit. Fluids, 21 (2001) 181-193.

[21] Ferreira, M. and Schwarz, C.E., *Super- and near-critical fluid phase behavior and phenomena of the ternary system* CO_2 *+ 1-decanol + n-tetradecane*, J. Chem. Thermodyn., 111 (2017) 88-99.

[22] Schwarz, C.E., Paulse, Q.H. and Knoetze, J.H.*, Phase equilibria of methyl esters in supercritical propane*, J. Supercrit. Fluids, 99 (2015) 61-67.

[23] Schwarz, C.E., and Chobanov, K.G., *Phase equilibria of linear saturated high molecular mass acids in supercritical ethane*, J. Supercrit. Fluids, 87 (2014) 40-49.

[24] Schwarz, C.E. and Knoetze, J.H., *Phase equilibrium measurements of long chain acids in supercritical carbon dioxide*, J. Supercrit. Fluids, 66 (2012) 36-48.

[25] Zamudio, M., Schwarz, C.E. and Knoetze, J.H., *Phase equilibria of branched isomers of* C_{10}*-alcohols and* C_{10}*-alkanes in supercritical carbon dioxide*, J. Supercrit. Fluids, 59 (2011) 14-26.

[26] Schwarz, C.E., Fourie, F.C.v.N. and Knoetze, J.H., *Phase equilibria of alcohols in supercritical fluids Part II: The effect of side branching on C_8 alcohols in supercritical carbon dioxide*, J. Supercrit. Fluids, 51 (2009) 128-135.

[27] Fourie, F.C.v.N., Schwarz, C.E. and Knoetze, J.H., *Phase equilibria of alcohols in supercritical fluids Part I. The effect of the position of the hydroxyl group for linear C_8 alcohols in supercritical carbon dioxide*, J. Supercrit. Fluids, 47 (2008) 161-167.

[28] Zamudio, M., *The Separation of Detergent Range Alkanes and Alcohol Isomers with Supercritical Carbon Dioxide*, PhD Dissertation, Stellenbosch University, South Africa, 2014.

[29] Zamudio, M., Schwarz, C.E. and Knoetze, J.H., *The effect of branched alcohol isomers on the separation of alkanes and alcohols with supercritical CO_2*, Poster communication, 13th European Meeting on Supercritical Fluids, The Hague, Netherlands, 2011.

[30] Schwarz, C.E., Bonthuys, G.J.K., Van Schalkwyk, R.F., Laubscher, D.L., Burger, A.J. and Knoetze, J.H., *Separation of alkanes and alcohols with supercritical fluids. Part II. Influence of process parameters and size of operating range*, J. Supercrit. Fluids, 58 (2011) 352-359.

[31] Schwarz, C.E., Nieuwoudt, I. and Knoetze, J.H., *Additional Pilot Plant Measurements with Incorporation of Reflux for the Fractionation of Wax Derivatives with Supercritical Propane*, Ind. Eng. Chem. Res., 49 (2010) 4462-4467.

[32] Lombard, J.E., *Thermodynamic modelling of hydrocarbon-chains and light-weight supercritical solvents*, MSc Thesis, Stellenbosch University, South Africa, 2015.

[33] De Villiers, A.J., Schwarz, C.E., Burger, A.J. and Kontogeorgis, G.M.*, Evaluation of the PC-SAFT, SAFT and CPA equations of state in predicting derivative properties of selected non-polar and hydrogen-bonding compounds*, Fluid Phase Equilib., 338 (2013) 1-15.

[34] Zamudio, M., Schwarz, C.E. and Knoetze, J.H., *Experimental measurement and modelling with Aspen Plus® of the phase behaviour of supercritical CO_2 + (n-dodecane + 1-decanol + 3,7-dimethyl-1-octanol)*, J. Supercrit. Fluids, 84 (2013) 132-145.

[35] Schwarz, C.E., De Villiers, A.J., McClune, C.B., Bonthuys, G.J.K., Burger, A.J. and Knoetze, J.H., *High pressure phase equilibrium measurements of long chain alcohols in supercritical ethane*, J. Supercrit. Fluids, 55 (2010) 554-565.

[36] Franken, H.H., Knoetze, J.H. and Schwarz, C.E., *Concurrent measurement of high-pressure binary phase equilibrium, density and dynamic viscosity*, J. Supercrit. Fluids, 133 (2018) 444-454.

[37] Franken, H.H., Knoetze, J.H. and Schwarz, C.E., *High-pressure binary phase equilibria, density and dynamic viscosity of 100 & 200 cSt polydimethylsiloxane (PDMS) with supercritical* CO_2, J. Supercritical Fluids, 139 (2018) 1-7.

[38] Franken, H.H., Knoetze, J.H. and Schwarz, C.E., *Hydrodynamics of a Packed Column Operated under Supercritical Conditions*, Chem. Eng. Trans., 69 (2018).

2. Background Literature

The literature review section contains an introduction to the key concepts in supercritical fluids and two-phase countercurrent column hydrodynamics. After these chapters currently available supercritical two-phase countercurrent hydrodynamic literature and correlations are discussed. Some of the basic, introductory literature presented below, in particular, a significant part of Section 2.1 to 2.3, is summarised from the preceding Master's study [1]. Each subsection adapted, improved upon or repurposed will be indicated at the start of the subsection.

2.1 Supercritical Fluids

The following section of basic background literature is adapted and improved upon from the preceding Masters Study [1].

A supercritical fluid is any substance above its critical temperature and pressure. The critical point of a pure compound lies at the end of the gas-liquid equilibrium curve and defines the critical temperature and pressure. Above this point, phase transitions disappear, and distinct liquid and gas phases do not exist. As a consequence, there is no clear physical delimitation of the supercritical phase, but rather an implied boundary. Despite this, the supercritical state is defined as a separate phase, as can be seen in Figure 2-1

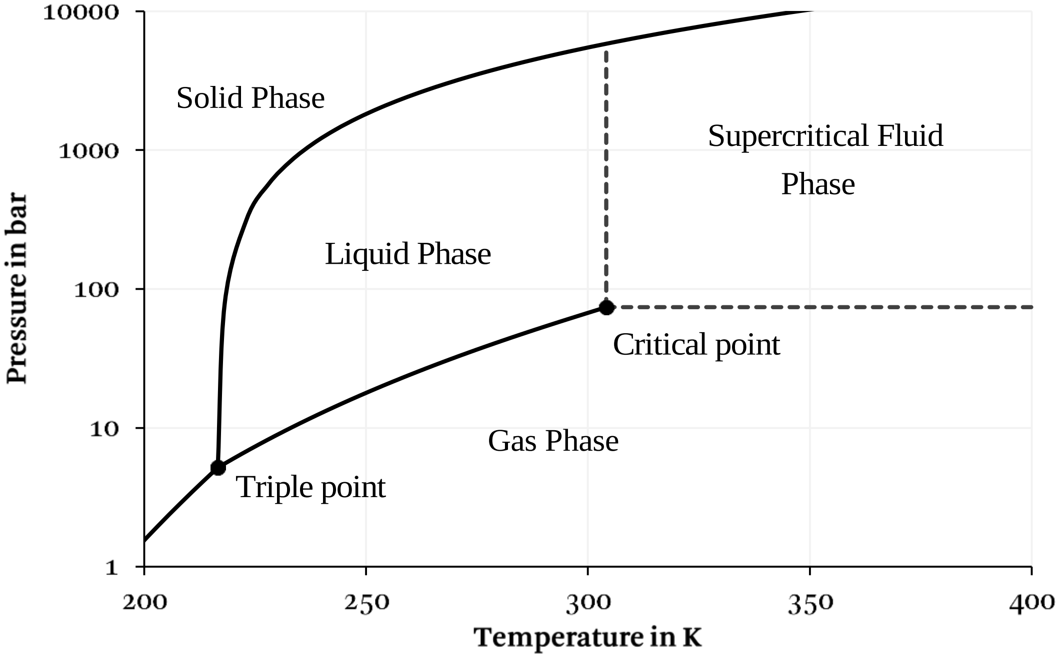

Figure 2-1: CO_2 pressure-temperature phase diagram.
(Drawn from data calculated by NIST WebBook using the equation of state proposed by Span and Wagner [2])

Supercritical fluids exhibit neither the expected behaviours of a gas, nor a liquid, but instead possess a set of properties describing an intermediate phase of matter. The supercritical phase has attributes somewhere between that of a liquid and a gas, for example being able to diffuse through solids like a gas and dissolve materials like a liquid.

2.1.1 Temperature and Pressure Dependence

The following section of basic background literature is repurposed from the preceding Masters Study [1].

According to Gibbs' phase rule [3], the properties of a single component, present in a single phase, can be defined using two intensive variables. The pressure and temperature represents the fundamental dependencies of a phase, with all subsequent terms derivable through thermodynamics. In order to define the dependence of the supercritical phase on temperature and pressure, one is kept constant while the other is varied.

At constant pressure, changes in temperature play a significant role in the supercritical phase. This is especially true close to the critical point where a slight isobaric change in temperature will cause disproportionally large changes in the density and viscosity of the fluid. This temperature dependence is seen in Figure 2-2 and Figure 2-3. An increase in temperature causes a decrease in density and viscosity, which corresponds with a more gas-like phase forming.

At constant temperature, the density and viscosity is also significantly influenced by the pressure. An increase in pressure leads to an increase in density and viscosity and a more liquid-like phase forming. Once again, close to the critical point, small changes in the pressure drastically affect the properties of the fluid, leading to rapid changes from gas-like to liquid-like behaviour and vice versa. This pressure dependence can be seen very well in Figure 2-2 and Figure 2-3 by following the property line at the critical temperature, where the density and viscosity change significantly with a small increase or decrease in pressure.

Density and viscosity are essential factors when investigating hydrodynamics as they directly influence the fluid flow of a supercritical phase and govern interactions between the supercritical phase and other phases.

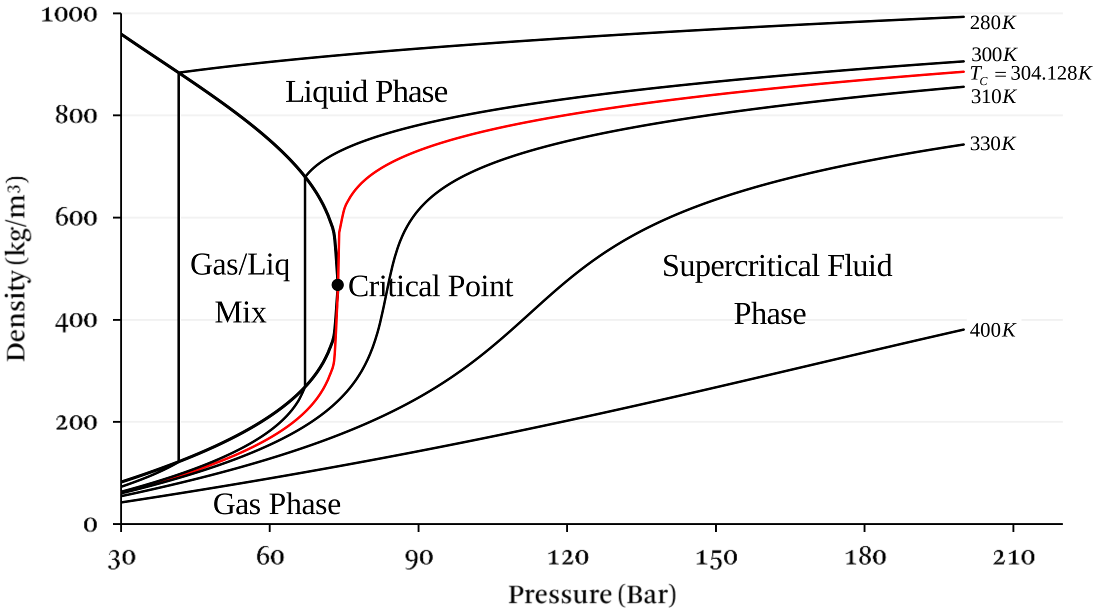

Figure 2-2: CO_2 density-pressure phase diagram at varied temperatures.
(Drawn from data calculated by NIST WebBook using the equation of state proposed by Span and Wagner [2])

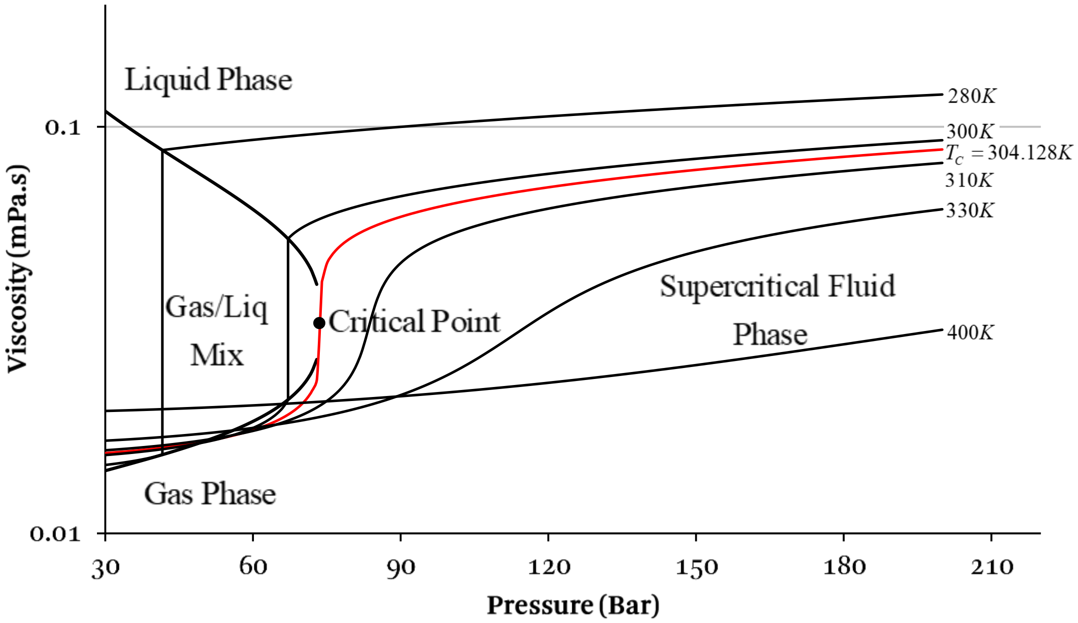

Figure 2-3: CO_2 viscosity-pressure phase diagram at varied temperatures.
(Drawn from data calculated by NIST WebBook using the viscosity model proposed by Fenghour et al. [4])

2.1.2 Typical Properties

The following section of basic background literature is repurposed from the preceding Masters Study [1].

The typical properties of a supercritical fluid are affected by its intermediate nature, the phenomenon of molecule clustering and the temperature and pressure dependence of its fluid properties. The individual properties of a supercritical fluid may be summarised as follows [5]:

The density of the phase can be gas-like or liquid-like, depending on the state relative to the critical point. The density usually tends more towards that of the corresponding liquid phase. As discussed in Section 2.1.1, the density increases with a decrease in temperature and/or an increase in pressure.

The viscosity is of intermediate value, falling between that of the liquid and the gas. Viscosity increases with a decrease in temperature and/or an increase in pressure. In this aspect, the supercritical phase is more liquid-like, with the temperature and pressure dependence being directly the inverse of that of a gas.

Thermal conductivity falls between the general values of the liquid and gaseous states of the compound. Thermal conductivity increases with a decrease in temperature and/or an increase in pressure. The temperature dependence corresponds with that of a liquid, but not with that of a gas.

Diffusivity also falls between that of the pure gas and liquid states, with values tending more towards a gas-like state. The diffusivity of supercritical fluids is up to five times higher than the liquid state. The high diffusivity contributes to higher effective mass transfer rates.

The surface tension of supercritical fluids is between that of the liquid and the gas, although values tend more towards that of the gas. It is an important variable when considering wetting in packed columns, where low surface tension is preferred. The surface tension decreases as the pressure increases and has a complicated relationship with temperature.

2.1.3 Advantages and Disadvantages of Supercritical Fluid Solvents

The following section of basic background literature is summarised and modified from the preceding Masters Study [1].

The advantages and disadvantages of fractionating with a supercritical fluid are discussed below. The advantages and disadvantages discussed are summarised from the literature [6, 7], unless otherwise referenced.

Using a supercritical fluid as a solvent holds several advantages over traditional systems. These include, but are not limited to, the following:

- Some supercritical solvents can be operated at low temperatures and even close to ambient temperatures, avoiding thermal degradation of labile components and high heating costs.
- Supercritical fluids are very flexible solvents with a wide range of separations achievable with variation in temperature and pressure. The operating conditions of a column can be fine-tuned to exactly meet the needs of a specific separation or changed during operation to compensate for an irregular feedstock.
- Supercritical fluids can exhibit a high degree of selectivity and can even distinguish between different molecules according to its chain length [8] and functional group [9]. This selectivity allows for more efficient processes and sharper separations.
- Generally, the properties of a supercritical solvent allows for higher mass transfer rates than possible in traditional solvents.
- The extracted solute is readily recovered, and the process leaves little to no residual solvent in the product.
- The solvent is readily recyclable with no significant theoretical losses. Therefore a fractionation process requires very little addition of fresh solvent during operation.
- Supercritical fluids are ordinarily less toxic and more environmentally friendly than the equivalent traditional solvents.

No process is without its disadvantages, and supercritical fluid processing is no exception. Some disadvantages are:

- Supercritical processes operate at much higher pressures than traditional separations. The higher operating pressure implies higher process equipment specification requirements and stricter safety and maintenance procedures.
- The technology is still immature, with well established, standardised design methods and operating philosophies few and far between.
- Supercritical phase behaviour is complicated because of the non-ideality and intrinsic asymmetric nature of the system.
- Supercritical extraction/fractionation is not easily modelled in commercially available process simulators.

Supercritical fractionation fulfils specialised roles niche areas, utilising the nature of supercritical fluids to execute challenging separations not possible with traditional means.

Before hydrodynamics under supercritical conditions are discussed, an overview of classical hydrodynamics is presented.

2.2 Overview of Two-Phase Countercurrent Column Hydrodynamics

The following section of basic background literature is adapted from the preceding Masters Study [1].

The Oxford dictionary defines hydrodynamics as: "The branch of science concerned with forces acting on or exerted by fluids" [10] and is a sub-category of Fluid Mechanics. The hydrodynamic capacity of a system is its range of operability [11]. Hydrodynamic capacity is delimited by the fluid flow rate combinations at which the column becomes hydrodynamically inoperable or where performance, typically mass transfer performance, becomes unacceptable [12, 13]. Hydrodynamics encompass, among others, the pressure drop over the column, liquid hold-up in the column and flow rates of the respective fluids, which is a function of the fluid properties and column internals.

As mentioned in the introduction, supercritical hydrodynamics fall between gas-liquid and liquid-liquid systems. The majority of the systems in literature have treated such systems similarly to distillation. Gas-liquid systems are also the predominant approach of this work, although the potential applicability of a liquid-liquid system approach cannot be denied. the following discussion delves deeper into a gas-liquid system, with a brief view on liquid-liquid systems in Section 2.2.5.

2.2.1 Packed Column Internals

The following section of basic background literature is adapted and improved upon from the preceding Masters Study [1].

Column internals increase the available surface area in a column and encourages contact between the respective phases. Mass transfer occurs at the interface between the phases, meaning the selection of the correct internal for a process is crucial.

A supercritical fractionation is analogous to a stripping or rectification column, where random and structured packings are typically the internal of choice. Random packing was developed as an alternative to tray columns [11], providing a reduction in pressure drop, increase in capacity and reduced liquid hold-up. Random packing consists of a multitude of discrete units of a specific geometry packed into a column. The column internals create a randomised bed with a large surface area. The specific traits of a particular packing depends on the geometry of the individual units.

Structured packing followed random packing, providing a more consistent and predictable solution. Structured packing consists of crimped layers of wire mesh, corrugated or metal gauze sheets. The sheets form a distinctive pattern, usually consisting of triangular or sinusoidal channels arranged in parallel to each other and at an oblique angle relative to the column. Tray setups, although not discussed here, can be constructed for small diameter columns in the form of cartridge trays. Cartridge trays are not readily available commercially as a standard option for the column sizes considered, leading to very high construction costs.

¼″ Dixon Rings were selected for this study. Dixon rings present a readily available, relatively cheap, small diameter random packing with high efficiency and low-pressure drop. Dixon rings are recommended for small diameter columns and have shown to be useful in 'difficult' separations [14].

2.2.2 Falling Films

The following section of basic background literature is expanded upon and improved from the preceding Masters Study [1].

In a column, the liquid flow over the packing elements is the easiest to predict, as adhesion forces in the liquid will cause the liquid to strive to maintain contact with column internals. This liquid flow is approximated as a falling film on the surface of the column packing.

In both structured and random packings, the lighter gaseous phase flows in the opposite direction, exerting a shear force on the falling film. This shear force works on the boundary between the fluids, causing pressure drop and characteristic flow patterns. This film flow was described by Mersmann [15] in his attempt to derive general considerations on the hydrodynamic behaviour of random packings. Three different film flow profiles are identified at increasing gas flow rates, as can be seen in Figure 2-4 [16].

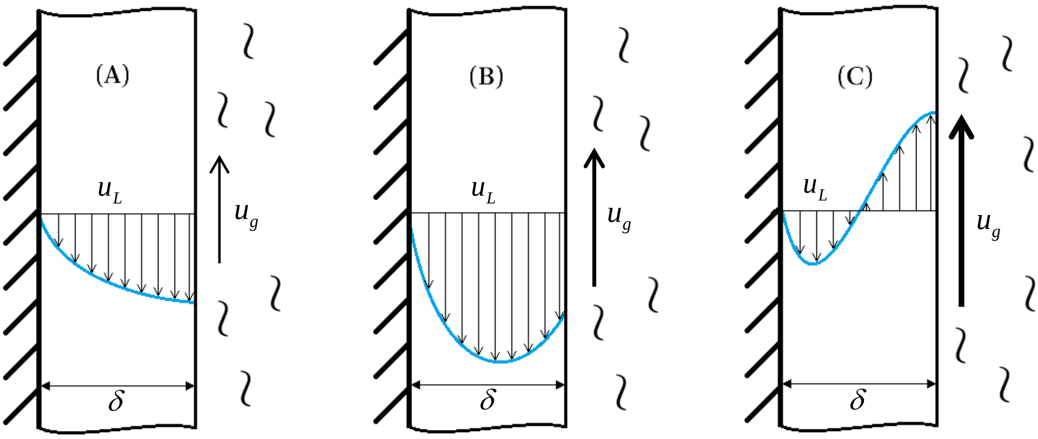

Figure 2-4: Film flow with A) negligible, B) strong and C) very strong gas counterflow. Drawn from the worded definition by Tilton in Perry's Chemical Engineers' Handbook [16].

At low gas flow rates (Figure 2-4A), the shear force is too small to affect liquid flow significantly. A liquid velocity gradient of zero is observed at the phase boundary. Increased gas flow (Figure 2-4B), causes significant interaction and a new velocity profile forms in the liquid. The liquid flow is somewhat hindered, but the net liquid flow is still in a downward direction. At very high gas velocities (Figure 2-4C), the force exerted by the gas is sufficient to entrain the liquid, driven by film instability, surface waves and droplet formation. The liquid flow is significantly impeded, and flooding occurs as soon as a net upward flow of liquid is reached.

Between each of these film flow regions, points of change are defined. Firstly, the loading point is the point at which the force exerted by the gas on the liquid becomes significant, and the rate of change in pressure drop with increasing flow rate starts to change. This shift happens between Figure 2-4A and Figure 2-4B. Secondly, the flooding point where a finite change in the liquid or gas flow causes the column to flood or, theoretically, for the pressure drop to tend to infinity [17, 18]. This shift happens between Figure 2-4B and Figure 2-4C.

The stability of films is a broad field of study and contributes to the fundamental understanding of column hydrodynamics. Falling films allow for the better understanding of interfacial phenomena such as driven by film instability, surface waves and droplet formation which in turn are crucial for selecting the assumptions and boundary conditions in the derivation of a model. Flooding can also be predicted using film theory.

2.2.2.1. Falling Films under Supercritical Conditions.

Limited work has been done on falling films under high pressure and supercritical conditions. The work of Guedes de Carvalo and Talaia [19] presents a summary of high-pressure work before 1998 and presents a flooding prediction for wetted wall columns.

Supercritical falling film work by Stockfleth and Brunner [20], found that falling films under supercritical conditions are not smooth and show ‘wavy’ behaviour even at low flow rates in agreement with prior literature [21]. The formation of wave crests, followed by droplet formation and flooding was observed with an increase in liquid flow. The determination of these transitions is important to identify potential flooding and the behaviour that causes it. Stockfleth et al. [20] found that Nusselt’s [22] equations could be used to describe the falling film flow, despite some of the assumptions of the equation not being valid for high pressure falling films.

This study approaches hydrodynamics through a more macroscopic approach through the measurement of pressure drop and liquid hold-up.

2.2.3 Pressure Drop

The following section of basic background literature is adapted from the preceding Masters Study [1].

The pressure drop over a column is one of the standard parameters measured in hydrodynamic investigations. It is measured over the column internals, with the highest pressure at the bottom of the column and the lowest at the top. It is dependent on the column internals, operating pressure, fluid properties and fluid flow rates and is easily measured and clearly defined. For a specific type of packing and column diameter under the same operating conditions, the pressure drop increases linearly with packed height [11]. With columns typically being of differing heights, the absolute pressure drop over a column is not a meaningful value, and it is related to a unit length (e.g. Pa/m).

This pressure drop per unit length, $\Delta P/H$, has a direct relationship with the separation efficiency, n_t/H , of a column. This dependency was initially discovered by Kirschbaum [23] and is shown in Equations {2-1, 2-2}:

$$\frac{\Delta P}{H} = \psi_{VL} \times \frac{u_G^2}{2} \times \frac{\rho_G}{d} \qquad \{2\text{-}1\}$$

$$\frac{n_t/H}{\psi_{VL}} \cong 0.13 \qquad \{2\text{-}2\}$$

where n_t/H is the number of theoretical stages per 1 m of packed height, ψ_{VL} the total resistance coefficient, u_G is the gaseous phase velocity, ρ_G the gaseous phase density and d the column diameter.

The pressure drop of a specific packing can be used along with these correlations to determine the column diameter needed for a specific application. Since Kirschbaum [23], correlating the pressure drop to efficiency has been further pursued by Billet and Mackoviak [24, 25, 26, 27].

As the pressure drop can be correlated with the separation efficiency, it is used not only to predict flooding but to determine the optimal operation point of the column. In the loading region, which will be discussed more thoroughly later in this section, efficiency increases with an increase in pressure drop. This trend typically continues to just before the flooding point, whereafter the efficiency drops drastically. Heuristics state that a typical operating point of 70% [28, 29] of the flooding point is to be advised. This operating point can be determined by using a GPDC (Generalized Pressure Drop Correlation) chart, the most common of these being the Sherwood-Lobo [13] correlation.

2.2.3.1. Dry and Wet Pressure Drop

The following section of basic background literature is adapted from the preceding Masters Study [1].

The measurement of pressure drop is divided into a dry and a wet pressure drop [11]. The dry pressure drop, $\Delta P_0/H$, is measured at a specific gas flow rate in the absence of liquids. The dry-bed pressure drop provides a measure of the pressure drop without two-fluid interactions, and hence without flooding and shear phenomena. It is important to remember to subtract the static head during any experimentation.

The wet or irrigated pressure drop, $\Delta P/H$, is measured during operation with both phases present. Here the fluids interact, exerting shear forces on each other, causing additional pressure drop over the column. The wet pressure drop is essential when designing countercurrent systems. The wet pressure drop is generally used in correlations and equations describing hydrodynamics, as it represents actual operating conditions.

Typical wet and dry pressure drop curves can be seen in Figure 2-5. The pressure drop is plotted against the gas capacity factor F_G , also called the vapour flow factor, which is defined as the gas velocity adjusted for the density of the gas. The gas capacity factor will be discussed in Section 2.4.

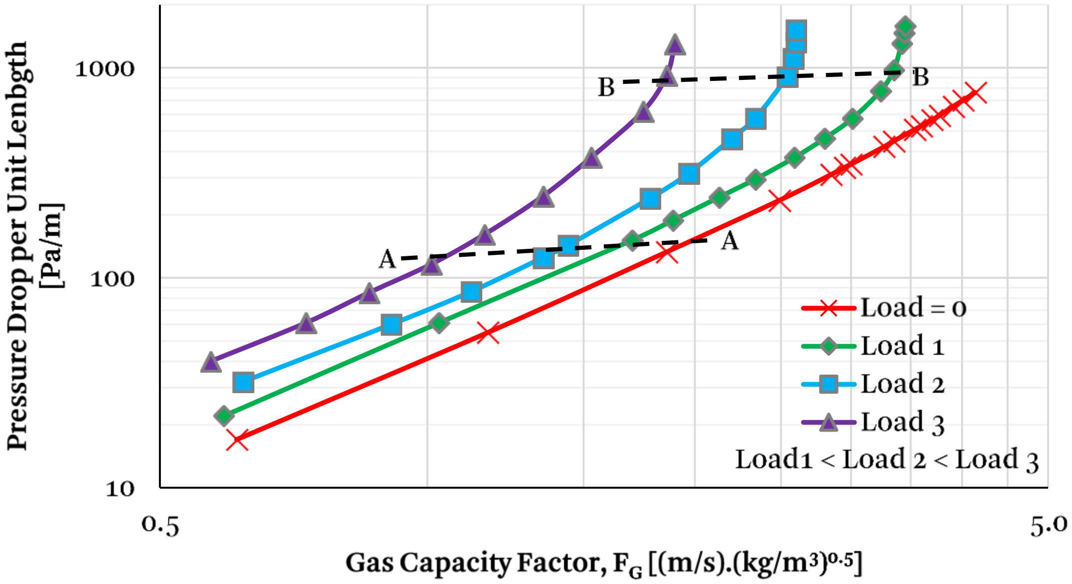

Figure 2-5: Typical pressure drop vs gas capacity factor. Drawn from data by Lamprecht [30]. 'Load' refers to the liquid load to the column, where Load = 0 being the no liquid flow case.

- The loading region: Here, the interaction between phases becomes significant, but not overwhelming, and the resulting shear forces cause an additional pressure drop. The rate of change in the pressure drop with increasing flow rate is no longer linear, but increases as a function of the gas capacity factor in this regime. The loading region is represented as the area between the A–A and B–B lines, being between the loading and flooding points. The loading regime presents the regime in which most columns are operated. In this regime, efficiency increases with an increase in pressure drop, up to the flooding point.

- The flooding region: The rapidly increasing pressure drop eventually yields a point where the value effectively tends to infinity (except at very low liquid loadings). This point is defined as the flooding point, and any points beyond this are seen as being in the flooding region. The area beyond the B–B line falls within this flow regime. The flooding point is not well defined, with separate researchers giving different definitions. The differences in definition in the literature means that the placement of line B–B is dependant on each researcher. Flooding and operability will be discussed in detail in Chapters 5 and 6.

2.2.3.2. Pressure Drop in Random vs Structured Packings

The following section of basic background literature is improved upon from the preceding Masters Study [1].

At the same gas capacity factor, the dry pressure drop behaves differently for random and structured packings. Apart from the noticeable changes due to different geometries, each packing type also responds differently to a change in column diameter. In a random packing, the pressure drop is typically independent of the column diameter (and is a function of the packing size to tower diameter ratio, typically 1:8), while in structured packing, the column diameter has been shown to have a significant effect in small diameter columns [31, 32], such as those used for supercritical work. The pressure drop over a column with structured packing drops with an increase in diameter.

Further research is needed to validate the premise for supercritical systems. As the columns used in supercritical fractionation are usually small in diameter, as discussed in Section 2.2.1, wall effects and the effect of structured vs random packing are important phenomena and merit further investigation. Wall effects are addressed in Chapter 6.

2.2.4 Liquid Hold-up

The following section of basic background literature is summarised from the preceding Masters Study [1].

If a column operating in the loading region exhibits an increase in the rate of change in pressure drop with increasing flow rate, it can be assumed that the shear forces between the phases have increased. If the shear forces increase while the liquid load to the column stays constant, the gas in the column will exert a net upward force on the liquid in the column. The system will then retain more liquid until the opposing force, exerted by gravity on the liquid, equals that of the upward shear force [12]. Hence a new equilibrium is achieved by allowing the liquid inventory in the column to increase.

This total retained liquid in a column is defined as the liquid hold-up. The liquid hold-up of a column, like the pressure drop, provides an indication of the hydrodynamic capacity of said column and, importantly, the residence time of the liquid. Like the pressure drop, the hold-up is also dependent on the column internals, operating pressure, fluid properties and fluid flow rates. The liquid hold-up is also normalised, in this case to the units of volume of hold-up per unit volume of packing, h_L (m^3/m^{-3}), to create a term that is translatable between systems.

2.2.4.1. Static and Dynamic Liquid Hold-up

The following section of basic background literature is partially adapted from the preceding Masters Study [1].

The liquid hold-up is divided into a static and a dynamic hold-up, which can each be measured separately. The static hold-up does not leave the column freely because of adhesion forces or being trapped by packing geometry. The static liquid hold-up is a constant value for a specific experimental setup and fluid combination. The dynamic hold-up is the liquid in the column retained due to flow phenomena such as viscosity, surface tension and shear forces caused by phase interaction. The difference between the two types can be seen in Figure 2-6.

The static hold-up, h_{Ls}, as seen in Figure 2- 6A, is caused by the forces between the gas, liquid, the surface of the packing and, depending on the orientation, the effect of gravity. For static hold-up to occur, these forces need to be in equilibrium. Said forces are in turn dependent on the liquid weight, surface tension, gravity and contact area. These factors can be lumped into a dimensionless number, the Bond number, Bo [33, 34]. Correlations exist that relate the Bond number to the static liquid hold-up, h_{Ls}, [35] and will be discussed in Section 2.4.

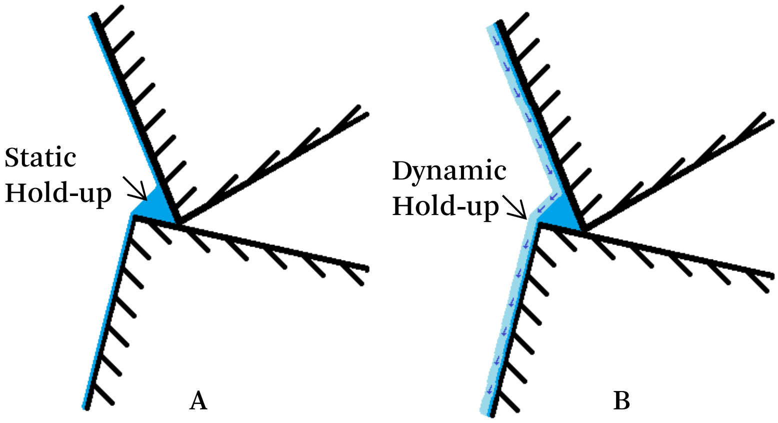

Figure 2-6: A) Static hold-up only and B) Dynamic and static hold-up.

The dynamic hold-up, h_{Ld} , constitutes the majority of the liquid in the column under regular operation. As can be seen in Figure 2-6B, the dynamic hold-up is in constant motion. Correlations used to describe the dynamic hold-up include the liquid Reynolds number and the Froude number, both modified for column flow, discussed later in Section 2.4

Adding the static and dynamic hold-up together yields the total liquid hold-up, h_L . Typical liquid hold-up curves can be seen in Figure 2-7. The liquid hold-up is plotted, like the pressure drop, against the gas capacity factor, F_G . As with the pressure drop, the trends in the liquid hold-up can also be correlated to the different film flow types, as described in Section 2.2.3.1. The curves are divided into three flow regimes by the loading point, line A–A and the flooding point, line B–B.

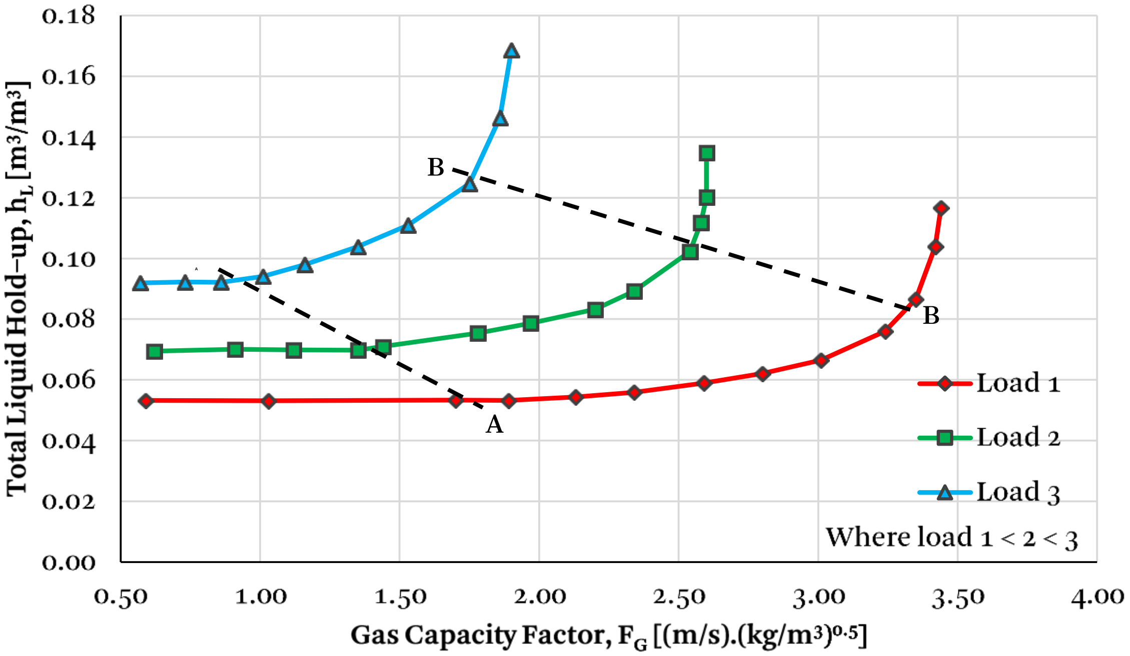

Figure 2-7: Typical liquid hold-up vs gas capacity factor. Drawn from data by Lamprecht [30]. 'Load' refers to the liquid load to the column, where Load = 0 being the no liquid flow case.

These flow regimes are described as follows [36, 18]:

- The pre-loading region: The area to the left of the loading point, A–A, where the interaction between phases is negligible. Here the liquid hold-up stays constant in this region, with the offset between different liquid loads dependent on the liquid load itself.
- The loading region: Interaction between phases becomes significant, causing the gas flow to exert a significant force on the liquid. The liquid hold-up increases exponentially as a function of the gas capacity factor. This region is defined as between the loading point, A–A, and the flooding point, B–B

- The flooding region: Here the shear forces exerted by the gas become overpowering and the liquid is entrained upwards in the column. The liquid hold-up rises sharply and effectively tends towards infinity. This area is defined as the flooding region and encompasses any points beyond the flooding point, B–B.

2.2.4.2. Droplet Entrainment

The following section of basic background literature is repurposed from the preceding Masters Study [1].

High gas flow rates cause high shear forces between the liquid and gas phases. When these shear forces exceed the downward forces, a net upward flow of liquid occurs, as discussed for film flow in Section 2.2.2. In these conditions, film stability deteriorates and surface waves, wave crest detachment, and droplet formation occurs. The shear force exceeds the cohesive forces of surface tension and viscosity in the liquid, causing loose droplets to be sheared from the falling liquid film. These droplets are then carried along with the gas flow until they either rejoin a falling film, collide with a column internal, or get carried out of the column with the exiting gas. The latter of these three possibilities can lead to the presence of unwanted components in the top gas product and is called entrainment. As the purpose of a column is to effect separation, this phenomenon is usually undesirable, as it leads to a decrease in efficiency. The packing geometry has a direct impact on entrainment, with smaller elements decreasing the extent of entrainment. [11]

2.2.5 Liquid-Liquid Extractions.

Liquid-liquid extraction is a separation technique that has been successfully used in industry for many years for applications where distillation is impractical or too costly [16]. In this process, droplets of a dispersed phase is passed through a continuous second phase in order to affect a separation.

Spray columns are the most basic of liquid-liquid solutions, in which the heavy and light liquids are sprayed across the column from opposite ends. This solution can allow for a lot of back- and axial mixing, which reduces the separation efficiency, with only one or two theoretical stages of extraction practical [16]. Packed columns can somewhat reduce these effects, allow better contact between the phases, as well as induce turbulence in the droplets and continuous phases. Columns with random packing, sieve trays or disk and doughnut setups are found in literature but are advised for large capacity, industrial applications with few equilibrium stages [16].

As soon as a higher efficiency or a larger number of equilibrium stages is required, a different solution is needed. As the surface area driving this separation is not dependent on the column internals, but instead on the number and size of droplets of the disperse phase, the majority of liquid-liquid solutions are mechanically agitated in some way to encourage droplet formation and decrease back- and axial mixing. This mechanical agitation takes different forms and helps to avoid the potential back- and axial mixing problems. This kind of mechanical agitation is difficult and costly at high pressures. Agitation through an inert gaseous phase is also found in literature, with gas-liquid-liquid systems having a larger impact.

It is important to note that the characteristics of liquid-liquid counter current equipment is scarce in literature [16] and the modes of operation are less well defined than that of gas-liquid systems. The number of variables that influence liquid-liquid extractions are significant and no attempts has been successful in establishing a method for estimating extraction rates, necessitating the piloting of any new systems [16]. This implies that, similarly to supercritical systems, random packing liquid-liquid extraction lacks for better design methods and models. Liquid-liquid extractions may be a better comparison to supercritical fluid systems under some conditions, especially when the supercritical phase density is high, but the body of knowledge to compare to in the available literature pales in comparison with gas-liquid systems.

2.3 Hydrodynamics under Supercritical Conditions

The following section of background literature is repurposed from the preceding Masters Study [1].

Studies in hydrodynamics under supercritical conditions can be roughly divided into the hydrodynamics around falling films, being the more phenomenological approach, and column hydrodynamics, considering the overall, macroscopic hydrodynamics effects in a column during operation, such as pressure drop and liquid hold-up. Of the two, the second is more directly relevant to practical application and operability and will be discussed here. As there is relatively little data available in literature, each of the contributions found will be discussed individually, with a summary of the findings in Table 2-1. For the sake of ease of reading the pressure range, temperature range, column sizes and exact packing types are summarised in Table 2-1 and not mentioned in text.

2.3.1 History of Hydrodynamics under Supercritical Conditions

The following section of background literature is improved upon from the preceding Masters Study [1].

The earliest paper found dealing with supercritical fractionation in packed columns is that of Peter and Tiegs [37], as referenced by Rathkamp et al. [38], presented at a conference in 1987. Although no mention of hydrodynamics is made, the study showed that supercritical fluid fractionation could achieve high degrees of efficiency in packed columns.

Table 2-1: Historically relevant investigations in literature showing column diameter, packing type and height, liquid and supercritical phases and temperature and pressure ranges [1].

Author(s) and Year Published	Column ID	Packing Used	Packed Height	Liquid Phase	Supercritical / Gas Phase	Pressure (MPa)	Temperature (K)
Systems investigating Hydrodynamics							
Krehenwinkel and Knapp [39]- [1987]	86 mm – 155 mm	15 mm Raschig rings	0.8 - 1.8 m	Metanol	Nitrogen	0.12 - 10 MPa	190 - 300 K
		15 mm Pall Rings		Water			
		10 mm, 15 mm Berl Saddles		Glycol			
		20 mm Novalox Saddles					
Seibert and Moosberg [40] - [1988]	98.8 mm	12.7 mm Raschig rings	1.68m	Isopropanol + Water	CO_2	8.2 – 15.2 MPa	297 - 318 K
		no. 15 Intalox saddles					
Sievers [41] - [1994]	36 mm	Montz-pak type A3	2 m	Water	CO_2	11.4 – 22 MPa	323 K
Woerlee [42] - [1997]	36 mm	Montz-pak type A3	2 m	Hexadecane	CO_2	8 – 17.3 MPa	323 - 343 K
Lim et al. [43]- [1995]	31.8 mm	Knit mesh packing	1.5 m	Ethanol + Water	CO_2	9.1 – 12.2 MPa	308 - 323 K
Machado [44] - [1998]	25 mm	Sulzer EX	1 m	Palm oil distillate	CO_2	20 - 29 MPa	333 - 373 K
Meyer [45] - [1998]	25 mm	Sulzer EX	1 m	Soybean oil	CO_2	10 - 30 MPa	313 - 393 K
	35 mm	Sulzer CY		Fish oil			
Budich and Brunner [46, 47] - [1999]	25 mm	Sulzer EX	1 m	Orange peel oil	CO_2	10 – 11.2 MPa	323 - 343 K
Stockfleth and Brunner [17, 48] - [1999] ; [53, 25] - [2001]	25 mm, 35 mm	5 x 0.5 mm Raschig rings	0.9 m	Water	CO_2	8 - 30 MPa	313 - 373 K
		15 mm Berl Saddles		α-Tocopherol			
		Sulzer CY		Olive oil deodorizer distillate			
		Sulzer EX					
Zacchi et al. [49]- [2008]	40 mm	Sulzer Mellapak 500.X	7.5 m	Rapeseed oil doped with Oleic acid	CO_2	20 - 26 MPa	333 K
		6 mm Wire mesh random packing manufactured					
Systems investigating efficiency and other noteworthy systems							
Peter and Tiegs [37] - [1984]	25.4 mm	Raschig rings	-	Oleic acid glycerides with Acetone entrainer	CO_2	13.7 MPa	343 K
		Drop distributor					
		Split-tube					
		Wire spirals					
		Sulzer gauze packing					
Rathkamp, Bravo and Fair [38] - [1987]	25.4 mm	6.4 mm Raschig rings	0.61 m	Ethanol + Water	CO_2	10.3 MPa	308 - 313 K
				Isopropanol + Water			

The first paper found considering high-pressure hydrodynamics in packed columns was by Krehenwinkel and Knapp [39], published in 1987. This paper measured pressure drop and flooding in an assortment of random packings. Although this research used subcritical nitrogen, it is worth mentioning as it is an in-depth hydrodynamic study concerned with a high pressure, high-density gaseous phase.

Rathkamp et al. [38] in 1987, followed closely by Seibert and Moosberg [40] in 1988, conducted research into the efficiency and energy requirements of columns operating with supercritical CO_2. Rathkamp et al. tested a dispersed gas phase column packed with Raschig rings and a spray column setup, finding the spray column to be the more efficient of the two. Seibert and Moosberg tested a column with sieve trays, Raschig rings, Intalox saddles and a spray column setup. They found the sieve trays to be the most efficient and the spray column the least efficient. Concerning hydrodynamics, Seibert and Moosberg measured the dynamic liquid hold-up for a CO_2 + isopropanol + water system. These two publications, while not yielding much value in the field of hydrodynamics, are of interest as they consider an overall view of the technology and show the trials and errors of early research. Further, they provide an indication of packing efficiencies and a conflicting view on the efficiency of spray columns vs packing.

The first hydrodynamic research on a structured packing, specifically Montz-pak type A3, was done by Sievers [41] in 1994, followed by Woerlee [42] in 1997, working on the same experimental setup. Woerlee [42] derived a model that proved suitable for supercritical use which will be tested in Section 2.4. These authors found that the measured flooding data points were not consistent with generalised pressure drop correlations, such as those proposed by Sherwood-Lobo [13] and Souders and Brown [50]. This inconsistency was attributed to the high solubility of CO_2 in the liquids used: namely water and hexadecane. Further, it has been shown that the generalised pressure drop correlation approach is flawed should not be used. The deviation illustrated the need for systems with low mutual solubility to determine the basic fundamental hydrodynamics, as will be discussed more thoroughly in Section 2.3.4.

Lim et al. [43] in 1995 investigated the mass transfer and liquid hold-up for an unnamed, knit mesh structured packing with an ethanol + water + CO_2 system. It was found that higher liquid hold-ups were observed at higher pressures.

Research shifted to systems with less soluble organic oils, as earlier research had problems isolating hydrodynamics due to high mutual phase solubility. Machado [44] in 1998, studied flooding using a palm oil distillate + CO_2 system with Sulzer EX laboratory packing and successfully measured flooding points consistent with the work by Woerlee [42]. Although it was not the explicit intention of Machado to reduce mutual solubility, it was a step in the right direction.

An in-depth investigation into hydrodynamics under supercritical conditions by Meyer [45] in 1998, using soybean oil + CO_2 and fish oil + CO_2 systems, using the same experimental setup as Machado [44]. Meyer not only measured the flooding point, as done by previous authors but also the pressure drop and some of the physical properties of the systems. Further, Meyer [45] compared his results with well-known flood point correlations of the time, namely those by Mersmann [15], Eckert [51] and Maćkowiak [52]. Meyer was the first to state explicitly that the models applicable at vacuum and standard pressures do not readily predict high-pressure systems ($P > 7$ MPa).

On the same column, Budich and Brunner [47] and Budich [46] investigated flooding in orange peel oil + CO_2 and water + ethanol + CO_2 systems. It was found that the orange peel oil exhibited similar trends as earlier research [42, 44], but the water + ethanol systems flooded much earlier than expected. The earlier flooding was attributed to the significant density differences between water (1000 kg/m^3), orange oil (~840 kg/m^3) and ethanol (790 kg/m^3), with the fluids with densities closer to the supercritical fluid density flooding later. This earlier flooding with higher liquid density is contrary to intuition, as well as trends in fractionation and distillation showcasing the error of using pure fluid properties as a benchmark for supercritical systems.

The next significant contribution was the PhD dissertation of Stockfleth [53], summarised in the work of Stockfleth and Brunner published in 1999 [48] and 2001 [17]. They investigated liquid hold-up, flooding, pressure drop, and foaming for water + CO_2, olive oil distillate + CO_2 and tocopherol + CO_2 systems. They concluded that supercritical fluid hydrodynamics is not fundamentally different from those at atmospheric pressure. The data collected were fitted with relative success to dry pressure drop, liquid hold-up and flooding data correlations adapted for the supercritical density. The correlations used will be discussed in more detail in Section 2.4.

Furthermore Stockfleth et al. [48] echoed the earlier assumption of Budich and Brunner [47] and Budich [46] that flooding is primarily dependent on the density of the liquid phase and packing geometry. Finally, it was found that foamability decreased decisively with increasing pressure, making it effectively negligible at certain conditions.

After the work of Stockfleth and Brunner, only one further investigation into supercritical fluid hydrodynamics has been done by Zacchi et al. [49], who investigated the efficiency and static and dynamic hold-up for a rapeseed oil + CO_2 system. The findings of this paper are in agreement with those of Stockfleth et al. [48, 17].

2.3.2 Trends Expected

The following section of background literature is summarised from the preceding Masters Study [1].

The following trends are expected in supercritical fluid hydrodynamics, summarised from the discussion Section 2.3.1:

- Dry-bed pressure drop will:
    - Increase with higher supercritical solvent feed rate.
    - Be higher than that of the same system at atmospheric conditions due to the higher density/viscosity of the supercritical phase.
    - Not differ significantly from the pressure drop of a wetted column.
- Wetted-bed pressure drop will:
    - Increase with higher supercritical solvent or liquid feed rate.
    - Be higher than the respective atmospheric dynamics due to the higher density/viscosity of the supercritical phase.
- Liquid hold-up will:
    - Increase with higher supercritical solvent or liquid feed rate.
    - Be primarily dependent on the liquid density.
    - Static hold-up typically decreases at high pressure due to the reduction in liquid surface tension [17].
    - High supercritical phase density produces significant reduction in the negative buoyancy [17] force exerted on the liquid phase, decreasing the nett downward force exerted on the liquid, which leads to higher total liquid hold-up than the respective atmospheric values.
- Flooding:
    - Is mutually dependent on the liquid and supercritical phase flow rates. For example, if liquid load 1 < load 2, then the system with load 2 will flood at a lower supercritical phase flow rate than that of the system with load 1. The inverse is also true, with the hypothetical supercritical load 1 < load 2, then load 2 will flood at a lower liquid flow rate than load 1.
    - Is primarily dependent on liquid density, according to Stockfleth et al. [48]. Thus systems with higher liquid densities will flood at lower supercritical flow rates.
- Foaming:
    - Is assumed negligible in supercritical fractionation columns [17], as foamability decreases significantly with increasing pressure.

2.3.3 Computational Fluid Dynamic Studies on Supercritical Hydrodynamics

The following section of background literature is repurposed from the preceding Masters Study [1].

As supercritical pilot plants are not widely available nor cheap to construct, sources of new data are limited. Data scarcity, along with increased use of computers and computational techniques, has led to the predictive modelling of supercritical systems becoming more common. Simulations investigating hydrodynamics can be found, although most of the modelling done is on mass transfer and thermodynamics [54, 55, 56, 57]. One recent study considers hydrodynamics and presents valuable insights [58].

Most relevant to this project is the work done by Fernandes et al. [59, 60]. They investigated the wet and dry pressure drop over a Sulzer EX packing using a commercial CFD (Computational Fluid Dynamics) software package, *Fluent*. Results obtained were compared with the experimental results of Meyer [45] and Stockfleth and Brunner [48, 17] and found to correlate very well. No simulations concerned with random packing were found.

2.3.4 The Effect of Mass-Transfer

The following section of basic background literature is summarised from the preceding Masters Study [1].

Although this study is focussed on hydrodynamics, mass transfer is the final goal of a fractionation column. Numerous investigations into supercritical mass transfer exist with extensive research into phase equilibria [61, 62, 63, 64, 65]. No single conclusive correlation for supercritical mass transfer has been developed [66].

Mass transfer will not be investigated in this work, however, it needs to be taken into consideration. As briefly mentioned in the introduction, mass transfer is to be either limited or fully accounted for during hydrodynamic investigations. Mass transfer directly affects the flow rate and properties of both phases, which in turn has a direct influence on column hydrodynamics.

Supercritical fluid systems typically possess mutual solubility, meaning that both phases will contain some of the other phase in solution. This mutual solubility affects the properties of both phases, causing a broader range of possible deviations, and ultimately complicating the interpretation of hydrodynamic results. Indeed, the mutual solubility is mentioned by literature as a significant problem in the determination of hydrodynamics, as the solubility significantly changes superficial flow rates and fluid properties [42]. The selection of an appropriate liquid/supercritical fluid system becomes essential to eliminate the solubility affecting at least one of the phases. Pure hydrodynamic data are still of value to systems where mass transfer occurs, as it can inform operability limits and proper equipment sizing.

2.4 Semi-Empirical Correlations for Hydrodynamics under Supercritical Conditions

Ideally, a model should be available that readily predicts hydrodynamics for a wide array of column internals and fluid properties. Such a model would significantly ease design procedures, providing reasonably accurate predictions of column behaviour without timeous and costly pilot work.

For atmospheric conditions, a wide array of established and validated hydrodynamic models are available. However, this is not the case for high-pressure applications, and even less so for supercritical applications. Models typically fail to predict the changes in the system affected by the significantly changed density, viscosity and surface tension of a supercritical fluid.

To the best of the author's knowledge, no models explicitly derived for supercritical application can be found in the open literature, and only two examples of modified models were found. Models covering the fluid property ranges under investigation are also few and far between. One model that has been adapted for supercritical use is a modification made by Stockfleth and Brunner [17] to the set of semi-empirical models Stichlmair et al. [67]. A second modified model, presenting a more phenomenological approach, is that by Woerlee [42]. More general models that are capable of predicting systems operating at high pressures, such as the SBD (Suspended Bed of Droplets) model by Maćkowiak [11], were found not applicable to columns with small diameters. Regardless of the model used, model approximations are typically based on three different simplified approximations of the column packing.

2.4.1 Model Structure Simplifications

For the approximation of hydrodynamics in packings, three different model structure simplifications are typically considered, namely the channel, beam and particle models [68, 17].

The channel model visualizes the packing as a solid body with equally spaced, round channels running through the packing from top to bottom. The channel diameters are approximated by using the hydraulic bed diameter, defined as:

$$d_H = 4 \in / a \qquad \{2\text{-}3\}$$

where $\in$ is the fractional void volume and a the packing surface area per unit volume. This model fails for high surface area packings, where the calculated channels start to overlap in order to emulate the large surface area.

The beam model is the exact opposite of the channel model, being a void space filled with equally spaced solid round beams. This model, being of similar nature as the channel model, falls victim to the same shortcomings.

The particle model sees the packing as a bed of round spheres with the sphere or particle diameter, d_p, calculated as in Equation {2-4}:

$$d_p = 6\frac{1-\in}{a} \tag{2-4}$$

This model solves the overlapping problem and is typically used in most modern models. It is, however, essential to adjust the particle diameter and specific surface area if the packing is liable to form dead volumes, for example, when using Raschig rings. This problem has been eliminated in most modern random packings [11].

2.4.2 Modified Stichlmair et al. Equations

Modified subcritical correlations have been used with relative success to approximate supercritical column design, even though they do not allow for the higher density, viscosity and surface tension of a supercritical fluid [66]. The only known example of a modified model is the set of equations prepared by Stockfleth and Brunner [17, 48], derived by modifying the well-known semi-empirical model set by Stichlmair et al. [67]. This set of equations is based on the particle model approximation and uses the particle diameter.

2.4.2.1. Dry Pressure Drop

The dry pressure drop can be calculated with a modified Ergun-type equation [68]. The Ergun equation expresses the friction factor in a packed column as a function of the Reynolds number. To calculate the friction factor itself, a modified version of the original equation proposed by Stichlmair et al. [67] and as used by Stockfleth et al [17, 48], is used. The Ergun equation is intended for a bed of spheres or relatively low porosity, which does not accurately model the majority of real systems, and is used in this work only as a comparison with Stockfleth et al. [17, 48]. This modification states that the friction factor, ψ, is proportional to $\in^{4.55}/(1-\in)$ instead of $\in^{3}/(1-\in)$, as determined by Rumpf and Gupte [69] for beds with $0.35 \leq \in \leq 0.7$.

The pressure drop and friction factor are calculated using Equation {2-5}:

$$\frac{\Delta P_0}{H} = \frac{3\psi \rho_G u_G^2 (1-\epsilon)}{4d_p \epsilon^{4.55}} \quad \text{and} \quad \psi = \frac{K_1}{\mathrm{Re}_G} + K_2 = \frac{4}{3}\frac{\Delta P_0 \epsilon^{4.55} d_p}{H(1-\epsilon)\rho_G u_G^2} \tag{2-5}$$

where $\Delta P_0/H$ defines the pressure drop per unit length of dry packing and ρ_G and u_G is the respective density and superficial velocity of the supercritical phase. The superficial velocity is calculated by dividing the volumetric flow rate by the column cross-sectional area. K_1 and K_2 are empirically determined constants that are dependent on the geometry of the packing used.

The gaseous phase Reynolds number [70], Re_G, as used in Equation {2-5}, is defined as:

$$\mathrm{Re}_G = \frac{u_G d_p \rho_G}{\mu_G} \tag{2-6}$$

where μ_G is the dynamic viscosity of the gaseous phase.

Constants K_1 and K_2 are determined by fitting experimental data to Equation {2-5}. The determined constants provide a generalised empirical equation capable of predicting the dry pressure drop for a specific packing. Values for all constants will be given at the end of this model discussion in Table 2-2.

2.4.2.2. Liquid Hold-up below the Loading Point

Liquid hold-up below the loading point is dependent on the interaction between the liquid and the packing and consists of a static and a dynamic element.

First, the static hold-up is discussed. The static hold-up is a function of the dimensionless Bond number, Equation {2-7}:

$$Bo = \frac{g\rho_L}{\sigma a^2} \tag{2-7}$$

and is dependent on gravity, g, liquid surface tension, σ, liquid density, ρ_L, and the packing surface area, a. The original Bond number was intended for a moving sheet of water, flowing over a known length. The equation here is slightly modified for use in column geometry by using the packing surface area per unit volume, a. Stockfleth did not modify the Bond number, but it would be prudent to substitute the liquid density, ρ_L, with a density difference to compensate for the buoyancy created by the supercritical phase:

$$\Delta\rho = \rho_L - \rho_G \tag{2-8}$$

The static hold-up is approximated as follows [53]:

$$h_{Ls} = 0.037 \in Bo^{-0.07} \text{ for } Bo < 1 \qquad \{2\text{-}9\}$$

$$h_{Ls} = 0.037 \in Bo^{-0.65} \text{ for } Bo \geq 1 \qquad \{2\text{-}10\}$$

The surface tension of a liquid is generally very low at high pressures [17], implying that the Bond number would have a high value. A high Bond number implies a small static liquid hold-up, leading to the static hold-up being considered negligible during further modelling.

The dynamic liquid hold-up below the loading point is predicted using the Reynolds and Froude numbers of the liquid phase. Firstly, the liquid Reynolds [53] number is modified from the classical Reynolds number [70] to allow for application in a column environment. This modification is done by substituting the surface area per unit volume of packing in the place of the typical length. This liquid Reynolds number, Re_L, provides a measure of the ratio of inertial to viscous forces in the liquid flowing over the column internals. The modified formula is seen in Equation {2-11}:

$$\mathrm{Re}_L = \frac{\rho_L u_L}{\mu_L a} \qquad \{2\text{-}11\}$$

where u_L is the superficial liquid velocity and μ_L the dynamic liquid viscosity. The superficial liquid velocity is calculated by dividing the volumetric flow rate by the cross-sectional area. If $\mathrm{Re}_L \geq 2$, the flow is expected to be turbulent with $\mathrm{Re}_L < 2$ indicating laminar flow [11].

The Froude number [53] provides a measure of the ratio of inertial forces to gravity and is similarly modified. The liquid Froude number in a column is as follows:

$$Fr_L = \frac{u_L^2 a}{g} \qquad \{2\text{-}12\}$$

The dynamic hold-up below the loading line is then calculated as follows [53]:

$$h_{Ld,0} = K_3 \left(\frac{Fr_L^2}{\mathrm{Re}_L} \right)^{K_4} \qquad \{2\text{-}13\}$$

where K_3 and K_4 are empirical parameters that are determined with an experimental data fit. The available regressed values can be seen in Table 2-2.

2.4.2.3. Wet Pressure Drop and Liquid Hold-up above the Loading Point

Above the loading point, the liquid hold-up and pressure drop becomes interdependent due to the significant interaction between the phases. Following the work of Stichlmair et al. [67], the irrigated or wet pressure drop per unit length, $\Delta P / H$, is calculated as:

$$\Delta P / H = \Delta P_0 / H\{[1- \in (1-h_{Ld} / \in)] / (1- \in)\}^{(2-C)/3}.(1-h_{Ld} / \in)^{-4.55} \qquad \{2\text{-}14\}$$

$$C = \frac{K_1 / \mathrm{Re}_G + K_2 / (2\sqrt{\mathrm{Re}_G})}{\psi} \qquad \{2\text{-}15\}$$

where K_1 and ψ is the same as that defined in Equation {2-5}. Note in the article by Stockfleth et al. [17], this formula is misreported even though it was applied correctly.

The dynamic liquid hold-up, h_{Ld}, is calculated in Equation {2-16}:

$$h_{Ld} = h_{Ld,0}\left[1+K_5(\Delta P / H.\rho_L.g)^{K_6}\right] \qquad \{2\text{-}16\}$$

with K_5 and K_6 yet a further set of empirically determined constants. The equation proposed by Stockfleth et al. [17] differs from the original equation by Stichlmair et al. [67] by substituting the liquid density, ρ_L, for the density difference between the liquid and supercritical phases, $\Delta\rho$, as can be seen in Equation {2-17}:

$$h_{Ld} = h_{Ld,0}\left[1+K_5(\Delta P / H.\Delta\rho.g)^{K_6}\right] \qquad \{2\text{-}17\}$$

This substitution is made to compensate for the significant buoyancy force exerted by the supercritical fluid on the liquid phase. This buoyancy force works upwards against the force of gravity. The use of the term alongside the gravitational constant justifies the difference between the phase densities as an appropriate substitution.

To calculate the pressure drop Equation {2-17} is substituted into Equation {2-14}, yielding an equation dependent only on pressure drop as variable. This equation can be solved iteratively to provide a pressure drop value and can be seen in Equation {2-18}:

$$\frac{\Delta P}{H} = \frac{\Delta P_0}{H}\frac{\left(\left[1-\varepsilon\left(1-{}^{h_{Ld}}\!/_{\varepsilon}\left\{1+K_5\left({}^{\Delta P}\!/_{H\,\Delta\rho\, g}\right)^{K_6}\right\}\right)\right)\right]\left(1-\varepsilon\right)^{-1}\right)^{\frac{2-C}{3}}}{\left(1-{}^{h_{Ld}}\!/_{\varepsilon}\left\{1+K_5\left({}^{\Delta P}\!/_{H\,\Delta\rho\, g}\right)^{K_6}\right\}\right)^{4,65}} \qquad \{2\text{-}18\}$$

The data presented by Stockfleth et al. [17] is very scattered and presented difficulty in presenting a precise model fit, leading to two fits presented with two sets of constants to predict the flooding and liquid hold-up, respectively. Stockfleth et al. attempted no prediction of pressure drop values. Further, the regressed parameters are not universal, but every packing/liquid set has its own set of parameters. Finally, it should be noted that K_6 was not calculated by Stockfleth et al. [17], but rather chosen as an educated guess and kept constant to simplify the problem. The reader is advised to consult the article by Stockfleth et al. [17] directly if more information is required.

The packing properties and derived constants by Stockfleth et al. [17] can be seen in Table 2-2. The narrowest packing, Sulzer EX, has the highest calculated friction factor while the widest packing, Sulzer CY, has the lowest. This difference is reflected in constants K_1 and K_2. The random packings, namely the Raschig rings and Berl saddles, presented with similar constants to the wider Sulzer CY despite having lower fractional void volumes and higher surface areas. Constants K_3 and K_4 are representative of liquid hold-up. The narrowest packings, being the Sulzer EX and the random packings, presented the same constants corresponding with a higher liquid hold-up. The wider Sulzer CY presented with smaller constants and a lower hold-up, in alignment with expectations. From the above, it can be seen that the random packings improved the liquid capacity of the column while keeping the pressure drop lower.

Table 2-2: Packing properties and derived constants for the equations used by Stockfleth et al. [17].

	Sulzer EX	Sulzer CY	Raschig Rings (5 x 0.5 mm)	Berl Saddles (5 mm)
Fractional Void Volume	0.86	0.96	0.82	0.61
Surface area	1850	860	3365	1520
Particle Diameter	0.45	0.35	0.34	1.5
K1	155	23	23	
K2	3.4	0.2	1.2	
K3	3.6	1.27	3.6	
K4	0.25	0.23	0.25	
K5	Dependant on packing and liquid - no universal constants found.			
K6				

2.4.2.4. Flooding

The flooding point is much debated in the literature with different researchers giving different definitions. The differences in definition in the literature means that the identification of the flooding point is dependant on the researcher. Flooding and column operability for this work will be discussed in detail in Chapters 5 and 6.

Stockfleth et al. [17] defines flooding as the point where a finite change in gas or liquid velocity causes an infinite change in the pressure drop or liquid hold-up. Mathematically this translates to where:

$$\frac{\delta \Delta P}{\delta \Delta P_0} = \infty \Leftrightarrow \frac{\delta \Delta P_0}{\delta \Delta P} = 0 \qquad \{2\text{-}19\}$$

To attempt a prediction of the flooding point, Stockfleth et al. [17] determined the derivative of Equation {2-18} and equated it to zero in Equation {2-20}:

$$0 = \left(\frac{\Delta P}{H \Delta \rho g}\right)^{-K6} - \frac{2.65 K_5 K_6 h_{Ld,0}}{\in - h_{Ld,0}\left[1 + K_5\left(\frac{\Delta P}{H \Delta \rho g}\right)^{K_6}\right]} - \frac{\left(\frac{2-C}{3}\right) K_5 K_6 h_{Ld,0}}{1 - \in + h_{Ld,0}\left[1 + K_5\left(\frac{\Delta P}{H \Delta \rho g}\right)^{K_6}\right]} \qquad \{2\text{-}20\}$$

Unfortunately, this model, although it is mechanistic in nature with a physical background, provided an inferior prediction of the flooding point data gathered by Stockfleth et al. [17].

As an alternative Stockfleth et al. [17] had relative success with a modified empirical Sherwood flooding diagram [71] used in conjunction with a correlation for flooding in pipes derived by Wallis [72]. The correlation by Wallis, as restructured by Woerlee [42], can be seen in Equation {2-21}:

$$F_G = \sqrt{H.g}\,\frac{K_7^2}{(1 + K_4\sqrt{\Phi})^2} \qquad \{2\text{-}21\}$$

with F_G being the gas capacity factor and Φ the flow parameter.

The gas capacity factor, F_G, is typically defined as:

$$F_G = u_G(\rho_G / (\rho_L - \rho_G))^{0.5} \qquad \{2\text{-}22\}$$

and the flow parameter, Φ, is defined as:

$$\Phi = L / G(\rho_G / \rho_L)^{0.5} \qquad \{2\text{-}23\}$$

where L is the liquid phase superficial mass flow rate and G the gaseous phase superficial mass flow rate. Both of these terms are calculated by dividing the phase mass flow rate by the cross-sectional area of the column.

2.4.2.5. Range of Model

The model proposed by Stockfleth and Brunner has only been proven for a minimal range of fluid properties. The limits of the ranges tested are shown below in Table 2-3.

Table 2-3: Range of parameters investigated in the Stichlmair et al. model [67], as modified by Stockfleth and Brunner [17].

Parameter	Units	Range
System Pressure	MPa	8 - 30
System Temperature	K	313 - 373
Pressure drop range	Pa/m	192 - 1549
Liquid Reynolds number	-	0.1 - 0.9
Column diameter	m	0.025 ; 0.035
Total surface area per unit volume	m²/m³	860 - 3365
Void fraction	m³/m³	0.61 - 0.96
Liquid density	kg/m³	855 - 1030
Dynamic liquid viscosity	mPa.s	0.283 - 0.653 ; 2.6 - 5.4
Surface tension	mN/m	23.2 - 27.9
Gaseous density	kg/m³	248 - 770
Gaseous viscosity	mPa.s	0.0037 - 0.0073

2.4.3 Maćkowiak Equations

The predictive SBD or Suspended Bed of Droplets model by Maćkowiak [11, 73] is based on the dependency between the flow resistance coefficient and packing shape. The liquid hold-up and pressure drop is predicted using a calculated gas velocity and liquid hold-up at flooding.

Some of the equations are based on the assumption of a solid body with channels, with the hydraulic diameter used for liquid hold-up. The pressure drop equations are based on the particle model and use the particle diameter.

2.4.3.1. Flooding Liquid Hold-up and -Gas Velocity

Maćkowiak [11, 73] proposes a calculation for the flooding liquid hold-up and gas velocity, also based on the work of Stichlmair [74]. The derivation of the terms will not be discussed here, but interested readers are advised to peruse the book by Maćkowiak, *Fluid Dynamics of Packed Columns,* [11].

The flooding liquid hold-up, $\mathrm{h}_{L,FL}$, is described by Equations {2-24} and {2-25}:

$$\mathrm{h}_{L,FL} = \in \times \frac{(1.44\lambda_0^2 + 0.8\lambda_0(1-\lambda_0))^{0.5} - 1.2\lambda_0}{0.4(1-\lambda_0)} \text{ for } \mathrm{Re}_L \geq 2 \qquad \{2\text{-}24\}$$

$$\mathrm{h}_{L,FL} = \in \times \frac{(1.25\lambda_0^2 + 0.48\lambda_0(1-\lambda_0))^{0.5} - 1.2\lambda_0}{0.24(1-\lambda_0)} \text{ for } \mathrm{Re}_L < 2 \qquad \{2\text{-}25\}$$

where λ_0 is the phase flow ratio at the flooding point, described as:

$$\lambda_0 = {}^{u_L}\!/\!_{u_{G,FL}} \text{ or } \lambda_0 = {}^{L\rho_G}\!/\!_{G\rho_L} \text{ at flooding conditions} \qquad \{2\text{-}26\}$$

The value for the liquid hold-up at the flooding point is interdependent with the gaseous phase velocity at flooding, $u_{G,FL}$. A simplified version of the equation derived by Maćkowiak [11], applicable to random packing for high-density gaseous flow, can be seen in Equation {2-27}:

$$u_{G,FL} = C_{FL} \in^{6/5} \left({}^{d_h}\!/_{d_T} \right)^{1/4} \left({}^{d_T \Delta\rho g}\!/_{\rho_G} \right)^{1/2} \left(1 - {}^{h_{L,FL}}\!/_{\in} \right)^{7/2} \left(\frac{\rho_G}{1.165} \right)^{0.18} \tag{2-27}$$

where, C_{FL} is the flooding point factor, d_h the hydraulic bed diameter and d_T the liquid droplet diameter.

The flooding point factor is a function of the resistance coefficient for single-phase flow of gas phase at flooding, ψ_{FL}, but can be assumed to be $C_{FL} \approx 0.5$ for classic, randomly filled packing elements, $C_{FL} \approx 0.55$ for modern, highly perforated packing elements, such as Hiflow rings and $C_{FL} \approx 0.615$ for structured perforated packings such as Mellapak 250 Y [11].

The liquid droplet diameter is defined as:

$$d_T = \sqrt{\frac{\sigma}{(\rho_L - \rho_G)g}} \tag{2-28}$$

where σ is the liquid surface tension.

Now that the flooding point has been established the column liquid hold-up can be calculated.

2.4.3.2. Liquid Hold-up

The liquid hold-up is calculated using the equations proposed by Mersmann and Deixler [75]. This set of equations first calculates the liquid hold-up below the loading point, after which the actual liquid hold-up is calculated with the help of the flooding liquid hold-up. The liquid hold-up below the loading line, $h_{Ld,0}$, can be calculated using Equation {2-29}:

$$h_{Ld,0} = 2.2\sqrt{B_L} \tag{2-29}$$

where B_L is the dimensionless liquid load, calculated using Equation {2-30}:

$$B_L = \left(\frac{u_L}{\in^3} \right) \left(\frac{1 - \in}{d_p} \right) \left(\frac{\mu_L}{\rho_L g^2} \right)^{1/3} \quad \text{for } B_L < 2 \times 10^{-5} \tag{2-30}$$

The liquid hold-up beyond the liquid line and up to the flooding point is described by Maćkowiak [73] as follows:

$$h_L = h_{L,FL} - (h_{L,FL} - h_{Ld,0})\left[1 - \left(\frac{F_G / F_{G,FL} - 0.65}{0.35}\right)\right]^{1/2} \qquad \{2\text{-}31\}$$

where $F_{G,FL}$ is the gas capacity factor at the flooding point. $F_{G,FL}$ can be calculated using Equation {2-27} to calculate the gaseous phase velocity at flooding, then substituting the calculated value into Equation {2-22}:

$$F_{G,FL} = u_{G,FL}(\rho_G / (\rho_L - \rho_G))^{0.5} \qquad \{2\text{-}22\}$$

2.4.3.3. Pressure Drop

Maćkowiak first suggested a model for wet pressure drop [73], followed later by a model for dry pressure drop [76]. The dry pressure drop can be calculated with Equation {2-32}:

$$\frac{\Delta P_0}{H} = (1 - \varphi_p)\left(\frac{1-\in}{\in^3}\right)\left(\frac{725.6}{\mathrm{Re}_G} + 3.203\right)\left(\frac{F_G^2}{d_p.K}\right) \qquad \{2\text{-}32\}$$

where K is the wall factor and φ_p is the packing form factor. The packing form factor represents the proportion of the perforated surface area and is experimentally determined. Tables containing extensive calculated and experimental form factor values are available in the work of Maćkowiak [11, 76].

The wall factor, K, considers the influence of the column wall on the resistance coefficient and can be calculated using Equation {2-33}:

$$K = \left(1 + \frac{2}{3}\left(\frac{1}{1-\in}\right)\left(\frac{d_p}{d}\right)\right)^{-1} \qquad \{2\text{-}33\}$$

The wet pressure drop can be calculated using a similar equation. Allowance for the pressure drop caused by the liquid hold-up is made, as can be seen in Equation {2-34, 2-35}:

$$\frac{\Delta P}{H} = 5.4\,\mathrm{Re}_L^{-0.14}\,\mu_P\left(\frac{1-\in}{\in^3}\right)\left(\frac{F_G^2}{d_p.K}\right)\left(1 + \frac{h_L}{1-\in}\right)\left(1 - \frac{h_L}{\in}\right)^{-3} \quad \text{for } 0.3 \le \mathrm{Re}_L \le 12.3 \qquad \{2\text{-}34\}$$

$$\frac{\Delta P}{H} = 3.8\mu_P\left(\frac{1-\in}{\in^3}\right)\left(\frac{F_G^2}{d_p.K}\right)\left(1 + \frac{h_L}{1-\in}\right)\left(1 - \frac{h_L}{\in}\right)^{-3} \quad \text{for } \mathrm{Re}_L > 12.3 \qquad \{2\text{-}35\}$$

where μ_P is the irrigated packing form factor. The irrigated packing form factor, like its dry counterpart, is an experimentally determined value. Tables containing extensive experimental irrigated packing form factor values are available in the work of Maćkowiak [11, 76].

2.4.3.4. Range of Model

The model proposed by Maćkowiak has been proven for an impressively wide range of fluid properties, but unfortunately mostly for parameters outside that of typical supercritical column systems. Firstly, the model is only proven for a minimum column diameter of 0.1 m – one to two orders of magnitude larger than the supercritical columns found by the author in the literature (Section 2.3.1). Secondly, the model is only valid for pressures up to 10 MPa, well below that of some supercritical fluid systems. Finally, highest gas density covered by the model is 3.6 kg/m^3, a full two orders of magnitude smaller than typical supercritical fluid densities. This compounds to a model that is unlikely to provide an accurate prediction. Nonetheless, the model is one of the few available hydrodynamic models capable of predicting at high pressures and provides an excellent example of a well-developed, current hydrodynamic model. The limits of the ranges tested are shown below in Table 2-4.

Table 2-4: Range of parameters investigated in the Maćkowiak [11] model as reported by Lamprecht [30].

Parameter	Units	Range
Pressure drop range	Pa/m	2 - 4000
System Pressure	MPa	0.00133 - 10
Liquid Reynolds number	-	0.15 - 200
Column diameter	m	0.1 - 1.4
Total surface area per unit volume	m^2/m^3	54 - 500
Void fraction	m^3/m^3	0.63 - 0.987
Liquid density	kg/m^3	660 - 1260
Dynamic liquid viscosity	mPa.s	0.2 - 8
Surface tension	mN/m	14 - 74.6
Gaseous density	kg/m^3	0.03 - 3.6
Gaseous viscosity	mPa.s	0.0065 - 0.0185

2.4.4 Woerlee Equations

The work of Woerlee [42] and Woerlee et al. [77] presents itself as a more macroscopic approach to hydrodynamics and has a different fundamental root than the equations used by Stockfleth. Woerlee successfully modelled a supercritical CO_2 + H_2O system using this set of equations.

The model is based on the assumption of inclined flow channels, similar to the work by Wallis [72], (using the hydraulic bed diameter) with annular flow. The model further assumes that the liquid flows in a uniform, laminar film down the channel walls. As the model derivation is intricate and does not add value to this work, only the effective equations are discussed below.

2.4.4.1. Dry Pressure Drop and Channel Angle of Inclination

Woerlee [42] describes the dry pressure drop, also using a modified Ergun-type equation [68]:

$$\frac{\Delta P_0}{H} = \psi.2.\rho_G.\left(\frac{u_G}{\in}\right)^2 \Big/ d_h \qquad \{2\text{-}36\}$$

where ψ is the packed bed friction factor. Please note that in the work of Woerlee [42] this equation is misreported; however it is stated correctly in later work [77] by the same author.

Woerlee uses the same basis for the friction factor as Stichlmair et al. (Equation {2-5}), with determined constant values for K_1 and K_2 of similar magnitude to those determined by Stockfleth for random packings. Woerlee does, however, recommend a different calculation of the friction factor that can be calculated using Equation{2-37}:

$$\psi = \frac{1}{4}\left(\frac{83.5}{\mathrm{Re}_G.\cos(\alpha)} + \frac{0.6556.\tan^2(\alpha) + 0.0142}{\cos(\alpha)}\right) \qquad \{2\text{-}37\}$$

where α is the effective angle of inclination of the hypothetical flow channel. The equation has several constants, some of which can be related to a physical basis. Firstly, the constant 83.5 relates to the laminar friction coefficient and has been determined experimentally by Woerlee [42] and Woerlee at al. [77]. Secondly, 0.0142 represents the infinite friction factor for a smooth pipe geometry and is derived from fundamentals. Lastly, 0.6556 is an empirical constant and is fitted with the data points.

The angle of inclination is pivotal in the determination of the model fit for wet pressure drop and the dependant liquid hold-up. Woerlee [42] suggests using dry pressure drop data to fit a value the angle of inclination. For the system investigated by Woerlee [42], a value for α of 51.5° was calculated.

It should be noted that in smaller diameter columns wall effects play a larger role. For the model by Woerlee [42], this manifests in more vertically directed flow as the hypothetical sloped channels have to 'turn' when meeting the wall. More vertical flow causes a smaller effective inclination angle for the packing. To account for the influence of the column wall, the effective angle of inclination is modified for random packings using Equation {2-38}:

$$\alpha = \alpha_0.\left(1 + \frac{4}{a.d}\right)^{-1} \qquad \{2\text{-}38\}$$

where α_0 is the effective angle of at an infinite column diameter. For structured columns, a different approach is followed to account for wall effects. As this work focusses on random packing, the reader is directed to the work of Woerlee [42] for further details.

2.4.4.2. Liquid Hold-up

As a channel model, the Woerlee model uses the assumption of a hydraulic diameter, d_h. During wetted operation the model uses a reduced hydraulic diameter, d_{int}, to represent the reduced flow area available to the gaseous flow. The ratio of these diameters can be used to calculate the liquid hold-up:

$$h_L = \in.\left(1-\frac{d_{\text{int}}^2}{d_h^2}\right) \tag{2-39}$$

The ratio between the two radii is used often in the model and is represented by θ, called the dimensionless interface radius number. θ is calculated as the reduced diameter over the hydraulic diameter:

$$\theta = \frac{d_{\text{int}}}{d_h} \tag{2-40}$$

where θ is calculated from the pressure drop. Unlike the prior calculations, the Woerlee model first needs to determine the pressure drop before the liquid hold-up can be calculated.

2.4.4.3. Wet Pressure Drop

The wet pressure drop is estimated through an iterative calculation. The Woerlee [42] set of equations calculate a theoretical superficial liquid flow using a guessed value for both θ and the pressure drop for each point. The equation itself using a derivation of the Navier-Stokes equation:

$$u_L = -\frac{(1-\theta^2)^2}{32\mu_L}.\left(\Delta\rho.g+\frac{\Delta P}{H}\right).\cos(\alpha).\text{d}_h^2 - \left[\frac{(1-\theta^2).d_h^2}{16\mu_L}.\left(\Delta\rho.g+\frac{\Delta P}{H}\right).\cos(\alpha)+u_{\text{int}}\right].\left(\theta^2+\frac{1-\theta^2}{2.\ln(\theta)}\right) \tag{2-41}$$

where u_{int} is the interfacial velocity between the two phases.

Interfacial velocity is calculated using Equation {2-42}, which is in turn derived through solving for the boundary conditions at the interface between the phases:

$$u_{\text{int}} = -\left(\Delta\rho.g+\frac{\Delta P}{H}\right).\cos(\alpha).\left(\theta^2\ln(\theta)+\frac{1-\theta^2}{2}\right).\frac{d_h^2}{8.\mu_L} \tag{2-42}$$

To close the iterative loop the pressure drop is solved for using Equation {2-43}:

$$\frac{\Delta P}{H}=-\frac{2.\psi}{\theta.d_h}.\rho_G.\left(\frac{u_G}{\in.\theta^2}-u_{\text{int}}.\cos(\alpha)\right)\left|\frac{u_G}{\in.\theta^2}-u_{\text{int}}.\cos(\alpha)\right| \qquad \{2\text{-}43\}$$

The residuals taken into account for the model iteration are 1) the difference between the guessed and calculated values for the pressure drop and 2) the selected and calculated superficial liquid flow rate. The residuals are minimised using a mathematical solver by varying the guessed pressure drop and dimensionless interface radius number.

2.4.5 Model Comparison

The discussed models were used to predict the available literature data [17]. Only the two main hydrodynamic factors are considered, being the liquid hold-up below the flooding line and the wet pressure drop.

Stockfleth et al. [17] provides data for a 25 mm column packed with 5 x 0.5 mm Raschig rings, operating with water and CO_2. The data are available at superficial gas velocities of 4, 8 and 12 mm/s over a range of superficial liquid velocities. Model constants were obtained from the literature. The system properties can be seen in Table 2-5.

Table 2-5: Column, packing and fluid properties used in the modelling exercise.

	Symbol	Description	Value
Column Properties	Packing	Column Internals	Raschig Rings 5 x 0.5 mm
	a (m^2/m^3)	Packing Surface Area per Volume	3365
	∈	Packing Void Fraction	82%
	d (m)	Column Diameter	0.025
Liquid Properties	ρ_L (kg/m^3)	Water Density	996.6
	μ_L (mPa.s)	Water Viscosity	0.6557
	σ (N/m)	Water Surface Tension	0.025
Supercritical Phase Properties	ρ_G (kg/m^3)	CO_2 Density	719.4
	μ_G (mPa.s)	CO_2 Viscosity	0.0587

2.4.5.1. Liquid Hold-up

First to be discussed is the liquid hold-up. The model predictions were determined and plotted against the available literature data in Figure 2-8.

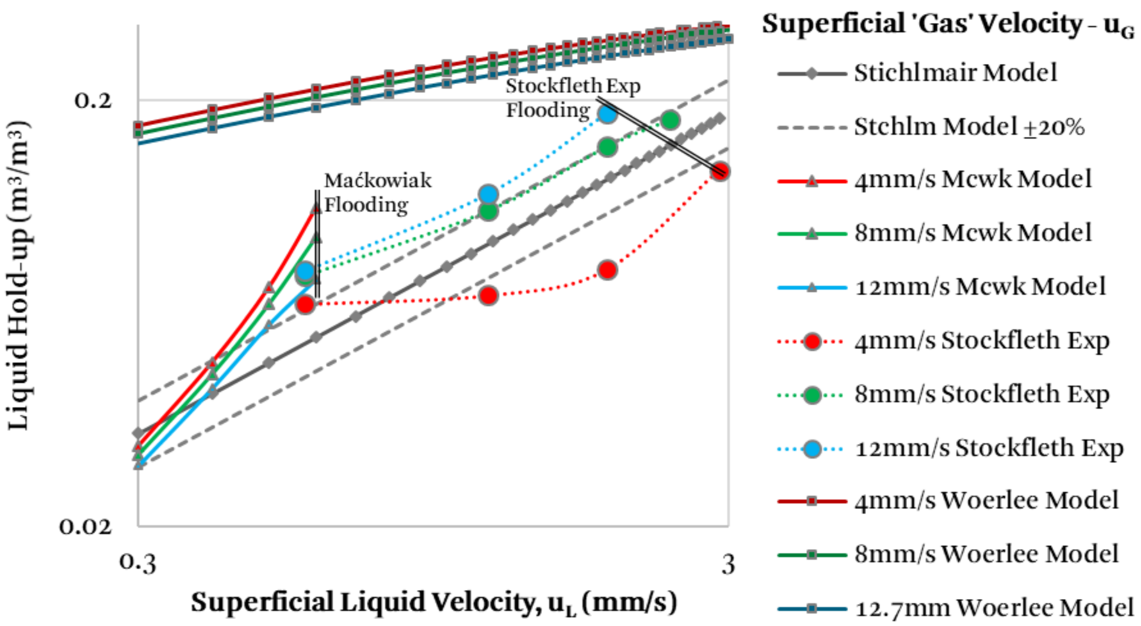

Figure 2-8: Liquid hold-up model predictions for the models by Stockfleth et al., Maćkowiak and Woerlee compared to the literature data by Stockfleth et al. [17]. Note the logarithmic axes. Flooding is indicated by a black, double line where applicable.

In Figure 2-8, the Maćkowiak model prediction shows a steep increase in hold-up compared to the Stichlmair et al. and Woerlee models and literature data. The different slope of the prediction indicates a different approach to predicting the hold-up. The model predicts a very low flooding point and falls short of the literature values. Compared to literature, it can be seen that this model fails to present even a decent approximation of reality. This poor prediction is not unexpected, as the system's conditions fall well outside of the parameters where the model has been validated.

The Stichlmair et al. model shows a better approximation, as can be expected by a fitted, semi-empirical model. Stichlmair et al. model predictions for all three superficial gas velocities rates were virtually collinear, presenting effectively the same solution. Hence, only one model prediction for the Stichlmair et al. model is presented in Figure 2-8. The lack of model variation agrees with Stockfleth's statement in the literature that the column operates in the pre-loading regime [48], where the gaseous flow does not influence the hold-up.

The Stichlmair et al. model prediction presents a similar slope as the literature data. However, the model fails to predict any of the individual literature data points accurately. The data has a large scatter, with the majority of the data falling well outside 20% of the model. The model deviated from the literature data with an average absolute deviation of 63.1 % and a maximum of 77.7 %.

The Stichlmair et al. model also predicts flooding at considerably higher liquid rates than reported in the literature. The model predicts the onset of flooding at a superficial liquid velocity of ~6.5 mm/s, in contrast with the literature flooding at ~1.9 - 2.9 mm/s. Flooding is also implied to be dependant on the Superficial liquid velocity [17], which the model fails to show during prediction.

The Woerlee model was calculated iteratively with calculation stopped as soon as the residuals reached <<0.1%. As the dry pressure drop data required to determine the angle of inclination is not available for the literature system, some assumptions had to be made. The angle of inclination was calculated by using the literature constants of $K_1 = 23$ and $K_2 = 1.2$ for the investigated packing and equating Equations {2-5} and {2-37}. An angle of inclination of 52.7° is calculated for the literature data, which agrees well with the reported value of 51.5° [42].

The Woerlee model overpredicts the liquid hold-up significantly, especially at lower superficial liquid flow rates, failing to produce a reasonable approximation of the literature data. The model deviated from the literature data with an average absolute deviation of 138.0 % and a maximum of 260.5 %

The Woerlee model shows the smallest slope of any of the models with little change in hold-up with increasing superficial liquid velocity. This difference in trend could indicate that the model parameters are incorrect, or an assumption made in the derivation of the model is not applicable. Further, t model shows a change in prediction with an increase in superficial 'gas' velocity, with higher superficial gas velocity presenting with a lower hold-up. This trend is the opposite of that observed in the literature data, with higher superficial gas velocities presenting with a higher liquid hold-up. This discrepancy implies that there is a fundamental assumption that is incorrect in both models.

The Woerlee model fails to predict any reasonable flooding point, with superficial liquid flow rate values four times higher than the experimental flooding still failing to show any signs of tending to flooding. Even in application, Woerlee did not use the model to predict flooding or any inoperability.

2.4.5.2. Wet Pressure Drop

The model predictions for the wet pressure drop were calculated.

It was found that the predictions of the Maćkowiak model fell well below literature values and those predicted by the Stichlmair et al. model. As the difference between the Maćkowiak model and literature was too big to compare graphically, the predicted and literature values are presented in Table 2-6.

Table 2-6: Wet pressure drop (Pa/m) – Model predictions for the models by Stichlmair et al., Woerlee and Maćkowiak compared to data by Stockfleth et al. [17].

	u_L mm/s	0.576	1.178	1.868	2.410
u_G = 4 mm/s	Exp data	192.8	241.6	308.4	436.3
	Stichlmair	54.19	77.00	108.9	134.0
	Woerlee	493.5	827.9	1207	1790
	Maćkowiak	0.1989	Flooded		
u_G = 8 mm/s	Exp data	271.8	359.5	380.4	517.6
	Stichlmair	172.0	258.3	385.9	520.0
	Woerlee	742.6	1096	1472	1759
	Maćkowiak	0.7222	Flooded		
u_G = 12 mm/s	Exp data	359.5	443.0	685.9	Flooded
	Stichlmair	364.3	579.8	962.1	
	Woerlee	1115	1529	1950	
	Maćkowiak	1.448	Flooded		

In Table 2- 6, it can be seen that neither model accurately predicted the pressure drop reported by literature.

The model by Maćkowiak, having a very low flooding point prediction, only succeeds in providing a prediction for the very lowest literature liquid flow rate. The predicted values are between two and three orders of magnitude less than the predicted values, hugely under predicting the pressure drop.

The Stichlmair et al. model provides a better quantitative fit to the literature data. That being said the model prediction still has several problems with providing a qualitative fit. The Woerlee model far overpredicts the pressure drop measured. The models are plotted in Figure 2-9 with the literature data for easy comparison.

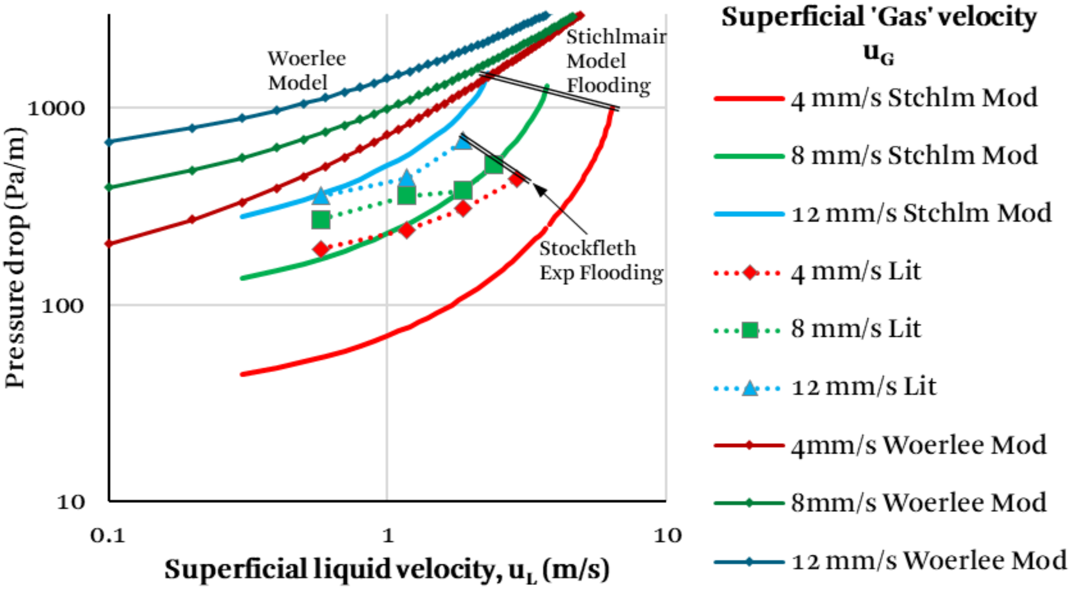

Figure 2-9: Pressure Drop model predictions using the Stichlmair et al. model; compared to the literature data by Stockfleth et al. [17]. Note the logarithmic axes. Flooding is indicated by a black, double line where applicable.

First, the performance of the Stichlmair model will be discussed. The model fails to predict the literature data at the lowest gas flow rate. The middle and higher flow rates provide better approximations of the actual pressure drop, with the models agreeing with the limited literature data with an average absolute deviation of 19.9 % and a maximum of 40.3 %. Including the data at 4 mm/s, the average absolute deviation shifts to 37.4 % and a maximum of 71.9 %. Figure 2-9 further shows that the Stichlmair model significantly overpredicts the flooding point. This overprediction is a significant shortcoming, as one of the primary purposes of a hydrodynamic model is to predict operability. Even considering that inaccuracies in hydrodynamics are typically large, the model prediction falls well outside acceptable limits.

The Woerlee model fails to predict the literature data as well, with the model overpredicting the pressure drop for all superficial liquid velocity flow rates. The model does, however, present a better approximation of the spread of the data. The model predicted pressure drops are closer to each other with increasing superficial liquid velocity, mimicking the experimental data better. The average absolute deviation of the model to the literature data is 231.3 % with a maximum of 310.3 %. Like with the liquid hold-up, the Woerlee model fails to present a reasonable prediction of flooding.

In conclusion, none of the tested models can be trusted to present a reliable prediction of the Stockfleth literature data, not even the fitted, semi-empirical Stichlmair et al. model or the more macroscopic Woerlee model. None of the tested models can be used to predict the operability limits and hydrodynamic capacity of the system. The lack of the models in producing a reliable prediction leaves definite room for improvement in the form of a new model or the comparison with further models to determine the applicability of the chosen model boundary conditions and assumptions.

2.5 Fluid Properties under Supercritical Conditions

The fluid properties of density and dynamic viscosity play a significant role in the modelling of hydrodynamic systems, as is evident from their frequent use in the preceding chapter. Fluid properties would be required for any modelling exercise and play a vital role in the interpretation of any hydrodynamic results. Under supercritical conditions, small changes in temperature and pressure can induce substantial changes in fluid properties for both the supercritical fluid and liquid phases. Fluid properties for both phases are not easily predicted using standard models [78].

Despite the importance of fluid properties in various applications, including hydrodynamics, there is a decided lack of data on the fluid properties of supercritical binary mixtures. This statement is echoed in the work of Stockfleth and Brunner [48] in 1999, although in recent years, an increase in data in the literature has been seen.

The literature data are split into either reporting on a saturated or an unsaturated fluid system. Unsaturated systems give valuable insight on how the fluid properties change with different degrees of saturation. Available literature data on unsaturated systems focus on the properties of the liquid phase only, with both density and viscosity data available [79-85]. Saturated systems give insight into the maximum deviation from the pure fluid property possible. Saturated fluid properties are used for any hydrodynamic modelling and are therefore of key interest to this study. The available literature also only focuses on the liquid phase properties [84-95], with a particular abundance of Poly[ethyleneglycol) data in the literature properties [90-95]. Saturation itself is a separate measure addressed in the study of phase equilibria. Many different methods are used to measure high-pressure phase equilibria with no single method being superior [79]. As mentioned in Section 2.3.4, phase equilibria are well researched and explained in the literature. As phase equilibria not the core focus of this work, the interested reader is directed to the extensive and thorough works of Dohrn et al. [61-63, 96] and the literature in Chapters 3 and 4.

Some authors have tried to circumvent the lack of saturated fluid property data by using mixing rules, equations of state or departure functions [5, 80]. Estimations have significant error margins, making their application unreliable, although the estimation of properties is a better practice than just using pure fluid properties.

The data in literature have significant shortcomings when considered for use in a hydrodynamic investigation. None of the systems found in the literature provided a full set of data (fluid properties and phase equilibria) in the desired fluid property ranges and exhibiting low mutual solubility. Significantly, no paper measuring the saturated supercritical fluid phase could be found. The solubility of the solute into the supercritical phase is especially relevant, as the highest density solvent is found at the top of the column. This can cause unstable operation and back mixing of the solvent [37, 42]. The supercritical phase properties would be required for any attempted hydrodynamic modelling. The different measurement methods for the fluid properties of interest, being density and dynamic viscosity, will be discussed in the literature for the first publication, Chapter 3.

2.6 Literature Shortcomings and Summary

In the evaluation of the available literature and semi-empirical approximations, several significant shortcomings can be identified. Focusing first on the existing literature, the following points of interest emerge.

Looking at the history of hydrodynamics under supercritical conditions, Section 2.3.1, it was seen that very little experimental work had been done on the hydrodynamics of supercritical systems. From the systems that were investigated, a few areas can be identified that lack the necessary depth of understanding in the literature.

Firstly, most of the studies fail to consider the effect of the mutual phase solubility in supercritical systems. If the solubility effect is mentioned, it is often not explicitly taken into consideration and solubilities as high as 40 wt% (gaseous phase into liquid) are dismissed as insignificant. This omission is a debatable assumption, as the properties of fluids with supercritical fluids have been shown to vary significantly with pressure, which would, in turn, magnify the effect of any solutes in the supercritical fluid. As an extension of this, no system adequately addressing the effect of mass transfer was found in the literature.

Secondly, precious little work has been reported in the open literature on random packings in supercritical conditions and none on modern random packings. Small diameter columns are typically used in supercritical columns. Structured and random packings are known to react differently to the column diameter, as discussed in Section 2.2.3, with random packings influenced less negatively by column diameter.

Thirdly, no investigation in the open literature has been found considering the effect of column diameter on hydrodynamics under supercritical conditions. At small diameters, wall effects may be significant. No hydrodynamic studies have been performed on columns below 25 mm ØI.

Fourthly and finally, no investigation on the effect of the supercritical fluid phase properties on column hydrodynamics, such as viscosity, has been done. Fluid properties have a significant impact on hydrodynamics and are valuable tools in hydrodynamic modelling.

Some further issues are identified when looking at the hydrodynamic model predictions under supercritical conditions. Firstly, no universal models were found in the open literature that can accurately predict supercritical hydrodynamics and operability limits, even though hydrodynamics under supercritical conditions have been said to be fundamentally no different than atmospheric hydrodynamics [17]. Secondly, no allowance was made in existing correlations for the higher viscosity and surface tension of the supercritical fluid, only for the density. None of the authors consulted mentioned if these properties were considered significant or taken into consideration.

With regards to the specific models investigated, several issues were identified which hamper the application of the modified semi-empirical correlation by Stockfleth [17, 48]. Firstly, very limited empirical constants are available for the equations used, with only Raschig rings and Berl saddles fitted for random packings. Secondly, and most importantly, the semi-empirical correlations have only been proven on a few select systems, and only for a limited range of fluid properties. On the other hand, the well known SBD by Maćkowiak [11, 73] fails to predict any property in the supercritical regime for the literature data. The Model by Woerlee overpredicts both the liquid hold-up and pressure drop, although the model showed better response to variation in the superficial supercritical fluid velocity than the Stockfleth model.

Finally, no system in the literature presents with the full complement of data required for a hydrodynamic study. A hydrodynamic study requires a well-defined system with the fluid properties known and the mass transfer defined. This requires the density, dynamic viscosity and phase equilibria of a system as a minimum. Ideally, the fluid properties of the system should compare to industrially relevant systems in order to present relevant results and outcomes.

2.7 Literature Conclusion

The lack of data and shortage of reliable models force industry to perform expensive and lengthy pilot plant studies in order to obtain a reliable design, decreasing the attractiveness of the technology. Pilot plant studies are likewise complicated by these shortcomings, due to the lack of correlations to provide an initial guess of the flooding point, loading point and operating conditions. These constraints necessitate a time consuming, expensive, and iterative process to gather data. It also causes difficulty in differentiating between hydrodynamics, mass transfer and thermodynamic effects in a particular system.

In order to address the shortcomings in literature, hydrodynamic data under supercritical conditions have to be collected and interpreted with the help of pilot plant studies. Only then can an investigation into the adaptation of an existing model, or derivation of a new model, be undertaken. The fluid properties of the saturated fluid phases are required to investigate and model hydrodynamics accurately while minimising mass transfer. A definite lack of saturated fluid properties in the literature highlights the need for such data to be gathered as well.

The above discussion leads to the first two objectives. As there is no viable system found in the literature to use in hydrodynamic experimentation, a system needs to be identified, and its fluid properties measured. Before this can be done, suitable equipment is needed for the identification of a system with low mutual solubility, followed by the measurement of the system phase equilibria and fluid properties at saturation.

References

[1] Franken, H.H., Establishment of a Supercritical Pilot Plant and the Hydrodynamics of Supercritical Countercurrent Columns;, Masters Dissertation, Stellenbosch University, Department of Process Engineering, (2014).

[2] Span, R. and Wagner, W., A New Equation of State for Carbon Dioxide Covering the Fluid Region from the Triple- Point Temperature to 1100 K at Pressures up to 800 MPa, J. Phys. Chem. Ref. Data, 25 (1996) 1509- 1596.

[3] Gibbs, J.W., On the Equilibrium of Heterogeneous Substances, Part 1, Trans. Conn. Acad. Arts Sci., 3 (1876) 108- 24.

[4] Fenghour, A.; Wakeham, W.A. and Vesovic, V., The Viscosity of Carbon Dioxide, J. Phys. Chem. Ref. Data, 27 (1998) 31- 44..

[5] Nieuwoudt, I., The Fractionation of High Molecular Weight Alkane Mixtures with Supercritical Fluids;, Ph.D. Dissertation, Stellenbosch University, Department of Process Engineering, (1994).

[6] Schwarz, C.E. and Knoetze, J.H., Design of Supercritical Fluid Processes for High Molecular Mass Petrochemicals, 'Supercritical Fluids', M. Belinsky (ed). Nova Science Publishers Inc., (2009).

[7] Schwarz, C.E., The processing of wax and wax additives in supercritical fluids, Ph.D. Dissertation, Stellenbosch University Department of Process Engineering, Stellenbosch, South Africa, (2005).

[8] Schwarz, C.E., Nieuwoudt, I. and Knoetze, J.H., Phase equilibria of long chain n- alkanes in supercritical ethane: Review, measurements and prediction, J. Supercrit. Fluids, 46 (2008) 226- 232.

[9] Schwarz, C.E., Fourie, F.C.v.N. and Knoetze, J.H., Phase equilibria of alcohols in supercritical fluids Part II. The effect of side branching on C8 alcohols in supercritical carbon dioxide, J. Supercrit. Fluids, 51 (2009) 128- 135.

[10] Oxford Dictionaries, Concise Oxford Dictionary of English, 11th Edition, Oxford University Press, Cape Town, South Africa, (2008).

[11] Maćkowiak, J., Fluid Dynamics of Packed Columns, Springer, Berlin, Germany, (2010).

[12] Eckert, J.S., How tower packings behave, Chem. Eng., 2 (1975) 70- 76.

[13] Lobo, W.E., Friend, L., Hashmall, F. and Zenz, F., Limiting capacity of dumped tower packings, Trans. Am. Inst. Chem. Engng., 41 (1945) 693- 710.

[14] Alford, R., Burns, M. and Burns, N., Dixon Rings- A Revolutionary Random Column Packing, Filtration 11 (2011) 218- 223.

[15] Mersmann, A., Zur Berechnung des Flutpunktes in Füllkörperschüttungen., Chem. Ing. Tech., 37 (1965) 218- 226.

[16] Tilton, J.N., Perry's Chemical Engineers' Handbook, 8th Edition, McGraw- Hill: New York, United States of America, (2010).

[17] Stockfleth, R. and Brunner, G., Holdup, Pressure Drop, and Flooding in Packed Countercurrent Columns for the Gas Extraction, Ind. Eng. Chem. Res., 40 (2001) 347- 356.

[18] Kister, H.Z., Distillation Design, McGraw- Hill, New York, United States of America, (1992).

[19] Guedes de Carvalho, J.R.F. and Talaia, M.A.R., Interfacial shear stress as a criterion for flooding in counter current film flow along vertical surfaces, Chem. Eng. Sci, 53 (1998) 2041- 2051.

[20] Stockfleth, R. and Brunner, G., Film Thickness, Flow Regimes, and Flooding in Countercurrent Annular Flow of a Falling Film at High Pressures, Ind. Eng. Chem. Res., 40 (2001) 6014- 6020.

[21] Moser, M. and Trepp, C., Investigating the Stability of Falling Films at Round Vertical Film Carriers Under High Pressure, Chem. Eng. Technol., 20 (1997) 612- 616 .

[22] Nusselt, W., Die Oberflachenkondensation des Wasserdampfes, Z. Ver. Dtsch. Ing., 60 (1916) 541- 546.

[23] Kirschbaum, E., Destillier und Rektifiziertechnik 4th Edition, Springer- Verlag, Berlin, Germany [as cited by: Maćkowiak, J. in Fluid Dynamics of Packed Columns, 2010], (1969).

[24] Billet, R., Industrielle Destillation, Weinheim: Chemie Verlag, Weinheim, Germany [as cited by: Maćkowiak, J. in Fluid Dynamics of Packed Columns, 2010].

[25] Billet, R. and Maćkowiak, J., Allgemeines Verfahren zur Berechnung der Trennwirkung von Füllkörperkolonnen, Chem.- Ing.- Techn., 55 (1983) 211- 213 [as cited by: Maćkowiak, J. in Fluid Dynamics of Packed Columns, 2010].

[26] Billet, R. and Maćkowiak, J., Neues Verfahren zur Auslegung von Füllkörperkolonnen für die Rektifikation., Verfahrenstechnik vt, 17 (1983) 203- 211, [as cited by: Maćkowiak, J. in Fluid Dynamics of Packed Columns, 2010].

[27] Billet, R. and Maćkowiak, J., How to use the absorption data for design and scale- up of packed column, Fette, Seifen, Anstrichmittel, 86 (1984) 349- 358 [as cited by: Maćkowiak, J. in Fluid Dynamics of Packed Columns, 2010].

[28] Turton, R.C., Bailie, R.C., Whiting, W.B. and Shaeiwitz, J.A., Analysis, Synthesis and Design of Chemical Processes, 3rd edition, Prentice Hall PTR, Boston, United States of America, (2009).

[29] Walas, S.M., Chemical Process Equipment - Selection and Design, Butterworth-Heinemann, Newton, Unites States of America, (1990).

[30] Lamprecht, S.M., Establishing a Facility to Measure Packed Column Hydrodynamics, Masters Dissertation, Stellenbosch University, Department of Process Engineering, (2010).

[31] Billet, R. and Maćkowiak, J., Application of Modern Packings in Thermal separation Processes, Chem. Eng. Technol., 11 (1988) 213- 227.

[32] Kuźniar, J. and Niżański, A., Investigations on Mellapak 250Y made of sheet metal (Orig. Polish), Simposium volume III: Rectification, Absorption, Extraction, (1999) p. 65- 74.

[33] Bond, W.N., The surface tension of a moving water sheet., Proc. Physical Society, 47 (1935) 549- 558.

[34] Hager, W.H., Wilfrid Noel Bond and the Bond number, J. Hydraul. Res., 50 (2012) 3- 9.

[35] Blass, E. and Kurtz, R., The influence of surface energy values on the two- phase counter-current packed columns with Raschig- Part I: fluid content. (orig. German), Process Eng., Vol. 10, p. 721, [as cited by: Maćkowiak, J. in Fluid Dynamics of Packed Columns, 2010], (1976).

[36] Billet, R. and Schultes, M., Fluid Dynamics and Mass Transfer in the Total Capacity Range of Packed Columns up to the Flood Point, Chem. Eng. Tech., 18 (1995) 371- 379.

[37] Peter, S. and Tiegs, C., International Symposium on High Pressure Chemical Engineering, Erlangen, West Germany. [as referenced by: Rathkamp, Bravo and Fair, Solvent Extr. Ion Exch., 3 (1987) 367], (1984).

[38] Rathkamp, P.J., Bravo, J.L. and Fair, J.R., Evaluation of Packed Columns in Supercritical Extraction Processes, Solv. Extr. Ion Exch., 5 (1987) 367- 391.

[39] Krehenwinkel, H. and Knapp, H., Pressure Drop and Flooding in Packed columns at High pressures, Chem. Eng. Tech., 10 (1987) 231- 242.

[40] Seibert, A.F. and Moosberg, D.G., Performance of Spray, Sieve Tray, and Packed Contactors for high Pressure Extraction, Sep. Sci. Tech., 23 (1988) 2049- 2063.

[41] Sievers, E.J., Pressure Drop and Flooding with a supercritical fluid, Ph.D. Dissertation, Technische Universität Delft, (1994).

[42] Woerlee, G.F., Hydrodynamics and Mass Transfer in Packed Columns and their Applications for Supercritical Separations;, Ph.D. Dissertation, Technische Universität Delft, (1997).

[43] Lim, J.S., Lee, Y.- W., Kim, J.- D, Lee, Y.Y. and Chun, H.- S., Mass- Transfer and Hydraulic Characteristics in Spray and Packed Extraction Columns for Supercritical Carbon Dioxide- Ethanol- Water System, J. Supercrit. Fluids, 8 (1995) 127.

[44] Machado, N.T., Fractionation of PFAD- Compounds in Countercurrent Columns Using Supercritical Carbon Dioxide as Solvent;, Ph.D. Dissertation, Technische Universität Hamburg - Harburg, (1998).

[45] Meyer, J.- T., Druckverlust und Flutpunkte in Hochdruckgegenstromkolonnen, Ph.D Dissertation, Technische Universität Hamburg - Harburg, (1998).

[46] Budich, M., Countercurrent Extraction of Citrus Aroma from Aqueous and Nonaqueous Solutions Using Supercritical Carbon Dioxide;, VDI- Verlag, Düsseldorf, Germany, (1999).

[47] M. a. B. G. Budich, Vapour- Liquid Equilibrium Data and Flooding Point measurements of the Mixture Carbon Dioxide + Orange Peel Oil, Fluid Phase Equilib., 158- 160 (1999) 759- 773.

[48] Stockfleth, R. and Brunner, G., Hydrodynamics of a Packed Countercurrent Column for the Gas Extraction, Ind. Eng. Chem. Res. 38 (1999) 4000- 4006.

[49] Zacchi, P., Calvo Bastida, S., Jaeger, P., Cocero, M.J. and Eggers, R., Countercurrent de-acidification of vegetable oils using supercritical CO2: Holdup and RTD experiments, J. Supercrit. Fluids, 45 (2008) 238- 244.

[50] Souders, M. and Brown, G.G., Design of Fractionating Columns, Entrainment and Capacity, Ind. Eng. Chem., 38 (1934) 98- 103.

[51] Eckert, J.S., Selecting the Proper Distillation Column Packing., Chem. Eng. Prog., 66 (1970) 39.

[52] Maćkowiak, J., Fluid dynamics of packings and columns with modern packings for gas / liquid systems (orig. German), Salle & Sauerland, Frankfurt, Germany, (1991).

[53] Stockfleth, R., Fluiddynamik in Hochdruckgegenstromkolonnen für die Gasextraktion;, Ph.D. Dissertation, Technical University of Hamburg - Harburg, (2001).

[54] Diaz, M.S. and Brignole, E.A., Modeling and optimization of supercritical fluid processes, J. Supercrit. Fluids, 47 (2009) 611- 618.

[55] Martín, A. and Cocero, M.J., Mathematical modeling of the fractionation of liquids with supercritical CO2 in a countercurrent packed column, J. Supercrit. Fluids, 39 (2007) 304-314.

[56] Ruivio, R., Paiva, A., Mota, J.P.B. and Simões, P., Dynamic model of a countercurrent packed column operating at high pressure conditions, J. Supercrit. Fluids, 32 (2004) 183-192.

[57] Reverchon, E. and Lacuzio, G., Supercritical desorption of bergamot peel oil from silica gel - Experiments and mathematical modelling, Chem. Eng. Sci., 52 (1997) 3553- 3559.

[58] Brockkötter, J. and Jupke, A., Modeling the fluid dynamics of a high- pressure extraction column.

[59] Fernandes, J., Simões, P.C., Mota, J.P.B. and Saatdijan, E., Application of CFD in the study of supercritical fluid extraction with structured packing: Dry pressure drop calculations, J. Supercrit. Fluids, 47 (2008) 17- 24.

[60] Fernandes, J., Lisboa, P.F., Simões, P.C., Mota, J.P.B. and Saatdijan, E., Application of CFD in the study of supercritical fluid extraction with structured packing: Wet pressure drop calculations, J. Supercrit. Fluids, 50 (2009) 61- 68.

[61] Dohrn, R., High- pressure fluid- phase equilibria: Experimental methods and systems investigated (1988- 1993), Fluid Phase Equilib., 106 (1995) 213- 282.

[62] Dohrn, R. and Christov, M., High- pressure fluid phase equilibria: Experimental methods and systems investigated (1994- 1999), Fluid Phase Equilib., 202 (2002) 153- 218.

[63] Dohrn, R., Peper, S. and Fonseca, J.M.S., High- pressure fluid- phase equilibria: Experimental methods and systems investigated (2000- 2004), Fluid Phase Equilib., 288 (2010) 1- 54.

[64] Dohrn, R., Fonseca, J.M.S. and Peper, S., High- pressure fluid- phase equilibria: Experimental methods and systems investigated (2005- 2008), Fluid Phase Equilib., 300 (2011) 1- 69.

[65] Peper, S., Fonseca, J.M.S. and Dohrn, R., High- pressure fluid- phase equilibria: Trends, recent developments and systems investigated (2009 - 2012), Fluid Phase Equilib., 484 (2019) 126- 224..

[66] Brunner, G., Counter- current separations, J. Supercrit. Fluids, 47 (2009) 574 - 582.

[67] Stichlmair, J., Bravo, J.L. and Fair, J.R., General model for prediction of pressure drop and capacity of countercurrent gas/liquid packed columns, Gas Sep. Purif., 3 (1989) 19- 28.

[68] Ergun, S., Fluid Flow through Packed Columns, Chem. Eng. Prog., 48 (1952) 89- 94.

[69] Rumpf, H.C.H. and Gupte, A.R., Einflüsse der Porosität und Korngrößenverteilung im Widerstandsgesetz der Porenströmung, Chem. Ing. Tech.,43 (1971) 367- 375.

[70] Reynolds, O., An Experimental Investigation of the Circumstances Which Determine Whether the Motion of Water Shall Be Direct or Sinuous, and of the Law of Resistance in Parallel Channels, Philos. Trans. Royal Soc., 174 (1883) 935- 982.

[71] Sherwood, T.K., Shipley, G.H. and Holloway, F.A.L., Flooding Velocities in Packed Columns, Ind. Eng. Chem., 30 (1938) 765- 769.

[72] Wallis, G.B., One- dimensional Two- phase Flow, McGraw- Hill: New York, United States of America, (1969).

[73] Maćkowiak, J., Pressure drop in irrigated packed columns, Chem. Eng. Process. 29 (1991) 93- 105.

[74] Stichlmair, J., Paper presented at the internal meeting of the Technical Committee "Thermal decomposition of gas and Liquid Mixtures", GVD VDI Society for Chemical Engineering, Bochum, (1983).

[75] Mersmann, A. and Deixler, A., Packungskolonnen, Chem.- Ing.- Techn., 56 (1986) 19- 31.

[76] Maćkowiak, J., Extended channel model for prediction of the pressure drop in single-phase flow in packed columns, Chem. Eng. Res. and Des., 87 (2009) 123- 134.

[77] Woerlee, G.F., Berends, J., Olujic, Z. and De Graauw, J., A comprehensive model for the pressure drop in vertical pipes and packed columns, Chem Eng J., 84 (2001) 367- 379..

[78] Brunner, G., Gas Extraction: An Introduction to Fundamentals of Supercritical Fluids and the Application to Separation Processes, Steinkopff, Darmstadt, 1994, ISBN: 978- 3- 662-07382- 7..

[79] Dohrn, R.; Fonseca, J.M.S. and Peper, S., Experimental Methods for Phase Equilibria at High Pressures, Annu. Rev. Chem. Biomol. Eng., 3 (2012) 343, 2012..

[80] De Haan, A.B., Supercritical Fluid Extraction of Liquid Hydrocarbon Mixtures, Ph.D. Dissertation, Technische Universität Delft, (1997)..

[81] Mertsch, R. and Wolf, B.A., Solutions of Poly(dimethylsiloxane) in Supercritical CO2: Viscometric and Volumetric Behavior, Macromolecules, 27 (1994) 3289–3294..

[82] Xiong, Y. and Kiran, E., Miscibility, density and viscosity of poly(dimethylsiloxane) in supercritical carbon dioxide, Polymer, 36 (1995) 4817- 4826..

[83] Dindar, C. and Kiran, E., High- Pressure Viscosity and Density of Polymer Solutions at the Critical Polymer Concentration in Near- Critical and Supercritical Fluids, Ind. Eng. Chem. Res., 41 (2002) 6354- 6362..

[84] Liu, K., Schuch, F. and Kiran, E., High- pressure viscosity and density of poly(methyl methacrylate)+ acetone and poly(methyl methacrylate)+ acetone+ CO2 systems, J. of Supercrit. Fluids, 39 (2006) 89–101..

[85] Bayraktar, Z. and Kiran, E., Miscibility, Phase Separation, and Volumetric Properties in Solutions of Poly(dimethylsiloxane) in Supercritical Carbon Dioxide, J. Appl. Polym. Sci., 75 (1999) 1397- 1403..

[86] Pensado, A.S., Pádua, A.A.H., Comuñas, M.J.P. and Fernández, J., Viscosity and density measurements for carbon dioxide+ pentaerythritol ester lubricant mixtures at low lubricant concentration, J. of Supercrit. Fluids. 44 (2008) 172–185..

[87] Jenab, E. and Temelli, F., Viscosity measurement and modeling of canola oil and its blend with canola stearin in equilibrium with high pressure carbon dioxide, J. of Supercrit. Fluids, 58 (2011) 7–14..

[88] Seifried, B. and Temelli, F., Use and limitations of a quartz crystal microbalance to measure viscosity of carbon dioxide- expanded fish oil fatty acid ethyl esters, J. of Supercrit. Fluids, 101 (2015) 104–109. .

[89] Ilieva, P., Kilzer, A. and Weidner, E., Measurement of solubility, viscosity, density and interfacial tension of the systems tristearin and CO2 and rapeseed oil and CO2, J. of Supercrit. Fluids, 117 (2016) 40–49..

[90] Kian, K. and Scurto, A.M., Viscosity of compressed CO2 - saturated n- alkanes: CO2/n- hexane, CO2/n- decane, and CO2/n- tetradecane, J. Supercrit. Fluids, 133 (2018) 411–420..

[91] Gourgouillon, D., Avelino, H.M.N.T., Fareleira, J.M.N.A. and Nunes da Ponte, M., Simultaneous viscosity and density measurement of supercritical CO2- saturated PEG 400, J. Supercrit. Fluids, 13 (1998) 177- 185..

[92] Hrnčič, M.K., Škerget, M. and Knez, Z., Density and viscosity of the binary polyethylene glycol/CO2 systems, J. Supercrit. Fluids, 95 (2014) 641- 668..

[93] Iguchi, M. Hiraga, Y., Kasuya, K., Aida, T.M., Watanabe, M., Sato, Y. and Smith, R.L., Viscosity and density of poly(ethylene glycol) and its solution with carbon dioxide at 353.2 K and 373.2 K at pressures up to 15 MPa, J. of Supercrit. Fluids, 97 (2015).

[94] Kravanja, G., Hrnčič, M.K., Škerget, M. and Knez, Z., Interfacial tension and gas solubility of molten polymer polyethylene glycol in contact with supercritical carbon dioxide and argon, J. Supercrit. Fluids, 108 (2016) 45- 55..

[95] Avelino, H.M.N.T., Fareleira, J.M.N.A., Gourgouillon, D., Igreja, J.M. and Nunes da Ponte, M., Viscosity of poly(ethyleneglycol) 200 [PEG 200] saturated with carbon dioxide, J. Supercrit. Fluids, 128 (2017) 300- 307..

[96] Kravanja, G., Knez, Z. and Hrnčič, M.K., Density, interfacial tension, and viscosity of polyethylene glycol 6000 and supercritical CO2, J. Supercrit. Fluids, 139 (2018) 72- 79..

[97] Lopes, J.M., Kareth, S., Bermejo, M.D., Martín, Á., Weidner, E. and Cocero, M.J., Experimental determination of viscosities and densities of mixtures carbon dioxide+ 1-allyl- 3- methylimidazolium chloride. Viscosity correlation, , J. of Supercrit. Fluids, 111 (2016) 91- 96.

3. Publication 1

Concurrent Measurement of High-Pressure Binary Phase Equilibrium, Density and Dynamic Viscosity.

H.H. Franken[a], J.H. Knoetze[a], C.E Schwarz[a, *]

[a] Department of Process Engineering, Stellenbosch University, Private Bag X1, Matieland,
7602, South Africa.

*Phone: +27 21 808 4487, Email: cschwarz@sun.ac.za

The Journal of Supercritical Fluids, 133 (2018) 444–454
Received 21 September 2017; Revised 13 November 2017; Accepted 14 November 2017

DOI: 10.1016/j.supflu.2017.11.008

Declaration by the candidate

Concerning Chapter 3, the nature and scope of my contribution(s) were as follows:

Nature of contribution	Contribution (%)
I was responsible for the equipment's conceptualisation, design, procurement, construction, commissioning, method development, experimental work and validation. I was also the primary author of the article, responsible for compiling the document and the submission and review process.	80%

The following co-authors contributed to Chapter 3:

Name	E-mail address	Contribution Nature	Contribution (%)
Cara E. Schwarz	cschwarz@sun.ac.za	Supervisor of student, HH Franken	12.5 %
Johannes H. Knoetze	jhk@sun.ac.za	Co-supervisor of student, HH Franken	7.5 %

Signature of candidate: Declaration with signature in possession of candidate and supervisor
Date : 20 January 2020

Declaration by co-authors

The undersigned hereby confirm that:

1. The declaration above accurately reflects the nature and extent of the contributions of the candidate and the co-authors to Chapter 3.

2. No other authors contributed to Chapter 3 besides those specified above.

3. Potential conflicts of interest have been revealed to all interested parties and that the necessary arrangements have been made to use the material in Chapter 3 of this dissertation.

Signature	Institutional affiliation	Date
Declaration with signature in possession of candidate and supervisor	Supervisor to the student, HH Franken at Stellenbosch University	20 January 2020
Declaration with signature in possession of candidate and supervisor	Co-Supervisor to the student, HH Franken at Stellenbosch University	20 January 2020

Preface

Experimental method detail (Safe Working Procedures), as well as an analysis and steps to eliminate or mitigate any risk (Task Risk Assessment), are presented in Appendix B. Safety information for all chemicals used can be found in Appendix C. A full description of the new equipment and its operating principles, safety considerations and technical data can be found in Appendix D. Technical data includes detailed documentation on: parts and materials, design drawings, design calculations, measurement equipment, calibrations and certifications, software and peripherals.

This paper addresses the first objective - To design, construct, commission, and verify equipment capable of simultaneously measuring the phase equilibria and fluid properties of density and dynamic viscosity at saturation under supercritical conditions. This requirement leads from the literature review, where the need for such data was highlighted and justified.

Abstract

New equipment offering a novel combination of concurrent binary phase equilibria, saturated fluid density and dynamic viscosity determination, was developed. The setup (P_{max} 35 MPa; T_{max} 393 K) includes a variable volume view cell to determine bubble/dew points and density, with a quartz-crystal resonator to measure dynamic viscosity. Phase equilibrium is determined visually, using a synthetically known composition (SynVisVar). Uncertainties in measurements are 0.06 MPa in pressure, < 0.0005 in mass fraction, and 0.2 K in temperature. Density is calculated to within < 0.003 of the value. The dynamic viscosity is determined by measuring the frequency shift over the quartz crystal, to within < 0.01 of the value. Equipment verification was done using n-dodecane and benzene at 0.1 - 30 MPa and 313 - 353 K while contributing to available benzene literature. Binary equilibrium measurements were verified using CO_2 + ethyl tetradecanoate while presenting new data on the dynamic viscosity and density of the saturated binary phase.

Keywords: Benzene; Supercritical CO_2; n-Dodecane; Ethyl tetradecanoate; Piezoelectric quartz; Viscometer

Highlights

- Equipment for the measurement of phase equilibria, dynamic viscosity and density.
- Rapid, concurrent measurement with excellent repeatability and accuracy.
- Novel density and dynamic viscosity data for benzene and CO_2+ethyl tetradecanoate.
- Supplementary electromechanical determination of bubble and dew points.
- Large fluid property variability under supercritical conditions vs pure components.

3.1 Introduction

A need for comprehensive equipment sizing and design methods for supercritical processes has become ever more pronounced. To develop these methods, a fundamental understanding of the mass transfer and transport phenomena in supercritical systems is required, each discussed separately below. Potential mass transfer in a system is determined by the system's phase equilibria, indicating the viability of separation and, if separation is possible, it quantifies the driving force behind said separation. Mass transfer addresses design concerns such as the operating pressure, temperature and method-specific considerations, such as the required number of separation stages in a separation column [1]. Mass transfer alone is, however, not sufficient when accounting for the physical size and geometry of equipment. To address this, the transport phenomena are investigated, with a particular focus in this study on physical properties and the dependent fluid dynamics. Fluid dynamic properties (e.g. density and viscosity), along with the potential equipment size and geometry, can be used to calculate the operating regime/range and the efficiency of a system. Efficiency and operating range are essential to design considerations, highlighting the associated importance of the fluid properties of density and viscosity [2]. In the supercritical regime, these fluid properties undergo substantial changes with small changes in temperature and pressure, significantly affecting fluid dynamics, which in turn requires revision and adjustment of design methodology and equipment geometry. These properties can also not easily be predicted using standard models [3].

Preciously little research on fluid properties and fluid dynamics under supercritical conditions has been done to date [4]. When investigating fluid dynamics with equipment sizing and design methods in mind, the fluid properties must be known and other transport phenomena, such as mass- and heat transfer, should be eliminated or fully quantified. This implies that phase equilibria and fluid property data are required to make informed decisions and reasonable deductions, necessitating their combined accurate measurement.

This paper aims to present and verify a new piece of equipment, proposing a novel combination of an established phase equilibrium determination method (dew/bubble point), supplemented with density and viscosity measurement at the point of equilibrium. To validate the equipment, the viscosity and density methods are used to gather pure component data for n dodecane and benzene for comparison with the literature, while contributing a higher resolution of data points at comparatively low temperatures and pressures. The equipment is then validated for the measurement of binary phase equilibria, using CO_2 + ethyl tetradecanoate, with new density and dynamic viscosity data for this binary system. The developed equipment simplifies and accelerates data acquisition towards further study into fluid dynamic properties by the concurrent measurement of properties. The gathered data ultimately provides a basis for equipment sizing and design methods to be developed, with future work aimed at fluid dynamics in packed columns operating under supercritical conditions.

Each of the measurement aspects of the equipment is discussed separately below.

3.1.1 Phase Equilibria

Many different methods are used to measure high-pressure phase equilibria with no single method being superior [5]. The measurement of phase equilibria is typically divided into analytical and synthetic methods. In analytical methods, the composition of the equilibrium phases is determined through a qualitative [1] measurement at a defined state. Synthetic methods investigate a mixture with a known composition, by manipulating the system's intensive properties to achieve equilibrium. Both methods are further subdivided into several subcategories. Interested readers are directed to the work of Dohrn et al. [5].

For this study, a high-pressure, variable volume cell was selected. This cell is comparably inexpensive to manufacture and simple to operate, providing a robust, flexible, and above all, tried and tested solution. The cell is equipped with a sight glass to visually observe and determine phase changes, per a synthetic-visual (SynVisVar) method. The operating procedure for such a cell is described in full by Schwarz and Nieuwoudt [6] and more recently in brief by Fourie et al. [7].

3.1.2 Viscosity

Viscosity is measured by applying a shear force to a fluid and measuring the resultant rate of deformation. Knowledge of a fluid's viscosity provides insight into the frictional forces during fluid transport, the turbulence of and mixing behaviour in a fluid, and falling film thickness, to name a few.

Viscosity measurement technology for the equipment has to conform to a few requirements. Firstly, the method must be capable of measuring saturated fluids under high pressure/supercritical conditions. Secondly, a non-disruptive measurement method is required, as any significant disturbance may potentially upset the phase equilibrium at the point of measurement [8]. Thirdly, the measurement method has to be integrated into a device concurrently measuring the phase equilibria and density of the same fluid state.

Most of the commonly used techniques can be dismissed out of hand when applying these metrics. Capillary tube viscometers can measure under high pressures but present several practical challenges. A rotational rheometer can provide high accuracy but presents

---

[1] This is in error and should read 'quantitative'.

mechanical sealing problems. Falling body or falling ball viscometers are commonly used, but present challenges to the accurate release, timing and detection of the falling body, with the range of shear rates limited by the size and geometry of the falling objects available. This leaves vibrational viscometers, such as the vibrating wire and crystal. [9]

The vibrating wire technique requires a wire, of known mass and dimensions, to be clamped between two fixed supports. The wire is suspended in a permanent magnetic field and excited by passing an AC signal through the wire, as per Faraday's Law. The wire can measure both viscosity and density through knowledge of the wire density, -geometry and -tension and the resonance frequency and bandwidth generated. [10]

The vibrating crystal technique exploits the converse piezoelectric effect of a quartz crystal, with a mechanical vibration induced in the crystal by a changing electrical field. The measurement principle is similar to that of a quartz microbalance (used in high accuracy scales), with the crystal resonance frequency shifting when a load, such as mass or viscous drag, is applied to the crystal. This method has been proven reliable up to 1000 MPa and 373 K for pure organic liquids [11], with method variables and constants effectively independent of pressure in the region of interest [12]. Density can also be derived from the crystal setup if the resonance bandwidth is measured, although this requires precise impedance analysis.

After consideration, the quartz crystal technique was selected. Firstly, it provided less variability compared to the vibrating wire, with the crystal dimensions fixed and finely machined by suppliers. In contrast, the wire geometry and mass are typically derived using a known viscosity, following the assumption of a perfect cylinder. Secondly, the wire was deemed to be more difficult to install into a removable unit, a requirement for easy cleaning, while keeping the wire tension constant. In contrast, the crystal setup provided a simple solution, with mobile, though sensitive connections to the crystal, immune to small distortions in the surrounding materials. To summarise, the crystal presents a more straightforward implementation and a more robust physical solution while providing a similar degree of accuracy.

Several different crystal types and techniques are available in the literature, but will not be discussed here for brevity's sake. For this work, a large, torsional crystal was selected[2]. A larger crystal possesses a lower resonant frequency and larger surface area, which in turn minimises the energy transmitted into the fluid. This lower transmitted energy fulfils the prescription of minimising the disturbance of the phase equilibria during measurement. Additionally, a lower frequency is also less likely to violate the assumption of a no-slip boundary condition at the interface between the fluid and the crystal.

---

[2] Appendix D.5.5 contains the relevant technical details of the selected crystal.

3.1.3 Density

The importance of density is self-explanatory, with the fluid property playing a central role in fluid dynamics and physical sizing. Density, per definition as mass per volume, is easily measured.

By loading a known mass into a known volume, the density of the system is known. The density measurement requires precise mass measurement and the determination or calibration of the volume, both easily possible with the selected high-pressure cell.

As an alternative, the quartz crystal viscometer has the added advantage of being capable of determining the density. This capability, however, requires additional equipment to determine the bandwidth such as impedance analysers and is beyond the scope of the current work.

3.2 Materials and Methods

3.2.1 Experimental Set-up

A high-pressure cell, seen in Figure 3-1, was designed and constructed according to ASME VIII DIV 1 for operation up to 35 MPa and 393 K. The majority of the components, including the high-pressure body and piston, were machined from stainless steel 316. Components under regular mechanical strain were machined from phosphor bronze to reduce the chance of thread and piston damage. After construction, the cell was cold pressure tested up to 75 MPa and certified for operation up to 35 MPa and 393 K by RITC (Pty) Ltd. After all calibrations, the cell working volume was determined to be 22.3–57.2 cm^3.

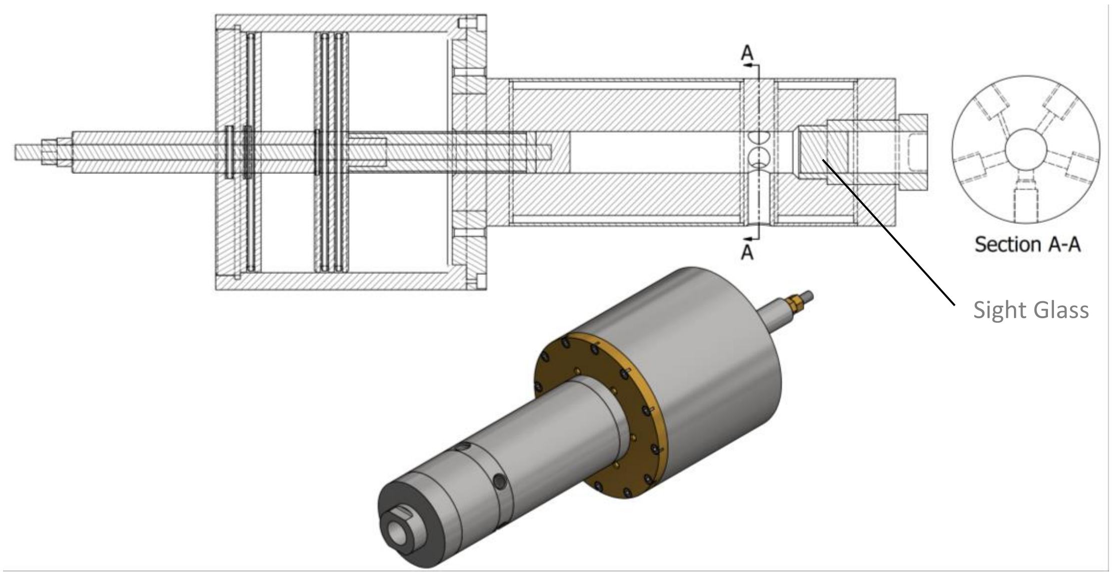

Figure 3-1: Longitudinal section of the high pressure, variable volume, view cell showing the low-pressure section (left) and high-pressure barrel (right). A cut through the barrel showing the various access ports can be seen on the far right.

The cell is stirred with a magnetic stirring bar. The bar is driven using an assembly of three electromagnets with a custom driver circuit, allowing variable stirring of the cell in any orientation.

In Figure 3-1, the five access ports into the cell, spaced equally around the circumference, are seen. The first port is drilled at an angle of 16° to the normal, to avoid direct fluid pressure on the internals while loading and fitted with a Swagelok needle valve (model: SS-20VM4-F4-A). This valve is used to load and unload gaseous solvent. The second port is fitted with a Conax Technologies sensor wire compression fitting (model: TG-24T-A2-G) and provides electrical connectivity to the quartz crystal assembly. The remaining three ports contain two temperature sensors and a pressure sensor. Temperature and pressure are logged using a Delta PLC and HMI setup. Any dead volume in the access ports is filled with custom Teflon or PEEK (polyether ether ketone) inserts and spacers depending on the need.

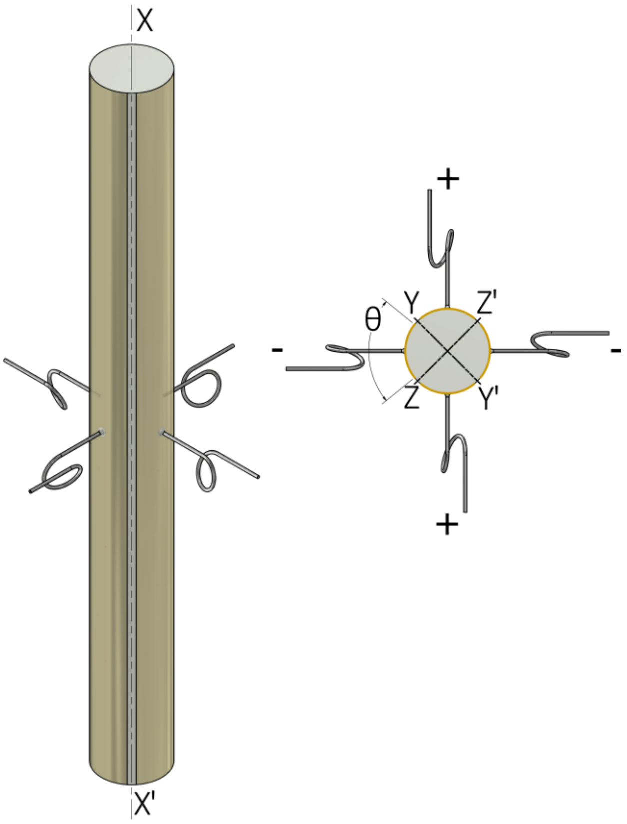

Figure 3-2: Cylindrical quartz crystal and electrode configuration for a torsional mode of vibration, shown from the side isometric and top views. The electrical connectivity (+, -), electrode area θ (80°) and the X, Y and Z crystallographic axes are indicated.

For the viscosity measurements, a cylindrical α-quartz, X-cut crystal cylinder of 50 mm length and 5 mm diameter was used. A schematic of the crystal is seen in Figure 3-2. Some authors [11, 13, 14] have published results and methods using this cut orientation and crystal size, with the original application reported in the work of Mason [15]. Previous researchers have successfully measured dynamic viscosity using a crystal of this geometry and mode of operation at extreme and delicate conditions such as extremely low-temperature liquid helium [13] and very high pressures [11]. The crystal is polished to an ultra-smooth finish and plated with four gold electrodes. The electrodes are deposited in quadrants of 80° along the circumference and for the full height of the crystal. The unplated regions lie in the Y- and Z-axes of the crystal, ensuring a torsional mode of vibration. Very thin wire leads are then attached to the centre of each electrode. This minimises the damping effect of the leads on the crystal during measurement. Each wire is looped once before connection to avoid strain on the leads and crystal. A short discussion of the crystal operation is found in Section 3.2.3.

A removable crystal 'cage' was designed and constructed to house the quartz crystal and provide electrical contact, as seen in Figure 3-3[1]*. The cage is constructed from stainless steel 316 and PEEK plastic, with 50-50 Indium/Tin soldering used to connect the wire leads to the cage. The crystal requires two electrical contacts, with opposing electrodes connected. One contact is provided by lining up one pair of opposing crystal cage 'bars' with a spring-loaded, gold, circuit board test probe (90° conical tip with 1 mm diameter), held in place by a tight-fit PEEK insert. The other end of the test probe is soldered to a Teflon coated wire, which is passed through the Conax wire seal to an external connector, providing the 'positive' contact. The other contact is provided by contacting the second pair of opposing 'bars' of the cage with the high-pressure cell wall, which is grounded to the measurement equipment, providing the 'neutral' contact.

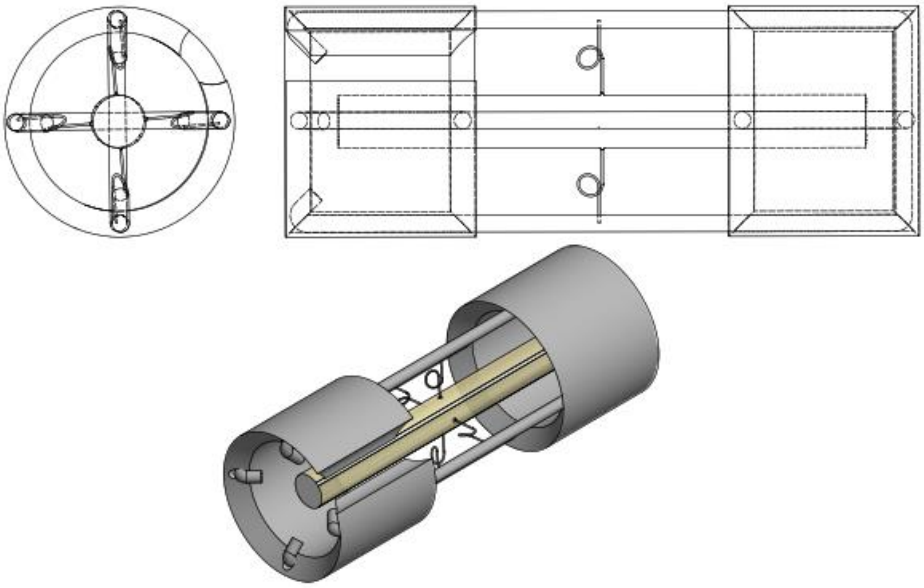

Figure 3-3: Removable crystal cage assembly, allowing for easy cleaning and crystal removal.

Using the electrical contacts the crystal can be operated in either a forced- or free-mode of vibration. The forced-mode implies that the crystal is continuously stimulated with an electric

---

[1] The crystal cage is inserted into the cell to ensure contact between the crystal and the measured fluid.

current and the resonance characteristics measured, while the free-mode analyses the damping of the crystal by the fluid, after the electric stimulation is switched off. For this work, the use of a forced-mode is selected, presenting the opportunity to continuously measure the crystal response through the appearance of a phase transition, providing additional information if correlated with the pressure.

3.2.2 Phase Equilibria Method

A detailed experimental procedure with regards to loading, operating, unloading, and cleaning high-pressure variable volume cells has been published previously [6, 7][2]. The experimental procedure can be briefly summarized as follows: A quantified mass of the liquid component is loaded into the cell. The cell is then closed, the piston seal tightened, and all air is removed using a vacuum pump and multiple flushes with CO_2. A quantified mass of CO_2 is then transferred into the cell. The cell is then heated to the first experimental temperature, pressurised, and allowed time to reach thermal equilibrium (approx. 1 h). After sufficient time the cell is slowly, isothermally depressurised while continually monitoring for phase transitions using an HD camera setup. Once a transition is observed and recorded, the cell is repressurised, and the process is repeated until the phase transitions are repeatedly observed to within 0.02 MPa. After measurements are completed at a set temperature, the temperature is increased to a new value. After sufficient time has passed to ensure thermal equilibrium (approx. 1 h), the measurement method is repeated until all desired temperatures are measured.

3.2.3 Dynamic Viscosity Theory and Method

When a suspended quartz crystal (as seen in Figure 3-3) is excited by an alternating current, a mechanical torsion is produced. This mechanical torsion induces transverse waves in the crystal of the same frequency as the electrical input (transverse waves cause displacement of the medium perpendicular to the direction of propagation of the wave). In a vacuum, where the wave cannot propagate further than the edge of the crystal, the crystal resonates at a characteristic frequency, f_o, the vacuum resonance. In this case, the only dissipation of energy is through the internal friction in the crystal and virtually negligible losses through the suspending wires. For the fundamental mode of vibration, the vacuum resonance for a torsional cylinder is described by:

$$f_o = \left(2 \cdot l \cdot (\rho_Q / C_{66})^{1/2}\right)^{-1} \qquad \{3\text{-}1\}$$

where l (m) is the crystal length, ρ_Q is the quartz density (2650 kg/m^3 – manufacturer value) and C_{66} is the appropriate crystal rigidity modulus for torsion (40.63 x 10^9 m^2/N – manufacturer value) [13].

---

[2] Full operating procedures for the cell can be found in Appendix B with technical specifications in Appendix D.

A vacuum resonance of ~39 kHz is predicted for the crystal selected for this work using Equation {3-1}. The vacuum resonance, density and geometry of the crystal are effectively independent of pressure in the range investigated in this work [16, 12]. Temperature, however, has a noticeable effect, necessitating the need to calibrate the crystal for different temperatures [11]. This calibration is achieved by measuring the vacuum resonance for each of the experimental temperatures. Measured vacuum resonances can be seen in Table 3-1.

When the crystal is placed in a fluid medium and excited, the generated transverse waves propagate into the fluid in the form of an ultrasonic wave. The ultrasonic wave is damped logarithmically in the fluid (assuming planar wave theory [17]), with the vibrations effectively extinguished only a few micrometres away from the surface. This damping affects the electrical response of the crystal, as per the converse piezoelectric effect, changing the crystal impedance and, hence, the loaded resonance, f_{res}. The degree of damping is directly related to the product of the dynamic viscosity and density of the fluid, and is expressed as:

$$f_o - f_{res} = k \cdot (\pi \cdot f_{res} \cdot \eta \cdot \rho_f)^{1/2} \qquad \{3\text{-}2\}$$

where η (Pa.s) is the dynamic viscosity, ρ_f (kg/m^3) the fluid density and k (m^2/kg) the electromechanical constant [11]. In the case of the equipment presented, k was calculated by placing the crystal in a liquid of known viscosity for each experimental temperature. For this, n-dodecane at atmospheric conditions was used. k was found to be temperature dependent, in agreement with literature [11]. Determined k vales can be found in Table 3-1.

Table 3-1: Determined constants k (determined using n-dodecane at atmospheric conditions) and f_o (measured at temperature, under vacuum).

Temperature (K)	Constant K (m²/kg)	Vacuum Resonance (Hz)
313.15	0.11839	39136.62
323.15	0.12249	39136.98
333.15	0.12290	39137.80
343.15	0.12972	39137.86
353.15	0.13204	39137.92

To experimentally determine the crystal resonance, be it under vacuum or load, a particular AC signal is introduced to the crystal, with the response of the crystal relative to the signal, indicated on an oscilloscope. The frequency is stepped through the frequency band where the resonance is expected, and the voltage drop over the crystal and the phase shift is recorded, using custom software developed in-house. The resonant frequency is identified at the minimum voltage and zero phase shift, using recorded data and visual confirmation on the oscilloscope. This measurement is repeated at least three times to ensure accuracy. The viscosity can then be calculated using Equation {3-2}, provided the density is known. Alternatively, the resonance bandwidth and crystal resistance can be used, allowing for the calculation of density and hence the viscosity. The density calculation, however, requires very accurate impedance measurement, not available in the current study. Interested readers are directed to the work of Mason [15] or Collings and McLaughlin [11].

Several different voltages (ranging from 1V to 5V) were applied to the quartz crystal at a set temperature and pressure to verify if the tested fluids were exhibiting Newtonian behaviour. The change in potential difference over the crystal causes a corresponding change in the vibration amplitude, which in turn produces a different shear rate. No variation in the measured viscosity beyond the reported uncertainty was noted, confirming Newtonian behaviour for the selected fluids in the range investigated.

The crystal resonance was continuously measured while approaching the phase change point to measure the properties of the binary system. It was found that, for a given mixture, the crystal resonance did not vary noticeably with pressure just above the phase transition point pressure (up to 0.8 MPa above). The final dynamic viscosity measurement was performed at a pressure range of 0.1 – 0.2 MPa higher than the determined phase transition point to ensure the crystal measured the saturated phase viscosity, without any residue from a second phase. The measurement was performed after allowing sufficient time to pass to be sure the system is in a single-phase equilibrium.

3.2.4 Density Method

To measure the density, the volume and the mass in the cell is required. The experimental mass loaded into the cell is weighed with high accuracy (see Section 3.2.2).

The volume of the variable volume cell is accurately calibrated using a known mass of CO_2[1]. The use of CO_2 provides a compromise between compressibility, accuracy and range of volumes possible with a single mass. The cell is loaded, as per the experimental procedure, with only CO_2. After loading the CO_2, the cell is allowed to reach equilibrium at a set temperature, and the piston position and pressure is noted. The cell volume is then changed through the application of nitrogen to the low-pressure chamber and the contents allowed to reach a new equilibrium, after which the changed pressure and piston position are noted. This process is repeated for the entire range of the piston movement. Hysteresis was investigated by both increasing and decreasing the volume and observing any discrepancy. A slight hysteresis was noticed and is factored into the uncertainty in the cell volume (see Section 3.2.5). The CO_2 specific volume

---

[1] The volume calibration can be seen in Appendix D.5.8.5.

corresponding to each of the measured states is then calculated using the CO_2 specific EOS by Span and Wagner [18]. The volume is then calculated and related to the measured piston position for the entire range. For experimental use, the relationship between the piston position and the volume is regressed, presenting a linear equation of almost perfect fit ($R^2 = 0.999$).

With both the mass and volume of an experimental system known, calculating the density is trivial. For density measurements at saturation, the density reported was noted just before the appearance of a phase transition, at the same conditions as the viscosity measurement.

3.2.5 Uncertainty

Uncertainties are primarily Type B standard uncertainties as defined by the Guide to the expression of uncertainty in measurement [19] unless stated otherwise.

Pressure is measured using an ONEhalf20 melt pressure transducer, model number: CT6MA-DLX-3.5CB. The pressure sensor is calibrated to a standard uncertainty of 0.02 MPa after each full experimental set, using a Barnett Industrial deadweight tester, itself calibrated to a standard uncertainty smaller than 0.01 MPa by Unique Metrology (Pty) Ltd. [a SANAS (South African National Accreditation System) accredited pressure metrology laboratory]. Considering all errors, including repeatability, sensor hysteresis, and human error, it is determined that the combined uncertainty is at worst 0.06 MPa of the phase equilibria pressure measurements.

Temperature is measured using two identical 4-wire PT 100 probes, sourced from WIKA Instruments. Both probes are directly in contact with the fluid medium, with one probe slightly protruding into the cell and the other slightly recessed. The probes are calibrated yearly to a standard uncertainty of <0.2 K by Thermon South Africa (Pty) Ltd., a SANAS and ISO 17011:2004; ISO 9001:2008 accredited temperature metrology laboratory.

Dynamic viscosity is measured using the crystal assembly. The X-cut quartz crystals were sourced from Boston Piezo Optics Inc., with the gold-plated electrodes and wire leads pre-installed. The crystal was machined to ± 0.003" (± 76 µm) on the diameter and ± 0.001" (± 25 µm) on the length. The gold electrode thickness is reported as 0.35 µm. The crystal is excited by an AC signal, generated by a RIGOL DG1022 signal generator, to a standard uncertainty of 1 µHz, ± 100 ppm of the signal per year. A Tektronix TDS2002 oscilloscope, with a sampling rate of 1.0 GS/s and accurate within ± 5 mV (± 3 % of the selected vertical range), is used to measure the response of the crystal. Combined uncertainties for the measurement of the dynamic viscosity value are calculated to be lower than 0.01 times the measured mPa.s value, considering the equipment uncertainty, combined with the variability between repeated measurements and deviation from known values.

The mass of the synthetic mixture loaded into the cell was weighed to within 0.0001 g for liquid samples and to within 0.001 g for the gas. A combined standard uncertainty of less than 0.0005 in the reported mass fractions was calculated.

The cell volume is measured using an Insize 300 mm single beam digital gauge (model: 1150-300) as LVDT (linear variable differential transformer), measuring the depth of the piston into the cell to within 0.01 mm. The piston head and shaft is constructed out of solid stainless, with the LVDT measuring the position of the shaft, and hence the piston face, directly. Accounting for a slight hysteresis noticed during calibration, the standard uncertainty of the measurement is taken to be within 0.03 mm. Considering the hysteresis, the uncertainty in the linear relation derived during calibration ($R^2 = 0.999$), the uncertainty in the mass loaded and the uncertainty in the CO_2 density predicted by the model, a combined uncertainty in the volume of <0.0025 is calculated. The volume is calibrated after each experimental set using pure CO_2.

The uncertainties in the mass and volume, as well as repeatability between values, are combined to form the uncertainty in the density measurement, calculated to be no greater than 0.003 times the density value.

3.2.6 Verification

To test and verify the equipment, two pure component systems and a saturated binary system under supercritical conditions were selected. The pure component systems are used to verify the density and dynamic viscosity measurement method while contributing data points to available literature in the range investigated. The binary system is used to validate the phase equilibria determination while contributing measurements for the dynamic viscosity and density, testing the property measurement method for binary systems and presenting a system with a full set of data.

n-Dodecane was chosen as the first pure component system, encompassing a relatively higher dynamic viscosity range (~0.6 - 1.5 mPa.s). Fluid property data for n-dodecane are available from several sources, measured with a range of viscosity and density determination methods (including an oscillating cylinder-, capillary-, falling ball- and vibrating wire viscometer) [20 - 22]. Models predicting both the density [23] and viscosity [24], approved by the National Institute of Standards and Technology (NIST) as Standard Reference Data (SRD), are available in the literature. Available literature presents a coherent picture, with data in close agreement in pressure and temperature for viscosity and density.

Benzene was chosen as the second pure component system, covering a lower dynamic viscosity range (~0.3 - 0.6 mPa.s). Fluid property data for benzene are available from several sources over a range of temperatures and pressures, using a range of viscosity and density determination methods (including a falling body-, vibrating wire- and torsional quartz crystal viscometer) [14, 25 - 28]. A NIST approved model predicting the density [29] is available, but no reliable model is found for the viscosity. The literature data points are spread at random in the pressure and temperature range investigated. Thus, the opportunity to contribute a more coherent range of values to the literature while verifying the method over a different viscosity range presents itself.

In both systems, the viscosity measurements were repeated at least three times to ensure accuracy and test repeatability. The repeated measurements showed excellent repeatability, excluding measurements discarded for electrical interference from the environment (where a common earth on the oscilloscope caused significant noise in the read value). Repeatability of the measured frequency for both systems was found to be < 0.0002 % and factored into the uncertainty in the viscosity measurement.

No binary systems found in available literature presented phase equilibria data accompanied by dynamic viscosity and density data at saturation for the property ranges under investigation. Further, no source was found presenting data on both the supercritical fluid and liquid-rich phases. Literature data are available, investigating polymers saturated with supercritical fluids [30], but the fluid properties differ significantly from those of typically separated organic components. The viscosities reported by the literature data are orders of magnitude higher and the densities significantly larger (~200 kg/m^3). Further, no attempt is made to quantify the properties of the supercritical fluid-rich phase.

The system CO_2 + ethyl tetradecanoate (CO_2 + ET) was the binary system chosen to validate the phase equilibria measurements, with properties expected in the range of typical organic systems. This system has published phase equilibria data [31], with pure component properties in the range of interest. High-pressure density [18, 32] and dynamic viscosity [33, 34] data are available in the literature for both pure components, providing a basis for comparison and discussion of the deviation of the binary properties from the pure component properties.

3.2.7 Materials Used

Details on the chemicals used are given in Table 3-2. Chemicals were used without further treatment or purification. The dynamic viscosity of the purchased n-dodecane and benzene were also measured at atmospheric conditions, for the experimental temperatures, using an Anton-Paar MCR501 Rheometer. The values are not presented here but were found to compare very well with the literature.

Table 3-2: Chemicals used in this study.

Chemical	Stated purity	Supplier	Product Number	CAS Number
Benzene	≥99.9%	Sigma Aldrich	270709-1L	71-43-2
CO_2	99.9999%	Air Products	K243C	124-38-9
n-Dodecane	≥99%	Sigma Aldrich	D221104-2.5L	112-40-3
Ethyl tetradecanoate (ethyl myristate)	≥99.0%	Sigma Aldrich	70090-100ML	124-06-1

3.3 Results and Discussion

The phase equilibria, density and dynamic viscosity results are summarised in Table 3-3 to Table 3-5, found at the end of the chapter, with each system discussed individually below.

3.3.1 n-Dodecane

The measured densities for n-dodecane are seen in Figure 3-4. The measured density data were found to agree very well with model predictions made using an empirical, Tait-type equation (using parameters derived by Caudwell et al.)[1] [20] and an isochoric equation of state (EOS) [23] predictions. Experimental results agreed, at worst, to within 0.24% of the predicted densities, with an average absolute deviation of 0.09% from the Tait equation (itself reported to be accurate to within 0.2% [20]). The models agreed with each other to within 0.04% of the predicted value. Due to the very close agreement with the model predictions, only the predictions derived from the Tait equation are shown in Figure 3-4. The residual plot of the experimental values relative to the predictive model can be seen in Figure 3-5. There is some systematic deviation visible, although the actual values of deviation are small. The deviation can be attributed to the materials of the cell expanding and contracting as the temperature changes, or the inclusion of minuscule amounts of air in capillary areas in the atmospheric measurement, leading to a small negative error at lower pressures.

The measured n-dodecane dynamic viscosity results are seen in Figure 3-6. The measured data were found to agree very well with the literature data [21, 22] and model predictions [24]. The experimental data follows the expected trends of an almost linear change with pressure, as seen in the work of Keramidi and Rastorguev [21]. A slight upward kurtosis is visible in the experimental data but falls within the uncertainty of the experimental method. Experimental results agreed, at worst, to within 1.18% of the model predicted viscosity, with an average absolute deviation of 0.39% relative to model predictions (the model itself has a reported accuracy of 3% [24]). The residual plot of the experimental and literature values relative to the predictive model can be seen in Figure 3-7. The experimental data fall tightly around the model prediction. In contrast, the work by Keramidi and Rastorguev [21] is consistently higher than

---

[1] Available literature data by Cauldwell et al [20] takes large jumps in pressure (40 MPa), making it difficult to directly compare with the experimental data. As the density of liquids follow a linear trend with pressure in the given range, the empirical model serves as a good comparison with literature data.

the predictive model. Values by Ducoulombier et al. [22] shows significant deviation, although little can be said of the over- or underprediction of data, due to the relatively few data points available in the range investigated.

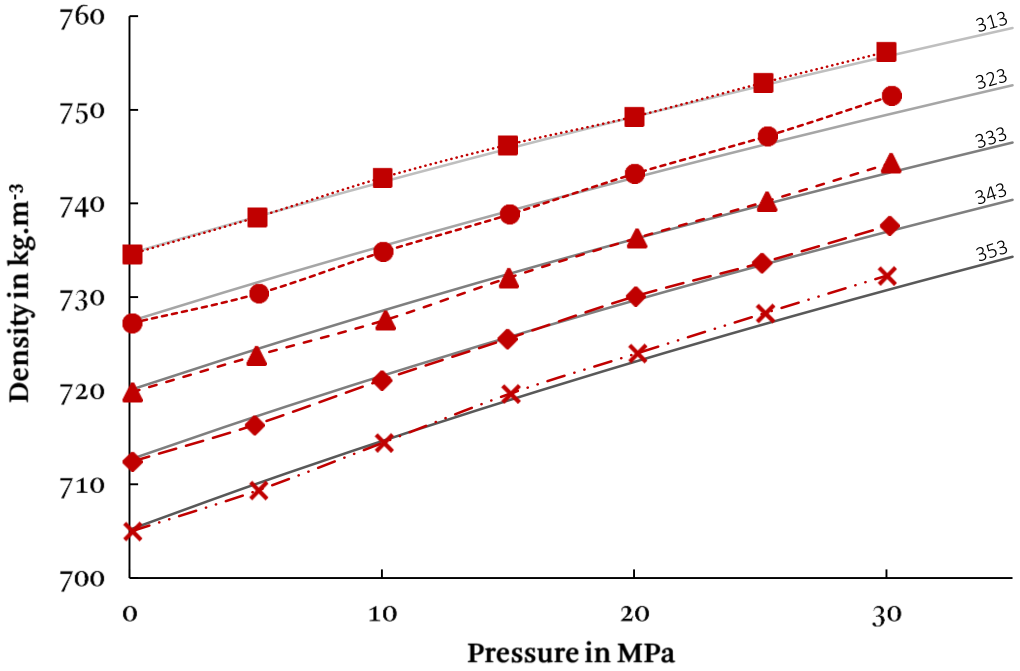

Figure 3-4: The density of n-dodecane.
Temperatures are marked as: ■ 313.15 K; ● 323.15 K; ▲ 333.15 K; ◆ 343.15 K; ✖ 353.15 K. Model predictions (solid lines) at the same temperatures are obtained from a modified Tait type equation with parameters as derived by Caudwell et al. [20].

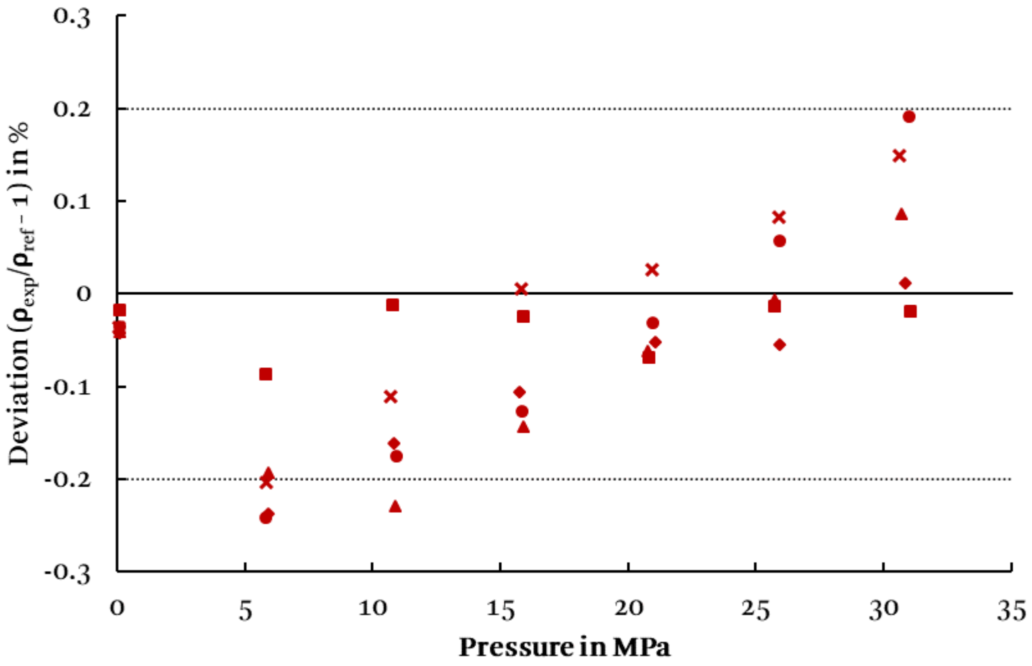

Figure 3-5: Deviations of the experimental density values from the predictive model (solid line) by Caudwell et al. [20]. Dotted lines indicate the confidence interval of the model.
Temperatures are marked as: ■ 313.15 K; ● 323.15 K; ▲ 333.15 K; ◆ 343.15 K; ✖ 353.15 K.

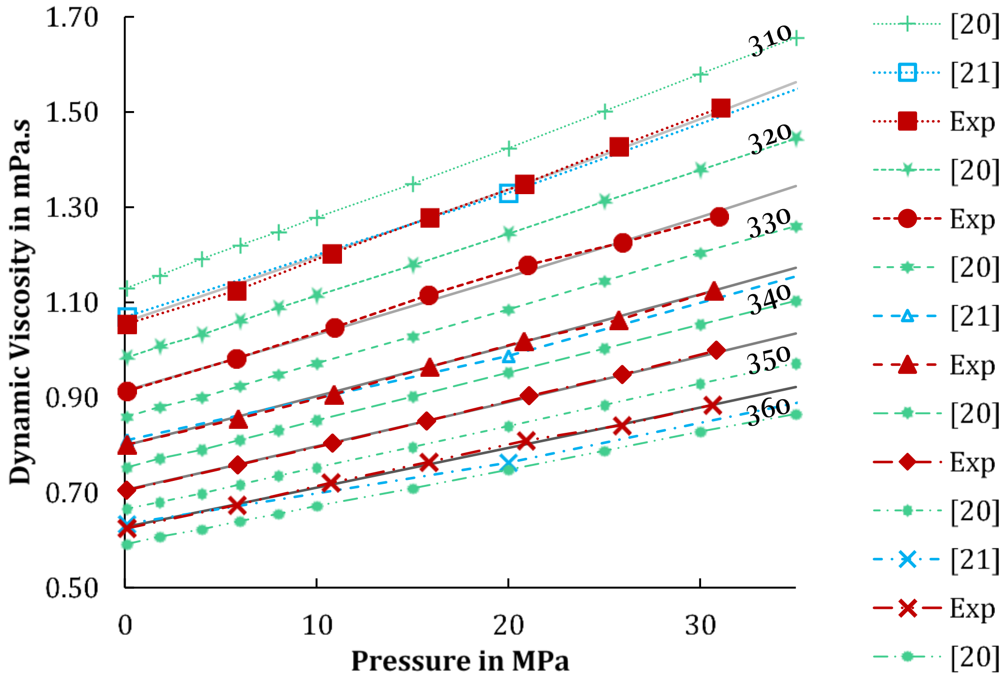

Figure 3-6: The dynamic viscosity of n-dodecane. Comparison with the literature by Keramidi and Rastorguev [21] and Ducoulombier et al. [22].
Temperatures are marked as:■/□ 313.15 K;● 323.15 K; ▲ /△ 333.15 K; ◆ 343.15 K; ✖ /✖ 353.15 K, with Keramidi represented by the symbols: ✚ /★ /✸ /✸ /✸ /✸ (310 K to 360 K in 10K intervals). Model predictions (solid lines) using the experimental temperatures are calculated using the model provided by Huber et al. [24].

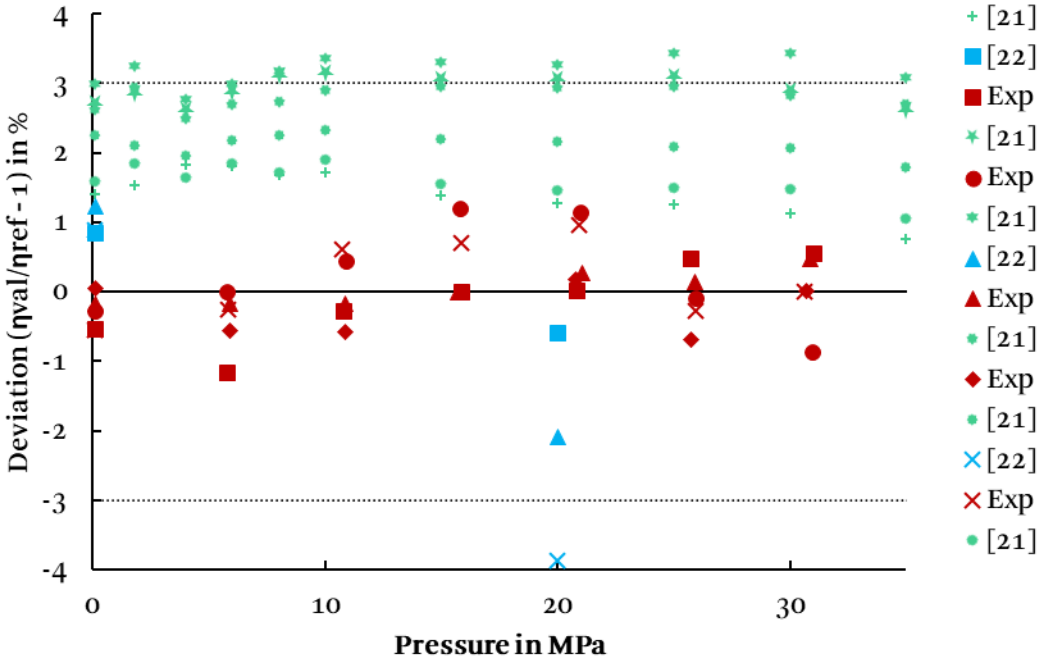

Figure 3-7: Deviations of the experimental and literature [21, 22] dynamic viscosity values from the available predictive model (solid line) by Huber et al. [24].
Dotted lines indicate the confidence interval of the model. Temperatures are marked as:■/□ 313.15 K; ● 323.15 K; ▲ /△ 333.15 K; ◆ 343.15 K; ✖ /✖ 353.15 K, with Keramidi and Rastorguev [21] represented by the symbols: ✚ /★/✸/✸/✸/✸ (310 K to 360 K in 10K intervals).

3.3.2 Benzene

The measured densities of benzene are seen in Figure 3-8. The measured density data were found to agree very well with the literature data [14, 25, 26] and isochoric EOS predictions [29]. It is important to note that two of the literature sources [14, 26] are derived from the third [25]. The model was seen to overpredict the measured experimental results slightly. Results agreed, at worst, to within 0.27% of the value, with an absolute average deviation of 0.10% relative to the EOS predicted density (the EOS has a reported accuracy of 0.24% in predicting the saturated liquid density of benzene). The residual plot of the experimental and literature values relative to the predictive model can be seen in Figure 3-9. As with the n-dodecane values, there is some small deviations, but the deviations are less systematic. In general, all experimental values tend to fall below the model predictions, except for a few outliers. As two of the sources [14, 26] were derived from the third [25], it can be seen that they agree closely in deviation. Some outliers are, however, seen in the literature values [26], falling well beyond the reported accuracy of the authors.

The measured benzene dynamic viscosity results are seen in Figure 3-10. The experimental data follow the expected trends of an almost linear change with pressure, with a slightly decreasing change in dynamic viscosity at higher temperatures [27, 28]. The measured data were found to agree with the literature [14, 26, 27, 28], with some deviation. There is doubt as to some of the literature sources [14, 28], as they are partially in disagreement with each other and some data are in disagreement with the measured data presented here. Significantly, the literature data fail to align with the atmospheric dynamic viscosity values. The atmospheric values are widely available and easily checked, and should directly line up with any measured high-pressure data at the same temperature. In contrast to the linear change in viscosity usually observed, these literature sources show a definite deviation from the atmospheric values, which is unexplained in the publications. The literature sources are found to deviate as far as 3.5% from both the atmospheric values as measured in-house and stated in the literature, while the data presented here agree to within 0.7 %. Considering the excellent agreement of the experimental and the literature data in the n-dodecane system, the agreement of the benzene density results with some of the literature ([26] and low temperature [28]), and the agreement of the viscosity results with the broader range of data presented by Mamedov [27], the data presented here are considered as reliable.

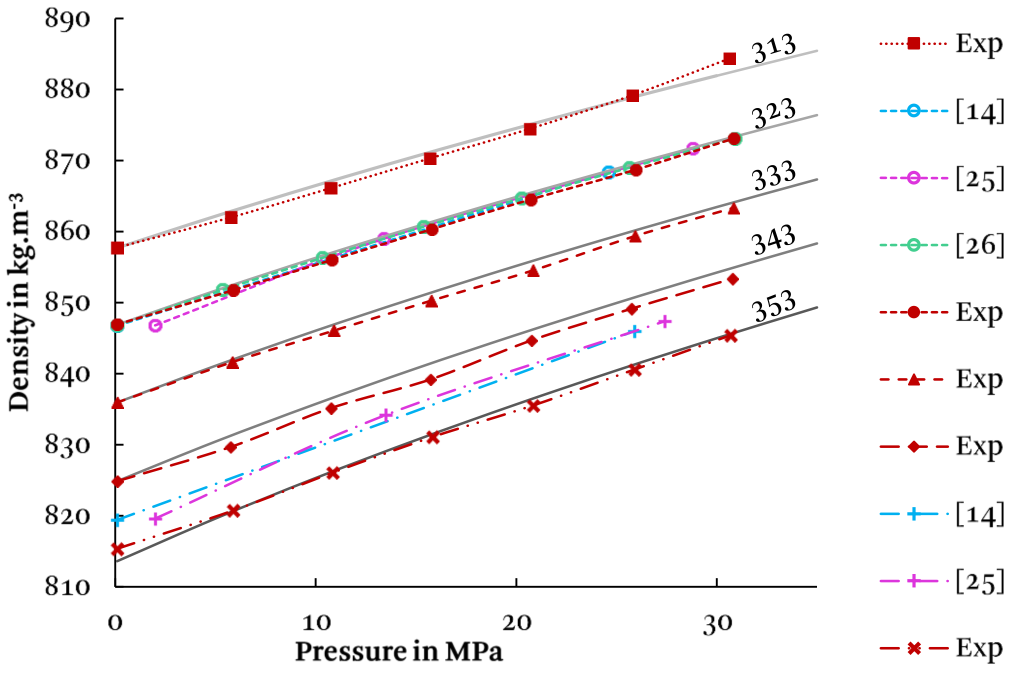

Figure 3-8: The density of benzene. Comparison with the literature by Dos Santos and Nieto De Castro [14] Kashiwagi et al. [25] and Assael et al. [26].

Temperatures are marked as: ■ 313.15 K; ● / ○ / ○ / ○ 323.15 K; ▲ 333.15 K; ◆ 343.15 K; ✚ / ✚ 348.15 K; ✖ 353.15 K. Model predictions at the experimental temperatures (Solid lines) were calculated using the model provided by Goodwin [29].

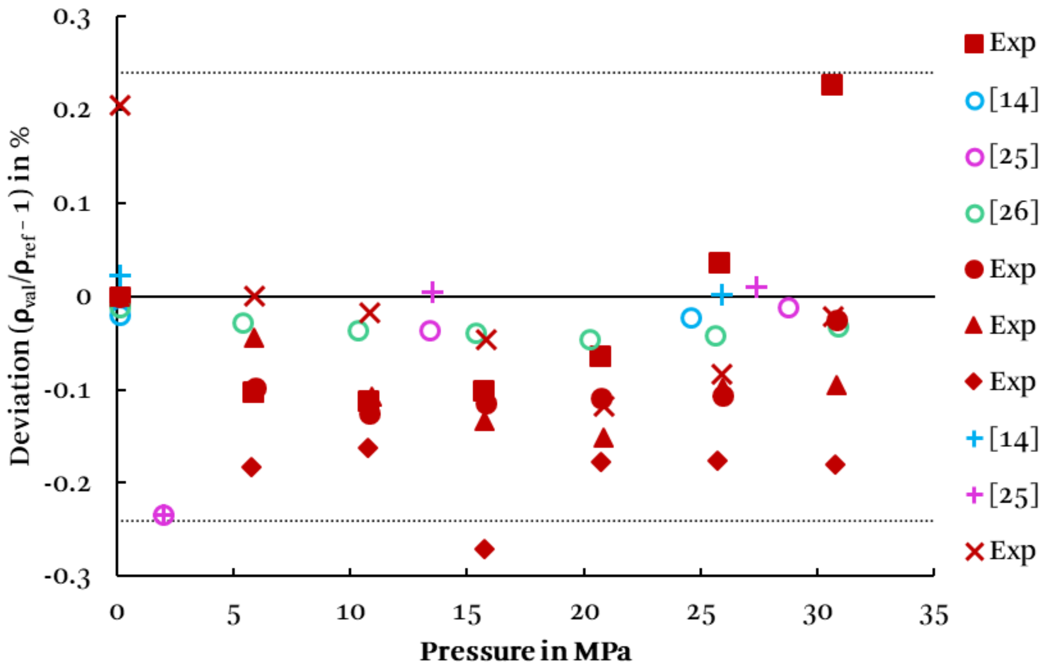

Figure 3-9: Deviations of the experimental density and literature [14, 25, 26] values from the predictive model (solid line) by Goodwin [29].

Dotted lines indicate the confidence interval of the model. Temperatures are marked as: ■ 313.15 K; ● / ○ / ○ / ○ 323.15 K; ▲ 333.15 K; ◆ 343.15 K; ✚ / ✚ 348.15 K; ✖ 353.15 K.

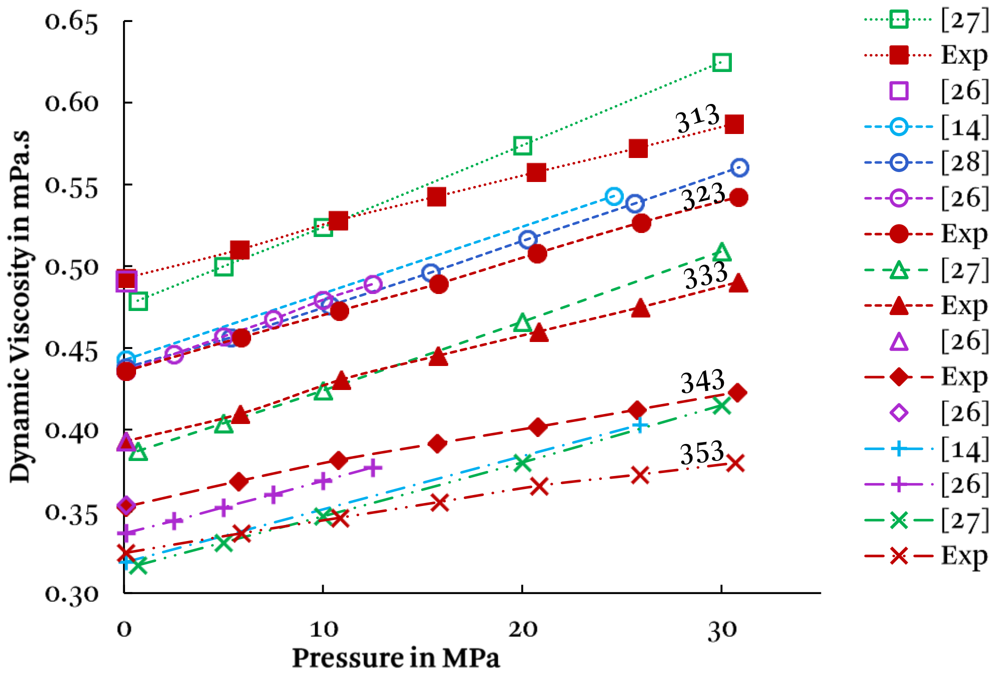

Figure 3-10: The dynamic viscosity of benzene. Comparison with the literature by Vieira Dos Santos and Nieto De Castro [14], Assael et al. [26], Mamedov et al. [27], and Hernández-Galván et al. [28]. Temperatures are marked as:■/□/□313.15 K;●/○/○/○ 323.15 K; ▲/△/△ 333.15 K; ◆/◇ 343.15 K; ✚/ ✚ 348.15 K; ✖/✖ 353.15 K.

3.3.3 CO_2 + Ethyl tetradecanoate

The measured phase equilibria results are seen in Figure 3-11. Phase transitions were determined visually. In a supporting capacity, the quartz crystal resonant frequency was monitored for any changes at the phase transition point. It was found that the resonance of the crystal drops with ~1.5 Hz for a dew point (indicating a higher net strain on the crystal), and increases with ~1 Hz at a bubble point (lower net strain). The electromechanical measurement of phase transition points using quartz piezoelectric sensors has been demonstrated in the literature [35, 36], providing a reliable, repeatable measurement that is not dependent on human interpretation. At some of the compositions, this point was found to be slightly higher (up to 0.15 MPa) than the visually observed point. The difference in result could potentially indicate the formation of a mist or microdroplets [8] that can sometimes be difficult to observe with the HD camera setup. At present, no definitive statement can be made as to which of the two methods are superior and further research in this regard is beyond the scope of the current work. All measured results presented here are determined visually to ensure consistency with literature, with the deviation in measurement between the electromechanical and visual methods indicated in Table 3-5

Experimental phase equilibria data follow the expected trends and agree well with the literature [31]. Some slight deviation with the data of Crampon et al. [31] is seen, however, other data published by Crampon for the CO_2 + ethyl octadecanote system shows similar deviation when compared to other sources [37, 38].

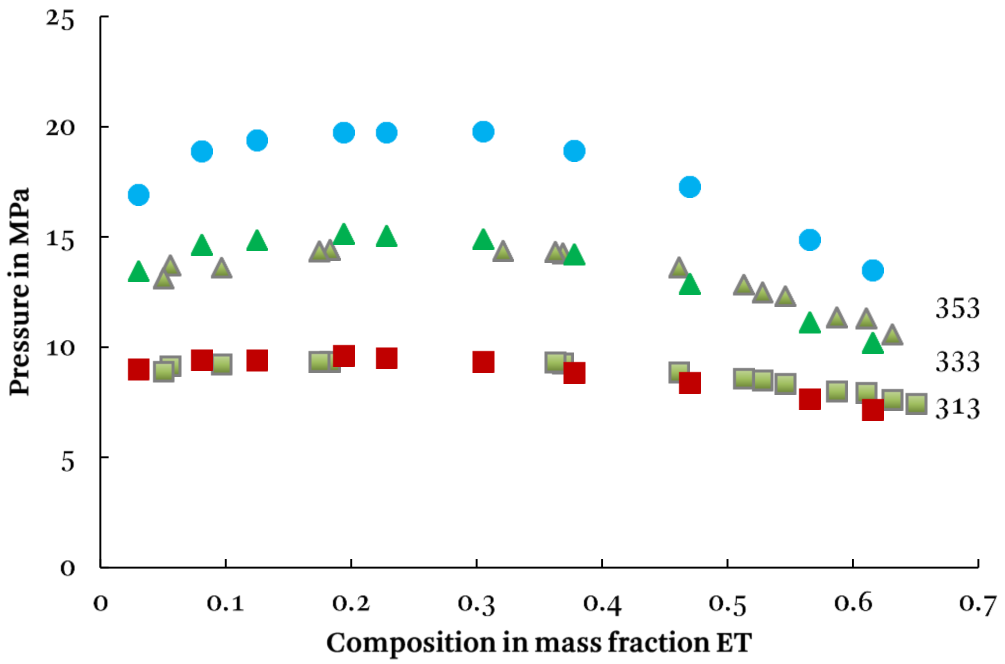

Figure 3-11: Phase equilibria data for the system CO_2 + ET. Comparison with the literature (grey markers) by Crampon et al. [31].
Temperatures are marked as: 🟥 / 🟩 313.15 K; ▲ / ▲ 333.15 K; ● 353.15 K.

The density of the system is dependent on the pressure, temperature and mixture composition. The density is plotted against the pressure, Figure 3-12, and composition, Figure 3-13. As there are no binary data available, the pure component densities are used to provide perspective of the deviations for the binary mixture density from that of the pure component properties under similar conditions. CO_2 data were generated using the CO_2 specific EOS by Span and Wagner [18], with ET data obtained from the literature [32].

In Figure 3-12, it is seen that the ET-rich equilibrium phases (filled markers – ET composition decreases from left to right) tend to have densities similar to that of pure ET, showing more significant deviation as more CO_2 is added, or as the temperature increases. In contrast, the CO_2-rich phase density (empty markers – ET composition decreases from top to bottom) is significantly affected by the dissolved ET. The CO_2-rich phase density changes significantly with composition, tending toward the pure ET density at higher ET concentrations, and the pure CO_2 density at low ET concentrations.

Figure 3-13 affirms the effect a change in composition has on the density. As expected, the density increases as the mixture fractions tend toward higher ET compositions. It is seen that the CO_2-rich phase density changes sharply with composition, with the ET-rich phase showing a much more gradual change.

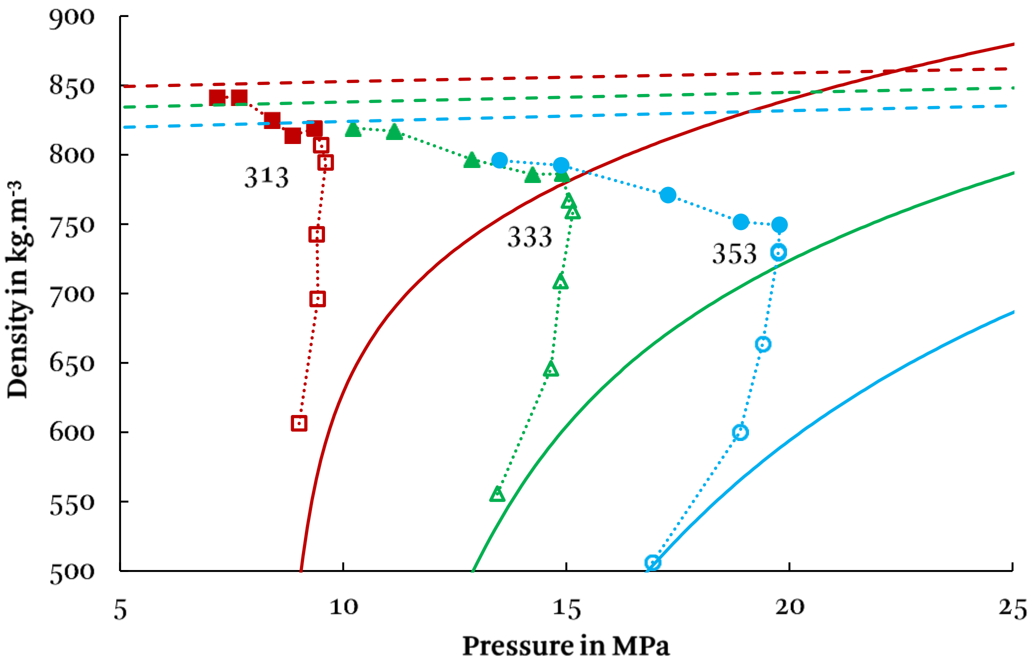

Figure 3-12: The density of system CO_2 + ET at saturation vs pressure.
Temperatures are marked as:■ 313.15 K; ▲ 333.15 K;● 353.15 K, filled markers indicate bubble-point phase transition, non-filled markers dew-point phase transition. Comparison with pure CO_2 density (Solid lines) predicted using the EOS of Span and Wagner [18] and ET data (Dashed lines) by Ndiaye et al. [32], both at the same experimental temperatures.

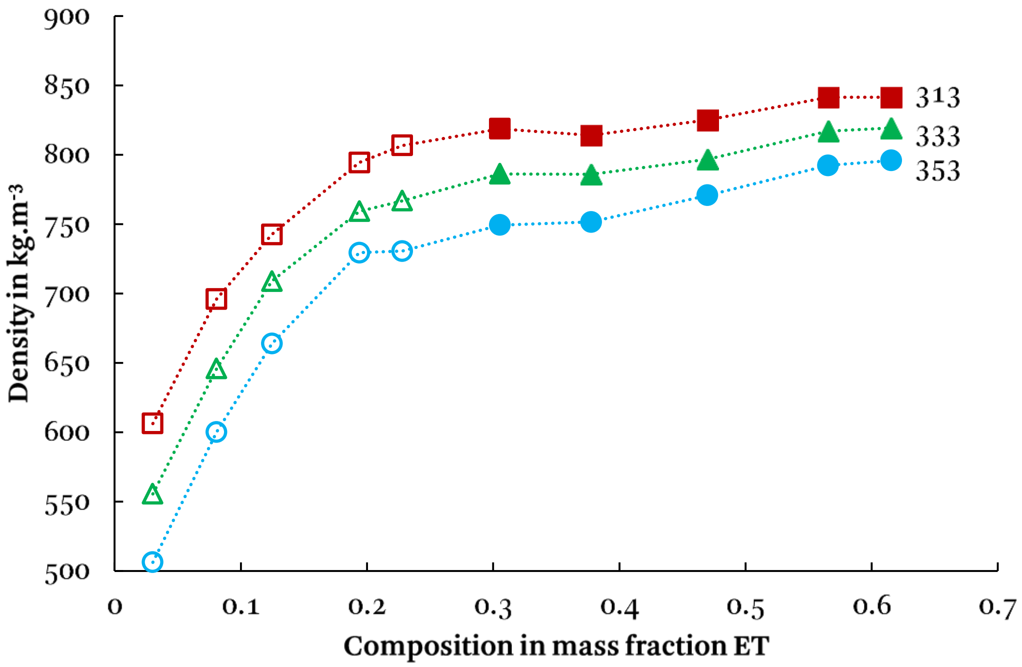

Figure 3-13: The density of system CO_2 + ET at saturation vs mass fraction ET.
Temperatures are marked as:■ 313.15 K; ▲ 333.15 K;● 353.15 K, filled markers indicate bubble-point phase transition, non-filled markers dew-point phase transition.

Like the density, the dynamic viscosity is dependent on pressure, temperature and mixture composition. The dynamic viscosity is plotted against the pressure, Figure 3-14, and composition, Figure 3-15. Pure component data were obtained from the literature [33, 34].

In Figure 3-14, the measured mixture dynamic viscosity is presented together with that of the pure components to provide perspective. The measured viscosity deviates with at least one order of magnitude from both the pure component values. This significant deviation shows that the inclusion of the second component into both the CO_2 and ET-rich phases has a significant effect on the properties of the bulk fluid. Further, the dynamic viscosity of the saturated phase becomes more pressure-dependent with an increase in temperature, as the phase saturation point itself becomes more temperature-dependent.

The results are plotted against the composition in Figure 3-15 to compare the change between the systems. As expected, the dynamic viscosity increases with an increase in ET concentration. At low ET concentrations (a CO_2-rich equilibrium phase), temperature and composition are seen to have relatively little effect. The small temperature dependence at low ET concentrations is affirmed by the pure CO_2 dynamic viscosity also showing a relatively small temperature dependence. On the contrary, high ET concentrations show a noticeable temperature dependence (also seen in the pure ET data in Figure 3-14), with higher temperatures causing lower dynamic viscosities. An increase in the ET concentration, predictably, leads to an increase in the dynamic viscosity.

It can be summarised that both phases, CO_2 and ET-rich, are affected by the absorption of the respective dissolved components. The CO_2-rich mixtures show a large density variability, but a relatively smaller viscosity deviation when compared to the pure component data. ET-rich mixtures show a smaller deviation regarding density from pure data, but a significant deviation regarding dynamic viscosity. These findings justify and strengthen the statement made in the introduction, namely that binary systems under supercritical conditions can have significant variation in fluid properties, necessitating the measurement of properties to encompass mass and transport properties adequately. This conclusion is in agreement with the recent findings of Avelino et al. [30] for the density and viscosity of a solute-rich phase poly(ethylene glycol) 200 saturated with supercritical CO_2.

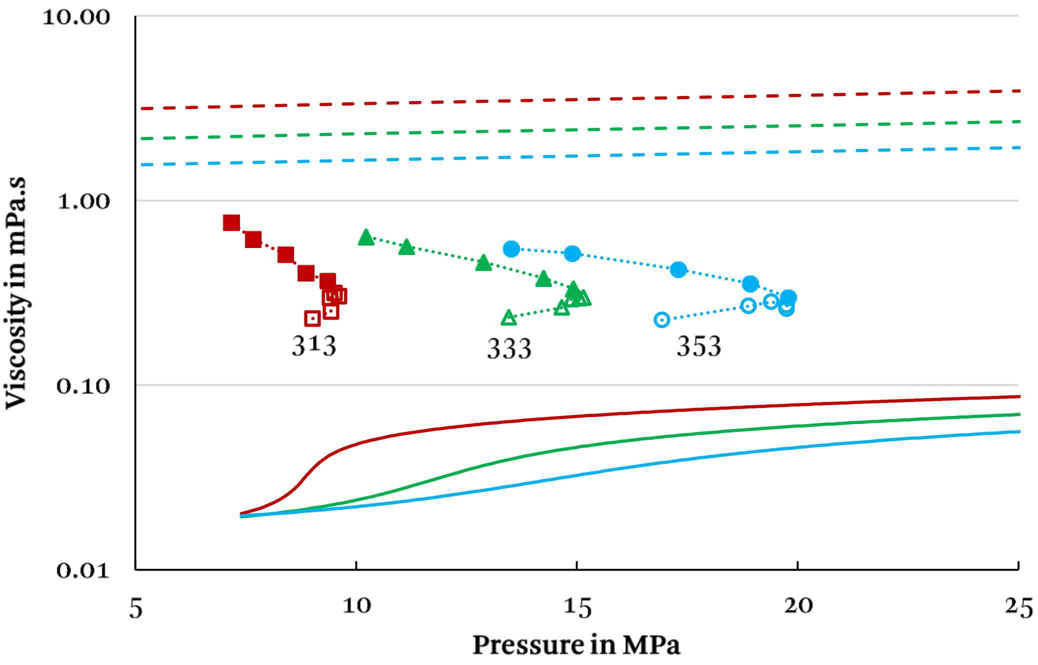

Figure 3-14: The dynamic viscosity of system CO_2 + ET at saturation vs pressure. Note the logarithmic scale.
Temperatures are marked as:■ 313.15 K; ▲ 333.15 K;● 353.15 K, filled markers indicate bubble-point phase transition, non-filled markers dew-point phase transition. Comparison with pure CO_2 dynamic viscosity (Solid lines) predicted using the model by Fenghour et al. [33] and ET data (Dashed lines) by Habrioux et al. [34]

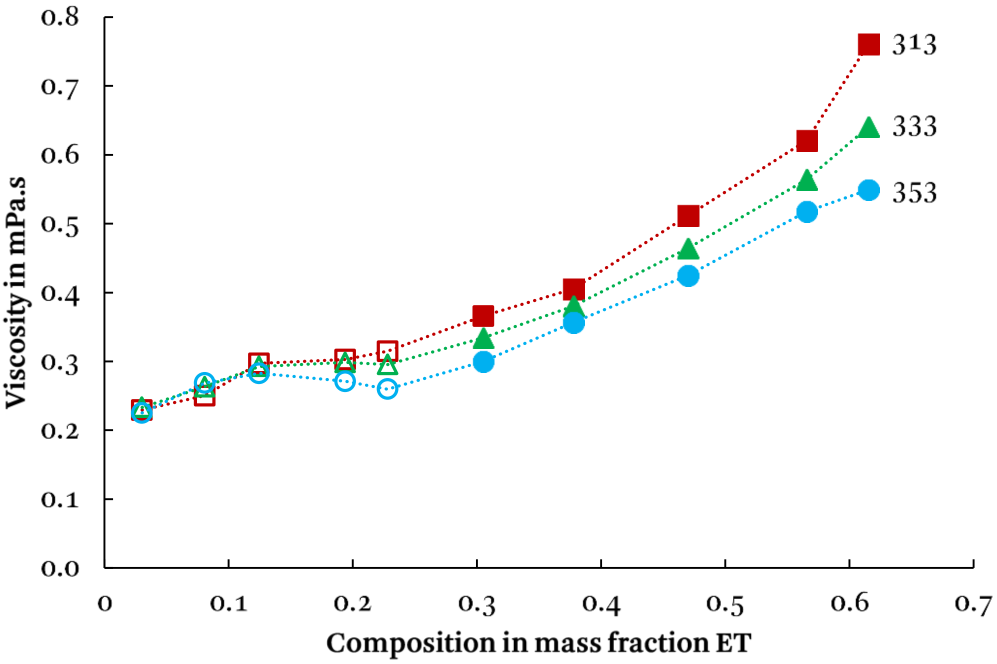

Figure 3-15: The dynamic viscosity of system CO_2 + ET at saturation vs mass fraction ET.
Temperatures are marked as:■ 313.15 K; ▲ 333.15 K;● 353.15 K, filled markers indicate bubble-point phase transition, non-filled markers dew-point phase transition.

3.4 Conclusions

An experimental setup was designed, constructed and commissioned, with the experimental methods and techniques verified against literature data. The equipment provides a novel solution to measuring concurrent phase equilibria, density and dynamic viscosity data in the supercritical regime. Firstly, the equipment was verified to measure accurate density and dynamic viscosity data, using the pure components n-dodecane and benzene. The n-dodecane system was found to agree closely with the literature, while the benzene experimental data were found to have disagreement with some literature data, explicated by inconsistencies and possible doubt in the literature. Secondly, the equipment was verified for the accurate measurement of phase equilibria by measuring phase transition data for the system CO_2 + ethyl tetradecanoate (ET) using a visual method (SynVisVar). Phase equilibria measurements were supplemented by electromechanical phase transition detection using the quartz oscillator, with further work required to determine which method is superior. Density and dynamic viscosity data were also measured for the CO_2 + ET binary system, demonstrating the significant deviation between the pure component and saturated fluid properties.

Acknowledgements

This work is based on the research supported in part by the National Research Foundation of South Africa (Grant specific unique reference number (UID) 88782). The authors acknowledge that opinions, findings and conclusions or recommendations expressed in any publication generated by the NRF supported research is that of the authors', and that the NRF sponsors accept no liability whatsoever in this regard.

Data Tables

Table 3-3: Experimental density and dynamic viscosity of n-dodecane.

Temperature (K)	Pressure (MPa)	Density (kg/m^3)	Viscosity (mPa.s)
313.2	0.10	734.6	1.055
313.2	5.82	738.5	1.125
313.2	10.80	742.8	1.204
313.2	15.88	746.3	1.279
313.2	20.83	749.3	1.350
313.2	25.75	752.9	1.429
313.2	31.06	756.2	1.510
323.2	0.10	727.2	0.910
323.2	5.80	730.4	0.979
323.2	10.93	734.8	1.044
323.2	15.84	738.8	1.112
323.2	20.99	743.2	1.175
323.2	25.95	747.2	1.222
323.2	30.98	751.5	1.276
333.2	0.10	719.9	0.802
333.2	5.90	723.8	0.857
333.2	10.89	727.6	0.909
333.2	15.88	732.1	0.966
333.2	20.79	736.3	1.021
333.2	25.74	740.2	1.065
333.2	30.71	744.3	1.127
343.2	0.10	712.5	0.704
343.2	5.90	716.3	0.758
343.2	10.84	721.1	0.803
343.2	15.74	725.5	0.850
343.2	21.09	730.1	0.903
343.2	25.94	733.7	0.948
343.2	30.86	737.6	0.998
353.2	0.10	705.0	0.624
353.2	5.84	709.4	0.673
353.2	10.73	714.5	0.720
353.2	15.84	719.7	0.763
353.2	20.93	724.0	0.808
353.2	25.93	728.3	0.840
353.2	30.64	732.3	0.883

$u(T) = 0.2$ K; $u(P) = 0.06$ MPa; $u_c(\rho) < 0.003 \cdot \rho$ kg/m^3; $u_c(\eta) \leq 0.01 \cdot \mu$ mPa.s

Table 3-4: Experimental density and dynamic viscosity of benzene.

Temperature (K)	Pressure (MPa)	Density (kg/m^3)	Viscosity (mPa.s)
313.2	0.10	857.7	0.493
313.2	5.79	862.0	0.510
313.2	10.74	866.1	0.528
313.2	15.69	870.3	0.543
313.2	20.68	874.5	0.558
313.2	25.79	879.2	0.572
313.2	30.63	884.4	0.587
323.1	0.10	846.9	0.436
323.1	5.89	851.8	0.456
323.1	10.81	856.0	0.473
323.2	15.79	860.3	0.489
323.2	20.73	864.5	0.508
323.2	25.96	868.7	0.527
323.2	30.85	873.1	0.542
333.2	0.10	835.9	0.393
333.1	5.84	841.6	0.410
333.1	10.91	846.1	0.431
333.2	15.76	850.3	0.445
333.2	20.83	854.5	0.460
333.1	25.93	859.4	0.475
333.1	30.83	863.3	0.490
343.2	0.10	824.8	0.353
343.2	5.75	829.7	0.369
343.2	10.76	835.1	0.381
343.1	15.72	839.2	0.392
343.1	20.76	844.7	0.402
343.1	25.75	849.1	0.412
343.1	30.78	853.4	0.423
353.1	0.11	815.3	0.325
353.1	5.91	820.7	0.337
353.2	10.85	826.0	0.346
353.2	15.85	831.1	0.356
353.2	20.85	835.5	0.366
353.2	25.90	840.6	0.373
353.2	30.69	845.4	0.380

$u(T) = 0.2$ K; $u(P) = 0.06$ MPa; $u_c(\rho) < 0.003\cdot\rho$ kg/m^3; $u_c(\eta) \leq 0.01\cdot\mu$ mPa.s

Table 3-5: Experimental saturation pressures for various binary mixtures of CO_2 + ET and the measured density and viscosity of the mixture at saturation. Values in brackets indicate the difference in phase transition measurement when using the electromechanical measurement compared to the optical measurement.

Temperature (K)	Mass fraction ET (g/g)	Pressure (MPa)	Density (kg/m^3)	Viscosity (mPa.s)
313.2	0.0302	8.98 (+0.04)	606.2	0.229
313.2	0.0807	9.40 (+0.04)	695.9	0.250
313.2	0.125	9.41 (+0.01)	742.5	0.297
313.2	0.194	9.59 (+0.02)	794.3	0.303
313.2	0.228	9.52 (+0.00)	806.7	0.315
313.2	0.305	9.39 (-0.02)	818.7	0.366
313.2	0.378	8.88 (-0.02)	814.0	0.405
313.2	0.470	8.44 (-0.04)	825.2	0.512
313.2	0.565	7.64 (+0.02)	841.4	0.621
313.2	0.616	7.17 (+0.00)	841.4	0.761
333.2	0.0302	13.38 (+0.08)	555.5	0.233
333.2	0.0807	14.61 (+0.05)	645.8	0.263
333.2	0.125	14.84 (+0.04)	708.9	0.293
333.2	0.194	15.12 (+0.03)	759.2	0.299
333.2	0.228	15.07 (-0.01)	766.9	0.296
333.2	0.305	14.93 (-0.02)	786.2	0.334
333.2	0.378	14.23 (+0.01)	786.0	0.380
333.2	0.470	12.85 (+0.03)	796.8	0.464
333.2	0.565	11.10 (+0.04)	817.0	0.564
333.2	0.616	10.22 (+0.02)	819.3	0.641
353.2	0.0302	16.80 (+0.13)	506.1	0.225
353.2	0.0807	18.74 (+0.15)	600.1	0.268
353.2	0.125	19.35 (+0.05)	663.8	0.283
353.2	0.194	19.72 (+0.03)	722.8	0.274
353.2	0.228	19.76 (-0.01)	730.6	0.260
353.2	0.305	19.76 (+0.02)	749.4	0.300
353.2	0.378	18.84 (+0.06)	751.5	0.356
353.2	0.470	17.27 (+0.02)	770.8	0.425
353.2	0.565	14.86 (+0.03)	792.3	0.518
353.4	0.616	13.45 (+0.06)	795.9	0.549

$u(T) = 0.2$ K; $u_c(x) < 0.0005$; $u(P) = 0.06$ MPa; $u_c(\rho) < 0.003 \cdot \rho$ kg/m^3; $u_c(\eta) \leq 0.01 \cdot \mu$ mPa.s

References

[1] Seader J.D. and Henley, E.J., *Separation Process Principles, 3rd Edition,* Wiley, Chichester, 2013, ISBN: 978-0-470-48183-7.

[2] Acheson, D. J., *Applied Hydrodynamics: An Introduction to Ideal and Real Fluid Flows*, CRC Press, Leiden, 2009, ISBN: 978-0-415-49271-3.

[3] Brunner, G., Gas Extraction: *An Introduction to Fundamentals of Supercritical Fluids and the Application to Separation Processes*, Steinkopff, Darmstadt, 1994, ISBN: 978-3-662-07382-7.

[4] Stockfleth, R. and Brunner, G*., Hydrodynamics of a Packed Countercurrent Column for the Gas Extraction*, Ind. Eng. Chem. Res., 38 (1999) 4000-4006.

[5] Dohrn, R.; Fonseca, J.M.S. and Peper, S., *Experimental Methods for Phase Equilibria at High Pressures*, Annu. Rev. Chem. Biomol. Eng., 3 (2012) 343, 2012.

[6] Schwarz, C.E. and Nieuwoudt, I., *Phase equilibrium of propane and alkanes: Part I. Experimental procedures, dotriacontane equilibrium and EOS modelling*, J. Supercrit. Fluids, 27 (2003) 133-144.

[7] Fourie, F.C.vN.; Schwarz, C.E. and Knoetze, J.H., *Phase equilibria of alcohols in supercritical fluids. Part I. The effect of the position of the hydroxyl group for linear C8 alcohols in supercritical carbon dioxide*, J. Supercrit. Fluids, 47 (2008) 161–167.

[8] Fourie, F.C.vN.; Schwarz, C.E. and Knoetze, J.H., *Analytic High-Pressure Phase Equilibria. Part II: Gas Chromatography and Sampling Method Develop*ment, Chem. Eng. Technol., 39 (2016) 1475-1483.

[9] Schaschke, C.J., *High pressure viscosity measurement with falling body type viscometers*, IRECHE, 2 (2010) 564-567.

[10] Tough, J.T.; McCormick, W.D. and Dash, J.G., *Viscosity of Liquid He II*, Phys. Rev., 132 (1963) 2373-2378.

[11] Collings, A.F. and McLaughlin, E., *Torsional Crystal Technique for the Measurement of Viscosities of Liquids at High Pressure*, Trans. Faraday Soc., 67 (1971) 340-352.

[12] Calderon, E.; Gauthier, M.; Decremps, F.; Hamel, G.; Syfosse, G. and Polian, A., *Complete determination of the elastic moduli of α-quartz under hydrostatic pressure up to 1 GPa: an ultrasonic study*, J. Phys. Condens. Matter, 19 (2007), 436228 (13pp).

[13] Webeler, R.W.H. and Hammer, D.C., *Damping of a torsional oscillator in liquid helium 4 and 3 from 0.4°Kto 2.5°K*, National Aeronautics and Space Administration, Washington, D.C., NASA technical note (1968) D-4381.

[14] Vieira Dos Santos, F.J. and Nieto De Castro, C.A., *Viscosity of Toluene and Benzene Under High Pressure*, Int. J. Thermophys., 18 (1997) 367-378.

[15] Mason, W.P., *Measurement of the Viscosity and Shear Elasticity of Liquids by Means of a Torsionally Vibrating Crystal*, Trans. ASME, 69 (1947) 359.

[16] Kimizuka, H.; Shigenobu, O.; Li, J. and Shibutani, Y., *Complete set of elastic constants of α-quartz at high pressure: A first-principles study*, Phys. Rev. B, 75 (2007) 054109 (6pp).

[17] Jackson, J.D., *Classical Electrodynamics, 3rd Edition*, Wiley, New York, 1999, ISBN: 978-0-471-30932-1.

[18] Span, R. and Wagner, W., *A New Equation of State for Carbon Dioxide Covering the Fluid Region from the Triple-Point Temperature to 1100 K at Pressures up to 800 MPa*, J. Phys. Chem. Ref. Data, 25 (1996) 1509-1596.

[19] Joint Committee for Guides in Metrology, *Evaluation of measurement data – Guide to the expression of uncertainty in measurement, JCGM 100:2008*, available at: http://www.iso.org/sites/JCGM/GUM/JCGM100/C045315e-html/C045315e.html, 2008 (accessed: 06 Nov 2017).

[20] Caudwell, D.r.; Trusler, J.P.M.; Vesovic, V. and Wakeham, W.A., *The Viscosity and Density of n-Dodecane and n-Octadecane at Pressures up to 200 MPa and Temperatures up to 473 K*, Int. J. Thermophys, 25 (2004) 1339-1352.

[21] Keramidi, A.S. and Rastorguev, Y.L., *Viskosität von Alkanen*, Izv. Vyssh. Uchebn. Zaved. Neft Gaz (1972) 61-66.

[22] Ducoulombier, D.; Zhou, H.; Boned, C.; Peyrelasse, J.; Saint-Guirons, H. and Xans, P., *Pressure (1-1000 bars) and Temperature (20-100 °C) Dependence of the Viscosity of Liquid Hydrocarbons*, J. Phys. Chem., 90 (1986) 1692-1700.

[23] Lemmon, E.W. and Huber, M.L., *Thermodynamic Properties of n-Dodecane*, Energy Fuels, 18 (2004) 960-967.

[24] Huber, M.L.; Laesecke, A. and Perkins, R., *Transport Properties of n-Dodecane*, Energy Fuels, 18 (2004) 968-975.

[25] Kashiwagi, H.; Fukunaga, H.; Tanaka, Y.; Kubota, H. and Makita, T., *Dielectric constant and density of (benzene + chlorobenzene) at high pressures*, J. Chem. Thermodyn., 15 (1983) 567-580.

[26] Assael, M.J.; Papadaki, M. and Wakeham, W.A., *Measurements of the Viscosity of Benzene, Toluene, and m-Xylene at Pressure up to 80 MPa*, Int. J. Thermophys., 12 (1991) 449-457.

[27] Mamedov, A.M.; Akhundov, T.S.; Ismail-Zade, S.M. and Tairov, A.D, *Viskosität von Benzen*, Izv. Vyssh. Uchebn. Zaved., Neft Gaz, 2 (1971) 74-76.

[28] Hernández-Galván, M.A.; García-Sánchez, F. and Macías-Salinas, R., *Liquid viscosities of benzene, n-tetradecane, and benzene + n-tetradecane from 313 to 393 K and pressures up to 60 MPa: Experiment and modelling*, Fluid Phase Equilib, 262 (2007) 51–60.

[29] Goodwin, R.D., *Benzene Thermophysical Properties from 279 to 900 K at Pressures to 1000 Bar*, J. Phys. Chem. Ref. Data, 17 (1988) 1541-1636.

[30] Avelino, H.M.N.T.; Fareleira, J.M.N.A.; Gourgouillon, D.; Igreja, J.M. and Nunes da Ponte, M., *Viscosity of poly(ethyleneglycol) 200 [PEG 200] saturated with carbon dioxide*, J. Supercrit. Fluids, 128 (2017) 300-307.

[31] Crampon, C.; Charbit, G. and Neau, E., *High-pressure apparatus for phase equilibria studies: solubility of fatty acid esters in supercritical* CO_2, J. Supercrit. Fluids, 16 (1999) 11-20.

[32] Ndiaye, E.I.; Habrioux, M.; Coutinho, J.A.P.; Paredes, M.L.L. and Daridon, J., *Speed of Sound, Density, and Derivative Properties of Ethyl Myristate, Methyl Myristate, and Methyl Palmitate under High Pressure*, J. Chem. Eng. Data, 58 (2013) 1371−1377.

[33] Fenghour, A.; Wakeham, W.A. and Vesovic, V., *The Viscosity of Carbon Dioxide*, J. Phys. Chem. Ref. Data, 27 (1998) 31-44.

[34] Habrioux, M.; Balize, J.; Galliero, G. and Darion, J., *Viscosities of Fatty Acid Methyl and Ethyl Esters under High Pressure: Methyl Myristate and Ethyl Myristate*, J. Chem. Eng. Data, 61 (2016) 398−403.

[35] Ke, J.; King, P.J.; George, M.W. and Poliakoff, M., *Method for Locating the Vapor-Liquid Critical Point of Multicomponent Fluid Mixtures Using a Shear Mode Piezoelectric Sensor*, Anal. Chem., 77 (2005) 85–92.

[36] Nie, J.; Liu, J. and Meng, X., *Dew point fast measurement in organic vapor mixtures using quartz resonant sensor*, Rev. Sci. Instrum., 88 (2017) 015005 (5pp).

[37] Brandalize, M.V.; Gaschi, P.S.; Mafra, M.R.; Ramos, L.P. and Corazza, M.L., *High-pressure phase equilibrium measurements and thermodynamic modeling for the systems involving* CO_2*, ethyl esters (oleate, stearate, palmitate) and acetone,* Chem. Eng. Res. Des., 92 (2014) 2814-2825.

[38] Barath, R.; Inomata, H.; Arai, K.; Shoji, K. and Noguchi, Y., *Vapor-liquid equilibria for binary mixtures of carbon dioxide and fatty acid ethyl esters*, Fluid Phase Equilib., 50 (1989) 315-327.

4. Publication 2

High-pressure Binary Phase Equilibria, Density and Dynamic Viscosity of 100 & 200 cSt Polydimethylsiloxane (PDMS) with Supercritical CO_2

H.H. Franken[a], J.H. Knoetze[a], C.E Schwarz[a, *]

[a] Department of Process Engineering, Stellenbosch University, Private Bag X1, Matieland, 7602, South Africa.

*Phone: +27 21 808 4487, Email: cschwarz@sun.ac.za

The Journal of Supercritical Fluids 139 (2018) 1–7
Received 29 January 2018; Revised 24 April 2018; Accepted 26 April 2018

DOI: 10.1016/j.supflu.2018.04.020

Declaration by the candidate

Concerning Chapter 4, the nature and scope of my contribution(s) were as follows:

Nature of contribution	Contribution (%)
I was responsible for conducting the experimental work and processing and interpreting the results. I was also the primary author of the article, responsible for compiling the document and the submission and review process.	80%

The following co-authors contributed to Chapter 4:

Name	E-mail address	Contribution Nature	Contribution (%)
Cara E Schwarz	cschwarz@sun.ac.za	Supervisor of student, HH Franken	10 %
Johannes H. Knoetze	jhk@sun.ac.za	Co-supervisor of student, HH Franken	10 %

Signature of candidate: Declaration with signature in possession of candidate and supervisor

Date : 20 January 2020

Declaration by co-authors

The undersigned hereby confirm that:

1. The declaration above accurately reflects the nature and extent of the contributions of the candidate and the co-authors to Chapter 4.

2. No other authors contributed to Chapter 4 besides those specified above.

3. Potential conflicts of interest have been revealed to all interested parties and that the necessary arrangements have been made to use the material in Chapter 4 of this dissertation.

Signature	Institutional affiliation	Date
Declaration with signature in possession of candidate and supervisor	Supervisor to the student, HH Franken at Stellenbosch University	20 January 2020
Declaration with signature in possession of candidate and supervisor	Co-Supervisor to the student, HH Franken at Stellenbosch University	20 January 2020

Preface

Experimental method detail (Safe Working Procedures), as well as an analysis and steps to eliminate or mitigate any risk (Task Risk Assessment), are presented in Appendix B. Safety information for all chemicals used can be found in Appendix C. Supporting and detailed method documentation for the equipment can be found in Appendix C, including all technical, safety and calibration data.

This paper addresses the second objective – A) Use the constructed equipment, presented in the previous chapter, to measure binary phase equilibria and property data with a supercritical fluid as one of the components. B) Use the measured data to identify experimental systems exhibiting low mutual solubility (reducing the effect of mass transfer), with fluid properties similar to that of industrially relevant processes. This requirement leads from the literature review, where the need for such data was highlighted and justified (Section 2.5).

Abstract

The phase equilibria and saturated fluid properties of CO_2 + PDMS (polydimethylsiloxane) systems were measured to investigate suitability for future hydrodynamic experiments. Two PDMS fluids graded at 100 cSt (Mw = 14 300, Mz = 22 000, ĐM = 1.59) and 200 cSt (Mw = 18 400, Mz = 53 000, ĐM = 4.72) were selected. Saturation pressure, and hence phase transition pressure, was determined for 1 – 70 wt% PDMS in CO_2 at 313 – 353 K using the variable volume view cell method (SynVisVar). The density and dynamic viscosity were measured at saturation using the quantified volume and mass, and the converse piezoelectric effect, respectively. In agreement with the literature, the phase equilibria showed complex phase behaviour. Additionally, fluid properties deviated significantly from that of the respective pure components. It was found that both systems exhibited low solubility in CO_2 (< 1 % above 20 MPa), with properties in the desired ranges (~900 – 800 kg.m^{-3} and ~0.7 – 7 mPa.s) for planned future hydrodynamic experiments.

Keywords: Supercritical CO_2, Piezoelectric Quartz, Polydimethylsiloxane (PDMS), Polymer, Silicone Oil, Viscometer

Highlights

- Complex phase behaviour and fluid property phenomena.
- Visual and electromechanical determination of phase transition points.
- New density and dynamic viscosity data for PDMS + CO_2.
- Large degree of polymer plasticization by the supercritical CO_2
- Large fluid property variability under supercritical conditions vs pure components.

4.1 Introduction

The need for comprehensive equipment sizing and design methods for fractionation- and extraction columns operating under supercritical conditions has become ever more pronounced. To develop these methods, a fundamental understanding of the mass transfer and transport phenomena in supercritical systems is required. Mass transfer is widely investigated in the literature, with phase equilibria providing insight into the operating pressure, temperature, and driving force for separation [1]. Additionally, several EOS (Equation of State) models capable of predicting phase equilibria under supercritical conditions exist in the literature [2]. However, data and models for physical properties and transport phenomena under supercritical conditions are decidedly scarcer.

Consequently, no comprehensive, predictive hydrodynamic models for columns operating under supercritical conditions exist. This deficiency forces the extensive piloting of any new applications and the significant overdesign of equipment to compensate for the lack of knowledge. To address this shortcoming, a thorough study of the fluid properties and hydrodynamics of these systems is required, allowing the creation of a knowledge base from where such models can be developed.

Two aspects are of particular concern when investigating hydrodynamics. Firstly, the fluid properties of the respective phases involved must be known. The fluid properties of density and viscosity are particularly important, as these properties are highly variable with changes in pressure and temperature under supercritical conditions [3]. This variability implies that small variations in pressure and/or temperature can significantly affect hydrodynamics. Further, this fluid property variability causes large deviations from model predictions using atmospheric fluid properties. Properties in the supercritical regime can also not easily be predicted under supercritical conditions using standard property models [4]. Secondly, mass- and heat transfer should be minimised or quantified when studying the hydrodynamics of a supercritical separation column. Minimising mass- and heat transfer allows one to isolate the hydrodynamic effects, providing a more communicable, fundamental representation of the system under investigation. Isolating the hydrodynamic effects proves a challenge in supercritical systems, with mutual solubility between the solvent and solute found to some extent in the majority of systems.

With the above discussion in mind, it is advantageous to select a supercritical fluid + fluid binary system with negligible mutual solubility for hydrodynamic studies. Adding this constraint eliminates some of the mass transfer concerns in a system, simplifying the eventual interpretation of results. Phase equilibria and fluid property data on systems presenting with no or negligible mutual solubility are decidedly scarce in the literature, with no suitable system presenting with a full complement of phase equilibria, and fluid property data in the appropriate ranges. To this end, equipment capable of concurrently measuring phase transitions, density, and dynamic viscosity of a loaded mixture was previously developed and verified [3].

This paper aims to make use of the equipment mentioned above to determine the suitability of two binary systems for future hydrodynamic study. Suitability is investigated by presenting a full set of phase equilibria, density and dynamic viscosity data. Firstly, these systems must exhibit relatively low to no mutual solubility, minimising the effect of other transport phenomena. Secondly, the systems should have fluid properties in ranges similar to that of typical industrially relevant systems where supercritical extraction / fractionation is used.

When selecting an appropriate system, several factors should be included in addition to the aforementioned low mutual solubility and appropriate fluid properties. Ideally, the component(s) should be low-cost, non-toxic and easy to handle, while exhibiting fluid properties close to that expected in a typical industrial system. To narrow down the options, CO_2 was selected as the supercritical solvent of choice. CO_2 is inexpensive, safe, and environmentally friendly and does not react with process components. Indeed CO_2 is seen as the most popular supercritical solvent [5] and is widely used in industry. CO_2 is also a poor solvent for some components, requiring very high pressures for total solubility, making it a good option for finding a system that limits mutual solubility, which in turn makes it a good option for hydrodynamic investigations.

The selection of a solute phase was also guided by the criteria of low mutual solubility, followed by cost, toxicity and handling ease. Non-volatile, apolar molecules were identified as viable compounds with straight-chained, unbranched polymers, being particularly promising [6]. Unbranched polymers are typically large, apolar molecules that exhibit very low volatility, potentially having very little to no solubility in the supercritical phase. Only limited knowledge of the density, viscosity, and phase equilibria of polymers with supercritical fluids is available in the literature [7]. There is, however, sufficient information available to guide the selection of a system for future hydrodynamic work, while leaving enough room to contribute to the knowledge base of the field.

Research has been done on the properties of low weight fractions of Polydimethylsiloxane (PDMS) in CO_2 [8 - 10], including density, and limited viscosity data [8, 11]. Available data in the literature [8, 9, 11, 12] indicates that the properties of the PDMS + CO_2 systems can, with some careful selection, fall in the desired ranges, while exhibiting a sufficiently small degree of mutual solubility at lower pressures. The literature data only covers low PDMS mixture fractions at unsaturated conditions, allowing for the contribution of a broader range of compositions at saturated conditions. For this study, two low molecular weight PDMS polymers, graded at 100 cSt and 200 cSt, were selected, henceforth referred to as PDMS 100 and PDMS 200. These relatively low viscosity, low molecular weight fluids were selected to achieve fluid properties (density & dynamic viscosity) in the desired ranges.

Beyond the planned use of the systems for future hydrodynamic study, the CO_2 + PDMS systems presented here are also of particular interest to carbon capture[1] [13] and pharmaceutical research [14], as well as providing insight to polymer processing and plasticization [7, 15], and oil recovery [16] through supercritical fluids.

This paper proceeds to present phase transitions, density and dynamic viscosity data on the two selected systems, CO_2 + PDMS 100 and CO_2 + PDMS 200. Saturation pressures are determined for compositions between 0.1 – 70 wt% PDMS at temperatures from 313,15 K to 353,15 K, with the fluid properties of density and dynamic viscosity determined for both the solute- and solvent-rich phases.

4.2 Materials and Methods

4.2.1 Experimental Equipment and Procedure

A previously verified high-pressure cell [3], operating up to 35 MPa and 393 K, was used in this study. The cell concurrently measures the phase equilibria, density, and dynamic viscosity of a loaded binary mixture. Each of these aspects and the equipment uncertainty are discussed in brief below, with interested readers referred to Franken et al. [3] for a detailed discussion.[2]

4.2.1.1. Phase Equilibria

Phase equilibria were investigated through the determination of phase transition points using a synthetic-visual (SynVisVar) method. A detailed experimental procedure with regards to phase equilibria determination has been published previously [17, 18], with only a summary presented here: A quantified mass of the liquid component was loaded into the cell. The cell was then closed, the piston seal tightened, and all air removed using a vacuum pump and multiple flushes with CO_2. A quantified mass of CO_2 was then transferred into the cell. The cell was then heated to the desired experimental temperature, pressurised, and allowed sufficient time to reach thermal equilibrium (approx. 1 h). Next, the cell was slowly, isothermally depressurised and the contents continually monitored for phase transitions using a sight glass and an HD camera setup. Once a transition was observed and recorded, the cell was repressurized, and the process repeated until the phase transitions were repeatedly observed

---

[1] Carbon capture refers to the capture of CO^2

[2] Detailed experimental procedures can be found in Appendix B

to within 0.02 MPa. After measurements were completed at a set temperature, the temperature was changed to a new value. After sufficient time passed to ensure thermal equilibrium, the measurement method was repeated until all desired temperatures were measured. In addition to the visual method, the phase transition was confirmed by monitoring for a distinct change in the resonance frequency of a cylindrical quartz crystal, used for the dynamic viscosity measurements. A decrease or increase in the frequency correlated with the appearance of a fluid with a respective higher or lower dynamic viscosity/density.

4.2.1.2. Density

The density was determined through quantification of the mass loaded into and volume of the cell during an experiment. The mass of the synthetic mixture loaded into the cell was weighed to within 0.0001 g for liquids and to within 0.001 g for the gas. The cell working volume (~22.3 – 53.4 cm^3) was measured using a digital height gauge as LVDT (linear variable differential transformer). The LVDT is directly connected to the one-piece cell piston, ensuring the accurate measurement of the volume. To calibrate the volume, a known mass of pure CO_2 was loaded into the cell, after which the cell was heated and pressurised. The piston position was then varied isothermally, and the resultant pressure noted. The temperature and measured pressure were then used to predict the phase density, using the CO_2 specific EOS of Span and Wagner [19]. Finally, the volume was calculated using the loaded mass and correlated to the specific piston position. This procedure was performed for the whole range of the piston, yielding a correlation between piston position and volume.

The density reported in this work was noted just before the appearance of a phase transition. The volume was calibrated after each experimental set using a known mass of pure CO_2 to ensure accuracy.

4.2.1.3. Dynamic Viscosity

The dynamic viscosity was determined with the quartz crystal cylinder, using a technique pioneered by Mason [20]. The crystal was excited using an AC signal of known frequency, applied to four gold electrodes running the length of the crystal. The cut of the quartz crystal and location of the electrodes causes the crystal to vibrate in a torsional mode at the same frequency, generating transverse waves (ultrasonic) that propagate into the surrounding fluid. These waves are damped by the fluid, affecting the electrical response of the crystal as per the converse piezoelectric effect.

The degree of damping is directly related to the dynamic viscosity/density product of the fluid, and is expressed as:

$$f_o - f_{res} = k \cdot (\pi \cdot f_{res} \cdot \eta \cdot \rho_f) \qquad \{4\text{-}1\}$$

where f_o (Hz) is the resonance of the crystal in a vacuum, f_{res} (Hz) is the resonance of the crystal under load, η (Pa.s) is the dynamic viscosity, ρ_f (kg/m^3) the fluid density and k (m^2/kg) a determined electromechanical constant [21]. f_o and k for each temperature were determined in the previous validation paper [3].

The applied frequency was stepped through the expected range to determine the resonant frequency of the crystal, while the voltage drop over the crystal and electrical phase shift was recorded. The resonant frequency was identified at a minimum in the voltage loss and zero phase shift, using the recorded data and visual confirmation on an oscilloscope. This measurement was repeated at least three times to ensure repeatability. From the resonant frequency and density, the dynamic viscosity can then be calculated using Eq. 1.

Several different voltages (ranging from 1V to 5V) were applied to the quartz crystal at each experimental composition to verify if the tested fluids were exhibiting Newtonian behaviour. The change in potential difference over the crystal causes a corresponding change in the vibration amplitude, which in turn produces a different shear rate. No variation in the measured dynamic viscosities beyond the reported accuracy was noted, validating the assumption of Newtonian behaviour.

4.2.1.4. Uncertainty

The uncertainties on the reported values are the same as reported in the equipment verification article [3]. Uncertainties are primarily Type B standard uncertainties as defined by the Guide to the expression of uncertainty in measurement [22] unless stated otherwise. A summary of uncertainties can be seen in Table 4-1.

Table 4-1: Reported accuracies.

Parameter	Uncertainty type	Propagated Error		Equation form
Pressure	Combined standard	0.06	MPa	$u(P) = 0.06$ MPa
Temperature	Standard	0.2	K	$u(T) = 0.2$ K
Mass - liquid	Standard	0.0001	g	$u(M_L) = 0.0001$ g
Mass - gas	Standard	0.001	g	$u(M_G) = 0.001$ g
Mass Fraction	Combined standard	< 0.0005	-	$u(x) < 0.0005$
Volume	Combined standard	< 0.25 %	ml	$u(v) = 0.0025 \cdot v$ ml
Density	Combined standard	< 0.3 %	kg/m^3	$u(\rho) < 0.003 \cdot \rho$ kg/m^3
Dynamic Viscosity	Combined standard	≤ 1 %	mPa.s	$u(\eta) \leq 0.01 \cdot \eta$ mPa.s

4.2.2 Materials Used

Details on the chemicals used are shown in Table 4-2. The PDMS used in this study were methyl group capped and effectively linear, with few side chains. Chemicals were used without further treatment or purification.

Table 4-2: Chemicals used in this study.

Chemical	Purity	Supplier	CAS Number
CO_2	99.9999%	Air Products	124-38-9
PDMS 100	Absolute	Xiameter PMX-200 (DOW Corning)	63148-62-9
PDMS 200	Absolute	Xiameter PMX-200 (DOW Corning)	63148-62-9

The dynamic viscosity of the purchased PDMS was measured under atmospheric conditions at the experimental temperatures, using an Anton-Paar MCR501 Rheometer. The measured values are reported in Table 4-3, later used as a comparison for the mixture values. The polymers were also tested for water content using Karl Fischer titration, reporting a water content smaller than the accuracy of the titration (0.1%).

Table 4-3: Experimental PDMS dynamic viscosity at atmospheric conditions.

	Temperature (K)	Dynamic Viscosity (mPa.s)
PDMS 100	313.15	79.4
	333.15	56.2
	353.15	41.2
PDMS 200	313.15	151.9
	333.15	108.8
	353.15	80.3

The molar weight averages and dispersity of both polymers were determined using size exclusion chromatography (SEC). The SEC system consists of a Waters 1515 isocratic pump, a Waters 717plus auto-sampler, Waters 600E system controller (run by Breeze Version 3.30 SPA) and a Waters in-line degasser AF. A Waters 410 differential refractometer is connected in series with a Waters 2487 dual-wavelength absorbance UV detector. Tetrahydrofuran [THF, HPLC grade, stabilised with 0.125% butylated hydroxytoluene (BHT)] is used as mobile phase, introduced at a flow rate of 1ml/min under the operating temperature of 30°C and an injection volume of 100 µl. Two PLgel (Polymer Laboratories) 5µm Mixed-C (300x7.5 mm) columns and a pre-column (PLgel 5 µm Guard, 50 x 7.5 mm) are used. Calibration is done using narrow polystyrene standards ranging from 580 to $2x10^6$ g/mol (Agilent Technologies), and all molecular weights were reported as polystyrene equivalents. Results of the SEC analysis are reported in Table 4-4. Both polymers presented with a single distribution peak, indicating that the polymer is unblended and favourable for use in phase equilibria experiments.

Table 4-4: Experimental PDMS molar weight averages and dispersity.

Chemical	Molecular Weight:			Dispersity - $Đ_M$
	Number Avg. - M_n (g/mol)	Weight Avg. - M_w (g/mol)	Higher Avg. - M_z (g/mol)	
PDMS 100	9 000	14 300	22 000	1.59
PDMS 200	3 900	18 400	53 000	4.72

4.3 Results and Discussion

The phase equilibria, density, and dynamic viscosity results are summarised in Table 4-5 and Table 4-6, found at the end of the chapter, with each system discussed individually below.

4.3.1 Phase Equilibria

The visual and electromechanical determinations correlated well, with the quartz crystal typically giving slightly higher values (on average 0.04 MPa and maximum 0.13 MPa) at some difficult to determine visual points at low PDMS concentrations. The discrepancy could potentially indicate the formation of a mist or microdroplets [23] that can sometimes be difficult to observe with the HD camera setup. In keeping with previous work, all results presented here are determined visually to ensure consistency.

The measured phase equilibria results for the two systems are seen in Figure 4-1 and Figure 4-2. Experimental phase equilibria data follow expected trends [13], with higher pressures required to achieve complete solution at higher temperatures. The individual curves for both PDMS 100 and PDMS 200 lean sharply to the left, indicating a low solubility of PDMS into the supercritical CO_2 phase. PDMS 200 is less soluble than PDMS 100, most probably due to the effect of the longer average polymer chain length, on solubility. Supercritical CO_2 is considerably more soluble into the PDMS phase, with 50 wt% of CO_2 soluble at ~12 MPa and 313 K for both fluids. The polymer chain length has only a small effect on the amount of CO_2 soluble into the liquid phase (on a mass basis) for the components investigated, with the PDMS 200 showing a slight increase in pressure required for solubility when compared to PDMS 100. The effect of the longer chain length on solubility can be explained by the decrease in polymer free volume with an increase in chain length [24].

A noticeable ‘bump’ in the solubility pressures can be seen at very low fractions of PDMS in both figures, being more noticeable in the PDMS 200 than in the PDMS 100. Indeed, this ‘bump’ is a potential indicator of complex phase behaviour occurring. Complex phase behaviour is not unusual in binary mixtures exhibiting a large degree of molecular asymmetry. Indeed, many polymer-supercritical solvent systems, and in particular CO_2 + PDMS [8, 9], have been shown to present type III phase behaviour [25], as classified by Konynenburg and Scott [26]. In particular, Bayraktar and Kiran [9] have shown that CO_2 + PDMS exhibits both a lower critical solution temperature (LCST) and upper critical solution temperature (UCST).

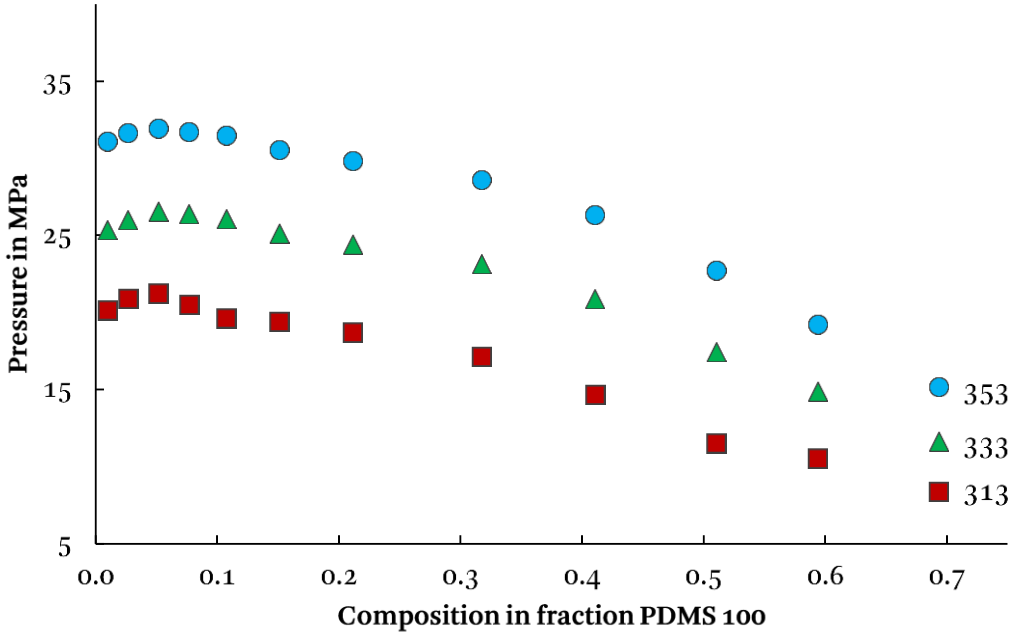

Figure 4-1- Phase equilibria data for the system CO_2 + PDMS 100. [9]
Temperatures are marked as: 🟥 **313.15 K;** ▲ **333.15 K;** ● **353.15 K.**

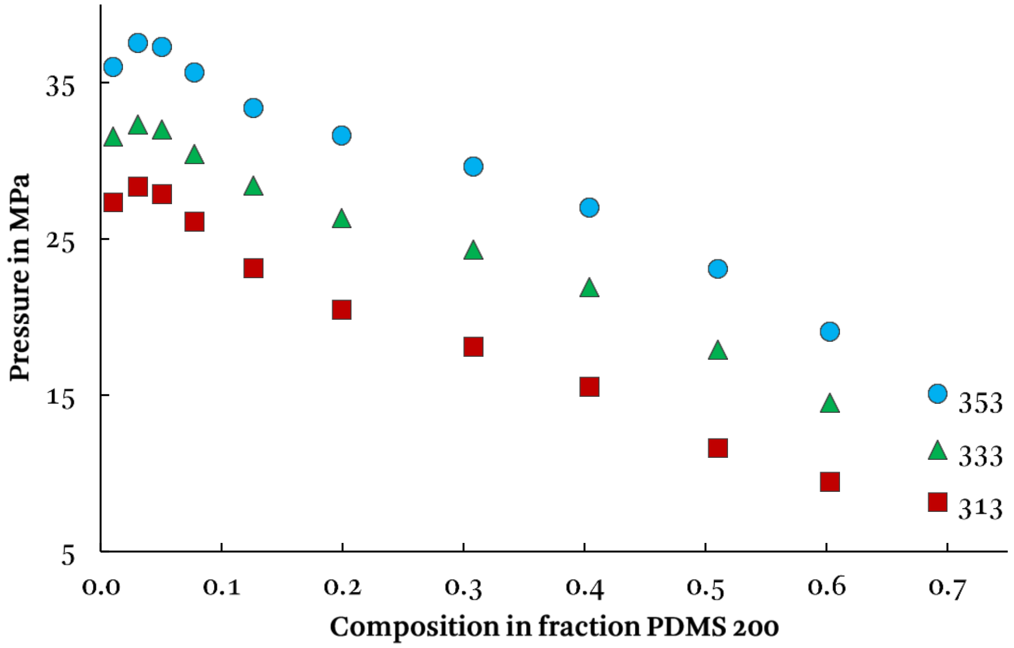

Figure 4-2- Phase equilibria data for the system CO_2 + PDMS 200. [9]
Temperatures are marked as: 🟥 **313.15 K;** ▲ **333.15 K;** ● **353.15 K**

---

[9] X-axis fractions refer to mass fraction

It can further be seen that the 'bump' is much more significant for the PDMS 200 system. It was noted during SEC analysis that the PDMS 200 presented with a much longer high molecular weight tail, as indicated by a large Mz (higher-average-molecular-weight) value. Xiong and Kiran [8] have shown that the phase equilibria of low fractions of PDMS in CO_2 (1 – 5 wt%) are sensitive to PDMS mixtures with high molecular weight tails. In particular, Xiong and Kiran showed that presence of a small amount of longer chains in the mixture significantly increases the dissolution pressures of the PDMS. In agreement with this, the measured PDMS 200 shows higher dissolution pressures at these low concentrations, even though its Mw (weight average molecular mass) value is very similar to that of the PDMS 100.

4.3.2 Density

The determined densities are plotted against pressure, Figure 4-3, Figure 4-4 and Figure 4-5, and composition (wt% PDMS), Figure 4-6 and Figure 4-7. Pure component data are generated to serve as a frame of reference using the CO_2 specific EOS by Span and Wagner [19] and a Tait type prediction for PDMS 100 by Fakhreddine and Zoller [27][10].

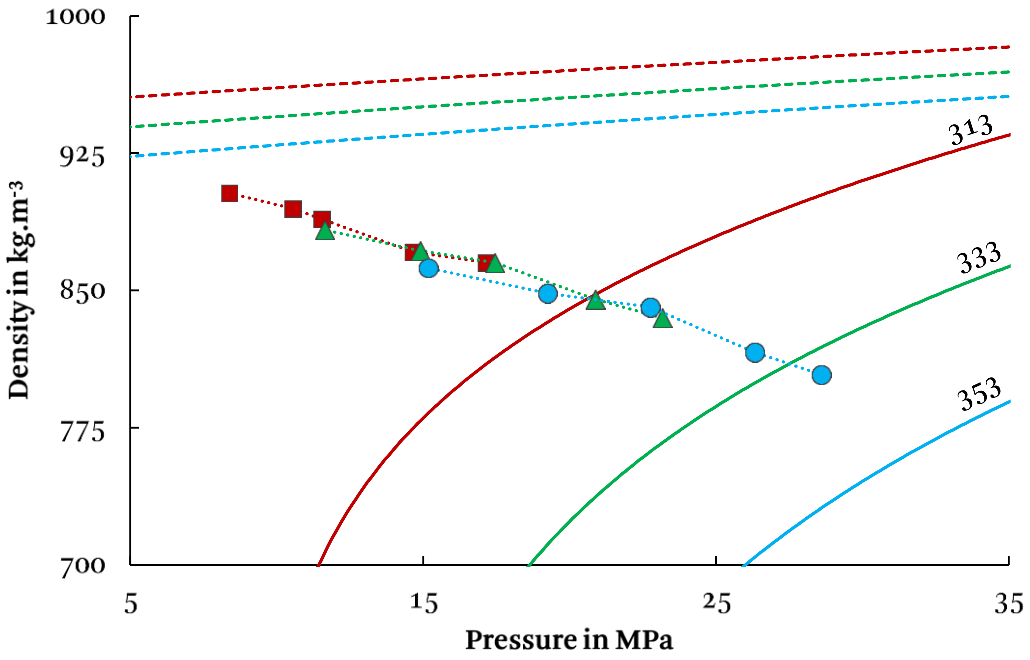

Figure 4-3- The density of system CO_2 + PDMS 100 at saturation vs pressure for the liquid-rich phase. Temperatures are marked as: ■ 313.15 K; ▲ 333.15 K; ● 353.15 K. Pure CO_2 density (solid lines), predicted using the EOS of Span and Wagner [19] and pure PDMS 100 density (dotted lines) predicted using the predictions of Fakhreddine and Zoller[27].

---

[10] As density changes linearly with an increase in pressure, knowledge of the density at ambient (supplier provided) and published PDMS density under pressure, used with an appropriate model, presents a sensible comparison.

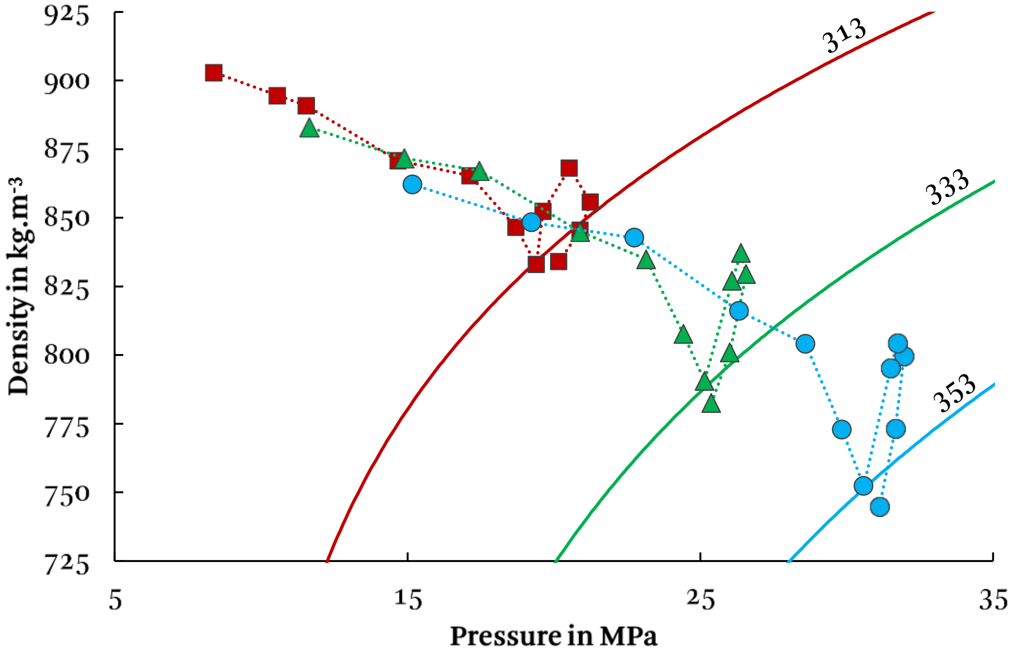

Figure 4-4: The density of system CO_2 + PDMS 100 at saturation vs pressure.
Temperatures are marked as: 🟥 313.15 K; ▲ 333.15 K; ● 353.15 K. Pure CO_2 density (Solid lines), predicted using the EOS of Span et al. [19].

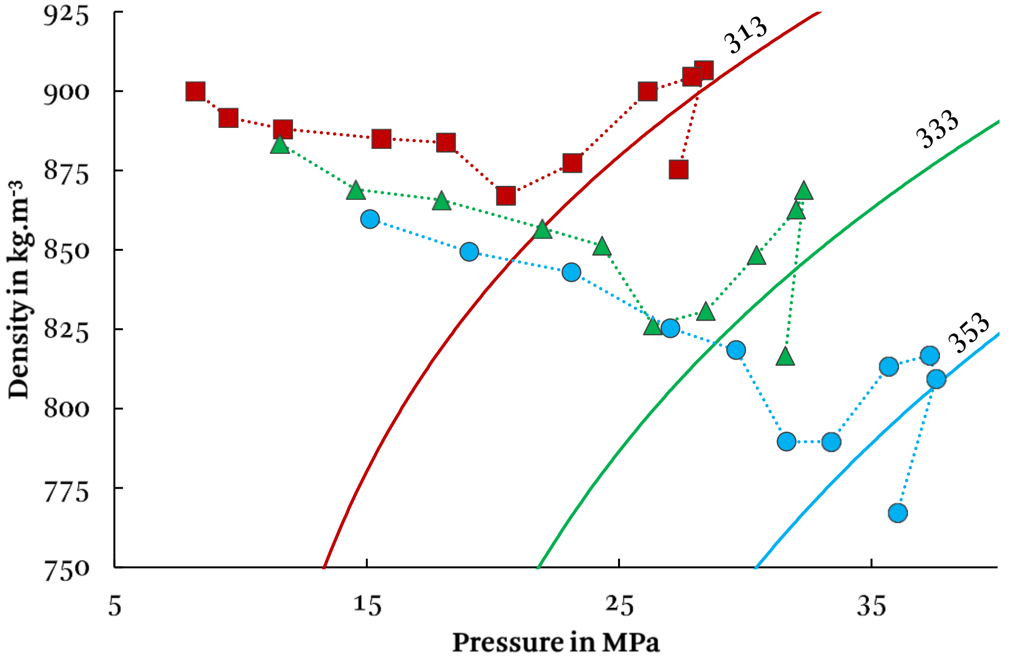

Figure 4-5- The density of system CO_2 + PDMS 200 at saturation vs pressure.
Temperatures are marked as: 🟥 313.15 K; ▲ 333.15 K; ● 353.15 K. Pure CO_2 density (Solid lines), predicted using the EOS of Span et al. [19].

Figure 4-3 presents a comparison of the pure component properties with the saturated liquid-rich data for PDMS 100. It can be seen that the polymer is plasticised by the inclusion of CO_2, with measured densities markedly lower than predicted pure-fluid densities. It is noteworthy that the density of the saturated, liquid-rich phases form a linear downward trend with an increase in pressure, and subsequently an increase in CO_2, despite different experimental temperatures. This trend is especially true for PDMS 100, with the solute-rich points of all three temperatures aligned. The same trend is visible for PDMS 200 for individual temperatures (see Figure 4-5), but with the trend shifting vertically up or down with a decrease or increase in temperature.

Figure 4-4 and Figure 4-5 present the saturated phase densities concerning pressure. As expected, an increase in CO_2 decreases the density. This downward trend continues for the liquid-rich compositions until the density reaches that of pure CO_2 at the same temperature and pressure. In contrast to the linear trend in the liquid-rich phase densities, the now gas-rich, low PDMS fractions exhibit a sharp increase and subsequent decrease in density. This density behaviour is a further indication of complex phase behaviour, with a sudden change in density, suggesting a change in the underlying phase behaviour. It can be seen that the effect is much more significant in the PDMS 200 system, suggesting that polymer chain length, and hence polymer free volume, play a role.

To better visualise the influence of changing phase behaviour on the density, see Figure 4-6 and Figure 4-7. A gradual decrease in density can be noted as the PDMS concentration decreases (from right to left). This trend is suddenly interrupted by an increase and subsequent decrease or 'bump' in density at low concentrations. This phenomenon corresponds directly to the 'bump' discussed in the phase equilibria data, caused by complex phase behaviour. Again it can be seen that the effect is more significant in PDMS 200 than for PDMS 100.

Measured densities fall in the range of ~900 - 800 $kg.m^{-3}$. This range corresponds to lighter organics such as oils and aromatics typically extracted with supercritical fluids, falling in an acceptable range for hydrodynamic investigation.

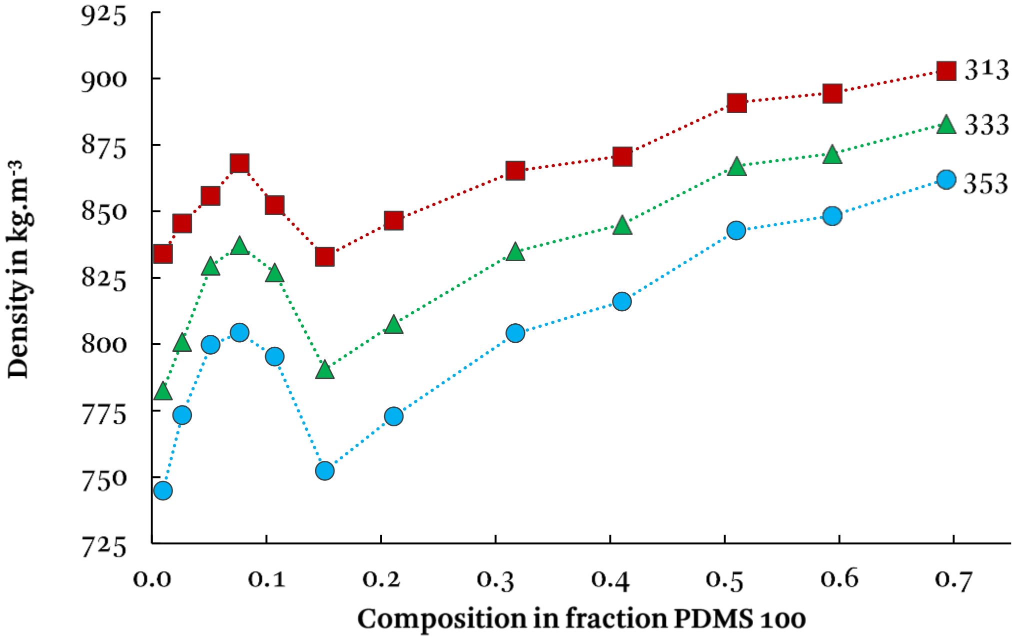

Figure 4-6- The density of system CO_2 + PDMS 100 at saturation vs mass fraction PDMS 100. Temperatures are marked as: ■ 313.15 K; ▲ 333.15 K; ● 353.15 K.

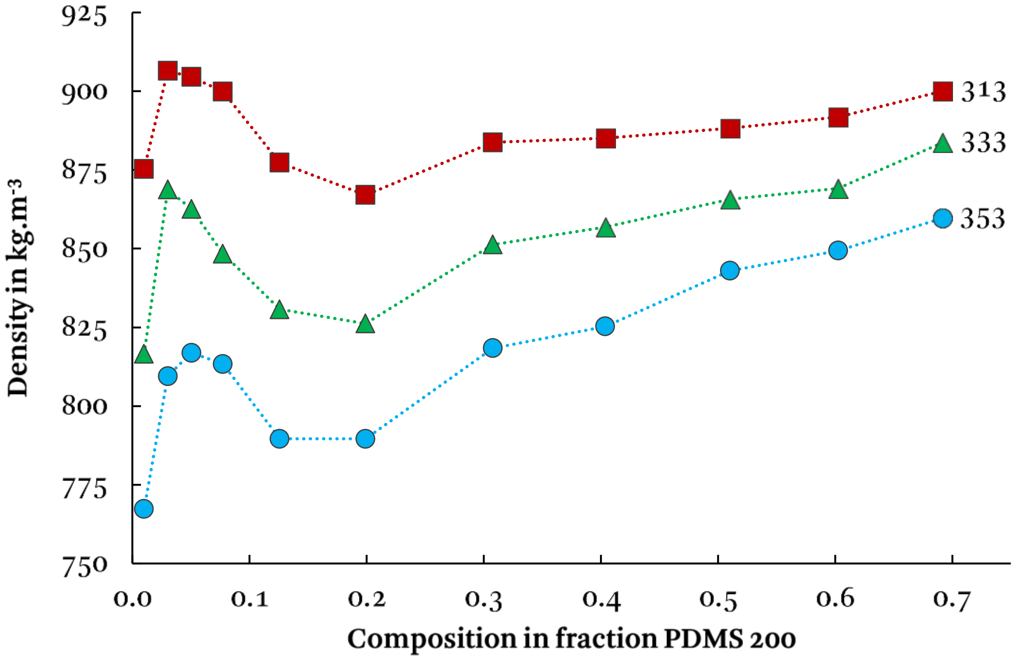

Figure 4-7- The density of system CO_2 + PDMS 200 at saturation vs mass fraction PDMS 200. Temperatures are marked as: ■ 313.15 K; ▲ 333.15 K; ● 353.15 K.

4.3.3 Dynamic Viscosity

The dynamic viscosity is plotted against the pressure, Figure 4-8 and Figure 4-9, and composition, Figure 4-10 and Figure 4-11. Pure CO_2 data are predicted using the CO_2 specific model by Fenghour et al. [28] and were used to provide perspective and serve as a frame of reference. Pure PDMS data were measured under atmospheric conditions, at the same experimental temperatures, to serve as a reference (Table 4-3).

From Figure 4-8 and Figure 4-9, it can be seen that the measured dynamic viscosities are significantly closer to that of pure CO_2 than pure PDMS reported in Table 4-3. This statement is made keeping in mind that the pure PDMS dynamic viscosity would not vary significantly with pressure [29]. This significant decrease in dynamic viscosity is further evidence of the large degree of plasticization caused by the inclusion of CO_2 into the PDMS.

The saturated phase dynamic viscosities follow a logarithmic trend, deviating only slightly at very low PDMS compositions where the gaseous phase becomes dominant. The start of the deviation coincides with the maximum density and –saturation pressure of the low PDMS fraction 'bump' discussed for phase equilibria and density. This phenomenon is further evident with respect to the composition in Figure 4-10 and Figure 4-11, with only the bottom three points deviating from the otherwise logarithmic trend.

In Figure 4-10 and Figure 4-11, a logarithmically decreasing change in dynamic viscosity can be noted as the PDMS concentration decreases (from right to left). Again, it can be seen that the polymer is plasticised by the supercritical CO_2, with the dynamic viscosity more than an order of magnitude smaller than the measured pure PDMS atmospheric values. Further, the PDMS-rich data points show some temperature dependence, with an increase leading to a lower dynamic viscosity, in agreement with the literature [8].

The measured dynamic viscosities of the liquid-rich phase covers a broad range, spanning from ~ 0.7 -7 mPa.s. This range proves sufficient for future hydrodynamic study, covering a wide possible range of properties.[11]

---

[11] In the ranges of shear possible and at the measured conditions, no non- Newtonian behaviour was observed. PDMS also did not display non- Newtonian behavior under experimental conditions.

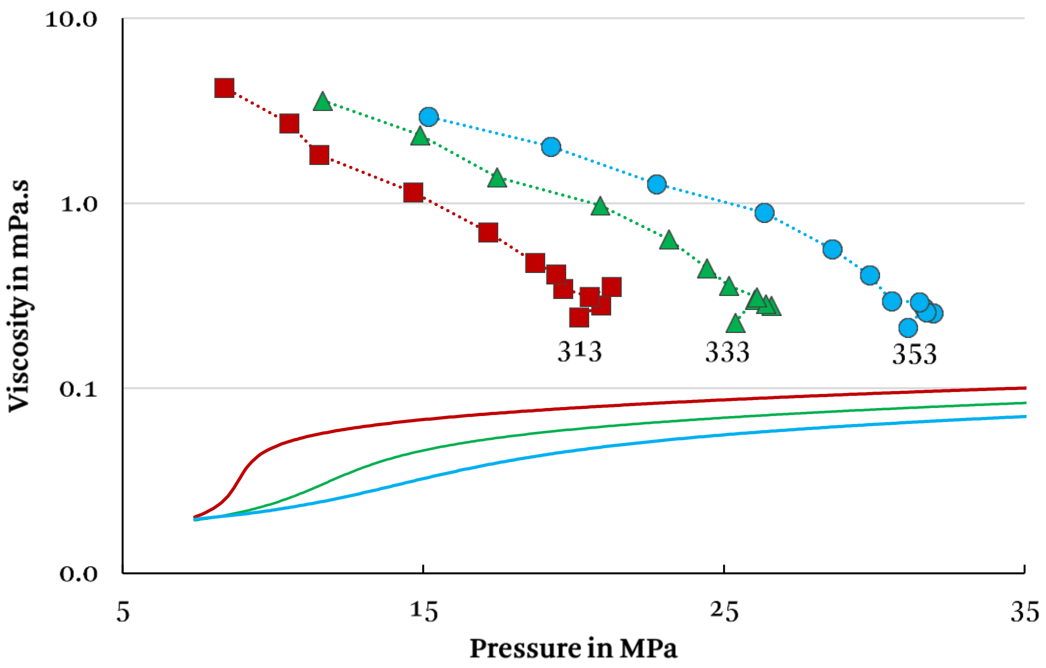

Figure 4-8: The dynamic viscosity of CO_2 + PDMS 100 at saturation vs pressure. Temperatures are marked as:■ 313.15 K; ▲ 333.15 K;● 353.15 K. Pure CO_2 dynamic viscosity (Solid lines) predicted using the model by Fenghour et al. [28]

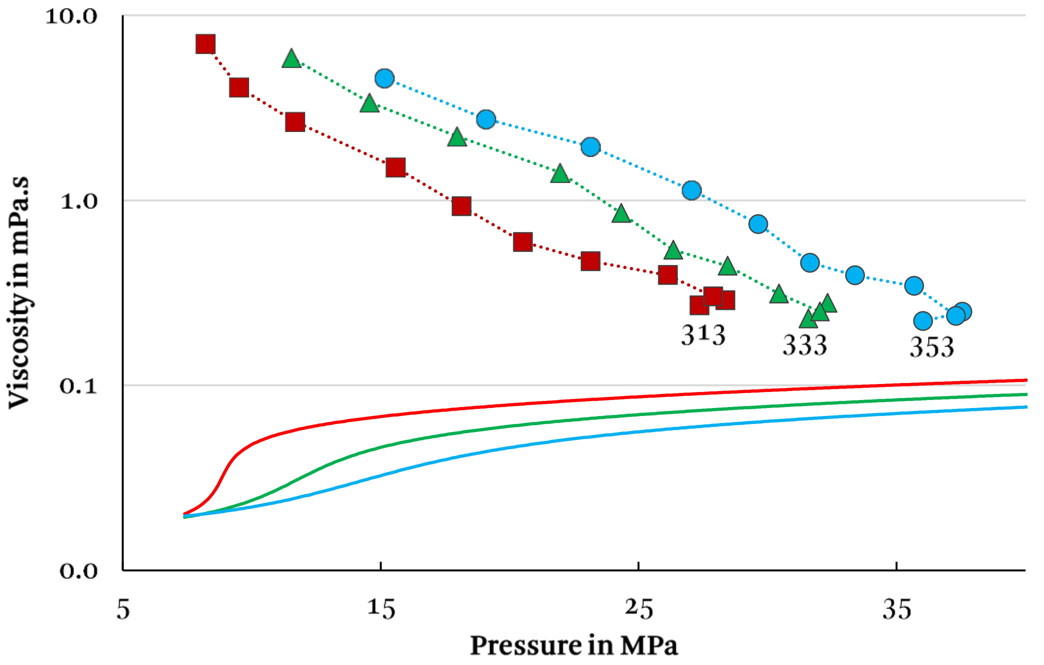

Figure 4-9: The dynamic viscosity of CO_2 + PDMS 200 at saturation vs pressure. Temperatures are marked as:■ 313.15 K; ▲ 333.15 K;● 353.15 K. Pure CO_2 dynamic viscosity (Solid lines) predicted using the model by Fenghour et al. [28]

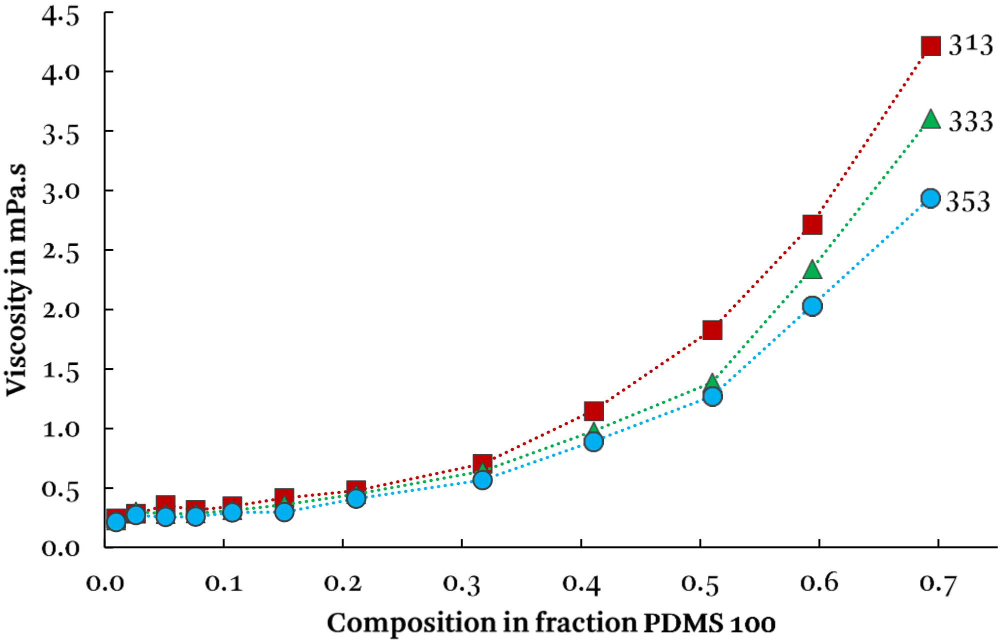

Figure 4-10: The dynamic viscosity of system CO_2 + PDMS 100 at saturation vs mass fraction PDMS 100. Temperatures are marked as: ■ 313.15 K; ▲ 333.15 K; ● 353.15 K.

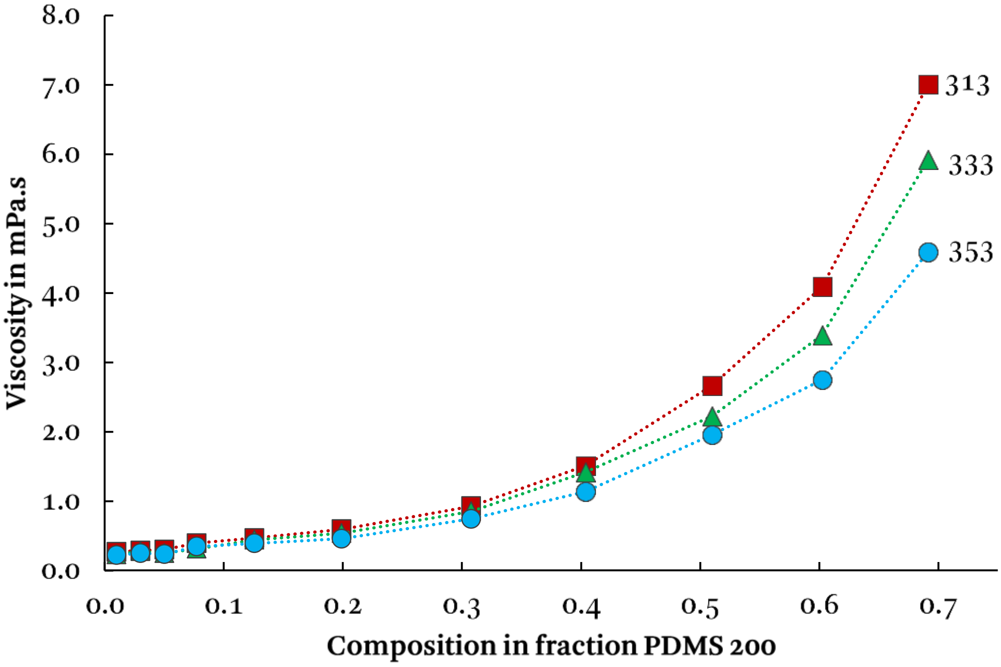

Figure 4-11: The dynamic viscosity of system CO_2 + PDMS 200 at saturation vs mass fraction PDMS 200. Temperatures are marked as: ■ 313.15 K; ▲ 333.15 K; ● 353.15 K.

4.4 Conclusions

The viability of two CO_2 + PDMS systems for future hydrodynamic investigations in supercritical packed columns was investigated. Phase equilibria were determined using a visual method (SynVisVar) in the temperature range of 313 - 353 K, with the phase properties of the density and the dynamic viscosity measured at saturation. Phase equilibria data displayed complex phase behaviour in agreement with literature. It was found that the molecular weight distribution of PDMS influenced phase behaviour and density, especially at low fractions of PDMS in CO_2, increasing the saturation pressure and density. Density data showed an inversion of the measured densities, with a sharp increase and decrease in density, at low PDMS fractions. This phenomenon coincided with an increase in saturation pressure due to complex phase behaviour.

The systems exhibited properties in applicable ranges for hydrodynamic study (~900 – 800 $kg.m^{-3}$ and ~0.7 - 7 mPa.s), with a low amount of PDMS soluble in the supercritical phase, minimising mutual solubility and hence eventual mass transfer. Operation of hydrodynamic experiments at lower pressures (~14 MPa) should prove sufficient to avoid the region of complex phase behaviour, while still presenting a range of properties to investigate.

Acknowledgements

This work is based on the research supported in part by the National Research Foundation of South Africa (Grant specific unique reference number (UID) 88782). The authors acknowledge that opinions, findings and conclusions or recommendations expressed in any publication generated by the NRF supported research is that of the authors', and that the NRF sponsors

Data Tables

Table 4-5: Experimental saturation pressures for binary mixtures of CO_2 + PDMS 100 and the measured density and dynamic viscosity of the mixture at saturation.

Temperature (K)	Mass frac PDMS 100	Pressure (MPa)	Density (kg/m³)	Dynamic Viscosity (mPa.s)
313.2	0.0097	20.2	834.0	0.242
313.2	0.0264	20.9	845.4	0.282
313.2	0.0514	21.3	855.7	0.299
313.2	0.0766	20.5	868.0	0.314
313.2	0.107	19.6	852.3	0.345
313.2	0.151	19.4	832.9	0.415
313.2	0.211	18.7	846.4	0.478
313.3	0.317	17.1	865.2	0.703
313.2	0.410	14.7	870.9	1.150
313.2	0.510	11.5	894.2	1.829
313.2	0.594	10.5	894.6	2.719
313.2	0.693	8.4	903.0	4.220
333.2	0.0097	25.4	782.6	0.227
333.2	0.0264	26.0	800.9	0.302
333.2	0.0514	26.6	829.5	0.281
333.2	0.0766	26.4	837.2	0.287
333.2	0.107	26.1	827.0	0.312
333.3	0.151	25.2	790.6	0.359
333.3	0.211	24.4	807.6	0.448
333.2	0.317	23.2	834.9	0.641
333.2	0.410	20.9	845.0	0.978
333.2	0.510	17.5	870.3	1.386
333.1	0.594	14.9	871.7	2.343
333.1	0.693	11.6	883.0	3.608
353.2	0.0097	31.1	744.8	0.214
353.2	0.0264	31.7	773.2	0.272
353.2	0.0514	32.0	799.7	0.255
353.2	0.0766	31.7	804.3	0.259
353.2	0.107	31.5	795.3	0.294
353.2	0.151	30.6	752.3	0.296
353.3	0.211	29.8	772.8	0.410
353.2	0.317	28.6	804.0	0.566
353.2	0.410	26.3	816.0	0.891
353.2	0.510	22.8	845.6	1.272
353.3	0.594	19.2	848.3	2.033
353.3	0.693	15.2	862.1	2.938

$u(T) = 0.2\ K;\ u_c(x) < 0.0005;\ u(P) = 0.06\ MPa;\ u_c(\rho) < 0.003 \cdot \rho\ kg/m^3;\ u_c(\eta) \leq 0.01 \cdot \eta\ mPa.s$

Table 4-6: Experimental saturation pressures for binary mixtures of CO_2 + PDMS 200 and the measured density and dynamic viscosity of the mixture at saturation.

Temperature (K)	Mass frac PDMS 200	Pressure (MPa)	Density (kg/m^3)	Dynamic Viscosity (mPa.s)
313.3	0.0100	27.37	875.2	0.269
313.3	0.0302	28.37	906.5	0.288
313.1	0.0504	27.90	904.5	0.301
313.2	0.0772	26.14	899.9	0.393
313.2	0.126	23.15	877.3	0.468
313.2	0.199	20.52	867.0	0.595
313.2	0.308	18.14	883.8	0.927
313.2	0.404	15.56	885.1	1.509
313.2	0.510	11.66	888.2	2.667
313.2	0.603	9.50	891.8	4.075
313.2	0.692	8.19	900.0	7.007
333.2	0.0100	31.59	816.6	0.229
333.3	0.0302	32.33	868.8	0.279
333.2	0.0504	32.03	862.6	0.250
333.2	0.0772	30.45	848.4	0.312
333.1	0.126	28.45	830.7	0.442
333.3	0.199	26.35	826.2	0.539
333.3	0.308	24.33	851.3	0.853
333.3	0.404	21.95	856.9	1.414
333.3	0.510	17.95	865.7	2.225
333.3	0.603	14.56	869.1	3.381
333.3	0.692	11.53	883.6	5.919
353.3	0.0100	36.03	767.3	0.222
353.3	0.0302	37.56	809.5	0.249
353.2	0.0504	37.31	816.9	0.237
353.4	0.0772	35.68	813.3	0.344
353.2	0.126	33.40	789.6	0.392
353.2	0.199	31.65	789.6	0.459
353.4	0.308	29.65	818.4	0.743
353.3	0.404	27.04	825.3	1.137
353.3	0.510	23.12	843.0	1.954
353.3	0.603	19.07	849.4	2.739
353.3	0.692	15.13	859.7	4.589

$u(T) = 0.2$ K; $u_c(x) < 0.0005$; $u(P) = 0.06$ MPa; $u_c(\rho) < 0.003 \cdot \rho$ kg/m^3; $u_c(\eta) \leq 0.01 \cdot \eta$ mPa.s

References

[1] Seader J.D. and Henley, E.J., *Separation Process Principles, 3rd Edition*, Wiley, Chichester, 2013, ISBN: 978-0-470-48183-7.

[2] Lombard, J.E., *Thermodynamic Modelling of Hydrocarbon-Chains and Light-Weight Supercritical Solvents*, Masters Thesis, Stellenbosch University, 2015, Retrieved from: http://hdl.handle.net/10019.1/96844.

[3] Franken, H.H., Knoetze, J.H. and Schwarz, C.E., *Concurrent measurement of high-pressure binary phase equilibrium, density and dynamic viscosity*, J. Supercrit. Fluids, 133 (2018) 444-454.

[4] Brunner, G., Gas Extraction, *An Introduction to Fundamentals of Supercritical Fluids and the Application to Separation Processes*, Steinkopff, Darmstadt, 1994, ISBN: 978-3-662-07382-7.

[5] Schwarz, C.E. and Knoetze, J.H., *Design of Supercritical Fluid Processes for High Molecular Mass Petrochemicals*, in: M.R. Belinsky (Ed.), Supercritical Fluids, Nova Science Publishers Inc., New York, 2009, ISBN: 978-1-60741-930-3.

[6] Kiran, E. and Zhuang, W., *Miscibility and Phase Separation of Polymers in Near- and Supercritical Fluids*, ACS Symp. Ser., 670 (1997) 2-36.

[7] Avelino, H.M.N.T., Fareleira, J.M.N.A., Gourgouillon, D., Igreja, J.M. and Nunes da Ponte, M., *Viscosity of poly(ethyleneglycol) 200 [PEG 200] saturated with carbon dioxide*, J. Supercrit. Fluids, 128 (2017) 300-307.

[8] Xiong, Y. and Kiran, E., *Miscibility, density and viscosity of poly(dimethylsiloxane) in supercritical carbon dioxide*, Polymer, 36 (1995) 4817-4826.

[9] Bayraktar, Z. and Kiran, E., *Miscibility, Phase Separation, and Volumetric Properties in Solutions of Poly(dimethylsiloxane) in Supercritical Carbon Dioxide*, J. Appl. Polym. Sci., 75 (1999) 1397-1403.

[10] Dindar, C. and Kiran, E., *High-Pressure Viscosity and Density of Polymer Solutions at the Critical Polymer Concentration in Near-Critical and Supercritical Fluids*, Ind. Eng. Chem. Res., 41 (2002) 6354-6362.

[11] Mertsch, R. and Wolf, B.A., *Solutions of Poly(dimethylsiloxane) in Supercritical CO_2: Viscometric and Volumetric Behavior*, Macromolecules, 27 (1994) 3289–3294.

[12] Garg, A., Gulari, E. and Manke, C.E., *Thermodynamics of Polymer Melts Swollen with Supercritical Gases*, Macromolecules, 27 (1994) 5643-5653.

[13] Koronaios, P., Stevenson, C., Warman, S., Enick, R. and Luebke, D., *Thermally Stable Silicone Solvents for the Selective Absorption of* CO_2 *from Warm Gas Streams That Also Contain* H_2 *and* H_2O, Energy Fuels, 30 (2016) 5901–5910.

[14] Johnston, K.P., Da Rocha, S.R.P., Lee, C.T, Li, G. and Yates, M.Z., *Colloid and Interface Science for* CO_2*-Based Pharmaceutical Processes*, in: York, P., Kompella, U.B. and Shekunov, B.Y. (Eds.), Supercritical Fluid Technology for Drug Product Development, Informa Healthcare, New York, 2008, 202-231, ISBN 0-8247-4805-0.

[15] Nalawade, S.P., Picchioni, F. and Janssen, L.P.B.M., *Supercritical carbon dioxide as a green solvent for processing polymer melts: Processing aspects and applications*, Prog. Polym. Sci., 31 (2006) 19–43.

[16] Björklund, E., Turner, C., Karlsson, L., Mathiasson, L., Björn, S and Skogsmo, J, *The Influence of Oil Extractability and Metal Part Geometry in Degreasing Processes Using Supercritical Carbon Dioxide*, J. Supercrit. Fluids, 9 (1996) 56-60.

[17] Schwarz, C.E. and Nieuwoudt, I., *Phase equilibrium of propane and alkanes: Part I. Experimental procedures, dotriacontane equilibrium and EOS modelling*, J. Supercrit. Fluids, 27 (2003) 133-144.

[18] Fourie, F.C.vN, Schwarz, C.E. and Knoetze, J.H., *Phase equilibria of alcohols in supercritical fluids. Part I. The effect of the position of the hydroxyl group for linear C8 alcohols in supercritical carbon dioxide*, J. Supercrit. Fluids, 47 (2008) 161–167.

[19] Span, R. and Wagner, W., *A New Equation of State for Carbon Dioxide Covering the Fluid Region from the Triple-Point Temperature to 1100 K at Pressures up to 800 MPa*, J. Phys. Chem. Ref. Data, 25 (1996) 1509-1596.

[20] Mason, W.P., *Measurement of the Viscosity and Shear Elasticity of Liquids by Means of a Torsionally Vibrating Crystal*, Trans. ASME, 69 (1947), pp.359.

[21] Collings, A.F. and McLaughlin, E., *Torsional Crystal Technique for the Measurement of Viscosities of Liquids at High Pressure*, Trans. Faraday Soc., 67 (1971) 340-352.

[22] Joint Committee for Guides in Metrology, *Evaluation of measurement data - Guide to the expression of uncertainty in measurement, JCGM 100:2008*, available

at: http://www.iso.org/sites/JCGM/GUM/JCGM100/C045315e-html/C045315e.html, 2008 (accessed 06 Nov 2017).

[23] Fourie, F.C.vN., Schwarz, C.E. and Knoetze, J.H., *Analytic High-Pressure Phase Equilibria. Part II: Gas Chromatography and Sampling Method Development*, Chem. Eng. Technol., 39 (2016) 1475-1483.

[24] Rudnick, J., Taylor, P. L., Litt, M. and Hopfinger, A. J., *Theory of free volume in polymers*, J. Polym. Sci. Polym. Phys. Ed., 17 (1979) 311–320.

[25] Kikic, I. and De Loos, T.W., *Thermodynamic Properties at High Pressure*, in: A. Bertucco, G.Vetter (Eds.), High Pressure Process Technology: Fundamentals and Applications, Elsevier, Amsterdam, 2001, ISBN: 978-0-444-50498-2.

[26] Konynenburg, P.H. and Scott, R.L., *Critical lines and phase equilibria in binary van der Waals mixtures*, Phil. Trans. R. Soc. A, 298 (1980) 495-540.

[27] Fakhreddine, A. and Zoller, P., *The Equation of State of a Polydimethylsiloxane Fluid*, J. Appl. Polym. Sci., 41 (1990) 1087-1093.

[28] Fenghour, A., Wakeham, W.A. and Vesovic, V., *The Viscosity of Carbon Dioxide*, J. Phys. Chem. Ref. Data, 27 (1998) 31-44.

[29] Schmelzer, J. W., Zanotto, E. D., and Fokin, V. M., *Pressure dependence of viscosity.*, J. Chem. Phys., 122 (2005) 074511.

5. Publication 3

Hydrodynamics of a Packed Column Operated under Supercritical Conditions

H.H. Franken[a], J.H. Knoetze[a], C.E Schwarz[a,]*

[a] Department of Process Engineering, Stellenbosch University, Private Bag X1, Matieland, 7602, South Africa.

*Phone: +27 21 808 4487, Email: cschwarz@sun.ac.za

Chemical Engineering Transactions, 69 (2018) 13-18
Published 1 October 2018

DOI: 10.3303/CET1869003

Declaration by the candidate

Concerning Chapter 5, the nature and scope of my contribution(s) were as follows:

Nature of contribution	Contribution (%)
I was responsible for conducting the experimental work and processing and interpreting the results. I was also the primary author of the article, responsible for compiling the document and the submission and review process.	80%

The following co-authors contributed to Chapter 5:

Name	E-mail address	Contribution Nature	Contribution (%)
Cara E Schwarz	cschwarz@sun.ac.za	Supervisor of student, HH Franken	10 %
Johannes H. Knoetze	jhk@sun.ac.za	Co-supervisor of student, HH Franken	10 %

Signature of candidate: Declaration with signature in possession of candidate and supervisor

Date : 20 January 2020

Declaration by co-authors

The undersigned hereby confirm that:

1. The declaration above accurately reflects the nature and extent of the contributions of the candidate and the co-authors to Chapter 5.

2. No other authors contributed to Chapter 5 besides those specified above.

3. Potential conflicts of interest have been revealed to all interested parties and that the necessary arrangements have been made to use the material in Chapter 5 of this dissertation.

Signature	Institutional affiliation	Date
Declaration with signature in possession of candidate and supervisor	Supervisor to the student, HH Franken at Stellenbosch University	20 January 2020
Declaration with signature in possession of candidate and supervisor	Co-Supervisor to the student, HH Franken at Stellenbosch University	20 January 2020

Preface

Experimental method detail (Safe Working Procedures), as well as an analysis and steps to eliminate or mitigate any risk (Task Risk Assessment), are presented in Appendix B. Safety information for all chemicals used can be found in Appendix C. For any further equipment detail the reader is directed to the preceding Master's study: *Establishment of a Supercritical Pilot Plant and the Hydrodynamics Of Supercritical Countercurrent Columns*, Master's Thesis, Stellenbosch University, Department of Process Engineering, 2014. The raw hydrodynamic data can be found in Appendix F.

This paper is a peer-reviewed paper, written for the Distillation Absorption 2018 conference series, and published in the Chemical Engineering Transactions journal. This article is intended as an initial snapshot of results. This issue of the journal published a selection of peer-reviewed papers from the conference, but the number of pages that could be included in the published version was severely limited. To present the results entirely in an in-depth discussion, a further journal publication is planned, as presented in Chapter 6, Manuscript 4. The reader is alerted to the fact that there is duplication between this paper and the manuscript in Chapter 6. The duplication is needed to create context and present a full set of data for the manuscript.

This paper uses the fluid properties and phase equilibrium data gathered in the preceding chapter to investigate hydrodynamics for a supercritical system. This paper starts to address the third objective - to measure hydrodynamic data, namely liquid hold-up and pressure drop, for the selected system(s). The hydrodynamics can then be used to determine A) the operability limits of the system and B) the influence of the fluid properties of viscosity and density on hydrodynamics. The investigation is incomplete and will be concluded in the following chapter.

Abstract

There is a lack of hydrodynamic data under supercritical conditions, in particular in systems that attempt to isolate hydrodynamics from mass transfer. This paper presents hydrodynamic data focusing on the characterisation of flooding. Two different flooding phenomena are identified using the column overheads, pressure drop and liquid hold-up of the system. It is further noted that the saturated fluid properties of density and dynamic viscosity play a significant role in flooding. A density difference of less than 250 kg/m^3 between phases and a decrease in liquid viscosity causes a shift from classical gas-liquid flooding to behaviour more analogous to that of liquid-liquid extraction columns.

5.1 Introduction

Supercritical fluids (SFs) are increasing in popularity as a solvent for various extraction, fractionation and absorption processes. Presenting an attractive alternative to traditional solvents, SFs are readily tuneable and capable of sharp, highly efficient separations while using less intrinsically harmful solvents. The application of the technology is, however, hampered by a lack of design methods and predictive models [1]. To develop these methods, a fundamental understanding of the mass transfer and transport phenomena in SF systems is required.

Mass transfer in SFs is widely investigated in the literature, with phase equilibria providing insight into the operating pressure, temperature, and driving force for separation [2]. Additionally, several EOS (Equation of State) models capable of reasonable predictions of phase equilibria under SF conditions exist in the literature [3]. However, data and models for physical properties and transport phenomena under SF conditions are decidedly scarcer. Consequently, no comprehensive, predictive hydrodynamic models for columns operating under SF conditions exist. This deficiency forces the extensive piloting of any new applications and significant overdesign of equipment to compensate for the lack of knowledge. A thorough study of the effect of fluid properties on the hydrodynamics of SF systems is required to address this shortcoming. Such a study would allow the creation of a knowledge base from which such models can be developed.

The available literature is very diverse and does not typically focus solely on hydrodynamics. Rathkamp et al. [4], researched the efficiency and energy requirements of columns operating with supercritical CO_2 using a water + EtOH system in a 25.4 mm column packed with 6.4 mm metal Raschig rings. Seibert and Moosberg [5], measured efficiency and liquid hold-up using a 98.8 mm column with sieve trays, 12.7 mm Raschig rings and #15 IMTP using a water + EtOH system. Sievers [6] and Woerlee [7], were among the first to measure flooding under SF conditions, using water and hexadecane respectively, in a 36 mm column packed with a gauze type packing, Montz-Pak type A3. Both authors explicitly state that SF hydrodynamics are not consistent with generalised pressure drop correlations of the time. Lim et al. [8], investigated liquid hold-up in a 31.8 mm column with a knit mesh packing. They observed a positive correlation between a rise in system pressure and a rise in the liquid hold-up. Machado [9], measured flooding points consistent with the work of Woerlee [7], using palm oil distillate in a 25 mm column, packed with Sulzer EX. Meyer [10], using the same experimental setup measured not only flooding but also the pressure drop and physical properties of soybean oil + CO_2 and fish oil + CO_2 systems. Meyer [10] compared his results with well-known flood point correlations [11 - 13] and concluded that models derived for vacuum- and lower pressure application do not readily predict high-pressure systems ($P > 7$ MPa). Buddich [14], and Buddich and Brunner [15], again using the same experimental setup, investigated orange peel oil + CO_2 and water + ethanol + CO_2 systems. Stockfleth and Brunner [16, 17], were the first and only to perform a full hydrodynamic study, investigating liquid hold-up, flooding, pressure drop and foaming for water + CO_2, olive oil distillate + CO_2 and tocopherol + CO_2 systems. Modifying the semi-empirical models proposed by Stichlmair et al. [18], they achieved relative success in empirically predicting hydrodynamic phenomena, except for flooding.

To investigate fundamental hydrodynamic behaviour, systems with quantified mass transfer and known fluid properties are required. Firstly, mass transfer directly affects effective fluid flow rates and fluid properties, complicating the interpretation of hydrodynamic results. The limited available literature on SF hydrodynamics has neglected the effect of mass transfer or used systems with fluid properties, either undefined or very different from that of a typical, commercially relevant system. Secondly, the fluid properties of density and dynamic viscosity are particularly important, as these properties are highly variable with changes in mixture composition, pressure and temperature under SF conditions [19]. This variability implies that small variations in pressure and temperature can significantly affect hydrodynamics. Further, this fluid property variability causes large deviations from predictions using atmospheric fluid properties. Fluid properties can also not easily be predicted under SF conditions using standard models [20].

No collection of literature sources cover all the required aspects of a suitable system, presenting both phase equilibria data and phase properties. To address this gap, a previous study was done [21]. In this study, a binary system with suitable phase behaviour was identified, and its fluid properties of saturated density and dynamic viscosity were measured. CO_2, as the most popular SF solvent, was used with 100 cSt PDMS (poly[dimethylsiloxane]) as the liquid phase. The system proved to exhibit properties in applicable ranges for hydrodynamic study (~900 – 800 $kg.m^{-3}$ and ~0.7 – 7 mPa.s), with only a meagre amount[12] of PDMS soluble in the SF phase. The low amount of PDMS soluble means that mutual solubility is minimised and hence eventual mass transfer. The data allows the investigation of hydrodynamics using a system with known fluid properties in ranges similar to that of real SF – solute systems.

This work aims to make use of the aforementioned CO_2 + PDMS 100 system to measure hydrodynamics under SF conditions on a pilot plant scale while minimising mutual solubility. Specifically, the paper focussed on the identification of flooding behaviour by interpreting the liquid percentage in the overheads, the liquid hold-up in the column packing, and the pressure drop over the packing. Further, the influence of the fluid properties on flooding was investigated. Notably, the experiments were performed using random packing, ¼ " Dixon Rings, while literature data are only available on structured packings.

---

[12] << 1 wt% PDMS in CO_2.

5.2 Materials and Methods

5.2.1 Experimental Equipment

A basic process flow diagram of the experimental pilot plant[13] is seen in Figure 5-1 with a legend in Table 5-1 a) and specifications for the pilot plant provided in Table 5-1 b). The pilot plant was assembled in-house and consisted of two columns. For the work presented here, only the larger diameter column, ID 38 mm, was used. The pilot plant can measure the liquid hold-up, pressure drop and column bottom- and overheads rates over a wide range of liquid- and SF solvent flow rates. From these measurements, flooding and entrainment can be identified. Pressure drop is measured using an Endress+Hauser Deltabar S PMD75 with an accuracy of 0.075 % of its range of 50 kPa. Temperature is measured by multiple J type thermocouples, accuracy ±1.5 K. SF. Mass flow rate is measured using a Micro Motion D12 flow sensor and RFT 9729 remote flow transmitter combo with an uncertainty of 0.2% of the rate. All electronic data are logged using a custom PLC setup. The liquid mass flow rate is determined from prior calibration of the pumps and confirmed by doing a liquid mass balance over the column.

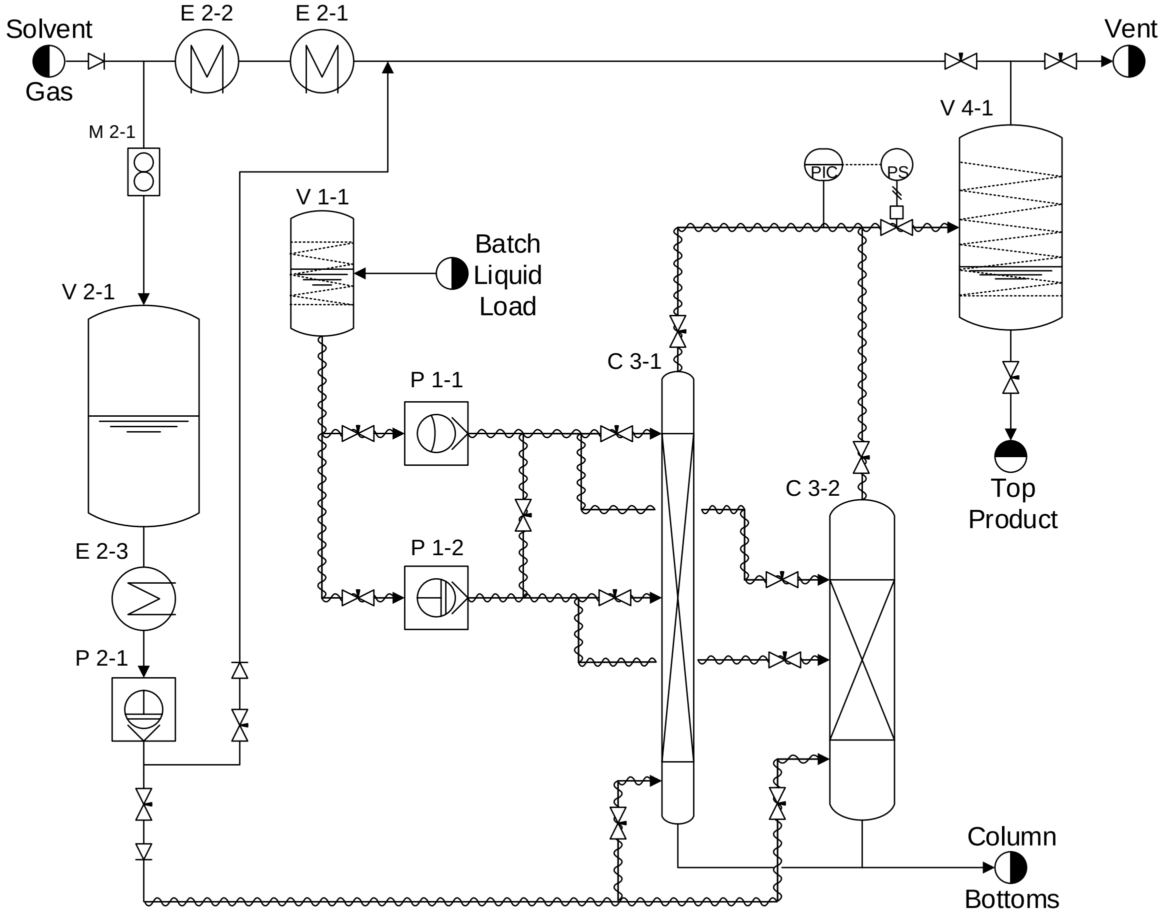

Figure 5-1: Schematic representation of the pilot plant set-up

---

[13] The construction, commissioning, method development and operation for this setup was part of a previous study [24]

Table 5-1 a) Legend for Figure 5-1.

Label	Description
V 1-1	Liquid Feed Tank
P 1-1	Small Capacity Diaphragm Pump
P 1-2	Large Capacity Piston Pump
E 2-1	Water Pre-cooler
E 2-2	Chilled Condenser
M 2-1	Mass Flow Meter
V 2-1	Solvent Buffer Tank
E 2-3	Pump Feed Chilled Pre-cooler
P 2-1	Solvent Diaphragm Pump
V 3-1	Bottoms Vessel
C 3-1	Small Diameter Column
C 3-2	Large Diameter Column
V 4-1	Overhead Product Separator Vessel

b) Pilot plant specifications.

Description	Values
Maximum system pressure	30 MPa
Maximum system temperature	473 K
Separator pressure	~5 MPa
Liquid flow rate range	0 - 8 ℓ/h
SF flow rate range	0 - 55 ℓ/h
Column C 3-1 Diameter	17 mm
Column C 3-1 Packed Height	3.5 m
Column C 3-2 Diameter	38 mm
Column C 3-2 Packed Height	1.5 m
Column Packing	1/4'' Dixon Rings
Packing void fraction - $\in$	91 %
Packing surface area	900 m^2/m^3
Particle diameter (const.) - d_p	0.6 mm

5.2.2 Materials Used

Details on the chemicals used are available in Table 5-2. The PDMS used in this study were methyl group capped and effectively linear, with few side chains. Chemicals were used without further treatment or purification. The phase transitions and fluid properties of the CO_2 + PDMS systems were determined in-house using a previously verified variable volume view cell [19]. Saturation, and hence phase transition, was determined for 1 - 70 wt% PDMS in CO_2 at 313 – 353 K using the visual static synthetic method (SynVisVar). The density and dynamic viscosity were measured for both the SF- and solute-rich phases using the quantified volume and mass, and the converse piezoelectric effect, respectively.

Table 5-2: Chemicals used in this study.

Chemical	Purity	Supplier	CAS Number
CO_2	99.95%	Afrox Oxygen Ltd.	124-38-9
PDMS 100	Absolute	Xiameter PMX-200 (DOW Corning)	63148-62-9

5.2.3 Experimental Considerations and Procedure

5.2.3.1. Pressure and Temperature Considerations

With an array of possible testing conditions, careful selection of the experimental conditions was required to ensure mass transfer is limited, and the physical properties fall in the desired ranges. Experiments were performed at 14 MPa to simplify the problem. This pressure ensured that the solubility of the PDMS into the SF phase is very low (<< 1 wt%) and the SF phase properties are effectively the same as that of pure CO_2 at the same pressure and temperature. CO_2 solubility into PDMS at these conditions is significant (~30 - 40 wt%), and must be taken into consideration. An experimental temperature of 333.15 K was selected as a starting point, with the temperature lowered in 5 K intervals for every subsequent experimental set. This decrease was continued until the column becomes inoperable due to flooding. Each change in temperature leads to a change in density and viscosity of the fluids.

5.2.3.2. Dry pressure drop

Before the packing was wetted, the dry bed pressure drop was measured. This measurement was done by operating the column with only SF CO_2 flow. After reaching stable, equilibrium flow, as indicated by a steady pressure drop over the column, the pressure drop was noted. The SF flow rate was then changed, and time was allowed to ensure a new equilibrium (~30 minutes). This procedure was repeated to provide dry pressure drop data over a full range of SF flow rates. The temperature was then changed and the process repeated until all the required experimental conditions were investigated.

5.2.3.3. Wet pressure drop and liquid hold-up

For a single liquid / SF flow rate combination, the column was first operated only with SF CO_2. After the column reached equilibrium with SF flow alone, the pressure drop over the column was noted, and the liquid feed started at a pre-calibrated rate. The column was then allowed to reach a new equilibrium, after which the pressure drop over the column was noted. All flow to the column was then shut off, with the pressure drop immediately after the shutdown noted and the hold-up diverted to separate it from the bottoms.[14] After allowing for sufficient time for all of the liquid hold-up to drain the column bottoms, tops and liquid hold-up were decanted and weighed. The flow rate combination and/or temperature is then changed as desired, after which the process was repeated to gather further data. The pressure drop reported here is the difference between the equilibrium value of the SF flow alone, subtracted from the maximum equilibrium value.[15]

5.3 Results and Discussion:

As the aim of this paper is to provide insight into the qualitative trends and phenomena, only representative results illustrating flooding are presented. Full sets of hydrodynamic data have been measured for the two PDMS systems and are reported elsewhere [22].

---

[14] A supplementary discussion on the bottoms removal method, liquid hold- up determination, and the involved equipment can be found in Appendix E.2

[15] An example of equilibrium determination and pressure drop can be found in Appendix E.1, including how the equipment was zeroed

5.3.1 Dry Pressure Drop

Measurements of the dry pressure drop behaviour of the packing are presented for 313.15 K, as seen in Figure 5-2. A model prediction is performed using a modified Ergun-type equation [18], with determined constants K1 = 459 and K2 = 4.11. These constants are of the same order of magnitude as that determined by Stockfleth and Brunner [17]. It is seen that the model predicts the data well, as expected with a fitted, semi-empirical equation. It is, however, of value to see that the data fall comfortably within a ± 20 % confidence interval of the model, indicating the pilot plant stability and repeatability.

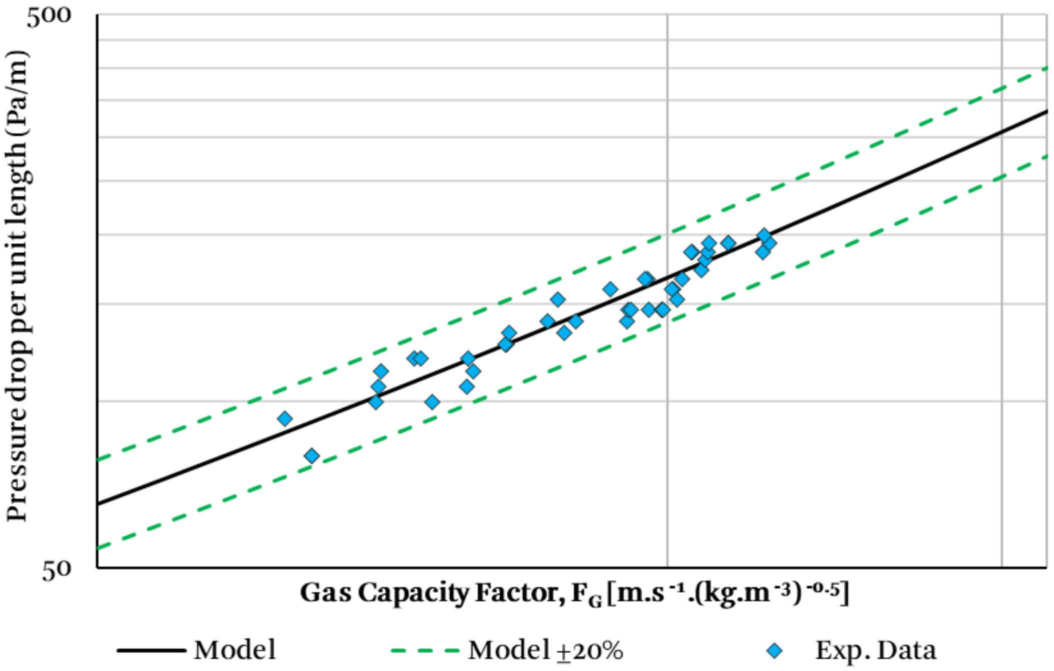

Figure 5-2: Dry pressure drop and model prediction at 14 MPa and 313.15 K for ¼ " Dixon Rings and SF CO_2[16].

5.3.2 Flooding Determination

There is no universal definition for flooding, and many of the definitions available in the literature are vague, impractical or arbitrary [23]. Flooding is defined for this work as the total hydrodynamic inoperability of a column, or, in other words, the point after which a column ceases to be an effective vessel for separation. This operability is determined by monitoring the mass fraction of liquid in the overheads, the pressure drop and the liquid hold-up. Typically flooding is accompanied by a sharp, sudden increase in the percentage of liquid in the overheads. A significant wt% increase (>80% of the value[17]) above the saturation of the fluid was deemed a possible indication of flooding, with further investigation into the pressure drop and

---

[16] The Gas capacity factor is calculated using: $F_G = u_G(\rho_G / (\rho_L - \rho_G))^{0.5}$

[17] The determination of the percentage is discussed in Section 6.2.4.

liquid hold-up used to confirm. An example of this can is seen in Figure 5-3, with unfilled markers indicating flooding from here on.

Two types of flooding behaviour were identified in the systems measured.

Firstly, flooding was observed that caused an increase in both the liquid percentage of the overheads, liquid hold-up and the pressure drop, concerning an increase in liquid feed rate. This type of flooding was found at high liquid rates and low SF flow rates and characteristically exhibited an intermittent, rapid rise and fall in the pressure drop of the column under 'equilibrium' conditions. This pressure instability is thought to be an indication of 'slugging' behaviour, with a continuous liquid phase layer forming in the column. This continuous liquid phase is then intermittently pushed out of the column by slugs of the SF phase rising through it. Alternatively, the liquid layer can build up high enough in the column to start exiting through the overheads. A large amount of liquid in the column would also correspond to a relatively higher pressure drop and higher liquid hold-ups before the column becomes inoperable. This behaviour can be seen in Figure 5-4 for the liquid hold-up of the 12.7 mm/s gas velocity system, showing a gradual increase in the hold-up followed by eventual flooding. Similar behaviour was observed for the pressure drop, omitted here due to spatial constraints[18]. This behaviour is similar to flooding in a 'classical' gas-liquid extraction column and agrees with the data gathered by Franken [24] for the system Polyethyleneglycol + CO_2.[19]

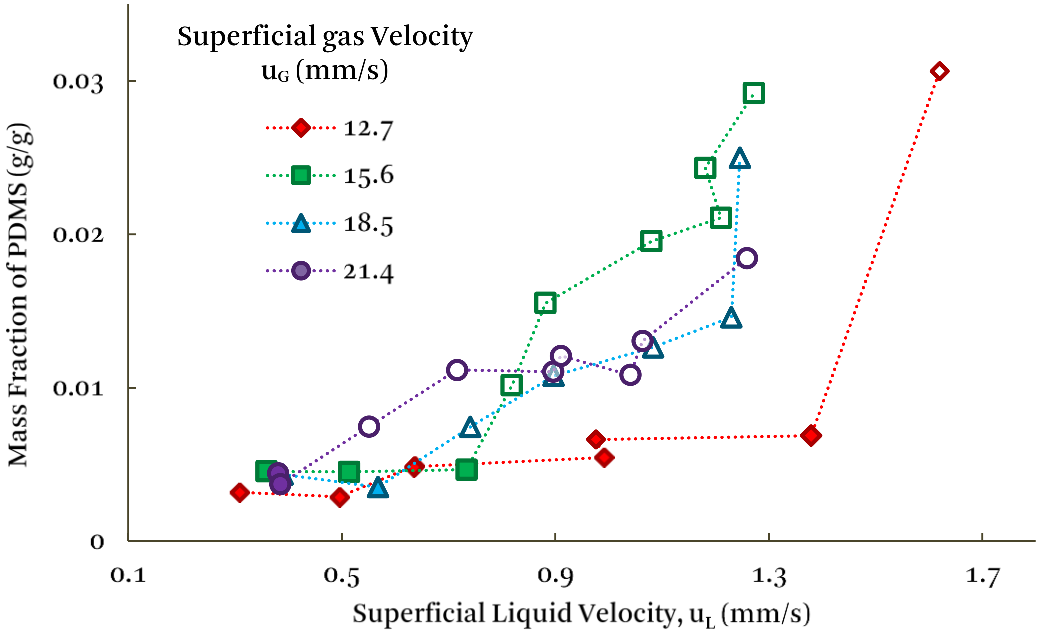

Figure 5-3: Mass fraction PDMS 100 cSt in the column overheads at 14 MPa and 313.15 K at various superficial gas velocities[20]

---

[18] See Figure 6-3 for the omitted details.

[19] Flooding definitions and determination is expanded upon and better explained in Section 6.2.4.

[20] Closed symbols represent unflooded data points while open symbols represent flooded data.

Secondly, flooding was identified that caused an increase in the liquid percentage in the overheads, a plateau in the liquid hold-up, and a maximum and subsequent decrease in the pressure drop, all with respect to an increase in liquid feed rate. This behaviour was noted in medium to high liquid- and SF flow rates, as can be seen for 15.6 - 21.4 mm/s range in Figure 5-4 for the liquid hold-up. This flooding occurred more readily when the density of the SF phase became similar to that of the saturated liquid, and the liquid dynamic viscosity decreased. The fluid property dependence is better seen in Figure 5-5, where the density difference between the phases varies from ~300 kg/m^3, ~250 kg/m^3 to ~200 kg/m^3 and the viscosity decreases from ~2.86 mPa.s, ~2.48 mPa.s to ~2.11 mPa.s, as the temperature decreases. The smaller difference in phase densities plays a significant role in the magnitude of buoyancy forces, while a decrease in the dynamic viscosity increases the mobility of the liquid phase. Together these changes in the fluid properties promote the entrainment of the liquid by the SF phase. This behaviour is more analogous to that found in liquid-liquid extraction columns.

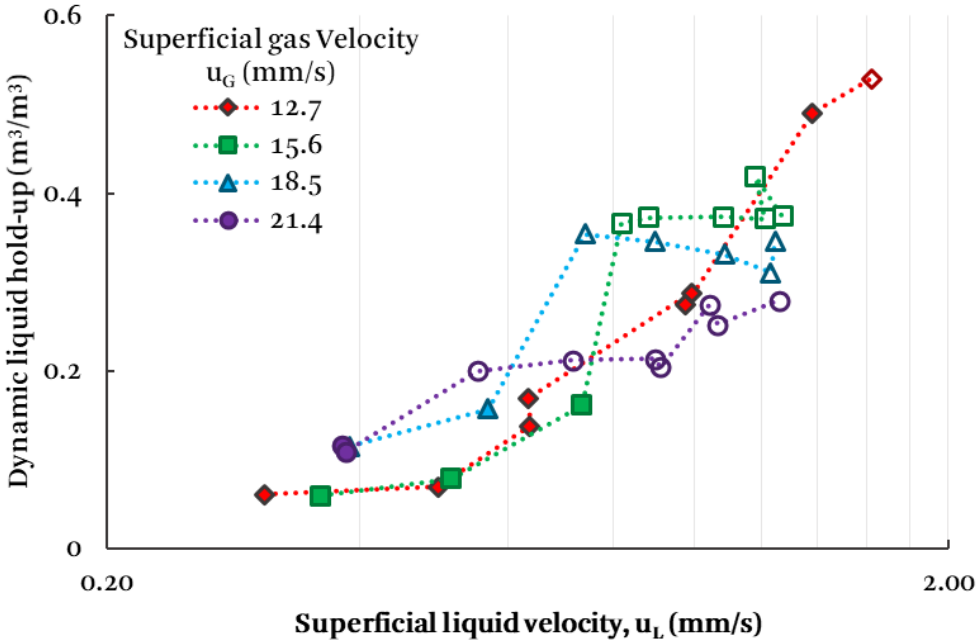

Figure 5-4: Dynamic liquid hold-up at 313.15 K and 14 MPa for CO_2 + PDMS 100 cSt.[20]

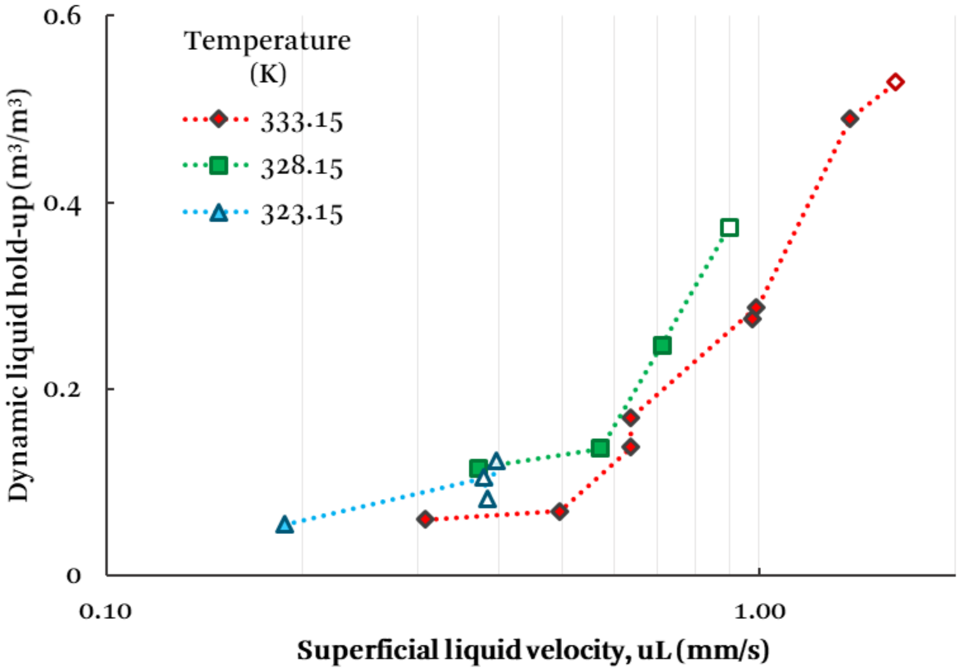

Figure 5-5: Dynamic liquid hold-up at u_G = 12.7 mm/s over three different temperature for CO_2 + PDMS 100 cSt.[20]

5.4 Conclusions

Pilot plant data were measured to identify flooding of a column with random packing, ¼ ” Dixon Rings, operated with a system optimised for low mutual mass transfer and fluid properties close to that of actual SF systems, namely CO_2 + 100 cSt poly(dimethylsiloxane). Flooding was identified using the liquid percentage in the overheads, the liquid hold-up in the column packing, and the pressure drop over the packing. Two different types of flooding phenomena were identified, respectively being analogous to gas-liquid and liquid-liquid columns. The shift between the flooding phenomena was accompanied by a decrease in the liquid phase viscosity and the density difference between the phases, with a difference in density of less than ~250 kg/m^3 proving significant.

Acknowledgements

This work is based on the research supported in part by the National Research Foundation of South Africa (Grant specific unique reference number (UID) 88782). The authors acknowledge that opinions, findings and conclusions or recommendations expressed in any publication generated by the NRF supported research is that of the authors’, and that the NRF sponsors accept no liability whatsoever in this regard.

References

[1] Schwarz, C.E., Knoetze, J.H., 2009, *Design of supercritical fluid processes for high molecular mass petrochemicals*, In: Belinsky, M.R. (Ed.), Supercritical Fluids, Nova Science Publishers, Hauppauge, New York, United States, ISBN: 978-1-60741-930-3

[2] Seader J.D., Henley, E.J., 2013, *Separation Process Principles, 3rd Edition*, Wiley, Chichester, ISBN: 978-0-470-48183-7.

[3] Lombard, J.E., 2015, *Thermodynamic modelling of hydrocarbon-chains and light-weight supercritical solvents*, Masters Thesis, Stellenbosch University, Stellenbosch, South Africa, Retrieved from: http://hdl.handle.net/10019.1/96844.

[4] Rathkamp, P.J., Bravo, J.L., Fair, J.R., 1987, *Evaluation of packed columns in supercritical extraction process*, Solvent Extr. Ion Exch., 3, 367.

[5] Seibert, A.F., Moosberg, D.G., 1988, *Performance of spray, sieve tray, and packed contactors for high pressure extraction*, Sep.Sci. Tech., 23, 2049.

[6] Sievers, E.J., 1994, *Pressure drop and flooding with a supercritical fluid*, PhD Dissertation, Technische Universität Delft, Delft, The Netherlands.

[7] Woerlee, G.F., 1997, *Hydrodynamics and mass transfer in packed columns and their applications for supercritical separations*, PhD Dissertation, Technische Universiteit Delft, Delft, The Netherlands.

[8] Lim, J.S., Lee, Y.-W., Kim, J.-W., Lee, Y.Y., Chun, H.-S., 1995, *Mass-transfer and hydraulic characteristics in spray and packed extraction columns for supercritical Carbon Dioxide-ethanol-water system*, J. Supercrit. Fluids, 8, 127.

[9] Machado, N.T., 1998, *Fractionation of PFAD - compounds in countercurrent columns using supercritical carbon dioxide as solvent*, PhD Dissertation, Technische Universität Hamburg – Harburg, Harburg, Germany.

[10] Meyer, J.-T., 1998, *Druckverlust und flutpunkte in hochdruckgegenstromkolonnen*, PhD Dissertation, Technische Universität Hamburg, Hamburg, Germany.

[11] Mersmann, A., 1965, *Zur berechnung des flutpunktes in füllkörperschüttungen.* Chem. Eng. Tech., 37, 218.

[12] Eckert, J.S., 1970, *Selecting the proper distillation column packing*, Chem. Eng. Prog., 66, 39.

[13] Maćkowiak, J. 1991, *Fluid dynamics of packings and columns with modern packings for gas/liquid systems* (orig. German), Salle & Sauerland, Frankfurt, Germany.

[14] Budich, M., 1999, *Countercurrent extraction of citrus aroma from aqueous and nonaqueous solutions using supercritical carbon dioxide*, Düsseldorf, Düsseldorf, Germany, VDI-Verlag.

[15] Budich, M., Brunner, G., 1999, *Vapour-liquid equilibrium data and flooding point measurements of the mixture carbon dioxide + orange peel oil*, Fluid Phase Equilib., 158, 759.

[16] Stockfleth, R., Brunner, G., 1999, *Hydrodynamics of a packed countercurrent column for the gas extraction*, Ind. Eng. Chem. Res., 38, 4000.

[17] Stockfleth, R., Brunner, G., 2001, *Holdup, pressure drop, and flooding in packed countercurrent columns for the gas extraction*, Ind. Eng. Chem. Res., 40, 347.

[18] Stichlmair, J., Bravo, J.L. Fair, J.R., 1989, *General model for prediction of pressure drop and capacity of countercurrent gas/liquid packed columns*, Gas Sep. Purif., 3, 19.

[19] Franken, H.H., Knoetze, J.H., Schwarz, C.E., 2018, *Concurrent measurement of high-pressure binary phase equilibrium, density and dynamic viscosity*, J. Supercritical Fluids, 133, 444

[20] Brunner, G., 1994, *Gas Extraction, An introduction to fundamentals of supercritical fluids and the application to separation processes*, Steinkopff, Darmstadt, ISBN: 978-3-662-07382-7.

[21] Franken, H.H., Knoetze, J.H. and Schwarz, C.E., *High-pressure binary phase equilibria, density and dynamic viscosity of 100 & 200 cSt polydimethylsiloxane (PDMS) with supercritical* CO_2*, J. Supercritical Fluids*, 139 (2018) 1-7, https://doi.org/10.1016/j.supflu.2018.04.020.

[22] Franken, H.H., 2020, *The Hydrodynamics of Supercritical Countercurrent Columns*, PhD Dissertation, Stellenbosch University, Stellenbosch, South Africa, (to be published, Mrt 2020).

[23] Kister, H.Z., 1992, *Distillation Design*, McGraw- Hill, New York, United States of America, ISBN 0-07-034909-6.

[24] Franken, H.H., 2014, *Establishment of a supercritical pilot plant and the hydrodynamics of supercritical countercurrent columns*, Masters Thesis, Stellenbosch Univerisity, Stellenbosch, South Africa, Retrieved from: http://hdl.handle.net/10019.1/95961

6. Manuscript 4

Influence of Fluid Properties on the Hydrodynamics and Operability of a Countercurrent Supercritical Packed Column

H.H. Franken[a], J.H. Knoetze[a], C.E Schwarz[a, *]

[a] Department of Process Engineering, Stellenbosch University, Private Bag X1, Matieland, 7602, South Africa.

*Phone: +27 21 808 4487, Email: cschwarz@sun.ac.za

To be submitted to Chemical Engineering Research and Design

Declaration by the candidate

With regard to Chapter 6, the nature and scope of my contribution(s) were as follows:

Nature of contribution	Contribution (%)
I was responsible for conducting the experimental work and processing and interpreting the results. I was also the primary author of the article, responsible for compiling the document and the submission and review process.	80%

The following co-authors contributed to Chapter 6:

Name	E-mail address	Contribution Nature	Contribution (%)
Cara E Schwarz	cschwarz@sun.ac.za	Supervisor of student, HH Franken	10 %
Johannes H Knoetze	jhk@sun.ac.za	Co-supervisor of student, HH Franken	10 %

Signature of candidate: Declaration with signature in possession of candidate and supervisor

Date : 20 January 2020

Declaration by co-authors

The undersigned hereby confirm that:

1. The declaration above accurately reflects the nature and extent of the contributions of the candidate and the co-authors to Chapter 6.

2. No other authors contributed to Chapter 6 besides those specified above.

3. Potential conflicts of interest have been revealed to all interested parties and that the necessary arrangements have been made to use the material in Chapter 6 of this dissertation.

Signature	Institutional affiliation	Date
Declaration with signature in possession of candidate and supervisor	Supervisor to the student, HH Franken at Stellenbosch University	20 January 2020
Declaration with signature in possession of candidate and supervisor	Co-Supervisor to the student, HH Franken at Stellenbosch University	20 January 2020

Preface

Experimental method detail (Safe Working Procedures), as well as an analysis and steps to eliminate or mitigate any risk (Task Risk Assessment), are presented in Appendix B. Safety information for all chemicals used can be found in Appendix C. For any further equipment detail the reader is directed to the preceding Master's study: *Establishment of a Supercritical Pilot Plant and the Hydrodynamics of Supercritical Countercurrent Columns*, Master's Thesis, Stellenbosch University, Department of Process Engineering, 2014. The raw hydrodynamic data can be found in Appendix F.

This paper uses the fluid properties, and phase equilibrium data gathered in Chapter 4 to investigate hydrodynamics for a supercritical system and serves as a stand-alone extension of Paper 3. This chapter presents significant findings on supercritical hydrodynamics and adds significant insight into the literature. This paper concludes the third objective - to measure hydrodynamic data, namely liquid hold-up and pressure drop, for the selected system(s). The hydrodynamics can then be used to determine A) the operability limits of the system and B) the influence of the fluid properties of viscosity and density on hydrodynamics.

Abstract

The hydrodynamic operability and the influence of fluid properties on hydrodynamics under supercritical conditions were investigated in a 38 mm diameter column packed with ¼ " Dixon rings. The column was operated using 100 cSt and 200 cSt Poly[dimethylsiloxane] (PDMS), with supercritical CO_2 at 14 MPa and 333 K, 328 K and 323 K respectively. The pressure drop, liquid hold-up and mass flow/fractions were measured. The column operability was determined for both binary systems over a range of liquid and supercritical fluid flow rates using the measured data. Three distinct types of inoperability were identified, namely liquid layer flooding, bubble column flooding and entrainment. It was found that liquid hold-up and pressure drop are not reliable indicators of operability in supercritical systems. Further, no observable loading operating regime was found (as defined for subcritical systems), with the column only operating in the pre-loading or inoperable (flooded/entrained) regimes. The influence of the density and dynamic viscosity on hydrodynamics was found to be complex, yet significant. Small changes in temperature caused substantial changes in fluid properties, having a significant impact on column operability. Column operability decreased with an increase in liquid viscosity and SF density, respectively.

Keywords: Flooding, Liquid Hold-up, Polydimethylsiloxane (PDMS), Pressure Drop, Supercritical CO_2, Dynamic Viscosity.

Highlights

- Liquid hold-up and pressure drop do not reliably indicate operability in SF fractionation columns.
- No observable “loading” operating regime was found under SF conditions.
- Changes in temperature had a significant impact on operability due to fluid property variation.
- Column operability range decreased with an increase in liquid viscosity and density.

6.1 Introduction

Supercritical fluids (SFs) present an attractive alternative to traditional solvents as a separation medium in extraction/fractionation columns. SFs are readily ‘tuneable’ and capable of effecting sharp, highly efficient separations while typically using less intrinsically harmful chemicals as a solvent. Further, SFs can differentiate hydrocarbons by chain length and functional group, accomplishing separations not easily accomplished by conventional means [1, 2].

The general adoption of SF technologies in fractionation columns has been hampered by, amongst others, a lack of holistic/comprehensive data and accurate design correlations. The lack of data available in the open literature on columns operating with SFs results in a shortage of design methods and predictive models for SF columns. A lack of methods and models means that any new application requires extensive piloting before it can be accepted as a commercially viable solution [3]. To develop new methods and models, a fundamental understanding of the transport phenomena in SF columns is required, particularly concerning hydrodynamics and mass transfer. However, several aspects hamper the development of new hydrodynamic and mass transfer models for operation at supercritical conditions.

Firstly, data and models for hydrodynamics in columns operating under SF conditions are scarce and, if found, only applicable to a particular system [4]. Secondly, studies on overall/dynamic mass transfer are scarce. Phase equilibria data are, however, more available in the literature, providing insights into the possible operating pressure, temperature, and driving force for separation [5]. Several EOS (Equation of State) models capable of correlating equilibria for an SF + a single liquid phase are available in the literature and can be used to predict some binary phase states [6]. Lastly, the physical properties of SF systems are found to be poorly investigated in the literature [7]. A lack of physical property data presents a challenge when selecting viable systems for hydrodynamic study, and creates difficulties in defining and describing different transport phenomena.

A thorough study of the effect of fluid properties on the hydrodynamics of SF systems is therefore warranted to help address the shortcomings in the literature. Such a study will aid in the creation of a knowledge base from which comprehensive, predictive hydrodynamic models can be developed in the future.

A system with quantified mass transfer and known fluid properties is required to investigate fundamental hydrodynamic behaviour. Firstly, mass transfer influences the effective fluid flow rates and fluid properties, complicating the isolation of hydrodynamic effects. Studies in the open literature concerning SF hydrodynamics are often not comprehensive. The literature either neglected the effect of mass transfer or used systems with fluid properties that are undefined or very dissimilar from that of typical, commercially relevant systems [8].

Secondly, knowledge of the fluid properties of density and viscosity of the co-existing phases are particularly important. Under SF conditions, small changes in mixture composition can substantially and suddenly change these fluid properties [9]. The compositions of the co-existing phases are in turn dependant on the pressure and temperature of the system, as per the phase rule. This temperature dependence implies that small changes in pressure and temperature can significantly affect hydrodynamics. Physical properties under SF conditions vary significantly from their atmospheric counterparts [9] and are not easily predicted using standard models [10].

In preparation of this hydrodynamic study, two binary systems with suitable phase behaviour (low mutual solubility) and appropriate fluid property ranges (relevant density and dynamic viscosity) were identified and measured [9]. CO_2 was chosen as the SF solvent, being the most widely used in industry, with two silicone oils, namely 100 cSt and 200 cSt PDMS (poly[dimethyl siloxane]), as the respective liquid phases. The selected silicone oils are non-volatile, apolar, straight-chained polymers that lends itself to low solubility in SF CO_2. The detail of the selection of these systems is discussed in a prior publication [9].

This work aims to use the CO_2 + PDMS systems above to measure hydrodynamics in a packed column under SF conditions on a pilot plant scale. Specifically, this paper focusses on defining column operability, and the influence of fluid properties thereon, by using the mass fraction liquid in the overheads, liquid hold-up in the column packing, and the pressure drop over the packed bed. From the mass fraction liquid in the overheads, column operability is determined, while the pressure drop and liquid hold-up are used to confirm and investigate the nature of the inoperability (flooding/entrainment) and hydrodynamic operating regimes. Finally, the influence of the fluid properties of density and dynamic viscosity, of both the liquid and SF phases, on the various hydrodynamic phenomena was investigated and discussed. Notably, experiments were performed using a random packing, ¼ " Dixon Rings. Data in the literature are predominantly available only on structured packing.

6.2 Materials and Methods

6.2.1 Experimental Equipment

A pilot plant capable of operation up to 30 MPa and 473 K was previously constructed in-house [11]. A basic process flow diagram of the experimental pilot plant is seen in Figure 6-1 with a legend in Table 6-1a). Specifications for the pilot plant are summarised in Table 6-1b), with packing variables provided by the supplier. The pilot plant consists of two columns, but for the work presented here, only the larger diameter column C 3-2 (38 mm diameter) was used to minimise wall effects. The setup is capable of measuring the pressure drop over the column, the liquid hold-up in the column, the rate of overheads and bottoms and the mass fraction liquid in the overheads.

6.2.2 Dry Pressure Drop Measurement

The dry bed pressure drop was measured while operating the column with only SF CO_2 flow. After reaching stable, equilibrium flow, as represented by a steady pressure drop over the column, the pressure drop was noted.[21] The SF flow rate was then changed, and time was allowed to ensure a new equilibrium. At the most, a measurably steady pressure drop was achieved after 30 minutes, confirmed by the measurement of the pressure drop over the column via an HMI/PLC Setup (averaged and recorded every 10 ms). This procedure was repeated to provide dry pressure drop data over a full range of SF flow rates over several days to ensure repeatability.

6.2.3 Wet Pressure Drop and Liquid Hold-up Measurement[22]

For a single liquid + SF flow rate combination, at a selected temperature and pressure, the column was first operated only with SF CO_2. After the column reached equilibrium with SF flow alone, the pressure drop over the column was noted, and the liquid feed started at a pre-determined rate. The start time of the liquid flow was noted. The column was then allowed to reach a new equilibrium, indicated by a steady pressure drop reading over the column for at least 5-10 minutes, after which the pressure drop was again noted. All flow to the column was then simultaneously shut off, the valves to Bottoms Vessel V 3-1 closed, and the time noted. The total runtime was then determined.

---

[21] An example of equilibrium determination can be found in Appendix E.1, including how the equipment was zeroed

[22] A supplementary discussion on the bottoms removal method, liquid hold- up determination, and the involved equipment can be found in Appendix E.2

The Bottoms Vessel V 3-1 was then drained and the liquid weighed, as well as the column tops from Overhead Product Separator Vessel V 2-1. The valve between the column and Bottoms

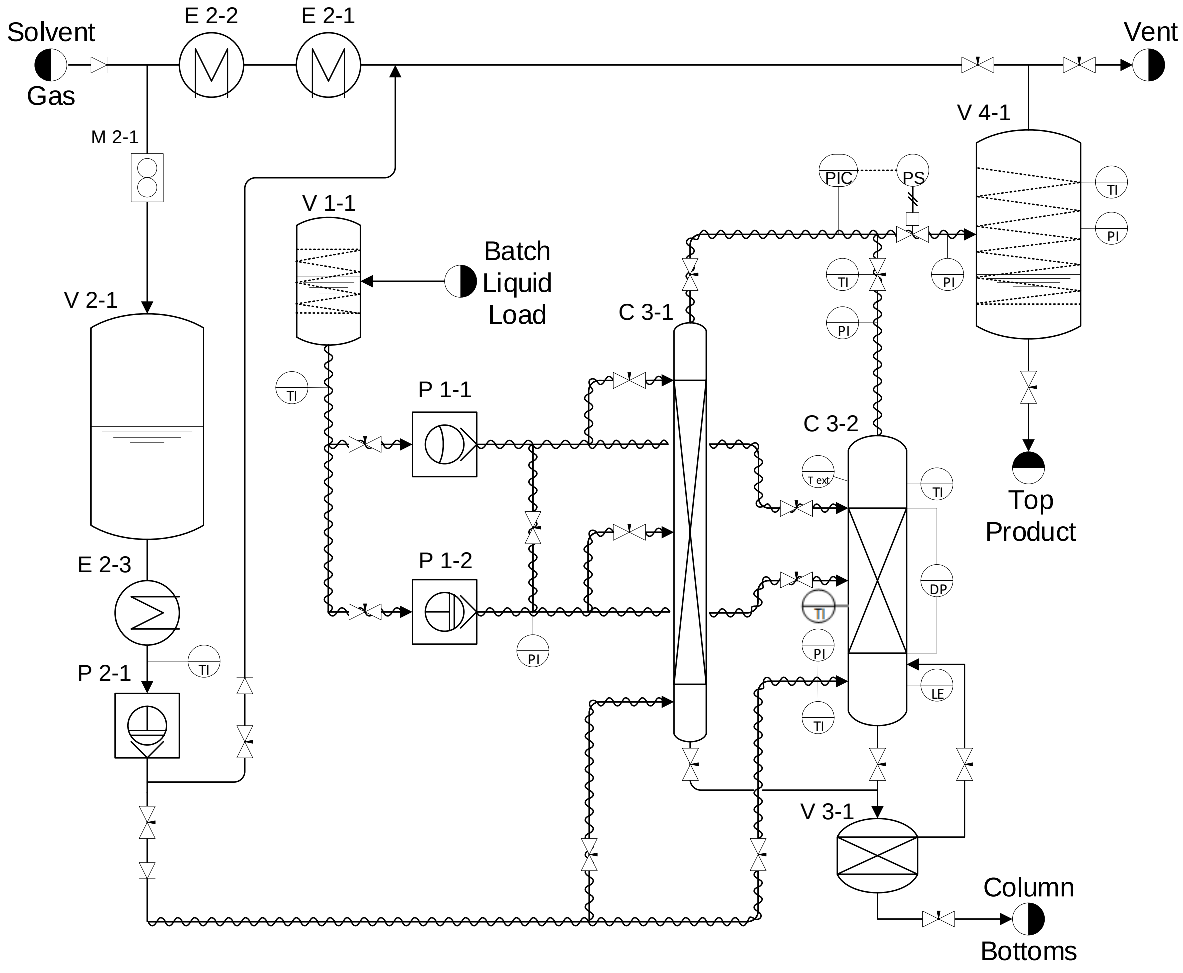

Figure 6-1- Schematic representation of the pilot plant set-up.

Table 6-1: a) Legend for Figure 1. **b) Pilot plant specifications.**

Label	Description
V 1-1	Liquid Feed Tank
P 1-1	Small Capacity Diaphragm Pump
P 1-2	Large Capacity Piston Pump
E 2-1	Water Pre-cooler
E 2-2	Chilled Condenser
M 2-1	Mass Flow Meter
V 2-1	Solvent Buffer Tank
E 2-3	Pump Feed Chilled Pre-cooler
P 2-1	Solvent Diaphragm Pump
V 3-1	Bottoms Vessel
C 3-1	Small Diameter Column
C 3-2	Large Diameter Column
V 4-1	Overhead Product Separator Vessel

Description	Values
Maximum system pressure	30 MPa
Maximum system temperature	473 K
Separator pressure	~5 MPa
Liquid flow rate range	0 - 8 ℓ/h
SF flow rate range	0 - 55 ℓ/h
Column C 3-1 Diameter	17 mm
Column C 3-1 Packed Height	3.5 m
Column C 3-2 Diameter	38 mm
Column C 3-2 Packed Height	1.5 m
Column Packing	1/4'' Dixon Rings
Packing void fraction - ϵ	91 %
Packing surface area	900 m^2/m^3
Particle diameter (const.) - d_p	0.6 mm

Vessel V 3-1 was then slowly opened to the column to allow the collected liquid hold-up to drain. The CO_2 feed was briefly resumed as needed to return the column to operating pressure and purge any liquid from the SF feed line. The hold-up was then slowly decanted and weighed. After no more liquid was decanted from the column for a 10-minute interval (with the time measured from the last liquid drained and then tested at roughly two-minute intervals), the column was deemed as drained, and the liquid hold-up noted. The drained liquid is tested to ensure that the dissolved gasses have evaporated, and is weighed as a solute, liquid only mass. The actual hold-up in the column is then calculated using the saturated fluid properties. The amount of gas soluble was found to be negligible even before degassing.

The experimental data are then used to calculate the actual liquid flow rates, using the overall runtime and recorded masses, as well as the respective component's mass fraction in the column bottoms and overheads. The mass balance over the column was checked using total mass drained from the column, compared to the expected mass [which was calculated using the selected pre-determined (calibrated) flow rate and runtime]. The flow rate combination and/or temperature was then changed as desired, after which the process was repeated to gather further data points. After every experimental set, the manually recorded pressure drop data were reviewed and inspected for stability using a comparison with the logged data captured by the HMI/PLC. The data review was to ensure data accuracy and stability in pressure, temperature and flow for every measurement.

6.2.4 Hydrodynamic Inoperability and Flooding/Entrainment

In this work, the hydrodynamic operability limits of the column and packing are investigated. The column is deemed hydrodynamically inoperable when it stops being a useful vessel for separation. Inoperability may be due to many different physical phenomena but is expected to be because of excessive liquid entrainment and liquid layer build-up/flooding. Both of these phenomena cause liquid to exit the column at the top, meaning the separation driven by phase behaviour alone is no longer possible.

During a mass transfer operation, the effectivity of a column increases as it approaches the inoperable state as the throughput and potential for interaction of the fluids is increased [12]. When the column reaches an inoperable state, its efficiency drastically decreases. Thus a column is ideally operated as close to inoperability as practically possible without causing flooding or excessive entrainment [12].

For this work, the column is deemed hydrodynamically inoperable at a particular datum through a series of checks done by holistically reviewing the full set of data. This definition avoids 'shortcut' rules of thumb for inoperability. A data point is suspected of inoperability if the mass fraction (solute) in the overheads exceeds 80% above the average mass fraction detected in other experiments at the same pressure and temperature, particularly those at very low liquid and SF flow rates where operability is expected, and the fraction falls within the solubility limits of the liquid. 80% is selected using phase behaviour data from prior work [9] and to allow for the accuracy of the equipment with regards to pressure- and temperature control, as well as the inherent variation and allowable entrainment expected in hydrodynamic experiments. This method uses data points where the column is known to be operable as a baseline to determine above operational liquid volumes in the overheads. A higher than average liquid fraction in the overheads (at known operable points) is a likely indicator of inoperability. This liquid fraction can indicate either entrainment, flooding or other hydrodynamic phenomena. Due to the lack of knowledge in supercritical systems, and the difficulty of visually confirming the physical processes, all the phenomena are grouped as inoperability. Regardless of the phenomenon, the column is no longer effecting a separation driven only by phase behaviour and is inoperable.

Data points that have been identified as potentially inoperable using the solute mass fraction data are then correlated to their respective pressure drop and liquid hold-up data. Therefore the main criteria is the fraction of liquid in the overheads, with the behaviour of the pressure drop and liquid hold-up relative to the rest of the body of data indicating whether the column has flooded, or if bulk entrainment is occurring. This definition ensures inoperability is connected to an actual measure of the column's ability to effect the required separation. The determination of operability will be discussed for each experimental system in the results section, separately.

6.2.5 Pressure and Temperature Considerations

For these experiments, an operating pressure of ~14 MPa and a temperature range of ~323.15 – 333.15 K was selected. These temperature/pressure combinations produce fluid properties similar to real, industrially applicable systems (~850 – 900 kg.m^{-3} and ~2 - 4.5 mPa.s). Further, these temperature/pressure combinations allow some overlap in the fluid properties, with similar densities having different viscosities. This fluid property overlap can be used to partially isolate the respective impacts of viscosity and density on hydrodynamics. The fluid properties for the saturated fluids used in the experiments are summarised in Table 6-2 across the temperature ranges investigated.

Table 6-2: Fluid properties for the respective saturated phases at 14 MPa [9]. The respective SF and liquid phases are indicated by their major components.

	100 cSt PDMS			200 cSt PDMS		
Saturated phase properties:	323.15 K	328.15 K	333.15 K	323.15 K	328.15 K	333.15 K
SF CO_2 Dynamic Viscosity (mPa.s)	0.0531	0.0474	0.0421	0.0531	0.0474	0.0421
PDMS Dynamic Viscosity (mPa.s)	2.11	2.48	2.86	3.40	3.87	4.42
SF CO_2 Density (kg/m^3)	672.2	618.5	561.4	672.2	618.5	561.4
PDMS Density (kg/m^3)	872.9	871.5	870.0	874.0	869.5	864.1
CO_2 mass frac in Liquid phase (g/g)	0.474	0.426	0.379	0.467	0.424	0.381
Phase density difference (kg/m^3)	200.7	253.0	308.6	201.8	251.0	302.7

$u(T) = 1.5$ K; $u_c(\rho_L) < 0.003 \cdot \rho$ kg/m^3; $u_c(\eta_L) \leq 0.01 \cdot \eta$ mPa.s

It is important to note that, contrary to intuition, the PDMS-rich liquid dynamic viscosity drops with a drop in temperature under isobaric conditions, meaning the fluid is more mobile at lower temperatures [9]. This viscosity drop is due to more CO_2 being soluble in the PDMS at lower temperatures, plasticising the polymer. The liquid density stays mostly unchanged with changes in temperature, while the SF density increases with a decrease in temperature [9].

The solubility of the solute into the supercritical phase is especially relevant to hydrodynamic studies, as the highest density solvent is found at the top of the column. This causes a density gradient that can cause unstable operation and back mixing of the solvent [13]. The selected system shows a minimal change in solvent density from pure properties, eliminating this potential problem and simplifying the interpretation of the hydrodynamics.

Finally, at 14 MPa, only a small amount of PDMS is soluble in the SF phase (<< 1 wt%). The low solubility ensures that the properties of the SF phase were assumed to be virtually identical to that of pure SF CO_2 at the same temperature and pressure [9]. The low PDMS solubility is also an advantage when determining hydrodynamic inoperability, as small increases in the overheads' liquid flow are easily detected. CO_2 solubility into the PDMS at these conditions was, however, still significant (~30 - 40 wt%) and was taken into consideration.

6.2.6 Column Wall Effects

The significance of potential wall effects in the column need to be addressed as the column is of a very small diameter. The estimated size of the boundary layer on the column wall, δ , can be calculated to serve as an indicator of possible column wall effects. The boundary layer can be calculated by [14]:

$$\delta = \left(\frac{3.\mu_L.D}{4.\rho_L.g} \right)^{1/3} \text{ for laminar flow, } \mathrm{Re}_L < 2100 \qquad \{6\text{-}1\}$$

where:

$$\mathrm{Re}_L = \frac{\rho_L.u_L.\mathrm{D}}{\mu_L} \qquad \{6\text{-}2\}$$

and μ_L is the liquid dynamic viscosity, D the column diameter, ρ_L the liquid density, g the gravitational acceleration = 9.81 m/s^2 and u_L the liquid superficial velocity.

As the effective liquid feed rates to the column are very low (maximum ~1.4mm/s), the Reynolds numbers during experiments were well within the bounds of laminar flow ($\mathrm{Re} \approx 1\text{-}30$). The maximum boundary layer thickness on the column wall was calculated using equation {6-1} was <1.7 mm, which is well below the column inner diameter of 38mm (~4.5% of D). This diameter calculates to a worst-case of 7-17% of the available cross-sectional area taken up by annular flow. The small boundary layer thickness assures that the column wall effects are unlikely to have a significant effect on the effective column diameter and hence on flooding/operability behaviour. The boundary layer on the packing is a different, much more complicated matter, dependant on the approximation of the packing, and will not be addressed in this paper as it is focussed on the determination of practical operability.

6.2.7 Measurement and Uncertainty

Uncertainties are primarily Type B standard uncertainties as defined by the Guide to the expression of uncertainty in measurement [15] unless stated otherwise. The interested reader is referred to the Guide for the standard calculation methods of uncertainties. Uncertainties are summarised in Table 6-3. Where relevant uncertainties are determined through repeated measurements, such as the temperature, pressure and liquid flow rate, to name a few.

Table 6-3: Reported uncertainties.

Parameter	Uncertainty type	Propagated Error		Equation form
Temperature	Combined Standard	1.5	K	$u_c(T) = 1.5$ K
Pressure	Combined Standard	0.4	MPa	$u_c(P) = 0.4$ MPa
Pressure Drop	Combined Standard	37.5	Pa	$u_c(\Delta P) = 37.5$ Pa
SF flow rate	Combined Standard	< 0.5%	mm/s	$u_c(u_G) = 0.005 \cdot u_G$ mm/s
Liquid flow rate	Combined Standard	< 6 %	mm/s	$u_c(u_L) = 0.06 \cdot u_L$ mm/s
Density	Combined Standard	< 0.3 %	kg/m³	$u_c(\rho) < 0.003 \cdot \rho$ kg/m³
Dynamic Viscoity	Combined Standard	≤ 1 %	mPa.s	$u_c(\eta) \leq 0.01 \cdot \eta$ mPa.s

6.2.7.1. Temperature

The temperature was measured throughout the pilot plant at crucial points, including along the length of the column, using J type thermocouples accurate to within 1.5 K. Temperature measurement points can be seen in Figure 6-1. Thermocouples were in direct contact with the fluids, unless indicated otherwise on Figure 6-1, to ensure accurate measurement and rapid response, while others measure on the external surface of vessels to measure longer-term temperature creep. Experiments were only performed after the pilot plant reached thermal equilibrium.

The thermocouples were calibrated before major experimental sets using a handheld Testo 720 PT 100; itself calibrated to a standard uncertainty of < 0.2 K by Thermon South Africa (Pty) Ltd. [a SANAS (South African National Accreditation System) and ISO 17011:2004; ISO 9001:2008 accredited laboratory]. The combined standard uncertainty in temperature was calculated as $u_c(T) = 1.5$ K.

6.2.7.2. Pressure

The pressure was measured and controlled at the top of the column using a pressure transducer with an uncertainty of 0.2 MPa [16]. The pressure transducer was calibrated to a standard uncertainty of 0.02 MPa before major experimental sets, using a Barnett Industrial deadweight tester, itself calibrated to a standard uncertainty smaller than 0.01 MPa by Unique Metrology (Pty) Ltd. (SANAS accredited). Considering repeatability, sensor hysteresis, control instability and human errors, it was determined that the combined standard uncertainty is at worst 0.4 MPa of the phase equilibria pressure measurements. Control instability and the sensor's inherent uncertainty are the most significant contributors. Therefore $u_c(P) = 0.4$ MPa.

6.2.7.3. Pressure drop

The pressure drop over the column is measured using an Endress+Hauser Deltabar S PMD75 DP Cell. The DP Cell is connected to the column via temperature-controlled capillary tubes. The unit was pre-calibrated by the supplier to within 0.075% of its 50 kPa range, being 37.5 Pa. Therefore the uncertainty in pressure drop is $u_c(\Delta P) = 37.5$ Pa.

6.2.7.4. SF and Liquid Flow Rates.

The CO_2 mass flow rate is measured as a liquid after the separator using a Micro Motion D12 flow sensor and an RFT 9729 remote flow transmitter. The unit is manufacturer calibrated for supercritical fluids and automatically corrects for temperature. The manufacturer reports the accuracy of the complete flow assembly as ±0.2% of the current mass flow rate plus ±0.01% of the sensor upper range limit. The mass flow is converted into a superficial SF velocity, u_G, through calculation. The combined standard uncertainty for the final value is $u_c(u_G) = 0.005\ u_G$ (mm/s)

The PDMS flow is delivered using a LEWA EL1 metering pump. The pump operates on a positive displacement principle, ensuring that an accurate volume is delivered for each pump stroke. The flow rate was manually calibrated, yielding a straight-line correlation for volumetric flow with $R^2 = 0.999$ and uncertainty of 0.016·slope. The liquid flow rate is validated by doing a mass balance over the column. Including the conversion to superficial liquid velocity, u_L, the combined standard uncertainty is calculated as $u_c(u_L) = 0.06\ u_L$ (mm/s)

6.2.7.5. Other

Other uncertainties are as quoted in the literature source for the fluid properties [9], being uncertainty in density and dynamic viscosity, are:

$u_c(\rho_L) < 0.003\ \rho_L$ kg/m^3 and $u_c(\eta_L) \leq 0.01\ \eta$ mPa.s.

6.2.8 Materials Used

Purities and suppliers of the materials used during experiments are summarised in Table 6-4. Chemicals were used without further treatment or purification. The PDMS used is methyl group capped and effectively linear, with few side chains. The phase transitions, density, and dynamic viscosity at saturation of the CO_2 + PDMS systems are published elsewhere and will not be discussed here [9].

Table 6-4: Chemicals used in this study.

Chemical	Purity	Supplier	CAS Number
CO_2	99.95%	Afrox Oxygen Ltd.	124-38-9
PDMS 100	Absolute	Xiameter PMX-200 (DOW Corning)	63148-62-9
PDMS 200	Absolute	Xiameter PMX-200 (DOW Corning)	63148-62-9

6.3 Results and Discussion

6.3.1 Dry Pressure Drop

Measurements of the dry pressure drop behaviour for this column has been reported in a prior publication [8], but results are depicted and expanded upon here to present a complete picture of the work performed.

The dry pressure drop per unit length of dry packing, $\Delta P_0/H$, was measured at 313.15 K. A model fit was done on the gathered data using a modified Ergun-type equation [17]. The equation expresses a packed column friction factor, ψ , as a function of the gaseous Reynolds number:

$$\frac{\Delta P_0}{H} = \frac{3\psi \rho_G u_G^2 (1-\in)}{4 d_p \in^{4.65}} \quad \text{or} \quad \psi = \frac{K_1}{\mathrm{Re}_G} + K_2 = \frac{4}{3} \frac{\Delta P_0 \in^{4.65} d_p}{H(1-\in)\rho_G u_G^2} \qquad \{6\text{-}3\}$$

where $\in$ is the fractional void volume, d_p the particle diameter (a packing dependant constant) and ρ_G and u_G the respective density and superficial velocity of the supercritical phase. The superficial velocity is calculated by dividing the volumetric flow rate by the column cross-sectional area. K_1 and K_2 are empirically determined constants that are dependent on the geometry of the packing used. For the gathered data, the model constants are determined as $K_1 = 459$ and $K_2 = 4.11$.

It is seen in Figure 6-2 that the model fit the data well, falling well within a 20% margin of error as expected from a fitted, semi-empirical equation. The model predicts the data to within 5.8 % average absolute deviation, with a maximum deviation of 15.1 %. The model fit serves to show that the data follows the expected trend and shows excellent repeatability and accuracy. Notably, the derived constants are of the same order of magnitude as those derived by Stockfleth and Brunner [18] (K_1 = 23-155; K_2 = 0.2-3.4) for a column operating under supercritical conditions with various packings.

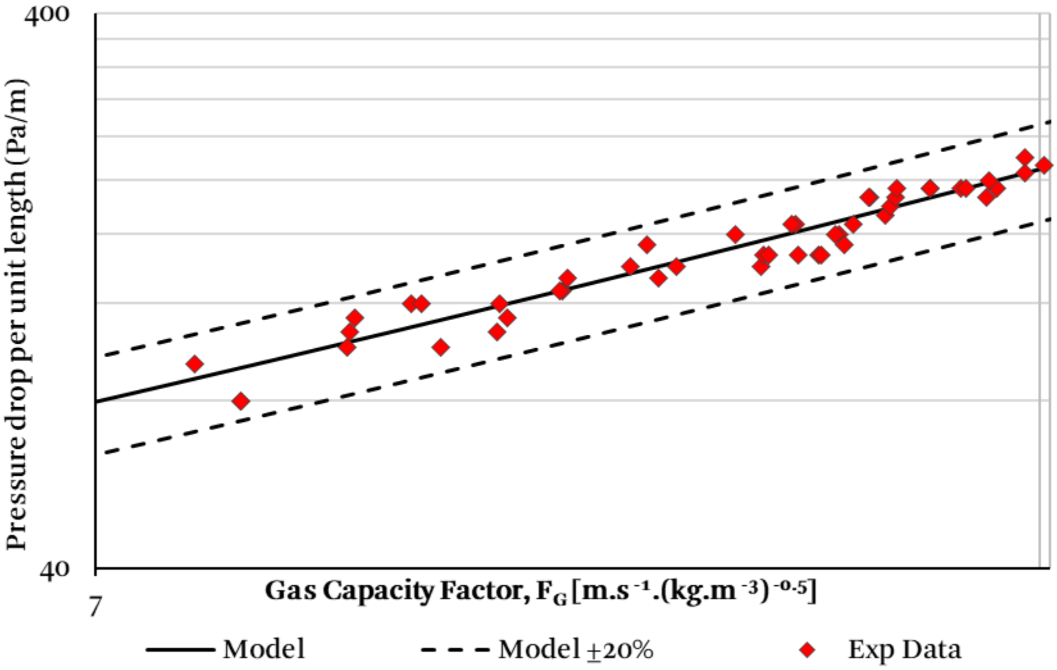

Figure 6-2: Dry pressure drop and model prediction at 14 MPa and 313.15 K for ¼ " Dixon Rings and SF CO_2. Note logarithmic axes.

After the wetted experiments, the liquid hold-up was allowed to drain between experiments and the pressure drop was again measured with only the SF phase on the 'wetted' column. It was found that the dry pressure drop data, with the column containing no liquid at all, showed no significant difference to the pressure drop data of a wetted column without liquid flow once equilibrium was reached. This result implies the column had negligible static hold-up, or the influence of any static hold-up remaining was insignificant. This observation is in agreement with the literature, with Stockfleth et al. [18] stating that static hold-up typically decreases to negligible levels at high pressure due to the reduction in liquid surface tension.

This agreement with the dry pressure drop proved a handy check to ensure no liquid was present in the DP Cell capillaries. The capillaries were purged between experiments, but any residual liquid in the capillaries would skew the differential pressure measurement. If a difference was detected, the capillaries were purged again, and the measurement repeated.

6.3.2 100 cSt PDMS + CO_2

Data were measured for the system 100 cSt PDMS + CO_2, henceforth shortened as the '100 cSt system'. The wet pressure drop, liquid hold-up, and mass fraction PDMS in the overheads are presented for individual temperatures and across four SF flow rates in Figure 6-3, with A) - C) at 333 K and D) - F) at 328 K. The system achieved inoperability rapidly at 323 K yielding only a single operable data point at low SF and liquid flow rates. No measurements were possible at lower temperatures. The data for 323.K experiments are presented and discussed when comparing data for a single SF flow rate over multiple temperatures, in Figure 6-5.

From Figure 6-3 A) + B), and D) + E) it is seen that the wet pressure drop over the column and liquid hold-up in the column show interaction for the 100 cSt system, with both the pressure drop and liquid hold-up increasing with an increase in the superficial velocity for most of the observed data. The more hold-up, the less of the cross-sectional area is available for supercritical fluid flow, and the higher the pressure drop. To provide a frame of reference for this reduction, the ratio of the superficial liquid and gas velocities at inoperability, u_G / u_L or G/L, is used.

It is important to note that the analysis of the experimental results is done from a framework of distillation / fractionation and gas-liquid systems. Comparison with liquid-liquid systems are made in specific instances where relevant. In truth, supercritical processes are neither purely gas-liquid like nor liquid-liquid like, however, the literature has stated that it is better to compare to gas-liquid systems [13]. This argument is based on the fact that supercritical fluids have a larger kinetic energy than potential energy, making it more analogous to the gas-liquid system.

Inoperability tended to occur more readily with increasing liquid flow rates, as expected [seen in Figure 6-3 C) and F)]. The operable range, however, varied significantly in magnitude between different temperatures and SF flow rates. Operability showed some dependence on SF flow, with operability tending to decrease with increasing SF flow. Operability also decreased with a decrease in temperature at a specific SF flow rate. Three modes of inoperability were identified with the help of pressure drop and liquid hold-up data. This discussion complements prior work which investigated flooding in particular, where two modes of flooding were identified for the same system [8]. It is important to note that the identified inoperability mechanisms, such as entrainment, liquid layer flooding and bubble column flooding, are purely hypothetical and could not be observed visually. There is, however, merit in trying to connect the observed behaviours back known column inoperability behaviours in an attempt to better understand and discuss the complexity of supercritical hydrodynamics.

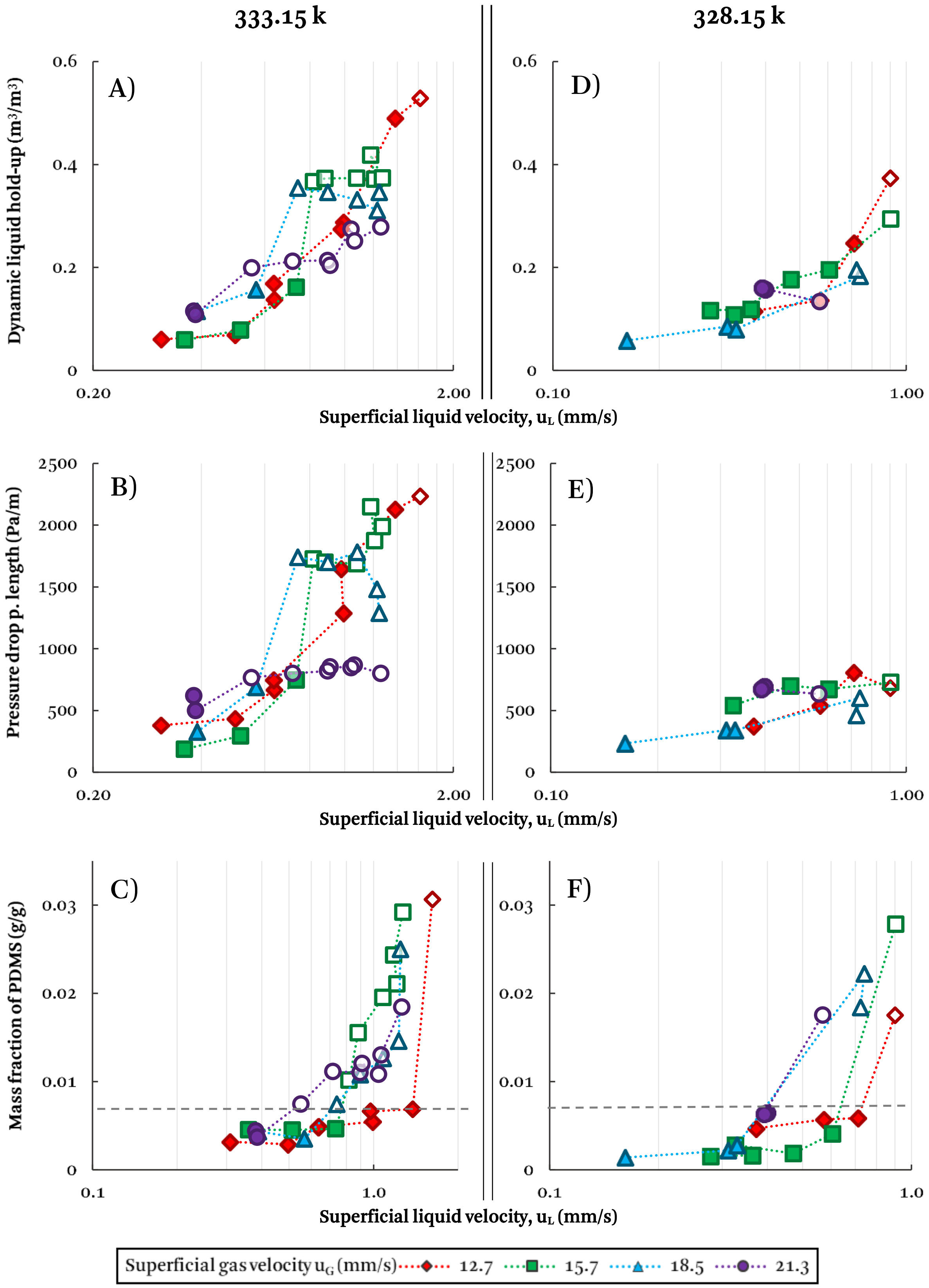

Figure 6-3: CO_2 + PDMS 100 cSt hydrodynamic data at 333.15 K (left) and 328.15 K (right). A) & D) Liquid Hold-up, B) & E) Pressure Drop and C) & F) Mass Fraction PDMS in the overheads. Note the logarithmic scale for the superficial liquid velocity in figures A), B), D) and E). All unfilled markers indicate states deemed as inoperable. The dashed line in figures C) and F) represents the 80% cut off line for operability.

Firstly, similar operability trends were found A) at high liquid rates and low SF flow rates at 333 K (u_G = 12.7 mm/s), and B) in all systems measured at lower temperatures (328 - 323 K). Under these conditions increasing the liquid flow caused a considerable step change in the mass fraction PDMS in the overheads, causing inoperability. Inoperability is accompanied by a disproportionately small step in the corresponding pressure drop and hold-up. The pressure drop and liquid hold-up showed a gradual increase, regardless of the operability, except for some of the data at lower temperatures where the pressure drop decreased after inoperability.

The first inoperability behaviour is attributed to the column flooding at the top, with the liquid layer on top of the packing being pushed out of the column through the overheads, causing the column to lose separation efficiency. This behaviour is similar to the "liquid layer flooding" reported by Stockfleth and Brunner [4]. For the system at 333 K and u_G = 12.7 mm/s specifically, inoperability was accompanied by an intermittent, fluctuating pressure drop over the column under 'equilibrium' conditions. As indicated in prior work [8], this pressure instability is thought to be an indication of "slugging" behaviour, see Figure 6-4.

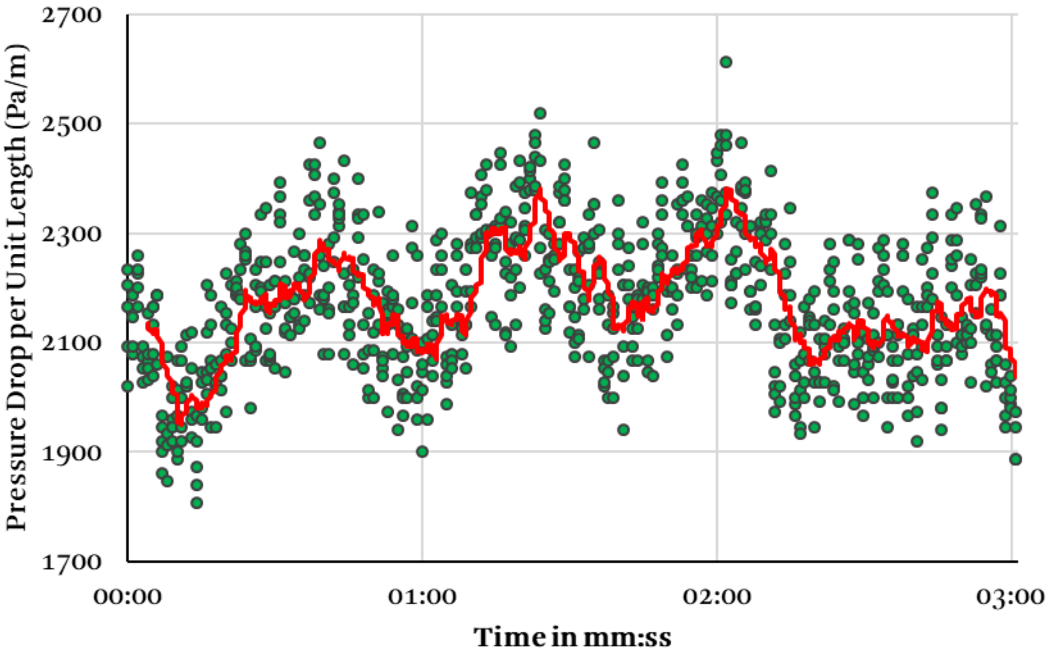

Figure 6-4: Pressure drop instability at inoperability, 333.15 K, u_G = 12.7 mm/s and u_L = 1.6 mm/s.

For this inoperability mode, a G/L ratio of ~8 for the 333 K system, ~12, 16, 23 and 35 for the 328 K system and ~30 for the 325 K system was found. For this mode of inoperability it seems as though there was no commonality in the fluid flow rate ratios at which flooding occurred, and indeed similar flooding behaviour was observed over a range of different fluid flow ratios for the 328 K system. The fluid flow ratio required to render the column inoperable increased as the superficial 'gas' velocity increased. Using a Souders-Brown [19] analysis, a maximum ‘vapour’ velocity can be calculated as 58 – 79 mm/s. These values are significantly higher than the superficial gas velocities investigated here. This strengthens the argument that inoperability is significantly affected by the fluid properties and that a gradual build-up of liquid is responsible for flooding in this case, as the interaction between the phases is not significant enough to cause rapid flooding. A higher supercritical phase velocity will, however, reduce the time required for the liquid build up to occur due to a higher nett upwards force. It is likely that entrainment plays a large role in some of the points with higher G/L ratios.

Secondly, inoperability was identified that caused a sharp increase in the liquid hold-up and pressure drop (with an increase of liquid flow rate). This behaviour was noted in medium liquid- and SF flow rates at 333.15 K, as is seen for 15.6 - 18.5 mm/s range in Figure 6-3 A) to C). The significant jump in pressure drop and hold-up is noteworthy. This behaviour is typically connected with flooding in atmospheric hydrodynamics, akin to the definition of a “finite change in the gas or liquid velocity causing an infinite change in the pressure drop or hold-up” [18]. The behaviour matches the “bubble column flooding” described by Stockfleth and Brunner [4] under supercritical conditions and is analogous to flooding found in liquid-liquid extraction columns, being sudden and significant. Without a way to visually confirm any of the behaviours, it is difficult to pinpoint the exact inoperability phenomenon, and further study is required to confirm. It is, however, hypothesised that for this behaviour the liquid in the column starts building up from the narrowest point in the packing, forming a continuous liquid phase in the column. From there, the liquid then propagates upwards causing flooding and inoperability. The overheads fraction in this state is dependent on when the experiment is terminated. As the column flooding was detected by monitoring the column overheads, the overheads will indicate flooding, the magnitude of the value has no inherent meaning.

For this inoperability mode, a G/L ratio of ~19-20 was found for both systems. As both systems had very similar ratio at which inoperability occurred it is likely that this system is rendered inoperable by the specific combinations of liquid and supercritical flow.

Finally, at the highest SF flow of $u_G = 21.4$ mm/s at 333.15 K, there is no significant step in either the liquid hold-up and pressure drop or the mass fraction in the overheads with inoperability. Instead, the pressure drop, hold-up and mass fraction PDMS gradually increased with an increase in liquid flow. It is hypothesised that this inoperability occurs when the SF flow is above a critical minimum; i.e. where the SF phase flow is fast and forceful enough to carry all but a trickle of the liquid PDMS directly out of the column. With most of the liquid ‘shortcutting’ to the overheads, the column does not get liquid building up in the packing, and the subsequent increase in the liquid hold-up and dependant pressure drop does not happen. Depending on the experiment, between 18 – 45 % of the liquid entering the column, exited through the overheads. This behaviour is analogous to entrainment, seen in atmospheric columns, although the behaviour observed here is somewhat more extreme. Entrainment adds the third mode of operability above the flooding observed in prior work [8]. It is believed this is due to the higher density and viscosity of the supercritical phase (to be discussed in more detail in Section 3.4).

For this inoperability mode, a the highest G/L ratio of ~39 was found. This is almost double that of the prior mode of inoperability and implies that the 'gas' is simply over powering the liquid flow in the column, in agreement with mass entrainment.

To further analyse the data, the typical hydrodynamic operating regimes are considered [12]. Firstly, the pre-loading zone is an operating regime ordinarily present at very low fluid flow rates where the interaction between phases is negligible. The pre-loading zone is identified through the change in hold-up and pressure drop with variation in fluid flow. Firstly, hold-up does not change with an increase in SF flow and increases linearly with an increase in liquid flow (seen as a slight curve on the single log axis graph). Secondly, pressure drop increases with an increase in liquid flow. The loading zone follows the pre-loading zone. In the loading zone, an increase of either the SF or liquid fluid flow rate increases both the liquid hold-up and pressure drop exponentially. Finally, the column is deemed flooded/entrained according to a chosen definition of hydrodynamic inoperability.

Applying these definitions to the gathered data, it is seen in Figure 6-3 A) and D) that the liquid hold-up, and even pressure drop, does not change significantly with an increase in SF flow (u_G) within the operable limits of the column. This lack of change suggests that the column is operating in the pre-loading regime in its operable limits. This observation is in agreement with published data by Stockfleth and Brunner [4]. Stockfleth and Brunner suggested that the loading zone is undetectably small in supercritical columns. It can, therefore, be postulated that the system was going from the no-interaction, pre-loading regime to an inoperable state almost immediately without a detectable transitional loading zone. The loading regime is a convention of atmospheric hydrodynamics, and it is argued that its absence can be attributed to the fluid properties of the SF solvent phase. The significance of the SF phase is supported by literature data, with atmospheric silicone oil + air data available [20] showing a clear loading regime, despite a much higher effective dynamic viscosity than that of this work. In particular, the relatively high dynamic viscosity and high density of the SF phase plays a role in fluid interaction phenomena like droplet entrainment, interfacial shear stress and the formation of surface waves on the fluid, all of which play a role in the system presenting a loading regime. The higher fluid property values can cause these phenomena to be much more significant than in an atmospheric system, causing the lack of an observable loading regime. The significance of the loading regime (and the flooding point) is a common and important assumption in the development of classical hydrodynamic models. The lack of a detectable loading regime can explain why classical hydrodynamic models do not work well for the prediction of supercritical systems in some cases. Indeed, the observation of a rapid change from operable to inoperable conditions in the system has parallels with liquid-liquid extraction systems, where no loading regime is found.

Comparing the data across temperatures at the same SF flow rate, it is seen in Figure 6-5 A) + B) that inoperability started at increasingly lower liquid flow rates with a drop in temperature. Indeed with a relatively slight change in temperature, the change in operability was significant; with each 5 K drop virtually halving the column capacity. This temperature dependence emphasises the statement made in the introduction that a small change in temperature can have a considerable impact on hydrodynamics due to changing fluid properties. The effect of fluid properties on the overall column hydrodynamics is discussed in Section 6.3.4.

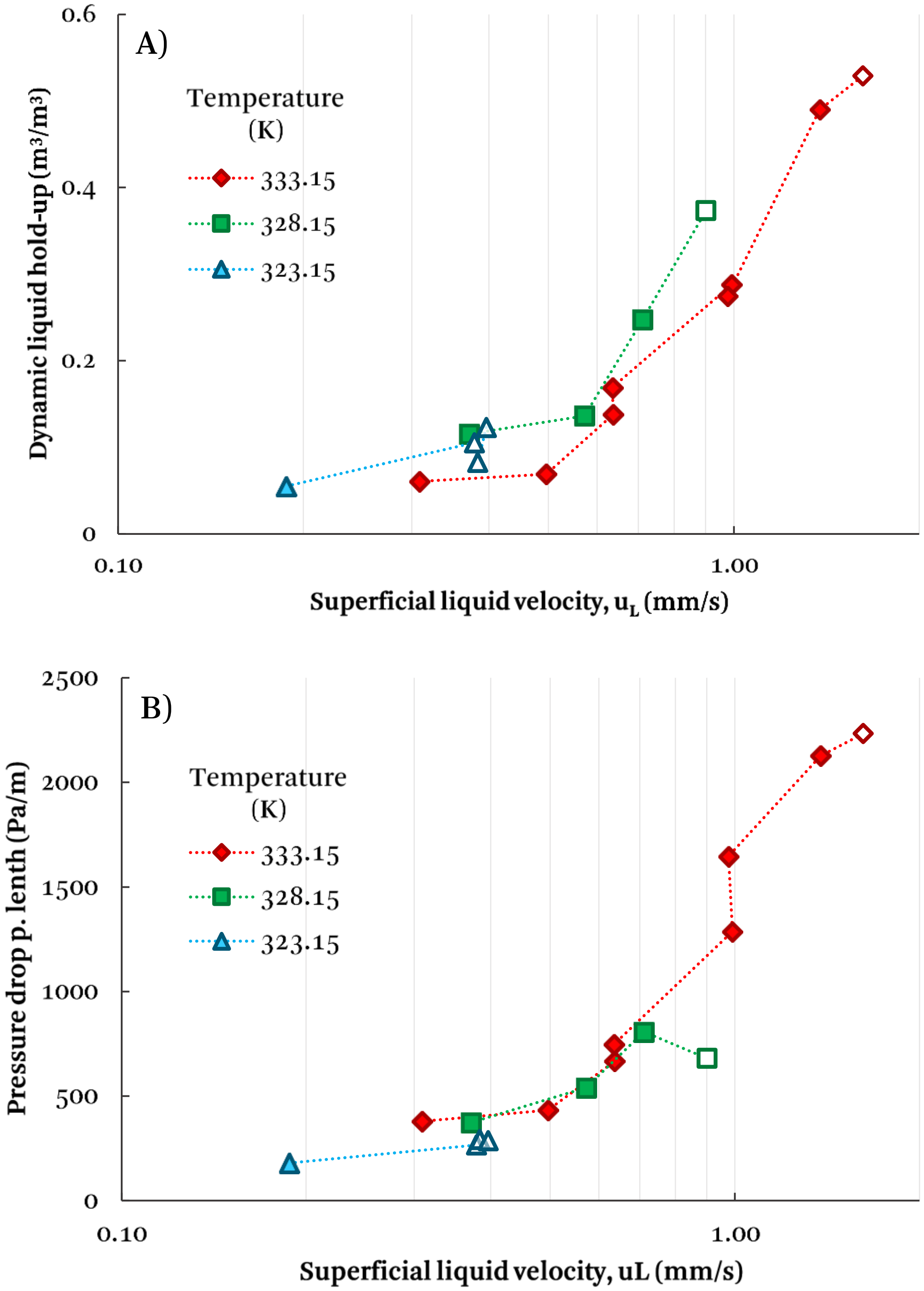

Figure 6-5: A) Dynamic liquid hold-up and B) pressure drop at $u_G = 12.7$ mm/s over three different temperatures for CO_2 + PDMS 100 cSt.
Note the logarithmic scale. All unfilled markers indicate states deemed as inoperable.

6.3.3 200 cSt PDMS + CO_2

Data were measured for the system 200 cSt PDMS + CO_2, henceforth shortened as the '200 cSt system'. Like the 100 cSt system, the 200 cSt system was also measured at 333 K, 328 K and 323 K. The wet pressure drop, liquid hold-up, and mass fraction PDMS in the overheads are presented for the individual temperatures across four SF flow rates in Figure 6-6, except for 323 K which again yielded only one operable datum which is displayed in Figure 6-7. The system's behaviour with changing temperature is presented for a single flow rate across all the temperatures in Figure 6-7.

As for the 100 cSt system, the wet pressure drop over the column and liquid hold-up in the column for the 200 cSt system are positively correlated, as seen in Figure 6-6 A) + B) and D) + E). Operability is again determined with the help of the mass fraction liquid in the overheads, seen in Figure 6-6 C) and F). The operability of the 200 cSt system shows different trends to that of the 100 cSt system. There is less variation in operability, with all the data points at a single temperature showing similar behaviour regardless of flow rate. Two modes of hydrodynamic inoperability are identified.

Firstly, operability for the measurements at lower temperatures (328 – 325 K), seems to match 'liquid layer flooding' behaviour found for the lower temperature 100 cSt data. Inoperability occurs with a similar significant step increase in the overheads mass fraction. There is, however, some difference, as the liquid hold-up and pressure drop tends to decrease after the inoperability limit. This drop at higher flow rates implies that some element of entrainment is involved, and takes over from the liquid layer flooding. A visual study of the system would be needed to define the flooding mechanism at these conditions appropriately.

For this inoperability mode, the G/L ratios show the same variation as in the 100 cSt system, with ratios of ~18, 22, 29 and 32 for the 328 K system and ~20 for the 325 K system. This similarity helps to draw parallels between the systems. Significantly, the flooding behaviour is now only found at lower temperatures, where the density difference between the phases is lower and buoyancy plays a larger role. It is likely that entrainment is playing a significant role in this mode of inoperability at higher superficial 'gas' flow rates

Secondly, the 333 K system displays behaviour similar to the entrainment type inoperability noted in the 100 cSt system at 333 K and u_G = 21.3 mm/s. There are no disproportionate jumps in pressure drop or hold-up noted with the onset of flooding. Instead, the behaviour is similar to that of the u_G = 21.4 mm/s 100 cSt system, pressure drop and liquid hold-up increased proportionally. G/L ratios of ~21, 26, 28 and 34 were found for the 333 K system. The values are high enough to agree with entrainment as a culprit in themode of inoperability.

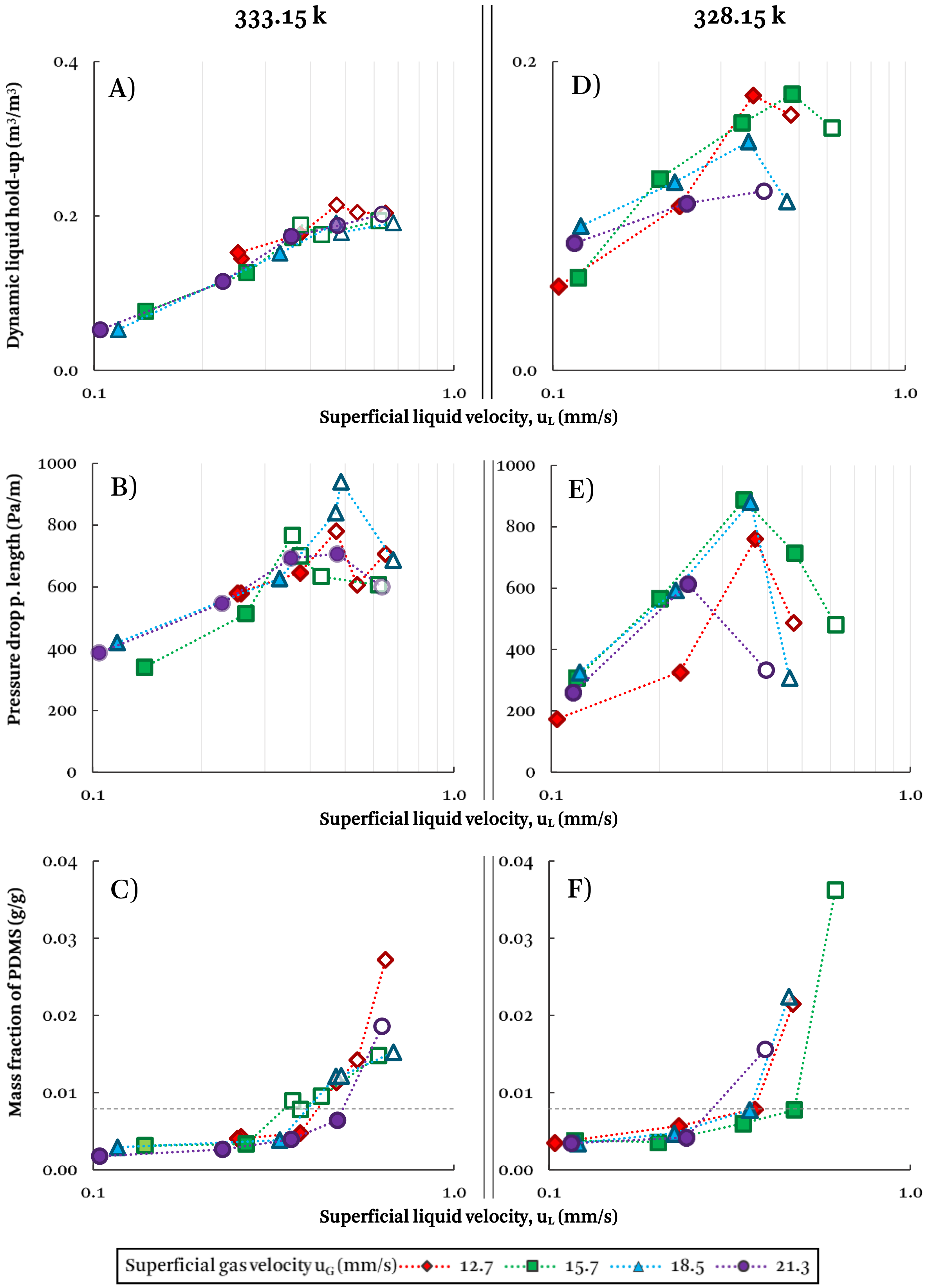

Figure 6-6: A) CO_2 + PDMS 200 cSt hydrodynamic data at 333.15 K (left) and 328.15 K (right) A) & D) Liquid Hold-up, B) & E) Pressure Drop and C) & F) Mass Fraction PDMS in the overheads. Note the logarithmic scale for the superficial liquid velocity in figures A), B), D) and E). All unfilled markers indicate states deemed as inoperable. The dashed line in figures C) and F) represents the 80% cut off line for operability.

Importantly, it is seen in Figure 6-6 that the liquid hold-up and pressure drop were not clear indicators of operability, failing to show a consistent pattern predicting a transition into an inoperable state. The pressure drop and hold-up either slightly plateaued and or decreased with an increase in liquid flow, contrary to typical behaviour at atmospheric conditions. Indeed, if only the pressure drop and liquid hold-up were used to analyse operability, a severe misrepresentation of the column capacity was possible. This potential for misprediction is also seen in the 100 cSt system, especially when comparing the very highest and lowest SF flow rate data in Figure 6-3 A) and B). Significantly, this shows that pressure drop and liquid hold-up alone cannot be used to define operability under supercritical conditions and knowledge of the mass transfer in the system and the overheads and/or bottoms compositions are required. The failure of pressure drop and hold-up to define operability emphasises some of the fundamental differences to atmospheric hydrodynamics. These differences are mainly driven by the very different set of fluid properties in an SF system (discussed in detail in Section 6.3.4).

Further analysing the overall curves, it is seen that the column was inoperable at much lower SF flow rates when compared to the equivalent 100 cSt systems. This reduced operability is attributed to the differences in phase properties between the two systems and will be discussed in Section 6.3.4.

Similar to the 100 cSt system, there is evidence of the column operating only in the pre-loading region, with hold-up and pressure drop data presenting as linear within operability limits. The hold-up data for the 200 cSt system is also linear between SF flow rates, with the different data sets coinciding with one another.

The 200 cSt system is seen to be less sensitive to temperature than the 100 cSt system when comparing the data in Figure 6-7. The operability range at 333 K and 328 K is very similar, while the 323 K system here also only yields one operable datum. The lack of a significant difference for the 200 cSt system opens up exciting possibilities for discussion of the influence of the fluid properties on hydrodynamics.

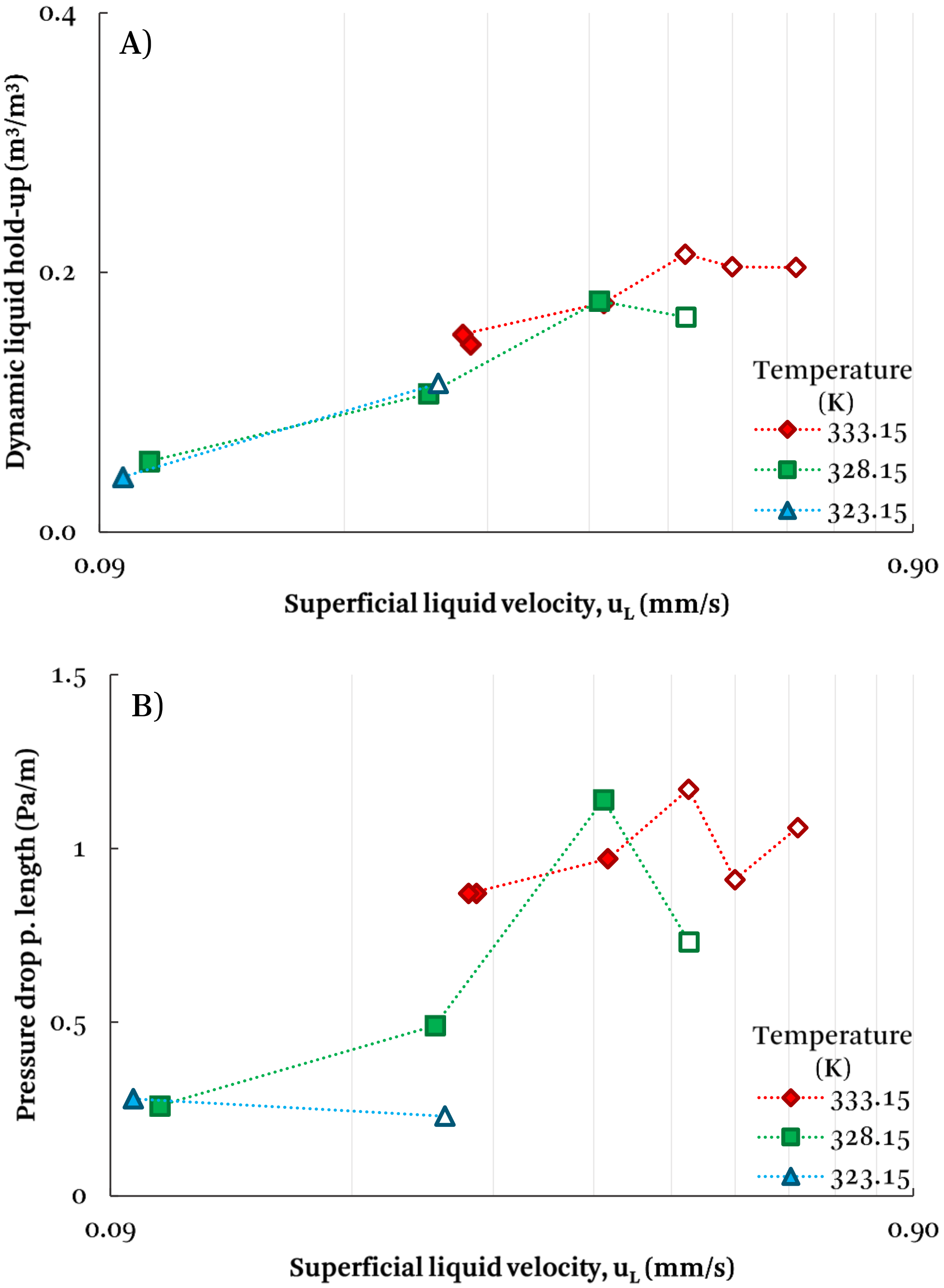

Figure 6-7: A) Dynamic liquid hold-up and B) pressure drop at $u_G = 12.7$ mm/s at three different temperatures for CO_2 + PDMS 200.
Note the logarithmic scale. All unfilled markers indicate states deemed as inoperable.

6.3.4 Influence of Fluid Properties on Hydrodynamics

In a prior publication, the effect of the change in the physical properties on hydrodynamics was briefly discussed for the system 100 cSt PDMS + CO_2 [8]. Notably, it was found that the column tended to inoperability more readily at lower temperatures where the density of the SF phase became closer to that of the saturated liquid, and the liquid dynamic viscosity decreased. Surface tension also changes with temperature, however, no conclusion could be made to its effect, as the values for the system were unknown.

For the 100 cSt system, the density difference between the phases varies from ~310 kg/m^3, ~250 kg/m^3 to ~200 kg/m^3, and the liquid dynamic viscosity decreases from ~2.86 mPa.s, ~2.48 mPa.s to ~2.11 mPa.s, as the temperature decreases from 333 K to 328 K to 323 K. The dynamic viscosity of the SF phase increases by ~25% as the temperature drops, approximately the same order of magnitude as the change in the liquid dynamic viscosity (as was shown in Table 6-2). It is hypothesised that as the temperature drops, several things happen to decrease the operability limits. 1) The smaller difference between the respective phase densities increases the effects of buoyancy, while 2), a decrease in the liquid dynamic viscosity increases the mobility of the liquid phase and 3) an increase of the SF dynamic viscosity increases the impact of interfacial phenomena. In the case of the 100 cSt system, all of these effects come together to induce column inoperability at lower temperatures.

The 200 cSt system provides us with the opportunity to separate the influence of the properties. Keeping in mind that as experiments were performed at the same temperature and pressure, the SF properties were the same for both systems. Considering the liquid properties of the 200 cSt system, the density difference over the experimental temperatures is virtually identical to the 100 cSt system, dropping from ~300 kg/m^3, ~250 kg/m^3 to ~200 kg/m^3. However, the dynamic viscosity is almost double that of the 100 cSt system, decreasing from ~4.42 mPa.s, ~3.87 mPa.s to ~3.40 mPa.s. The higher liquid dynamic viscosity of the 200 cSt system, while the other fluid properties are virtually identical to the 100 cSt system, allows us to isolate the effect of the liquid dynamic viscosity.

Combining Figure 6-5 and Figure 6-7, the two systems are directly compared in Figure 6-8. It is immediately evident that the 200 cSt system's operability is limited to much lower liquid flow rates than the 100 cSt system. Further, the 200 cSt system had significantly higher liquid hold-ups for similar flow conditions, although the pressure drop stayed very similar to that of the 100 cSt system (taking different inoperability behaviours into account). CO_2 solubility is similar for both systems, as can be seen from the similarity in system density and literature [9].

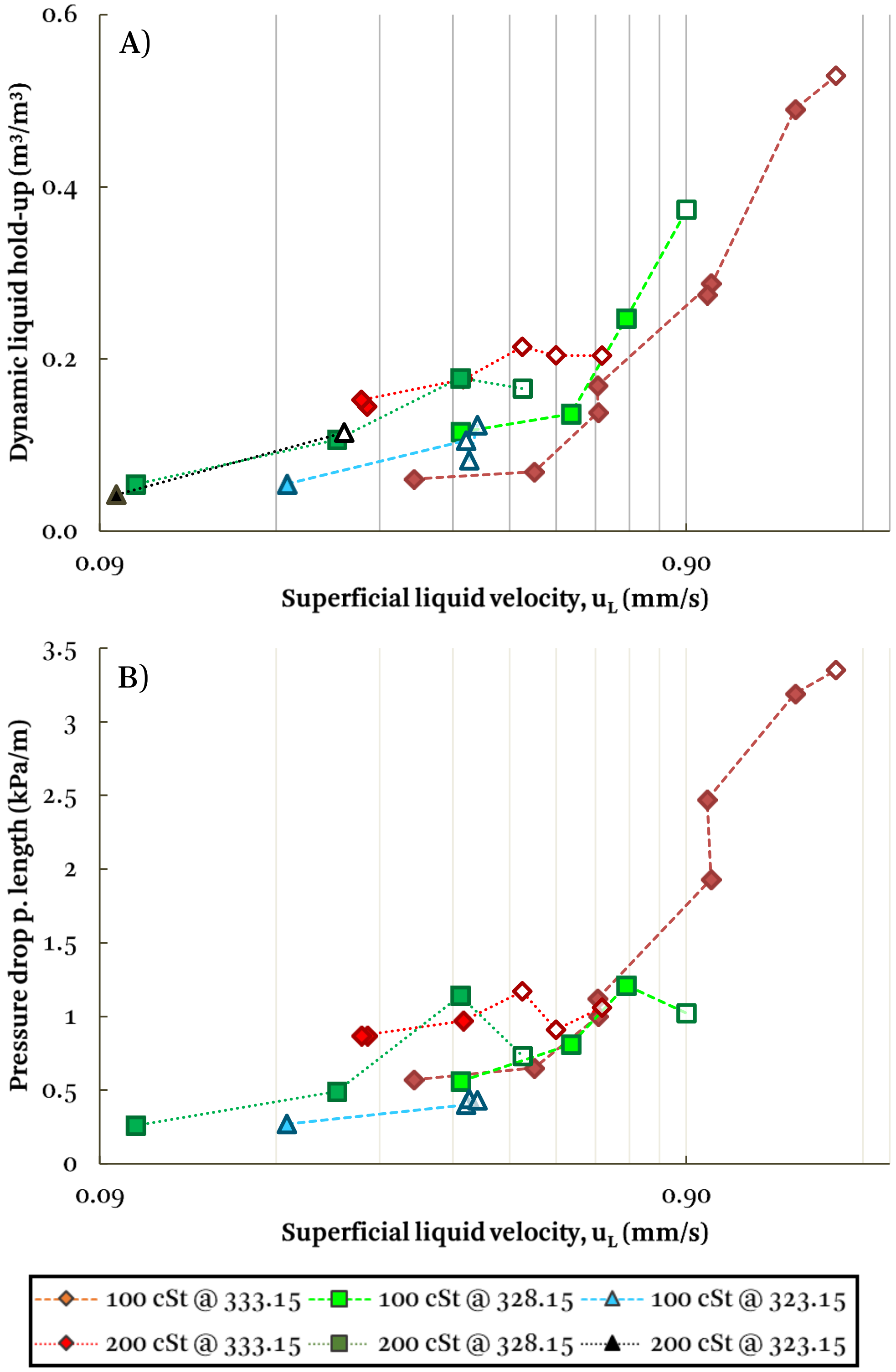

Figure 6-8: A) Dynamic liquid hold-up and B) pressure drop at $u_G = 12.7$ mm/s for three different temperatures for both the 100 cSt and 200 cSt systems.
Note the logarithmic scale. All unfilled markers indicate states deemed as inoperable.

The differences can be attributed to the different liquid dynamic viscosities, with other known fluid properties between the systems virtually identical, and the operating parameters unchanged. Surface tension also plays a significant role in film stability and droplet size, but as it could not be quantified for this work, it will be left out of this discussion. It is seen that a higher liquid viscosity decreases the column operability and increases the hold-up capacity. Liquid viscosity is directly related to the cohesive forces between molecules in the liquid [21]. Firstly, under atmospheric conditions a higher dynamic viscosity and cohesion would make it harder to shear off droplets, making entrainment less likely, and increasing the wettability of the system. Secondly, the higher viscosity also increases the thickness of the theoretical boundary layer, effectively increasing the liquid in the column while reducing the available flow area for the SF phase. In both cases, the liquid hold-up increases with an increase in viscosity. The above reasoning applies to SF systems, as substantiated by the data presented here.

Further investigating the influence of the properties, the change in hydrodynamic behaviour should be addressed. It is seen in Figure 6-8, in B) in particular, that the 100 cSt system at 333 K presented a more extensive operability range than any of the other systems. When comparing the system to its 200 cSt equivalent, at the same density difference and SF properties, it is seen that the higher dynamic viscosity (4.42 mPa.s vs 2.86 mPa.s) severely limits the operability. However, viscosity is not the only influencing factor. Comparing the 100 cSt system at 333 K with two systems having viscosities just lower and higher, 1) 2.48 mPa.s for the 100 cSt system at 328 K and 2) 3.40 mPa.s the 200 cSt system at 323 K, it is seen that the both of the other systems have a smaller operable range. The linear change in viscosity does not lead to a linear change in operability. This nonlinearity implies that liquid dynamic viscosity alone does not mandate the operability of the column. Between these systems, the density difference between phases changes from ~300 kg/m^3, ~250 kg/m^3 to ~200 kg/m^3. As the density difference decreases the operability of the column also dramatically decreases. The primary source of the change in density difference comes from the SF phase density. Therefore in agreement with prior work [8], the SF phase density also plays a significant role in the column operability.

Indeed, the interplay of dynamic viscosity and density seems to be complicated, and both have a significant influence on operability. The influence of viscosity provides a new perspective when compared the work of Stockfleth and Brunner [4], who stated that density prevails over all other fluid properties when determining operability. However, further data, modelling and numeric investigation are required to expound on this paper's findings and disentangle the effects of viscosity and density.

6.4 Conclusions

New hydrodynamic pilot plant data for operability, liquid hold-up and pressure drop, were gathered using a 38 mm diameter column packed with ¼" Dixon Rings and operated under supercritical fluid phase conditions. Two PDMS + CO_2 systems of differing fluid properties were used, namely a 100 cSt PDMS and a 200 cSt PDMS system. Both systems were previously identified as systems with low mutual mass transfer and with physical properties close to that of actual SF systems, making them appropriate for hydrodynamic investigation.

Hydrodynamic operability was investigated for both systems by using the mass fraction of liquid in the overheads, with the liquid hold-up and pressure drop used to confirm. The 200 cSt system was found to have a much smaller operability range than the 100 cSt system, with this ascribed to the difference of viscosity between the two systems. The pressure drop and hold-up were also used to discuss potential phenomena that caused the column to become hydrodynamically inoperable (unable to effect a separation). Three different potential mechanisms of the column inoperability were postulated, namely liquid layer flooding, bubble column flooding and entrainment. No one system or fluid property could be connected to variability in operability phenomena, and further research is recommended.

Several observations on supercritical hydrodynamics were made using the data. 1) The supercritical systems displayed no observable loading region – in agreement with Stockfleth and Brunner [4]. This lack of an observable loading region is thought to be due to the elevated fluid properties of the SF system. The higher density and viscosity of the SF system increases the intensity of inter-fluid/interfacial phenomena. 2) Relatively small temperature changes can have significant effects on the hydrodynamics and column operability due to the variation of fluid properties, and 3) Pressure drop and liquid hold-up proved unreliable predictors of operability limits under supercritical conditions. This inability to predict operability limits is in contrast with typical atmospheric systems. Pressure drop is often used to measure and predict hydrodynamic operability in atmospheric columns.

Finally, the impact of variations in the fluid properties of density and dynamic viscosity on the hydrodynamics was investigated. It was found that an increase in the liquid viscosity while keeping other properties constant, decreased the operable range of the column. Further, a higher liquid viscosity caused a higher liquid hold-up, while at a similar pressure drop over the column. Additionally, a higher liquid density also decreased the operable range. Together, viscosity and density have a significant, yet complex influence on hydrodynamics under the conditions investigated.

Nomenclature:

δ	Boundary layer (m)
$\Delta P_0/H$	Dry pressure drop per unit length of dry packing (Pa/m)
D	Column diameter (m)
$d_p = 6\frac{1-\in}{a}$	Particle diameter [a packing dependant constant] (m)
$\in$	Fractional void volume
$K_1,\ K_2$	Empirically determined constants
ρ_G	SF density (kg/m^3)
ρ_L	Liquid density (kg/m^3)
Re_G	Gaseous Reynolds number
Re_L	Liquid Reynolds number
u_G	SF superficial velocity (m/s)
u_L	Liquid superficial velocity (m/s)
μ_L	Liquid dynamic viscosity (Pa.s)
ψ	Packed column friction factor

Funding

This work is based on the research supported in part by the National Research Foundation of South Africa (Grant specific unique reference number (UID) 88782). The authors acknowledge that opinions, findings and conclusions or recommendations expressed in any publication generated by the NRF supported research is that of the authors', and that the NRF sponsors accept no liability whatsoever in this regard.

References

[1] Schwarz, C.E., Nieuwoudt, I. and Knoetze, J.H., *Phase equilibria of long chain n- alkanes in supercritical ethane: Review, measurements and prediction*, J. Supercrit. Fluids, 46 (2008) 226- 232.

[2] Schwarz, C.E., Fourie, F.C.v.N. and Knoetze, J.H., *Phase equilibria of alcohols in supercritical fluids Part II. The effect of side branching on C8 alcohols in supercritical carbon dioxide*, J. Supercrit. Fluids, 51 (2009) 128-135.

[3] Schwarz, C.E. and Knoetze, J.H., *Design of Supercritical Fluid Processes for High Molecular Mass Petrochemicals*, in: M.R. Belinsky (Ed.), Supercritical Fluids, Nova Science Publishers Inc., New York (2009) ISBN: 978-1-60741-930-3.

[4] Stockfleth, R. and Brunner, G., *Hydrodynamics of a Packed Countercurrent Column for the Gas Extraction*, Ind. Eng. Chem. Res., 38 (1999) 4000-4006.

[5] Seader J.D. and Henley, E.J., *Separation Process Principles, 3rd Edition*, Wiley, Chichester (2013) ISBN: 978-0-470-48183-7.

[6] Lombard, J.E., *Thermodynamic Modelling of Hydrocarbon-Chains and Light-Weight Supercritical Solvents*, Masters Thesis, Stellenbosch University, 2015. Retrieved from: http://hdl.handle.net/10019.1/96844.

[7] Franken, H.H., Knoetze, J.H. and Schwarz, C.E., *Concurrent measurement of high-pressure binary phase equilibrium, density and dynamic viscosity*, J. Supercrit. Fluids, 133 (2018) 444-454.

[8] Franken, H.H., Knoetze, J.H. and Schwarz, C.E., *Hydrodynamics of a Packed Column Operated under Supercritical Conditions*, Chem. Eng. Trans., 69 (2018).

[9] Franken, H.H., Knoetze, J.H. and Schwarz, C.E., *High-pressure binary phase equilibria, density and dynamic viscosity of 100 & 200 cSt polydimethylsiloxane (PDMS) with supercritical* CO_2, J. Supercritical Fluids, 139 (2018) 1-7.

[10] Brunner, G., *Gas Extraction, An Introduction to Fundamentals of Supercritical Fluids and the Application to Separation Processes*, Steinkopff, Darmstadt (1994) ISBN: 978-3-662-07382-7.

[11] Franken, H.H., *Establishment of a supercritical pilot plant and the hydrodynamics of supercritical countercurrent columns*, Masters Thesis, Stellenbosch University, Stellenbosch, South Africa, 2014.

[12] Maćkowiak, J., *Fluid Dynamics of Packed Columns*, Springer, Berlin, Germany, 2010.

[13] Woerlee, G.F. *Hydrodynamics and Mass Transfer in Packed Columns and their Applications for Supercritical Separations*, PhD Dissertation, Technische Universitát Delft., 1997.

[14] Tilton, J.N. Perry's Chemical Engineers' Handbook, 8th Edition; McGraw-Hill New York, United States of America, 2010

[15] Joint Committee for Guides in Metrology, *Evaluation of measurement data - Guide to the expression of uncertainty in measurement, JCGM 100:2008*, available at: http://www.iso.org/sites/JCGM/GUM/JCGM100/C045315e-html/C045315e.html, 2008 (accessed 06 Nov 2017).

[16] Schwarz, C.E., *The processing of wax and wax additives with supercritical fluids*, PhD Thesis, Stellenbosch University, 2005.

[17] Stichlmair, J., Bravo, J.L. and Fair, J.R., *General model for prediction of pressure drop and capacity of countercurrent gas/liquid packed columns*, Gas Sep. Purif., 3 (1989) 19-28.

[18] Stockfleth, R. and Brunner, G., *Holdup, Pressure Drop, and Flooding in Packed Countercurrent Columns for the Gas Extraction*, Ind. Eng. Chem. Res., 40 (2001) 347-356.

[19] Souders, M. and Brown, G. G. *Design of Fractionating Columns, Entrainment and Capacity*, Ind. Eng. Chem., 38 (1934) 98-103.

[20] Minne, U.L., Burger, A.J. and Schwarz, C.E., *The Effect of Fluid Properties and Packing Size on the Hydrodynamics of Packed Columns,* Chem. Eng. Trans., 69 (2018) 31-36.

[21] Reid, R.C. and Sherwood, T.K., *The Properties of Gases and Liquids: Their estimation and correlation*, McGraw-Hill Book Company, New York, (1966) ISBN: 978-0-070-51789-9.

7. Hydrodynamic Model Evaluation vs Experimental Data

The fourth objective of evaluating likely hydrodynamic models is addressed using the gathered hydrodynamic data. This builds towards the overarching theme of establishing a basis for future model development.

The models by Stichlmair et al. [1], Maćkowiak [2], and Woerlee [3], as discussed in Section 2.4, were used to calculate predictions. Checking model predictions against the experimental data serves to determine the viability of the models in predicting supercritical hydrodynamics. As a reminder, all the models fit the data of Stockfleth [4] poorly.

No model development will be done in this work, although new constants are regressed where appropriate. The system properties used during modelling are summarised in Table 7-1.

Table 7-1: Column, packing and fluid properties from the experimental work.

	Symbol	Description	Value
Column Properties	Packing	Column Internals	¼ ” Dixon rings
	a (m^2/m^3)	Packing Surface Are per Volume	900
	$\in$	Packing Void Fraction	91%
	d (m)	Column Diameter	0.038
Liquid Properties	ρ_L (kg/m^3)	PDMS Density	864.1-874.0
	μ_L (mPa.s)	PDMS Viscosity	2.11-4.42
	σ (N/m)	PDMS Surface Tension	N/A
Supercritical Phase Properties	ρ_G (kg/m^3)	CO_2 Density	561.4-672.2
	μ_G (mPa.s)	CO_2 Viscosity	0.0421-0.0531
Determined Constants	K_1	Formula Constant	459
	K_2	Formula Constant	4.11

7.1 Liquid Hold-up

7.1.1 Maćkowiak Model Prediction

The SBD model by Maćkowiak [2] (see Section 2.4.3) could not be used in full, as it requires the surface tension of the liquid to predict hold-up and pressure drop. However, due to there being no observable loading zone for the system investigated, (see Section 6.3.2) it can be assumed that all the points below the flooding point are in the pre-loading zone. The hold-up below the flooding point can be calculated using the dimensionless liquid load, B_L, using Equations {2-29} and {2-30}, as described in Section 2.4.3.2. It should be noted that the physical properties of the supercritical phase fall outside of the model range, although the liquid properties fall comfortably within range.

$$h_{Ld,0} = 2.2\sqrt{B_L} \qquad \{2\text{-}29\}$$

$$B_L = \left(\frac{u_L}{\in^3}\right)\left(\frac{1-\in}{d_p}\right)\left(\frac{\mu_L}{\rho_L g^2}\right)^{1/3} \text{ for } B_L < 2\times10^{-5} \qquad \{2\text{-}30\}$$

The model was applied to all available experimental fluid flow rates and physical property combinations. The model predictions were effectively co-linear across the temperatures and fluids investigated, as the liquid properties between the systems varied only marginally. For discussion purposes, the prediction for the 100 cSt PDMS system at 333.15 K is seen in Figure 7-1 along with experimental data.

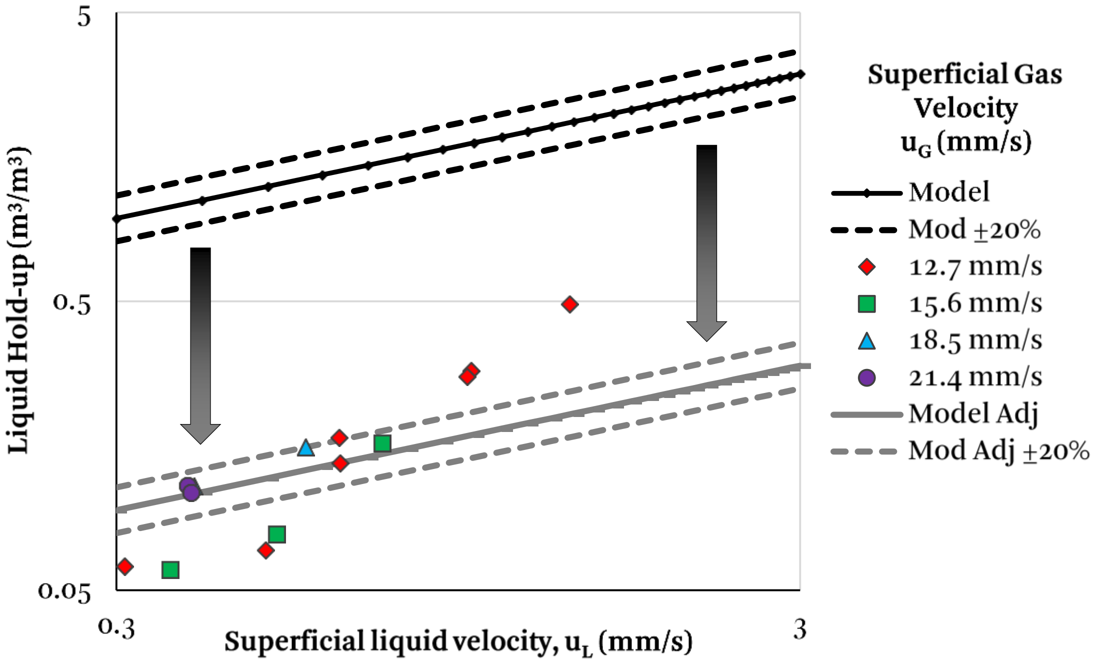

Figure 7-1: Maćkowiak liquid hold-up model predictions of unflooded data using the dimensionless liquid load, B_L, for the experimental data of the 100 cSt PDMS system at 333.15 K and 14 MPa. Two model fits are presented, obtained by manipulating equation {2-29}, A) using the literature constant of 2.2 and B) the adjusted model using the determined constant of 0.22. Note the logarithmic axes.

It is seen that the model significantly overpredicts the experimental data, with the prediction an order of magnitude larger than the gathered experimental data. In an attempt to create a better fit, the empirical constant value of 2.2 in Equation {2-29} was regressed to fit the data better, seen as the adjusted model in Figure 7-1. A regressed value of 0.22 led to the smallest average absolute deviation (33.3 %). The regressed value fits within the order of magnitude estimation used by Buchanan [5]:

$$h_{Ld,0} \simeq C_1 \left(\mathrm{Re}_L / \mathrm{Fr}_L \right)^{1/3} \tag{7-1}$$

where C_1 is the estimated constant. C_1 was found to have a range of 0.20 - 1.86 for the experimental data presented in Figure 7-1. The wide range of the constant, compared to similar estimations for atmospheric work [5], implies a poor fit of the model.

The poor model fit is confirmed in Figure 7-1, with the model failing to provide a good qualitative fit to the data, or predict the slope of the liquid hold-up data. The liquid hold-up seems to have a fundamental difference with the model presented by Maćkowiak [2], with the assumption that $h_{Ld,0} \approx f\left(B_L^{0.5}\right)$ not accurate for the supercritical system investigated.

7.1.2 Stichlmair et al. Model Prediction

Next, the Stichlmair et al. [1] model prediction was used to predict the hold-up. Equation {2-11}, as presented in Section 2.4.2.2, was applied to the unflooded data points to determine constants K_3 and K_4 for both systems:

$$h_{Ld,0} = K_3 \left(\frac{Fr_L^2}{\mathrm{Re}_L} \right)^{K_4} \tag{2-11}$$

The model prediction, along with the experimental data, is seen in Figure 7- 2 for the 100 cSt system and in Figure 7- 3 for the 200 cSt system. The constants were determined using unflooded data points.

In both cases, the models fit the data well considering the accuracy expected with hydrodynamic results. The 100 cSt system agrees with an average absolute deviation of 20.8 % and a maximum of 47.9 % to the model. The high gas flow rate data points fall outside the prediction of the model, corresponding with the hypothesised entrainment behaviour. If these points are ignored, the model presents a good fit with an average absolute deviation of 14.0 % and a maximum of 34.1 % to the model. The better fit implies that there is a shift in hydrodynamic behaviour with a change in the supercritical fluid flow rate that the model fails to predict.

The 200 cSt system agrees within 8.2 % (average absolute deviation) with a maximum of 22.7 %. Both of these data/model fits are significantly better than the fit of the Stichlmair et al. [1] correlation to the data of Stockfleth et al. [4] (average absolute deviation = 63.1 %, maximum = 77.7 %). The data of Stockfleth shows significant differences between individual superficial supercritical flow rates driving the discrepancy between the model and the data. The majority of the experimental data of this work falls within the ±20% confidence interval of the model and does not vary much with variation in the superficial supercritical flow rate. This agrees with the observation that the model does not vary significantly in the range of superficial supercritical flow rates investigated, as discussed in Section 2.4.5.

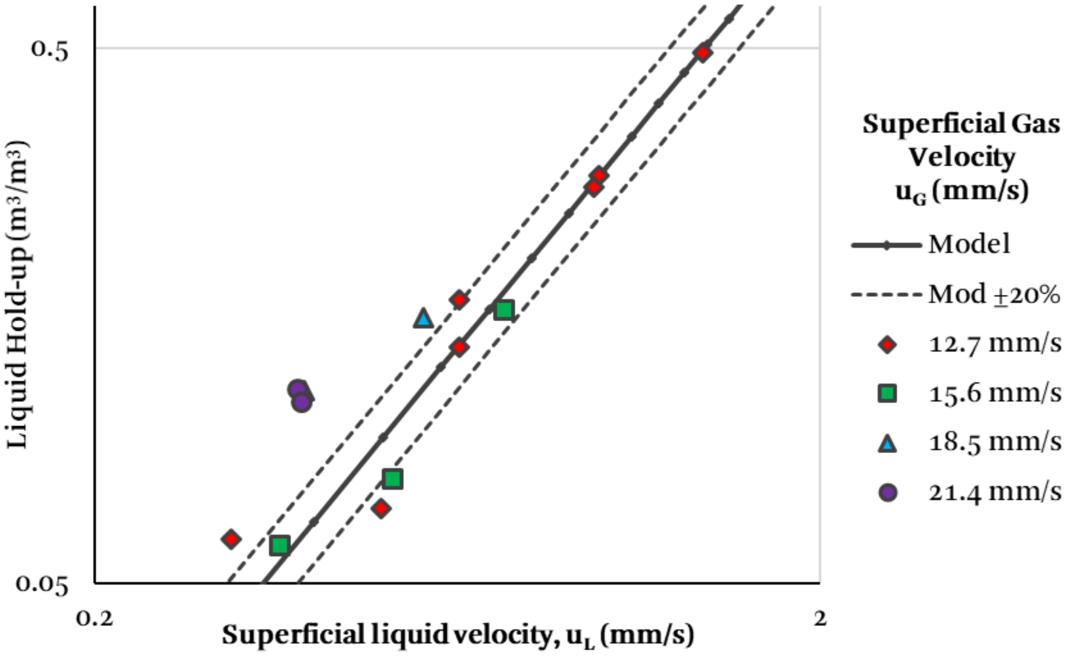

Figure 7-2: Stichlmair liquid hold-up model predictions for the experimental data of the 100 cSt system at 333.15 K and 14MPa.

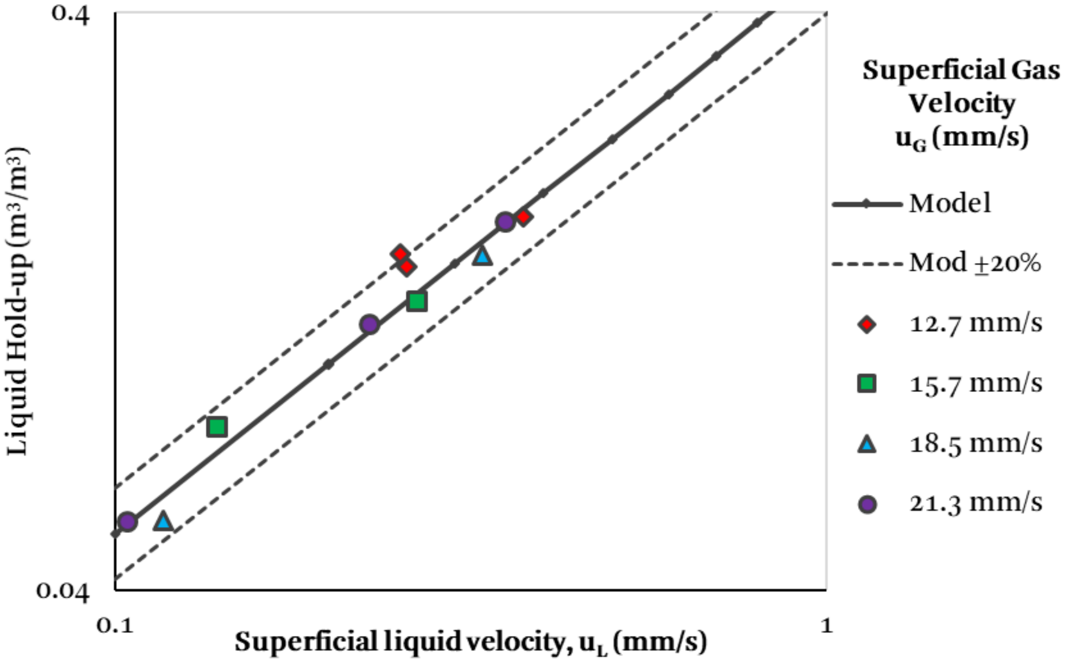

Figure 7-3: Stichlmair et al. liquid hold-up model predictions for the experimental data of the 200 cSt system at 333.15 K and 14 MPa

The best-fit constants for the experimental data were determined as $K_3 = 4141$ and $K_4 = 0.546$ for the 100 cSt PDMS system and $K_3 = 124$ and $K_4 = 0.326$ for the 200 cSt PDMS system. These constants were applicable across the temperatures investigated. Constant ranges found in the literature are $K_3 = 1.1 - 3.6$ and $K_4 = 0.17 - 0.25$ for both non-supercritical systems and the system of Stockfleth [4]. Constant K_3 serves as a proportional adjustment, while K_4 serves to tweak the kurtosis of the prediction at lower superficial liquid flow rates. The determined constants are significantly larger than those found in the literature [4]. There are several differences between the systems that can potentially explain the high values.

The literature and experimental systems are compared in an attempt to explain the significant difference in the constant values. For the values of Stockfleth [4], the reader is referred to Table 2-5. It is important to note that the data presented by Stockfleth [4] have lower liquid hold-ups (~0.06 - 0.15 m^3/m^3) compared to the liquid hold-ups measured in this study (~0.05 – 0.5 m^3/m^3) at similar superficial fluid velocities. The main differences between the literature and experimental systems are the column diameter and internals used and the fluid properties.

Firstly, the packing used by Stockfleth has a much larger surface area than the packing used in this study (3365 m^2/m^3 vs 900 m^2/m^3). A larger surface area suggests a higher liquid hold-up in the pre-loading regime (see equation {2-13}, Section 2.4.2.2). Secondly, the column used by Stockfleth has a smaller diameter than the column used in this study at 25 mm vs the 38 mm, respectively. A smaller column diameter has a proportionally bigger wall surface area relative to the overall column volume, and wall effects can play a more significant role. If both systems were operated with the same liquid at the same liquid rate, the expectation is that the column/internal combination used by Stockfleth should have the higher liquid hold-up. The experimental and literature data shows that the opposite is true and the fluid properties remain as the primary influencer of the liquid hold-up.

Concerning the fluid properties, there are several aspects to consider. The Stockfleth data were gathered at a lower system pressure and lower temperature, meaning the supercritical phase's density and viscosity is higher than that of the experimental data (see Figure 2-2 and Figure 2-3). The viscosity is only marginally higher and should not have a significant influence. The density is more significant with the literature system about ~160 kg/m^3 higher than the experimental system. The liquid density for the Stockfleth system is also ~130 kg/m^3 higher than that of this work, meaning the effective density difference between the supercritical and liquid phases, $\Delta\rho$, is very similar to the experimental system (~290 kg/m^3). The only remaining fluid property available for comparison is the liquid viscosity. The liquid viscosity for CO_2

saturated PDMS is an order of magnitude larger than the water viscosity reported by Stockfleth. The liquid viscosity is proportionally related to liquid hold-up (see equation {2-13}, Section 2.4.2.2).

The same can be said when comparing the two experimental systems (Section 6.3.4). The liquid viscosity is the only significant difference between the two systems, with all the other known fluid properties being very similar. Despite this, the viscosity of the two systems differ significantly (0.6557 mPa.s vs 2.86 - 4.42 mPa.s).

It can, therefore, be concluded that the main difference between the systems, the liquid dynamic viscosity, is responsible for the higher liquid hold-up.

7.1.3 Woerlee Model Prediction

The Woerlee model depends on the iterative solving of the pressure drop before the calculation of the liquid hold-up. For the sake of continuity, the liquid hold-up is discussed first.

First, the angle of inclination for the hypothetical channels need to be calculated before determining the liquid drop and pressure drop. The angle of inclination is determined empirically using dry pressure drop data and the equations {2-36} to {2-38}. At first, an attempt was made to calculate the angle of inclination using the literature derived constant of 0.6556 for equation {2-37}. Using the literature constant led to a calculated α_0 of 67.1° and an α of 60.1°. This value of α had a poor model fit, with the model predicting the data to an absolute average deviation of 21.0 % (average absolute deviation) with a maximum of 30.0 %.

To attempt to obtain a better model fit both the empirical constant and the angle of inclination is allowed to vary during the parameter regression. Varying both constants presents a much better model fit with a model constant of 0.153, an α_0 of 77.4° and an α of 69.3°. The difference of the calculated angle of inclination can be ascribed to differences in physical properties (similar to the discussion above in Section 7.1.2) as well as packing geometry. This model fits the data to within an absolute average deviation of 5.8 % (average absolute deviation) with a maximum of 14.1 %, which is a slightly better fit than the Stockfleth model (See Section 6.3.1). The model fit can be seen in Figure 7-4.

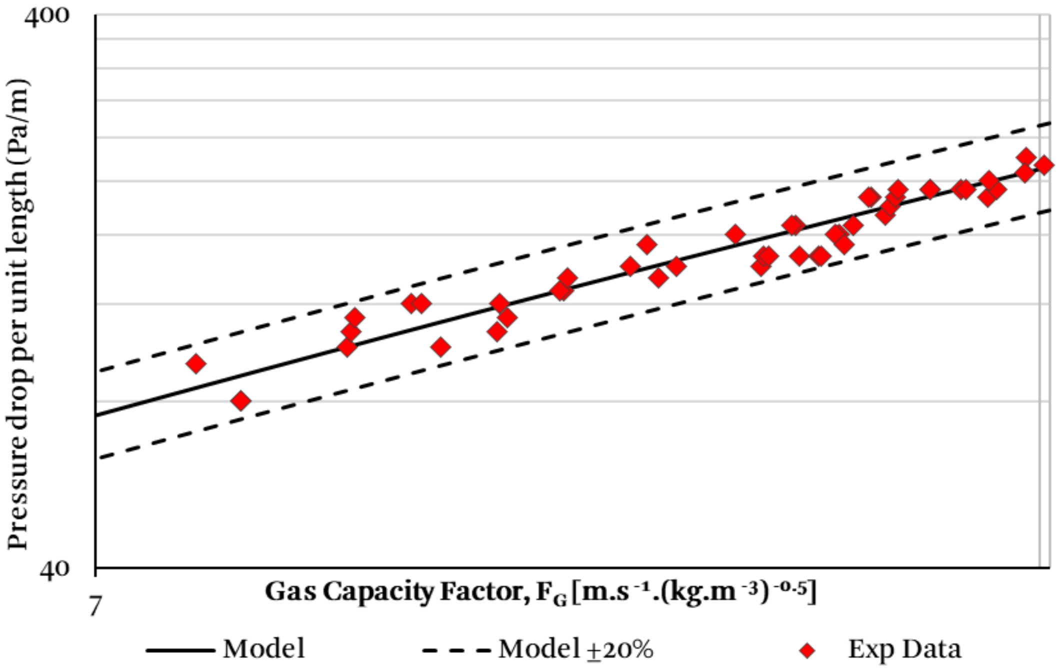

Figure 7-4: Woerlee dry pressure drop and model prediction at 14 MPa and 313.15 K for ¼ " Dixon Rings and SF CO_2. Note logarithmic axes.

The pressure drop and liquid hold-up is calculated through an iterative process using the calculated angle of inclination. The iteration was halted as soon as calculation residuals were <<0.1%. The liquid hold-up data and model prediction can be seen in Figure 7-5 and Figure 7-6.

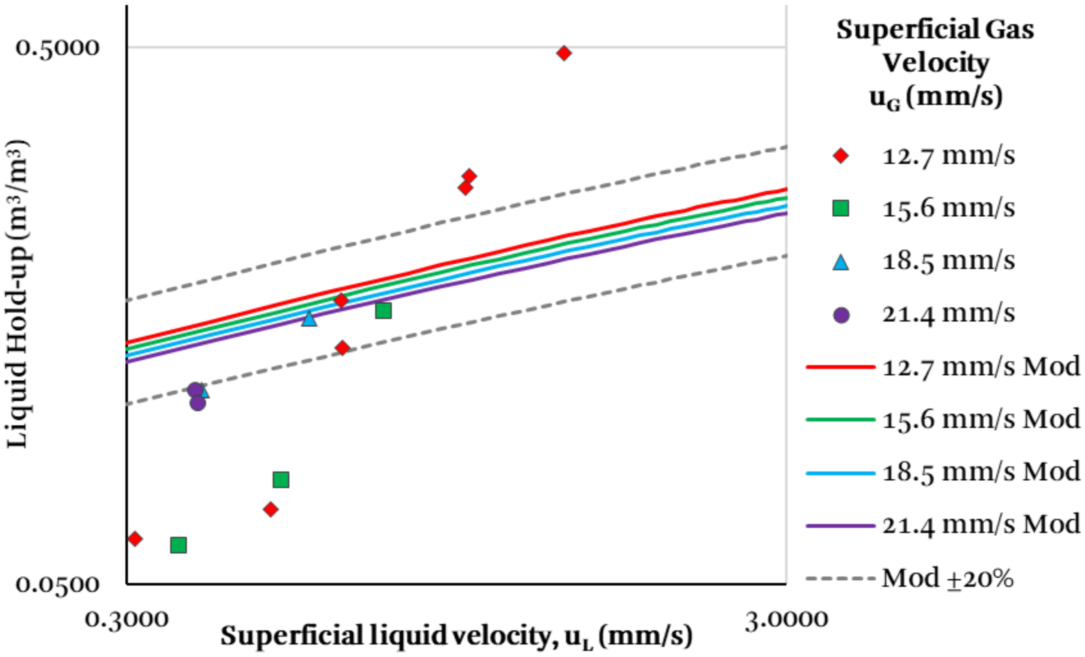

Figure 7-5: Woerlee liquid hold-up model predictions for the experimental data of the 100 cSt system at 333.15 K and 14 MPa

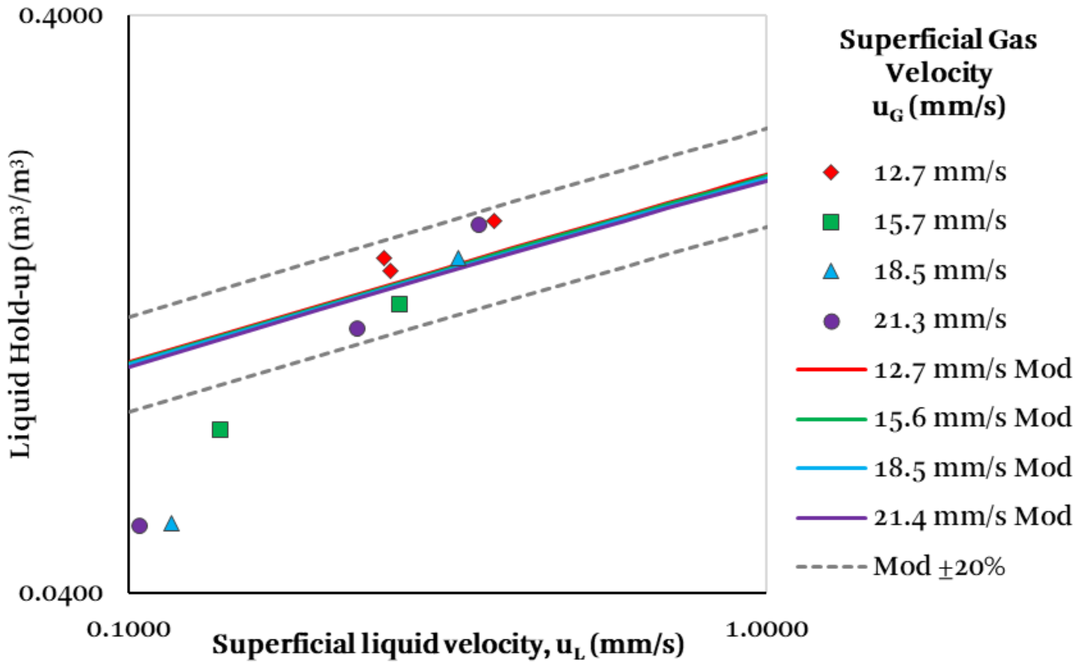

Figure 7-6: Woerlee liquid hold-up model predictions for the experimental data of the 100 cSt system at 333.15 K and 14 MPa

The prediction using the Woerlee model follows a different trend than the gathered liquid hold-up data for both PDMS + CO_2 systems. This difference in trend was noted during the comparison with the available literature data as well. The 100 cSt system is not predicted well, with an average absolute deviation of 50.4 % and a maximum deviation of 138.4 % from the data. Through what may be coincidence, the model predicts the higher superficial liquid velocity data points of the 200 cSt system fairly well, with an average absolute deviation of29.8 % and a maximum deviation of 96.1 % from the data. It is noteworthy that a model with very little empiricism could predict values similar to that of the experimental liquid hold-up.

To attempt a better model fit, the angle of inclination was manually varied, with no significant improvement in the fit. As the angle of inclination is the only input that is not calculated iteratively, except of course for the physical properties, no other simple options are available to attempt to better the model fit.

The 100 cSt model shows more variation with changes in the superficial supercritical fluid velocity than the 200 cSt. The two model predictions are also very close to each other. As the major change between the two systems is the viscosity of the liquid phase, the prediction shows that the model does successfully compensate for liquid viscosity.

The range of the calculated dimensionless interface value decreases from 0.920 to 0.889 for the 100 cSt system and from 0.943 to 0.909 for the 200 cSt system with increasing superficial liquid velocity. These values, compare well with the estimation of the wall effects in Section 6.2.6, where a lowest dimensionless interface number of 0.910 can be calculated. The lower numbers predicted by the model is due to the restrictive influence of the column packing.

7.1.4 Hold-up Model Comparison

To present a comparison, all three models for the 100 cSt system are presented together in Figure 7-7.

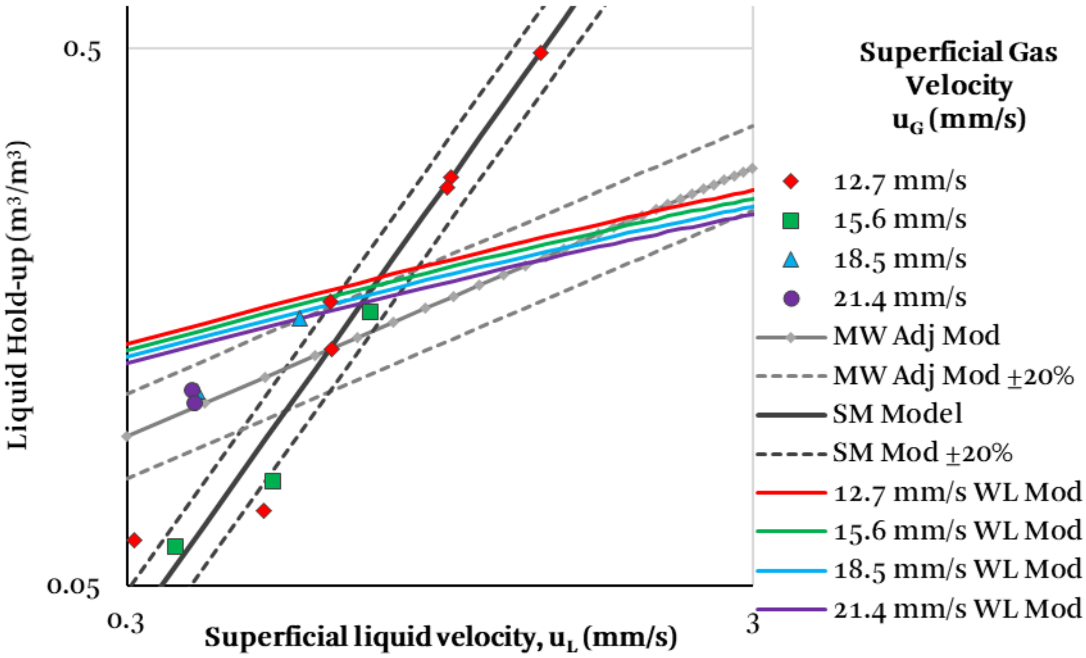

Figure 7-7: The comparison of the predicted hold-up for the three tested models against the experimental data.

It can be seen that the models present very different trends and approximations to the data, with the model by Stichlmair et al. coming the closest to a prediction. None of the models, however, present a good approximation. The Stichlmair et al. model predicts the steepest increase in hold-up, followed by the Maćkowiak model and then by the Woerlee model.

7.2 Pressure Drop

The Maćkowiak model [2] requires the liquid surface tension in order to calculate the flooding point and from there, the pressure drop (see equations {2-24} to {2-35}, Section 2.4.3). As it was not within the scope of this project to measure surface tension, and no reliable way was found in the literature to estimate it, no prediction could be made using this model.

The remaining two models both have all the inputs needed to calculate the preddure drop. The model of Woerlee [3] was used as is, with the calculated angle of inclanation from the dry presure drop. The Stichlmair et al. [1] model was applicable, but some simplifications were possible.

7.2.1 Stichlmair et al. Model Adjustments

The conclusion that the experimental systems had no detectable loading regime creates the opportunity to simplify the modelling of the pressure drop significantly.

According to Stichlmair et al., the pressure drop in the column is described by Equation {2-14}, as discussed in Section 2.4.2.3:

$$\Delta P / H = \Delta P_0 / H\{[1 - \in (1 - h_{Ld} / \in)] / (1 - \in)\}^{(2-C)/3} . (1 - h_{Ld} / \in)^{-4.55} \qquad \{2\text{-}14\}$$

where:

$$h_{Ld} = h_{Ld,0}\left[1 + K_5 (\Delta P / H . \Delta \rho . g)^{K_6}\right] \qquad \{2\text{-}17\}$$

These equations are interdependent and require iterative calculation to solve. As the loading regime is not observable in the system, as determined in Chapter 6 and reported in the literature [6], it is said that $h_{Ld} = h_{Ld,0}$. This assumption is as per the definition of the two terms to attempt a simplification of the model in line with experimental observations. As there is no loading regime observable, the assumption is that the hold-up, h_{Ld}, would equal that of a pre-loading system, $h_{Ld,0}$, for the operable points. This assumption eliminates the interdependency of the pressure drop and liquid hold-up equations. Eliminating the interdependency simplifies the calculation of the pressure drop significantly, with no iterative calculations needed and no need to fit data to determine constants K_5 and K_6. Stockfleth et al. [4] indicated great difficulty in determining these constants due to the iterative calculations needed, assuming a value for one constant and only regressing the other.

The modified model is used to again predict the literature data, with Figure 2-9, Section 2.4.5.2, redrawn. The new model prediction is plot alongside the old in the redrawn figure, Figure 7-8.

It is seen in Figure 7-8 that the assumption does not dramatically impact the model prediction. Deviation is only seen at higher superficial liquid velocities, close to the flooding point. In the area of interest where the literature data lies, the two model variants agree to within 1.2 % (average absolute deviation) with a maximum deviation of 9.3 %.

The drawback of this assumption is that the model can no longer predict flooding through iterative calculation. From the analysis of the data in Section 6.3, it was seen that flooding was not consistent for the system and other modes of inoperability also played a significant role. Therefore it is challenging to define a strict flooding regime to predict operability and further research to better differentiate between the phenomena and their causes is required.

Stockfleth et al. [4] defined flooding as: "*Throughout this paper, a liquid layer of 50 mm height on the uppermost packing element is the indicator for a flooding point.*" This definition is an arbitrary and system-specific indicator of flooding. A column could have 50mm of liquid at the top of the packing, while still being useful as a separation vessel. As discussed in Section 5.3.2, system-specific definitions were avoided and this work defines flooding as the total hydrodynamic inoperability of a column, or, in other words, the point after which a column ceases to be a useful vessel for separation. Importantly, the definition presented by literature could explain the difference between the predicted and measured flooding in Figure 7-8.

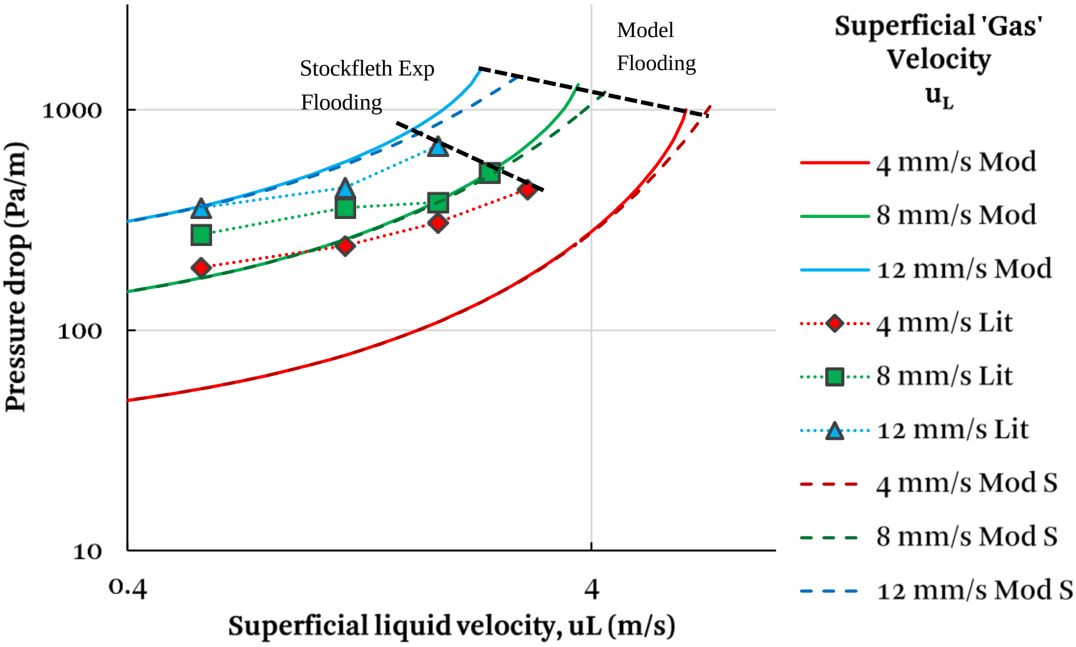

Figure 7-8: Pressure Drop model predictions using the Stichlmair et al. model (Mod) as well as the model using the simplification (Mod S), compared to the literature data by Stockfleth et al. [4] at 313 K and 12 MPa. Note the logarithmic axes.

7.2.2 Stichlmair et al. Model Prediction

Predictions were made for the 100 cSt and 200 cSt experimental systems, using the adjusted equation:

$$\Delta P / H = \Delta P_0 / H\{[1-\in(1-h_{Ld,0}/\in)]/(1-\in)\}^{(2-C)/3}.(1-h_{Ld,0}/\in)^{-4.55} \qquad \{7\text{-}2\}$$

The wet pressure drop model predictions for the 100 cSt systems are seen in Figure 7-9 at 333.15 K. The model provided a poor fit with 272.3 % average absolute deviation and a maximum deviation of 2281 %.

It is seen in Figure 7-9 that the model seemed to predict a similar trend as that of the data, but with an offset. To attempt a better fit to the model, Equation {2-14} was further modified:

$$\Delta P / H = K_7.\Delta P_0 / H\{[1-\in(1-h_{Ld,0}/\in)]/(1-\in)\}^{(2-C)/3}.(1-h_{Ld,0}/\in)^{-4.55} \qquad \{7\text{-}3\}$$

with K_7 a proportional constant to adjust the fit. Constants for K_7 were derived using a least-squares fit to the unflooded data points for both experimental systems. For the 100 cSt system, the constant was determined as $K_7 = 0.27$ and for the 200 cSt system as $K_7 = 0.26$. The agreement of these constants shows that there is an underlying accord between the systems, with the new model fits presented in Figure 7-10 and Figure 7-11.

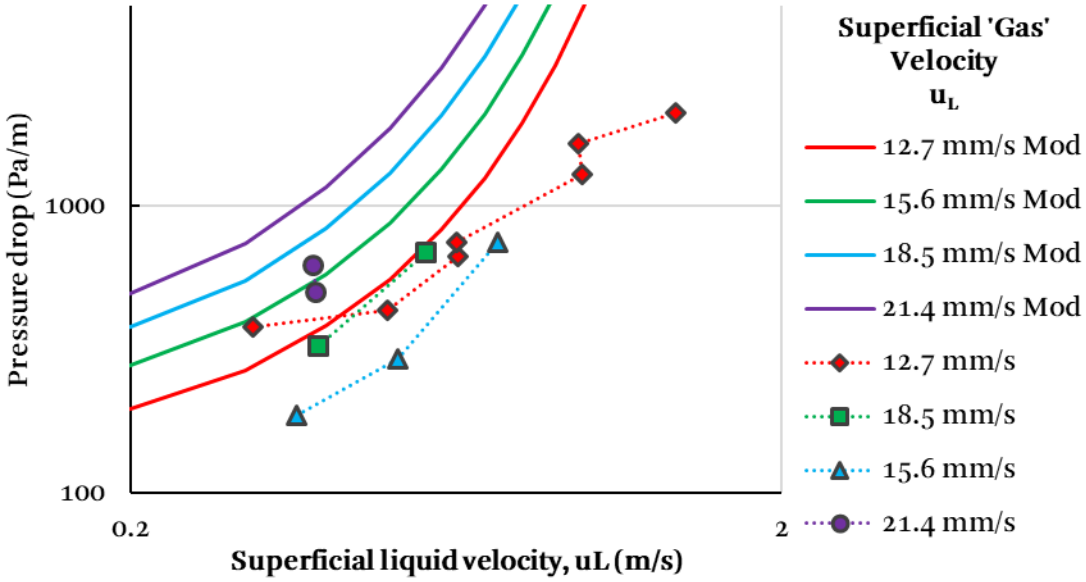

Figure 7-9: Pressure Drop model predictions using the Stichlmair et al. model (modified to operate below the loading line); compared to experimental data for the 100 cSt system at 333.15 K. Note the logarithmic axes.

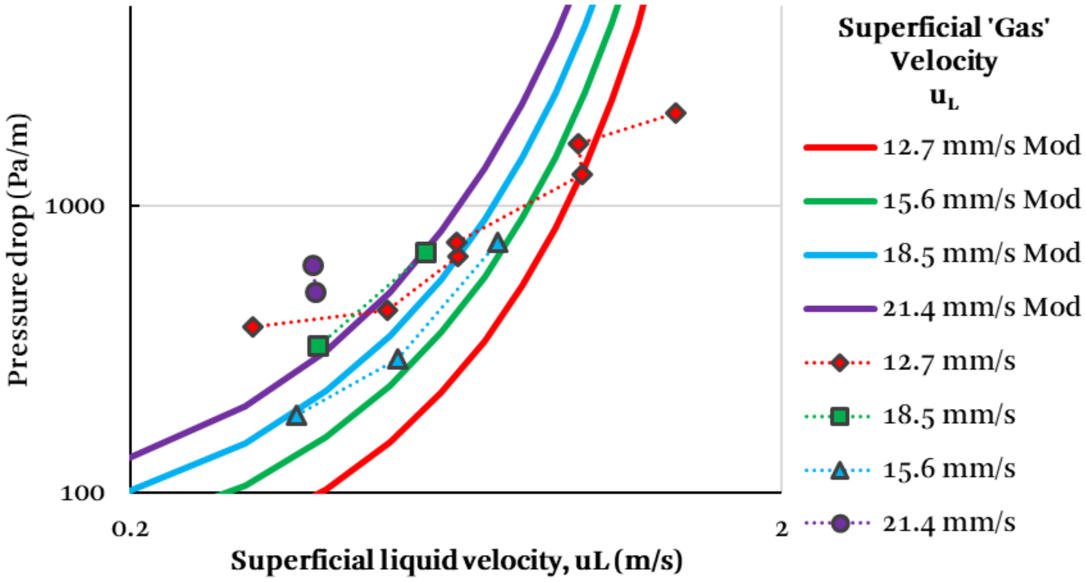

Figure 7-10: Stichlmair et al. 100 cSt pressure drop prediction and experimental data at 333.15 K and 14 MPa.

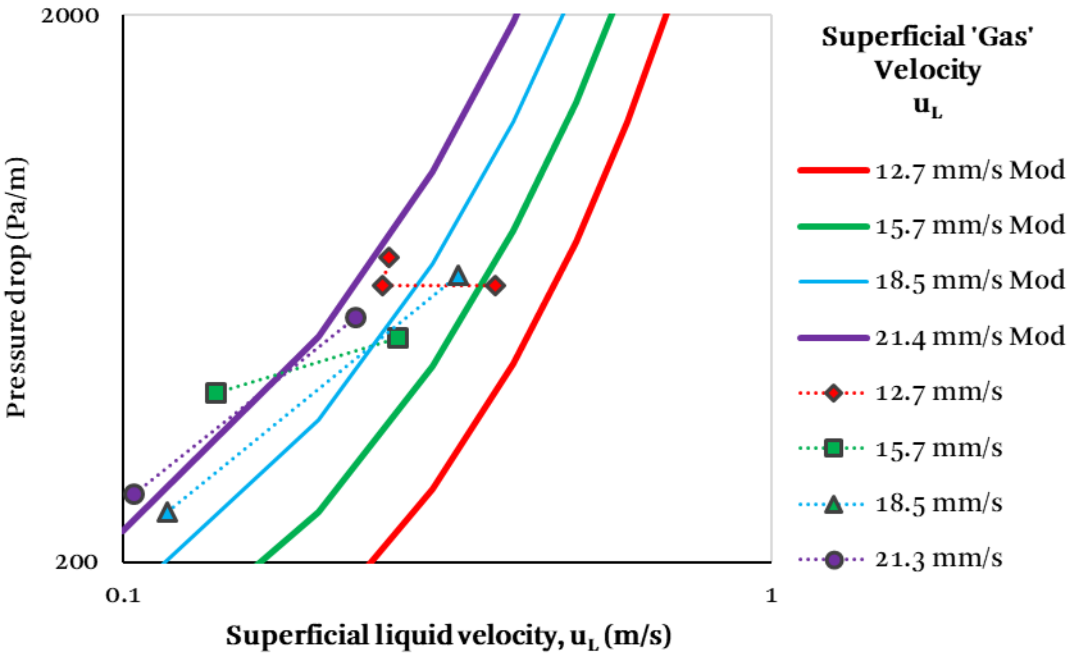

Figure 7-11: Stichlmair et al. 100 cSt pressure drop prediction and experimental data at 333.15 K and 14 MPa.

The models show much better predictions of the data but still fail to present an accurate view of either system. The 100 cSt adjusted model agrees with an average absolute deviation of 78.1 % and a maximum of 543.0 % to the experimental data. The 200 cSt adjusted model agrees within 48.7 % (average absolute deviation) with a maximum of 170.9 %. Both of these data fits are still worse than the fit of the Stichlmair et al. correlation to the data of Stockfleth (average absolute deviation = 37.4 %, maximum = 71.9 %).

The model predicts a progressively higher pressure drop with an increase in superficial supercritical velocity. The experimental pressure drop does not show the same trend. Linking back to the discussion on inoperability behaviour in Section 6.3, it is stated that the experimental data shows complex behaviour concerning changing superficial supercritical velocity. The presence of complex behaviour means the system potentially needs a more sophisticated approach to its modelling than is presented here.

Neither model could predict the pressure drop or operability limits for the experimental data. This lack of a prediction is despite the statement in the literature that there is no fundamental difference between supercritical and classical hydrodynamics.

7.2.3 Woerlee Model Prediction

As the model by Woerlee does not make any differentiation on the pressure drop below or above the loading line no simplification from the experimentally observed behaviour is possible. The wet pressure drop was determined iteratively, as described in Section 7.1.3. The model prediction can be seen with the experimental data in Figure 7-12 and Figure 7-13 for the two PDMS systems.

The model predicts pressure drop values of similar magnitude to the experimental data of the 100 cSt system. This is interesting, as the model has not been fitted to the system, like the prediction by the Stichlmair model, but predicted it using only the fluid and column/packing properties. The only place where the model had an empirical influence was at the determination of the angle of inclination, which was determined using dry pressure drop data.

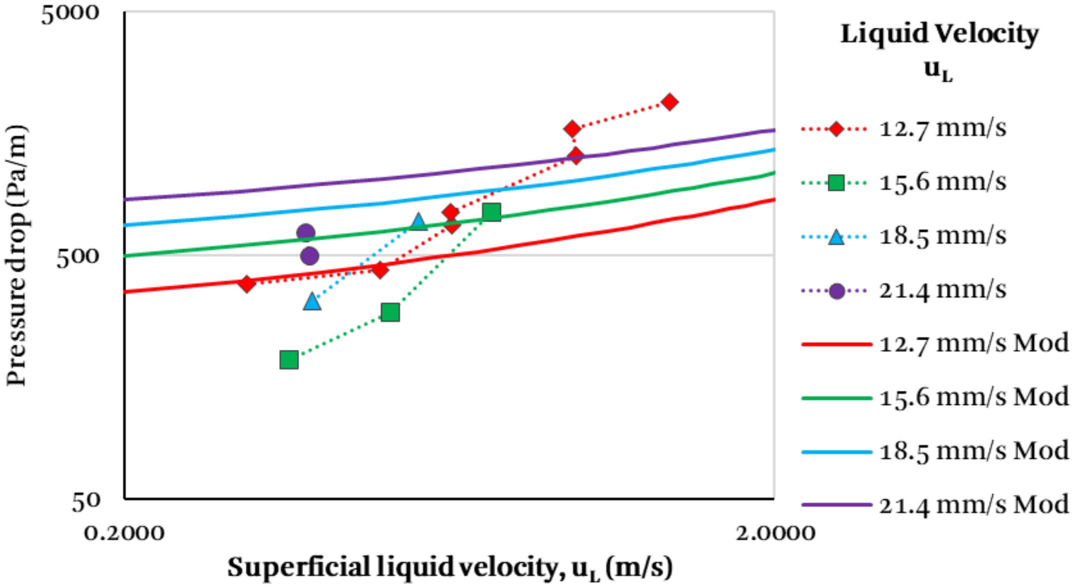

Figure 7-12: Woerlee pressure drop model predictions for the 100 cSt system at 333.15 K. Note the logarithmic axes.

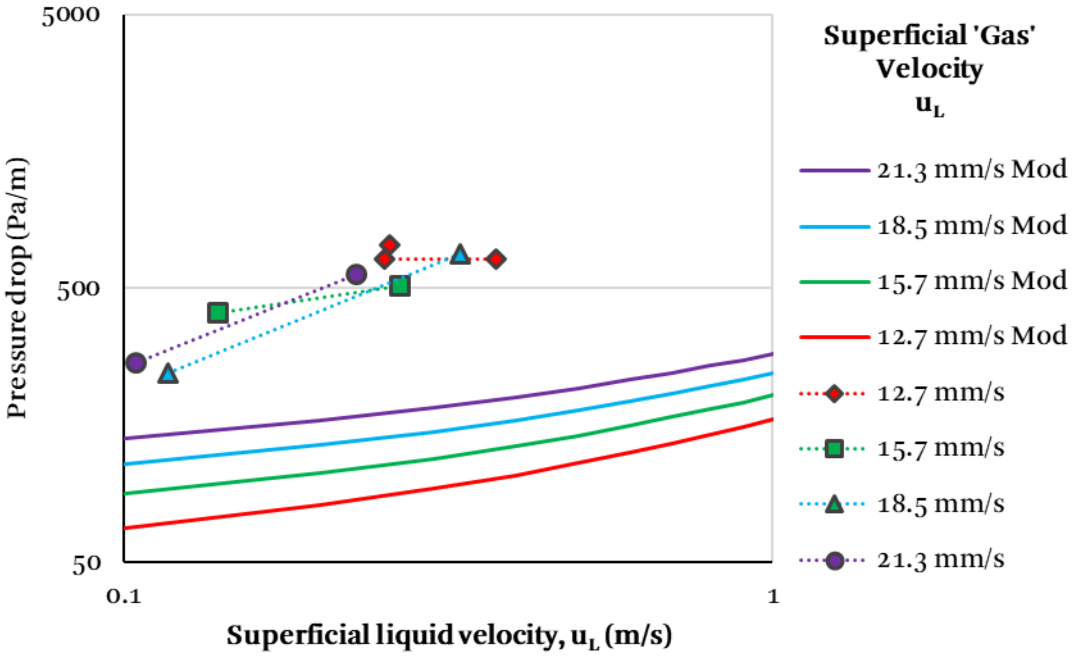

Figure 7-13: Woerlee pressure drop model predictions for the 200 cSt system at 333.15 K. Note the logarithmic axes.

The 200 cSt model, on the other hand fails to present a decent approximation of the pressure drop, under predicting the pressure drop significantly. Variation in the angle of inclination, like with the liquid hold-up, did not provide a significantly better fit to the data for either system.

As a whole the Woerlee model fails to present a decent prediction of the experimental system, showing a different trend than the experimental data and deviating significantly from the data. The 100 cSt model prediction showed an average absolute deviation of 61.7 % and a maximum of 203.7 % to the experimental data. This is a somewhat better fit than the modified Stichlmair model, but still not accurate enough to trust with a prediction. The 200 cSt system had an average absolute deviation of 73.0 % and a maximum deviation of 87.9 % from the experimental data.

The fact that the model prediction could achieve even a rough approximation of the system is, however, noteworthy, as there is very little empiricism in the model. This shows that may be some merit in comparing to atmospheric models, however changes need to be made to accurately predict the data. The two systems together paint a good picture of the potential pitfalls, with the model seeming to coincide with the data at the 100 cSt system and completely failing to get close to the 200 cSt system.

Similar to the Stichlmair et al. model and contrary to the experimental data, the Woerlee model also predicts a progressively higher pressure drop with an increase in superficial supercritical velocity.

7.2.4 Pressure Drop Model Comparison

To present a comparison, the models by Stichlmair et al. and Woerlee are presented together for the 100 cSt system in Figure 7-14, keeping in mind the Maćkowiak model could not present a prediction.

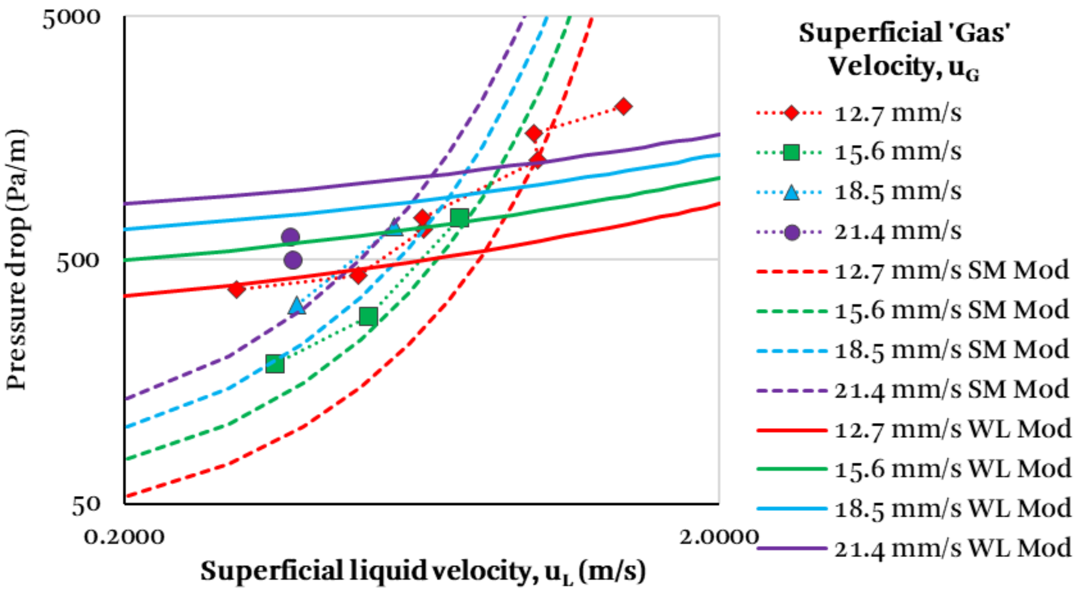

Figure 7-14: The comparison of the predicted pressure drop for the two tested that delivered predictions models against the experimental data.

It can be seen that the models present very different trends and approximations to the data, with the model by Woerlee coming the closest to a prediction. Neither models presents a good approximation. The Stichlmair et al. model predicts the steepest increase in pressure drop, with a significant exponential element visible. The model by Woerlee is more moderate with changing superficial liquid velocity, showing a smaller increase in pressure drop. Both models are similarly spaced with regards to increasing superficial supercritical fluid velocity in the figure.

7.3 Supercritical Hydrodynamics vs Atmospheric Hydrodynamics

An overview of the work to date is required to address the 5th objective: to test if the experimental results conform to the expectations of classical hydrodynamic systems. The majority of work in the literature has compared gathered results with gas-liquid models and interpretations. Meyer [7] was the first to state explicitly that the models applicable at vacuum and standard pressures do not readily predict high-pressure systems (P > 7 MPa). Stockfleth [6] states that there is no fundamental difference between classical hydrodynamics and hydrodynamics under supercritical conditions, as discussed in Section 2.3.1. Woerlee [3] states that it is preferred to compare supercritical systems to atmospheric columns due to the molecules of a supercritical fluid having a larger kinetic than potential energy. The statements by the literature sources seem diverse, and the opinion of Meyer seems to disagree with the other literature. Some of the findings of this study are used to test the hypothesis and its validity to the experimental results.

It is hypothesised that the system measured in this work, as well as supercritical systems in general, do not conform to classical hydrodynamics for several reasons.

Firstly, the loading zone is not detectable. Classical hydrodynamics display a measurable loading zone where the interactions between the phases are significant. In the experimental system, as well as the literature data by Stockfleth [4], the loading zone is not observed.

Secondly, pressure drop and liquid hold-up are found to be unreliable indicators of operability at supercritical conditions (Section 6.4). This observation is contrary to classical hydrodynamic systems where pressure drop is correlated with the separation efficiency. Pressure drop in classical hydrodynamics is used not only to predict flooding but also to determine the optimal operation point of the column. The same is not possible in the measured supercritical system, with several different operability limits occurring close to each other with variations in the fluid flow rates. The prediction of operability was also not possible for the presented literature by Stockfleth [4].

Thirdly, the investigated hydrodynamic models are unable to predict the pressure drop under supercritical conditions, despite making allowances for the elevated fluid properties of the supercritical fluid. The Woerlee model came close using a model with limited empiricism, but still failed to present a sensible approximation. Indeed pressure drop data showed complex behaviour concerning fluid flow rates, in contrast with the simple, straight forward trends found in classical hydrodynamics.

Fourthly, the investigated classical hydrodynamic models are unable to predict operability limits and flooding drop under supercritical conditions. Flooding in classical hydrodynamics are consistent for a given set of fluid properties. The same can not be said concerning the experimental system measured, with the operability range of the column varying wildly, despite the fluid properties staying constant.

On the contrary, the model fit by Woerlee was able to predict values in the same order of magnitude as the experimentally determined data with very little to no empirical fitting of the data. The model however fails to present a accurate prediction of either liquid hold-up or pressure drop.

In conclusion, there is not enough information, either in this publication or in literature, to definitively state that hydrodynamics under supercritical conditions are fundamentally equivalent to atmospheric hydrodynamics. The deviations discussed above, along with discrepancies noted in the literature, require further investigation to determine the underlying fundamentals. Prior literature sources have all compared to atmospheric hydrodynamics and presented different outcomes.

References

[1] Stichlmair, J., Bravo, J. and Fair, J., *General model for prediction of pressure drop and capacity of countercurrent gas/liquid packed columns*, Gas Sep. Purif., 3 (1989) 19-28.

[2] Maćkowiak, J., *Fluid Dynamics of Packed Columns*, Springer, Berlin, Germany, 2010.

[3] Woerlee, G.F. *Hydrodynamics and Mass Transfer in Packed Columns and their Applications for Supercritical Separations*, PhD Dissertation, Technische Universität Delft., 1997.

[4] Stockfleth, R. and Brunner, G., *Holdup, Pressure Drop, and Flooding in Packed Countercurrent Columns for the Gas Extraction*, Ind. Eng. Chem. Res., 40 (2001) 347-356.

[5] Buchanan, J.E. *Holdup in Irrigated Ring-Packed Towers Below the Loading Point*, J. Ind. Eng. Chem. Fundamentals, 6 (1967) 400-407.

[6] Stockfleth, R., *Fluiddynamik in Hochdruckgegenstromkolonnen für die Gasextraktion*, PhD Dissertation, Technical University of Hamburg - Harburg, 2001.

[7] Meyer, J.-T., *Druckverlust und Flutpunkte in Hochdruckgegenstromkolonnen*; PhD Dissertation, Technische Universität Hamburg - Harburg., 1998.

8. Conclusions

8.1 Conclusions from Literature - Chapter 2:

Chapter 2 focused on information available in the literature. After some introductory literature, a thorough literature survey of hydrodynamics under supercritical conditions was performed. It was found that the literature had several shortcomings.

Firstly, data concerning hydrodynamics under supercritical conditions are scarce, with only a handful of publications addressing the topic. Some points of concern were noted after reviewing the available literature. 1) The literature only covers a small range of fluid properties in the saturated liquid and supercritical phases. Further, the investigated property ranges do not overlap with typical, industrially relevant systems. 2) Very little work has been performed on random packings 3) Previous studies used fluid systems where significant mutual solubility was possible. The high mass transfer obscures hydrodynamic effects and complicates the interpretation of results. 4) No studies investigating the effect of fluid properties on supercritical hydrodynamics were found. The fluid properties have a significant effect on hydrodynamics and are known to be highly variable in supercritical systems.

Secondly, concerning the modelling of hydrodynamics under supercritical conditions, it was found that there are no models available for columns operating with supercritical fluids. Hydrodynamics under supercritical conditions are not readily predicted by models applicable at normal and vacuum pressures, even though the literature states that hydrodynamics under supercritical conditions are not fundamentally different from atmospheric hydrodynamics. Models that can potentially predict the hydrodynamics at elevated conditions are scarce with only two potential models, by Stichlmair et al. and Maćkowiak, identified. The selected models were tested against literature data. Neither model could fully predict hydrodynamics under supercritical conditions and even the semi-empirical Stichlmair et al. model, adjusted for supercritical fluids, failed to present reasonable approximations of the data. It is concluded that, to the best of the author's knowledge, no correlations are available that can accurately predict hydrodynamics, especially flooding/operability, under supercritical conditions.

Thirdly, no system in literature encompassed the full set of fluid property and phase equilibria data required for hydrodynamic experimentation. Fluid properties play a key role in the modelling of hydrodynamic systems, while phase equilibria give an indication of the possible mass transfer.

The lack of data and shortcomings in the literature forces industry to rely on pilot plant studies for data, decreasing the attractiveness of the technology. The literature survey identifies the shortcomings and justifies further study and investigation.

The objectives of this study were to:

1. Design, construct, commission, and verify equipment capable of simultaneously measuring the phase equilibria and fluid properties of density and dynamic viscosity at saturation under supercritical conditions.
2. Use the constructed equipment to measure binary phase equilibria and property data with a supercritical fluid as one of the components. Use the measured data to identify experimental systems exhibiting low mutual solubility (reducing the effect of mass transfer), with fluid properties similar to that of industrially relevant processes.
3. Measure hydrodynamic data, namely liquid hold-up and pressure drop, for the selected system(s). The hydrodynamics can then be used to determine A) the operability limits of the system and B) the influence of the fluid properties of viscosity and density on hydrodynamics.
4. Compare the gathered hydrodynamic data to available models to determine their accuracy in predicting supercritical hydrodynamics.
5. To test the literature hypothesis that supercritical hydrodynamics are fundamentally similar to atmospheric systems.

8.2 Objective 1 - Chapter 3

Chapter 3 focused on the conceptualisation, design, commissioning and validation of the equipment required to measure high-pressure phase equilibria and fluid properties. This work directly addresses the first objective of the study.

The designed variable volume cell, fitted with an electromechanical quartz crystal for fluid property determination, presented a novel solution to measure phase equilibria and the fluid properties concurrently. The equipment can measure fluid properties at saturation for a fluid up to 35 MPa and 393 K. The equipment was successfully validated for the measurement of phase equilibria, density and dynamic viscosity. Verification was first done with single-component fluids to verify the property measurement method. 1) n-Dodecane density and dynamic viscosity data were measured with excellent agreement with predictive models and literature. 2) Benzene density showed excellent agreement to predictive models and literature data. Viscosity agreed well with literature data, but with some explained deviation. The excellent agreement with literature single-phase data validated confidence in the measurement method, as well as served to verify the equipment.

The equipment was also successfully validated for the measurement of binary systems using the system CO_2 + ethyl tetradecanoate. For the measurement of phase equilibrium data, excellent agreement was achieved with literature, while adding new data at a higher temperature (353.15 K). A method was developed for the measurement of saturated fluid properties (density and dynamic viscosity) at high pressures, for both the liquid solute phase and supercritical fluid solvent phase. The measured fluid properties were compared to pure-component data as a sense check, as there were no saturated binary-system fluid properties to compare to in literature. The both the gathered density and dynamic viscosity data were successfully compared to pure component data, with the saturated binary phase properties showing the expected trends.

With the equipment validated and successfully measuring binary fluid properties at saturation, the first objective was achieved. The next step was to gather a full set of data fluid property and phase equilibrium data for a selected system.

8.3 **Objective 2 - Chapter 4**

Chapter 4 focused on the identification and description of appropriate systems for hydrodynamic study. This work addressed the second objective – to measure binary phase equilibria and property data for a supercritical fluid system with a) low mutual solubility and b) fluid properties in the desired ranges.

Polydimethylsiloxane (PDMS) with CO_2, the most popular supercritical solvent, was identified as the binary system. The literature data predicted low solubility and desirable fluid properties for this combination, making it an ideal candidate. Two PDMS liquids, rated at 100 cSt and 200 cSt were selected and characterised using size exclusion chromatography.

Phase equilibrium data were measured at 313 – 353 K for both PDMS + CO_2 systems with excellent consistency shown by the data. The SynVisVar visual method, as well as the electromechanical response of the quartz crystal, was used to determine equilibria. The electromechanical and optical measurements showed close agreement. Phase equilibrium data showed complex phase behaviour of type III for the binary system, as predicted by the literature. The two experimental systems were confirmed to exhibit the desired low mutual solubility. PDMS solubility into the supercritical fluid phase was very low. The solubility of CO_2 into the PDMS was still significant and affected the liquid properties.

Both the saturated fluid density and dynamic viscosity for both the liquid and supercritical fluid phases were measured. Both fluid properties showed evidence of the complex phase behaviour noted in the phase equilibria. Density data also showcased the effects of the significant solubility of CO_2 into the PDMS phase, with the saturated liquid density closer to the CO_2 phase than that of the pure liquid at higher pressures. Further, density data were found to be in a range similar to that of lighter organics and oils typically extracted with supercritical fluids (~900 - 800 kg.m^{-3}). Dynamic viscosity data were measured with a wide range of viscosities noted (~ 0.7 - 7 mPa.s). The PDMS polymers were shown to be plasticised by the supercritical CO_2, showing viscosities much closer to that of supercritical CO_2 than of liquid PDMS.

Reviewing the gathered data hydrodynamic experiments at 14 MPa were suggested. This pressure provided a mix of properties that enabled some differentiation between the influence of density and viscosity, due to an overlap in properties between the two systems. This pressure also ensured operation well below the pressure where the complex phase behaviour occurs.

This publication delivered a full complement of data for the PDMS + CO_2 systems for phase equilibria, density and dynamic viscosity with fluid properties falling in the desired ranges. This fulfilled the second objective and provided the necessary data required to progress into a hydrodynamic investigation.

8.4 **Objective 3 - Chapters 5 and 6**

Chapter 5 presented an initial publication on the measured supercritical hydrodynamics and focussed primarily on flooding behaviour in the PDMS 100 system. Chapter 6 expanded on Chapter 5, presenting a full complement of hydrodynamic data for both the PDMS systems. Chapter 6 considered operability instead of just flooding, adding entrainment and added a discussion on the influence of fluid properties.

Together these two chapters address the fourth objective – to measure pressure drop and liquid hold-up, determine the operability limits of the system, as well as the impact of fluid properties on hydrodynamics.

Hydrodynamic data in the form of the dry and wet pressure drop, liquid hold-up, mass flow through the column and component mass fractions in the product streams were measured for both the 100 cSt and 200 cSt PDMS systems.

The measured dry pressure drop data for the ¼ ” Dixon Ring packing was presented. It was found that dry pressure drop data showed no significant difference to the pressure drop of a wetted column. The lack of a difference indicated that the column and packing had a negligible static hold-up, in agreement with literature. A semi-empirical Ergun-type model was fitted to the data. The data were found to fall comfortably within the ±20 % interval of the model with derived model constants agreeing well with literature.

Liquid hold-up and wet pressure drop data were presented for both the 100 cSt and 200 cSt PDMS systems. It was seen that small changes in temperature had significant effects on the hydrodynamics of the system. This volatility was attributed to the significant variation of fluid properties. The fluid properties also played a significant role in the operability of the column. Three modes of inoperability were identified using the pressure drop and liquid hold-up data for both systems. 1) "Liquid layer flooding", being similar flooding found in 'classical' gas-liquid extraction columns. This inoperability mode was noted for both the 100 cSt and 200 cSt systems measured at 325.15 K and 328.15 K., as well as high liquid rates and low supercritical fluid flow rates at 333.15 K for the 100 cSt system. 2) "Bubble column flooding", which exhibited a sharp increase in the liquid hold-up and pressure drop at flooding, was similar to the flooding found in liquid-liquid columns. This behaviour was noted in medium liquid- and SF flow rates at 333.15 K for the 100 cSt system. 3) "Entrainment" was found at the highest supercritical fluid flow rates with most of the liquid 'shortcutting' the column and exiting directly through the column overheads. This inoperability mode was noted at high supercritical flow rates at 333.15 K for both systems

Significantly, a loading zone was not detected under supercritical conditions for the systems investigated. The hydrodynamic behaviour progressed directly from a pre-loading zone to an inoperable zone, regardless of the mode of inoperability or fluid properties. The failure to observe a loading zone is in agreement with literature observations and proved an essential observation for later modelling.

Lastly, the impact of the fluid properties on hydrodynamics were discussed. Differences in flooding modes and operability limits were attributed to different fluid flow rates, as well as differences in the fluid properties. In an attempt to isolate the impact of fluid properties, the two systems were compared at a single superficial supercritical fluid velocity, as the literature predicted changing liquid superficial velocity to have a negligible impact.

With regards to density, it was seen when comparing the two systems that the density difference between the phases, played a significant role in hydrodynamic behaviour. The elevated density of the supercritical fluid creates significant buoyancy forces which can lead to premature flooding and rapid entrainment. The difference between the liquid and supercritical phase density was an indicator of flooding, with a difference in density of less than ~250 kg/m^3 proving significant. Lower density differences between phases led to smaller operable ranges for both systems, and it was not possible to operate efficiently at a density difference lower than ~200 kg/m^3.

With regards to dynamic viscosity, it was found that an increase in the liquid viscosity while keeping other properties constant decreased the operable range of the column. Operability for the 200 cSt system was limited to much lower superficial liquid flow rates at the same superficial supercritical flow when compared to the 100 cSt system. The reduced hydrodynamic capacity was directly linked to the increased liquid viscosity, as the supercritical fluid properties were identical between the systems and the liquid densities did not differ significantly. The liquid viscosity was found in this work to play a significant role in hydrodynamics. The significance of viscosity was a new finding, with literature only mentioning density as a major contributor to hydrodynamics in supercritical systems.

The interplay of density and viscosity and their influence on hydrodynamics under supercritical systems are complex and merits further investigation.

The above points contributed to the fulfilment of the third objective. Hydrodynamic data were gathered, and multiple inoperability phenomena were identified in a single system. The impact of both the density and dynamic viscosity on the system was discussed. The gathered data were next compared to available models.

8.5 **Objective 4 - Chapter 7.1 and 7.2**

Chapter 7 compared the gathered data to the three models, the Stichlmair et al., Woerlee and Maćkowiak models. Comparisons to literature data were made where appropriate. This works towards the fourth objective - to compare the gathered hydrodynamic data to available models to determine their accuracy in predicting supercritical hydrodynamics:

The models were first used to predict liquid hold-up in the pre-loading region, below the loading line. The Maćkowiak model proved ineffective in predicting the liquid hold-up below the loading line. The model significantly over-predicted the experimental data and failed to predict the experimentally measured slope and trend of the data. An attempt was made to regress a new empirical constant to provide a better model fit. Despite fitting the model to the data, the prediction of the experimental results was unsuccessful due to the lack of the model even providing a qualitative fit to the experimental data. The modified Stichlmair et al. model provided an excellent fit to the liquid hold-up below the loading line for both systems. The excellent model fit was in contrast to the poor fit provided by the literature data. The better fit of the experimental data, when compared to that of the literature data, was attributed to the highly empirical nature of the model, as well as data of Stockfleth having large variations between individual superficial supercritical flow rates. The experimental data of this study showed little variation with changing superficial supercritical flow rates, in agreement with the model prediction. The model by Woerlee presented with a different slope than the literature data and failed to provide a prediction. It is, however, noteworthy that the model by Woerlee could predict hold-up values of similar magnitude to the experimental data with minimal empiricism in the model. The liquid hold-up of the experimental system was also found to be higher than the literature data at similar fluid flow rates. The increased liquid hold-up was found to not be due to column internals, but rather the difference in fluid properties between the systems, in particular, the liquid viscosity.

The pressure drop was modelled next. The Maćkowiak model required liquid surface tension (which was not measured or available in the literature) in order to predict pressure drop or flooding. Hence no further sensible predictions were made using this particular model. Before attempting a fit using the Stichlmair et al. pressure drop model, the calculations were simplified to take the lack of an observable loading zone into account. The simplification led to a much easier equation to solve and removed the need to calculate iteratively or derive further constants. The modification was tested against the unmodified model prediction of the literature values, with an excellent fit achieved in the area of interest. The modified model was found to present a poor prediction of the experimental data but presented with a similar qualitative trend. The model was, therefore, further modified with the addition of a constant to scale it to the experimental data. The derived constants for the two systems agreed very well, despite the differences in the constants derived for the liquid hold-up prediction feeding into the pressure drop equations. The scaled model fits did not agree well with the experimental data. The model predicted considerable variation in the pressure drop concerning the superficial supercritical velocity, with higher velocities predicting higher pressure drops. The same variation was not present in the experimental results, with the data showing more complex behaviour with regards to superficial supercritical velocity than the model could predict. The Woerlee model presented an order of magnitude prediction of the pressure drop op the 100 cSt system, but failed to predict the 200 cSt system. Again the model has a noteably different trend to its data when compared to the experimental data, showing a slower increase in pressure drop with an increase in superficial liquid velocity. The performance of the Woerlee model is noteworthy, as it managed order of magnitude predictions of some of the data with a very limited empirical element. this agreement shows there are some similarity between gas-liquid systems, but that the tested models do not have the sophistication to predict supercritical fluids.

In conclusion, no model could predict the pressure drop or operability limits for the experimental data. This lack of a prediction is found despite the statement in the literature that there is no fundamental difference between supercritical and classical hydrodynamics.

Although this work does not delve into the development of models and their fundamental structures, some conjectures can be made with regards to the development of future models. With sufficient data and insight, a 'generalized' correlation should be possible, such as the likes of the Makoviak model. This does, however require a lot of data with empirical constants for the different possible packings, fluids and fluid properties and is extremely research intensive and becomes unreliable as soon as one exceeds the boundaries of the model. This has been achieved for ‘classical’ systems within limits and should be possible for supercritical systems, although the level of intricacy and detail remains to be seen as more data are gathered.

8.6 **Objective 5 - Chapter 7.3**

A comparison between supercritical hydrodynamics and atmospheric hydrodynamics was made to test the hypothesis that supercritical hydrodynamics are fundamentally similar to atmospheric systems. Previous authors have provided contrasting views, firstly stating that classical hydrodynamical models can not predict supercritical systems, while secondly stating there is no fundamental difference between sub- and supercritical hydrodynamics. If there is no fundamental difference, then classical hydrodynamic models should be applicable, as long as the model is adjusted for the fluid properties of the supercritical fluid.

Three conclusions made during this study cast doubt on the fundamental similarity. Firstly, the lack of a detectable loading zone is in contrast with classical hydrodynamics. In classical hydrodynamics, the loading zone is present and plays a significant role in column operability and efficiency. Secondly, pressure drop and liquid hold-up were found to be unreliable predictors of operability in the supercritical systems investigated. This observation is in contrast with classical hydrodynamics, where pressure drop and liquid hold-up are well-established measures of operability. Thirdly, the investigated classical hydrodynamic models cannot predict pressure drop, flooding, or hydrodynamic capacity for the supercritical systems investigated. This lack is despite applying changes to compensate for elevated fluid properties of the supercritical phase.

On the contrary, the model fit by Woerlee was able to predict values in the same order of magnitude as the experimentally determined data with very little to no empirical fitting of the data. This ability of the model to present a rough prediction implies that there is some fundamental agreement in the model assumptions and what is happening in the experimental system. The model however fails to present an accurate prediction of either liquid hold-up or pressure drop, implying that further work is required.

None of the above points explicitly prove or disprove a fundamental difference between supercritical and classical hydrodynamics. They do, however, raise reasonable doubts that need to be addressed before the literature statement is assumed correct. Currently, there is insufficient information available to ascertain if there are fundamental differences between classical and supercritical hydrodynamics. It was concluded that further research is needed to delve into the differences before a conclusion can be reached.

8.7 Conclusions in Summary

The overarching aim of this study was to:

Investigate hydrodynamics in countercurrent columns operating under supercritical conditions, while laying groundwork for the eventual development of accurate predictive models and design methods.

This work started with a review of basic literature, hydrodynamics under supercritical conditions, available predictive models and fluid properties under supercritical conditions. The literature review identified the need for a) hydrodynamic data under supercritical conditions and b) a full set of fluid property data gathered implicitly for hydrodynamic study. The second point served as a departure point for the successful design, construction and verification of equipment capable of measuring suitable fluid property and phase data. The equipment was used to gather data on two PDMS + CO_2 systems that exhibited the desired properties at 313 – 353 K. The experimental systems were selected to isolate hydrodynamic behaviour by minimising the effect of mass transfer while providing the opportunity to isolate the influence of different fluid properties. Importantly, the equipment and measured systems were communicated to academia in the form of two publications.

The gathered fluid property and phase data were then used to define a set of hydrodynamic, pilot plant experiments. Operability behaviour and the influence of fluid properties on the hydrodynamic capacity were determined. Three different modes of inoperability were identified in a single system. Both viscosity and density were found to have a significant influence on the hydrodynamic capacity of the column. The density difference between the two phases proved an indicator of operability, with a lower difference reducing the operability. An increase in viscosity increased the liquid hold-up and decreased column operability. Importantly, no loading operating regime was identified for the system.

The gathered data were next used to evaluate the Stichlmair et al. and Maćkowiak models. Neither model could predict the pressure drop or operability limits for the experimental data, despite attempts to tweak the models and fit empirical constants.

The work was concluded by testing the literature hypothesis that supercritical hydrodynamics are fundamentally similar to atmospheric systems. The hypothesis cannot be proved or disproved with the available data, although doubts were raised as to the fundamental similarity.

As a whole, this work can serve as a launching platform for future research into supercritical hydrodynamics. The created equipment can rapidly measure data to create a broader base of fundamental fluid properties for use in hydrodynamic study. The investigated influence of the fluid properties on hydrodynamic capacity can guide the selection of further research, to deconstruct and investigate different influences on hydrodynamics properly. The presentation of hydrodynamic data and the evaluation of available models provide a starting point for model development. As a whole, this work presents novel insights into hydrodynamics countercurrent columns operating under supercritical conditions.

Finally, addressing the concerns raised in this work on the fundamental similarities/differences between classical and supercritical hydrodynamics can guide the development of models. If there are no fundamental differences, an in-depth review of available models and the modifications needed to adjust for the elevated supercritical properties is required. If the phenomena are fundamentally different, the creation of new models is needed.

9. Recommendations

Based on the results and conclusions from this study, several recommendations on areas of future study and investigation are made. These include:

- An in-depth comparison of the electromechanical phase equilibria determination compared to optical SynVisVar method. The electromechanical determination could be valuable for systems that are difficult to determine visually or have been shown to form mist/microdroplets. Additionally, the comparison can serve as a method comparison and help identify and eliminate systematic error in measurements for either method.
- To modify the fluid property equipment to measure the quartz crystal bandwidth. This modification will allow the electromechanical determination of the saturated fluid's density. This measurement should provide a more accurate determination of the saturated fluid density and serve to reduce the measurement equipment uncertainty.
- Modifying the fluid property equipment to measure speed of sound data for the saturated fluid. The quartz crystal used in the cell can potentially gather this data with some further modification and the development of peripherals. This data would prove invaluable to the thermodynamic modelling of the system.
- Thermodynamic modelling of the saturated fluid properties can help to start understanding the fundamentals of saturated fluid properties under supercritical conditions. In particular, the properties of the saturated binary phase when compared with the respective pure fluid properties can be of value to determine if rules of thumb or correlations can be created to predict saturated fluid properties. Rules of thumb or correlations could ease the selection of appropriate systems and assist in the creation of design equations for industrial systems.
- The creation of a range of PDMS fluids with a small amount of longer chains added to raise the dissolution pressure of the liquid artificially. Such fluids can serve to provide a range of various fluid properties while exhibiting the desired low mutual solubility. With some experimentation and planning, custom fluids can be created to investigate desired fluid properties accurately. Investigating a range of fluids, while determining the phase envelopes, can also provide valuable insight into the influence of progressively longer polymer chains on phase equilibria and how it influences complex phase behaviour.
- The further measurement of low mutual solubility systems for use in hydrodynamic studies to further broaden the selection of fluid properties available. An improved variety of fluid properties merits further hydrodynamic pilot plant experiments planned

using a proper statistical design of experiments (DOE). A proper statistical study designed to determine the influence of fluid and column properties on hydrodynamics can indicate significant components that can, in turn, be used with the Buckingham π theorem to identify appropriate dimensionless numbers to use in the creation of applicable hydrodynamic models. A full review of possible models and their fundamental nature could be used to select the correct assumptions and boundary conditions to develop a new model.

- The pilot plant setup has several high-pressure sight glasses built into the column. With the correct equipment, such as a small-bore HD camera, inoperability phenomena such as flooding and entrainment, can be observed during experimentation. This investigation would provide valuable insight into the hydrodynamics of supercritical systems.
    - Flooding and entrainment can be studied with visual confirmation. This study could serve to validate the proposed flooding behaviours of this work, as well as to confirm the complex inoperability behaviour found in the system.
    - Fluid-packing interactions can be observed to determine the wetting of the packing with regards to specific fluid properties and liquid retention time/dispersion studies can be done by injecting dyes using the second fluid feed pump.
- The further measurement of hydrodynamic pilot plant data to build up a broad database of pilot plant data to serve as a basis for the creation of hydrodynamic models for supercritical systems. This measurement can assist in judging the hypothesis that classical hydrodynamics and supercritical hydrodynamics are fundamentally similar.

10. Consolidated Reference List

Acheson, D. J., *Applied Hydrodynamics: An Introduction to Ideal and Real Fluid Flows*, CRC Press, Leiden, 2009, ISBN: 978-0-415-49271-3.	Pub 1 [2]
Alford, R., Burns, M. and Burns, N., Dixon Rings- A Revolutionary Random Column Packing, Filtration 11 (2011) 218-223.	Lit [14]
Arai, Y., Sako, T. and Takebayashi, Y., *Supercritical fluids - Molecular interactions, Physical Properties and New Applications*, Springer: London, England, 2002.	Int [9]
Assael, M.J.; Papadaki, M. and Wakeham, W.A., *Measurements of the Viscosity of Benzene, Toluene, and m-Xylene at Pressure up to 80 MPa*, Int. J. Thermophys., 12 (1991) 449-457.	Pub 1 [26]
Avelino, H.M.N.T., Fareleira, J.M.N.A., Gourgouillon, D., Igreja, J.M. and Nunes da Ponte, M., *Viscosity of poly(ethyleneglycol) 200 [PEG 200] saturated with carbon dioxide*, J. Supercrit. Fluids, 128 (2017) 300-307.	Lit [94]; Pub 1 [30]; Pub 2 [7]
Barath, R.; Inomata, H.; Arai, K.; Shoji, K. and Noguchi, Y., *Vapor-liquid equilibria for binary mixtures of carbon dioxide and fatty acid ethyl esters*, Fluid Phase Equilib., 50 (1989) 315-327.	Pub 1 [38]
Bayraktar, Z. and Kiran, E., *Miscibility, Phase Separation, and Volumetric Properties in Solutions of Poly(dimethylsiloxane) in Supercritical Carbon Dioxide*, J. Appl. Polym. Sci., 75 (1999) 1397-1403.	Lit [84]; Pub 2 [9]
Berche, B., Henkel, M. and Kenna, R., *Critical phenomena: 150 years since Cagniard de la Tour*, J. Phys. Stud, 13 (2009) 1-4.	Int [16]
Billet, R. and Maćkowiak, J. *Allgemeines Verfahren zur Berechnung der Trennwirkung von Füllkörperkolonnen.* Chem.-Ing.-Techn., 55 (1983) 211-213 [as cited by: Maćkowiak, J. in Fluid Dynamics of Packed Columns, 2010].	Lit [25]
Billet, R. and Maćkowiak, J. *Application of Modern Packings in Thermal separation Processes.* Chem. Eng. Technol., 11 (1988) 213-227.	Lit [31]
Billet, R. and Maćkowiak, J. *How to use the absorption data for design and scale-up of packed column.* Fette, Seifen, Anstrichmittel, 86 (1984) 349-358 [as cited by: Maćkowiak, J. in Fluid Dynamics of Packed Columns, 2010].	Lit [27]
Billet, R. and Maćkowiak, J. *Neues Verfahren zur Auslegung von Füllkörperkolonnen für die Rektifikation.* Verfahrenstechnik vt, 17 (1983) 203-211, [as cited by: Maćkowiak, J. in Fluid Dynamics of Packed Columns, 2010].	Lit [26]
Billet, R. and Schultes, M. *Fluid Dynamics and Mass Transfer in the Total Capacity Range of Packed Columns up to the Flood Point.* Chem. Eng. Tech., 18 (1995) 371-379.	Lit [36]
Billet, R. *Industrielle Destillation.* Weinheim : Chemie Verlag, Weinheim, Germany [as cited by: Maćkowiak, J. in Fluid Dynamics of Packed Columns, 2010].	Lit [24]
Björklund, E., Turner, C., Karlsson, L., Mathiasson, L., Björn, S and Skogsmo, J, *The Influence of Oil Extractability and Metal Part Geometry in Degreasing Processes Using Supercritical Carbon Dioxide*, J. Supercrit. Fluids, 9 (1996) 56-60.	Pub 2 [16]
Blass, E. and Kurtz, R. *The influence of surface energy values on the two-phase counter-current packed columns with Raschig-Part I: fluid content. (orig. German).* Process Eng., Vol. 10, p. 721, [as cited by: Maćkowiak, J. in Fluid Dynamics of Packed Columns, 2010], (1976).	Lit [35]
Bond, W.N. *The surface tension of a moving water sheet.* Proc. Physical Society, 47 (1935) 549-558.	Lit [33]
Brandalize, M.V.; Gaschi, P.S.; Mafra, M.R.; Ramos, L.P. and Corazza, M.L., *High-pressure phase equilibrium measurements and thermodynamic modeling for the systems involving CO₂, ethyl esters (oleate, stearate, palmitate) and acetone,* Chem. Eng. Res. Des., 92 (2014) 2814-2825.	Pub 1 [37]
Bright, F.V. and McNally, M.E., *Supercritical Fluid Technology - Theoretical and Applied Approaches to Analytical Chemistry*, ACS Symposium Series, Vol. 488, Washington DC, United States of America, 1992.	Int [12]
Brockkötter, J. and Jupke, A., *Modeling the fluid dynamics of a high-pressure extraction column*, J. Supercrit. Fluids, 154 (2019) 140636.	Lit [58]
Brunner, G. *Counter-current separations.* J. Supercrit. Fluids, 47 (2009) 574 - 582.	Int [8]; Lit [66]
Brunner, G., 1994, *Gas Extraction, An introduction to fundamentals of supercritical fluids and the application to separation processes*, Steinkopff, Darmstadt, ISBN: 978-3-662-07382-7.	Pub 3 [20]
Brunner, G., *Gas Extraction: An Introduction to Fundamentals of Supercritical Fluids and the Application to Separation Processes*, Steinkopff, Darmstadt, 1994, ISBN: 978-3-662-07382-7.	Lit [78]; Pub 1 [3]; Pub 2 [4]; MS 4 [10]
Buchanan, J.E. *Holdup in Irrigated Ring-Packed Towers Below the Loading Point*, J. Ind. Eng. Chem. Fundamentals, 6 (1967) 400-407.	Ch 7 [5]
Budich, M. and Brunner, G. *Vapour-Liquid Equilibrium Data and Flooding Point measurements of the Mixture Carbon Dioxide + Orange Peel Oil.* Fluid Phase Equilib., 158-160 (1999) 759-773.	Lit [47]
Budich, M. *Countercurrent Extraction of Citrus Aroma from Aqueous and Nonaqueous Solutions Using Supercritical Carbon Dioxide,* VDI-Verlag, Düsseldorf, Germany, (1999).	Lit [46]; Pub 3 [14]
Budich, M., Brunner, G., 1999, *Vapour-liquid equilibrium data and flooding point measurements of the mixture carbon dioxide + orange peel oil*, Fluid Phase Equilib., 158, 759.	Pub 3 [15]
Calderon, E.; Gauthier, M.; Decremps, F.; Hamel, G.; Syfosse, G. and Polian, A., *Complete determination of the elastic moduli of α-quartz under hydrostatic pressure up to 1 GPa: an ultrasonic study*, J. Phys. Condens. Matter, 19 (2007), 436228 (13pp).	Pub 1 [12]

Caudwell, D.r.; Trusler, J.P.M.; Vesovic, V. and Wakeham, W.A., *The Viscosity and Density of n-Dodecane and n-Octadecane at Pressures up to 200 MPa and Temperatures up to 473 K*, Int. J. Thermophys, 25 (2004) 1339-1352.	Pub 1 [20]
Collings, A.F. and McLaughlin, E., *Torsional Crystal Technique for the Measurement of Viscosities of Liquids at High Pressure*, Trans. Faraday Soc., 67 (1971) 340-352.	Pub 1 [11]; Pub 2 [21]
Crampon, C.; Charbit, G. and Neau, E., *High-pressure apparatus for phase equilibria studies: solubility of fatty acid esters in supercritical CO_2*, J. Supercrit. Fluids, 16 (1999) 11-20.	Pub 1 [31]
De Haan, A.B. *Supercritical Fluid Extraction of Liquid Hydrocarbon Mixtures.* Ph.D. Dissertation, Technische Universität Delft, (1997).	Lit [97]
De Villiers, A.J., Schwarz, C.E., Burger, A.J. and Kontogeorgis, G.M.*, Evaluation of the PC-SAFT, SAFT and CPA equations of state in predicting derivative properties of selected non-polar and hydrogen-bonding compounds*, Fluid Phase Equilib., 338 (2013) 1-15.	Int [33]
Diaz, M.S. and Brignole, E.A. *Modeling and optimization of supercritical fluid processes.* J. Supercrit. Fluids, 47 (2009) 611-618.	Lit [54]
Dindar, C. and Kiran, E., *High-Pressure Viscosity and Density of Polymer Solutions at the Critical Polymer Concentration in Near-Critical and Supercritical Fluids*, Ind. Eng. Chem. Res., 41 (2002) 6354-6362.	Lit [81]; Pub 2 [10]
Dohrn, R. and Christov, M. *High-pressure fluid phase equilibria: Experimental methods and systems investigated (1994-1999).* Fluid Phase Equilib., 202 (2002) 153-218.	Lit [62]
Dohrn, R. *High-pressure fluid-phase equilibria: Experimental methods and systems investigated (1988-1993).* Fluid Phase Equilib., 106 (1995) 213-282.	Lit [61]
Dohrn, R., Fonseca, J.M.S. and Peper, S. *High-pressure fluid-phase equilibria: Experimental methods and systems investigated (2005-2008).* Fluid Phase Equilib., 300 (2011) 1-69.	Lit [64]
Dohrn, R., Peper, S. and Fonseca, J.M.S. *High-pressure fluid-phase equilibria: Experimental methods and systems investigated (2000-2004).* Fluid Phase Equilib., 288 (2010) 1-54.	Lit [63]
Dohrn, R.; Fonseca, J.M.S. and Peper, S., *Experimental Methods for Phase Equilibria at High Pressures*, Annu. Rev. Chem. Biomol. Eng., 3 (2012) 343, 2012.	Lit [96]; Pub 1 [5]
Du Rand, M. and Nieuwoudt, I., *Measurement of phase equilibria of supercritical ethane and paraffins*, J. Supercrit. Fluids, 21 (2001) 181-193.	Int [20]
Ducoulombier, D.; Zhou, H.; Boned, C.; Peyrelasse, J.; Saint-Guirons, H. and Xans, P., *Pressure (1-1000 bars) and Temperature (20-100 °C) Dependence of the Viscosity of Liquid Hydrocarbons*, J. Phys. Chem., 90 (1986) 1692-1700.	Pub 1 [22]
Eckert, J.S. *How tower packings behave.* Chem. Eng., 2 (1975) 70-76.	Int [7]; Lit [12]
Eckert, J.S. *Selecting the Proper Distillation Column Packing.* Chem. Eng. Prog., 66 (1970) 39.	Lit [51]; Pub 3 [12]
Ergun, S. *Fluid Flow through Packed Columns.* Chem. Eng. Prog., 48 (1952) 89-94.	Lit [68]
Fakhreddine, A. and Zoller, P., *The Equation of State of a Polydimethylsiloxane Fluid*, J. Appl. Polym. Sci., 41 (1990) 1087-1093.	Pub 2 [27]
Fenghour, A.; Wakeham, W.A. and Vesovic, V. *The Viscosity of Carbon Dioxide.* J. Phys. Chem. Ref. Data, 27 (1998) 31-44.	Lit [4]; Pub 1 [33]; Pub 2 [28]
Fernandes, J., Lisboa, P.F., Simões, P.C., Mota, J.P.B. and Saatdijan, E. *Application of CFD in the study of supercritical fluid extraction with structured packing: Wet pressure drop calculations.* J. Supercrit. Fluids, 50 (2009) 61-68.	Lit [60]
Fernandes, J., Simões, P.C., Mota, J.P.B. and Saatdijan, E. *Application of CFD in the study of supercritical fluid extraction with structured packing: Dry pressure drop calculations.* J. Supercrit. Fluids, 47 (2008) 17-24.	Lit [59]
Ferreira, M. and Schwarz, C.E., *Super- and near-critical fluid phase behavior and phenomena of the ternary system CO_2 + 1-decanol + n-tetradecane*, J. Chem. Thermodyn., 111 (2017) 88-99.	Int [21]
Fourie, F.C.v.N., Schwarz, C.E. and Knoetze, J.H., *Phase equilibria of alcohols in supercritical fluids Part I. The effect of the position of the hydroxyl group for linear C_8 alcohols in supercritical carbon dioxide*, J. Supercrit. Fluids, 47 (2008) 161-167.	Int [27]; Pub 1 [7]; Pub 2 [18]
Fourie, F.C.vN.; Schwarz, C.E. and Knoetze, J.H., *Analytic High-Pressure Phase Equilibria. Part II: Gas Chromatography and Sampling Method Develop*ment, Chem. Eng. Technol., 39 (2016) 1475-1483.	Pub 1 [8]; Pub 2 [23]
Franken, H.H. *Establishment of a Supercritical Pilot Plant and the Hydrodynamics of Supercritical Countercurrent Columns,* Masters Dissertation, Stellenbosch University, Department of Process Engineering, (2014).	Int [10]; Lit [1]; MS 4 [11]
Franken, H.H., 2020, *The Hydrodynamics of Supercritical Countercurrent Columns*, PhD Dissertation, Stellenbosch University, Stellenbosch, South Africa, (to be published, Mrt 2020).	Pub 3 [22]
Franken, H.H., Knoetze, J.H. and Schwarz, C.E., *Concurrent measurement of high-pressure binary phase equilibrium, density and dynamic viscosity*, J. Supercrit. Fluids, 133 (2018) 444-454.	Int [36]; Pub 2 [3]; Pub 3 [19]; MS 4 [7]
Franken, H.H., Knoetze, J.H. and Schwarz, C.E., *High-pressure binary phase equilibria, density and dynamic viscosity of 100 & 200 cSt polydimethylsiloxane (PDMS) with supercritical CO_2*, J. Supercritical Fluids, 139 (2018) 1-7.	Int [37]; Pub 3 [21]; MS 4 [9]
Franken, H.H., Knoetze, J.H. and Schwarz, C.E., *Hydrodynamics of a Packed Column Operated under Supercritical Conditions*, Chem. Eng. Trans., 69 (2018).	Int [38]; MS 4 [8]
Garg, A., Gulari, E. and Manke, C.E., *Thermodynamics of Polymer Melts Swollen with Supercritical Gases*, Macromolecules, 27 (1994) 5643-5653.	Pub 2 [12]
Gibbs, J.W. *On the Equilibrium of Heterogeneous Substances, Part 1.* Trans. Conn. Acad. Arts Sci., 3 (1876) 108-24.	Lit [3]
Goodwin, R.D., *Benzene Thermophysical Properties from 279 to 900 K at Pressures to 1000 Bar*, J. Phys. Chem. Ref. Data, 17 (1988) 1541-1636.	Pub 1 [29]

Gourgouillon, D., Avelino, H.M.N.T., Fareleira, J.M.N.A. and Nunes da Ponte, M., *Simultaneous viscosity and density measurement of supercritical CO2-saturated PEG 400*, J. Supercrit. Fluids, 13 (1998) 177-185.	Lit [90]
Guedes de Carvalho, J.R.F. and Talaia, M.A.R. *Interfacial shear stress as a criterion for flooding in counter current film flow along vertical surfaces.* Chem. Eng. Sci, 53 (1998) 2041-2051.	Lit [19]
Habrioux, M.; Balize, J.; Galliero, G. and Darion, J., *Viscosities of Fatty Acid Methyl and Ethyl Esters under High Pressure: Methyl Myristate and Ethyl Myristate*, J. Chem. Eng. Data, 61 (2016) 398−403.	Pub 1 [34]
Hager, W.H. *Wilfrid Noel Bond and the Bond number.* J. Hydraul. Res., 50 (2012) 3-9.	Lit [34]
Hernández-Galván, M.A.; García-Sánchez, F. and Macías-Salinas, R., *Liquid viscosities of benzene, n-tetradecane, and benzene + n-tetradecane from 313 to 393 K and pressures up to 60 MPa: Experiment and modelling*, Fluid Phase Equilib, 262 (2007) 51–60.	Pub 1 [28]
Hrnčič, M.K., Škerget, M. and Knez, Z., *Density and viscosity of the binary polyethylene glycol/CO2 systems*, J. Supercrit. Fluids, 95 (2014) 641-668.	Lit [91]
Huber, M.L.; Laesecke, A. and Perkins, R., *Transport Properties of n-Dodecane*, Energy Fuels, 18 (2004) 968-975.	Pub 1 [24]
Iguchi, M. Hiraga, Y., Kasuya, K., Aida, T.M., Watanabe, M., Sato, Y. and Smith, R.L., *Viscosity and density of poly(ethylene glycol) and its solution with carbon dioxide at 353.2 K and 373.2 K at pressures up to 15 MPa*, J. of Supercrit. Fluids, 97 (2015).	Lit [92]
Ilieva, P., Kilzer, A. and Weidner, E., *Measurement of solubility, viscosity, density and interfacial tension of the systems tristearin and CO2 and rapeseed oil and CO2*, J. of Supercrit. Fluids, 117 (2016) 40–49.	Lit [88]
Jackson, J.D., *Classical Electrodynamics, 3rd Edition*, Wiley, New York, 1999, ISBN: 978-0-471-30932-1.	Pub 1 [17]
Jenab, E. and Temelli, F., *Viscosity measurement and modeling of canola oil and its blend with canola stearin in equilibrium with high pressure carbon dioxide*, J. of Supercrit. Fluids, 58 (2011) 7–14.	Lit [86]
Johnston, K.P., Da Rocha, S.R.P., Lee, C.T, Li, G. and Yates, M.Z., *Colloid and Interface Science for CO_2-Based Pharmaceutical Processes*, in: York, P., Kompella, U.B. and Shekunov, B.Y. (Eds.), Supercritical Fluid Technology for Drug Product Development, Informa Healthcare, New York, 2008, 202-231, ISBN 0-8247-4805-0.	Pub 2 [14]
Joint Committee for Guides in Metrology, *Evaluation of measurement data – Guide to the expression of uncertainty in measurement, JCGM 100:2008*, available at: http://www.iso.org/sites/JCGM/GUM/JCGM100/C045315e-html/C045315e.html, 2008 (accessed: 06 Nov 2017).	Pub 1 [19]; Pub 2 [22]; MS 4 [15]
Kashiwagi, H.; Fukunaga, H.; Tanaka, Y.; Kubota, H. and Makita, T., *Dielectric constant and density of (benzene + chlorobenzene) at high pressures*, J. Chem. Thermodyn., 15 (1983) 567-580.	Pub 1 [25]
Ke, J.; King, P.J.; George, M.W. and Poliakoff, M., *Method for Locating the Vapor-Liquid Critical Point of Multicomponent Fluid Mixtures Using a Shear Mode Piezoelectric Sensor*, Anal. Chem., 77 (2005) 85–92.	Pub 1 [35]
Keramidi, A.S. and Rastorguev, Y.L., *Viskosität von Alkanen*, Izv. Vyssh. Uchebn. Zaved. Neft Gaz (1972) 61-66.	Pub 1 [21]
Kian, K. and Scurto, A.M., *Viscosity of compressed CO2 -saturated n-alkanes: CO2/n-hexane, CO2/n-decane, and CO2/n-tetradecane*, J. Supercrit. Fluids, 133 (2018) 411–420.	Lit [89]
Kikic, I. and De Loos, T.W., *Thermodynamic Properties at High Pressure*, in: A. Bertucco, G.Vetter (Eds.), High Pressure Process Technology: Fundamentals and Applications, Elsevier, Amsterdam, 2001, ISBN: 978-0-444-50498-2.	Pub 2 [25]
Kimizuka, H.; Shigenobu, O.; Li, J. and Shibutani, Y., *Complete set of elastic constants of α-quartz at high pressure: A first-principles study*, Phys. Rev. B, 75 (2007) 054109 (6pp).	Pub 1 [16]
Kiran, E. and Zhuang, W., *Miscibility and Phase Separation of Polymers in Near- and Supercritical Fluids*, ACS Symp. Ser., 670 (1997) 2-36.	Pub 2 [6]
Kirschbaum, E. *Destillier und Rektifiziertechnik 4th Edition.* Springer-Verlag, Berlin, Germany [as cited by: Maćkowiak, J. in Fluid Dynamics of Packed Columns, 2010], (1969).	Lit [23]
Kister, H.Z. *Distillation Design.* McGraw-Hill, New York, United States of America, (1992).	Lit [18]; Pub 3 [23]
Konynenburg, P.H. and Scott, R.L., *Critical lines and phase equilibria in binary van der Waals mixtures*, Phil. Trans. R. Soc. A, 298 (1980) 495-540.	Pub 2 [26]
Koronaios, P., Stevenson, C., Warman, S., Enick, R. and Luebke, D., *Thermally Stable Silicone Solvents for the Selective Absorption of CO_2 from Warm Gas Streams That Also Contain H_2 and H_2O*, Energy Fuels, 30 (2016) 5901−5910.	Pub 2 [13]
Kravanja, G., Hrnčič, M.K., Škerget, M. and Knez, Z., *Interfacial tension and gas solubility of molten polymer polyethylene glycol in contact with supercritical carbon dioxide and argon*, J. Supercrit. Fluids, 108 (2016) 45-55.	Lit [93]
Kravanja, G., Knez, Z. and Hrnčič, M.K., *Density, interfacial tension, and viscosity of polyethylene glycol 6000 and supercritical CO2*, J. Supercrit. Fluids, 139 (2018) 72-79.	Lit [95]
Krehenwinkel, H. and Knapp, H. *Pressure Drop and Flooding in Packed columns at High pressures.* Chem. Eng. Tech., 10 (1987) 231-242.	Lit [39]
Kuźniar, J. and Niżański, A. *Investigations on Mellapak 250Y made of sheet metal (Orig. Polish).* Simposium volume III: Rectification, Absorption, Extraction, (1999) 65-74.	Lit [32]
Lamprecht, S.M. *Establishing a Facility to Measure Packed Column Hydrodynamics.* Masters Dissertation, Stellenbosch University, Department of Process Engineering, (2010).	Int [5]; Lit [30]
Lemmon, E.W. and Huber, M.L., *Thermodynamic Properties of n-Dodecane*, Energy Fuels, 18 (2004) 960-967.	Pub 1 [23]
Lim, J.S., Lee, Y.-W., Kim, J.-D, Lee, Y.Y. and Chun, H.-S. *Mass-Transfer and Hydraulic Characteristics in Spray and Packed Extraction Columns for Supercritical Carbon Dioxide-Ethanol-Water System.* J. Supercrit. Fluids, 8 (1995) 127.	Lit [43]; Pub 3 [8]
Liu, K., Schuch, F. and Kiran, E., *High-pressure viscosity and density of poly(methyl methacrylate)+ acetone and poly(methyl methacrylate)+ acetone+ CO2 systems, J. of Supercrit. Fluids*, 39 (2006) 89–101.	Lit [82]
Lobo, W.E., Friend, L., Hashmall, F. and Zenz, F. *Limiting capacity of dumped tower packings.* Trans. Am. Inst. Chem. Engng., 41 (1945) 693-710.	Lit [13]
Lombard, J.E., *Thermodynamic modelling of hydrocarbon-chains and light-weight supercritical solvents*, MSc Thesis, Stellenbosch University, South Africa, (2015).	Int [32]; Pub 2 [2]; Pub 3 [3]; MS 4 [6]

Lopes, J.M., Kareth, S., Bermejo, M.D., Martín, Á., Weidner, E. and Cocero, M.J., *Experimental determination of viscosities and densities of mixtures carbon dioxide+ 1-allyl-3-methylimidazolium chloride. Viscosity correlation*, J. of Supercrit. Fluids, 111 (2016) 91-96.	Lit [83]
Machado, N.T. *Fractionation of PFAD-Compounds in Countercurrent Columns Using Supercritical Carbon Dioxide as Solvent,* Ph.D. Dissertation, Technische Universität Hamburg - Harburg, (1998).	Lit [44]; Pub 3 [9]
Maćkowiak, J. *Extended channel model for prediction of the pressure drop in single-phase flow in packed columns.* Chem. Eng. Res. and Des., 87 (2009) 123-134.	Lit [76]
Maćkowiak, J. *Fluid dynamics of packings and columns with modern packings for gas / liquid systems (orig. German).* Salle & Sauerland, Frankfurt, Germany, (1991).	Lit [52]; Pub 3 [13]
Maćkowiak, J. *Pressure drop in irrigated packed columns.* Chem. Eng. Process. 29 (1991) 93-105.	Lit [73]
Maćkowiak, J., *Fluid Dynamics of Packed Columns*, Springer, Berlin, Germany, 2010.	Int [4]; Lit [11]; MS 4 [12]; Ch 7 [2]
Mamedov, A.M.; Akhundov, T.S.; Ismail-Zade, S.M. and Tairov, A.D, *Viskosität von Benzen*, Izv. Vyssh. Uchebn. Zaved., Neft Gaz, 2 (1971) 74-76.	Pub 1 [27]
Martín, A. and Cocero, M.J. *Mathematical modeling of the fractionation of liquids with supercritical CO2 in a countercurrent packed column.* J. Supercrit. Fluids, 39 (2007) 304-314.	Lit [55]
Mason, W.P., *Measurement of the Viscosity and Shear Elasticity of Liquids by Means of a Torsionally Vibrating Crystal*, Trans. ASME, 69 (1947) 359.	Pub 1 [15]; Pub 2 [20]
Mersmann, A. and Deixler, A. *Packungskolonnen.* Chem.-Ing.-Techn., 56 (1986) 19-31.	Lit [75]
Mersmann, A. *Zur Berechnung des Flutpunktes in Füllkörperschüttungen.* Chem. Ing. Tech., 37 (1965) 218-226.	Lit [15]; Pub 3 [11]
Mertsch, R. and Wolf, B.A., *Solutions of Poly(dimethylsiloxane) in Supercritical CO_2: Viscometric and Volumetric Behavior*, Macromolecules, 27 (1994) 3289–3294.	Lit [79]; Pub 2 [11]
Meyer, J.-T. *Druckverlust und Flutpunkte in Hochdruckgegenstromkolonnen.* Ph.D Dissertation, Technische Universität Hamburg - Harburg, (1998).	Lit [45]; Pub 3 [10]; Ch 7 [7]
Minne, U.L., Burger, A.J. and Schwarz, C.E., *The Effect of Fluid Properties and Packing Size on the Hydrodynamics of Packed Columns,* Chem. Eng. Trans., 69 (2018) 31-36.	MS 4 [20]
Moser, M. and Trepp, C. *Investigating the Stability of Falling Films at Round Vertical Film Carriers Under High Pressure.* Chem. Eng. Technol., 20 (1997) 612-616 .	Lit [21]
Nalawade, S.P., Picchioni, F. and Janssen, L.P.B.M., *Supercritical carbon dioxide as a green solvent for processing polymer melts: Processing aspects and applications*, Prog. Polym. Sci., 31 (2006) 19–43.	Pub 2 [15]
Ndiaye, E.I.; Habrioux, M.; Coutinho, J.A.P.; Paredes, M.L.L. and Daridon, J., *Speed of Sound, Density, and Derivative Properties of Ethyl Myristate, Methyl Myristate, and Methyl Palmitate under High Pressure*, J. Chem. Eng. Data, 58 (2013) 1371–1377.	Pub 1 [32]
Nie, J.; Liu, J. and Meng, X., *Dew point fast measurement in organic vapor mixtures using quartz resonant sensor*, Rev. Sci. Instrum., 88 (2017) 015005 (5pp).	Pub 1 [36]
Nieuwoudt, I. *The Fractionation of High Molecular Weight Alkane Mixtures with Supercritical Fluids,* Ph.D. Dissertation, Stellenbosch University, Department of Process Engineering, (1994).	Int [2]; Lit [5]
Nieuwoudt, I., and Du Rand, M., *Measurement of phase equilibria of supercritical carbon dioxide and paraffins*, J. Supercrit. Fluids, 22 (2002) 185-199.	Int [19]
Nusselt, W. *Die Oberflachenkondensation des Wasserdampfes.* Z. Ver. Dtsch. Ing., 60 (1916) 541-546.	Lit [22]
Oxford Dictionaries. *Concise Oxford Dictionary of English, 11th Edition.* Oxford University Press, Cape Town, South Africa, (2008).	Lit [10]
Pensado, A.S., Pádua, A.A.H., Comuñas, M.J.P. and Fernández, J., *Viscosity and density measurements for carbon dioxide+ pentaerythritol ester lubricant mixtures at low lubricant concentration*, J. of Supercrit. Fluids. 44 (2008) 172–185.	Lit [85]
Peper, S., Fonseca, J.M.S. and Dohrn, R. *High-pressure fluid-phase equilibria: Trends, recent developments and systems investigated (2009 - 2012).* Fluid Phase Equilib., 484 (2019) 126-224.	Lit [65]
Peter, S. and Tiegs, C. International Symposium on High Pressure Chemical Engineering, Erlangen, West Germany. [as referenced by: Rathkamp, Bravo and Fair, Solvent Extr. Ion Exch., 3 (1987) 367], (1984).	Lit [37]
Rathkamp, P.J., Bravo, J.L. and Fair, J.R. *Evaluation of Packed Columns in Supercritical Extraction Processes.* Solv. Extr. Ion Exch., 5 (1987) 367-391.	Lit [38]; Pub 3 [4]
Raveendran, P., Ikushima, Y. and Wallen, S.L., *Polar Attributes of Supercritical Carbon Dioxide*, Acc. Chem. Res., 38 (2005) 478-485.	Int [13]
Reid, R.C. and Sherwood, T.K., *The Properties of Gases and Liquids: Their estimation and correlation*, McGraw-Hill Book Company, New York, (1966) ISBN: 978-0-070-51789-9.	MS 4 [21]
Reverchon, E. and Lacuzio, G. *Supercritical desorption of bergamot peel oil from silica gel - Experiments and mathematical modelling.* Chem. Eng. Sci., 52 (1997) 3553-3559.	Lit [57]
Reynolds, O. *An Experimental Investigation of the Circumstances Which Determine Whether the Motion of Water Shall Be Direct or Sinuous, and of the Law of Resistance in Parallel Channels.* Philos. Trans. Royal Soc., 174 (1883) 935-982. Philosophical Transactions of the Royal Society, 174 (1883) 935-982.	Lit [70]
Rudnick, J., Taylor, P. L., Litt, M. and Hopfinger, A. J., *Theory of free volume in polymers*, J. Polym. Sci. Polym. Phys. Ed., 17 (1979) 311–320.	Pub 2 [24]
Ruivio, R., Paiva, A., Mota, J.P.B. and Simões, P. *Dynamic model of a countercurrent packed column operating at high pressure conditions.* J. Supercrit. Fluids, 32 (2004) 183-192.	Lit [56]
Rumpf, H.C.H. and Gupte, A.R. *Einflüsse der Porosität und Korngrößenverteilung im Widerstandsgesetz der Porenströmung.* Chem. Ing. Tech.,43 (1971) 367-375. Chem. -Ing. -Tech., 43 (1971) 367-375 [as cited by: Stockfleth, R. in Fluiddynamik in Hochdruckgegenstromkolonnen für die Gasextraktion; Ph.D. Dissertation, Technical University of Hamburg - Harburg, 2001].	Lit [69]

Saito, S., *Research activities on supercritical fluid science and technology in Japan—A review*, J. Supercrit. Fluids, 8 (1995) 177-204.	Int [11]
Schaschke, C.J., *High pressure viscosity measurement with falling body type viscometers*, IRECHE, 2 (2010) 564-567.	Pub 1 [9]
Schmelzer, J. W., Zanotto, E. D., and Fokin, V. M., *Pressure dependence of viscosity.*, J. Chem. Phys., 122 (2005) 074511.	Pub 2 [29]
Schwarz, C.E. and Knoetze, J.H. *Design of Supercritical Fluid Processes for High Molecular Mass Petrochemicals.* 'Supercritical Fluids', M. Belinsky (ed). Nova Science Publishers Inc., (2009).	Int [1]; Lit [6]; Pub 2 [5]; Pub 3 [1]; MS 4 [3]
Schwarz, C.E. and Knoetze, J.H., *Phase equilibrium measurements of long chain acids in supercritical carbon dioxide*, J. Supercrit. Fluids, 66 (2012) 36-48.	Int [24]
Schwarz, C.E. and Nieuwoudt, I., *Phase equilibrium of propane and alkanes: Part I. Experimental procedures, dotriacontane equilibrium and EOS modelling*, J. Supercrit. Fluids, 27 (2003) 133-144.	Pub 1 [6]; Pub 2 [17]
Schwarz, C.E. *The processing of wax and wax additives in supercritical fluids.* Ph.D. Dissertation, Stellenbosch University Department of Process Engineering, Stellenbosch, South Africa, (2005).	Lit [7]; MS 4 [16]
Schwarz, C.E., and Chobanov, K.G., *Phase equilibria of linear saturated high molecular mass acids in supercritical ethane*, J. Supercrit. Fluids, 87 (2014) 40-49.	Int [23]
Schwarz, C.E., Bonthuys, G.J.K., Van Schalkwyk, R.F., Laubscher, D.L., Burger, A.J. and Knoetze, J.H., *Separation of alkanes and alcohols with supercritical fluids. Part II. Influence of process parameters and size of operating range*, J. Supercrit. Fluids, 58 (2011) 352-359.	Int [30]
Schwarz, C.E., De Villiers, A.J., McClune, C.B., Bonthuys, G.J.K., Burger, A.J. and Knoetze, J.H., *High pressure phase equilibrium measurements of long chain alcohols in supercritical ethane*, J. Supercrit. Fluids, 55 (2010) 554-565.	Int [35]
Schwarz, C.E., Fourie, F.C.v.N. and Knoetze, J.H., *Phase equilibria of alcohols in supercritical fluids Part II: The effect of side branching on C_8 alcohols in supercritical carbon dioxide*, J. Supercrit. Fluids, 51 (2009) 128-135.	Int [26]; Lit [9]; MS 4 [2]
Schwarz, C.E., Nieuwoudt, I. and Knoetze, J.H., *Additional Pilot Plant Measurements with Incorporation of Reflux for the Fractionation of Wax Derivatives with Supercritical Propane*, Ind. Eng. Chem. Res., 49 (2010) 4462-4467.	Int [31]
Schwarz, C.E., Nieuwoudt, I. and Knoetze, J.H., *Phase equilibria of long chain n-alkanes in supercritical ethane: Review, measurements and prediction*, J Supercrit. Fluids, 46 (2008) 226-232.	Int [17]; Lit [8]; MS 4 [1]
Schwarz, C.E., Nieuwoudt, I. and Knoetze, J.H., *Phase equilibrium of propane and alkanes Part III: Beyond hexacontane*, J. Supercrit. Fluids, 41 (2007) 327-334.	Int [18]
Schwarz, C.E., Paulse, Q.H. and Knoetze, J.H., *Phase equilibria of methyl esters in supercritical propane*, J. Supercrit. Fluids, 99 (2015) 61-67.	Int [22]
Seader J.D. and Henley, E.J., *Separation Process Principles, 3rd Edition,* Wiley, Chichester, 2013, ISBN: 978-0-470-48183-7.	Pub 1 [1]; Pub 2 [1]; Pub 3 [2]; MS 4 [5]
Seibert, A.F. and Moosberg, D.G. *Performance of Spray, Sieve Tray, and Packed Contactors for high Pressure Extraction.* Sep. Sci. Tech., 23 (1988) 2049-2063.	Int [3]; Lit [40]; Pub 3 [5]
Seifried, B. and Temelli, F., *Use and limitations of a quartz crystal microbalance to measure viscosity of carbon dioxide-expanded fish oil fatty acid ethyl esters*, J. of Supercrit. Fluids, 101 (2015) 104–109.	Lit [87]
Sherwood, T.K., Shipley, G.H. and Holloway, F.A.L. *Flooding Velocities in Packed Columns.* Ind. Eng. Chem., 30 (1938) 765-769.	Int [6]; Lit [71]
Sievers, E.J. *Pressure Drop and Flooding with a supercritical fluid.* Ph.D. Dissertation, Technische Universität Delft, (1994).	Lit [41]; Pub 3 [6]
Souders, M. and Brown, G.G. *Design of Fractionating Columns, Entrainment and Capacity.* Ind. Eng. Chem., 38 (1934) 98-103.	Lit [50]; MS 4 [19]
Span, R. and Wagner, W., *A New Equation of State for Carbon Dioxide Covering the Fluid Region from the Triple-Point Temperature to 1100 K at Pressures up to 800 MPa*, J. Phys. Chem. Ref. Data, 25 (1996) 1509-1596.	Int [15]; Lit [2]; Pub 1 [18]; Pub 2 [19]
Stichlmair, J. *Paper presented at the internal meeting of the Technical Committee " Thermal decomposition of gas and Liquid Mixtures"*. GVD VDI Society for Chemical Engineering, Bochum, (1983).	Lit [74]
Stichlmair, J., Bravo, J.L. and Fair, J.R. *General model for prediction of pressure drop and capacity of countercurrent gas/liquid packed columns.* Gas Sep. Purif., 3 (1989) 19-28.	Lit [67]; Pub 3 [18]; MS 4 [17]; Ch 7 [1]
Stockfleth, R. and Brunner, G. *Film Thickness, Flow Regimes, and Flooding in Countercurrent Annular Flow of a Falling Film at High Pressures.* Ind. Eng. Chem. Res., 40 (2001) 6014-6020.	Lit [20]
Stockfleth, R. and Brunner, G. *Holdup, Pressure Drop, and Flooding in Packed Countercurrent Columns for the Gas Extraction.* Ind. Eng. Chem. Res., 40 (2001) 347-356.	Lit [17]; Pub 3 [17]; MS 4 [18]; Ch 7 [4]
Stockfleth, R. and Brunner, G. *Hydrodynamics of a Packed Countercurrent Column for the Gas Extraction.* Ind. Eng. Chem. Res. 38 (1999) 4000-4006.	Lit [48]; Pub 1 [4]; Pub 3 [16]; MS 4 [4]

Stockfleth, R. *Fluiddynamik in Hochdruckgegenstromkolonnen für die Gasextraktion,* Ph.D. Dissertation, Technical University of Hamburg - Harburg, (2001).	Lit [53]; Ch 7 [6]
Tilton, J.N. *Perry's Chemical Engineers' Handbook.* 8th Edition, McGraw-Hill: New York, United States of America, (2010).	Lit [16]; MS 4 [14]
Tough, J.T.; McCormick, W.D. and Dash, J.G., *Viscosity of Liquid He II*, Phys. Rev., 132 (1963) 2373-2378.	Pub 1 [10]
Turton, R.C., Bailie, R.C., Whiting, W.B. and Shaeiwitz, J.A. *Analysis, Synthesis and Design of Chemical Processes, 3rd edition.* Prentice Hall PTR, Boston, United States of America, (2009).	Lit [28]
Vieira Dos Santos, F.J. and Nieto De Castro, C.A., *Viscosity of Toluene and Benzene Under High Pressure*, Int. J. Thermophys., 18 (1997) 367-378.	Pub 1 [14]
Wagner, W., Saul, A and Pruss, A., *International Equations for the Pressure along the Melting and along the Sublimation Curve for Ordinary Water Substance*, J. Phys. Chem. Ref. Data, Vol 23, No 3, 1994	Int [14]
Walas, S.M. *Chemical Process Equipment - Selection and Design.* Butterworth-Heinemann, Newton, Unites States of America, (1990).	Lit [29]
Wallis, G.B. *One-dimensional Two-phase Flow.* McGraw-Hill: New York, United States of America, (1969).	Lit [72]
Webeler, R.W.H. and Hammer, D.C., *Damping of a torsional oscillator in liquid helium 4 and 3 from 0.4°Kto 2.5 °K*, National Aeronautics and Space Administration, Washington, D.C., NASA technical note (1968) D-4381.	Pub 1 [13]
Woerlee, G.F. *Hydrodynamics and Mass Transfer in Packed Columns and their Applications for Supercritical Separations,* Ph.D. Dissertation, Technische Universität Delft, (1997).	Lit [42]; MS 4 [13]; Ch 7 [3]
Woerlee, G.F., 1997, *Hydrodynamics and mass transfer in packed columns and their applications for supercritical separations*, PhD Dissertation, Technische Universiteit Delft, Delft, The Netherlands.	Pub 3 [7]
Woerlee, G.F., Berends, J., Olujic, Z. and De Graauw, J., *A comprehensive model for the pressure drop in vertical pipes and packed columns*, Chem Eng J., 84 (2001) 367-379.	Lit [77]
Xiong, Y. and Kiran, E., *Miscibility, density and viscosity of poly(dimethylsiloxane) in supercritical carbon dioxide*, Polymer, 36 (1995) 4817-4826.	Lit [80]; Pub 2 [8]
Zacchi, P., Calvo Bastida, S., Jaeger, P., Cocero, M.J. and Eggers, R. *Countercurrent de-acidification of vegetable oils using supercritical CO2: Holdup and RTD experiments.* J. Supercrit. Fluids, 45 (2008) 238-244.	Lit [49]
Zamudio, M., Schwarz, C.E. and Knoetze, J.H., *Experimental measurement and modelling with Aspen Plus® of the phase behaviour of supercritical* CO_2 *+ (n-dodecane + 1-decanol + 3,7-dimethyl-1-octanol)*, J. Supercrit. Fluids, 84 (2013) 132-145.	Int [34]
Zamudio, M., Schwarz, C.E. and Knoetze, J.H., *Phase equilibria of branched isomers of* C_{10}*-alcohols and* C_{10}*-alkanes in supercritical carbon dioxide*, J. Supercrit. Fluids, 59 (2011) 14-26.	Int [25]
Zamudio, M., Schwarz, C.E. and Knoetze, J.H., *The effect of branched alcohol isomers on the separation of alkanes and alcohols with supercritical* CO_2, Poster communication, 13th European Meeting on Supercritical Fluids, The Hague, Netherlands, 2011.	Int [29]
Zamudio, M., *The Separation of Detergent Range Alkanes and Alcohol Isomers with Supercritical Carbon Dioxide*, PhD Dissertation, Stellenbosch University, South Africa, 2014.	Int [28]

Appendix A: Conference Presentations and Posters

All conference presentations and posters are available in this section.

A.1 Presentation - 15th European Meeting on Supercritical Fluids (EMSF 2016) 212
A.2 Poster - 10th World Congress of Chemical Engineering (WCCE 2017) 216
A.3 Poster - 30th European Symposium on Applied Thermodynamics 218
A.4 Presentation - 11th International Conference on Distillation & Absorption 220

A.1 Presentation - 15th European Meeting on Supercritical Fluids (EMSF 2016)

A 1.1 EMSF 2016 Abstract

With increasing application of supercritical fluid fractionation in industry, there is a need for comprehensive data for equipment design purposes. Although phase equilibria data can be easily measured and supply sufficient information regarding the thermodynamic limits of separation, it does not account for the hydrodynamics of separation processes. Fluid properties can change drastically in the supercritical regime, significantly affecting hydrodynamic properties and, hence, design considerations.

A novel piece of equipment, constructed for the simultaneous measurement of binary phase equilibria in the supercritical regime, as well as the viscosity and density of a single-phase at saturation, is presented. The setup consists of a variable volume static view cell to determine equilibrium, and a quartz crystal microbalance to measure fluid properties. Design allows operation up to 35 MPa and 473 K.

Phase equilibrium is determined using a well-established visual method with an uncertainty smaller than 0.1 MPa. The composition of the binary mixture is determined with a maximum uncertainty of 0.01 of the value, and the temperature is measured with a maximum uncertainty of 0.2 K. Viscosity and density is determined measuring the frequency shift and electrical impedance over the quartz microbalance, after which fundamental piezoelectric equations are applied to calculate property values. Uncertainties as low as 0.01 of the value for viscosity and density are possible, as the measurement is dependent on the physical dimensions and characteristics of the crystal and, hence, the sensor requires no calibration.

Pure component viscosity and density measurements were verified using benzene. Additionally, the viscosity, density and phase equilibria data of the system CO_2 + PEG 400 were measured and compared to published data. The experimental setup is thus able to generate reliable phase equilibrium, viscosity and density data within the above-mentioned uncertainties.

A 1.2 EMSF 2016 Presentation

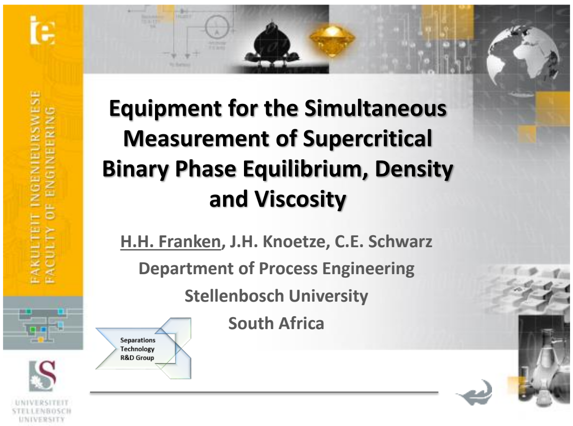

FAKULTEIT INGENIEURSWESE
FACULTY OF ENGINEERING

Equipment for the Simultaneous Measurement of Supercritical Binary Phase Equilibrium, Density and Viscosity

H.H. Franken, J.H. Knoetze, C.E. Schwarz
Department of Process Engineering
Stellenbosch University
South Africa

Separations Technology R&D Group

UNIVERSITEIT STELLENBOSCH UNIVERSITY

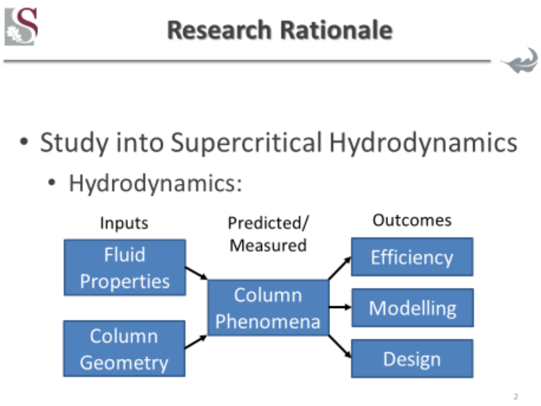

Research Rationale

- Study into Supercritical Hydrodynamics
  - Hydrodynamics:

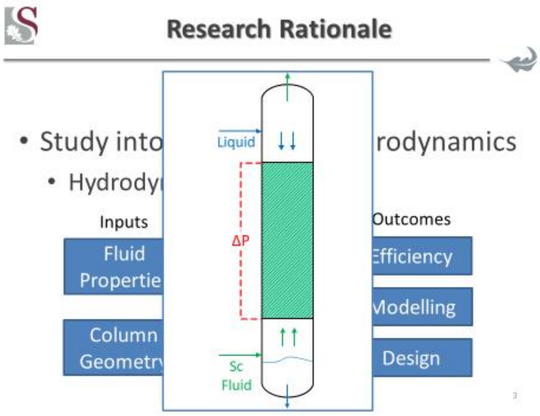

Research Rationale

- Study into rodynamics
  - Hydrody

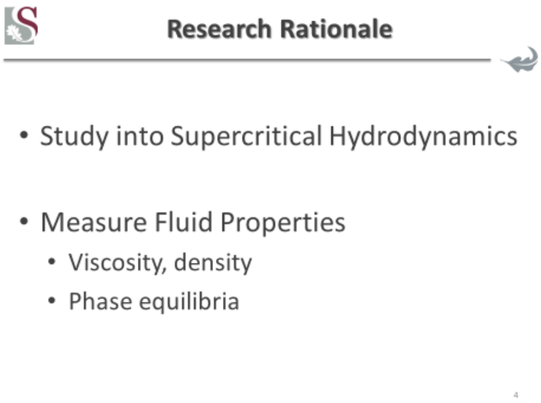

Research Rationale

- Study into Supercritical Hydrodynamics
- Measure Fluid Properties
  - Viscosity, density
  - Phase equilibria

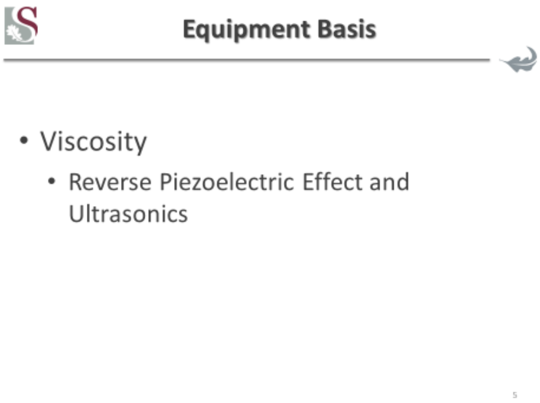

Equipment Basis

- Viscosity
  - Reverse Piezoelectric Effect and Ultrasonics

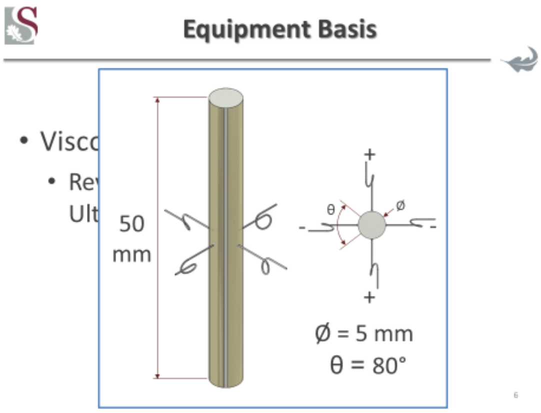

Equipment Basis

- Visc
  - Re
    Ult

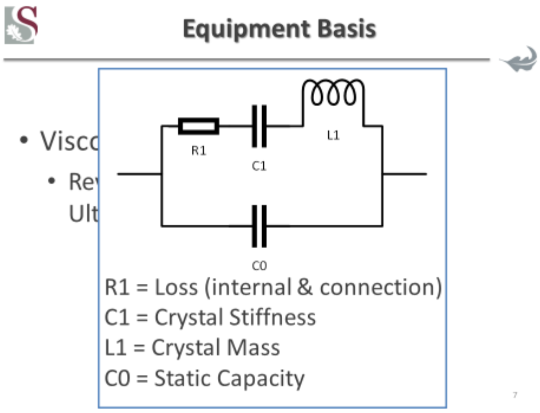

Equipment Basis

- Visc
  - Re
    Ult

R1 = Loss (internal & connection)
C1 = Crystal Stiffness
L1 = Crystal Mass
C0 = Static Capacity

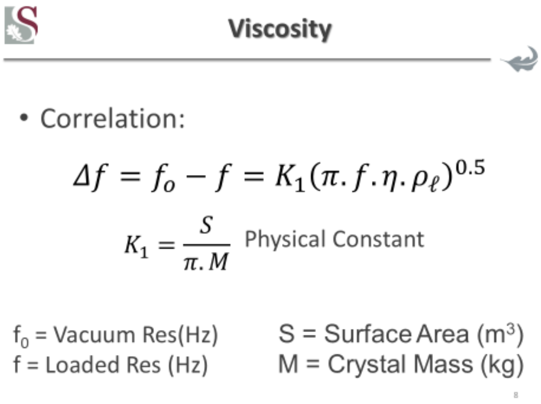

Viscosity

- Correlation:

$$\Delta f = f_o - f = K_1(\pi.f.\eta.\rho_\ell)^{0.5}$$

$$K_1 = \frac{S}{\pi.M}$$ Physical Constant

f_0 = Vacuum Res(Hz)
f = Loaded Res (Hz)

S = Surface Area (m^3)
M = Crystal Mass (kg)

Measurement electronics

- Signal generated by RIGOL DG1022
  - Accuracy 1 µHz ± 100 ppm in 1 year
- Response Measured using Tektronix TDS2002
  - 1.0 GS/s; ± 1mV;
- USB connectivity with Python coding.

Crystal Specifics

- Expends 1.99µW (@1V)
- Dissipates to e^{-1} in 0.24 µm
- Theoretical Resonance 39156.2 Hz

Vacuum resonance

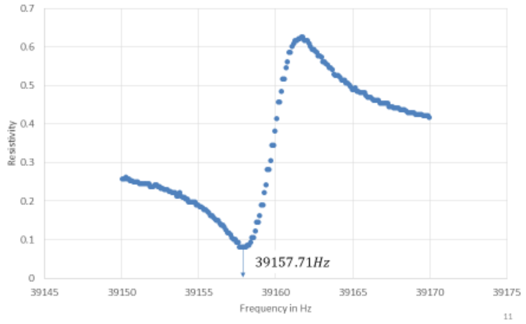

Fluid Resonance

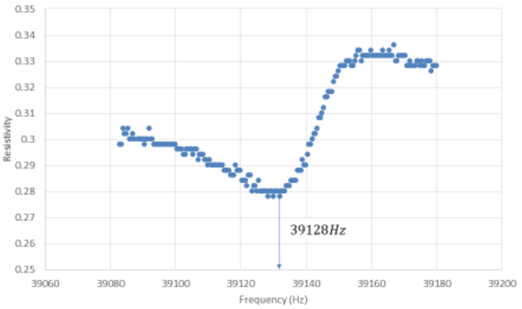

Resonance attenuation

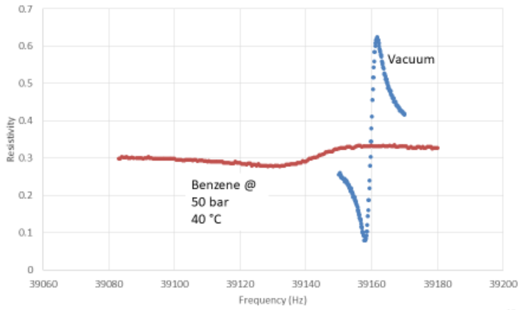

Equipment Basis

- Viscosity
  - Reverse Piezoelectric Effect/Ultrasonics
- Phase equilibria & density
  - SynVis – Variable Volume View cell

View Cell

- View Cell:

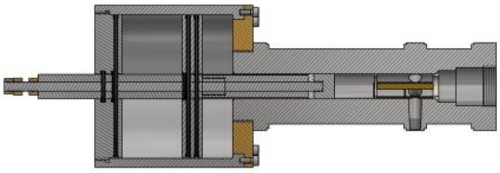

View Cell Specifics

- ±0.1°C with two probes
- ± 0.2 bar
- Delta PLC logging
- Mass within 0.01g
- Electromagnetic stirring

Equipment

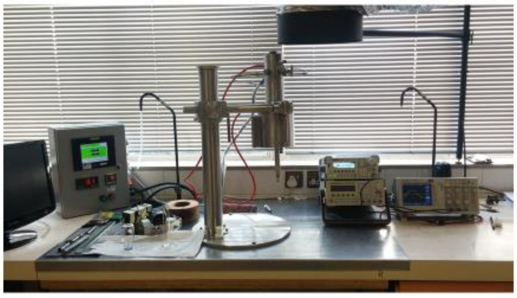

Validation - Benzene

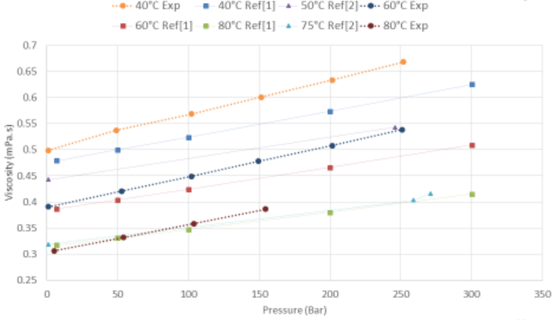

Ref [1] Hernández-Galván, Miguel A., Fernando García-Sánchez, and Ricardo Macías-Salinas. *Fluid Phase Equilibria* 262.1-2 (2007): 51-60.
Ref [2] Vieira dos Santos, F. J. and C. A. Nieto de Castro. *International Journal of Thermophysics* 18.2 (1997): 367-378.

Validation - Benzene

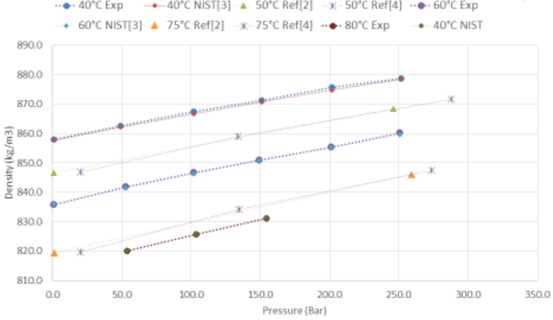

Ref [3] "Isothermal Properties For Benzene". NIST Chemistry WebBook. N.p., 2016. Web. 5 May 2016
Ref [4] Kashiwagi, H., Fukunaga, T., Tanaka, Y., Kubota, H. and Makita, T. *The Journal of Chemical Thermodynamics*, 15.6 (1983), pp.567-580.

Validation - 1-Octanol & CO_2

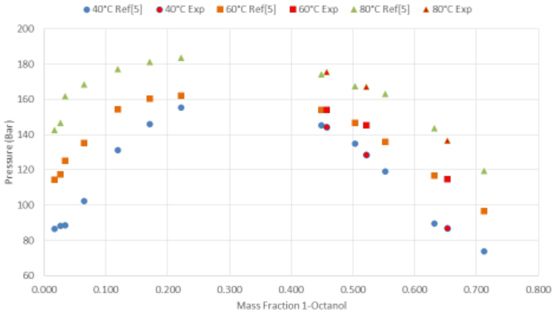

Ref [5] Fourie, F.C.v.N., C.E. Schwarz, and J.H. Knoetze. The Journal of Supercritical Fluids 47.2 (2008): 161-167.

Validation - 1-Octanol & CO_2

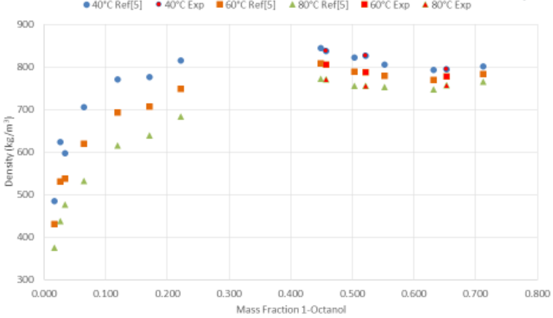

Ref [5] Fourie, F.C.v.N., C.E. Schwarz, and J.H. Knoetze. The Journal of Supercritical Fluids 47.2 (2008): 161-167.

Viscosity - 1-Octanol & CO_2

Temperature	Massfraction Solute	Resonance Frequency	Viscosity
˚C		Hz	mPa.s
40	0.635	39101	2.003
	0.522	39104	1.725
	0.466	39121	0.790
60	0.635	39111	1.488
	0.522	39123	0.826
	0.466	39127	0.638
80	0.635	39120	1.285
	0.522	39130	0.777
	0.466	39130	0.762

Challenges

- Wire connection & Crystal removability
- Crystal leads
- Measurement Sensitivity (Impedance)

Future Outcomes

- Implement Impedance analysis
  - Density determination
- Phase change detection.

A.2 Poster - 10th World Congress of Chemical Engineering (WCCE 2017)

A 2.1 WCCE 2017 Abstract

Data for phase equilibria in supercritical fluids are widely available, supplying sufficient information regarding the thermodynamic limits of separation. Phase equilibria do not, however, give information on the hydrodynamic effects and limits of separation processes. Hydrodynamics, being the study of fluids in motion, play a role in the design and sizing of equipment and is a function of the fluid properties (typically density and viscosity). With fluid properties capable of drastic and unexpected changes in the supercritical regime, hydrodynamic concerns under these conditions can have a significant impact on design considerations.

When investigating the hydrodynamics of a system, mass transfer must be limited and the fluid properties, e.g. viscosity and density, must be known. Concerning mass transfer, very little data are available on solutes that have slight to no mutual solubility, as is favourable for such an investigation. In cases where low solubility data are available, density and viscosity is typically not reported.

As part of a hydrodynamic study, this paper presents data on the phase equilibrium, density and viscosity of Polydimethylsiloxane (PDMS, or colloquially silicone oil) in CO_2. Chemicals are sourced from DOW Chemicals as unbranched, methyl group capped polymers. Two oils, graded at 100 cSt and 200 cSt, is investigated.

The setup used to measure the data consists of a variable volume static view cell to determine equilibrium, and a quartz crystal microbalance to measure fluid properties. The design of the variable volume view cell allows operation up to 35 MPa and 473 K. Phase equilibrium is determined with a well-established visual method, using a synthetically known composition (SynVisVar). Uncertainties smaller than 0.1 MPa in pressure, 0.01 of the mass fractions of the binary mixture and 0. K in temperature are expected. Viscosity and density is determined measuring the frequency shift and electrical impedance over the quartz microbalance, after which fundamental piezoelectric equations are applied to calculate property values. Uncertainties as low as 0.01 of the value for viscosity and density are possible. The solubility limits of the systems studied were defined, and density and viscosity measurements conducted. The compounds were found to meet the demands of the hydrodynamic study, yielding viscosities and densities under supercritical conditions that are comparable to industrially relevant supercritical process fluids.

A 2.2 WCCE 2017 Poster

Concurrent Measurement of High Pressure Phase Equilibria, Density and Viscosity of PDMS in Supercritical CO_2

H.H. Franken, J.H. Knoetze, C.E. Schwarz*
Department of Process Engineering, Stellenbosch University, Private Bag X1, Matieland 7602, South Africa
* Tel: +27 21 808-4203, e-mail: cschwarz@sun.ac.za

Objectives

1. Introduce equipment capable of measuring the phase equilibria, viscosity and density of a mixture under supercritical conditions.
2. Present measured fluid property and miscibility data, in preparation of future fluid dynamic studies.

Overall Problem Statement

- A lack in design methods & predictive models exists for bulk mass transfer devices (e.g. packed columns) operating under supercritical (SC) conditions.
- This hampers the technology growth, necessitating overdesign and extensive, expensive, piloting for new systems.
- To address this, a thorough study of system transport phenomena is required.
- With fluid dynamics in particular, there is a lack in available data and suitable systems.

Equipment Developed

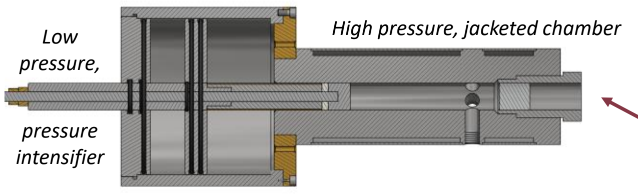

High Pressure Cell

Phase Equilibria (Bubble/Dew point)

Visual phase change determination with high pressure, variable volume cell (Maximum 35 MPa and 373 K)

- Isothermal pressure change of a synthetic mixture
- Supporting electro-mechanical readings with Quartz resonator
- Accurate within 0.06 MPa and 0.2 K

Density Determination

- Calibrated volume (within 0.02 ml)
- Mass loaded (±0.001 g - gas; ±0.0001 g - liquid)
- Accurate to within 0.8 kg/m^3

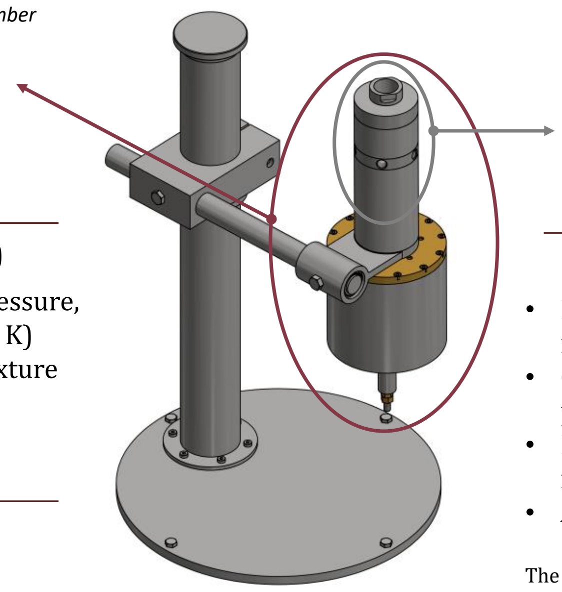

Equipment assembly

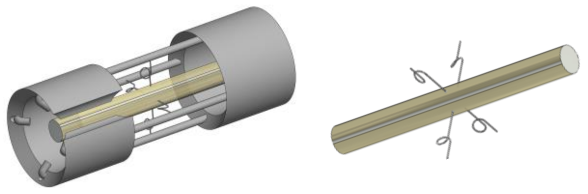

Quartz Crystal Inside Holder *Quartz Crystal Cylinder*

Dynamic Viscosity Measurement

- Determined by monitoring the damping of a resonating quartz crystal
- Operates on the principle of the converse piezoelectric effect and planar wave theory
- Excited using an AC signal, inducing a torsional mode of vibration
- Accurate to within ≤ 1% of the mPa.s value

The equipment was verified[1] using pure n-dodecane and benzene to confirm the viscosity & density methods and ethyl myristate to measure phase equilibria and density/viscosity for binary systems.

Experimental Results

Phase Equilibria

- Type III complex phase behaviour [2]
- Mutual solubility:
  - Low PDMS in CO_2 (<0.4wt% @15MPa)
  - High CO_2 in PDMS (>50wt% @15MPa)

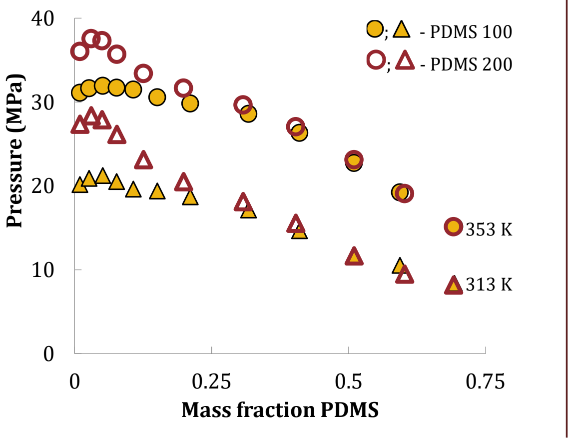

Density

- Shows effects of complex phase behaviour with density variation at low composition fractions
- Higher MW leads to larger deviation

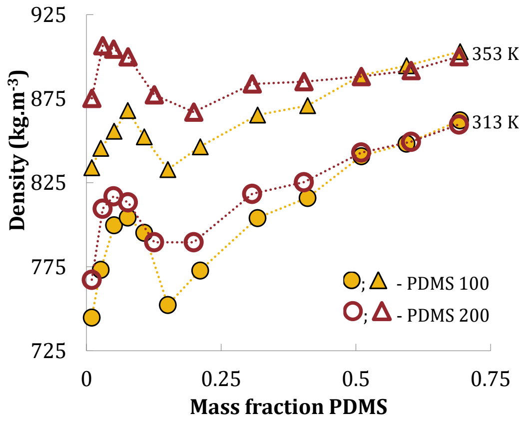

Dynamic Viscosity

- Low fractions tend to pure CO_2 viscosity.
- Decreases with increasing CO_2 concentration, illustrating high degree of polymer plasticization

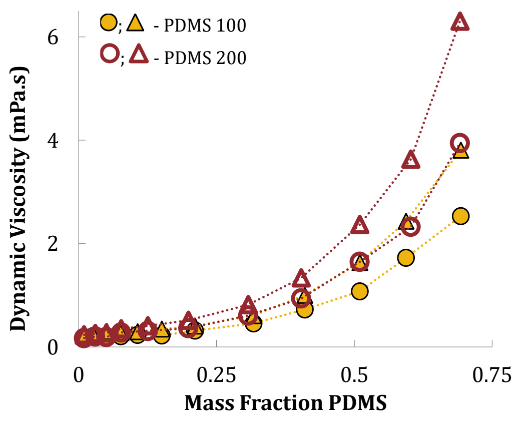

System Selection

- SC CO_2 – most popular SC fluid
- 2 Poly(dimethylsiloxanes) - 100 & 200 cSt
  - Low solubility in SC CO_2
  - Properties in the desired range for future fluid dynamic studies

Conclusions

1. Equipment was presented capable of measuring concurrent phase equilibria, density and viscosity data in the supercritical regime.
2. Two CO_2+PDMS systems were investigated and fluid properties and equilibria were quantified. VLLE behaviour was found, as predicted by literature[2].

The density and viscosity values measured, confirmed that the components are **suitable for the characterization of fluid dynamics** in packed columns under SC conditions.

References:
[1] Franken, H.H.; Knoetze, J.H. and Schwarz, C.E., submitted to J Supercrit. Fluids, (2017).
[2] Xiong, Y. and Kiran, E., Polymer, 36 (1995) 4817-1826

Acknowledgements: This work is based on the research supported in part by the National Research Foundation of South Africa (Grant specific unique reference number (UID) 88782). The authors acknowledge that opinions, findings and conclusions or recommendations expressed in any publication generated by the NRF supported research are that of the authors, and that the NRF sponsors accepts no liability whatsoever in this regard.

A.3 Poster - 30th European Symposium on Applied Thermodynamics (ESAT 2017)

A 3.1 ESAT 2017 Abstract

Within the field of supercritical fluids, phase equilibrium data are becoming more widely available, supplying sufficient information regarding the thermodynamic driving force for the separation of mixtures. There is, however, preciously little information on the physical properties of these mixtures (e.g. density and viscosity) and dependent phenomena (e.g. hydrodynamics) under supercritical conditions. This lack of information necessitates the extensive piloting of any new application, limiting the quick and easy practical application of potential new separation processes.

This paper presents the details of equipment that simultaneously measures phase transitions and the saturated fluid properties of density and viscosity to start addressing this problem. Phase transitions are determined visually using a variable volume view cell (SynVisVar). Uncertainties in phase measurements are 0.06 MPa in pressure, <0.0005 in mass fraction, and 0.2 K in temperature. Density is calculated accurately to within <0.8 kg/m^3, using the mass loaded and the calibrated cell volume. The dynamic viscosity is determined by measuring the frequency shift over a quartz microbalance, accurate to within <1% of the value.

Phase equilibria, density and viscosity data for two polydimethylsiloxane + supercritical CO_2 mixtures, are presented. In agreement with the literature, the phase equilibria showed complex phase behaviour. Fluid properties deviated significantly from that of the respective pure components, with density differing by up to 600 kg.m^{-3} and viscosity differing by more than an order of magnitude. Due to these large deviations, behaviour predicted using pure fluid properties can differ significantly from reality. Further, it was found that both systems exhibited low solubility in CO_2 (<1% above 20 MPa), with properties in the desired ranges (~900 - 800 kg.m^{-3} and ~0.7 - 7 mPa.s) for planned future work. This includes measuring hydrodynamics in a packed column under supercritical conditions to determine the influence of density and viscosity in order to improve design procedures for supercritical fluid fractionation.

Keywords: Piezoelectric Quartz, Physical properties, Silicone Oil, Viscometer

A 3.2 ESAT 2017 Poster

Concurrent Measurement of High Pressure Phase Equilibria, Density and Dynamic Viscosity of PDMS in Supercritical CO2

H.H. Franken, J.H. Knoetze, C.E. Schwarz*
Department of Process Engineering, Stellenosch University, Private Bag X1, Matieland 7602, South Africa
* Tel: +27 21 808-4485, e-mail: cschwarz@sun.ac.za

Objectives

Present measured density, dynamic viscosity and miscibility data on PDMS 100 and 200 in saturated with supercritical CO_2, in preparation of future fluid dynamic studies.

Overall Problem Statement

- A lack in design methods & predictive models exists for bulk mass transfer devices (e.g. packed columns) operating under supercritical (SC) conditions.
- This hampers the technology growth, necessitating overdesign and extensive, expensive, piloting for new systems.
- With fluid dynamics in particular, there is a lack in available data and suitable systems.

Equipment Developed

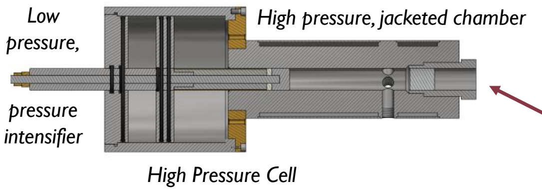

High Pressure Cell

Phase Equilibria (Bubble/Dew point)

Visual phase change determination with high pressure, variable volume cell (Maximum 35 MPa and 373 K)

- Isothermal pressure change of a synthetic mixture
- Supporting electro-mechanical readings with Quartz resonator
- Accurate within 0.06 MPa and 0.2 K

The equipment was verified[1] using pure n-dodecane and benzene to confirm the viscosity & density methods and ethyl myristate to measure phase equilibria and density/viscosity for binary systems.

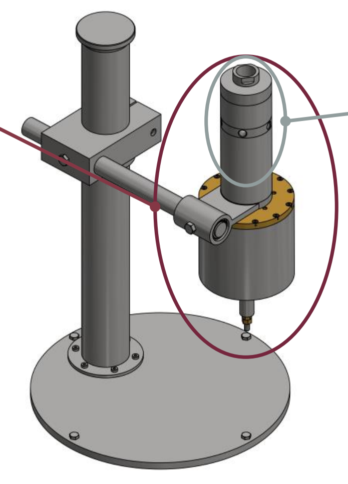

Equipment assembly

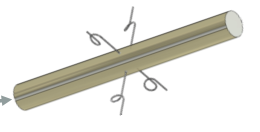

Quartz Crystal Cylinder

Dynamic Viscosity Measurement

- Determined by moni-toring the damping of a resonating quartz crystal
- Operates on the principle of the converse piezoelectric effect and planar wave theory
- Excited using an AC signal, inducing a torsional mode of vibration
- Accurate to within ≤ 1% of the mPa.s value

Density Determination

- Calibrated volume (within 0.02 ml)
- Mass loaded (±0.001 g - gas; ±0.0001 g - liquid)
- Accurate to within 0.8 kg/m[3]

Experimental Results

Phase Equilibria[3]

- Type III complex phase behaviour [2]
- Mutual solubility:
  - Low PDMS in CO_2 (<0.4wt% @15MPa)
  - High CO_2 in PDMS (>50wt% @15MPa)

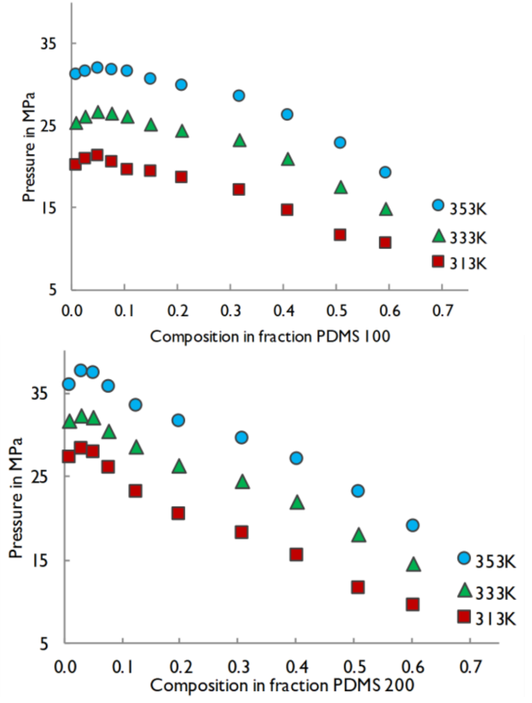

Density[3]

- Shows effects of complex phase behaviour with density variation at low composition fractions
- Higher MW leads to larger deviation

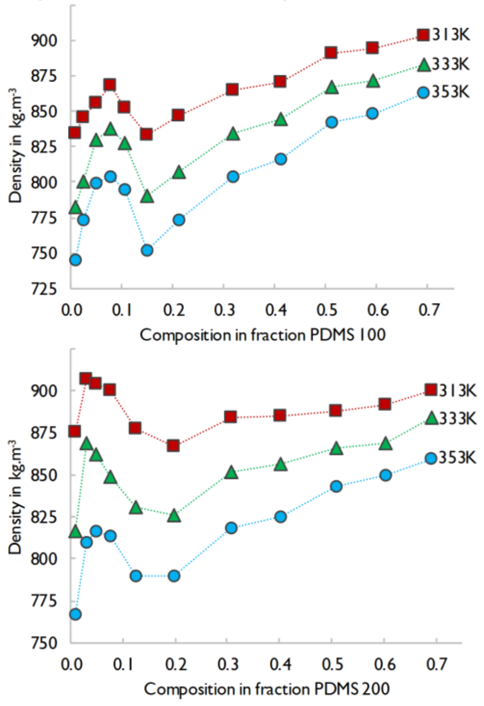

Dynamic Viscosity[3]

- Low fractions tend to pure CO_2 viscosity.
- Decreases with increasing CO_2 concentration, illustrating high degree of polymer plasticization

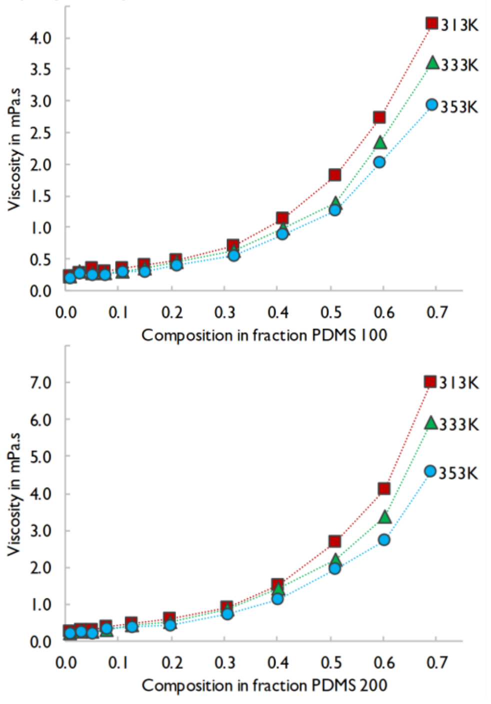

System Selection

- SC CO_2 – most popular SC fluid
- 2 Poly(dimethylsiloxanes) - 100 & 200 cSt
  - Low solubility in SC CO_2
  - Properties in the desired range for future fluid dynamic studies

Conclusions

Supercritical CO_2+PDMS was investigated and the fluid properties of density and dynamic viscosity of the liquid at saturation were quantified. The density and viscosity values measured, confirmed that the components are **suitable for the characterization of fluid dynamics** in packed columns under SC conditions.

References:
1 Franken, H.H.; Knoetze, J.H. and Schwarz, C.E., J. Supercrit. Fluids 133, (2018), 444-454
2 Xiong, Y. and Kiran, E., Polymer, 36 (1995) 4817-1826
3 Franken, H.H.; Knoetze, J.H. and Schwarz, C.E., J. Supercrit. Fluids 139, (2018), 1-7

Acknowledgements: This work is based on the research supported in part by the National Research Foundation of South Africa (Grant specific unique reference number (UID) 88782). The authors acknowledge that opinions, findings and conclusions or recommendations expressed in any publication generated by the NRF supported research are that of the authors, and that the NRF sponsors accepts no liability whatsoever in this regard.

A.4 Presentation - 11th International Conference on Distillation & Absorption (DA 2018)

A 4.1 DA 2018 Abstract

Supercritical fluids (SFs) are increasing in popularity as a solvent medium for various extraction and absorption columns. Presenting an attractive alternative to traditional solvents, SFs are readily tuneable and capable of sharp, highly efficient separations while using less intrinsically harmful solvents. The application of the technology is, however, hampered by a lack of design methods and predictive models, resulting in overdesign and extensive piloting of any new applications. To address this shortcoming, thorough investigation into the mass transfer and transport phenomena of such systems are required. Mass transfer is widely investigated in the literature, with several models capable of generating reasonable predictions. Transport phenomena, specifically hydrodynamics and fluid properties under SF conditions are, on the other hand, largely unexplored with no comprehensive predictive models available.

To investigate fundamental fluid dynamic behaviour, systems with very little to no mass transfer and with known fluid properties are preferred. Mass transfer directly affects effective fluid flow rates and fluid properties, complicating the interpretation of fluid dynamic results. Available literature on SF hydrodynamics has neglected the effect of mass transfer or used systems with fluid properties very different from that of a typical, commercially relevant system. Additionally, research is only available on structured packing, even though random packing presents a much cheaper solution for the small column diameters typically used (20-150 mm).

The presented work aims to improve fundamental knowledge of fluid dynamic phenomena in packed columns under SF conditions by considering both fluid properties and fluid dynamic behaviour. Firstly, binary systems with suitable phase behaviour were identified, and their fluid properties, specifically density and dynamic viscosity, measured. The systems selected were CO_2, as the most popular SF solvent, with 100 cSt and 200 cSt PDMS (poly[dimethylsiloxane]), respectively. This allowed hydrodynamics to be investigated using a system with known fluid properties, similar to real SF – solute systems. Secondly, pressure drop, flooding and liquid hold-up data, over a range of fluid flows and for different random packings (Propak and Dixon rings) were measured. The results show that the fluid phase viscosity and the difference in phase densities have a significant effect. The presented data form a basis for future fluid dynamic modelling of columns under SF conditions, with relevant fluid properties providing a more direct equivalence to industrially relevant systems.

A 4.1 DA 2018 Presentation

*Presentation prepared and presented by prof C.E. Schwarz.

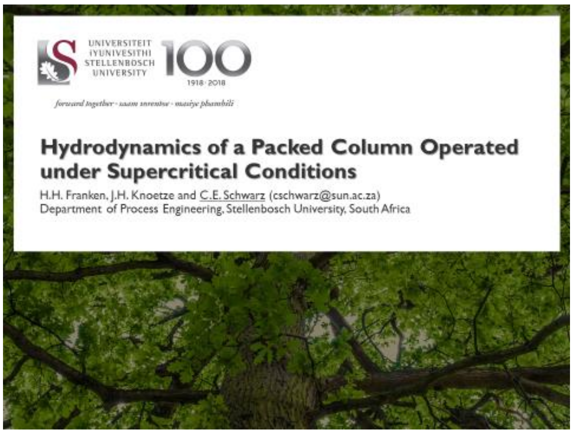

UNIVERSITEIT iYUNIVESITHI STELLENBOSCH UNIVERSITY 100 1918·2018

forward together · saam vorentoe · masiye phambili

Hydrodynamics of a Packed Column Operated under Supercritical Conditions

H.H. Franken, J.H. Knoetze and C.E. Schwarz (cschwarz@sun.ac.za)
Department of Process Engineering, Stellenbosch University, South Africa

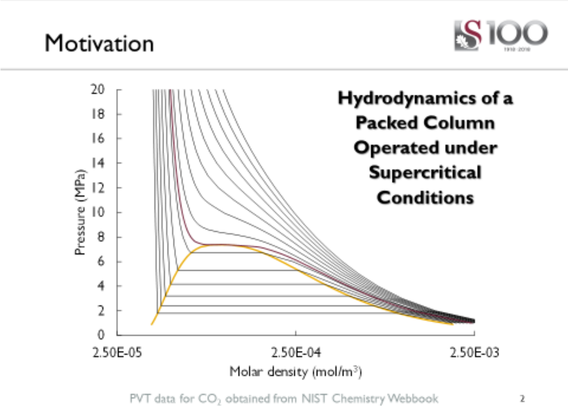

Motivation

Hydrodynamics of a Packed Column Operated under Supercritical Conditions

PVT data for CO_2 obtained from NIST Chemistry Webbook

Aim and Objectives

- **Investigation into hydrodynamic behaviour of packed columns operated under supercritical conditions using the system CO_2 + PDMS100**
  - CO_2: Supercritical / high pressure fluid
  - PDMS100: High molecular mass liquid (100 cSt poly[dimethylsiloxane)
  - Low solubility of PDMS100 in CO_2
  - PDMS properties similar to typical fluid to be fractionated

1. **Measurement of solubility, density and viscosity**
2. **Hydrodynamic measurements**
3. **Hydrodynamic modelling**

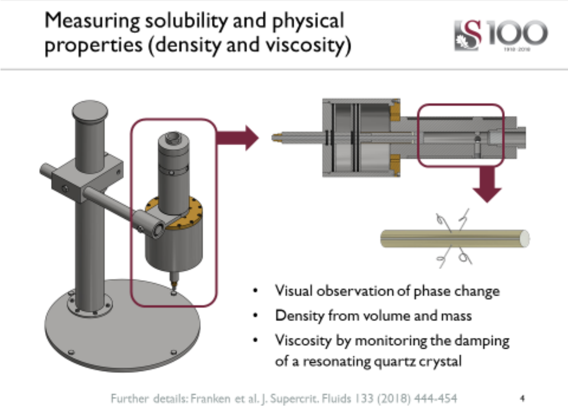

Measuring solubility and physical properties (density and viscosity)

- Visual observation of phase change
- Density from volume and mass
- Viscosity by monitoring the damping of a resonating quartz crystal

Further details: Franken et al. J. Supercrit. Fluids 133 (2018) 444-454

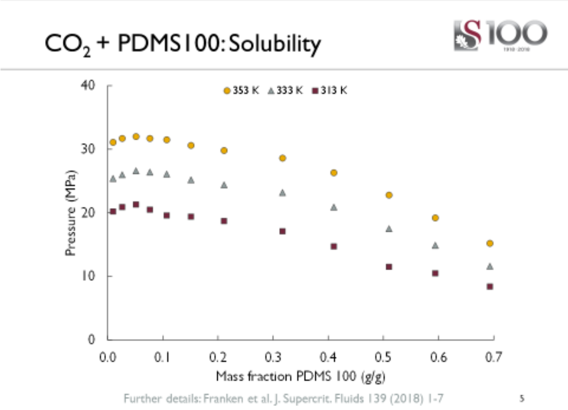

CO_2 + PDMS100: Solubility

Further details: Franken et al. J. Supercrit. Fluids 139 (2018) 1-7

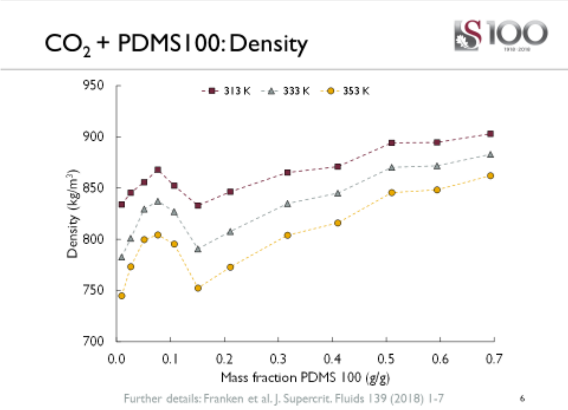

CO_2 + PDMS100: Density

Further details: Franken et al. J. Supercrit. Fluids 139 (2018) 1-7

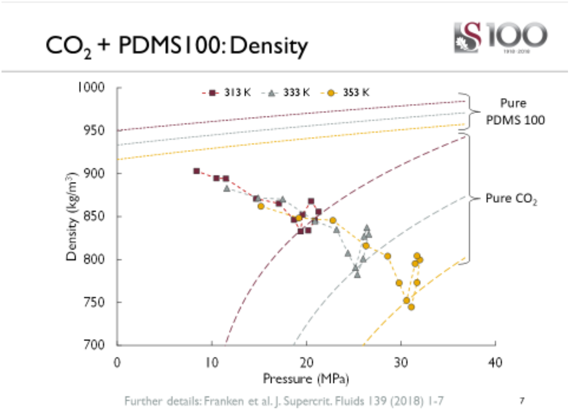

CO_2 + PDMS100: Density

Further details: Franken et al. J. Supercrit. Fluids 139 (2018) 1-7

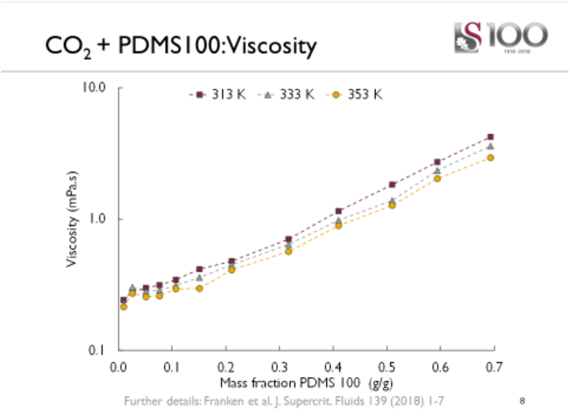

CO_2 + PDMS100: Viscosity

Further details: Franken et al. J. Supercrit. Fluids 139 (2018) 1-7

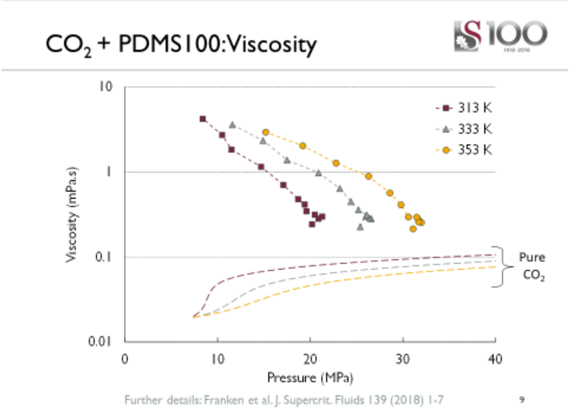

CO_2 + PDMS100: Viscosity

Further details: Franken et al. J. Supercrit. Fluids 139 (2018) 1-7

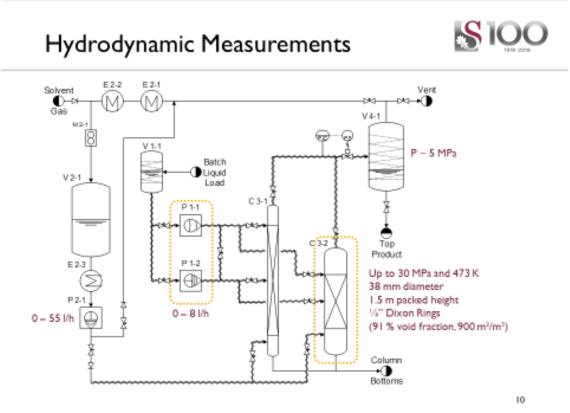

Hydrodynamic Measurements

Up to 30 MPa and 473 K
38 mm diameter
1.5 m packed height
¼" Dixon Rings
(91 % void fraction, 900 m^2/m^3)

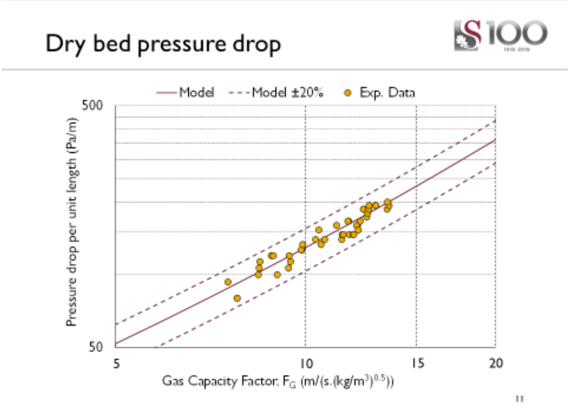

Dry bed pressure drop

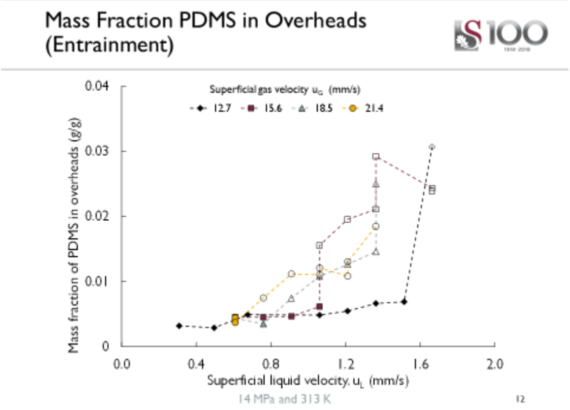

Mass Fraction PDMS in Overheads (Entrainment)

14 MPa and 313 K

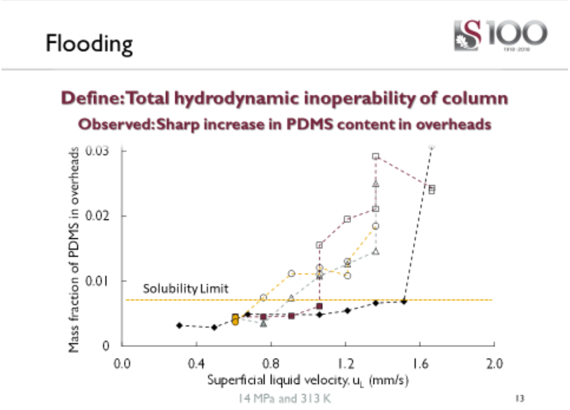

Flooding

Define: Total hydrodynamic inoperability of column

Observed: Sharp increase in PDMS content in overheads

14 MPa and 313 K

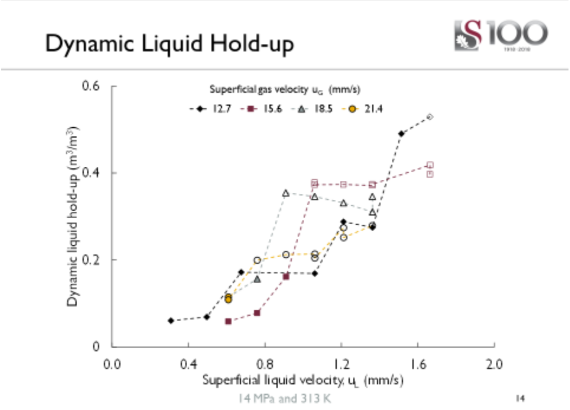

Dynamic Liquid Hold-up

14 MPa and 313 K

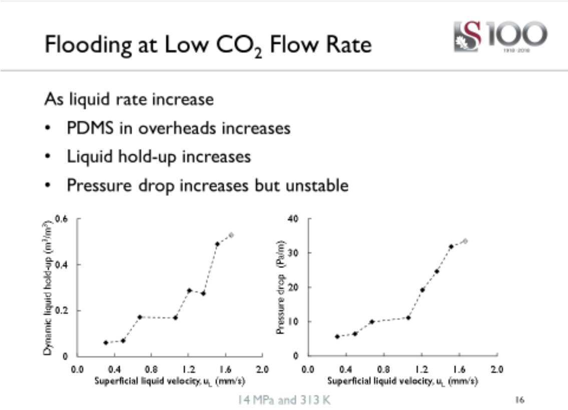

Flooding at Low CO_2 Flow Rate

As liquid rate increase

- PDMS in overheads increases
- Liquid hold-up increases
- Pressure drop increases but unstable

14 MPa and 313 K

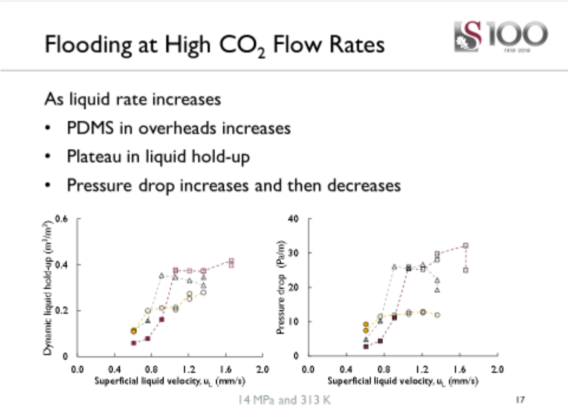

Flooding at High CO_2 Flow Rates

As liquid rate increases

- PDMS in overheads increases
- Plateau in liquid hold-up
- Pressure drop increases and then decreases

14 MPa and 313 K

Outcome

1. **Measurement of solubility, density and viscosity**
    - Low solubility of PDMS100 in CO_2
    - Moderate solubility of CO_2 in PDMS100
    - Small difference in density of co-existing phases
    - Viscosity varies with two orders of magnitude
    - Similar study on PDMS200 already completed
2. **Hydrodynamic measurements**
    - Flooding: Sharp increase in PDMS100 in overheads
    - Flooding behaviour depends on relative CO_2 flow rate
    - Future: Analyse PDMS200 data
3. **Hydrodynamic modelling**
    - Hydrodynamic modelling of data obtained

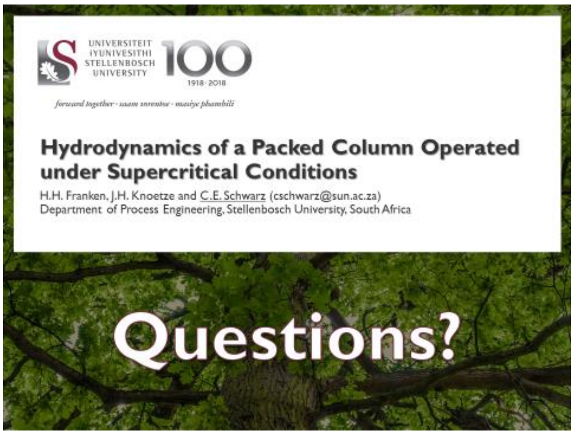

UNIVERSITEIT
iYUNIVESITHI
STELLENBOSCH
UNIVERSITY
100
1918 · 2018

forward together · saam vorentoe · masiye phambili

Hydrodynamics of a Packed Column Operated under Supercritical Conditions

H.H. Franken, J.H. Knoetze and C.E. Schwarz (cschwarz@sun.ac.za)
Department of Process Engineering, Stellenbosch University, South Africa

Questions?

Appendix B: Safe Working Procedures and Task Risk Assessment

The Stellenbosch Chemical Engineering Department drives a standard approach to safety through the requirement of a Safe Working Procedure (SWP) and Task Risk Assessment (TRA) documentation. The documentation of both pieces of equipment, namely the high-pressure view cell viscometer and the supercritical distillation column pilot plant, is found in this section.

All equipment was designed and built with future use in mind. The following procedures are structured in such a way as to be easily accessible for future users and not only applicable to this study.

B.1 High-pressure Gas Bomb handling procedure – CO_2 226
B.1.1. SWP - High-pressure Gas Bomb 226
B.1.2. TRA - High-pressure Gas Bomb 228
B.2 High-Pressure Viscosity Measurement View Cell 229
B.2.1. SWP – High-Pressure Viscosity View Cell – Loading 229
B.2.2. TRA – High-Pressure Viscosity View Cell– Loading 232
B.2.3. SWP – High-Pressure Viscosity View Cell – Experimental 233
B.2.4. TRA – High-Pressure Viscosity View Cell – Experimental 235
B.2.5. SWP – High-Pressure Viscosity View Cell – Unloading/Cleaning 236
B.2.6. TRA – High-Pressure Viscosity View Cell – Unloading/Cleaning 239
B.3 Large Supercritical Pilot Plant 241
B.3.1. For first-time users 241
B.3.2. SWP – Large Supercritical Pilot Plant – Start-up 242
B.3.3. TRA – Large Supercritical Pilot Plant – Start-up 247
B.3.4. SWP – Large Supercritical Pilot Plant – Experimental 248
B.3.5. TRA – Large Supercritical Pilot Plant – Experimental 252
B.3.6. SWP – Large Supercritical Pilot Plant – Shutdown/Clean-up 253
B.3.7. TRA – Large Supercritical Pilot Plant – Shutdown/Clean-up 256

B.1 High-pressure Gas Bomb Handling Procedure – CO_2

B.1.1 SWP - High-pressure Gas Bomb

Scope

This document outlines the handling of high-pressure gas bombs used to load equilibrium cells. The filling and safe storage of these bombs are also described. Equipment specific loading is described in the SWP of the particular equipment.

a) Authorisation

- Prof C.E. Schwarz to approve on any work prior to commencement.
- Training is required for the high-pressure process environment and lab procedures. Prof Schwarz to sign off on completed training.
- Due to high pressures and extreme conditions, all operators are to sign on the SWP before commencing any work.

b) Hazards

- High pressures (up to 70 Bar)
- High-pressure gas leaks or rapid gas expansion.
- Low temperatures on the gas bomb due to rapid expansion

Highest remaining residual risk rating: M

c) Personal Protective Equipment (PPE) *[minimum PPE required to be worn by all personnel working on task]*

- Safety glasses.
- Lab coat.
- Closed shoes.
- Kevlar gloves when handling the cold gas bomb.

d) Maintenance requirements

- Yearly Deadweight testing. Log testing on SharePoint. Signed off by Prof Schwarz.
- Soapy water leak detection monthly. Log sheet kept in lab and signed off by Prof Schwarz.
- Daily inspection of cell valves for leaks and damage.

UNDERTAKING THE TASK:

e) Step-by-step Procedure

Preparation and Precautions:

- Ensure the following is available: Kevlar Gloves, various spanners (Shifter and size 15).
- Be sure to do any venting of the bomb in well-ventilated areas. When venting explosive gas, ensure no ignition sources such as running motors or electric equipment is present.
- Be sure never to over tighten the valves, as this can cause permanent damage to the valve seat and stem.
- Inspect the work area to ensure that it is clean and safe before starting work.

Procedure Steps:

1. Use only a bomb labelled for the solvent to be used.
2. Ensure the gas bomb is close to empty by opening the venting valve. Close both valves securely to avoid moisture or air from entering.
3. Place the empty gas bomb in a designated freezer to reach a freezing temperature. Low temperatures aid the loading procedure.
4. When the gas bomb has cooled sufficiently, remove from the freezer using the Kevlar Gloves to avoid freezer burn.
5. Connect the gas bomb to the appropriate solvent gas cylinder, using a no.15 spanner and Swagelok fitting. (Do not use a shifter, as this damages the nuts and thread).
6. Be sure that all the gas bomb valves are closed.
7. Open the cylinder main valve and wait for the line to fill.
8. Close the cylinder valve and slightly loosen the Swagelok connection in order to purge any remaining air. After venting tighten the Swagelok connection again.
9. Open the gas cylinder main valve, then the bomb side valve.
10. Wait a few moments for the bomb to fill.
11. If it is necessary to purge the bomb, follow these steps:
    a. Close the gas bomb side valve.
    b. Close the gas cylinder main valve.
    c. Vent the bomb using the bottom valve. After the bomb has been vented, close the bottom valve and redo the filling procedure from *step 9* onward.
12. After the bomb has been filled (and vented if required) close gas bomb side valve, then the cylinder main valve. Do not overtighten the valves, as this causes damage to the valve seat and stem.
13. Slowly loosen the Swagelok connection, allowing the pressure in the line to escape.
14. Once the pressure has been vented, disconnect the gas bomb from the cylinder.
15. Vent a small amount of gas from the bomb.
16. The bomb will have condensation on the outer body, which could contaminate the loading process or cause inaccurate weighing. Dry the bomb as best possible using lab paper, compressed air, and/or drying with a hairdryer, especially before accurate weighing.
17. The bomb is ready for use in the loading procedure of any of several pieces of equipment.

f) Clean-up Procedures (including any waste disposal)

18. After use, vent the bomb to just above atmospheric. Securely close valves and replace the bomb in the designated freezer for future use.
19. Do any venting of the bomb in well-ventilated areas. When venting explosive gasses, ensure no ignition sources such as running motors or electric equipment is in vicinity of operation.

B.1.2 TRA - High-pressure Gas Bomb

STEP 1.					
Project / Task Name:	Gas bomb handling – CO_2 – Loading Procedure	**Work Area:**	Lab C 301	**Research group**	SepTech
Project / Task Description:	This document outlines the risks involved in the loading and handling of high pressure gas bombs used to load equilibrium cells, using the SWP rev.1.			**Revision Number**	1

STEP 2.		**STEP 3.**	**STEP 4.**	**STEP 5.**	**STEP 6.**	**STEP 7.**	**STEP 8.**			**ST EP 12.**
			RISK RANKING				**RESIDUAL RISK**			
Ref No.	**SPECIFIC TASK / ACTIVITY STEPS**	**IDENTIFY POTENTIAL HAZARDS**	**Consequence**	**Likelihood**	**Risk Rating**	**RISK CONTROL MEASURES** • *Hierarchy of Control – Elimination, Substitution, Isolation, Engineering, Administration, Personal Protection.* • *Additional information can be attached.*	**Consequence**	**Likelihood**	**Residual Risk**	**Actioner / Initials**
1	Use Chemicals – CO_2 ; Steps 2, 8, 11, 18, 19 and in case of risks [3, 4, 5]	Chemical Exposure Hazard – CO_2	2	3	M(8)	Proper training. Foreknowledge of the chemicals concerned. Consult MSDS sheets attached. Adequate ventilation. Correct PPE.	2	1	L(3)	*
2	Use tools (Spanners), ; Steps 5, 8, 13	Incorrect tool use / tool failure - Injury	2	1	L(3)	Proper training. Using the correct tool for the job. Correct PPE.	2	1	L(3)	*
3	Equipment inherent risk; Steps 7 to 18	High pressure –Leak	3	2	M(9)	Proper training and regular inspection. Regular testing of the equipment. Correct PPE reduces consequence.	2	1	L(3)	*
4	Equipment inherent risk; Steps 7 to 18	High Pressure – Equipment Failure Causing Explosive Decompression	3	1	M(6)	Proper training and inspection. Regular testing. Safety in design. Correct PPE.	3	1	M(6)	*
5	Venting of Bomb; Steps 2, 8, 11, 15, 18	High Pressure – Uncontrolled Rapid Expansion.	2	3	M(8)	Proper training. Correct PPE.	2	1	L(3)	*
6	Touching low temperature bomb; Steps 3 to 14, 17	Very low temperatures - Injury.	1	3	L(2)	Proper training. Correct PPE.	1	2	L(2)	*
				STEP 9.		**Highest Remaining Residual Risk**			**M**	

*Actioners : Training in equipment and PPE use must be implemented by Prof Schwarz, as well as enforcing inspection, maintenance and testing.
Operators must implement safe operations, perform regular testing and conform to lab safety and PPE requirements. Operators must familiarize themselves with relevant MSDS sheets and safety procedures, as well as the SWP.

B.2 High-Pressure Viscosity Measurement View Cell

B.2.1 SWP – High-Pressure Viscosity View Cell – Loading Procedure

Scope

This document outlines the loading procedure of the High-Pressure Cell for Viscosity Measurement in Lab C301 in the Department of Chemical Engineering.

a) Authorisation

- Prof C.E. Schwarz is to approve any work prior to commencement.
- Training is required for the high-pressure process environment and lab procedures. Prof Schwarz to sign off on completed training.
- Due to high pressures and extreme conditions, all operators are to sign the SWP before commencing any work.

b) Hazards

- High pressures (up to 350 Bar)
- High temperatures on the cell and thermostatic bath
- High-pressure gas leaks or rapid gas expansion.
- Heavy load handling
- Chemicals handling

Highest remaining residual risk rating: M

c) Personal Protective Equipment (PPE) *[minimum PPE required to be worn by all personnel working on task]*

- Safety glasses.
- Lab coat.
- Closed shoes.
- Kevlar gloves when handling the gas bomb.
- Latex/nitrile gloves when handling chemicals – chemical-specific.

d) Emergency Response/First aid requirements

- In case of Power Failure – decrease cell pressure using the nitrogen vent valves. Ascertain the nature of the interruption and act accordingly. Fully vent the cell for more prolonged interruptions, or ensure safe stasis for a short interruption.
- In case of fire – Close nitrogen Cylinder. If possible vent the nitrogen line, then the cell contents. Switch of all electric equipment at the plug. Evacuate quickly and safely.
- In case of emergency shutdown, follow SWP for Unloading, steps 1 to 9.

e) Maintenance Requirements:

Regular inspection:

- Visual inspection of the cell is required between experimental runs. This includes checking the screw threads, the sight glass, seals and general surfaces of the cell for wear and tear or damage.
- If the cell requires maintenance, refer to the plant manual for specific maintenance procedures.

Regular testing and calibration:

- Ensure that regular cell volume calibrations are conducted to ensure accuracy between projects and especially after any alterations, modifications or maintenance to the equipment.
- Ensure that pressure sensor calibrations are conducted six-monthly or after any alterations, modifications or maintenance to the equipment.
- Ensure that the cell is hydrostatically tested six-monthly or after any alterations, modifications or maintenance to the equipment.
- Test that the pressure relief valve is functional and set at the appropriate value every six months, or after any alterations or maintenance.
- Ensure the temperature sensors are calibrated yearly by a SANS certified company
- A log of all test and calibration results should be kept in the plant manual and SharePoint. A maintenance schedule is also to be kept in the manual for purposes of reference and audit.

UNDERTAKING THE TASK:

f) Step-by-step Procedure

Preparation/Precautions:

- Ensure the following are available: Kevlar Gloves and Appropriate Gas Bomb – see SWP for loading a gas bomb, hairdryer, various spanners (Shifter, sizes 13, 15, 17, 18 and 19), vacuum pump.
- Check the Task risk assessment for specific chemicals to be used (solvent gas and solute fluid/solid)
- Check that the cell is not hot and under pressure!
- Inspect the work area to ensure that it is clean and safe before starting work.

Procedure Steps:

1. Check that pressure indicated is at the reading that indicates atmospheric and that cell valve is open. If it is not already removed, remove the piston section.
2. Inspect the cell chamber and piston head/seal for any impurities and dirt [If cleaning is required, please refer to the unloading/cleaning SWP for this equipment.]
3. Ensure the cell is securely fastened in an upright position with the sight glass at the bottom.
4. After checking that the magnetic stirrer bar and crystal cage is clean and dry, add them to the cell. Ensure that the crystal cage makes electrical contact.
5. Add the desired amount of solute (calculated from the desired mass fraction), weighed accurate 0.001g to the cell chamber.
6. Screw the piston section onto the cell chamber. Ensure that the piston can be lifted high enough to easily attach it to the cell chamber (a platform is provided for shorter individuals if needed).

7. Tighten the nuts on the shaft to ensure proper sealing. Rotate the cell to a horizontal position.
8. Attach the vacuum pump and gas bomb to the cell valve, using the manifold (Ensure O-rings are present), and start the vacuum pump in order to evacuate the cell. Monitor the cell with the camera to ensure no solute is removed from the cell by evaporation.
9. Close the vacuum pump valve inlet and stop the pump in order to avoid gas going through the pump when loading.
10. Ensure that the fan extractor is turned on and placed on the top of the cell before flushing the in order to remove the remaining air in the cell.
11. The cell is flushed up to six times with solvent gas. The solvent gas is loaded from a gas bomb into the cell in small amounts using the appropriate manifold. The gas is then purged from the cell to just above the pressure displayed when the cell is open to the atmosphere, after which a new batch of solvent gas can be loaded for further purging. [Please see the appropriate SWP for the loading of gas bombs].
12. The gas cylinder is then safely removed and weighed to an accuracy of 0.01g. Ensure the bomb is dry to ensure an accurate weight.
13. The required amount of gas is calculated, and the gas bomb is vented under a fan extractor/exhaust to the appropriate mass.
14. Reconnect the gas bomb to the manifold (ensure O-ring is present). Evacuate the manifold using the vacuum pump.
15. Heat the gas bomb using the available hairdryer.
16. Load the gas from the bomb into the cell using the appropriate valves while heating the gas bomb and manifold.
17. After gas has been loaded into the cell, close the valve to the cell and gas bomb.
18. Vent the manifold and remove the gas bomb.
19. Weigh the gas bomb to determine the amount of solvent loaded into the cell. If an incorrect amount has been loaded, vent the cell and restart the procedure from step 9, after reloading the gas bomb.
20. Remove the manifold and put a blank nut on the valve.
21. Turn on the thermostatic bath circulation, after setting the bath to the appropriate temperature.
22. Attach any insulation required, position the magnetic stirrer assembly and turn stirring on.
23. Connect the height gauge to the piston side body for piston position determination.
24. Connect the nitrogen line, ensuring an O-ring seal is fitted.
25. Make sure that the nitrogen gas cylinder is safely fastened to the room wall and check that the regulator on the nitrogen gas cylinder is set to deliver a low pressure (barely closed).
26. Pressurise the cell just enough so as the fluid forms one homogeneous phase by closing (turn clockwise) the regulator on the nitrogen gas cylinder.

g) Clean-up Procedures (including any waste disposal)

None, no waste generated in loading procedure. Follow procedures for chemical handling for any spills or unneeded leftovers.

B.2.2 TRA - High-Pressure Viscosity Measurement View Cell – Loading Procedure

STEP 1.					
Project / Task Name:	High Pressure Viscosity Measurement View Cell – Loading Procedure	**Work Area:**	Lab C 301	**Research group**	SepTech
Project / Task Description:	This document outlines the risks involved in the loading procedure of the high pressure cell for Viscosity Measurement, using the SWP rev.1.			**Revision**	1

STEP 2.		**STEP 3.**	**STEP 4.**	**STEP 5.**	**STEP 6.**	**STEP 7.**	**STEP 8.**			**ST EP 12.**
			RISK RANKING			**RISK CONTROL MEASURES** • *Hierarchy of Control – Elimination, Substitution, Isolation, Engineering, Administration, Personal Protection.* • *Additional information can be attached.*	**RESIDUAL RISK**			
Ref No.	**SPECIFIC TASK / ACTIVITY STEPS**	**IDENTIFY POTENTIAL HAZARDS**	**Consequence**	**Likelihood**	**Risk Rating**		**Consequence**	**Likelihood**	**Residual Risk**	**Actioner / Initials**
1	Lifting Cell; Steps 1, 3, 6, 7	Heavy load – injury.	2	1	L(3)	Proper training. Use platforms provided. Ask for assistance.	2	1	L(3)	*
2	Using liquid chemicals ; Steps 1, 2, 5 and in case of risks [5, 6, 7]	Chemical Exposure Hazard	2	3	M(8)	Proper training. Foreknowledge of the chemicals concerned. Consult MSDS sheets attached. Adequate ventilation. Correct PPE.	2	1	L(3)	*
3	Using CO_2 ; Steps 1, 5, 8, 11 - 14, 18 and in case of risks [5, 6, 7]	Chemical Exposure Hazard – CO_2	2	3	M(8)	Proper training. Foreknowledge of the chemicals concerned. Consult MSDS sheets attached. Adequate ventilation. Correct PPE.	2	1	L(3)	*
4	Using tools; Steps 7, 8, 12, 14, 20, 22 - 24, 25	Incorrect tool use / tool failure - Injury	2	1	L(3)	Proper training. Using the correct tool for the job. Correct PPE.	2	1	L(3)	*
5	Equipment inherent risk; Steps 8 - 27	High pressure –Leak	3	2	M(9)	Proper training and regular inspection. Regular testing of the equipment. Correct PPE.	2	2	L(3)	*
6	Equipment inherent risk; Steps 8 - 27	High Pressure – Equipment Failure causing explosive decompression.	3	1	M(6)	Proper training and inspection. Regular testing. Safety in design. Correct PPE.	3	1	M(6)	*
7	Venting of Cell and Bomb; Steps 11, 13, 16, 18	High Pressure – Uncontrolled Rapid Expansion.	2	3	M(8)	Proper training and procedure. Proper Ventilation/extraction. Correct PPE.	2	1	L(3)	*
8	Equipment inherent risk; Steps 15 - 18	High Heat – Light Burns.	2	2	L(5)	Equipment has built in safety. Proper training. Correct PPE.	2	1	L(3)	*
9	Equipment inherent risk; General	High Voltage – Three phase motor	3	2	M(9)	Equipment has built in safety. Protective shielding. Correct PPE.	3	1	M(6)	*
				STEP 9.		**Highest Remaining Residual Risk**			**M(6)**	

*Actioners : Training in equipment and PPE use must be implemented by Prof Schwarz, as well as enforcing inspection, maintenance and testing. Operators must implement safe operations, perform regular testing and conform to lab safety and PPE requirements. Operators must familiarize themselves with relevant MSDS sheets and safety procedures, as well as the SWP.

B.2.3 SWP - High-Pressure Viscosity View Cell - Experimental

Scope

This document outlines the measuring procedure of the High-Pressure Cell for Viscosity Measurement in Lab C301 in the Department of Chemical Engineering.

a) **Authorisation**

- Prof C.E. Schwarz is to approve any work prior to commencement.
- Training is required for the high-pressure process environment and lab procedures. Prof Schwarz to sign off on completed training.
- Due to high pressures and extreme conditions, all operators are to sign the SWP before commencing any work.

b) **Hazards**

- High pressures (up to 350 Bar)
- High temperatures on the cell and thermostatic bath
- High-pressure gas leaks or rapid gas expansion.

Highest remaining residual risk rating: M

c) **Personal Protective Equipment (PPE)** *[minimum PPE required to be worn by all personnel working on task]*

- Safety glasses.
- Lab coat.
- Closed shoes.

d) **Emergency Response/First aid requirements**

- In case of Power Failure – decrease cell pressure using the nitrogen vent valves. Ascertain the nature of the interruption and act accordingly. Fully vent the cell for more prolonged interruptions, or ensure safe stasis for a short interruption.
- In case of fire – Close nitrogen Cylinder. If possible vent the nitrogen line, then the cell contents. Switch of all electric equipment at the plug. Evacuate quickly and safely.
- In case of emergency shutdown, follow SWP for Unloading, steps 1 to 9.

e) **Maintenance Requirements:**

Regular inspection:

- Visual inspection of the cell is required between experimental runs. This includes checking the screw threads, the sight glass, seals and general surfaces of the cell for wear and tear or damage.
- If the cell requires maintenance, refer to the plant manual for specific maintenance procedures.

Regular testing and calibration:

- Ensure that regular cell volume calibrations are conducted to ensure accuracy between projects and especially after any alterations, modifications or maintenance to the equipment.
- Ensure that pressure sensor calibrations are conducted six-monthly or after any

alterations, modifications or maintenance to the equipment.

- Ensure that the cell is hydrostatically tested six-monthly or after any alterations, modifications or maintenance to the equipment.
- Test that the pressure relief valve is functional and set at the appropriate value every six months, or after any alterations or maintenance.
- Ensure the temperature sensors are calibrated yearly by a SANS certified company
- A log of all test and calibration results should be kept in the plant manual and SharePoint. A maintenance schedule is also to be kept in the manual for purposes of reference and audit.

UNDERTAKING THE TASK:

f) Step-by-step Procedure

Preparation/Precautions:

- Inspect the work area to ensure that it is clean and safe before starting work.
- Ensure the following are available: High-resolution camera and optical fibre light source, screen display.
- Make sure that temperature and pressure readings are stable and thermal equilibrium has been reached.

Procedure Steps:

1. Place the camera endoscope through the dedicated hole of the cell. Make sure that the optical fibre and camera cable are not interlaced or pinched.
2. Turn on the camera, light source and the screen display.
3. Adjust the camera endoscope focus and position to see the entirety of the cell.
4. Decrease the regulator pressure and slowly reduce the pressure of the cell by opening and closing the release valve on the nitrogen gas line in small, slow amounts until a second phase starts to form. The transition point is observed visually on the monitor and the pressure, temperature, piston position (height gauge) and the number of phases, as well as their apparent type, are recorded.
5. Pressurise the cell back into the one-phase region by adjusting the regulator (turn clockwise) on the nitrogen gas cylinder.
6. Iteratively repeat *step 4 and 5* in order to locate the exact pressure point when phase transition takes place with a 0.2 bar accuracy (bisection method).
7. After the transition point is determined, use the oscilloscope and signal generator to determine the viscosity resonance frequency at a pressure just above, at and below the transition point by varying the signal.
8. The pressure, temperature, piston position and phase criteria should be recorded at all times and especially at this final point.
9. Once the transition point has been determined, the cell can be adjusted for the next temperature to be studied, by doing the following:
    a. Repeat *step 5 – pressurise the cell into the one-phase region.*
    b. Change the set point of the thermostatic bath to the next temperature to be studied and make sure that the cell contents remain in the one-phase region.
    c. Turn off the camera, the light source, the optical fibre and the screen display and gently put away the camera.
10. Wait for temperature and pressure stabilisation and repeat the measuring procedure from *step 1.*

g) Clean-up Procedures (including any waste disposal)

None, no waste generated in measuring procedure.

B.2.4 TRA - High-Pressure Viscosity View Cell - Experimental

STEP 1.					
Project / Task Name:	High Pressure Viscosity Measurement View Cell – Experimental Procedure	**Work Area:**	Lab C 301	**Research group**	SepTech
Project / Task Description:	This document outlines the risks involved in the Experimental procedure of the high pressure cell for viscosity measurement, using the SWP rev.1.			**Revision Number**	1

STEP 2.		**STEP 3.**	**STEP 4.**	**STEP 5.**	**STEP 6.**	**STEP 7.**	**STEP 8.**			**STEP 12.**
			RISK RANKING			**RISK CONTROL MEASURES** • *Hierarchy of Control – Elimination, Substitution, Isolation, Engineering, Administration, Personal Protection.* • *Additional information can be attached.*	**RESIDUAL RISK**			
Ref No.	**SPECIFIC TASK / ACTIVITY STEPS**	**IDENTIFY POTENTIAL HAZARDS**	**Consequence**	**Likelihood**	**Risk Rating**		**Consequence**	**Likelihood**	**Residual Risk**	**Actioner / Initials**
1	Using CO_2 ; In case of Risks [2, 3]	Chemical Exposure Hazard – CO_2	2	3	M(8)	Proper training. Foreknowledge of the chemicals concerned. Consult MSDS sheets attached. Adequate ventilation. Correct PPE.	2	1	L(3)	*
2	Equipment inherent risk; Steps 1 - 10	High pressure –Leak	3	2	M(9)	Proper training and regular inspection. Regular testing of the equipment. Correct PPE reduces consequence.	2	1	L(3)	*
3	Equipment inherent risk; Steps 1 - 10	High Pressure – Equipment Failure Causing Explosive Decompression	3	1	M(6)	Proper training and inspection. Regular testing. Safety in design. Correct PPE.	3	1	M(6)	*
4	Equipment inherent risk; Steps 4, 6,	High Pressure – Uncontrolled Rapid Expansion.	2	3	M(8)	Proper training. Correct PPE can reduce consequence..	2	1	L(3)	*
5	Equipment inherent risk; Steps 1 - 10	High Heat – Light Burns.	2	2	L(5)	Equipment has built in safety. Proper training. Correct PPE.	2	1	L(3)	*
6	Equipment inherent risk; General	High Voltage – Three phase motor	3	2	M(9)	Equipment has built in safety. Protective shielding. Correct PPE.	3	1	M(6)	*
7	Measurement Equipment Failure; Steps 1-10	Signal generator failure – High voltage breakthrough	3	1	M(8)	Equipment has built in safety. Inspect Regularly.	3	1	M(6)	*
				STEP 9.		**Highest Remaining Residual Risk**			**M(6)**	

*Actioners : Training in equipment and PPE use must be implemented by Prof Schwarz, as well as enforcing inspection, maintenance and testing. Operators must implement safe operations, perform regular testing and conform to lab safety and PPE requirements. Operators must familiarize themselves with relevant MSDS sheets and safety procedures, as well as the SWP.

B.2.5 SWP - High-Pressure Viscosity View Cell – Unloading/Cleaning

Scope

This document outlines the Unloading and Cleaning procedure of the High-Pressure Cell for Viscosity Measurement in Lab C301 in the Department of Chemical Engineering.

a) Authorisation

- Prof C.E. Schwarz is to approve any work prior to commencement.
- Training is required for the high-pressure process environment and lab procedures. Prof Schwarz to sign off on completed training.
- Due to high pressures and extreme conditions, all operators are to sign the SWP before commencing any work.

b) Hazards

- High pressures (up to 350 Bar)
- High temperatures on the cell and thermostat bath
- High-pressure gas leaks or rapid gas expansion.
- Heavy load handling
- Chemicals handling

Highest remaining residual risk rating: M

c) Personal Protective Equipment (PPE) *[minimum PPE required to be worn by all personnel working on task]*

- Safety glasses.
- Lab coat.
- Closed shoes.
- Latex/nitrile gloves when handling chemicals.

d) Emergency Response/First aid requirements

- In case of Power Failure – decrease cell pressure using the nitrogen vent valves. Ascertain the nature of the interruption and act accordingly. Fully vent the cell for more prolonged interruptions, or ensure safe stasis for a short interruption.
- In case of fire – Close nitrogen Cylinder. If possible vent the nitrogen line, then the cell contents. Switch of all electric equipment at the plug. Evacuate quickly and safely.
- In case of emergency shutdown, follow SWP for Unloading, steps 1 to 9.

e) Maintenance Requirements:

Regular inspection:

- Visual inspection of the cell is required between experimental runs. This includes checking the screw threads, the sight glass, seals and general surfaces of the cell for wear and tear or damage.
- If the cell requires maintenance, refer to the plant manual for specific maintenance procedures.

Regular testing and calibration:

- Ensure that regular cell volume calibrations are conducted to ensure accuracy between projects and especially after any alterations, modifications or maintenance to the equipment.
- Ensure that pressure sensor calibrations are conducted six-monthly or after any alterations, modifications or maintenance to the equipment.
- Ensure that the cell is hydrostatically tested six-monthly or after any alterations, modifications or maintenance to the equipment.
- Test that the pressure relief valve is functional and set at the appropriate value every six months, or after any alterations or maintenance.
- Ensure the temperature sensors are calibrated yearly by a SANS certified company
- A log of all test and calibration results should be kept in the plant manual and SharePoint. A maintenance schedule is also to be kept in the manual for purposes of reference and audit.

UNDERTAKING THE TASK:

f) Step-by-step Procedure

Preparation/Precautions:

- Ensure the following are available: Appropriate Cleaning chemicals (Xylene and Methanol), Appropriate glass flask for draining, various spanners (Shifter, sizes 13, 17, 18 and 19).
- Turn on and position the extraction fan piping to extract any vapours that might escape.
- Inspect the work area to ensure that it is clean and safe before starting work.

Procedure Steps:

1. Once the final measurement has been made, the pressure in the cell is released by fully opening the release valve on the nitrogen cylinder and closing the regulator.
2. The cell is cooled to a safe temperature (e.g. 40°C) by turning off the thermostatic bath circulation to allow natural cooling.
3. Turn off the magnetic stirrer and remove the stirrer and any insulation material.
4. Disconnect the nitrogen gas line from the cell, after ensuring all pressure is vented at the nitrogen cylinder
5. Remove the height gauge.
6. Once the cell has cooled, remove any further equipment (like temperature probes) and rotate the cell so that the cell inlet valve points downwards.
7. Turn on the extractor hood and position the piping over the cell.
8. Remove the blank nut from the cell valve and slowly drain the contents of the cell into an appropriate flask
9. Check the pressure reading on the cell is at the pressure displayed when the cell is open to the atmosphere, and the draining valve is fully open.
10. Once the content has been drained, completely open the inlet valve of the cell and rotate the cell until the piston section is at the top.
11. Free the shaft and seal by loosening the nuts and tapping on the end of the shaft until it moves downward.
12. Remove the piston section.
13. Place a large waste pan under the cell to capture any stray drops.
14. Rotate the cell body until the opening is facing downward, catching any remaining fluid in the cell in an appropriate flask.
15. While turning the cell into the downward-facing position, care must be taken not to lose the magnetic stirrer bar. Remove the magnetic stirrer bar and set aside for

cleaning. Carefully remove the crystal cage and set aside for cleaning.

g) Clean-up Procedures (including any waste disposal)

The cleaning procedure is the following:

16. Discard any fluids into the general waste container after checking chemical compatibility and completing the waste identification form on the waste container.
17. A large waste pan, matching the cleaning solvent to be used, is placed under the cell opening to collect cleaning chemicals.
18. First, flush the cell with xylene through the cell valve and the cell opening in order to remove any solute left inside.
19. The fluid in the waste pan (mainly xylene) is then discarded into a specific xylene container.
20. Change the waste pan to match the new cleaning solvent.
21. Next, the cell is flushed with methanol through the cell valve and the cell opening in order to remove the remaining chemicals.
22. The collected fluid (mainly methanol) is then discarded into a specific methanol container.
23. The piston head, stirrer and crystal cage can be cleaned using the same rinse procedure, catching any fluids in a waste pan.
24. Compressed air is used to remove traces of the cleaning agents inside the cell and its valve.
25. Dry and wipe any remaining impurities from the cell with tightly rolled lab paper.
26. Use Compressed air to remove any paper fibres.
27. Turn off the thermostat bath and cooling water.
28. Leave the extractor fan over the cell for at least 30 minutes to remove any remaining solvent vapours.

B.2.6 TRA - High-Pressure Viscosity View Cell - Unloading/Cleaning

STEP 1.					
Project / Task Name:	High Pressure Viscosity Measurement View Cell – Unloading and Cleaning Procedure	**Work Area:**	Lab C 301	**Research group**	SepTech
Project / Task Description:	This document outlines the risks involved in the loading procedure of the high pressure cell Viscosity Measurement, using the SWP rev.1.			**Revision**	1

STEP 2.		**STEP 3.**	**STEP 4.**	**STEP 5.**	**STEP 6.**	**STEP 7.**	**STEP 8.**			**STEP 12.**
			RISK RANKING			**RISK CONTROL MEASURES** • *Hierarchy of Control – Elimination, Substitution, Isolation, Engineering, Administration, Personal Protection.* • *Additional information can be attached.*	**RESIDUAL RISK**			
Ref No.	**SPECIFIC TASK / ACTIVITY STEPS**	**IDENTIFY POTENTIAL HAZARDS**	**Consequence**	**Likelihood**	**Risk Rating**		**Consequence**	**Likelihood**	**Residual Risk**	**Actioner / Initials**
1	Lifting Cell; Steps 6, 10, 12, 14	Heavy loads – injury.	2	1	L(3)	Proper training. Use platforms provided. Ask for assistance.	2	1	L(3)	*
2	Using Liquid Chemicals; Steps 8 - 16; and in case of risks [7,8,9]	Chemical Exposure Hazard	2	3	M(8)	Proper training. Foreknowledge of the chemicals concerned. Consult MSDS sheets attached. Adequate ventilation. Correct PPE.	2	1	L(3)	*
3	Using CO_2 ; Steps 8 - 12; and in case of risks [7,8,9]	Chemical Exposure Hazard – CO_2	2	3	M(8)	Proper training. Foreknowledge of the chemicals concerned. Consult MSDS sheets attached. Adequate ventilation. Correct PPE.	2	1	L(3)	*
4	Using Isopropanol; Steps 17 - 19, 23 - 25	Chemical Exposure Hazard – Isopropanol	2	3	M(8)	Proper training. Foreknowledge of the chemicals concerned. Consult MSDS sheets attached. Adequate ventilation. Correct PPE.	2	1	L(3)	*
5	Using Chemicals; Steps 20 - 25	Chemical Exposure Hazard – Methanol	3	3	H(16)	Proper training. Foreknowledge of the chemicals concerned. Consult MSDS sheets attached. Adequate ventilation. Correct PPE.	3	1	M(6)	*
6	Using tools (spanners, hammer, pliers); Steps 4 - 6, 8, 11	Incorrect tool use / tool failure - Injury	2	1	L(3)	Proper training. Using the correct tool for the job. Correct PPE.	2	1	L(3)	*
7	Equipment inherent risk; Steps 1 - 10	High pressure –leak	3	2	M(9)	Proper training and regular inspection. Regular testing of the equipment. Correct PPE.	2	1	L(3)	*

Continued on the next page...

STEP 2.		STEP 3.	STEP 4.	STEP 5.	STEP 6.	STEP 7.	STEP 8.			STEP 12.
Ref No.	**SPECIFIC TASK / ACTIVITY STEPS**	**IDENTIFY POTENTIAL HAZARDS**	**RISK RANKING**			**RISK CONTROL MEASURES** • *Hierarchy of Control – Elimination, Substitution, Isolation, Engineering, Administration, Personal Protection.* • *Additional information can be attached.*	**RESIDUAL RISK**			**Actioner / Initials**
			Consequence	**Likelihood**	**Risk Rating**		**Consequence**	**Likelihood**	**Residual Risk**	
8	Equipment inherent risk; Steps 1 - 10	High Pressure – Equipment Failure causing explosive decompression	3	1	M(6)	Proper training and inspection. Regular testing. Safety in design. Correct PPE.	3	1	M(6)	*
9	Venting Cell; Steps 1, 8	High Pressure – Uncontrolled Rapid Expansion.	3	4	H(17)	Proper training. Proper Ventilation/extraction. Correct PPE.	2	3	M(8)	*
10	Equipment inherent risk; Steps 2 - 5	High Heat – Burns.	2	2	L(5)	Equipment has built in safety. Proper training. Correct PPE.	2	1	L(3)	*
11	Equipment inherent risk; General	High Voltage – Three phase motor	3	2	M(9)	Equipment has built in safety. Protective shielding. Correct PPE.	3	1	M(6)	*
				STEP 9.		**Highest Remaining Residual Risk**			**M (6,8, 10)**	

*Actioners : Training in equipment and PPE use must be implemented by Prof Schwarz, as well as enforcing inspection, maintenance and testing. Operators must implement safe operations, perform regular testing and conform to lab safety and PPE requirements. Operators must familiarize themselves with relevant MSDS sheets and safety procedures, as well as the SWP.

B.3 Large Supercritical Pilot Plant

B.3.1 For First-time Users

Before a new operator operates the pilot plant for the first time, it is advised that they adhere to the following procedure. This will ensure that the pilot plant is kept in good working order and that the new user operates it safely.

1. Get familiarised with the pilot plant manual, especially the relevant safety documents and the process description.
2. Do a cursory check for leaks, especially heating oil, or apparent damage to the system.
3. Check if any pressure remains in the system from previous experiments. If pressure is present, vent in a safe manner.
4. Check the system maintenance schedule if any maintenance is due and perform as instructed in the pilot plant manual.
5. Check both the gearbox and hydraulic oil levels of the pumps and the heating oil level of the oil heaters, H1 and H2, and top up if required. The appropriate oils are recorded in the pilot plant manual.
6. Check if the system is clean, especially the feed vessel, V 1-1, and the separator vessel, V 4-1.
7. Check what kind of packing is in the column(s) and if the packing is clean. If needed, change the packing type as described in the pilot plant manual. If the packing is changed, a pressure test of the column is advised, followed by an air scouring as described in step 10.
8. Check if the optical level sensors and sapphire cones are clean.
9. If in any of the above three steps, the pilot plant is found in an unsatisfactory state, determine an appropriate cleaning solvent such as ethanol or warm soapy water. Avoid acetone as it can damage seals in the system. The chosen solvent is loaded into the feed vessel, V 1-1 and separator, V 4-1, and circulated by turning on the liquid and solvent feed pumps, P 1-1, P 1-2 and P 2-1. Manual cleaning of the separator is required. If required, the oil heaters, H1 and H2, can be turned on to aid in cleaning.
10. If the system is cleaned with a solvent, ensure the system is purged of the solvent by washing with pure water and/or scouring with compressed air. Scouring by air is done by connecting the compressed air hose to valve NV 1-1 for the liquid feed lines, NV 3-3 and NV 3-4 for Column 3-1 and 3-2 respectively, and NV 4-2 or NV 4-3 for the solvent section.
11. If any connections are loosened during cleaning or inspection, ensure that they are tightly fastened afterwards.
12. Ensure the cooling fans and radiators of the pump motors, heaters and refrigeration condenser are clean for optimal operation. Compressed air can be used to remove any loose dirt.
13. If a leak on the system is suspected, see the plant manual section for leak trouble-shooting.

B.3.2 SWP - Large Supercritical Pilot Plant - Start-up

Scope

This document outlines the Startup procedure of the Large Supercritical Pilot Plant in Lab C118 in the Department of Chemical Engineering.

a) Authorisation

- Prof C.E. Schwarz is to approve any work prior to commencement.
- Training is required for the high-pressure process environment and lab procedures. Prof Schwarz to sign off on completed training.
- Due to high pressures and extreme conditions, all operators are to sign the SWP before commencing any work.

b) Hazards

- High pressures (up to 350 Bar)
- High temperatures (up to 80 °C)
- High-pressure gas leaks or rapid gas expansion.
- High Noise Levels when heaters are in operation
- Chemicals handling

Highest remaining residual risk rating: M

c) Personal Protective Equipment (PPE) *[minimum PPE required to be worn by all personnel working on task]*

- Safety glasses.
- Lab coat.
- Closed shoes.
- Hearing protection.
- Hardhat when crane is in operation or work is done on higher levels.
- Insulating gloves when handling hot/cold surfaces.
- Latex/nitrile gloves when handling chemicals – chemical-specific.

d) Emergency Response/First aid requirements

- In case of Power Failure – the system is designed to safely self-contain through a series of fail-open/fail close and one-way valves. Decrease pressure in the column/high-pressure sections. Determine if the failure is long term and vent/secure the plant if needed, or secure a safe stasis for shorter interruptions.
- In case of fire – Close CO_2 Cylinder. If possible, turn the system off at the control box/Switchboard and vent CO_2 inventory. Evacuate quickly and safely.
- In case of cooling water failure, identify duration and if prolonged effect a safe shutdown as per the shutdown procedure.
- In case of emergency shutdown, follow SWP for Shutdown, steps 1, 2, 4, 7 and 8.

e) Maintenance Requirements:

Regular inspection:

- Visual inspection of the pilot plant is required between experimental runs. This includes checking for any leaks, wear and tear, or damage.
- If the pilot plant requires maintenance, refer to the plant manual for specific maintenance procedures.

Regular testing and calibration:

- Ensure that pressure sensor calibrations are conducted six-monthly or after any significant alterations, modifications or maintenance to the equipment.
- Ensure that the high-pressure side of the pilot plant is hydrostatically tested yearly, or after any alterations, modifications or maintenance to the equipment.
- Test that the pressure relief valves are functional and set at the appropriate value every six months, or after any alterations or maintenance.
- Ensure the temperature sensors are calibrated yearly.
- A log of all test and calibration results should be kept in the plant manual and in SharePoint. A maintenance schedule is also to be kept in the manual for purposes of reference and audit.

UNDERTAKING THE TASK:

f) Step-by-step Procedure

Preparation/Precautions:

- Inspect the work area to ensure that it is clean and safe before starting work.
- Do a cursory check for leaks, especially heating fluid or apparent damage to the system.
- Check the Task risk assessment for specific chemicals to be used (solvent gas and solute fluid/solid)
- Check if any pressure remains in the system from previous experiments. If pressure is present vent safely.
- Check both the gearbox and hydraulic oil levels of the pumps and the heating fluid level of the heaters and top up if required. The appropriate oils are recorded in the plant manual.
- If in any of the above steps the plant is found in an unsatisfactory state, refer to the plant shutdown/cleaning SWP.
- **NB:** While the plant is operating at pressures above the critical point, and the high-pressure loop is in operation, the operator must monitor the plant at all times.

Procedure Steps:

The following steps should be performed when preparing to start a run on the pilot plant (after doing the needed preparation and taking precautions as specified above):

1. Switch on the main power supply to the pilot plant.
2. Ensure that a flash drive with the correct file system (FAT 32) and sufficient free space is plugged into the HMI system to record the logging data.
3. Check that the compressed air valve, UV3, is open and delivers sufficient pressure. To check the air supply, open the utility nozzle air valve, UV 2 and observe if sufficient pressure is present.
4. Ensure that valves BV1-1, BV1-2 and NV1-1 are closed.
5. Place the liquid feed/solute into the feed vessel, V 1-1. If the component is prone to

evaporation or hygroscopic, add the lid and screw down tightly.

   a. In some cases, the solute feed pumps require priming with solute. This can be done by the following procedure:
   b. Open NV1-2 through NV 1-5.
   c. Ensure vessel V 1-1 is tightly closed.
   d. Turn on the pumps individually in the liquid feed section of the HMI system.
   e. Apply gentle air pressure to the tank through the top valve, until liquid appears at valve NV1-4.
   f. Turn all pumps off and close valves NV1-2 to 1-5.

6. Switch on heaters H1 and H2 and input the desired temperatures into the heaters, noting that the actual temperature is about 15°C below the heater set-point for heater H1 and 5-10°C above for heater H2 (at time of writing).
   a. Allow for sufficient time for the system to reach thermal equilibrium. It is advised that this is done at least 2 hours in advance for lower temperatures (up to 60°C) and the previous day for higher temperatures (up to 200°C), to allow for sufficient heating time. For temperatures above 80 °C ensure the heaters is filled with heating oil, not water.
7. Connect the Liquid hold-up tank to the bottom of the selected column and ensure valves NV5-1 and NV5-2 are closed.
8. Switch on the cooling water at the cooling water mains and open valves UV 1 and UV 2 to allow for cooling water flow.
9. Switch on the refrigeration unit on the refrigeration control panel. Ensure that the set temperatures are correct for the selected solvent, as specified in Table C- 1. Allow for 15-30 minutes for the refrigeration to reach operating temperatures.

Table C-1: Refrigerator temperature and controller set values for different supercritical fluids.

	Condenser		**Pump Suction**	
Supercritical Fluid	Temperature (°C)	Controller Setting	Temperature (°C)	Controller Setting
CO_2	5 - 22	10	-2 - 9	10
Ethane	5 - 22	10	-2 - 9	10
Propane	15 - 30	20	10 - 20	20
Butane	25 - 40	25	20 - 30	25

The system is now ready for the loading and priming of the solvent section. This is done as follows:

10. Turn on the extractor fans in the lab in case of a gas leak.
11. Before loading solvent ensure that the following valves are fully closed: NV1-1 through 1-7, NV2-2, NV2-4, NV3-1 through 3-10, NV4-1 through 4-4.
12. Check that the following valves are fully open: NV2-1, NV2-3, and NV2-5.
13. If needed, adjust the regulator valve, SV 2-1, in the solvent recycle loop. For a start-up, it is advised that the valve is fully open.
14. When connecting a new cylinder, first close valve NV2-1 and connect the cylinder. Open the cylinder main valve, followed by opening valve NV2-1. Open the valve slowly, especially when operating with carbon dioxide, to avoid ice forming in the lines.
15. If a new solvent is used, the system should be vented. This is done in the following manner:
    a. Open valves NV2-2, NV3-1, NV3-2,NV 3-9, NV 3-10, NV4-1 and override CV 4-1 on the separator section on the HMI. If the valve is overridden, the button will turn green.
    b. Briefly open valves NV2-4, NV3-3, NV3-4, NV4-2 and NV4-3.

   c. After this, reclose the valves NV2-2, NV 3-1, NV3-2, NV 3-9, NV 3-10 and NV4-1 and return control to CV 4-1 by pressing the override button again. If the override function is off, the button will appear yellow.

16. Ensure the stroke length for the solvent feed pump, P 2-1, is set to ~10mm.
17. To load solvent, select the 'Start-up' sequence on gas feed section on the HMI. This will bypass specific alarms and allow the P 2-1 to be turned on to start circulating the solvent.
18. Turn on Solvent pump P 2-1 on the HMI in the gas feed section as soon as sufficient liquid is in the solvent tank.
19. Monitor the gas feed pressure on local pressure indicator PI 2-1. If the pressure increases significantly above the gas bottle pressure, switch off the pump immediately.
20. Wait for the solvent to reach an acceptable liquid level, as can be observed in the level gauge. A level of three quarters is recommended for standard operation. Close NV 2-1 to ensure an accurate mass flow reading and press the "Start-up" button to re-enable said alarms.
21. Slowly open Valves NV4-1, NV4-4 and either valves NV3-1 and NV3-9 for operating column C 3-1 or NV3-2 and NV3-10 for column C 3-2.
22. Set the pressure set point for the control valve SV 2-1 to a value just above the currently circulating solvent pressure as read from PI 3-1. This is done in the separator section on the HMI.
23. Slowly close valve NV2-3 to close the solvent recycle loop.
24. Increase the set point for the control valve stepwise by about 10 bar to the selected column pressure, allowing for the system to adjust for a few minutes between steps. See Table C- 2 for recommended minimum values for a few supercritical solvents.

Table C- 2: Solvent critical pressure and suggested minimum operating pressure.

Supercritical Solvent	Critical Pressure (bar)	Suggested Minimum Pressure (bar)
CO_2	73.8	±90
Ethane	42.5	±60
Propane	50.6	±70
Butane	38.0	±60

25. Allow the system to run for five minutes to allow the gas to circulate.
26. The solvent feed pump, P 2-1, can now be adjusted to the appropriate setting by manually turning the solvent feed pump dial. Fine-tuning of the flow rate with respect to the mass flow sensor is advised. Remember to lock the pump safety lever at the appropriate setting.
27. If the control valve response is unsatisfactory or too big, the momentary pressure drop caused by control valve CV4-1 can be choked by partially closing NV 4-1. This provides backpressure, which keeps the pressure drop from fluctuating wildly. Note that if this is applied, the column pressure has to be monitored carefully to avoid pressure build-up.
28. For very low solvent flow rates, the recycle loop can be kept open and throttled to provide a smaller net flow:
    a. First, allow the pilot plant to reach steady-state at an intermediate solvent flow value. It is essential to ensure a constant flow for this operation mode.
    b. Note the current mass flow value.
    c. Turn on the 'Bypass'-option on the gas feed section of the HMI. Input the current average mass flow into the box as prompted. The calculated mass flow value should now appear as a separate block below the current mass flow and should currently be averaging around zero (adjust until this is achieved).

   d. Now open valve NV2-3 and adjust the regulator valve SV 2-1 until the desired calculated mass flow is obtained. Note that the calculated mass flow in this option is inaccurate and should be used with discretion. Do not adjust the pump flow rate or any throttling valves, as this will render the calculated value meaningless.

29. Ensure that no significant pressure build-up occurs beyond the extraction pressure. This is done by monitoring PIC 4-1 on the HMI or the local pressure indicators PI 3-1 and PI 4-1. If this occurs, turn off pumps and immediately vent the column at valves NV3-3 and NV3-4 for columns C3-1 and C 3-2 respectively.
30. Optimise the column pressure by changing the set point if required. If the drop in pressure from the opening and closing of the control valve CV 4-1 is too large, back pressure can be applied by partially closing NV 4-1.
31. The system is now ready to start an extraction or a hydrodynamic experiment

g) Clean-up Procedures (including any waste disposal)

None, no waste generated in startup procedure. Follow procedures for chemical handling for any spills or unneeded leftovers.

B.3.3 TRA - Large Supercritical Pilot Plant - Start-up

STEP 1.					
Project / Task Name:	Large Supercritical Pilot Plant – Startup Procedure	**Work Area:**	Lab C 118	**Research group**	SepTech
Project / Task Description:	This document outlines the risks involved in the startup procedure of the Large Supercritical Pilot Plant, using the SWP rev.1.1			**Revision Number**	1.1

STEP 2.		**STEP 3.**	**STEP 4.**	**STEP 5.**	**STEP 6.**	**STEP 7.**	**STEP 8.**			**STEP 12.**
			RISK RANKING				**RESIDUAL RISK**			
Ref No.	**SPECIFIC TASK / ACTIVITY STEPS**	**IDENTIFY POTENTIAL HAZARDS**	**Consequence**	**Likelihood**	**Risk Rating**	**RISK CONTROL MEASURES** • *Hierarchy of Control – Elimination, Substitution, Isolation, Engineering, Administration, Personal Protection.* • *Additional information can be attached.*	**Consequence**	**Likelihood**	**Residual Risk**	**Actioner / Initials**
1	Solvent: Using CO_2, in case of risks [3, 4, 5]	Chemical Exposure Hazard – CO_2	2	3	M(8)	Proper training. Foreknowledge of the chemicals concerned. Consult MSDS sheets attached. Adequate ventilation. Correct PPE.	2	1	L(3)	*
2	Solute: Using Silicone Oil; Step 5	Chemical Exposure Hazard – Silicone Oil	2	3	M(8)	Proper training. Foreknowledge of the chemicals concerned. Consult MSDS sheets attached. Adequate ventilation. Correct PPE.	2	1	L(3)	*
3	Equipment inherent risk; From step 14 onward.	High Pressure –Leak	3	2	M(9)	Proper training and regular inspection. Regular testing of the equipment. Correct PPE reduces consequence.	3	2	M(9)	*
4	Equipment inherent risk; From step 14 onward.	High Pressure – Equipment Failure Causing Explosive Decompression	4	1	M (10)	Proper training and inspection. Regular testing. Safety in design. Correct PPE.	4	1	M (10)	*
5	Venting of solvent; Step 15.	High Pressure – Uncontrolled Rapid Expansion.	2	3	M(8)	Proper training. Correct PPE can reduce consequence..	2	1	L(3)	*
6	Equipment inherent risk; From step 7 onward.	High Heat – Light Burns.	2	2	L(5)	Equipment has built in safety. Proper training. Correct PPE.	2	1	L(3)	*
7	Equipment inherent risk; From step 9 onward.	Low Temperatures – Frost burns	2	2	L(5)	Proper training. Correct PPE.	2	1	L(3)	*
8	Equipment inherent risk; General	High Voltage – Three phase power	3	2	M(9)	Equipment has built in safety. Protective shielding. Correct PPE.	3	1	M(6)	*
9	Equipment inherent risk; General	Heights – 2 Story setup	3	2	M(9)	Proper training – maintain 3-point contact. Correct PPE.	3	1	M(6)	*
10	Equipment inherent risk; General	High noise levels	2	3	M(8)	Proper training. Correct PPE.	3	1	M(6)	*
				STEP 9.		**Highest Remaining Residual Risk**			**M (10)**	

*Actioners : Training in equipment and PPE use must be implemented by Prof Schwarz, as well as enforcing inspection, maintenance and testing.
Operators must implement safe operations, perform regular testing and conform to lab safety and PPE requirements. Operators must familiarize themselves with relevant MSDS sheets and safety procedures, as well as the SWP.

B.3.4 SWP - Large Supercritical Pilot Plant - Experimental

Scope

This document outlines the Experimental procedure of the Large Supercritical Pilot Plant in Lab C118 in the Department of Chemical Engineering.

a) Authorisation

- Prof C.E. Schwarz is to approve any work prior to commencement.
- Training is required for the high-pressure process environment and lab procedures. Prof Schwarz to sign off on completed training.
- Due to high pressures and extreme conditions, all operators are to sign the SWP before commencing any work.

b) Hazards

- High pressures (up to 350 Bar)
- High temperatures (up to 80 °C)
- High-pressure gas leaks or rapid gas expansion.
- High Noise Levels when heaters are in operation
- Chemicals handling

Highest remaining residual risk rating: M

c) Personal Protective Equipment (PPE) *[minimum PPE required to be worn by all personnel working on task]*

- Safety glasses.
- Lab coat.
- Closed shoes.
- Hearing protection.
- Hardhat when crane is in operation or work is done on higher levels.
- Insulating gloves when handling hot/cold surfaces.
- Latex/nitrile gloves when handling chemicals – chemical-specific.

d) Emergency Response/First aid requirements

- In case of Power Failure – the system is designed to safely self-contain through a series of fail-open/fail close and one-way valves. Decrease pressure in the column/high-pressure sections. Determine if the failure is long term and vent/secure the plant if needed, or secure a safe stasis for shorter interruptions.
- In case of fire – Close CO_2 Cylinder. If possible, turn the system off at the control box/Switchboard and vent CO_2 inventory. Evacuate quickly and safely.
- In case of cooling water failure, identify duration and if prolonged effect a safe shutdown as per the shutdown procedure.
- In case of emergency shutdown, follow SWP for Shutdown, steps 1, 2, 4, 7 and 8.

e) Maintenance Requirements:

Regular inspection:

- Visual inspection of the pilot plant is required between experimental runs. This includes checking for any leaks, wear and tear, or damage.
- If the pilot plant requires maintenance, refer to the plant manual for specific maintenance procedures.

Regular testing and calibration:

- Ensure that pressure sensor calibrations are conducted six-monthly or after any significant alterations, modifications or maintenance to the equipment.
- Ensure that the High-pressure side of the pilot plant is hydrostatically tested yearly, or after any alterations, modifications or maintenance to the equipment.
- Test that the pressure relief valves are functional and set at the appropriate value every six months, or after any alterations or maintenance.
- Ensure the temperature sensors are calibrated yearly.
- A log of all test and calibration results should be kept in the plant manual and in SharePoint. A maintenance schedule is also to be kept in the manual for purposes of reference and audit.

UNDERTAKING THE TASK:

f) Step-by-step Procedure

Preparation/Precautions:

- Inspect the work area to ensure that it is clean and safe before starting work.
- Do a cursory check for leaks, especially high-pressure gas or heating fluid, or apparent damage to the system.
- Check the Task risk assessment for specific chemicals to be used (solvent gas and solute fluid/solid)
- Follow all steps in the preceding Startup SWP.
- **NB:** While the plant is operating at pressures above the critical point, and the high-pressure loop is in operation, the operator must monitor the plant at all times.

Procedure Steps:

The pilot plant can be operated in a Standard Countercurrent Mode, with an optional, supplementary Hydrodynamic Mode. Both are discussed below separately.

Standard operation of the plant can be achieved as follows:

1. Ensure that the liquid feed level is high enough in the feed vessel, V 1-1 and that the vessel is open to the atmosphere to prevent a vacuum from forming. In the case of fluids that prove difficult to pump or are prone to evaporation, pressurised air or nitrogen pressure can be applied to the feed vessel.
2. Open valve BV1-1 and NV1-2 to use the small capacity feed pump, P 1-1, or valve BV1-2 and NV 1-3 for the large capacity feed pump, P 1-2. For flows between 0 and 2ℓ the small pump is recommended, while for flows between 2 and 8ℓ, the larger pump is advised.
3. Open the relevant valves to select the feed position for the chosen column:
    a. Column C 3-1:
        i. Top Feed: Valves NV1-7 and NV3-6.
        ii. Middle feed: Valves NV1-6 and NV3-8.

    b. Column C 3-2:
        i. Top feed: Valves NV 1-7 and NV 3-5.
        ii. Middle feed: Valves NV 1-6 and NV 3-7.
4. In order to allow pressure to be read in the liquid feed pressure gauge (and in some cases allow for liquid flow) open valve NV 1-5.
5. Set the relevant liquid feed pump to the required setting. The required setting can be obtained by consulting the pump calibration curves in the plant manual.
   (for hydrodynamic experiments skip from here to step 11)

6. Turn on the chosen feed pump in the liquid feed section of the HMI.
7. For extended runs, monitor the level in feed vessel V 1-1 and top up as needed. If the feed is to be heated, add in small amounts or preheat the liquid before adding it to the vessel.
8. Periodically decant and measure the column bottoms to avoid build-up. Column C 3-2 has a level sensor that will warn of build-up. It is advised that column C 3-1 is timed and periodically drained with respect to the liquid feed rate.
9. Periodically decant and measure the built-up liquid from the separator, V 4-1, by opening valve NV4-2. The separator has a big volume and typically only needs emptying at the end of a run. In the case of the separator becoming full, a level sensor will warn the operator.
10. Periodically check the liquid solvent level in solvent feed tank V2-1 to ensure the system does not run dry.

The following procedures are for the measurement of hydrodynamic data, being pressure drop and liquid hold-up.

11. Turn the solvent feed rate to the first supercritical phase flow rate required.
12. Ensure the column bottoms, hold-up tank and separator are drained.
13. Allow the system time to reach equilibrium. Equilibrium is determined by monitoring the pressure drop over the column and the liquid solvent mass flow rate. As soon as the respective trends stop fluctuating for an extended period, equilibrium is assumed. This can take up to an hour.
14. Check the liquid/solute feed rate to ensure it is at the desired level. Turn on the pump while noting the starting time of the run.
15. Again monitor the pressure drop over the column to determine the new equilibrium state with the liquid/solute flow included.
16. Periodically decant and weigh and/or measure the volume the column bottoms and overheads, as dictated by the liquid flow rate. This can be done without disturbing the equilibrium, by isolating the liquid hold-up tank and decanting from it.
17. As soon as equilibrium is reached, note the current time on the HMI system. The system pressure drop, temperature and solvent flow rate can later be averaged from logged data at/or around this time.
18. The following procedure is used to measure liquid hold-up:
    a. After equilibrium is reached, drain all of the liquid from the bottom of the column/hold-up tank, as stated in step 16.
    b. Once all the liquid has drained, stop the liquid feed pump and open NV 2-3 to bypass the solvent immediately.
    c. Allow time for the liquid in the packing to drain out. This process is dependent on the packing geometry and the viscosity of the fluid and can take a significant amount of time. Keep completely draining the hold-up at set intervals until the liquid captured becomes negligible. Weigh and/or measure the volume of the hold-up.
    d. Briefly close NV 2-3 to pump solvent to the column to evacuate any remaining liquid hold-up from the solvent feed pipe that may have accumulated. Allow for

some time to settle and drain the column again.

19. Change the liquid feed rate to a higher level and repeat steps 14 to 18.
20. As soon as the liquid overheads show sharp increases, it can be assumed that the column has flooded. Level sensor L 3-2 should also be indicating a liquid level. Flooding concludes the measurement at a specific liquid flow rate. It is, however, advised to measure a few further data points to confirm that flooding has occurred and provide a complete picture of a system.
21. To measure at a different solvent flow rate, adjust the solvent feed pump and repeat the procedure from step 12 onward.

NB: All the required readings such as temperature, pressure, solvent flow rate and pressure drop are recorded onto the flash drive, by the HMI system. After an experimental set, the flash drive must be removed safely, to avoid data loss, by using the main screen, where after the data can be recovered using a computer. The recovered data can be compared to the time values noted during the experiment to identify the exact data required.

NOTE: The hold-up and bottoma are calculated from the drained mass. The solubility of CO_2 at atmospheric conditions is typically minute as the CO_2 flashes off. To determine if a significant amount of CO_2 remains in the bottoms, samples from different conditions should be weighed, then degassed in a vacuum. After degassing the samples are weighed again to determine if a significant amount of CO_2 remained in the samples. The mass of the liquid in the column is projected using the binary phase properties measured in the prior high pressure cell experiments.

g) Clean-up Procedures (including any waste disposal)

None, no waste generated in experimental procedure. Follow procedures for chemical handling for any spills or unneeded leftovers.

B.3.5 TRA - Large Supercritical Pilot Plant - Experimental

STEP 1.					
Project / Task Name:	Large Supercritical Pilot Plant – Experimental Procedure	**Work Area:**	Lab C 118	**Research group**	SepTech
Project / Task Description:	This document outlines the risks involved in the Experimental procedure of the Large Supercritical Pilot Plant, using the SWP rev.1.1			**Revision Number**	1.1

STEP 2.		**STEP 3.**	**STEP 4.**	**STEP 5.**	**STEP 6.**	**STEP 7.**	**STEP 8.**			**STEP 12.**
			RISK RANKING				**RESIDUAL RISK**			
Ref No.	**SPECIFIC TASK / ACTIVITY STEPS**	**IDENTIFY POTENTIAL HAZARDS**	**Consequence**	**Likelihood**	**Risk Rating**	**RISK CONTROL MEASURES** • *Hierarchy of Control – Elimination, Substitution, Isolation, Engineering, Administration, Personal Protection.* • *Additional information can be attached.*	**Consequence**	**Likelihood**	**Residual Risk**	**Actioner / Initials**
1	Solvent: Using CO_2, Steps 8-10, 12, 16, 18 and in case of risks [3, 4, 5]	Chemical Exposure Hazard – CO_2	2	3	M(8)	Proper training. Foreknowledge of the chemicals concerned. Consult MSDS sheets attached. Adequate ventilation. Correct PPE.	2	1	L(3)	*
2	Solute: Using Silicone Oil; Steps 7-10, 12, 16, 18 and in case of risks [3, 4, 5]	Chemical Exposure Hazard – Silicone Oil	2	3	M(8)	Proper training. Foreknowledge of the chemicals concerned. Consult MSDS sheets attached. Adequate ventilation. Correct PPE.	2	1	L(3)	*
3	Equipment inherent risk; All steps	High Pressure –Leak	3	2	M(9)	Proper training and regular inspection. Regular testing of the equipment. Correct PPE reduces consequence.	3	2	M(9)	*
4	Equipment inherent risk; All steps	High Pressure – Equipment Failure Causing Explosive Decompression	4	1	M (10)	Proper training and inspection. Regular testing. Safety in design. Correct PPE.	4	1	M (10)	*
5	Equipment inherent risk; Steps 8-10, 12, 16, 18	High Pressure – Uncontrolled Rapid Expansion.	2	3	M(8)	Proper training. Correct PPE can reduce consequence..	2	1	L(3)	*
6	Equipment inherent risk; General	High Heat – Light Burns.	2	2	L(5)	Equipment has built in safety. Proper training. Correct PPE.	2	1	L(3)	*
7	Equipment inherent risk; General	Low Temperatures – Frost burns	2	2	L(5)	Proper training. Correct PPE.	2	1	L(3)	*
8	Equipment inherent risk; General	High Voltage – Three phase power	3	2	M(9)	Equipment has built in safety. Protective shielding. Correct PPE.	3	1	M(6)	*
9	Equipment inherent risk; General	Heights – 2 Story setup	3	2	M(9)	Proper training – maintain 3-point contact. Correct PPE.	3	1	M(6)	*
10	Equipment inherent risk; General	High noise levels	2	3	M(8)	Proper training. Correct PPE.	3	1	M(6)	*
				STEP 9.		**Highest Remaining Residual Risk**			**M (10)**	

*Actioners : Training in equipment and PPE use must be implemented by Prof Schwarz, as well as enforcing inspection, maintenance and testing. Operators must implement safe operations, perform regular testing and conform to lab safety and PPE requirements. Operators must familiarize themselves with relevant MSDS sheets and safety procedures, as well as the SWP.

B.3.6 SWP - Large Supercritical Pilot Plant - Shutdown/Clean-up

Scope

This document outlines the Shutdown and Clean-up procedure of the Large Supercritical Pilot Plant in Lab C118 in the Department of Chemical Engineering.

1. **Authorisation**

- Prof C.E. Schwarz is to approve any work prior to commencement.
- Training is required for the high-pressure process environment and lab procedures. Prof Schwarz to sign off on completed training.
- Due to high pressures and extreme conditions, all operators are to sign the SWP before commencing any work.

2. **Hazards**

- High pressures (up to 350 Bar)
- High temperatures (up to 80 °C)
- High-pressure gas leaks or rapid gas expansion.
- High Noise Levels when heaters are in operation
- Chemicals handling

Highest remaining residual risk rating: M

3. **Personal Protective Equipment (PPE)** *[minimum PPE required to be worn by all personnel working on task]*

- Safety glasses.
- Lab coat.
- Closed shoes.
- Hearing protection.
- Hardhat when crane is in operation or work is done on higher levels.
- Insulating gloves when handling hot/cold surfaces.
- Latex/nitrile gloves when handling chemicals – chemical-specific.

4. **Emergency Response/First aid requirements**

- In case of Power Failure – the system is designed to safely self-contain through a series of fail-open/fail close and one-way valves. Decrease pressure in the column/high-pressure sections. Determine if the failure is long term and vent/secure the plant if needed, or secure a safe stasis for shorter interruptions.
- In case of fire – Close CO_2 Cylinder. If possible, turn the system off at the control box/Switchboard and vent CO_2 inventory. Evacuate quickly and safely.
- In case of cooling water failure, identify duration and if prolonged effect a safe shutdown as per the shutdown procedure.
- In case of emergency shutdown, follow SWP for Shutdown, steps 1, 2, 4, 7 and 8.

a) Maintenance Requirements:

Regular inspection:

- Visual inspection of the pilot plant is required between experimental runs. This includes checking for any leaks, wear and tear, or damage.
- If the pilot plant requires maintenance, refer to the plant manual for specific maintenance procedures.

Regular testing and calibration:

- Ensure that pressure sensor calibrations are conducted six-monthly or after any significant alterations, modifications or maintenance to the equipment.
- Ensure that the High-pressure side of the pilot plant is hydrostatically tested yearly, or after any alterations, modifications or maintenance to the equipment.
- Test that the pressure relief valves are functional and set at the appropriate value every six months, or after any alterations or maintenance.
- Ensure the temperature sensors are calibrated yearly.
- A log of all test and calibration results should be kept in the plant manual and in SharePoint. A maintenance schedule is also to be kept in the manual for purposes of reference and audit.

UNDERTAKING THE TASK:

5. Step-by-step Procedure

Preparation/Precautions:

- Inspect the work area to ensure that it is clean and safe before starting work.
- Do a cursory check for leaks, especially high-pressure gas or heating fluid, or apparent damage to the system.
- Check the Task risk assessment for specific chemicals to be used (solvent gas and solute fluid/solid)
- **NB:** While the plant is operating at pressures above the critical point and the high-pressure loop is in operation the operator must monitor the plant at all times.

Procedure Steps:

Once an experimental run is complete, the following procedure should be followed:

20. Turn off the appropriate liquid feed pump on the HMI liquid feed section.
21. Close the valves used to feed the liquid to the column:
    a. Column C 3-1:
        i. Top feed: Valve NV 3-6.
        ii. Middle Feed: Valve NV 3-8.
    b. Column C 3-2:
        i. Top feed: Valve NV 3-5.
        ii. Middle Feed: Valve NV 3-7.
22. Allow the solvent to circulate for a further 20 minutes, especially in the case of an extraction run. This removes any remaining light product in the column and top product line. Continue draining column bottoms and overheads as needed.
23. Relieve any remaining pressure in the liquid feed line by draining the line at valve NV1-4.
24. If needed, drain any remaining liquid feed in the feed tank, V 1-1, by opening valve NV1-1
25. If the solvent gas is to be reused, it can be stored in the system. The following

measures should be taken:

  a. Reduce the column set pressure in 10 bar steps to the solvent tank pressure.
  b. Close valve NV2-5 to keep the liquid solvent from leaving the buffer tank, V 2-1. The check valve CHV2-3 will prevent flow into the separator. It is not critical but advised to close the following valves to isolate equipment and decrease the effect of possible leaks: NV2-2, NV2-3, NV3-1, NV3-2, NV3-9, NV3-10, NV4-1 and NV4-3.
  c. Drain the column used by opening valve NV 3-3 for column C 3-1 and valve NV 3-4 for column C 3-2 and catching any remaining liquid. If no more liquid exits the column, the system can be fully depressurised if desired.
  d. Drain the separator by opening valve NV 4-3, again catching any remaining liquid. If no more liquid exits the separator, the system can be fully depressurised if desired.
  e. The solvent is now safe to store until the next run.

26. If the solvent is not to be stored, follow steps 7.a, c. and d., after which the solvent buffer tank, V 2-1, can be depressurised by opening valve NV 2-4. Ensure proper ventilation and a slow depressurisation to avoid the valves from icing over.
27. Turn off the solvent pump, P 2-1, in the gas feed section of the HMI.
28. Turn off the oil heaters H1 and H2
29. After allowing for a further 10 minutes turn off the refrigeration system, R1, followed by the cooling water.
30. Turn off the control panel and the pilot plant mains.

6. Clean-up Procedures (including any waste disposal)

31. Discard any fluids into the general waste container after checking chemical compatibility and completing the waste identification form on the waste container.
32. If a different liquid/solute is to be used with the pilot plant the plant has to be washed in preparation.
    a. Determine an appropriate cleaning solvent such as ethanol or warm soapy water.
    b. The chosen solvent is loaded into the feed vessel, V 1-1 and separator, V 4-1, and circulated by turning on the liquid and solvent feed pumps, P1-1, P1-2 and P2-1. After which the solvent can be drained from the column bottoms, separator and gas buffer tank.
    c. Manual cleaning of the separator is required.
    d. If required, the oil heaters, H1 and H2, can be turned on to aid in cleaning.
33. If the system is cleaned with a solvent, ensure the system is purged of the solvent by washing with pure water and/or scouring with compressed air.
    e. Scouring by air is done by connecting the compressed air hose to valve NV1-1 for the liquid feed lines, NV3-3 and NV3-4 for Column 3-1 and 3-2 respectively, and NV4-2 or NV4-3 for the solvent section.
34. If any connections are loosened during cleaning or inspection, ensure that they are tightly fastened afterwards.
35. Ensure the cooling fans and radiators of the pump motors, heaters and refrigeration condenser are clean for optimal operation. Compressed air can be used to remove any loose dirt.
36. If a leak on the system is suspected, see the plant manual section for leak trouble-shooting.

B.3.7 TRA - Large Supercritical Pilot Plant - Shutdown/Clean-up

STEP 1.					
Project / Task Name:	Large Supercritical Pilot Plant – Shutdown and Cleanup Procedure	**Work Area:**	Lab C 118	**Research group**	SepTech
Project / Task Description:	This document outlines the risks involved in the Shutdown and Cleanup procedure of the Large Supercritical Pilot Plant, using the SWP rev.1.1			**Revision Number**	1.1

STEP 2.		STEP 3.	STEP 4.	STEP 5.	STEP 6.	STEP 7.	STEP 8.			ST EP 12.
Ref No.	**SPECIFIC TASK / ACTIVITY STEPS**	**IDENTIFY POTENTIAL HAZARDS**	**RISK RANKING**			**RISK CONTROL MEASURES** • *Hierarchy of Control – Elimination, Substitution, Isolation, Engineering, Administration, Personal Protection.* • *Additional information can be attached.*	**RESIDUAL RISK**			**Actioner / Initials**
			Consequence	**Likelihood**	**Risk Rating**		**Consequence**	**Likelihood**	**Residual Risk**	
1	Solvent: Using CO_2, Steps 3, 6, 7 and in case of risks [5, 6, 7]	Chemical Exposure Hazard – CO_2	2	3	M(8)	Proper training. Foreknowledge of the chemicals concerned. Consult MSDS sheets attached. Adequate ventilation. Correct PPE.	2	1	L(3)	*
2	Solute: Using Silicone Oil; Steps 3, 4, 5, 12 and in case of risks [5, 6, 7]	Chemical Exposure Hazard – Silicone Oil	2	3	M(8)	Proper training. Foreknowledge of the chemicals concerned. Consult MSDS sheets attached. Adequate ventilation. Correct PPE.	2	1	L(3)	*
3	Cleaning Fluid: Using Methanol; Steps 13, 14 and in case of risks [5, 6, 7]	Chemical Exposure Hazard – Silicone Oil	3	3	H (16)	Proper training. Foreknowledge of the chemicals concerned. Consult MSDS sheets attached. Adequate ventilation. Correct PPE.	3	1	M(6)	*
4	Equipment inherent risk; Potentially All steps	High Pressure –Leak	3	2	M(9)	Proper training and regular inspection. Regular testing of the equipment. Correct PPE reduces consequence.	3	2	M(9)	*
5	Equipment inherent risk; Potentially All steps	High Pressure – Equipment Failure Causing Explosive Decompression	4	1	M (10)	Proper training and inspection. Regular testing. Safety in design. Correct PPE.	4	1	M (10)	*
6	Equipment inherent risk; Steps 3, 6, 7	High Pressure – Uncontrolled Rapid Expansion.	2	3	M(8)	Proper training. Correct PPE can reduce consequence..	2	1	L(3)	*
7	Equipment inherent risk; Steps 1-9 and 13	High Heat – Light Burns.	2	2	L(5)	Equipment has built in safety. Proper training. Correct PPE.	2	1	L(3)	*

Continued on the next page...

STEP 2.		**STEP 3.**	**STEP 4.**	**STEP 5.**	**STEP 6.**	**STEP 7.**	**STEP 8.**			**STEP 12.**
Ref No.	**SPECIFIC TASK / ACTIVITY STEPS**	**IDENTIFY POTENTIAL HAZARDS**	**RISK RANKING**			**RISK CONTROL MEASURES** • *Hierarchy of Control – Elimination, Substitution, Isolation, Engineering, Administration, Personal Protection.* • *Additional information can be attached.*	**RESIDUAL RISK**			**Actioner / Initials**
			Consequence	**Likelihood**	**Risk Rating**		**Consequence**	**Likelihood**	**Residual Risk**	
8	Equipment inherent risk; Steps 1-10	Low Temperatures – Frost burns	2	2	L(5)	Proper training. Correct PPE.	2	1	L(3)	*
9	Equipment inherent risk; General	High Voltage – Three phase power	3	2	M(9)	Equipment has built in safety. Protective shielding. Correct PPE.	3	1	M(6)	*
10	Equipment inherent risk; General	Heights – 2 Story setup	3	2	M(9)	Proper training – maintain 3-point contact. Correct PPE.	3	1	M(6)	*
11	Equipment inherent risk; General	High noise levels	2	3	M(8)	Proper training. Correct PPE.	3	1	M(6)	*
				STEP 9.		**Highest Remaining Residual Risk**			**M (10)**	

*Actioners : Training in equipment and PPE use must be implemented by Prof Schwarz, as well as enforcing inspection, maintenance and testing.
Operators must implement safe operations, perform regular testing and conform to lab safety and PPE requirements. Operators must familiarize themselves with relevant MSDS sheets and safety procedures, as well as the SWP.

Appendix C: Safety and Certification Forms

The Material Safety Data Sheet or MSDS forms for all the substances used in this study are gathered in this section. This exercise was performed before handling any of the chemicals to ensure proper training before encountering any of the fluids. MSDS sheets are available freely online and it is of utmost importance to consult and communicate available data to ensure safe handling,

The following MSDS's are compiled from various free sources to assemble sheets that are as complete as possible. These sources include:

http://cepsa.ca/, https://fscimage.fishersci.com/, https://www.cdhfinechemical.com/, https://www.spectrumchemical.com/, https://www.labchem.com/

The order of appearance is as follows:

C.1 MSDS for CO_2 260
C.2 MSDS for Benzene 262
C.3 MSDS for n-Dodecane 264
C.4 MSDS for Ethyl Tetradecanoate 266
C.5 MSDS for PDMS 100 cSt / PDMS 200 cSt 268
C.6 MSDS for Methanol 270
C.7 MSDS for Xylene 272
C.8 MSDS for Isopropanol 274

C.1 MSDS for CO_2

Material Safety Data Sheet

Section 1 - Product information

Product Identifier:	CO_2	**Manufacturer/Supplier:**	Merck Chemicals
Synonyms:	Carbon dioxide	**Identified uses:**	Laboratory chemicals
Chemical Formula:	CO_2		Chemical Intermediates

Section 2 Ingredients/Identity information

Component	**CAS No**	**Percentage**	**Hazardous**
Carbon Dioxide	124-38-9	99.9%	No

Section 3 Physical/Chemical Characteristics

Physical State:	Gas/Liquid	**Molar Weight:**	44.011 g/mole
Odour:	Odourless	**Specific Gravity:**	1.977 x 10^{-3}
Taste:	Not available	**Sublimation Temp:**	-79°C
Colour:	Colourless	**Vapour Pressure:**	n/a
pH:	n/a		
Solubility in Water:	Soluble		

Section 4 Fire and Explosion Hazard Data

Flammability of the Product:	n/a
Auto-Ignition Temperature:	n/a
Flash point:	n/a
Flammable Limits:	n/a
Extinguishing Media:	n/a
Explosion Hazards	Passing carbon dioxide over a mixture of sodium peroxide and aluminium or magnesium may explode.

Section 5 Reactivity Data

Stability:	Product is stable.
Instability Temperature	Not Available
Conditions of Instability:	Incompatible materials.
Substance incompatibility:	Certain reactive metals, hydrides, moist caesium monoxide
Corrosivity:	Non Corrosive
Special remarks	None

Continues on next page...

(MSDS C.1 CO_2, continues)

Section 6 Health Hazard Data
Potential Acute Health Effects:
Carbon dioxide is the most powerful cerebral vasodilator known. Inhaling large concentrations causes rapid circulatory insufficiency leading to coma and death.
Potential Chronic Health Effects:
CARCINOGENIC EFFECTS: Not known or anticipated. MUTAGENIC EFFECTS: Not known or anticipated. TERATOGENIC EFFECTS: Exposure of female rats to 60,000 ppm carbon dioxide for 24 hours has produced toxic effects to the embryo and fetus in pregnant rats. Toxic effects to the reproductive system have been observed in other mammalian species at similar concentrations. Repeated or prolonged exposure is not known to aggravate medical condition.
Toxicological Information:
LC50 Rat Inhalation - 470 000 ppm with an 30 min exposure time

Section 7 First Aid Measures
Eye Contact:
Check for and remove any contact lenses. In case of contact, immediately flush eyes with plenty of water for at least 15 minutes. Cold water may be used. Get medical attention if irritation occurs.
Skin Contact:
Wash with soap and water. Cover the affected skin with an emollient. Get medical attention if irritation develops. Cold water may be used.
Frostbite
Try to warm up the frozen tissues and seek medical attention.
Inhalation:
If inhaled, remove to fresh air. If not breathing, give artificial respiration. If breathing is difficult, give oxygen. Get medical attention.
Ingestion:
n/a

Section 8 Precautions for Safe Handling and Use
Handling:
Wash thoroughly after handling. Do not puncture or incinerate container. Use equipment rated for cylinder pressure. Close valve after each use and when empty. Protect cylinders from physical damage; do not drag, roll, slide, or drop. Avoid contact with eyes, skin, and clothing. Prevent entrapment of liquid in closed systems or piping without pressure relief devices. Keep container tightly closed. Avoid inhalation. Use with adequate ventilation.
Storage
Cylinders should be stored upright, with valve protection cap in place, and firmly secured to prevent falling or being knocked over. Cylinder temperatures should not exceed 52 °C.

Section 9 Accidental Release Measures
Immediately contact emergency personnel. Keep unnecessary personnel away. Use suitable protective equipment. Shut off gas supply if this can be done safely. Isolate area until gas has dispersed.

C.2 MSDS for Benzene

Material Safety Data Sheet

Section 1 - Product information

Product Identifier:	Benzene	**Manufacturer/Supplier:**	Sigma Aldrich
Synonyms:	Benzol	**Identified uses:**	Laboratory solvent
	Cyclohexa-1,3,5-triene		Chemical Intermediates
	1,3,5-Cyclohexatriene		Manufacture of Substances
Chemical Formula:	C_6H_6		

Section 2 Ingredients/Identity information

Component	**CAS No**	**Percentage**	**Hazardous**
Benzene	71-43-2	>99.9%	Yes

Section 3 Physical/Chemical Characteristics

Physical State:	Liquid	**Molar Weight:**	78.114 g/mole
Odour:	Aromatic, gasoline-like	**Specific Gravity:**	0.8765
Taste:	Not available	**Melting range:**	5.53°C
Colour:	Clear	**Boiling point:**	80.1°C
pH:	n/a	**Vapour Pressure:**	12.7 kPa at 25 °C
Solubility in Water:	1.84 g/L at 30 °C		

Section 4 Fire and Explosion Hazard Data

Flammability of the Product:	Highly flammable liquid and vapour.
Auto-Ignition Temperature:	497.78 °C
Flash point:	Closed Cup: -11.0°C
Explosive Limits:	1.2–7.8%
Extinguishing Media:	Use water spray, alcohol-resistant foam, dry chemical or carbon dioxide.
Explosion Hazards	Flash back possible over considerable distance., Container explosion may occur under fire conditions.

Section 5 Reactivity Data

Stability:	Product is stable.
Instability Temperature	Not Available
Conditions of Instability:	Incompatible materials, high heat, flames or sparks.
Substance incompatibility:	Acids, Bases, Halogens, Strong oxidizing agents, Metallic salts.
Corrosivity:	Non Corrosive
Special remarks	Handre with extreme care

Continues on next page...

(MSDS C.2 Benzene, continues)

Section 6 Health Hazard Data

Potential Acute Health Effects:

Benzene is considered very toxic; probable human oral lethal dose would be 50-500 mg/kg. Human inhalation of approximately 20,000 ppm (2% in air) was fatal in 5-10 minutes.

Potential Chronic Health Effects:

CARCINOGENIC EFFECTS: May cause cancer. Positive evidence from human epidemiological studies. A1 - Confirmed Human Carcinogen. MUTAGENIC EFFECTS: May cause genetic defects. DNA Inhibition: Human, Leukocyte = 2200 umol/L.; DNA Inhibition: Human, HeLa cell = 2200 umol/L.; TERATOGENIC EFFECTS: Inhalation, rat: TCLO = 50 ppm/24H (female 7-14 day(s) after conception) Effects on Embryo or Fetus - extra-embryonic structures (e.g., placenta, umbilical cord) and Effects on Embryo or Fetus - fetotoxicity (except death, e.g., stunted fetus).; Inhalation,mouse: TCLo = 5 ppm (female 6-15 day(s) after conception) Effects on Embryo or Fetus - cytological changes (including somatic cell genetic material) and Specific Developmental Abnormalities - blood and lymphatic systems (including spleen and marrow).

Toxicological Information:

LD50 Oral - Rat - male - > 2.000 mg/kg; LC50 Inhalation - Rat - female - 4 h - 43,7 mg/l; LD50 Dermal - Rabbit - male and female - > 8.260 mg/kg;

Section 7 First Aid Measures

Eye Contact:

Check for and remove any contact lenses. In case of contact, immediately flush eyes with plenty of water for at least 15 minutes. Cold water may be used. Get medical attention.

Skin Contact:

Wash with soap and water. CGet medical attention. Cold water may be used.

Inhalation:

If inhaled, remove to fresh air. If not breathing, give artificial respiration. If breathing is difficult, give oxygen. Get medical attention.

Ingestion:

Do NOT induce vomiting unless directed to do so by medical personnel. Never give anything by mouth to an unconscious person. Rinse mouth with water. Call a physician immediately. Loosen tight clothing such as a collar, tie, belt or waistband.

Section 8 Precautions for Safe Handling and Use

Handling:

Avoid exposure - obtain special instructions before use.Avoid contact with skin and eyes. Avoid inhalation of vapour or mist. Keep away from sources of ignition - No smoking.Take measures to prevent the build up of electrostatic charge.

Storage

Store in cool place. Keep container tightly closed in a dry and well-ventilated place. Containers which are opened must be carefully resealed and kept upright to prevent leakage. Store away from heat and sources of ignition.

Section 9 Accidental Release Measures

Use personal protective equipment. Avoid breathing vapours, mist or gas. Ensure adequate ventilation. Remove all sources of ignition. Evacuate personnel to safe areas. Beware of vapours accumulating to form explosive concentrations. Vapours can accumulate in low areas.Prevent further leakage or spillage if safe to do so. Do not let product enter drains. Discharge into the environment must be avoided.

C.3 MSDS for n-Dodecane

Material Safety Data Sheet

Section 1 - Product information

Product Identifier:	n Dodecane	**Manufacturer/Supplier:**	Sigma Aldrich
Synonyms:	Bihexyl	**Identified uses:**	Laboratory chemicals
	Dihexyl		
	Adakane 12		
	Duodecane		
Chemical Formula:	$CH_3(CH_2)_{10}CH_3$		

Section 2 Ingredients/Identity information

Component	**CAS No**	**Percentage**	**Hazardous**
n Dodecane	112-40-3	>99%	Yes

Section 3 Physical/Chemical Characteristics

Physical State:	Liquid	**Molar Weight:**	170.34 g/mole
Odour:	Gasoline-like to odorless	**Specific Gravity:**	0.7495
Taste:	Not available	**Melting range:**	-10.0 to -9.3°C
Colour:	Clear	**Boiling point:**	214 to 218 °C
pH:	n/a	**Vapour Pressure:**	18 Pa at 25 °C
Solubility in Water:	Insoluble in water.		

Section 4 Fire and Explosion Hazard Data

Flammability of the Product:	Combustible at high temperature or in presence of sparks or open flames
Auto-Ignition Temperature:	Not available
Flash point:	Closed Cup: 71°C
Flammable Limits:	Lower explosion limit: 0,6 % (v)
Extinguishing Media:	SMALL FIRE: Use DRY chemical powder.
	LARGE FIRE: Use water spray, fog or foam.
Explosion Hazards	Not available

Section 5 Reactivity Data

Stability:	Product is stable.
Instability Temperature	Not Available
Conditions of Instability:	Incompatible materials (strong oxidisers), high heat.
Substance incompatibility:	Reactive with oxidising agents, acids, alkalis
Corrosivity:	Non Corrosive
Special remarks	Hydrophilic, Hygroscopic

Continues on next page...

(MSDS C.3 n-Dodecane, continues)

Section 6 Health Hazard Data

Potential Acute Health Effects:

Slightly hazardous in case of skin contact (irritant, permeator), eye contact (irritant), ingestion or inhalation.

Potential Chronic Health Effects:

CARCINOGENIC EFFECTS: Not known or anticipated. MUTAGENIC EFFECTS: Not known or anticipated. TERATOGENIC EFFECTS: Not available. Repeated or prolonged exposure is not known to aggravate any medical condition.

Toxicological Information:

LD50 Oral - Rat - male and female - > 5.000 mg/kg; LC50 Inhalation - Rat - male and female - 4 h - > 4.951 mg/m3; LD50 Dermal - Rabbit - male and female - > 5.000 mg/kg

Section 7 First Aid Measures

Eye Contact:

Check for and remove any contact lenses. In case of contact, immediately flush eyes with plenty of water for at least 15 minutes. Cold water may be used. Get medical attention if irritation occurs.

Skin Contact:

Wash with soap and water. Cover the affected skin with an emollient. Get medical attention if irritation develops. Cold water may be used.

Inhalation:

If inhaled, remove to fresh air. If not breathing, give artificial respiration. If breathing is difficult, give oxygen. Get medical attention.

Ingestion:

Do NOT induce vomiting unless directed to do so by medical personnel. Never give anything by mouth to an unconscious person. Rinse mouth with water. If large quantities of this material are swallowed, call a physician immediately. Loosen tight clothing such as a collar, tie, belt or waistband.

Section 8 Precautions for Safe Handling and Use

Handling:

Wash thoroughly after handling. Remove contaminated clothing and wash before reuse. Avoid contact with eyes, skin, and clothing. Keep container tightly closed. Avoid ingestion and inhalation. Use with adequate ventilation.

Storage

Keep in a tightly closed container, stored in a cool, dry, ventilated area. Protect against physical damage. Containers which are opened must be carefully resealed and kept upright to prevent leakage. Handle and store under inert gas. Observe all warnings and precautions listed for the product.

Section 9 Accidental Release Measures

Personal Precautions

Use personal protective equipment. Avoid breathing vapours, mist or gas. Ensure adequate ventilation. Remove all sources of ignition. Evacuate personnel to safe areas. Beware of vapours accumulating to form explosive concentrations. Vapours can accumulate in low areas. Prevent further leakage or spillage if safe to do so. Do not let product enter drains.

Spill cleanup

Contain spillage, and then collect with an electrically protected vacuum cleaner or by wetbrushing and place in container for disposal according to local regulations. Keep in suitable, closed containers for disposal.

C.4 MSDS for Ethyl Tetradecanoate

Material Safety Data Sheet

Section 1 - Product information

Product Identifier:	Ethyl Tetradecanoate	**Manufacturer/Supplier:**	Sigma Aldrich
Synonyms:	Ethyl myristate	**Identified uses:**	Laboratory chemicals
			Manufacture of substances
Chemical Formula:	$C_{16}H_{32}O_2$		

Section 2 Ingredients/Identity information

Component	CAS No	Percentage	Hazardous
Ethyl myristate	124-06-1	>99.0%	No

Section 3 Physical/Chemical Characteristics

Physical State:	Liquid	**Molar Weight:**	256.42 g/mole
Odour:	Slight	**Specific Gravity:**	0.861
Taste:	Not available	**Melting range:**	11 to 12°C
Colour:	Clear	**Boiling point:**	178 to 180 °C
pH:	n/a	**Vapour Pressure:**	Not available
Solubility in Water:	Insoluble in water.		

Section 4 Fire and Explosion Hazard Data

Flammability of the Product:	Combustible at high temperature or in presence of sparks or open flames
Auto-Ignition Temperature:	315°C
Flash point:	Closed Cup: 113°C
Flammable Limits:	Lower explosion limit: 0,6 % (v)
Extinguishing Media:	Use water spray, alcohol-resistant foam, dry chemical or carbon dioxide.
Explosion Hazards	Not available

Section 5 Reactivity Data

Stability:	Product is stable.
Instability Temperature	Not Available
Conditions of Instability:	Incompatible materials (strong oxidisers), high heat.
Substance incompatibility:	Reactive with oxidising agents, acids, alkalis
Corrosivity:	Non Corrosive
Special remarks	

Continues on next page...

(MSDS C.4 Ethyl Tetradecanoate, continues)

Section 6 Health Hazard Data
Potential Acute Health Effects:
Slightly hazardous in case of skin contact (irritant, permeator), eye contact (irritant), ingestion or inhalation.
Potential Chronic Health Effects:
CARCINOGENIC EFFECTS: Not known or anticipated. MUTAGENIC EFFECTS: Not known or anticipated. TERATOGENIC EFFECTS: Not available. Repeated or prolonged exposure is not known to aggravate any medical condition.
Toxicological Information:
No data available

Section 7 First Aid Measures
Eye Contact:
Check for and remove any contact lenses. In case of contact, immediately flush eyes with plenty of water for at least 15 minutes. Cold water may be used. Get medical attention if irritation occurs.
Skin Contact:
Wash with soap and water. Cover the affected skin with an emollient. Get medical attention if irritation develops. Cold water may be used.
Inhalation:
If inhaled, remove to fresh air. If not breathing, give artificial respiration. If breathing is difficult, give oxygen. Get medical attention.
Ingestion:
Do NOT induce vomiting unless directed to do so by medical personnel. Never give anything by mouth to an unconscious person. Rinse mouth with water. If large quantities of this material are swallowed, call a physician immediately. Loosen tight clothing such as a collar, tie, belt or waistband.

Section 8 Precautions for Safe Handling and Use
Handling:
Wash thoroughly after handling. Remove contaminated clothing and wash before reuse. Avoid contact with eyes, skin, and clothing. Keep container tightly closed. Avoid ingestion and inhalation. Use with adequate ventilation.
Storage
Keep in a tightly closed container, stored in a cool, dry, ventilated area. Protect against physical damage. Containers which are opened must be carefully resealed and kept upright to prevent leakage. Handle and store under inert gas. Observe all warnings and precautions listed for the product.

Section 9 Accidental Release Measures
Personal Precautions
Use personal protective equipment. Avoid breathing vapours, mist or gas. Ensure adequate ventilation. Remove all sources of ignition. Evacuate personnel to safe areas. Beware of vapours accumulating to form explosive concentrations. Vapours can accumulate in low areas. Prevent further leakage or spillage if safe to do so. Do not let product enter drains.
Spill cleanup
Contain spillage, and then collect with an electrically protected vacuum cleaner or by wetbrushing and place in container for disposal according to local regulations. Keep in suitable, closed containers for disposal.

C.5 MSDS for PDMS 100 cSt / PDMS 200 cSt

Material Safety Data Sheet

Section 1 - Product information

Product Identifier:	Poly(dimethylsiloxane)	**Manufacturer/Supplier:**	Sigma Aldrich
Synonyms:	Dimethylpolysiloxane	**Identified uses:**	Laboratory chemicals
	Dimethicone		Manufacture of substances
	PDMS		
Chemical Formula:	$(CH_3)_3SiO[SiO(CH_3)_2]_nSi(CH_3)_3$		

Section 2 Ingredients/Identity information

Component	**CAS No**	**Percentage**	**Hazardous**
Poly(dimethylsiloxane)	9016-00-6	Absolute	No

Section 3 Physical/Chemical Characteristics

Physical State:	Liquid	**Molar Weight:**	Variable
Odour:	Odourless	**Specific Gravity:**	0.964 / 0.967
Taste:	Not available	**Melting range:**	-28°C / -287°C
Colour:	Clear	**Boiling point:**	Not available
pH:	n/a	**Vapour Pressure:**	7 hPa at 20 °C
Solubility in Water:	Not available		

Section 4 Fire and Explosion Hazard Data

Flammability of the Product:	Combustible at high temperature or in presence of sparks or open flames
Auto-Ignition Temperature:	No data available
Flash point:	Open Cup: 326°C
Flammable Limits:	No data available
Extinguishing Media:	Use water spray, alcohol-resistant foam, dry chemical or carbon dioxide.
Explosion Hazards	Not available

Section 5 Reactivity Data

Stability:	Product is stable.
Instability Temperature	Not Available
Conditions of Instability:	Incompatible materials (strong oxidisers), high heat.
Substance incompatibility:	Reactive with oxidising agents, acids, alkalis
Corrosivity:	Non Corrosive
Special remarks	Hygroscopic

Continues on next page...

(MSDS C.5 PDMS 100 cSt / PDMS 200 cSt, continues)

Section 6 Health Hazard Data

Potential Acute Health Effects:

Slightly hazardous in case of skin contact (irritant, permeator), eye contact (irritant), ingestion or inhalation.

Potential Chronic Health Effects:

CARCINOGENIC EFFECTS: Not known or anticipated. MUTAGENIC EFFECTS: Not known or anticipated. TERATOGENIC EFFECTS: Not available. Repeated or prolonged exposure is not known to aggravate any medical condition.

Toxicological Information:

No data available

Section 7 First Aid Measures

Eye Contact:

Check for and remove any contact lenses. In case of contact, immediately flush eyes with plenty of water for at least 15 minutes. Cold water may be used. Get medical attention if irritation occurs.

Skin Contact:

Wash with soap and water. Cover the affected skin with an emollient. Get medical attention if irritation develops. Cold water may be used.

Inhalation:

If inhaled, remove to fresh air. If not breathing, give artificial respiration. If breathing is difficult, give oxygen. Get medical attention.

Ingestion:

Do NOT induce vomiting unless directed to do so by medical personnel. Never give anything by mouth to an unconscious person. Rinse mouth with water. If large quantities of this material are swallowed, call a physician immediately. Loosen tight clothing such as a collar, tie, belt or waistband.

Section 8 Precautions for Safe Handling and Use

Handling:

Wash thoroughly after handling. Remove contaminated clothing and wash before reuse. Avoid contact with eyes, skin, and clothing. Keep container tightly closed. Avoid ingestion and inhalation. Use with adequate ventilation.

Storage

Keep in a tightly closed container, stored in a cool, dry, ventilated area. Protect against physical damage. Containers which are opened must be carefully resealed and kept upright to prevent leakage. Observe all warnings and precautions listed for the product.

Section 9 Accidental Release Measures

Personal Precautions

Use personal protective equipment. Avoid breathing vapours, mist or gas. Ensure adequate ventilation. Remove all sources of ignition. Prevent further leakage or spillage if safe to do so.

Spill cleanup

Contain spillage, and then collect with an electrically protected vacuum cleaner or by wetbrushing and place in container for disposal according to local regulations. Keep in suitable, closed containers for disposal.

C.6 MSDS for Methanol

Mat+A1:D37erial Safety Data Sheet

Section 1 - Product information

Product Identifier:	Methanol	**Manufacturer/Supplier:**	Sigma Aldrich
Synonyms:	Carbinol; Columbian spirits; Hydroxymethane; Methyl alcohol; Methyl hydrate; Methyl hydroxide; Methylic alcohol; Methylol; Pyroligneous spirit; Wood alcohol; Wood naphtha; Wood spirit; MeOH	**Identified uses:**	Laboratory solvent Chemical Intermediates Manufacture of Substances
Chemical Formula:	CH_3OH		

Section 2 Ingredients/Identity information

Component	**CAS No**	**Percentage**	**Hazardous**
Methanol	67-56-1	>95%	Yes

Section 3 Physical/Chemical Characteristics

Physical State:	Liquid	**Molar Weight:**	32.04 g/mole
Odour:	Pungent	**Specific Gravity:**	0.792
Taste:	Not available	**Melting range:**	-97.6°C
Colour:	Clear	**Boiling point:**	64.7°C
pH:	n/a	**Vapour Pressure:**	13.2 kPa at 20 °C
Solubility in Water:	completely miscible		

Section 4 Fire and Explosion Hazard Data

Flammability of the Product:	Highly flammable liquid and vapour.
Auto-Ignition Temperature:	455.0 °C
Flash point:	Closed Cup: 9.7°C
Explosive Limits:	6 - 36 %(V)
Extinguishing Media:	Use water spray, alcohol-resistant foam, dry chemical or carbon dioxide.
Explosion Hazards	Explosion limits: 6 - 36 %(V)

Section 5 Reactivity Data

Stability:	Product is stable.
Instability Temperature	Not Available
Conditions of Instability:	Incompatible materials, high heat, flames or sparks.
Substance incompatibility:	Acid chloridess, Acid anhydrides, Oxidizing agents, Alkali metals, Reducing agents, Acids, Bases
Corrosivity:	Non Corrosive
Special remarks	Handre with extreme care

Continues on next page...

(MSDS C.6 Methanol, continues)

Section 6 Health Hazard Data

Potential Acute Health Effects:

Methanol is considered toxic; Dizziness, Drowsiness, metabolic acidosis, Blurred vision, Seizures, Coma, Blindness, Death. LDLO Oral - Human - 143 mg/kg Remarks: Lungs, Thorax, or Respiration:Dyspnea. Ingestion may cause gastrointestinal irritation, nausea, vomiting and diarrhoea.

Potential Chronic Health Effects:

Causes damage to organs.
CARCINOGENIC EFFECTS: None known. MUTAGENIC EFFECTS: None known. TERATOGENIC EFFECTS: Damage to fetus not classifiable

Toxicological Information:

LD_{50} Oral - Rat - 1.187 - 2.769 mg/kg; LC_{50} Inhalation - Rat - 4 h - 128,2 mg/l; LC_{50} Inhalation - Rat - 6 h - 87,6 mg/l ; LD_{50} Dermal - Rabbit - 17.100 mg/kg

Section 7 First Aid Measures

Eye Contact:

Check for and remove any contact lenses. In case of contact, immediately flush eyes with plenty of water for at least 15 minutes. Cold water may be used. Get medical attention.

Skin Contact:

Wash with soap and water. Get medical attention immediately. Cold water may be used.

Inhalation:

If inhaled, remove to fresh air. If not breathing, give artificial respiration. If breathing is difficult, give oxygen. Get medical attention.

Ingestion:

Do NOT induce vomiting unless directed to do so by medical personnel. Never give anything by mouth to an unconscious person. Rinse mouth with water. Call a physician immediately. Loosen tight clothing such as a collar, tie, belt or waistband.

Section 8 Precautions for Safe Handling and Use

Handling:

Avoid exposure - obtain special instructions before use.Avoid contact with skin and eyes. Avoid inhalation of vapour or mist. Keep away from sources of ignition - No smoking.Take measures to prevent the build up of electrostatic charge.

Storage

Store in cool place. Keep container tightly closed in a dry and well-ventilated place. Containers which are opened must be carefully resealed and kept upright to prevent leakage. Store away from heat and sources of ignition.

Section 9 Accidental Release Measures

Use personal protective equipment. Avoid breathing vapours, mist or gas. Ensure adequate ventilation. Remove all sources of ignition. Evacuate personnel to safe areas. Beware of vapours accumulating to form explosive concentrations. Vapours can accumulate in low areas.Prevent further leakage or spillage if safe to do so. Do not let product enter drains. Discharge into the environment must be avoided.Contain spillage, and then collect with non-combustible absorbent material, (e.g. sand, earth, diatomaceous earth, vermiculite) and place in container for disposal according to local / national regulations.

C.7 MSDS for Xylene

Material Safety Data Sheet

Section 1 - Product information

Product Identifier:	Xylene	**Manufacturer/Supplier:**	Sigma Aldrich
Synonyms:	Xylol	**Identified uses:**	Laboratory solvent
	Dimethylbenzene		Chemical Intermediates
Chemical Formula:	C_8H_{10}		Manufacture of substances

Section 2 Ingredients/Identity information

Component	CAS No	Percentage	Hazardous
Xylene	1330-20-7	>95%	Yes

Section 3 Physical/Chemical Characteristics

Physical State:	Liquid	**Molar Weight:**	106.168 g/mole
Odour:	Odourless	**Specific Gravity:**	0.861
Taste:	Not available	**Melting range:**	13.2°C
Colour:	Clear	**Boiling point:**	138.35°C
pH:	n/a	**Vapour Pressure:**	24 hPa at 37.7 °C
Solubility in Water:	Insoluble		

Section 4 Fire and Explosion Hazard Data

Flammability of the Product:	Flammable liquid and vapour.
Auto-Ignition Temperature:	528 °C
Flash point:	Closed Cup: 27°C
Explosive Limits:	1.1 - 7 %(V)
Extinguishing Media:	Use water spray, alcohol-resistant foam, dry chemical or carbon dioxide.
Explosion Hazards	Explosion limits: 1.1 - 7 %(V)

Section 5 Reactivity Data

Stability:	Product is stable.
Instability Temperature	Not Available
Conditions of Instability:	Incompatible materials, high heat, flames or sparks.
Substance incompatibility:	Strong Oxidizing agents, Acids, Bases.
Corrosivity:	Non Corrosive
Special remarks	Handle with extreme care

Continues on next page...

(MSDS C.7 Xylene, continues)

Section 6 Health Hazard Data

Potential Acute Health Effects:

May be fatal if swallowed and enters airways. Harmful in contact with skin or if inhaled. Causes skin irritation. Causes serious eye irritation. May cause respiratory irritation. May cause damage to organs (Central nervous system, Liver, Kidney) through prolonged or repeated exposure if inhaled.

Potential Chronic Health Effects:

Causes damage to organs.
CARCINOGENIC EFFECTS: Group 3: Not classifiable as to its carcinogenicity to humans. MUTAGENIC EFFECTS: None known. TERATOGENIC EFFECTS: Damage to fetus not classifiable

Toxicological Information:

LD50 Oral - Rat - 3.523 mg/kg; LC50 Inhalation - Rat - 4 h - 5000 ppm; LD50 Dermal - Rabbit - 12.126 mg/kg;

Section 7 First Aid Measures

Eye Contact:

Check for and remove any contact lenses. In case of contact, immediately flush eyes with plenty of water for at least 15 minutes. Cold water may be used. Get medical attention.

Skin Contact:

Wash with soap and water. Get medical attention immediately. Cold water may be used.

Inhalation:

If inhaled, remove to fresh air. If not breathing, give artificial respiration. If breathing is difficult, give oxygen. Get medical attention.

Ingestion:

Do NOT induce vomiting unless directed to do so by medical personnel. Never give anything by mouth to an unconscious person. Rinse mouth with water. Call a physician immediately. Loosen tight clothing such as a collar, tie, belt or waistband.

Section 8 Precautions for Safe Handling and Use

Handling:

Avoid exposure - obtain special instructions before use.Avoid contact with skin and eyes. Avoid inhalation of vapour or mist. Keep away from sources of ignition - No smoking. Take measures to prevent the build up of electrostatic charge.

Storage

Store in cool place. Keep container tightly closed in a dry and well-ventilated place. Containers which are opened must be carefully resealed and kept upright to prevent leakage. Store away from heat and sources of ignition.

Section 9 Accidental Release Measures

Use personal protective equipment. Avoid breathing vapours, mist or gas. Ensure adequate ventilation. Remove all sources of ignition. Evacuate personnel to safe areas. Beware of vapours accumulating to form explosive concentrations. Vapours can accumulate in low areas.Prevent further leakage or spillage if safe to do so. Do not let product enter drains. Discharge into the environment must be avoided.Contain spillage, and then collect with non-combustible absorbent material, (e.g. sand, earth, diatomaceous earth, vermiculite) and place in container for disposal according to local / national regulations.

C.8 MSDS for Isopropanol

Material Safety Data Sheet

Section 1 - Product information

Product Identifier:	Isopropanol	**Manufacturer/Supplier:**	Sigma Aldrich
Synonyms:	Isopropyl alcohol; 2-Propanol; Propan-2-ol; Rubbing alcohol; sec-Propyl alcohol; s-Propanol; IPA	**Identified uses:**	Laboratory solvent Manufacture of substances
Chemical Formula:	C_3H_8O		

Section 2 Ingredients/Identity information

Component	**CAS No**	**Percentage**	**Hazardous**
Isopropanol	67-63-0	>95%	Yes

Section 3 Physical/Chemical Characteristics

Physical State:	Liquid	**Molar Weight:**	60.096 g/mole
Odour:	Alcohol-like	**Specific Gravity:**	0.786
Taste:	Not available	**Melting range:**	-89°C
Colour:	Clear	**Boiling point:**	82.6°C
pH:	n/a	**Vapour Pressure:**	43.2 hPa at 20 °C
Solubility in Water:	Completely soluable		

Section 4 Fire and Explosion Hazard Data

Flammability of the Product:	Highly flammable liquid and vapour.
Auto-Ignition Temperature:	425 °C
Flash point:	Closed Cup: 12.0°C
Explosive Limits:	2 - 12.7 %(V)
Extinguishing Media:	Use water spray, alcohol-resistant foam, dry chemical or carbon dioxide.
Explosion Hazards	Explosion limits: 2 - 12.7 %(V)

Section 5 Reactivity Data

Stability:	Product is stable.
Instability Temperature	Not Available
Conditions of Instability:	Incompatible materials, high heat, flames or sparks. Direct sunlight
Substance incompatibility:	Strong Oxidizing agents, Acid anhydrates, Aluminium, Halogenated compounds, Acids, Bases.
Corrosivity:	Non Corrosive
Special remarks	Handle with extreme care

Continues on next page...

(MSDS C.8 Isopropanol, continues)

Section 6 Health Hazard Data

Potential Acute Health Effects:

Causes serious eye irritation. May cause drowsiness or dizziness.

Potential Chronic Health Effects:

CARCINOGENIC EFFECTS: Group 3: Not classifiable as to its carcinogenicity to humans. MUTAGENIC EFFECTS: None known. TERATOGENIC EFFECTS: Damage to fetus not classifiable. Central nervous system depression, prolonged or repeated exposure can cause:, Nausea, Headache, Vomiting, narcosis, Drowsiness, Overexposure may cause mild, reversible liver effects., Aspiration may lead to:, Lung oedema, Pneumonia

Toxicological Information:

LD50 Oral - Rat - 5.045 mg/kg; Remarks: Behavioral:Altered sleep time (including change in righting reflex). Behavioral:Somnolence (general depressed activity). LC50 Inhalation - Rat - 8 h - 16000 ppm; LD50 Dermal - Rabbit - 12.800 mg/kg

Section 7 First Aid Measures

Eye Contact:

Check for and remove any contact lenses. In case of contact, immediately flush eyes with plenty of water for at least 15 minutes. Cold water may be used. Get medical attention.

Skin Contact:

Wash with soap and water. Get medical attention immediately. Cold water may be used.

Inhalation:

If inhaled, remove to fresh air. If not breathing, give artificial respiration. If breathing is difficult, give oxygen. Get medical attention.

Ingestion:

Do NOT induce vomiting unless directed to do so by medical personnel. Never give anything by mouth to an unconscious person. Rinse mouth with water. Call a physician immediately. Loosen tight clothing such as a collar, tie, belt or waistband.

Section 8 Precautions for Safe Handling and Use

Handling:

Avoid exposure - obtain special instructions before use.Avoid contact with skin and eyes. Avoid inhalation of vapour or mist. Keep away from sources of ignition - No smoking. Take measures to prevent the build up of electrostatic charge.

Storage

Store in cool place. Keep container tightly closed in a dry and well-ventilated place. Containers which are opened must be carefully resealed and kept upright to prevent leakage. Store away from heat and sources of ignition.

Section 9 Accidental Release Measures

Use personal protective equipment. Avoid breathing vapours, mist or gas. Ensure adequate ventilation. Remove all sources of ignition. Evacuate personnel to safe areas. Beware of vapours accumulating to form explosive concentrations. Vapours can accumulate in low areas.Prevent further leakage or spillage if safe to do so. Do not let product enter drains. Discharge into the environment must be avoided. Contain spillage, and then collect with an electrically protected vacuum cleaner or by wet-brushing and place in container for disposal according to local regulations.

Appendix D: High-Pressure Viscosity Measurement View Cell Design

A part of the PhD went into designing, commissioning and verifying the fluid property measurement of the high pressure, saturated fluids. This chapter encompasses all the details around the equipment, design considerations, drawings, calibrations and certifications.

D.1 Background

D.2 Equipment Description

D.3 Operating Principles

D.4 Safety Considerations

D.5 Technical Data

D.1 Background

The cell was designed and built to meet the need of measuring fluid properties (density and viscosity) at the point of phase equilibrium for a binary system under supercritical conditions. The design was done in-house, based on existing high-pressure cells in the department and calculated using ASME Sec VIII, Div 2 for a cylindrical pressure vessel for Stainless Steel 316. The design was validated and certified by RITC inspection in 2016 (See section D.5.4).

The cell is colloquially dubbed as “Amethystos”, a character from Greek mythology, as a nod toward the quartz resonator used for viscosity measurements. In Greek mythology, Dionysus, the god of intoxication, was pursuing a maiden named Amethystos, who refused his affections. Amethystos prayed to the gods to remain chaste, which the goddess Artemis granted and transformed her into a pure white stone. Humbled by Amethystos's desire to remain chaste, Dionysus poured wine over the stone as an offering, dyeing the crystals purple.

D.2 Equipment Description

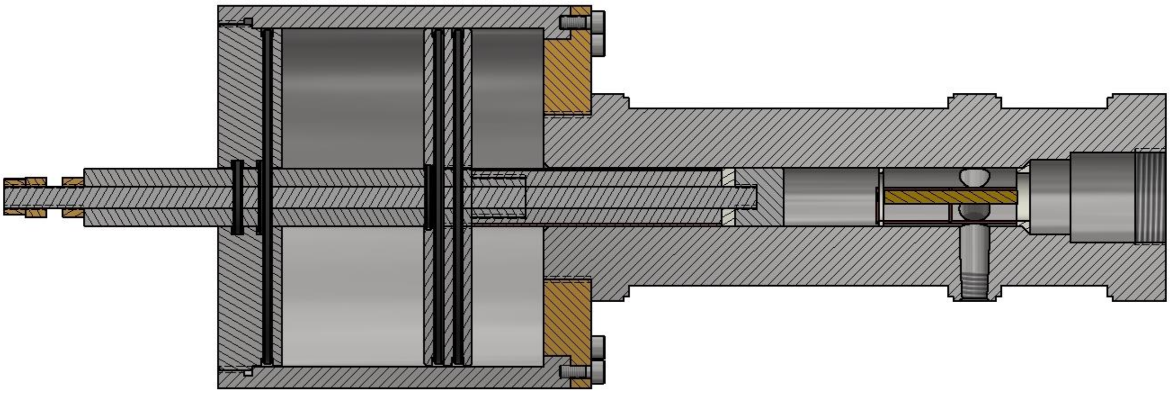

Figure D- 1: High-pressure view cell sketch

The cell is made up of a high-pressure chamber, low-pressure chamber and an atmospheric chamber. A basic concept sketch is seen in Figure D- 1, showing a cross-section of the assembled cell, with the high-pressure chamber on the right, atmospheric in the middle, and low pressure on the left. A moving piston connects the low- and high-pressure chambers. The low-pressure section and pistons can be unscrewed and removed to allow loading, cleaning and service of the cell.

Pressure is introduced at a controlled rate into the low-pressure section using a nitrogen cylinder and regulator. This method allows the piston assembly to act as a pressure intensifier with an area ratio between the two piston heads of about 32,62 : 1. Pressure is monitored using a melt pressure transducer by ONEhalf20, chosen for its small dead volume.

The temperature of the high-pressure chamber is controlled using a fluid-filled jacket, fed with water from a thermostatic bath. Temperature is monitored using two 4wire PT 100 pressure transducers from Wika.

Stirring is effected in the high-pressure chamber using a stirring bar and three electromagnets, driven by a custom driving circuit

A cylindrical quartz crystal is inserted into the high-pressure section, where its resonant frequency and resistance is determined. The determined values are used to calculate the viscosity and density of the fluid in contact with the crystal. The crystal is mounted in a removable, custom cage and is electrically connected to measurement equipment using a delicate spring-loaded assembly. The sealing of the electrical wires is achieved using a Conax fitting.

D.3 Operating Principles

D.3.1 General Operation

General operation is described in a set of instruction in Appendix B. The reader is directed thereto for the general cell loading and operating procedures.

D.3.2 Phase Equilibria Method

The cell determines equilibrium and solubility using a Synthetic, Visual method. For more details on the method, the reader is directed to the work of Schwarz and Nieuwoudt [*J. Supercrit. Fluids, 27* (2003) 133-144].

The experimental procedure is briefly summarized as follows: A quantified mass of the liquid component is loaded into the cell. The cell is then closed, the piston seal tightened, and all air is removed using a vacuum pump and multiple flushes with CO_2. A quantified mass of CO_2 is then transferred into the cell. The cell is then heated to the first experimental temperature, pressurised, and allowed time to reach thermal equilibrium (approx. 1 h). After sufficient time the cell is slowly, isothermally depressurised while continually monitoring for phase transitions using an HD camera setup. Once a transition is observed and recorded, the cell is repressurized, and the process is repeated until the phase transitions are repeatedly observed to within 0.02 MPa. After measurements are completed at a set temperature, the temperature is increased to a new value. After sufficient time has passed to ensure thermal equilibrium (approx. 1 h), the measurement method is repeated until all desired temperatures are measured.

In other words: a known binary mixture is loaded into the cell, and the temperature and pressure is controlled, with the volume allowed to vary. The cell is then visually inspected to observe any phase change. The visual measurement is supplemented by using the crystal resonance to determine phase change.

D.3.3 Viscosity Measurement Method

The phase equilibria method is similar to that used by Collings and McLaughlin [*Trans. Faraday Soc., 67* (1971) 340-352].

The method is discussed in detail in Section 3.2.3. The Equipment details are discussed in Section D.5.9.

D.4 Safety Considerations

D.4.1 High Pressure

High pressure is the leading risk in the High-Pressure Viscosity Measurement View Cell setup. It is imperative that the operator remembers that high pressure implies that a large amount of potential energy is stored in the system - enough energy to cause severe injury or harm. This risk has been reduced during design, but can also be reduced by safe operation.

D.4.1.1 Safety During Design

The cell is divided into two parts, a low pressure and a high-pressure zone.

The high-pressure side cell has been designed to withstand pressures well over the maximum operating pressure. The cell is to be used at a maximum pressure of 300 bar and a temperature of 100 °C. Using ASME Sec VIII Div 1 to calculate the vessel thickness for a cylindrical pressure vessel, ID 22mm, under the given maximum conditions, a minimum vessel thickness of 4.8 mm is calculated. A vessel thickness of 22.4 mm is selected using a +2x safety factor, meaning a maximum pressure > 700 bar can safely be contained at 100 °C. A thickness of 18 mm is selected for the piston head using similar principles. Stainless steel 316 was used in all load-bearing pressure components.

All connected pressure fittings are NPT thread with Teflon seals. Swagelok valves and fittings are used where applicable. The Swagelok® components used are rated at 500 bar.

The low-pressure side is calculated similarly, except for a maximum pressure of 10 bar, resulting in a 127.3 mm ID cylinder with 8.35 mm walls. This wall thickness translates into a pressure of >10 bar that could be safely contained. The low-pressure side is pressurised using a 40 bar nitrogen cylinder controlled with a regulator.

The low-pressure side is connected to the high-pressure side via a piston setup. The low-pressure side is used to pressurise the high-pressure side through a piston assembly with a ratio of 32.48:1. A pressure relief valve is installed on the low-pressure side to avoid overpressure and set to ±10.7 bar, which translates to the maximum operating pressure of 350 bar in the high-pressure side. A manual relief valve is also available to reduce the pressure if needed.

The maximum pressure the regulator can provide of 20 bar can safely be contained by the low-pressure side, with the resultant maximum pressure in the high-pressure side of 650 bar also containable.

In both the pressure zones, redundant safety has been applied concerning pressure. Not only has the system been designed and tested for pressures exceeding the working pressure, but the design and operating philosophies have been set up to ensure further safety.

D.4.1.2 Safety During Operation

It is crucial to ensure that the two pressure zones operate within their specifications. The pressure on the high-pressure side is monitored by an installed pressure sensor. The low-pressure side is monitored on a gauge on the pressure regulator. If overpressure occurs immediately remove pressure using the manual relief valve.

D.4.2 High Temperature

The cell can operate at a maximum of 100 °C, due to the low-temperature solder used in the crystal assembly. 100 °C is not an excessively high temperature but can be enough to cause burns

D.4.2.1 Safety During Design

The cell is heated using a water circulated from a heating bath through a welded jacket.

The water in the heating bath will boil at 100 °C, making this the effective maximum possible. The liquid level in the heating bath will drop below the heater's minimum level, causing the heater to shut down.

D.4.2.2 Safety During Operation

During standard operation, direct contact with hot areas are not required, but if it becomes necessary, the use of insulated gloves are recommended. All equipment around the cell and heating bath should be treated as if hot. Under no circumstances should hot water connections be unscrewed during operation, as this can cause the hot water to spray out. If a heating fluid leak occurs during operation, stop the process and allow the system to cool down before attempting to repair the leak.

D.4.3 Flammability and Explosion

The hazard of flammable or explosive solvents are not directly relevant to this project but has to be considered as a future possibility.

All of the major components in the cell are designed according to explosion-proof standards, and each piece of equipment is earthed to avoid static build-up and electrical sparks. The sensors on the cell can in future be explosion-proofed by adding safety barriers to the control box.

D.4.4 Viscosity Measurement Equipment

D.4.4.1 Safety During Design

The oscilloscope and frequency generator are unable of generating currents or voltages that can harm a human. Both units are self-contained and have built-in safety and overvoltage protection.

D.4.4.2 Safety During Operation

The piezoelectric component is to be operated between 0.5 V and 5 V AC. The current is minimised to avoid the piezoelectric element expending significant energy into the medium. Currents around 0.2 μC is expected.

D.5 Technical Data

This section contains the cell and equipment technical specifications and drawings. This includes any calculations, certificates and certifications.

D.5.1. Low-pressure and Atmospheric Chamber and Piston Assembly 285
D.5.2. High-Pressure Chamber 299
D.5.3. Design Calculations and Drawing review 306
D.5.4. RITC Certification 328
D.5.5. Quartz Crystal and Crystal Holder 329
D.5.6. Cell Stand Design Drawings 338
D.5.7. Temperature Control 346
D.5.8. Measurement and Calibration Data 347
D.5.9. HD Camera Setup 369
D.5.10. Magnetic Stirrer 370
D.5.11. Viscosity Measurement Equipment and Software 378

D.5.1 Low-Pressure and Atmospheric Chamber and Piston Assembly

Figure D- 2: Low-pressure chamber with the included piston assembly.

The low-pressure chamber and atmospheric chamber is, in essence, the same chamber, separated by the moving piston assembly. If the one chamber is at minimum volume, the other will be at maximum, and vice versa.

During operation, the low-pressure chamber is filled with nitrogen at a controlled rate and pressure to generate a higher pressure in the high-pressure section.

Specifications:

Capacity:	0 – 900 ml
Max Service Pressure:	~10.13 bar (designed for 40 bar)
Max Service Temperature	Atmospheric to +100 °C

Seals:

1 x Viton O-ring	[200-248; dimension of 120.24x3.53 mm] – Purchased at Allseal.
2 x Viton O-ring	[200-212; dimension of 21.80x3.53 mm] – Purchased at Allseal.
1 x Teflon seal	In house – see drawings.
2 x Viton O-ring	[200-248; dimension of 120.24x3.53 mm] – Purchased at Allseal.

Materials:

Stainless Steel 316; Phosphor Bronze

D.5.1.1 Design Drawings

This section contains the following Design Drawings:

D.5.1.1.1. Low-Pressure Chamber 287
D.5.1.1.2. Height Gauge Holder 288
D.5.1.1.3. Low-Pressure Side Cap 289
D.5.1.1.4. High-Pressure Chamber Side Cap 290
D.5.1.1.5. High-Pressure Piston Head 291
D.5.1.1.6. High-Pressure Piston Seal 292
D.5.1.1.7. High-Pressure Piston Rod 293
D.5.1.1.8. High-Pressure Side Sleeve 294
D.5.1.1.9. High-Pressure Side Bronze Sleeve 295
D.5.1.1.10. Low-Pressure Side Sleeve 296
D.5.1.1.11. Low-Pressure Piston Disk 297
D.5.1.1.12. Completed Assembly 298

D.5.1.1.1 Low-pressure Chamber

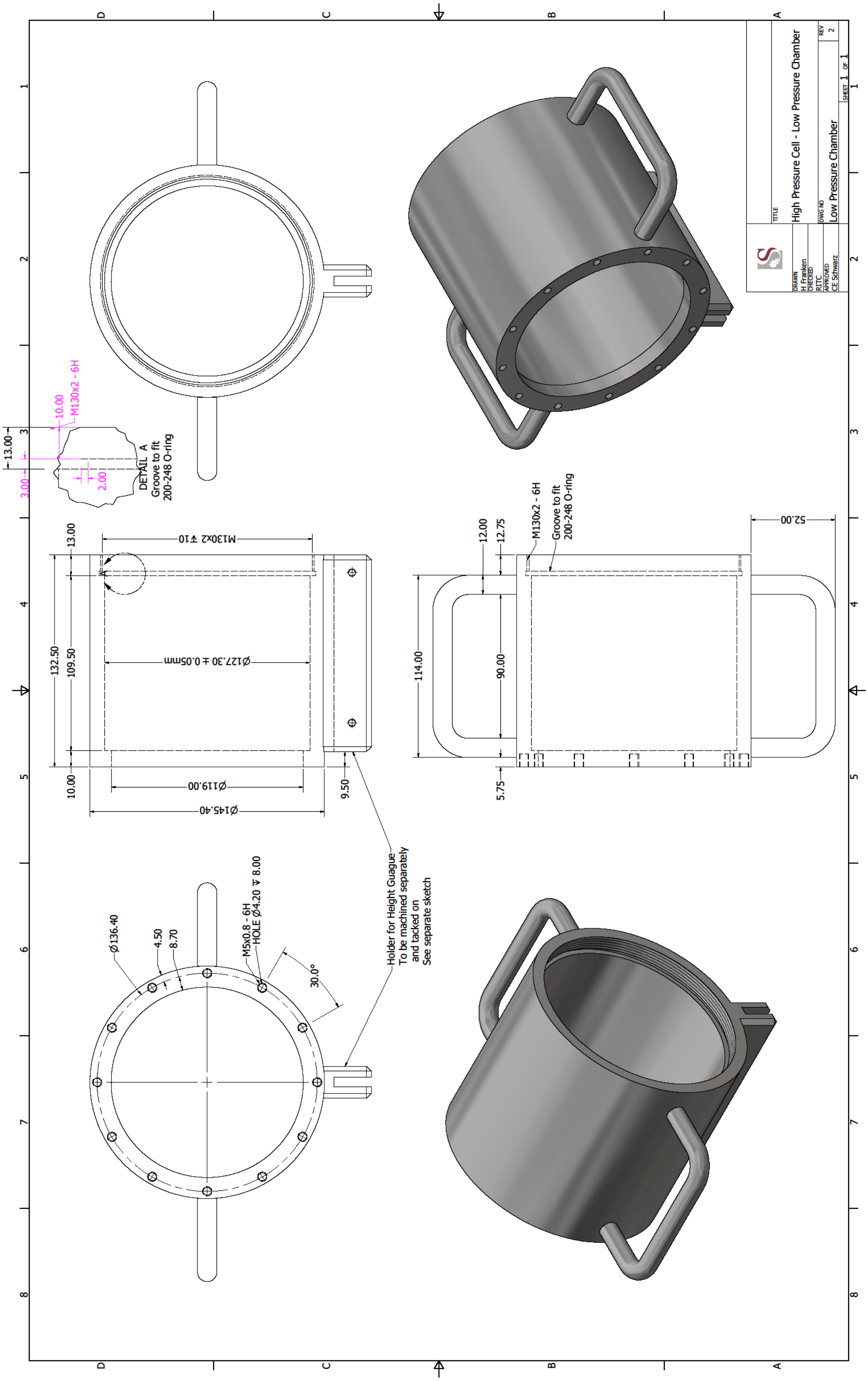

D.5.1.1.2 Height Gauge Holder

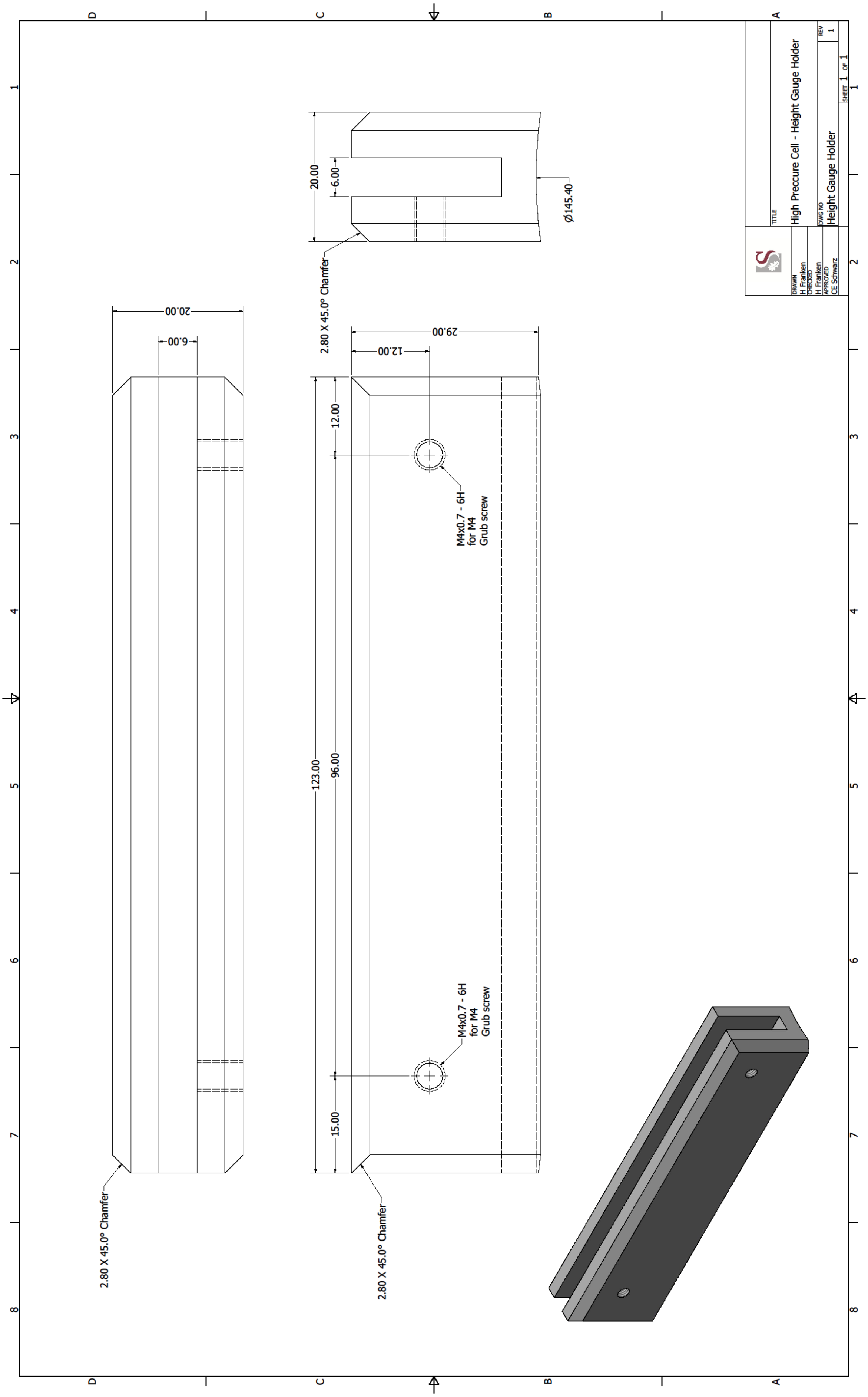

D.5.1.1.3 Low-Pressure Side Cap

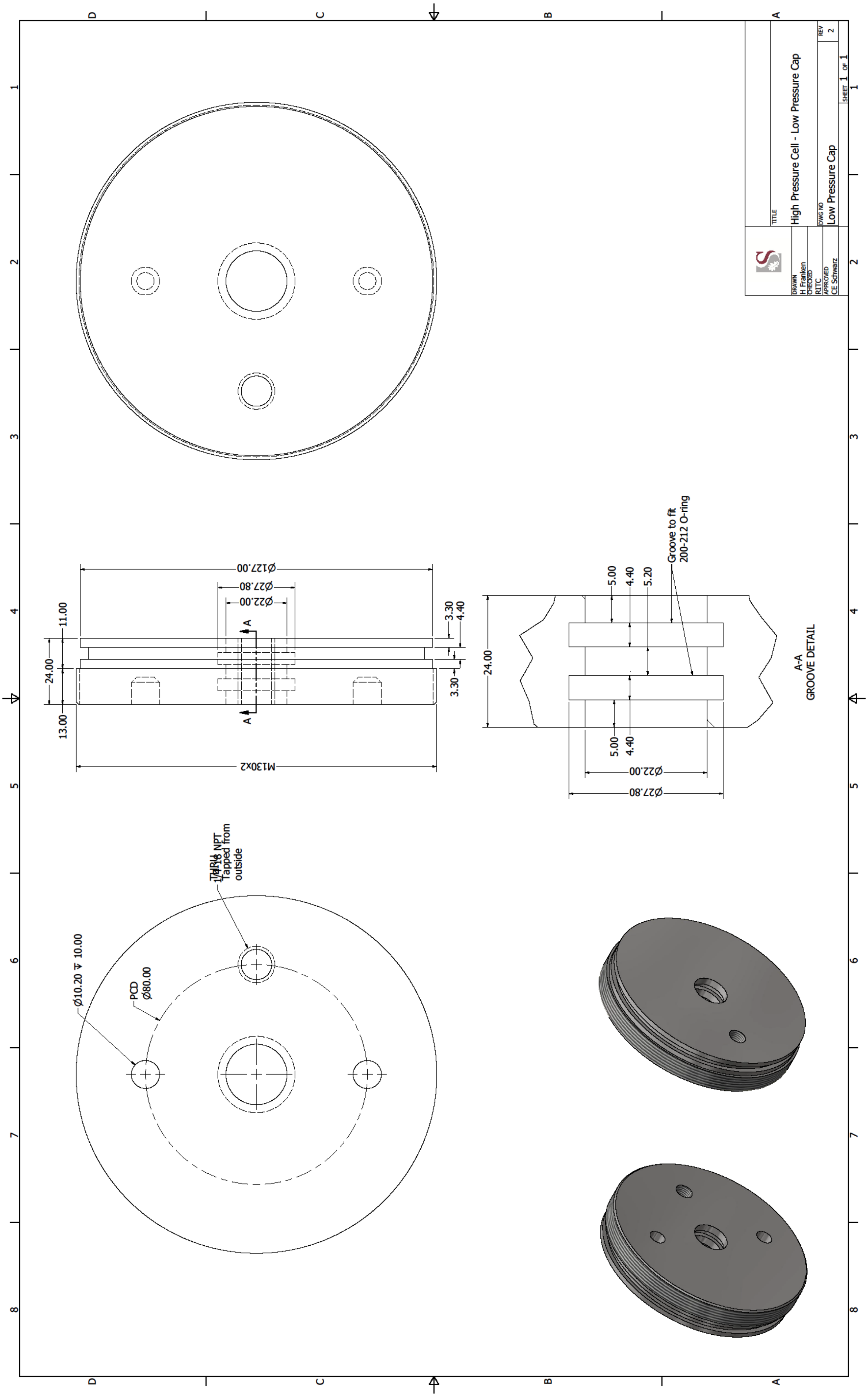

D.5.1.1.4 High-Pressure Chamber Side Cap

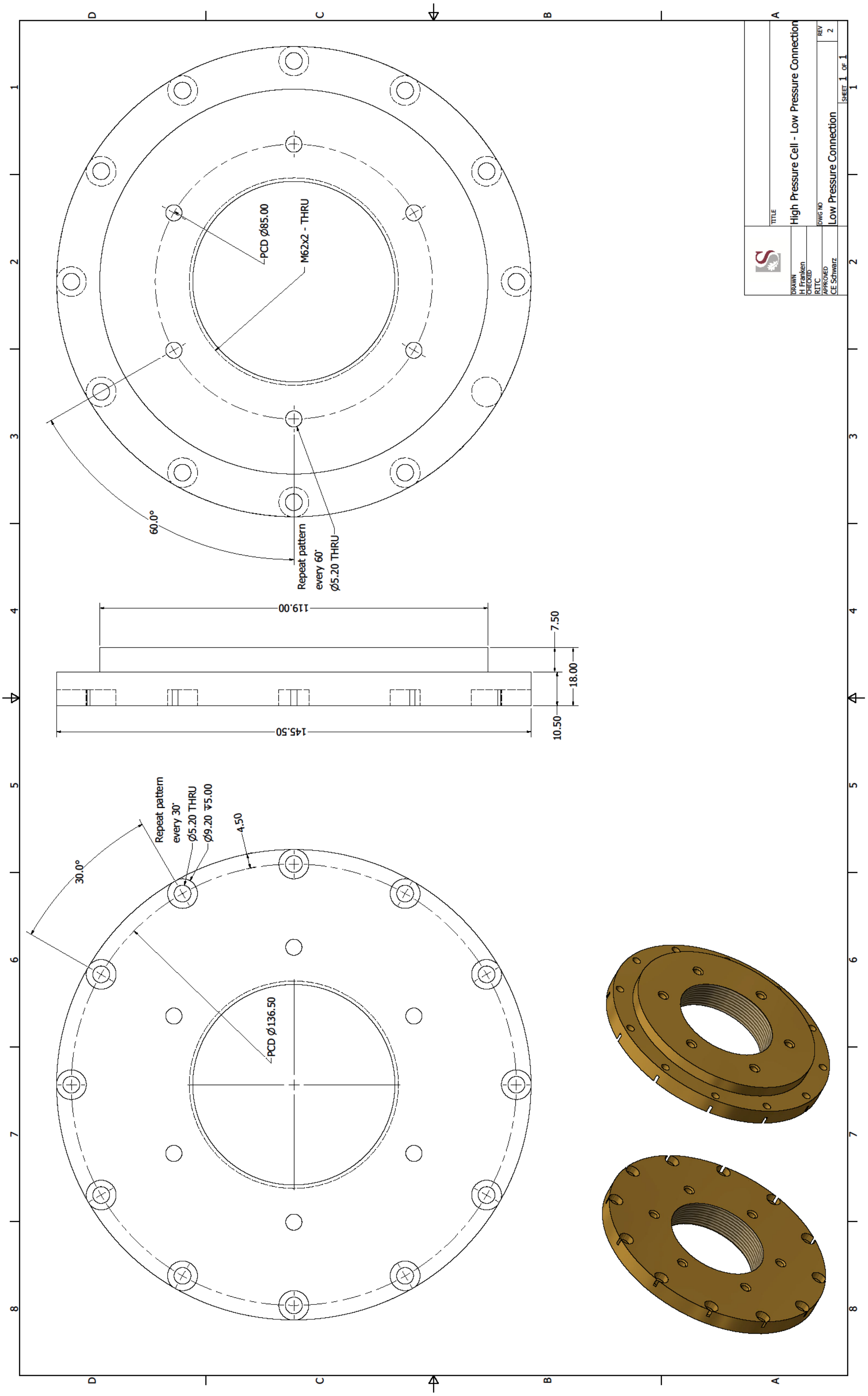

D.5.1.1.5 High-Pressure Piston Head

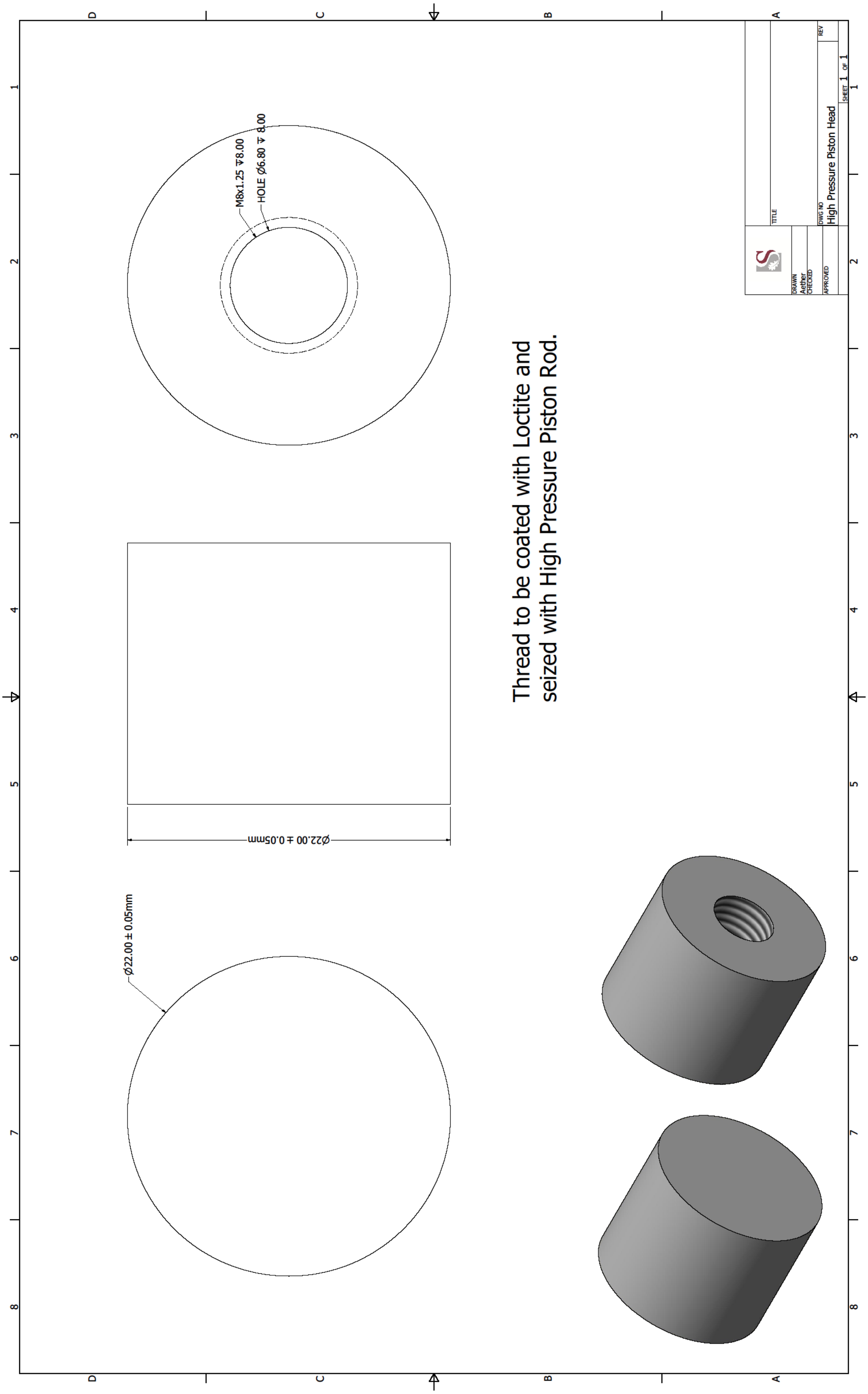

Thread to be coated with Loctite and seized with High Pressure Piston Rod.

D.5.1.1.6 High-Pressure Piston Seal

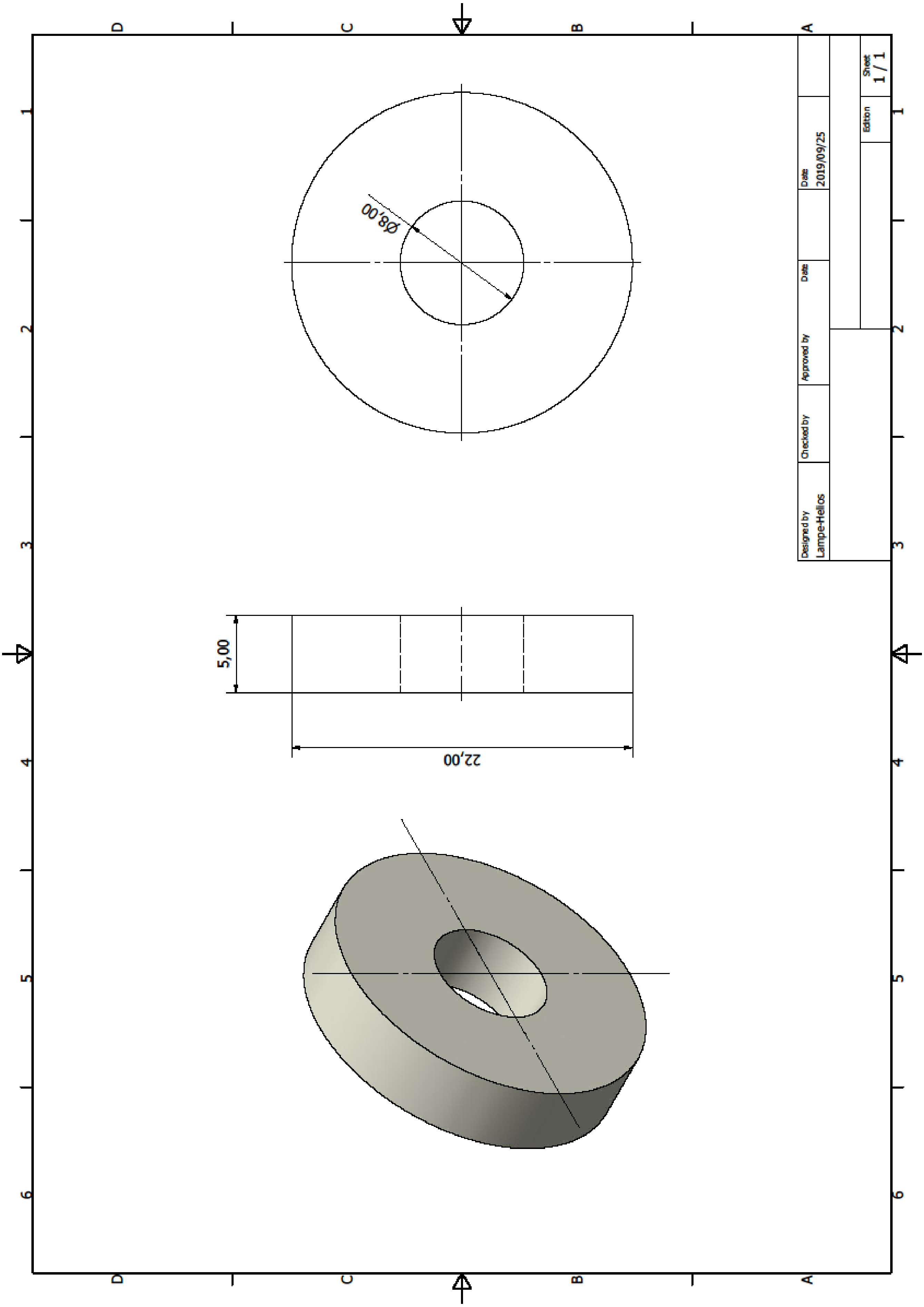

D.5.1.1.7 High-Pressure Piston Rod

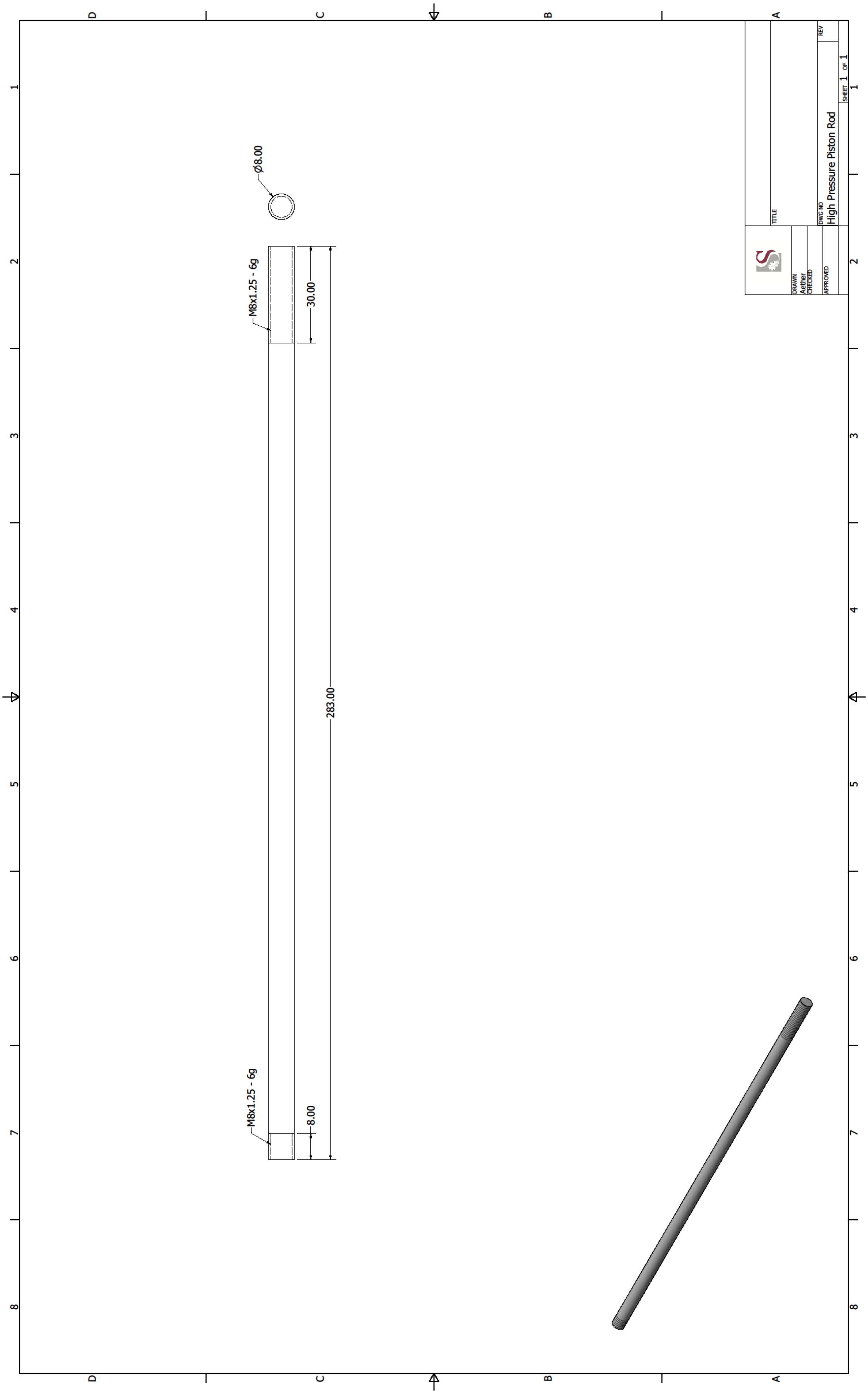

D.5.1.1.8 High-Pressure Side Sleeve

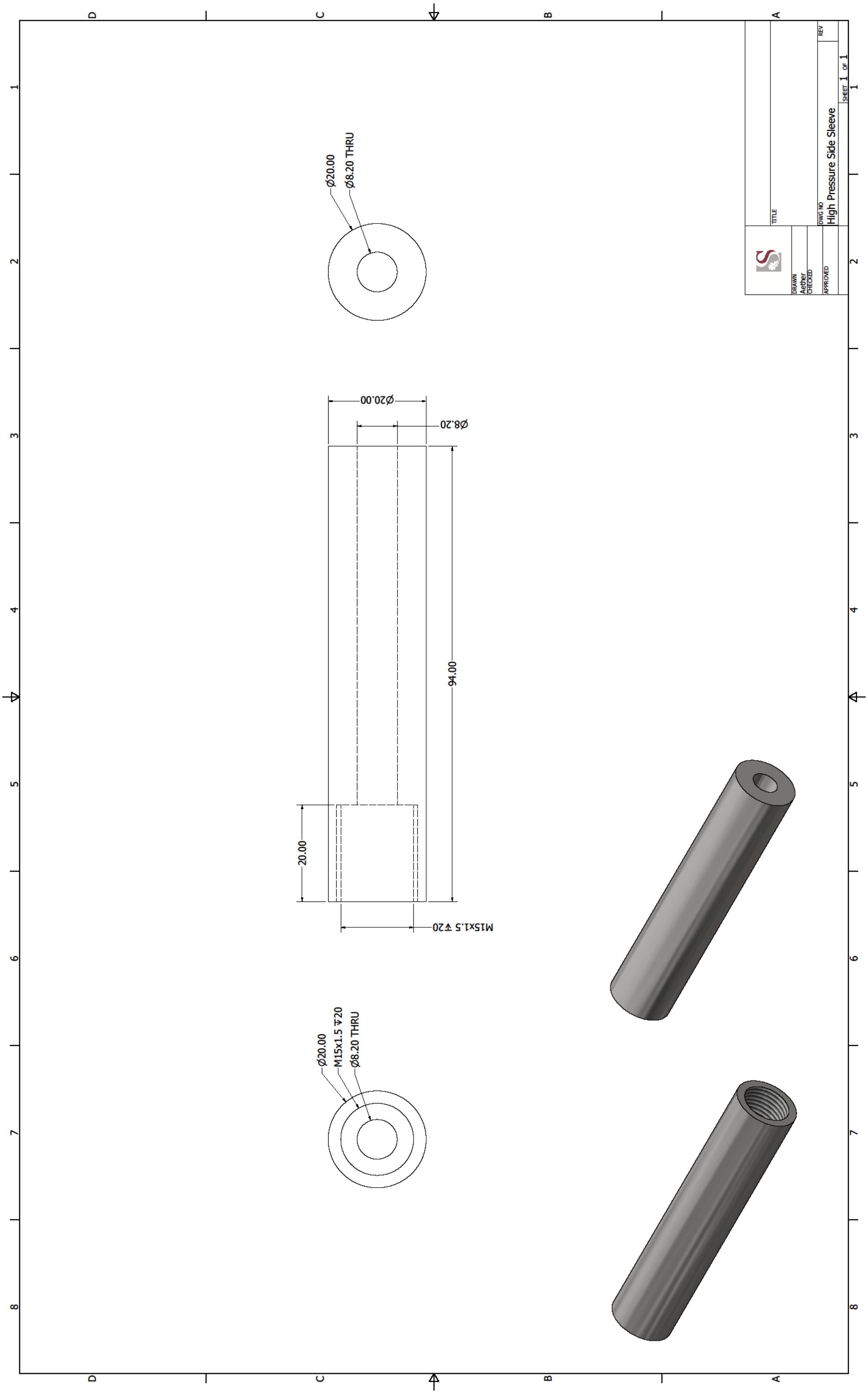

D.5.1.1.9 High-Pressure Side Bronze Sleeve

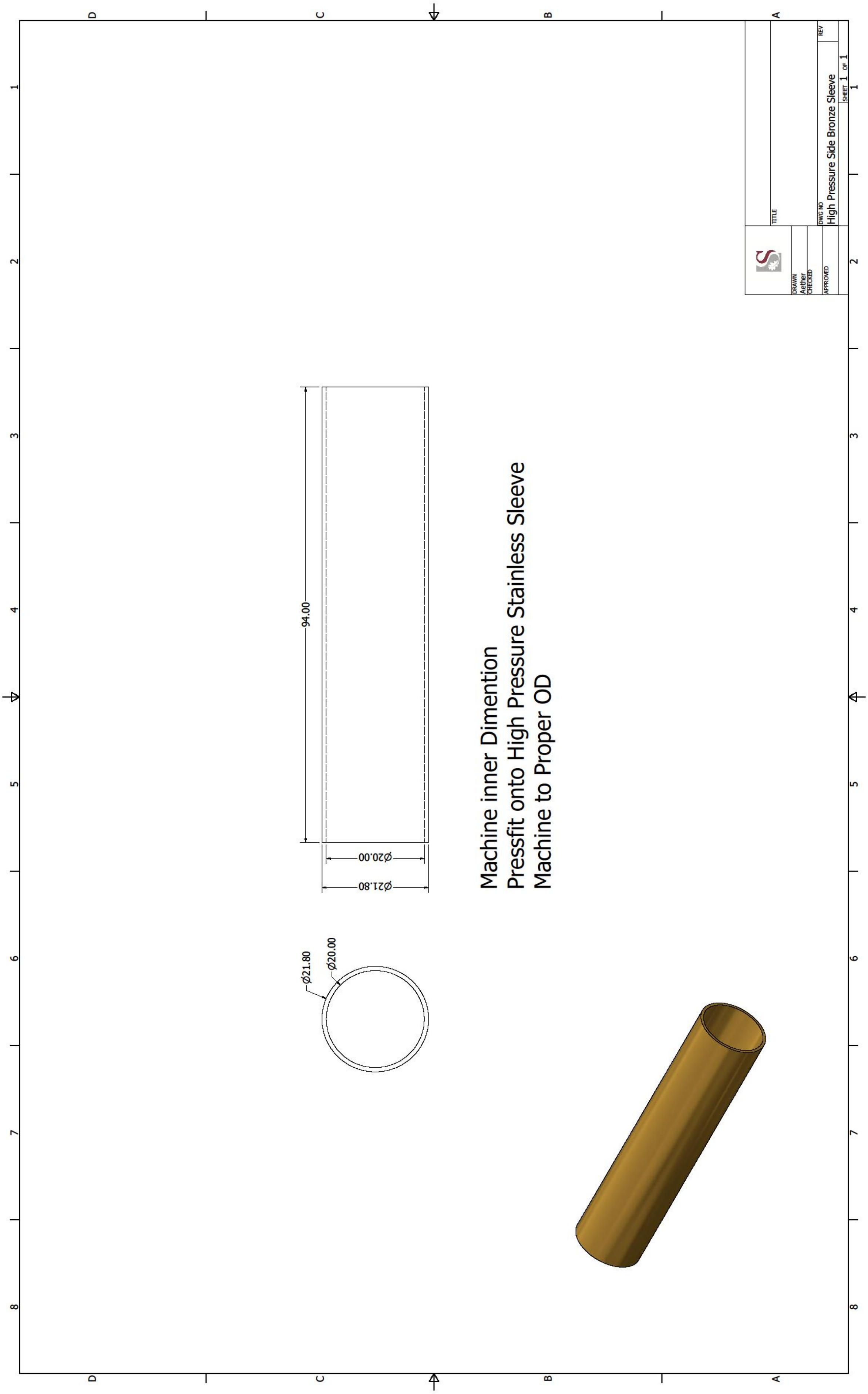

Machine inner Dimention
Pressfit onto High Pressure Stainless Sleeve
Machine to Proper OD

D.5.1.1.10 Low-Pressure Side Sleeve

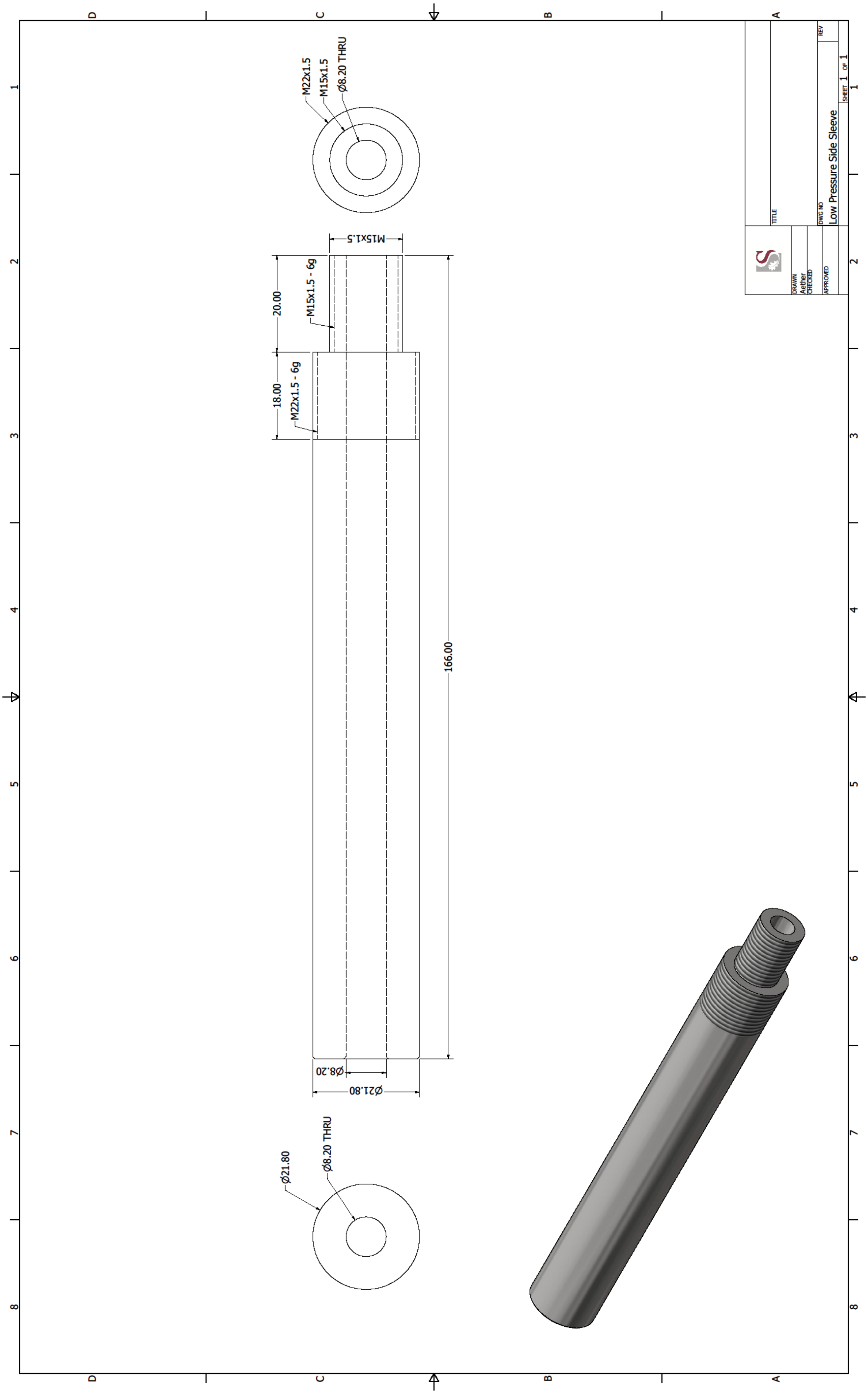

D.5.1.1.11 Low-Pressure Piston Disk

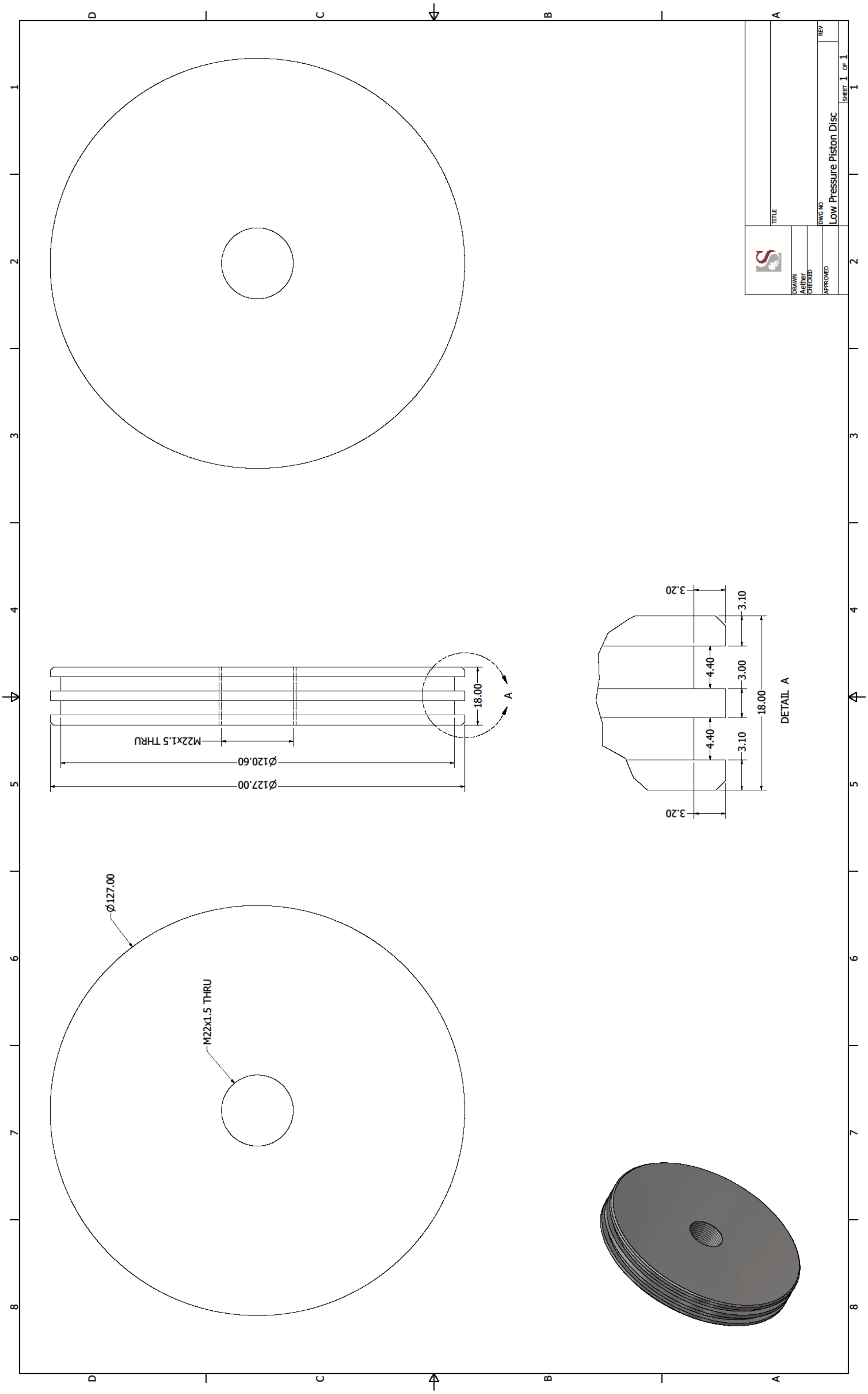

D.5.1.1.12 Completed Assembly

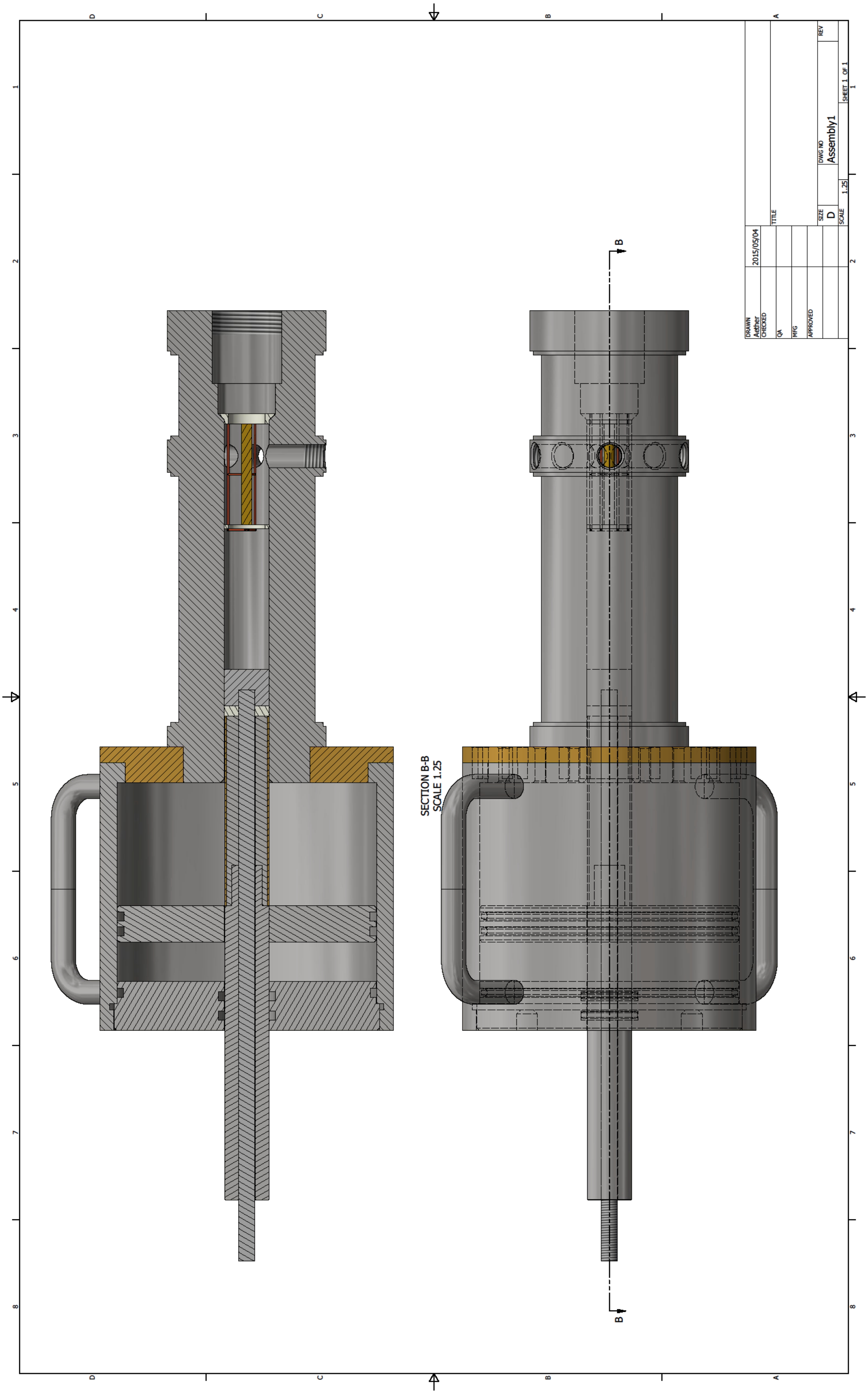

D.5.2 High-Pressure Chamber

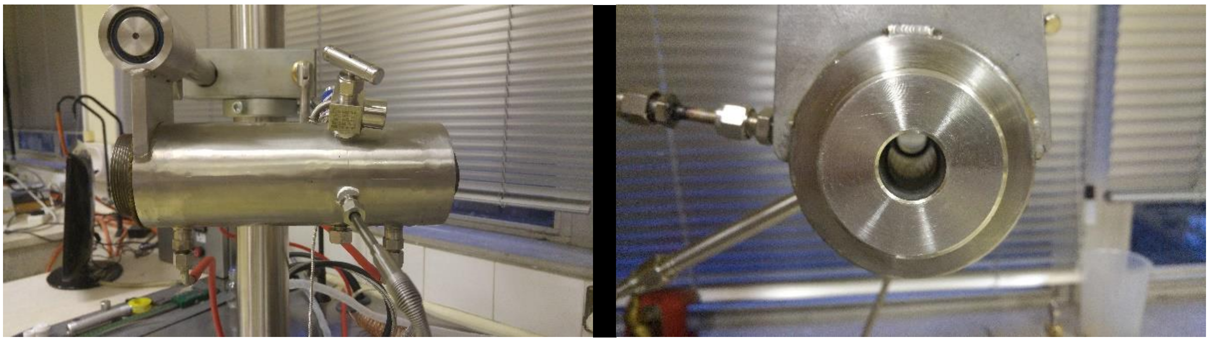

Figure D- 3: High-Pressure Chamber mounted on the cell stand.

The high-pressure chamber contains the experimental sample and viscosity measurement crystal. The section screws into the low pressure and atmospheric chamber, with the piston assembly high-pressure side going into the high-pressure chamber. Several fittings and equipment pieces screw into the chamber. Custom Teflon inserts were manufactured for the fittings where appropriate to minimise dead volume.

Specifications:

Capacity:	26 – 58 ml
Max Service Pressure:	350 bar (designed and certified for 500 bar)
Max Service Temperature	Atmospheric to +100 °C
High temperature jacketing	
Sight glass –	742.0106 Sieber Sitec.
Material:	Stainless Steel 316L (See Material Certificate in Section D.5.2.2)

D.5.2.1 Design Drawings

This section contains the following Design Drawings:

D.5.2.1.1. High-Pressure Chamber 301

D.5.2.1.2. High-Pressure Chamber – Hole Details 302

D.5.2.1.3. High-Pressure Chamber – Honing Details 303

D.5.2.1.4. Pressure Plug For Testing 304

D.5.2.1.1 High-Pressure Chamber

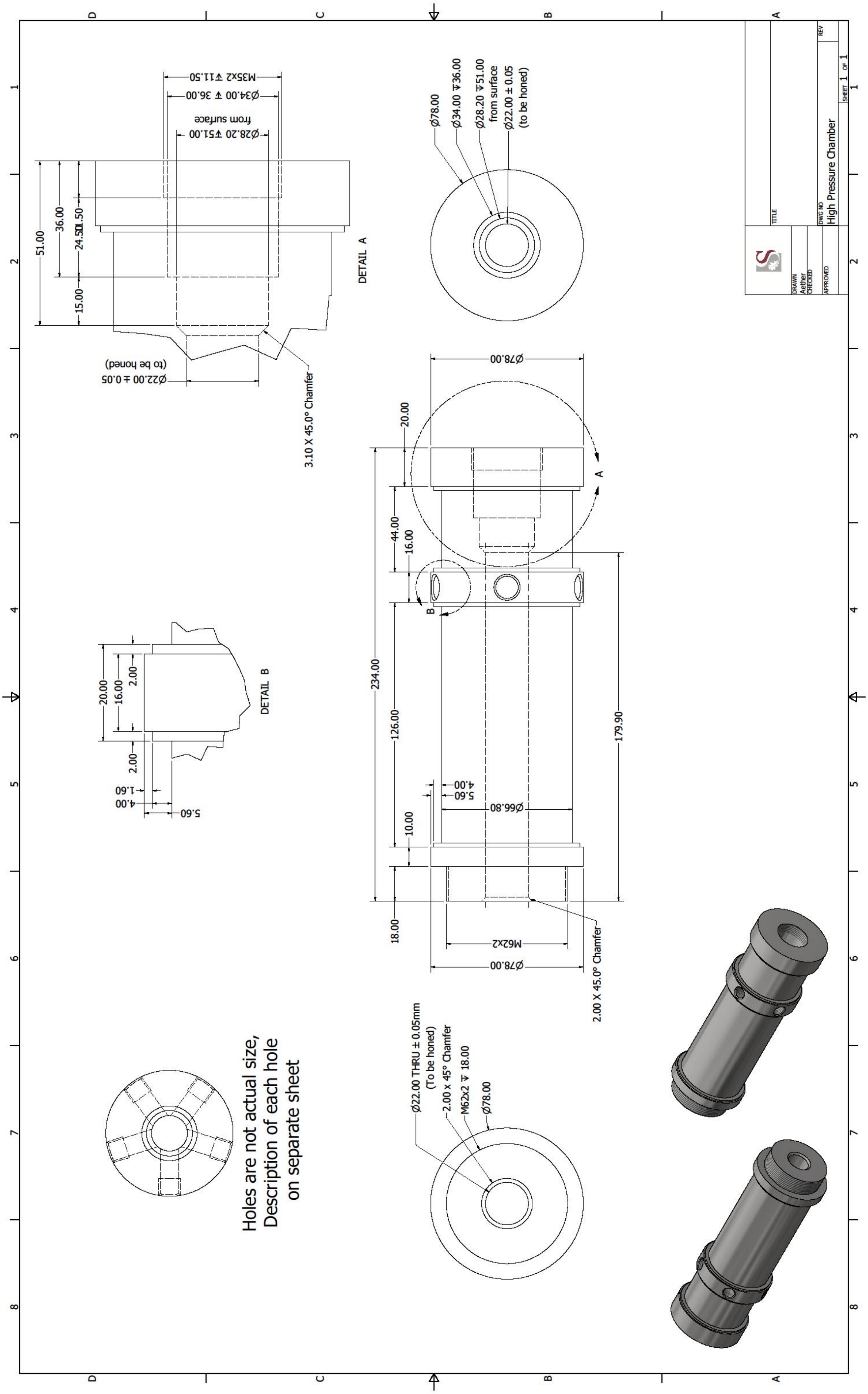

D.5.2.1.2 High-Pressure Chamber - Hole Details

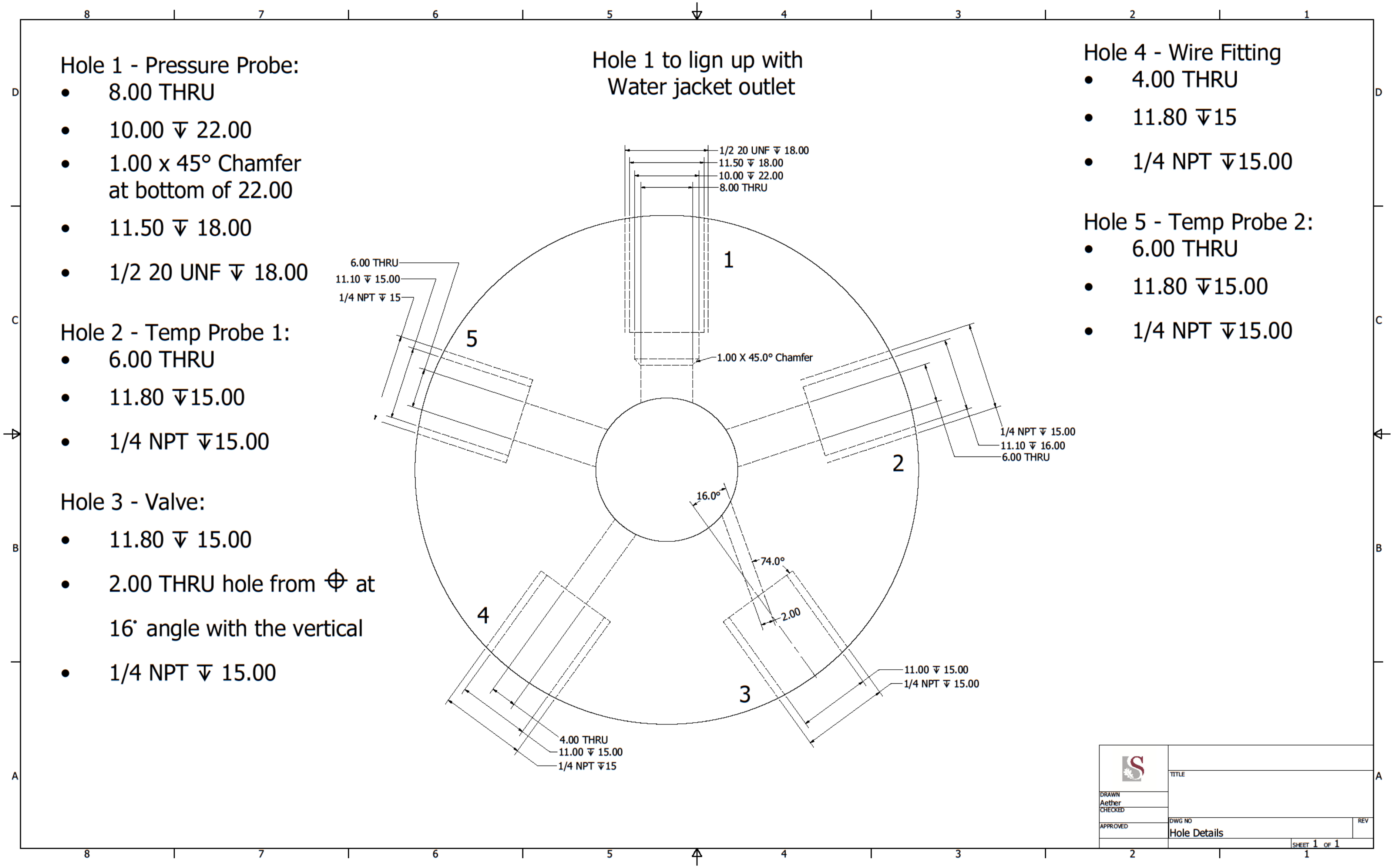

Hole 1 - Pressure Probe:
- 8.00 THRU
- 10.00 ↧ 22.00
- 1.00 x 45° Chamfer at bottom of 22.00
- 11.50 ↧ 18.00
- 1/2 20 UNF ↧ 18.00

Hole 2 - Temp Probe 1:
- 6.00 THRU
- 11.80 ↧15.00
- 1/4 NPT ↧15.00

Hole 3 - Valve:
- 11.80 ↧ 15.00
- 2.00 THRU hole from ⌖ at 16˚ angle with the vertical
- 1/4 NPT ↧ 15.00

Hole 1 to lign up with Water jacket outlet

Hole 4 - Wire Fitting
- 4.00 THRU
- 11.80 ↧15
- 1/4 NPT ↧15.00

Hole 5 - Temp Probe 2:
- 6.00 THRU
- 11.80 ↧15.00
- 1/4 NPT ↧15.00

D.5.2.1.3 High-Pressure Chamber - Honing Details

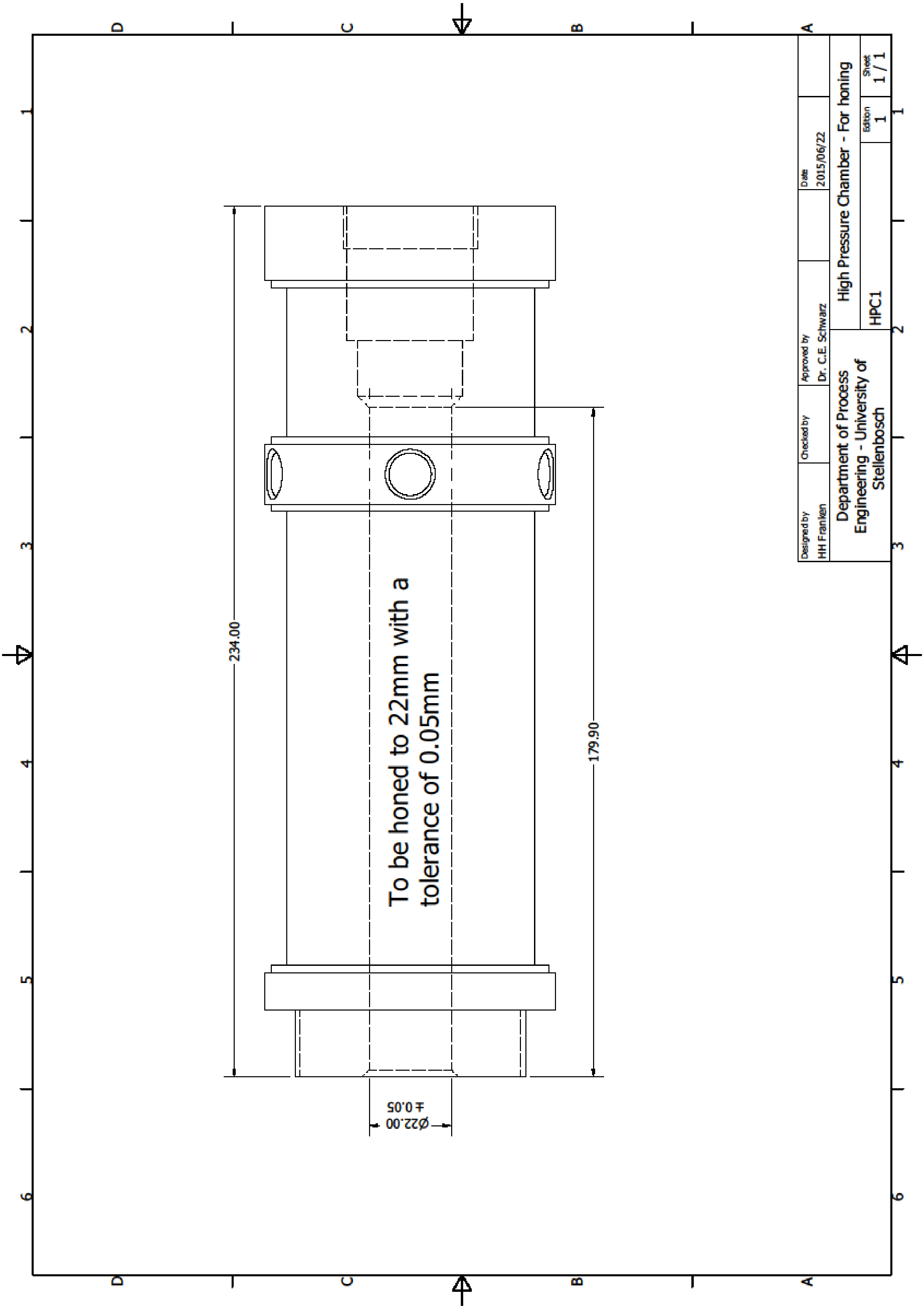

D.5.2.1.4 Pressure Plug for Testing

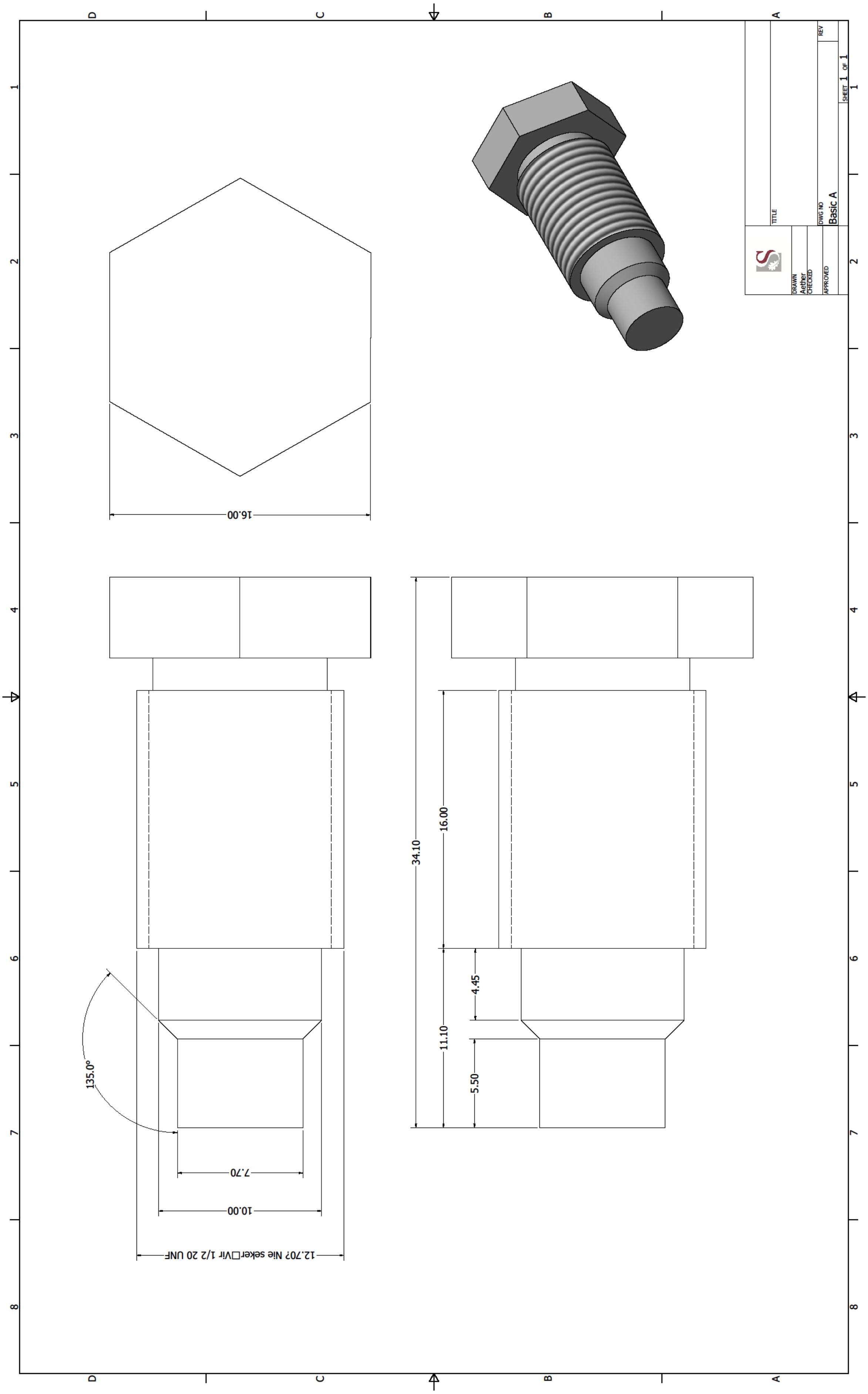

D.5.2.2 High-Pressure Barrel Material Certificate

The below material certificate is fir the high-pressure barrel and is required for certification purposes.

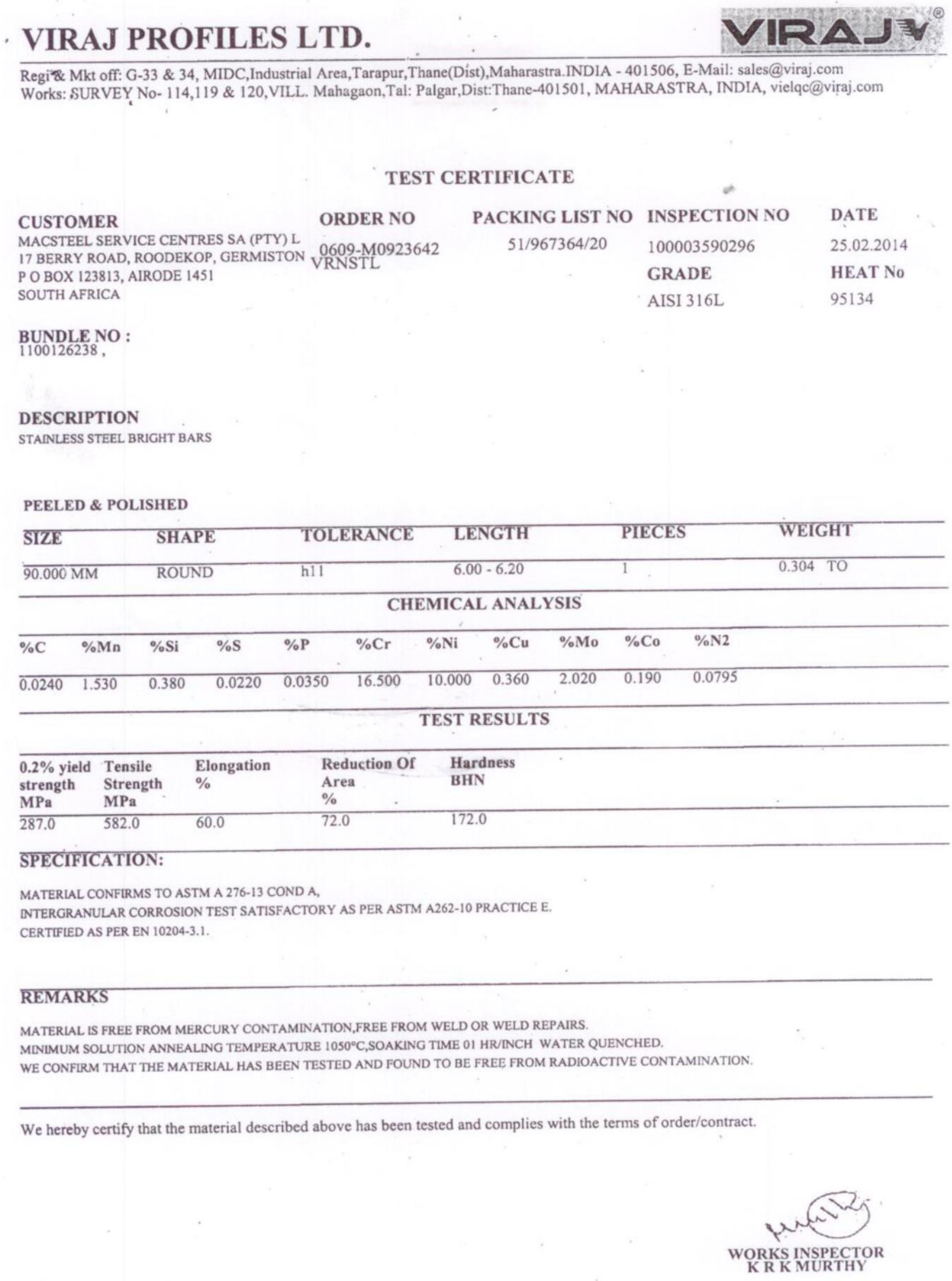

VIRAJ PROFILES LTD.

Regi & Mkt off: G-33 & 34, MIDC,Industrial Area,Tarapur,Thane(Dist),Maharastra.INDIA - 401506, E-Mail: sales@viraj.com
Works: SURVEY No- 114,119 & 120,VILL. Mahagaon,Tal: Palgar,Dist:Thane-401501, MAHARASTRA, INDIA, vielqc@viraj.com

TEST CERTIFICATE

CUSTOMER
MACSTEEL SERVICE CENTRES SA (PTY) L
17 BERRY ROAD, ROODEKOP, GERMISTON
P O BOX 123813, AIRODE 1451
SOUTH AFRICA

ORDER NO	PACKING LIST NO	INSPECTION NO	DATE
0609-M0923642 VRNSTL	51/967364/20	100003590296	25.02.2014
		GRADE	**HEAT No**
		AISI 316L	95134

BUNDLE NO :
1100126238 ,

DESCRIPTION
STAINLESS STEEL BRIGHT BARS

PEELED & POLISHED

SIZE	SHAPE	TOLERANCE	LENGTH	PIECES	WEIGHT
90.000 MM	ROUND	h11	6.00 - 6.20	1	0.304 TO

CHEMICAL ANALYSIS

%C	%Mn	%Si	%S	%P	%Cr	%Ni	%Cu	%Mo	%Co	%N2
0.0240	1.530	0.380	0.0220	0.0350	16.500	10.000	0.360	2.020	0.190	0.0795

TEST RESULTS

0.2% yield strength MPa	Tensile Strength MPa	Elongation %	Reduction Of Area %	Hardness BHN
287.0	582.0	60.0	72.0	172.0

SPECIFICATION:

MATERIAL CONFIRMS TO ASTM A 276-13 COND A,
INTERGRANULAR CORROSION TEST SATISFACTORY AS PER ASTM A262-10 PRACTICE E.
CERTIFIED AS PER EN 10204-3.1.

REMARKS

MATERIAL IS FREE FROM MERCURY CONTAMINATION,FREE FROM WELD OR WELD REPAIRS.
MINIMUM SOLUTION ANNEALING TEMPERATURE 1050°C,SOAKING TIME 01 HR/INCH WATER QUENCHED.
WE CONFIRM THAT THE MATERIAL HAS BEEN TESTED AND FOUND TO BE FREE FROM RADIOACTIVE CONTAMINATION.

We hereby certify that the material described above has been tested and complies with the terms of order/contract.

WORKS INSPECTOR
K R K MURTHY

D.5.3 Design Calculations and Drawing Review

This section contains the design calculations and drawing review for the Low-Pressure Chamber.

Calculations were first performed in-house according to ASME VIII, then independently validated by Schreuder Engineering Services.

D.5.3.1. In-house Pressure Vessel Calculations 307
D.5.3.2. Design and Drawing Review 313
D.5.3.3. Low-Pressure Chamber Design Calculation Report 316
D.5.3.4. High-Pressure Chamber Design Calculation Report 323

D.5.3.1 In-house Pressure Vessel Calculations

Low-pressure chamber shell calculation:

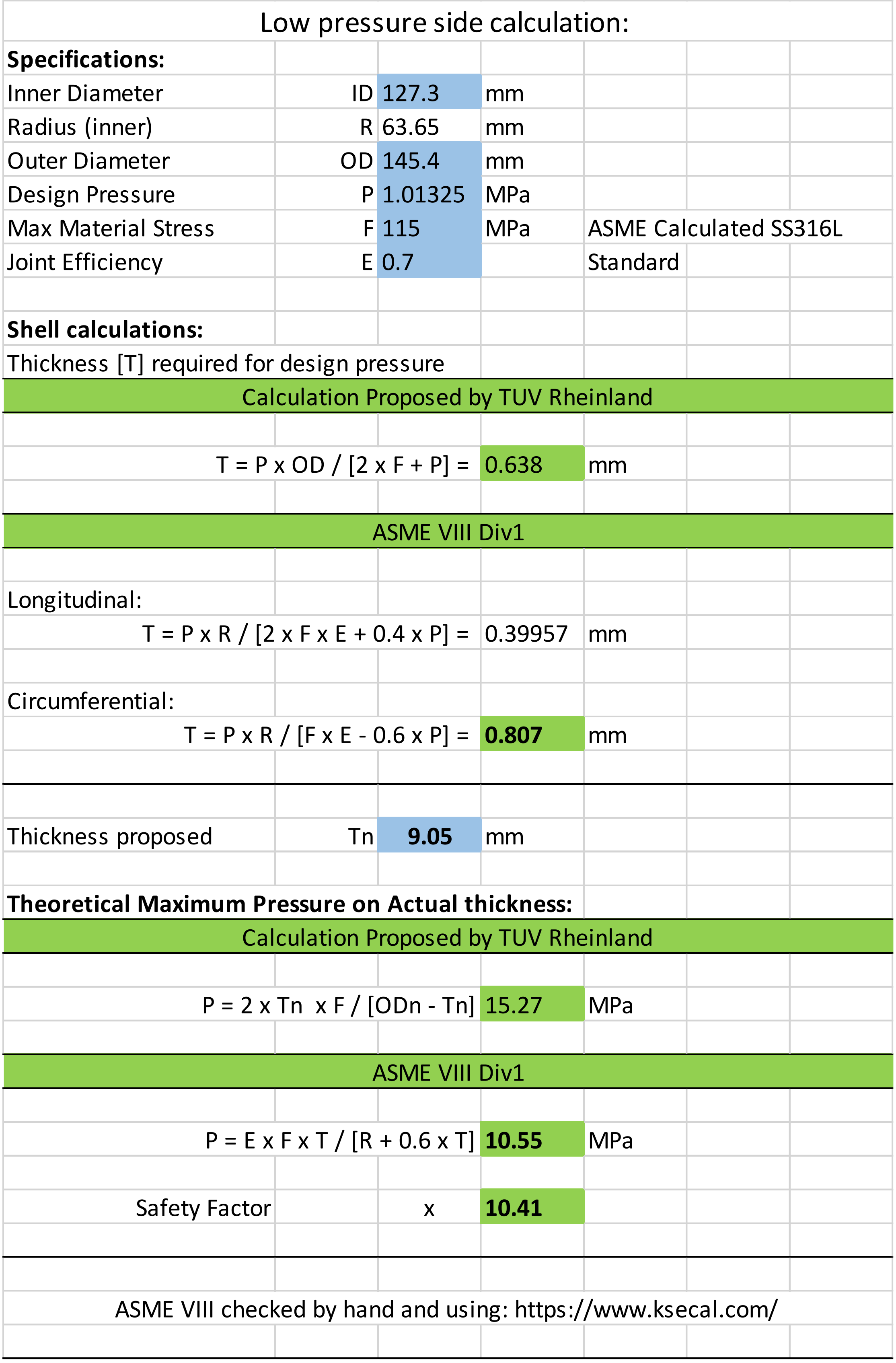

Low pressure side calculation:

Specifications:				
Inner Diameter	ID	127.3	mm	
Radius (inner)	R	63.65	mm	
Outer Diameter	OD	145.4	mm	
Design Pressure	P	1.01325	MPa	
Max Material Stress	F	115	MPa	ASME Calculated SS316L
Joint Efficiency	E	0.7		Standard

Shell calculations:

Thickness [T] required for design pressure

Calculation Proposed by TUV Rheinland

T = P x OD / [2 x F + P] = 0.638 mm

ASME VIII Div1

Longitudinal:

T = P x R / [2 x F x E + 0.4 x P] = 0.39957 mm

Circumferential:

T = P x R / [F x E - 0.6 x P] = **0.807** mm

Thickness proposed Tn **9.05** mm

Theoretical Maximum Pressure on Actual thickness:

Calculation Proposed by TUV Rheinland

P = 2 x Tn x F / [ODn - Tn] 15.27 MPa

ASME VIII Div1

P = E x F x T / [R + 0.6 x T] **10.55** MPa

Safety Factor x **10.41**

ASME VIII checked by hand and using: https://www.ksecal.com/

Low-pressure chamber Screw Cap calculation:

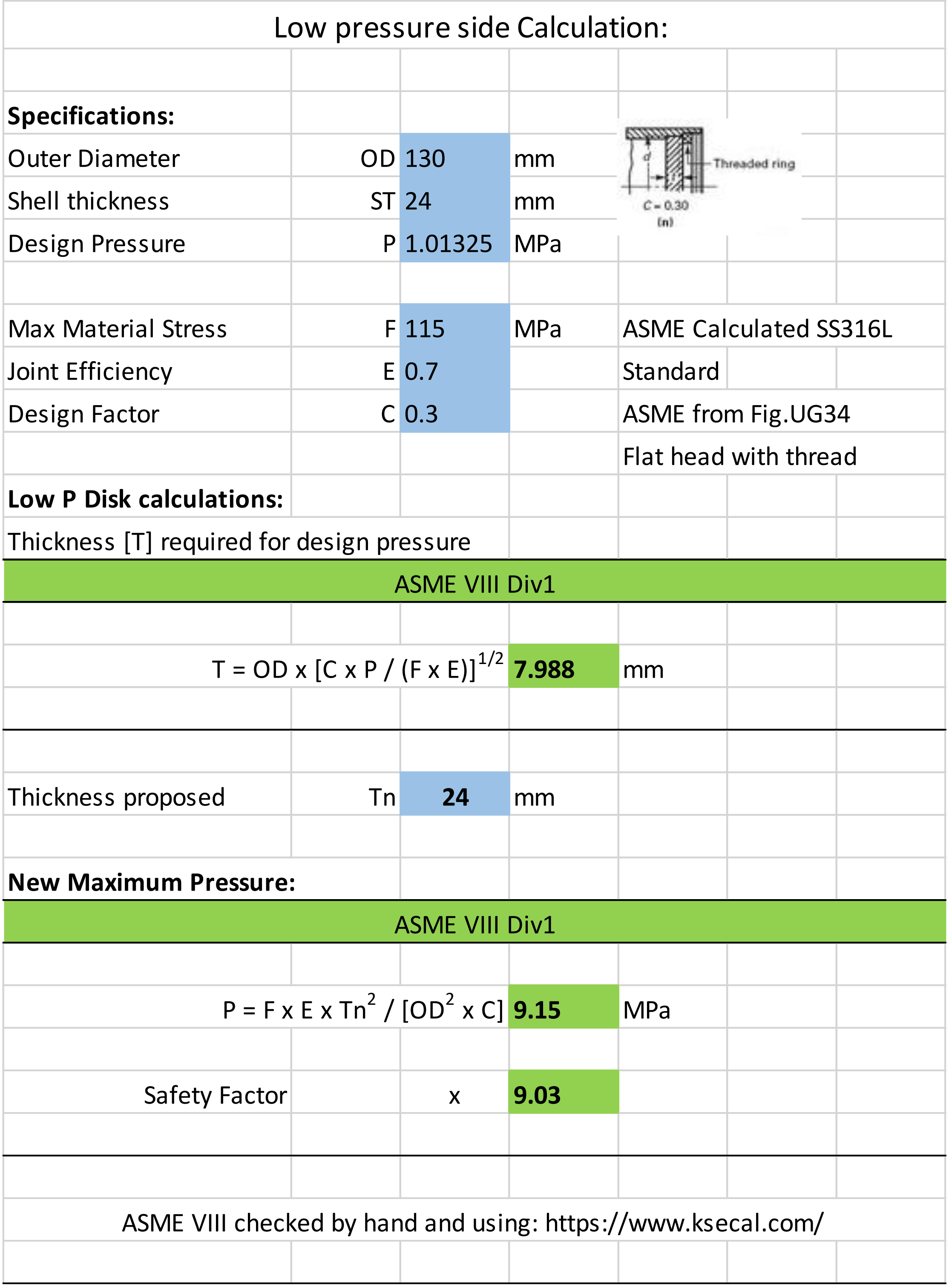

Low pressure side Calculation:

Specifications:				
Outer Diameter	OD	130	mm	
Shell thickness	ST	24	mm	
Design Pressure	P	1.01325	MPa	
Max Material Stress	F	115	MPa	ASME Calculated SS316L
Joint Efficiency	E	0.7		Standard
Design Factor	C	0.3		ASME from Fig.UG34
				Flat head with thread
Low P Disk calculations:				
Thickness [T] required for design pressure				
ASME VIII Div1				
$T = OD \times [C \times P / (F \times E)]^{1/2}$		**7.988**	mm	
Thickness proposed	Tn	**24**	mm	
New Maximum Pressure:				
ASME VIII Div1				
$P = F \times E \times Tn^2 / [OD^2 \times C]$		**9.15**	MPa	
Safety Factor	x	**9.03**		
ASME VIII checked by hand and using: https://www.ksecal.com/				

High-Pressure-Chamber-Side Cap:

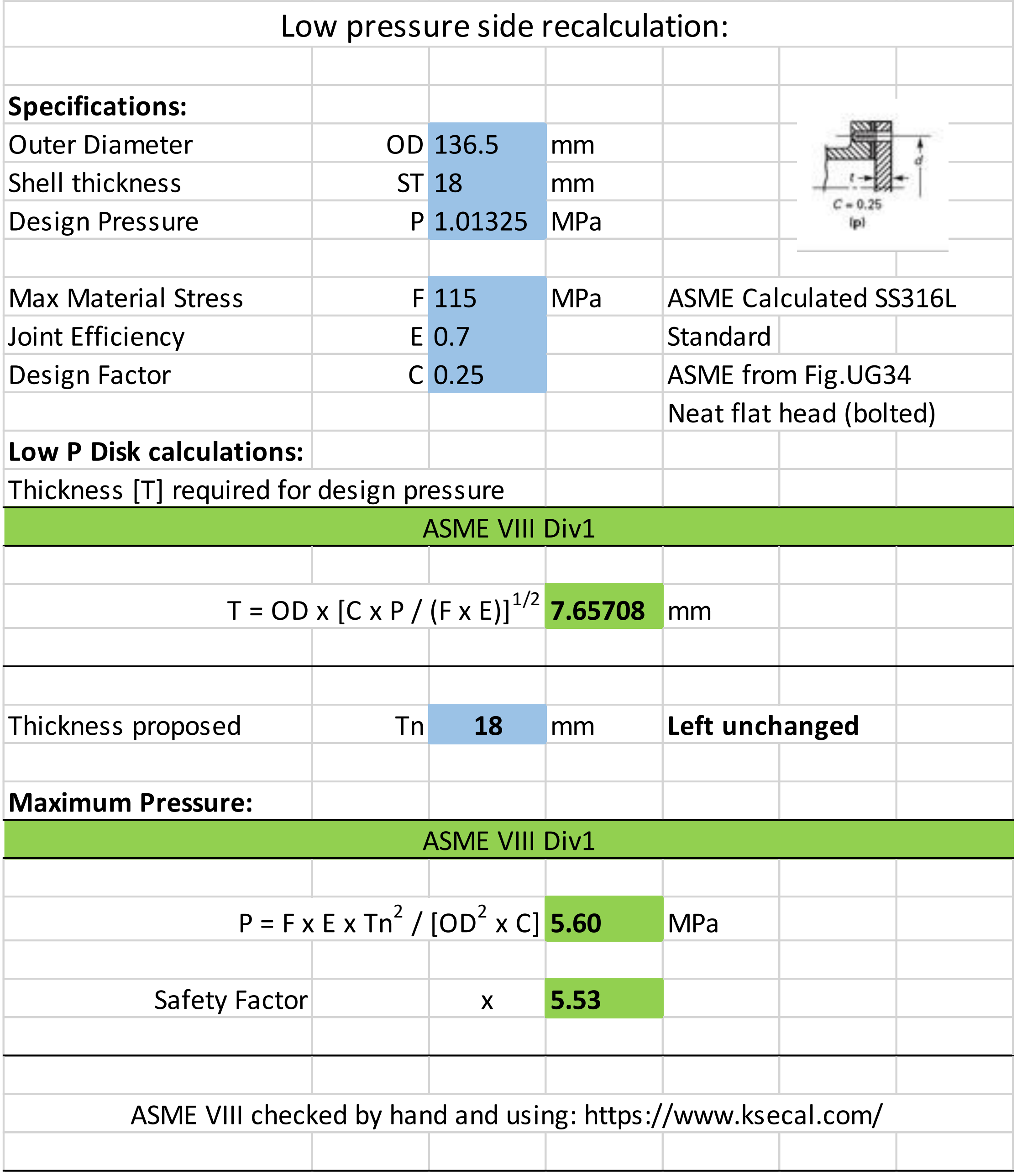

Low pressure side recalculation:

Specifications:				
Outer Diameter	OD	136.5	mm	
Shell thickness	ST	18	mm	
Design Pressure	P	1.01325	MPa	
Max Material Stress	F	115	MPa	ASME Calculated SS316L
Joint Efficiency	E	0.7		Standard
Design Factor	C	0.25		ASME from Fig.UG34
				Neat flat head (bolted)
Low P Disk calculations:				
Thickness [T] required for design pressure				
ASME VIII Div1				
$T = OD \times [C \times P / (F \times E)]^{1/2}$			**7.65708**	mm
Thickness proposed	Tn	**18**	mm	**Left unchanged**
Maximum Pressure:				
ASME VIII Div1				
$P = F \times E \times Tn^2 / [OD^2 \times C]$			**5.60**	MPa
Safety Factor		x	**5.53**	
ASME VIII checked by hand and using: https://www.ksecal.com/				

High-pressure chamber shell calculation:

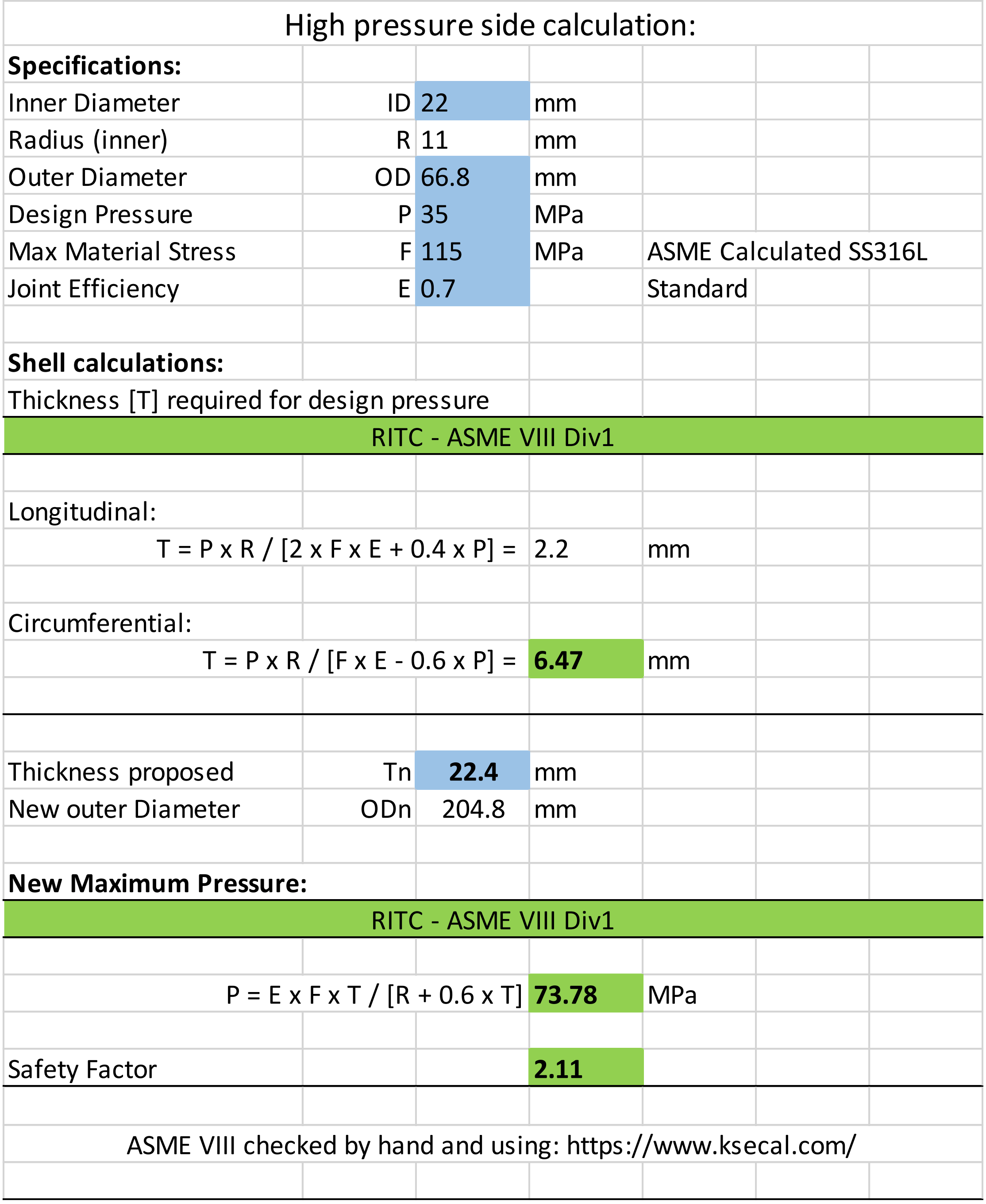

High pressure side calculation:				
Specifications:				
Inner Diameter	ID	22	mm	
Radius (inner)	R	11	mm	
Outer Diameter	OD	66.8	mm	
Design Pressure	P	35	MPa	
Max Material Stress	F	115	MPa	ASME Calculated SS316L
Joint Efficiency	E	0.7		Standard
Shell calculations:				
Thickness [T] required for design pressure				
RITC - ASME VIII Div1				
Longitudinal:				
T = P x R / [2 x F x E + 0.4 x P] =			2.2	mm
Circumferential:				
T = P x R / [F x E - 0.6 x P] =			**6.47**	mm
Thickness proposed	Tn	**22.4**	mm	
New outer Diameter	ODn	204.8	mm	
New Maximum Pressure:				
RITC - ASME VIII Div1				
P = E x F x T / [R + 0.6 x T]			**73.78**	MPa
Safety Factor			**2.11**	
ASME VIII checked by hand and using: https://www.ksecal.com/				

High-pressure chamber shell calculation – narrowest point:

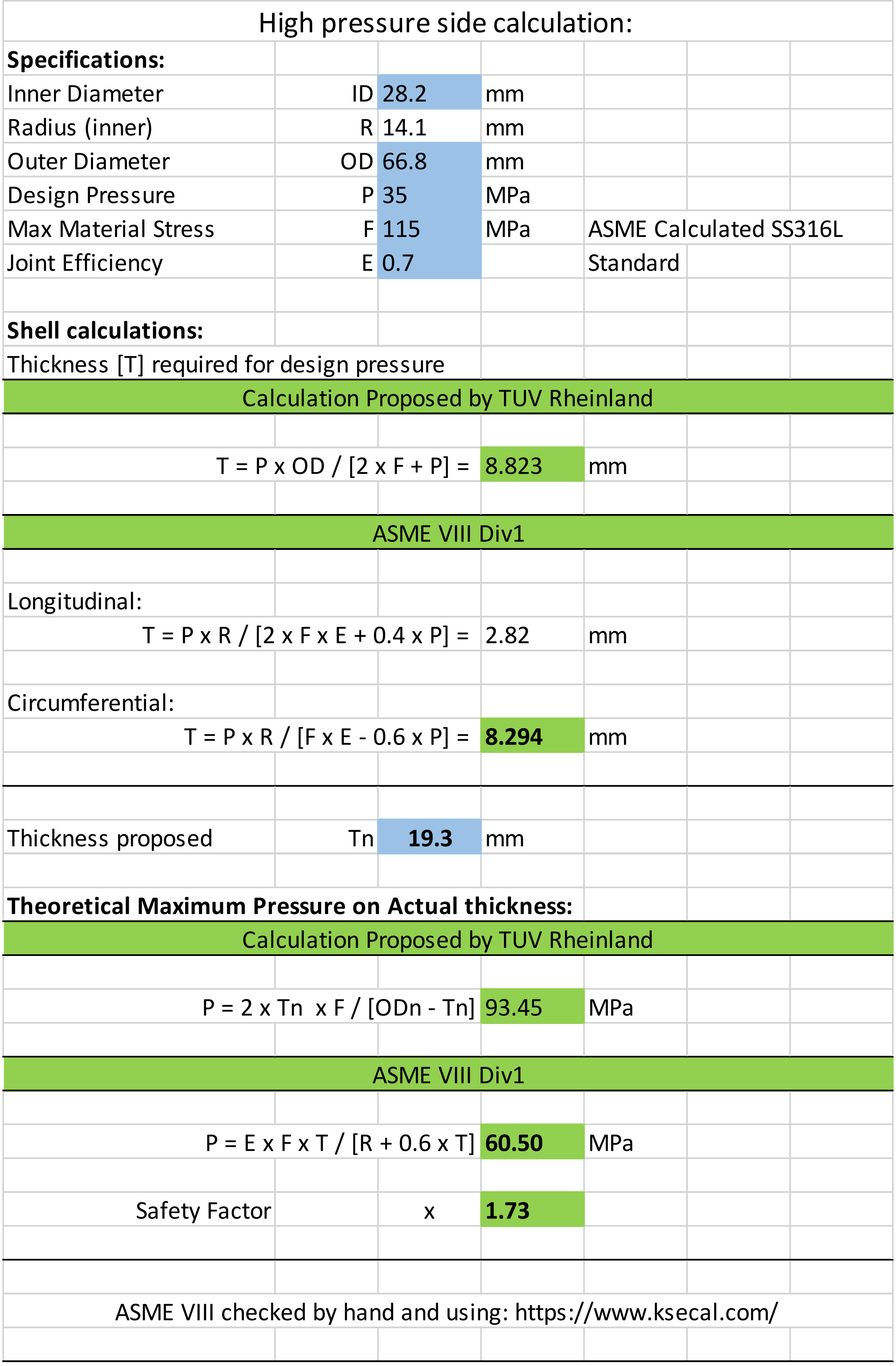

High pressure side calculation:				
Specifications:				
Inner Diameter	ID	28.2	mm	
Radius (inner)	R	14.1	mm	
Outer Diameter	OD	66.8	mm	
Design Pressure	P	35	MPa	
Max Material Stress	F	115	MPa	ASME Calculated SS316L
Joint Efficiency	E	0.7		Standard
Shell calculations:				
Thickness [T] required for design pressure				
Calculation Proposed by TUV Rheinland				
T = P x OD / [2 x F + P] =		8.823	mm	
ASME VIII Div1				
Longitudinal:				
T = P x R / [2 x F x E + 0.4 x P] =		2.82	mm	
Circumferential:				
T = P x R / [F x E - 0.6 x P] =		**8.294**	mm	
Thickness proposed	Tn	**19.3**	mm	
Theoretical Maximum Pressure on Actual thickness:				
Calculation Proposed by TUV Rheinland				
P = 2 x Tn x F / [ODn - Tn]		93.45	MPa	
ASME VIII Div1				
P = E x F x T / [R + 0.6 x T]		**60.50**	MPa	
Safety Factor	x	**1.73**		
ASME VIII checked by hand and using: https://www.ksecal.com/				

High pressure piston head calculation:

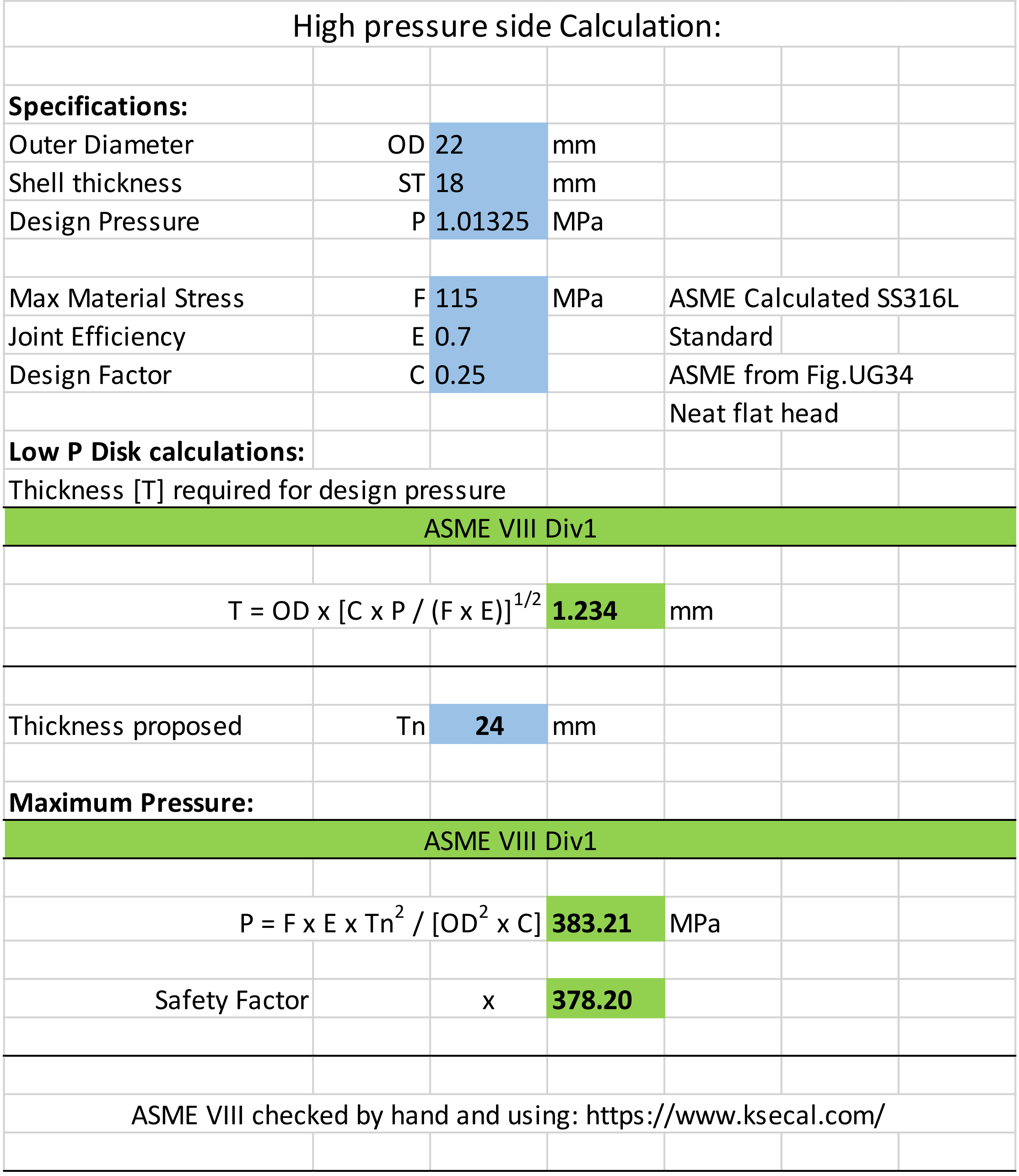

High pressure side Calculation:						
Specifications:						
Outer Diameter	OD	22	mm			
Shell thickness	ST	18	mm			
Design Pressure	P	1.01325	MPa			
Max Material Stress	F	115	MPa	ASME Calculated SS316L		
Joint Efficiency	E	0.7		Standard		
Design Factor	C	0.25		ASME from Fig.UG34		
				Neat flat head		
Low P Disk calculations:						
Thickness [T] required for design pressure						
ASME VIII Div1						
$T = OD \times [C \times P / (F \times E)]^{1/2}$			**1.234**	mm		
Thickness proposed	Tn	**24**	mm			
Maximum Pressure:						
ASME VIII Div1						
$P = F \times E \times Tn^2 / [OD^2 \times C]$			**383.21**	MPa		
Safety Factor		x	**378.20**			
ASME VIII checked by hand and using: https://www.ksecal.com/						

D.5.3.2 Design and Drawing Review

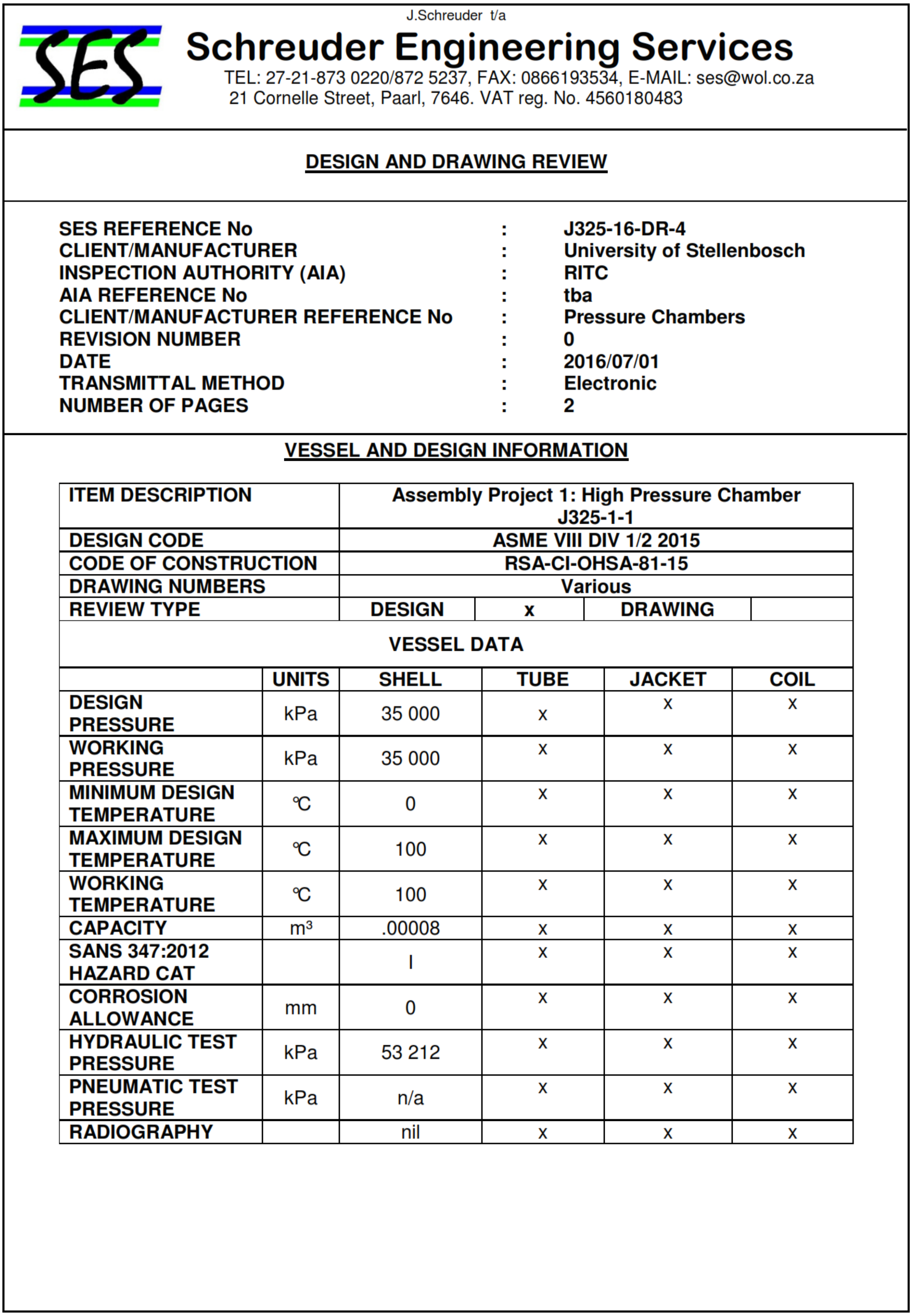

J.Schreuder t/a

Schreuder Engineering Services

TEL: 27-21-873 0220/872 5237, FAX: 0866193534, E-MAIL: ses@wol.co.za
21 Cornelle Street, Paarl, 7646. VAT reg. No. 4560180483

DESIGN AND DRAWING REVIEW

SES REFERENCE No : J325-16-DR-4
CLIENT/MANUFACTURER : University of Stellenbosch
INSPECTION AUTHORITY (AIA) : RITC
AIA REFERENCE No : tba
CLIENT/MANUFACTURER REFERENCE No : Pressure Chambers
REVISION NUMBER : 0
DATE : 2016/07/01
TRANSMITTAL METHOD : Electronic
NUMBER OF PAGES : 2

VESSEL AND DESIGN INFORMATION

ITEM DESCRIPTION	Assembly Project 1: High Pressure Chamber J325-1-1			
DESIGN CODE	ASME VIII DIV 1/2 2015			
CODE OF CONSTRUCTION	RSA-CI-OHSA-81-15			
DRAWING NUMBERS	Various			
REVIEW TYPE	DESIGN	x	DRAWING	

VESSEL DATA

	UNITS	SHELL	TUBE	JACKET	COIL
DESIGN PRESSURE	kPa	35 000	x	x	x
WORKING PRESSURE	kPa	35 000	x	x	x
MINIMUM DESIGN TEMPERATURE	℃	0	x	x	x
MAXIMUM DESIGN TEMPERATURE	℃	100	x	x	x
WORKING TEMPERATURE	℃	100	x	x	x
CAPACITY	m^3	.00008	x	x	x
SANS 347:2012 HAZARD CAT		I	x	x	x
CORROSION ALLOWANCE	mm	0	x	x	x
HYDRAULIC TEST PRESSURE	kPa	53 212	x	x	x
PNEUMATIC TEST PRESSURE	kPa	n/a	x	x	x
RADIOGRAPHY		nil	x	x	x

SOLE PROPRIETER: J. SCHREUDER

ITEM DESCRIPTION	**Assembly Project 1: Low Pressure Chamber J325-1-2**			
DESIGN CODE	**ASME VIII DIV 1/2 2015**			
CODE OF CONSTRUCTION	**RSA-CI-OHSA-81-15**			
DRAWING NUMBERS	**Various**			
REVIEW TYPE	**DESIGN**	**x**	**DRAWING**	

VESSEL DATA

	UNITS	**SHELL**	**TUBE**	**JACKET**	**COIL**
DESIGN PRESSURE	kPa	1 013	x	x	x
WORKING PRESSURE	kPa	1 013	x	x	x
MINIMUM DESIGN TEMPERATURE	°C	0	x	x	x
MAXIMUM DESIGN TEMPERATURE	°C	100	x	x	x
WORKING TEMPERATURE	°C	100	x	x	x
CAPACITY	m³	.001	x	x	x
SANS 347:2012 HAZARD CAT		SEP	x	x	x
CORROSION ALLOWANCE	mm	0	x	x	x
HYDRAULIC TEST PRESSURE	kPa	1 608	x	x	x
PNEUMATIC TEST PRESSURE	kPa	n/a	x	x	x
RADIOGRAPHY		nil	x	x	x

REVIEW STATUS

2A

1 :	**REVIEWED WITH NO COMMENTS**	**2:**	**REVIEWED WITH COMMENTS**
A:	**MANUFACTURING MAY PROCEED**	**B:**	**HOLD FABRICATION**
C:	**REVISE AND RESUBMIT**	**D:**	**SUBMIT FINAL DOCUMENT**

COMMENTS

1. The drawing provided was not fully dimensioned and not all relevant information is available on the drawing. This review is therefore based on the information received and interpretations made from the drawings. It is therefore essential that the AIA verify that information critical to the vessel integrity. We have worked from the assumption that the bodies will be machined from solid round bar and that the endcaps will be manufactured from plate.

REVISION RECORD

NUMBER	DATE ISSUED	REVIEWED BY	SIGNED
1	2016-07-02	J.Schreuder	J. Schreuder Pr Eng (mech) MSAIW MSAIMechE ecsa reg no 2012/0472
2	2016-07-14	J.Schreuder	J. Schreuder Pr Eng (mech) MSAIW MSAIMechE ecsa reg no 2012/0472
3	2016-07-14	J.Schreuder	J. Schreuder Pr Eng (mech) MSAIW MSAIMechE ecsa reg no 2012/0472

J. Schreuder Pr Eng (mech) MSAIW MSAIMechE
ecsa reg no 2012/0472

J. Schreuder t/a Schreuder Engineering Services: J. Schreuder Pr. Eng (mech) MSAIW MSAIMechE

This review is based on the information received and does not absolve the Fabricator, Designer or their Agents from their contractual and legal obligations regarding correct design, drawing, detailing, fabrication and installation. Design software, Designcalcs® from Computer Engineering is used for ASME VIII DIV1 design verification.

CALCULATIONS

D.5.3.3 Low-Pressure Chamber Design Calculation Report

Schreuder Engineering Services
21 Cornelle Street Paarl 7645,

Date Printed: 04/11/2016

CUSTOMER
University of Stellenbosch

,

VESSEL LOCATION
University of Stellenbosch

,

VESSEL DESCRIPTION
Assembly Project 1: Low Pressure Chamber

Vessel designed per the ASME Boiler & Pressure Vessel Code,
Section VIII, Division 1, 2015 Edition
with DesignCalcs, Version: 2016.2

Job No: J325-1-2

NAMEPLATE INFORMATION

Vessel MAWP:	1.0130 MPa at 100 ℃
MDMT:	0 ℃ at 1.0130 MPa
Serial Number(s):	____________________
National Board Number(s):	____________________
Year Built:	2016
Radiography:	NONE
Postweld Heat Treated:	NONE

Signatures

______________________________ Date: 03 / 11 / 2016

J. Schreuder Pr Eng (mech) MSAIW MSAIMechE
ecsa reg no 2012/0472

Schreuder Engineering Services
21 Cornelle Street Paarl 7645,

Date Printed: 04/11/2016

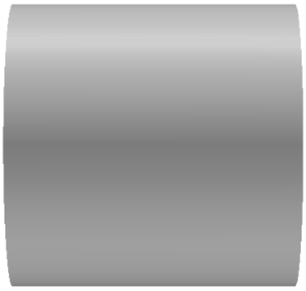

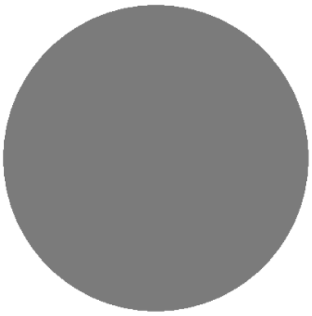

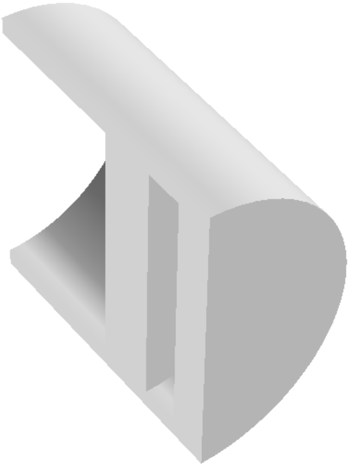

Schreuder Engineering Services

Shell 1

Customer: **University of Stellenbosch**
Job No: J325-1-2
Number: 1

Number: 1
Mark Number: S1

Date Printed: 04/11/2016

Cylindrical Shell Design Information

Design Pressure:	1.0130	MPa	Design Temperature:	100	℃
Static Head:	0.0000	MPa	Long. Joint Efficiency:	70	%
Shell Material:	SA-479 Gr. 304 S30400		Factor B Chart:	HA-1	
			Material Stress (hot):	113.00	MPa
Shell Length:	132.50	mm	Material Stress (cold):	138.00	MPa
			Compressive Stress:	88.92	MPa
Corrosion Allowance:	0.00	mm	Actual Circumferential Stress:	11.90	MPa
External Corrosion Allowance:	0.00	mm	Actual Longitudinal Stress:	5.23	MPa
Inside Diameter (new):	127.30	mm			
Inside Diameter (corroded):	127.30	mm	Specific Gravity:	1.00	
Shell Surface Area:	0.06	sq. m	Weight of Fluid:	1.69	kg
Shell Estimated Volume:	0.00	cu. m	Total Flooded Shell Weight:	5.47	kg
Circ. Joint Efficiency:	70	%	Shell Weight:	3.79	kg

Minimum Design Metal Temperature Data

Minimum Design Metal Temperature: 0 ℃
Material is exempt from impact testing per UHA-51(d)

Design Thickness Calculations

Longitudinal Stress Calculations per Paragraph UG-27(c)(2)

$$\mathbf{t} = \frac{PR}{2SE + 0.4P} = \frac{1.0130 * 63.65}{2 * 113.00 * 0.70 + 0.4 * 1.0130}$$

= Greater Of (0.41(Calculated), 1.50(Minimum Allowed)) + 0.00 (corrosion) + 0.00 (ext. corrosion) = minimum of **1.50** mm

Circumferential Stress Calculations per UG-27(c)(1)

$$\mathbf{t} = \frac{PR}{SE - 0.6P} = \frac{1.0130 * 63.65}{113.00 * 0.70 - 0.6 * 1.0130}$$

= Greater of (0.83(Calculated), 1.50(Minimum Allowed)) + 0.00 (corrosion) + 0.00 (ext. corrosion) = minimum of **1.50** mm

Extreme Fiber Elongation Calculation per Paragraph UHA-44 and Table UG-79-1

$$\textbf{Elongation} = \frac{50t}{Rf} = \frac{50 * 8.35}{67.83}$$

= elongation of **6.16** %

MAWP for this Shell Section Only

$$\mathbf{P} = \frac{SEt}{R + 0.6t} = \frac{113.00 * 0.70 * 8.35}{63.65 + 0.6 * 8.35}$$

= maximum design pressure of **9.6196** MPa

External loads do not control design.

Nominal Shell Thickness Selected = **8.35** mm

Schreuder Engineering Services

Head 1

Customer: **University of Stellenbosch**
Job No: J325-1-2
Number: 1

Number: 1
Mark Number: H1

Date Printed: 04/11/2016

Flat Head Design Information

Design Pressure:	1.0130 MPa		Design Temperature:	100	℃
Static Head:	0.0000 MPa		Joint Efficiency:	70	%
Head Material:	SA-479 Gr. 304 S30400				
			Material Stress (hot):	113.00	MPa
Corrosion Allowance:	0.00	mm	Material Stress (cold):	138.00	MPa
External Corrosion Allowance:	0.00	mm	Actual Head Stress:	18.75	MPa
Head Location:	Right				
Diameter (D):	144.00	mm			
Head Factor C :	0.2500				
UG-34 Head Configuration:	p				
Head Surface Area:	0.02	sq. m	Specific Gravity:	1.00	
Head Estimated Volume:	0.00	cu. m	Weight of Fluid:	0.00	kg
Head Weight:	2.62	kg	Total Flooded Head Weight:	2.62	kg

Minimum Design Metal Temperature Data

Minimum Design Metal Temperature: 0 ℃
Material is exempt from impact testing per UHA-51(d)

Design Thickness Calculations

Design Thickness Calculations per UG-34(c)(2)

$$\mathbf{t} = d * \sqrt{\frac{CP}{SE}} = 144.00 * \sqrt{\frac{0.2500 * 1.0130}{113.00 * 0.70}} = 8.15 + 0.00 \text{ (corrosion)} + 0.00 \text{ (ext. corrosion)} = \text{minimum of } \mathbf{8.15} \text{ mm}$$

MAWP per UG-32 for this Head Only

$$\mathbf{P} = \frac{SEt^2}{d^2C} = \frac{113.00 * 0.70 * 20.00^2}{144.00^2 * 0.2500} = \mathbf{6.1034} \text{ MPa}$$

External loads do not control design.

Nominal Head Thickness Selected = **20.00** mm

Schreuder Engineering Services

Head 2

Customer: **University of Stellenbosch**
Job No: J325-1-2
Number: 2

Number: 2
Mark Number: H2

Date Printed: 04/11/2016

Flat Head Design Information

Design Pressure:	1.0130 MPa	Design Temperature:	100 ℃
Static Head:	0.0000 MPa	Joint Efficiency:	70 %
Head Material:	SA-240 Gr. 304 S30400		
		Material Stress (hot):	113.00 MPa
Corrosion Allowance:	0.00 mm	Material Stress (cold):	138.00 MPa
External Corrosion Allowance:	0.00 mm	Actual Head Stress:	20.38 MPa
Head Location:	Left		
Diameter (D):	130.00 mm		
Inside Diameter (corroded) :	130.00 mm	Head Factor C :	0.7500
UG-34 Head Configuration:	q		
Head Surface Area:	0.01 sq. m	Specific Gravity:	1.00
Head Estimated Volume:	0.00 cu. m	Weight of Fluid:	0.00 kg
Head Weight:	3.20 kg	Total Flooded Head Weight:	3.20 kg

Minimum Design Metal Temperature Data

Minimum Design Metal Temperature: 0 ℃
Material is exempt from impact testing per UHA-51(d)

Design Thickness Calculations

Design Thickness Calculations per UG-34(c)(2)

$$t = d * \sqrt{\frac{CP}{SE}} = 130.00 * \sqrt{\frac{0.7500 * 1.0130}{113.00 * 0.70}} = 12.74 + 0.00 \text{ (corrosion)} + 0.00 \text{ (ext. corrosion)}$$

= minimum of **12.74** mm

MAWP per UG-32 for this Head Only

$$P = \frac{SEt^2}{d^2C} = \frac{113.00 * 0.70 * 30.00^2}{130.00^2 * 0.7500}$$

= **5.6166** MPa

External loads do not control design.

Nominal Head Thickness Selected = **30.00** mm

Schreuder Engineering Services

Customer: **University of Stellenbosch**
Job No: J325-1-2
Number: -1

Date Printed: 04/11/2016

MDMT Report by Components

Design MDMT is 0 °C

Component	Material	Curve	Pressure	MDMT
Shell 1	SA-479 Gr. 304 S3040			Exempt per UHA-51(d)
Head 2	SA-240 Gr. 304 S3040			Exempt per UHA-51(d)
Head 1	SA-479 Gr. 304 S3040			Exempt per UHA-51(d)

The required design MDMT of 0 °C has been met or exceeded for the calculated MDMT values.

ASME Flanges Are Not Included in MDMT Calculations.

Schreuder Engineering Services

Assembly Project 1: Low Pressure Chamber

Customer: **University of Stellenbosch**
Job No: J325-1-2
Number: -1

Date Printed: 04/11/2016

MAWP Report by Components

Component	Design Pressure	Static Head	Vessel MAWP New & Cold UG-98(a)	Component MAWP Hot & Corroded UG-98(b)	Vessel MAWP Hot & Corroded UG-98(a)
Shell 1	1.0130 MPa	0.0000 MPa	11.7479 MPa	9.6196 MPa	9.6196 MPa
Head 2	1.0130 MPa	0.0000 MPa	6.8592 MPa	5.6166 MPa	5.6166 MPa
Head 1	1.0130 MPa	0.0000 MPa	7.4537 MPa	6.1034 MPa	6.1034 MPa

NC = Not Calculated Inc = Incomplete

Summary

Component with the lowest vessel MAWP(New & Cold) : **Head 2**
The lowest vessel MAWP(New & Cold) : **6.8592** MPa

Component with the lowest vessel MAWP(Hot & Corroded) : **Head 2**
The lowest vessel MAWP(Hot & Corroded) : **5.6166** MPa

Pressures are exclusive of any external loads.

Flange pressures listed here do not consider external loadings

Schreuder Engineering Services

Customer: **University of Stellenbosch**
Job No: J325-1-2

Number: -1

Date Printed: 04/11/2016

Summary Information

	Dry Weight	Flooded Weight
Shell	3.79 kg	5.47 kg
Head	5.81 kg	5.81 kg
Totals	9.60 kg	11.29 kg

	Volume
Shell	0.00 cu. m
Head	0.00 cu. m
Totals	0.00 cu. m

	Area
Shell	0.06 sq. m
Head	0.03 sq. m
Totals	0.09 sq. m

Schreuder Engineering Services

Customer: **University of Stellenbosch**
Job No: J325-1-2

Number: -1

Date Printed: 04/11/2016

Hydrostatic Test Information Par. UG-99(b)
Gauge at Top

Component	Const.	x	STest	/	SDesign	x	Pressure	=	Component Hydro Test Pressure
Head 1	1.3	x	138.00	/	113.00	x	1.0130	=	**1.6082**
Head 2	1.3	x	138.00	/	113.00	x	1.0130	=	1.6082
Shell 1	1.3	x	138.00	/	113.00	x	1.0130	=	1.6082

Calculated Test Pressure: 1.6082 MPa

Special Notes:

This calculation assumes one chamber.

This calculation is limited by the lowest component pressure per chamber.

D.5.3.4 High-Pressure Chamber Design Calculation Report

Schreuder Engineering Services
21 Cornelle Street Paarl 7645,

Date Printed: 04/11/2016

CUSTOMER
University of Stellenbosch

,

VESSEL LOCATION
University of Stellenbosch

,

VESSEL DESCRIPTION
Assembly Project 1: High Pressure Chamber

Vessel designed per the ASME Boiler & Pressure Vessel Code,
Section VIII, Division 1, 2015 Edition
with DesignCalcs, Version: 2016.2

Job No: J325-1

NAMEPLATE INFORMATION

Vessel MAWP: 35.0000 MPa at 100 ℃
MDMT: 0 ℃ at 35.0000 MPa

Serial Number(s): ____________________

National Board Number(s): ____________________
Year Built: 2016
Radiography: NONE
Postweld Heat Treated: NONE

Signatures

Schreuder ____________________ Date: 03 / 11/ 2016

J. Schreuder Pr Eng (mech) MSAIW MSAIMechE
ecsa reg no 2012/0472

Schreuder Engineering Services
21 Cornelle Street Paarl 7645,

Date Printed: 04/11/2016

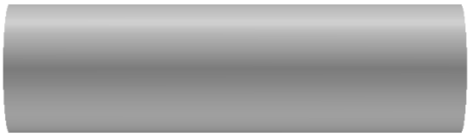

Schreuder Engineering Services

Shell 1

Customer: **University of Stellenbosch**
Job No: J325-1
Number: 1

Number: 1
Mark Number: S1

Date Printed: 04/11/2016

Cylindrical Shell Design Information

Design Pressure:	35.0000 MPa	Design Temperature:	100 ℃
Static Head:	0.0000 MPa	Long. Joint Efficiency:	70 %
Shell Material:	SA-479 Gr. 316 S31600	Factor B Chart:	HA-2
		Material Stress (hot):	118.00 MPa
Shell Length:	234.00 mm	Material Stress (cold):	138.00 MPa
		Compressive Stress:	104.55 MPa
Corrosion Allowance:	0.00 mm	Actual Circumferential Stress:	66.53 MPa
External Corrosion Allowance:	0.00 mm	Actual Longitudinal Stress:	8.26 MPa
Inside Diameter (new):	28.20 mm		
Inside Diameter (corroded):	28.20 mm	Specific Gravity:	1.00
Shell Surface Area:	0.05 sq. m	Weight of Fluid:	0.15 kg
Shell Estimated Volume:	0.00 cu. m	Total Flooded Shell Weight:	5.56 kg
Circ. Joint Efficiency:	70 %	Shell Weight:	5.41 kg

Minimum Design Metal Temperature Data

Minimum Design Metal Temperature: 0 ℃
Material is exempt from impact testing per UHA-51(d)

Design Thickness Calculations

Longitudinal Stress Calculations per Paragraph UG-27(c)(2)

$$t = \frac{PR}{2SE + 0.4P} = \frac{35.0000 * 14.10}{2 * 118.00 * 0.70 + 0.4 * 35.0000} = 2.75 + 0.00 \text{ (corrosion)} + 0.00 \text{ (ext. corrosion)}$$

= minimum of **2.75** mm

Circumferential Stress Calculations per UG-27(c)(1)

$$t = \frac{PR}{SE - 0.6P} = \frac{35.0000 * 14.10}{118.00 * 0.70 - 0.6 * 35.0000} = 8.01 + 0.00 \text{ (corrosion)} + 0.00 \text{ (ext. corrosion)}$$

= minimum of **8.01** mm

Extreme Fiber Elongation Calculation per Paragraph UHA-44 and Table UG-79-1

$$\textbf{Elongation} = \frac{50t}{Rf} = \frac{50 * 19.30}{23.75}$$

= elongation of **40.63** %

MAWP for this Shell Section Only

$$P = \frac{SEt}{R + 0.6t} = \frac{118.00 * 0.70 * 19.30}{14.10 + 0.6 * 19.30}$$

= maximum design pressure of **62.0787** MPa

External loads do not control design.

Nominal Shell Thickness Selected = **19.30** mm

Schreuder Engineering Services

Customer: **University of Stellenbosch**
Job No: J325-1

Number: -1

Date Printed: 04/11/2016

MDMT Report by Components

Design MDMT is 0 °C

Component	Material	Curve	Pressure	MDMT
Shell 1	SA-479 Gr. 316 S3160			Exempt per UHA-51(d)

The required design MDMT of 0 °C has been met or exceeded for the calculated MDMT values.

ASME Flanges Are Not Included in MDMT Calculations.

Schreuder Engineering Services

Assembly Project 1: High Pressure Chamber

Customer: **University of Stellenbosch**
Job No: J325-1

Number: -1

Date Printed: 04/11/2016

MAWP Report by Components

Component	Design Pressure	Static Head	Vessel MAWP New & Cold UG-98(a)	Component MAWP Hot & Corroded UG-98(b)	Vessel MAWP Hot & Corroded UG-98(a)
Shell 1	35.0000 MPa	0.0000 MPa	72.6005 MPa	62.0787 MPa	62.0787 MPa

NC = Not Calculated Inc = Incomplete

Summary

Component with the lowest vessel MAWP(New & Cold) : **Shell 1**
The lowest vessel MAWP(New & Cold) : **72.6005** MPa

Component with the lowest vessel MAWP(Hot & Corroded) : **Shell 1**
The lowest vessel MAWP(Hot & Corroded) : **62.0787** MPa

Pressures are exclusive of any external loads.

Flange pressures listed here do not consider external loadings

Schreuder Engineering Services

Customer: **University of Stellenbosch**
Job No: J325-1

Number: -1

Date Printed: 04/11/2016

Summary Information

	Dry Weight	Flooded Weight
Shell	5.41 kg	5.56 kg
Totals	5.41 kg	5.56 kg

	Volume
Shell	0.00 cu. m
Totals	0.00 cu. m

	Area
Shell	0.05 sq. m
Totals	0.05 sq. m

Schreuder Engineering Services

Customer: **University of Stellenbosch**
Job No: J325-1

Number: -1

Date Printed: 04/11/2016

Hydrostatic Test Information Par. UG-99(b)
Gauge at Top

Component	**Const.**	**x**	**STest**	**/**	**SDesign**	**x**	**Pressure**	**=**	**Component Hydro Test Pressure**
Shell 1	1.3	x	138.00	/	118.00	x	35.0000	=	**53.2119**

Calculated Test Pressure: 53.2119 MPa

Special Notes:

This calculation assumes one chamber.

This calculation is limited by the lowest component pressure per chamber.

D.5.4 RITC Certification

UNIVERSITEIT
STELLENBOSCH
UNIVERSITY

CERTIFICATE OF MANUFACTURE

High Pressure Phase Equilibria Cell

We hereby certify that the below referenced pressure vessel has been designed, constructed and tested in accordance with RSA/CI/OHSA 8.1 2015 and complies with the requirements of the OHS Act pressure equipment regulations and SANS 347 2012 edition 2.

MANUFACTURER: University of Stellenbosch **DATE:** 25 July 2016

INSPECTION AUTHORITY: RITC (Pty)Ltd **DATE:** 25 July 2016

PE 518
C[illegible]V 602

VESSEL TYPE: High Pressure Phase Equilibria Cell
SERIAL NUMBER: J325-1-1
OPERATING MEDIUM : Gas
CAPACITY: 0.00055 m^3
SANS 347 HAZ CAT: I
DESIGN PRESSURE: 35000KPA
DESIGN TEMPERATURE: 0°C - 100°C
MATERIAL OF CONSTRUCTION: AISI 316L
HYDROSTATIC TEST PRESSURE: 53212KPA
DATE OF TEST: 20 July 2016

24869-01

D.5.5 Quartz Crystal and Crystal Holder

Figure D- 4 Quartz crystal cage with mounted crystal.

This section contains the details of the Quartz Crystal.

Crystals were purchased from Boston Piezo-Optics. The crystal is X-cut, polished to an ultra-smooth finish and plated with four gold electrodes. The electrodes are deposited in quadrants of 80° along the circumference and for the full height of the crystal. The unplated regions lie in the Y- and Z-axes of the crystal, ensuring a torsional mode of vibration. Very thin wire leads are then attached to the centre of each electrode. The thin wires minimise the damping effect of the leads on the crystal during measurement. Each wire is looped once before connection to avoid strain on the leads and crystal.

Specifications:

Diameter: 0.197" +/- .003"
Length: 1.969" +/- .001"
Alignment: X-Cut
Density: 2650 kg/m^3
Cristal Rigidity C_{66}: 40.63×10^9 m^2/N

D.5.5.1 Crystal Holder Design Drawings

A removable crystal ‘cage’ was designed and constructed to house the quartz crystal and provide electrical contact. The cage is constructed from stainless steel 316 and PEEK plastic, with 50-50 Indium/Tin soldering used to connect the wire leads to the cage. The crystal requires two electrical contacts, with opposing electrodes connected. One contact is provided by lining up one pair of opposing crystal cage ‘bars’ with a spring-loaded, gold, circuit board test probe (90° conical tip with 1 mm diameter), held in place by a tight-fit PEEK insert. The other end of the test probe is soldered to a Teflon coated wire, which is passed through the Conax wire seal (model: TG-24T-A2-G) to an external connector, providing the ‘positive’ contact. The other contact is provided by contacting the second pair of opposing ‘bars’ of the cage with the high-pressure cell wall, which itself is grounded to the measurement equipment, providing the ‘neutral’ contact.

This section contains the following Design Drawings:

D.5.5.1.1. In Cell Crystal Assembly Dock 331
D.5.5.1.2. Upper Crystal Cage Ring 332
D.5.5.1.3. Lower Crystal Cage Ring 333
D.5.5.1.4. Stainless Steel Wire Profile and Measurements 334
D.5.5.1.5. Assembled Crystal Cage and Crystal 335
D.5.5.1.6. Assembled Crystal Cage and Crystal Close-up 336
D.5.5.1.7. Wire Fitting Seals and Rework 337

D.5.5.1.1 In Cell Crystal Cage Dock

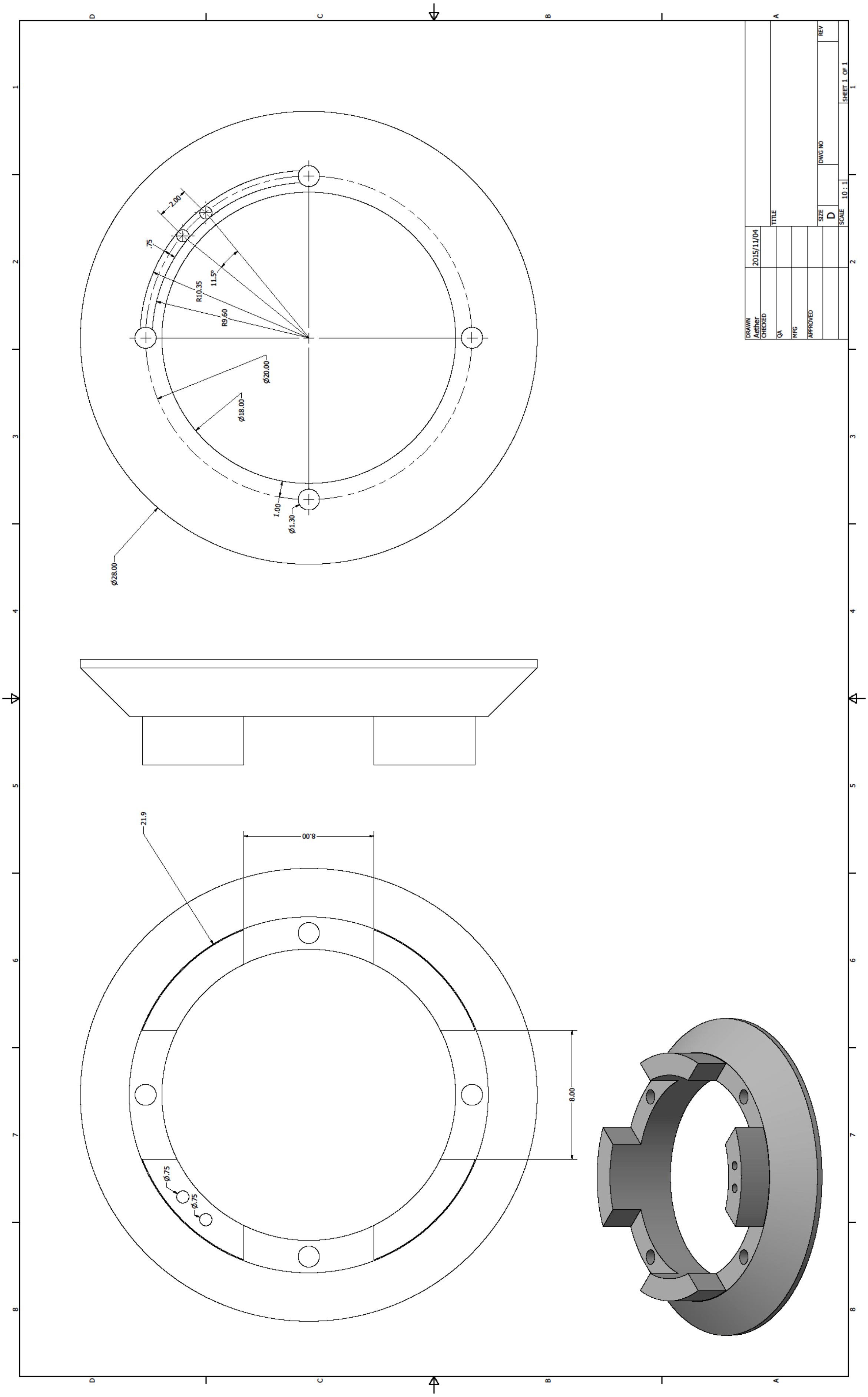

D.5.5.1.2 Upper Crystal Cage Ring

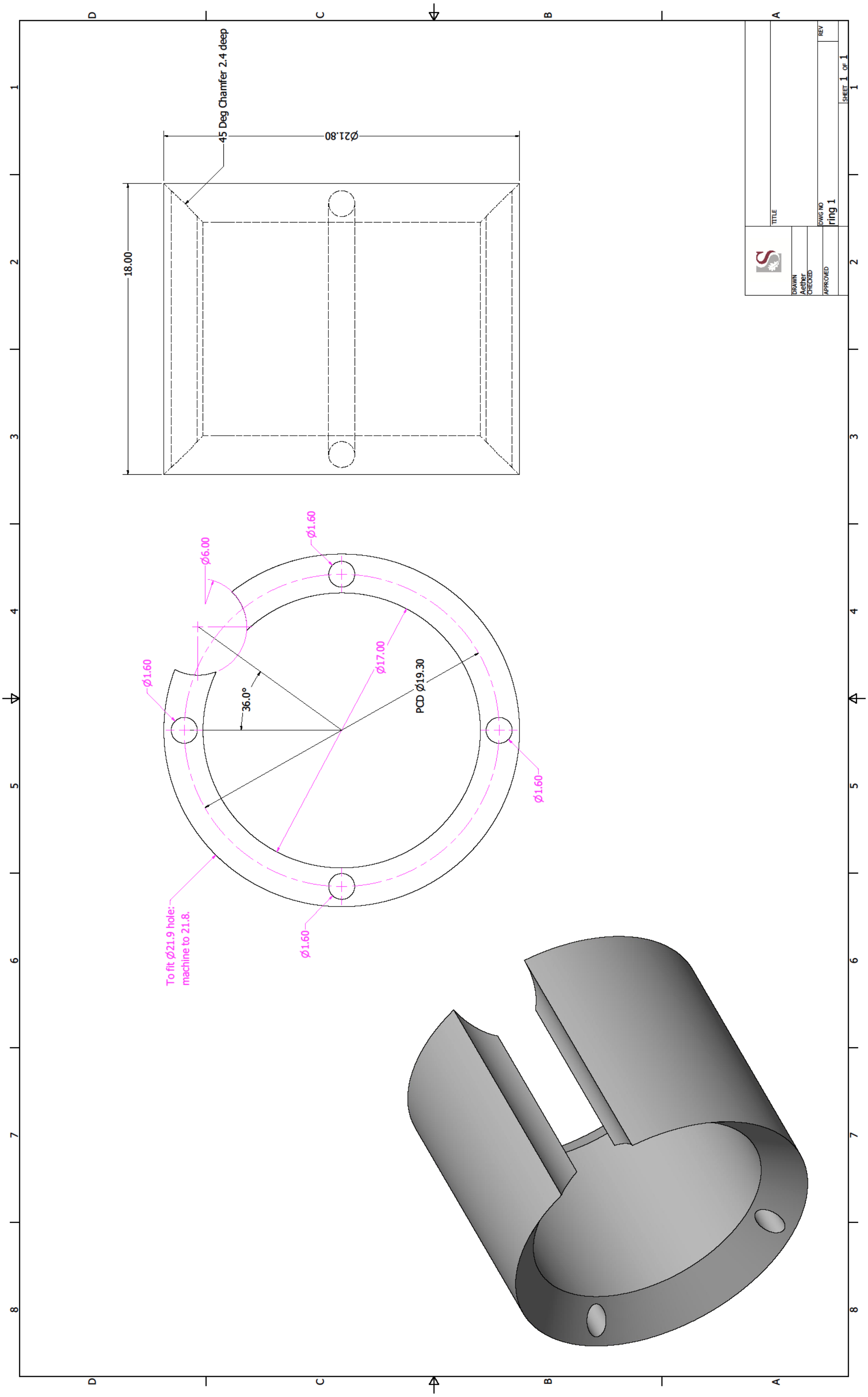

D.5.5.1.3 Lower Crystal Cage Ring

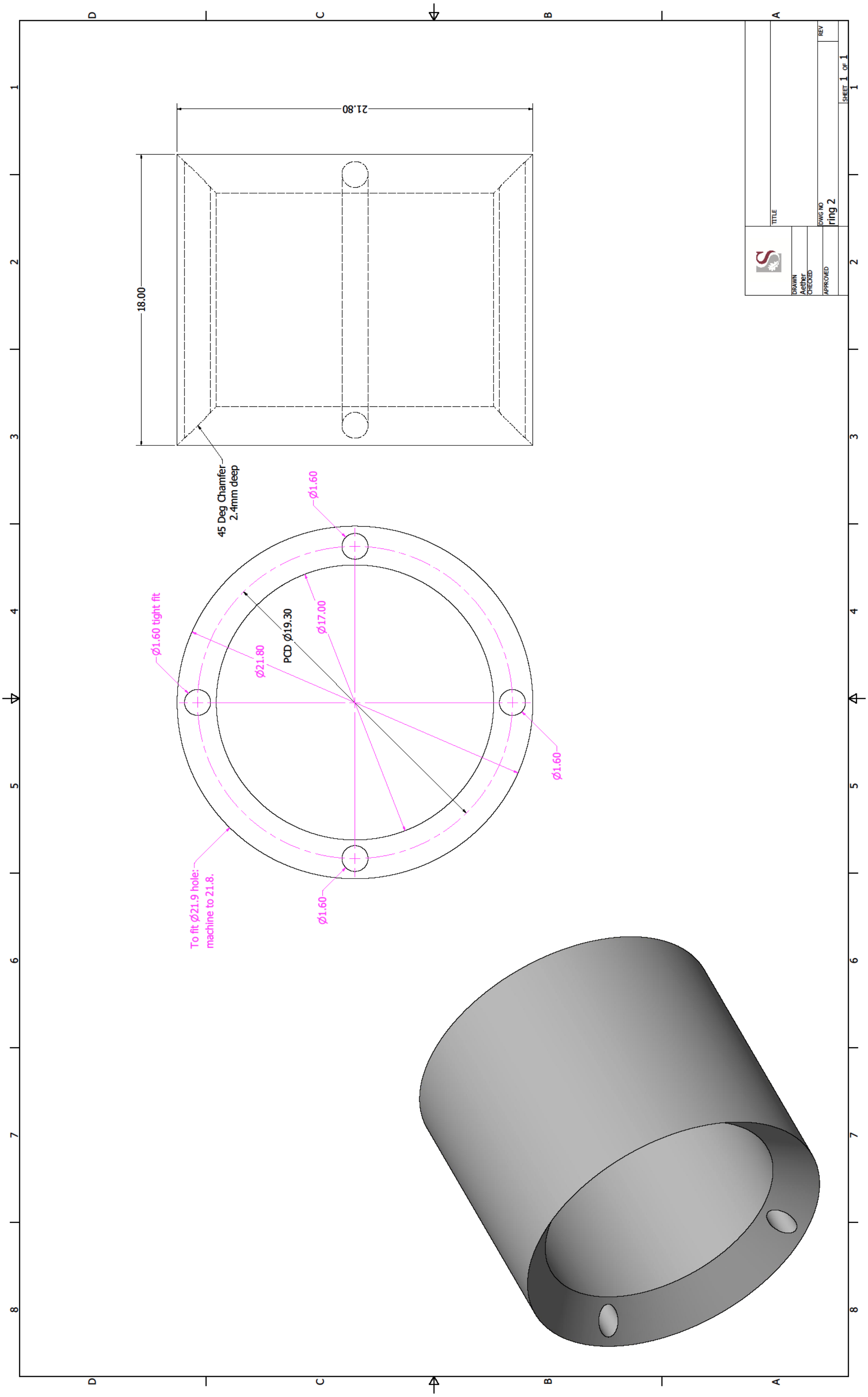

D.5.5.1.4 Stainless Steel Wire Profile and Measurements

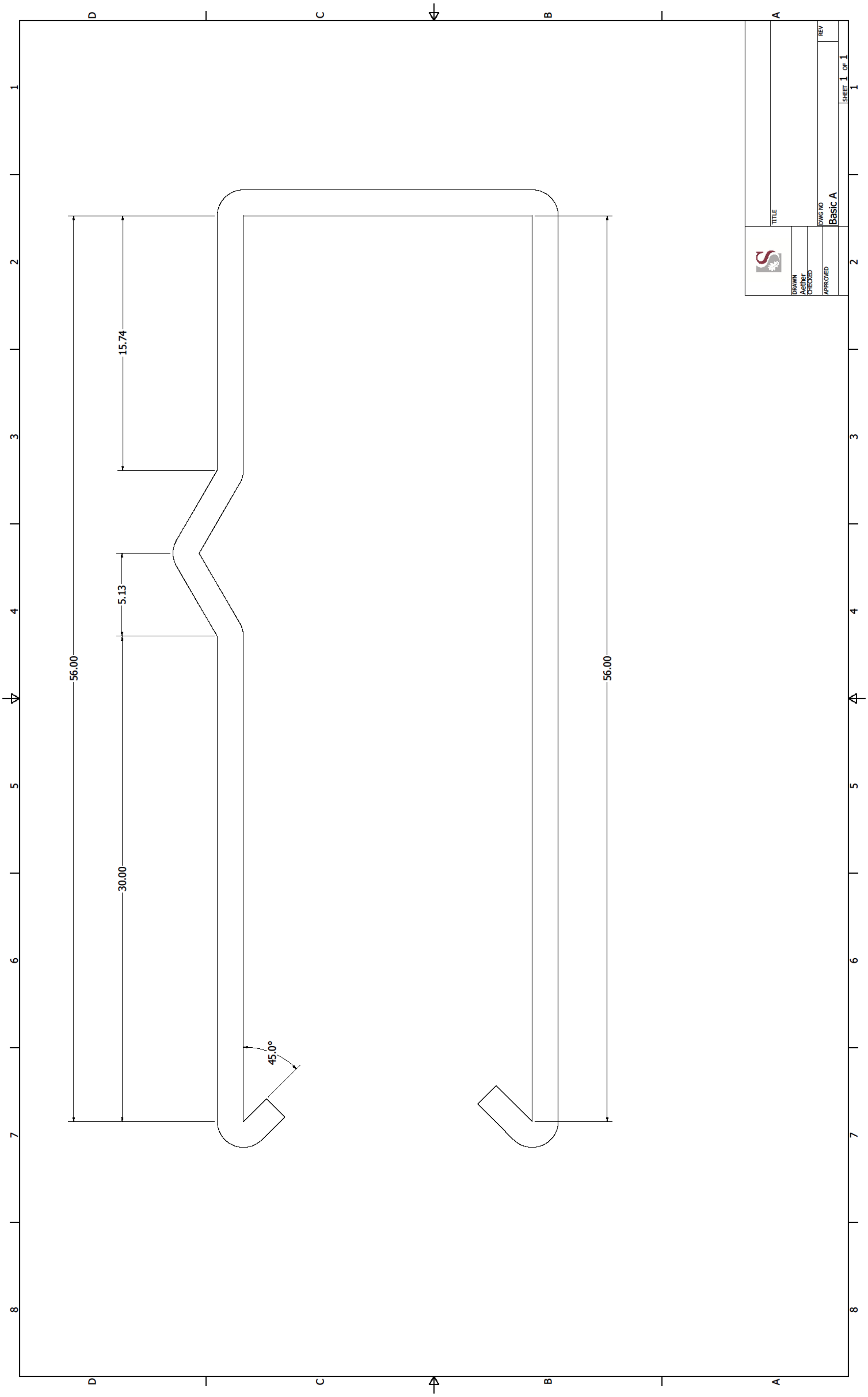

D.5.5.1.5 Assembled Crystal Cage and Crystal

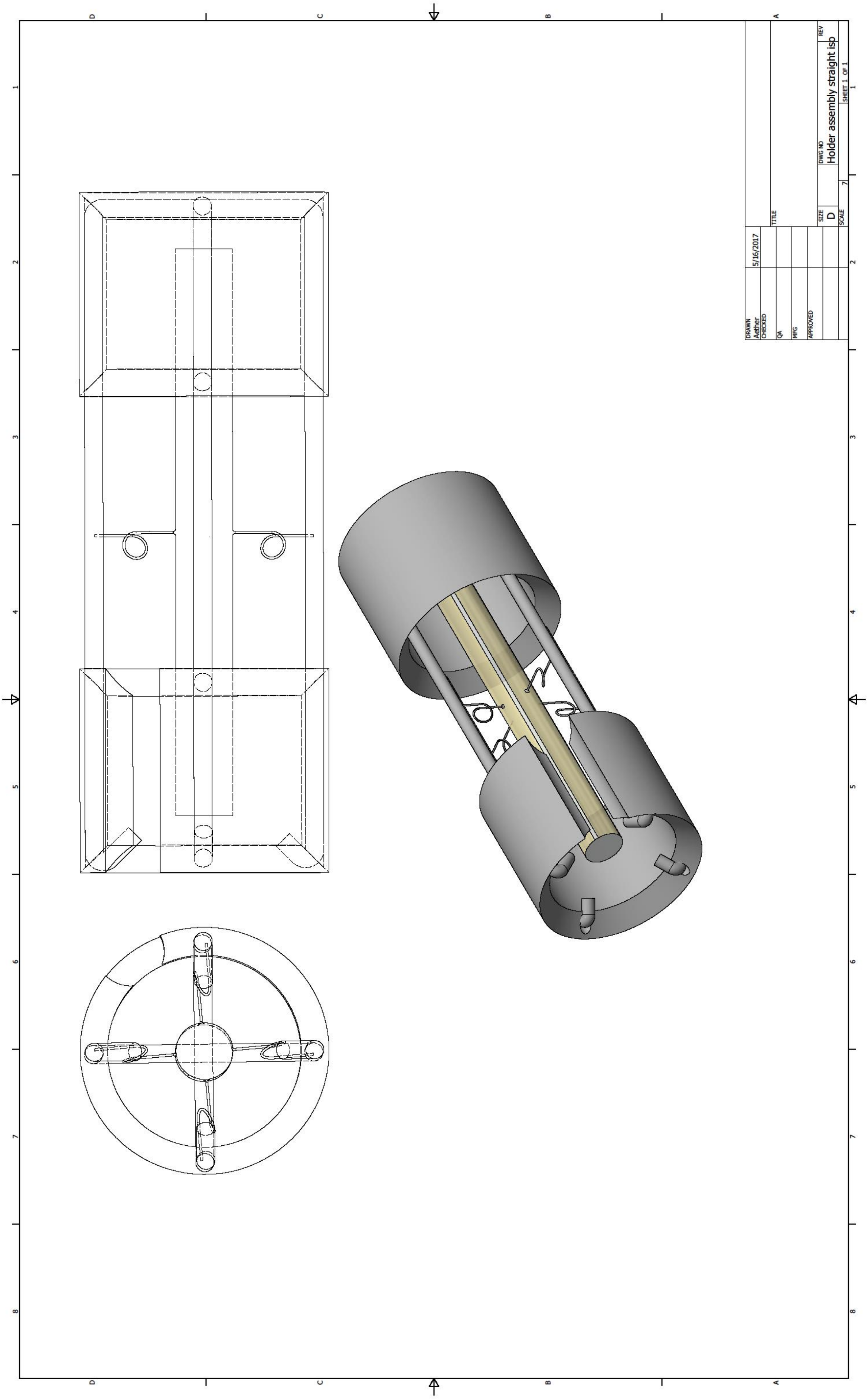

D.5.5.1.6 Assembled Crystal Cage and Crystal Closeup

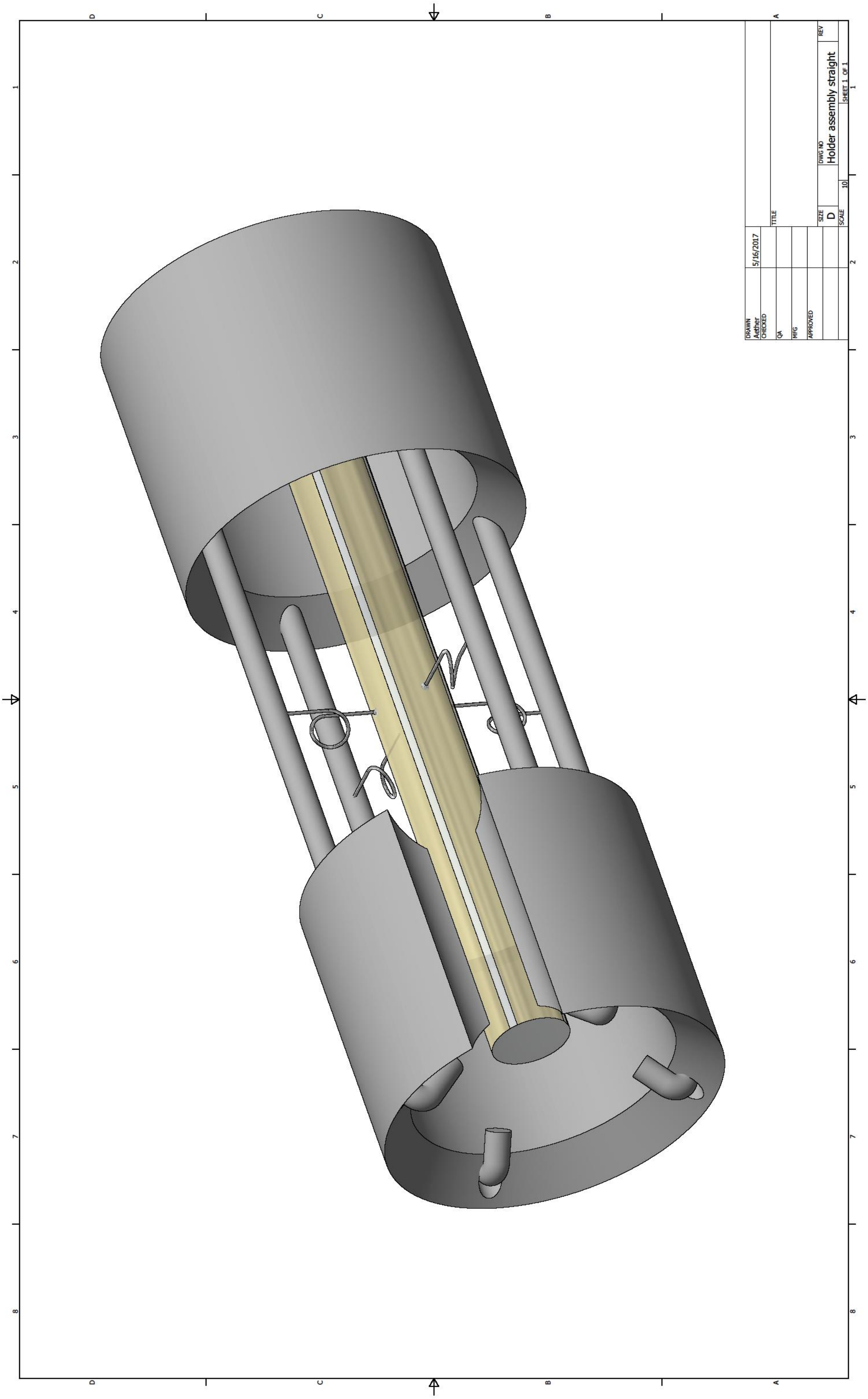

D.5.5.1.7 Wire Fitting Seals and Rework

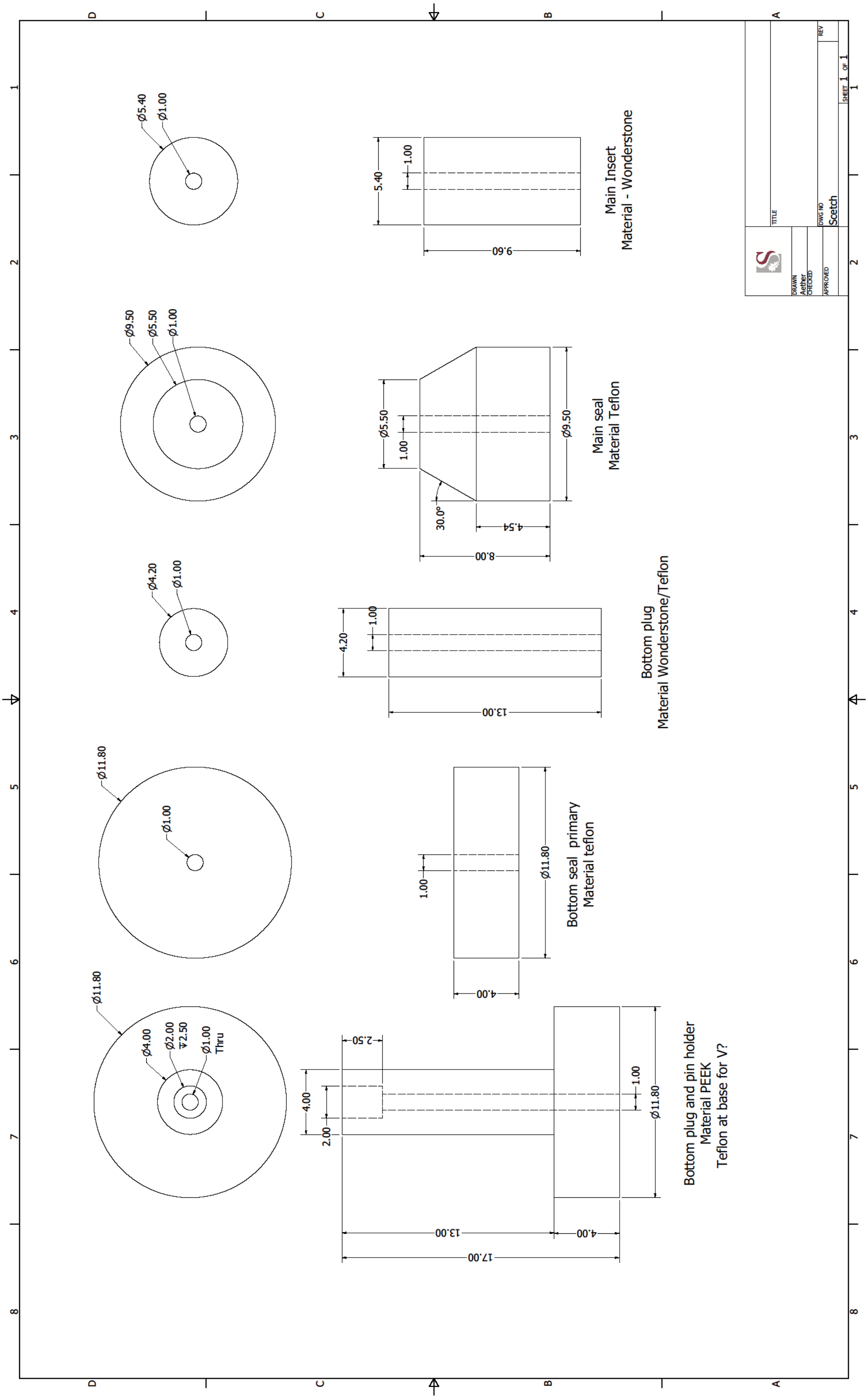

D.5.6 Cell Stand Design Drawings

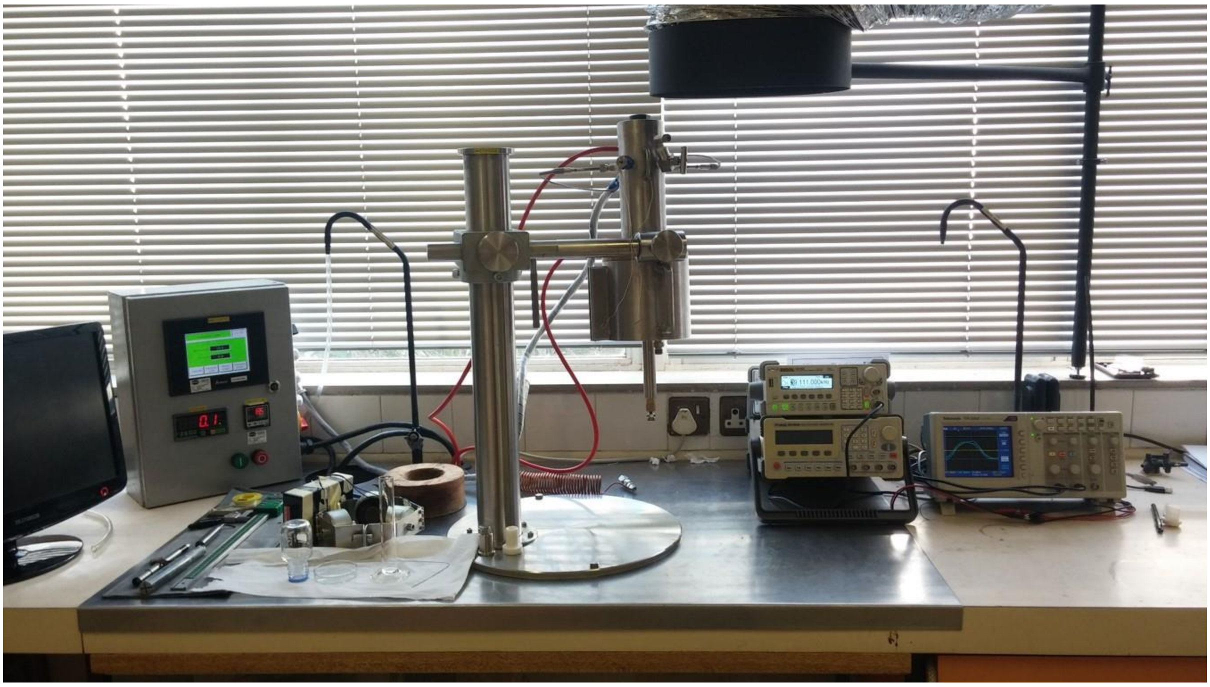

Figure D- 5: Finished high-pressure cell assembly – note the stand in the centre

A custom stand was constructed to mount the cell and allow for manoeuvrability, easy cleaning and an upright operating position. Non-standard, precision parts are listed here.

This section contains the following Design Drawings:

D.5.6.1. Top Cell Height Block 339
D.5.6.2. Top Cell Height Block 340
D.5.6.3. Bearing Collar 341
D.5.6.4. Cell Flange 342
D.5.6.5. Cell Rod 343
D.5.6.6. Assembled Stand 344
D.5.6.7. Assembled Stand and Cell 345

D.5.6.1 Top Cell Height Block

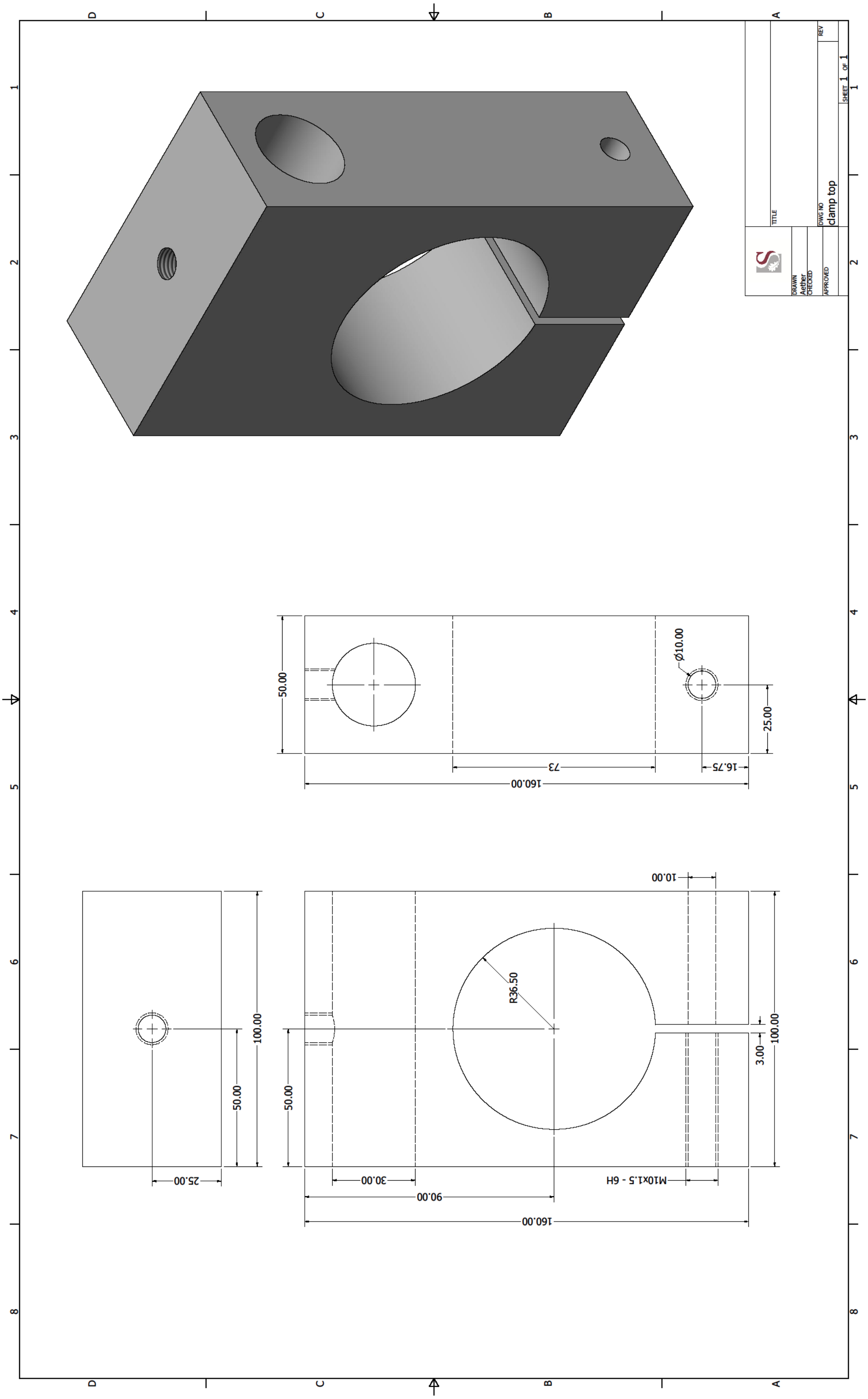

D.5.6.2 Bottom Cell Height Block

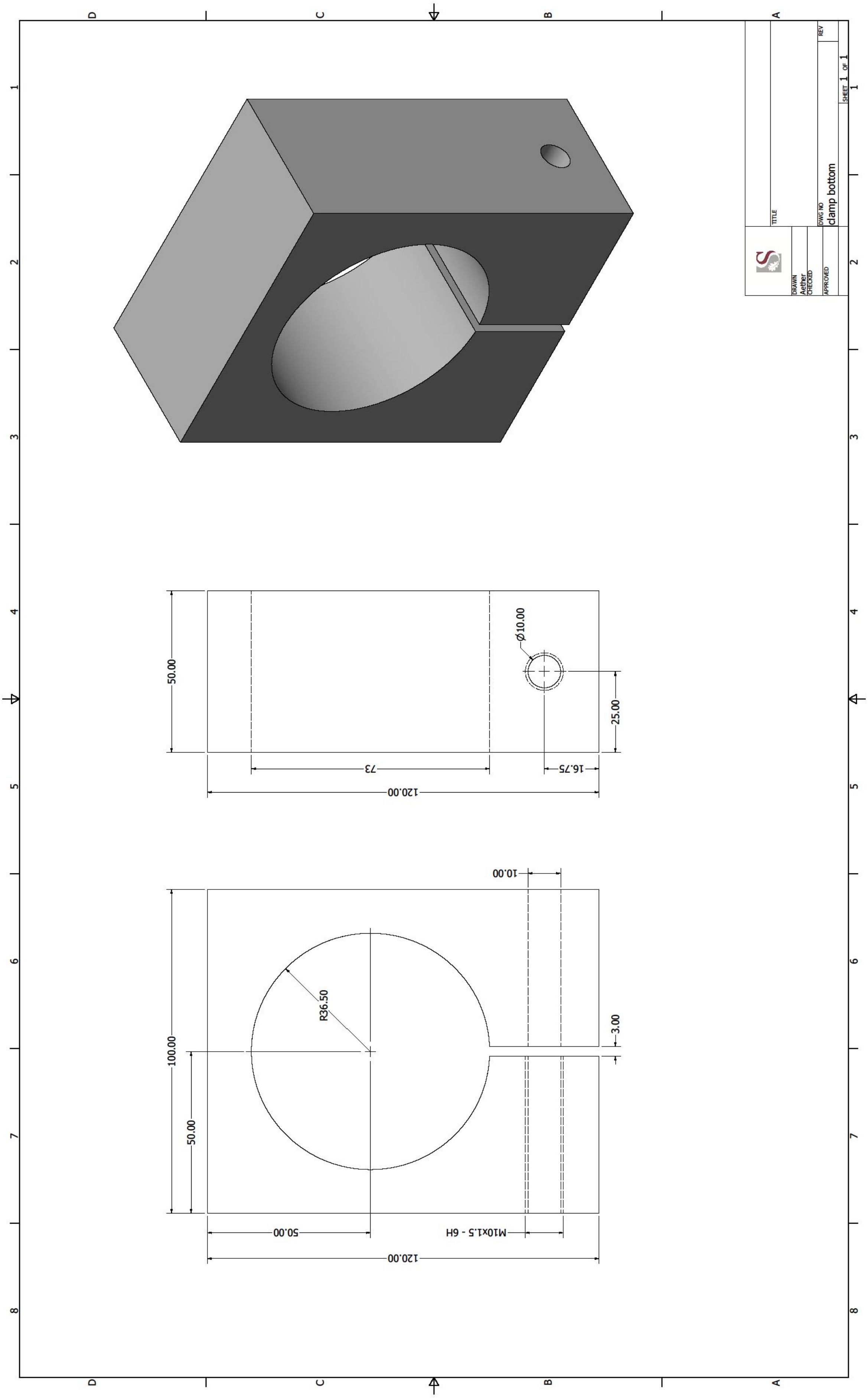

D.5.6.3 Bearing Collar

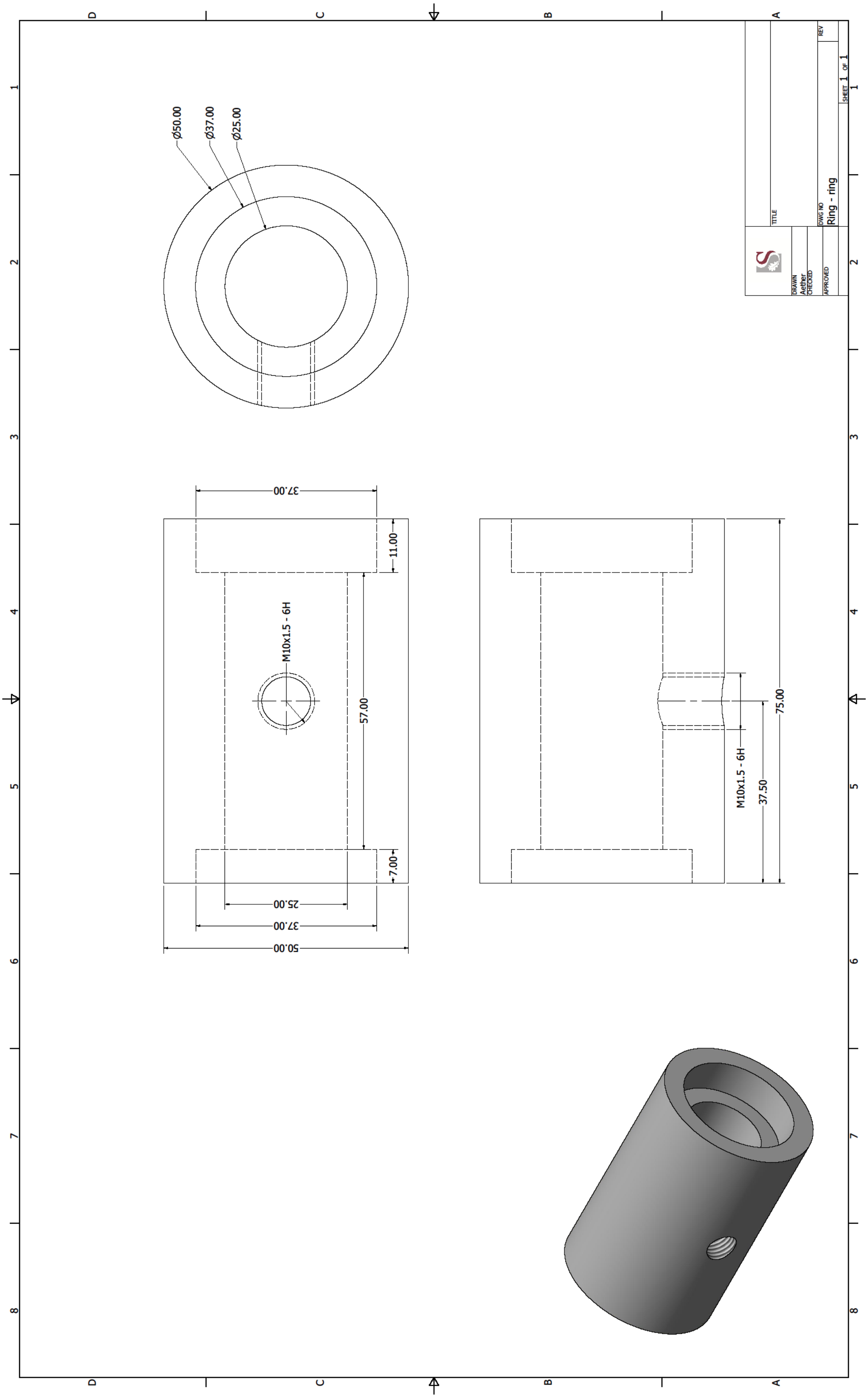

D.5.6.4 Cell Flange

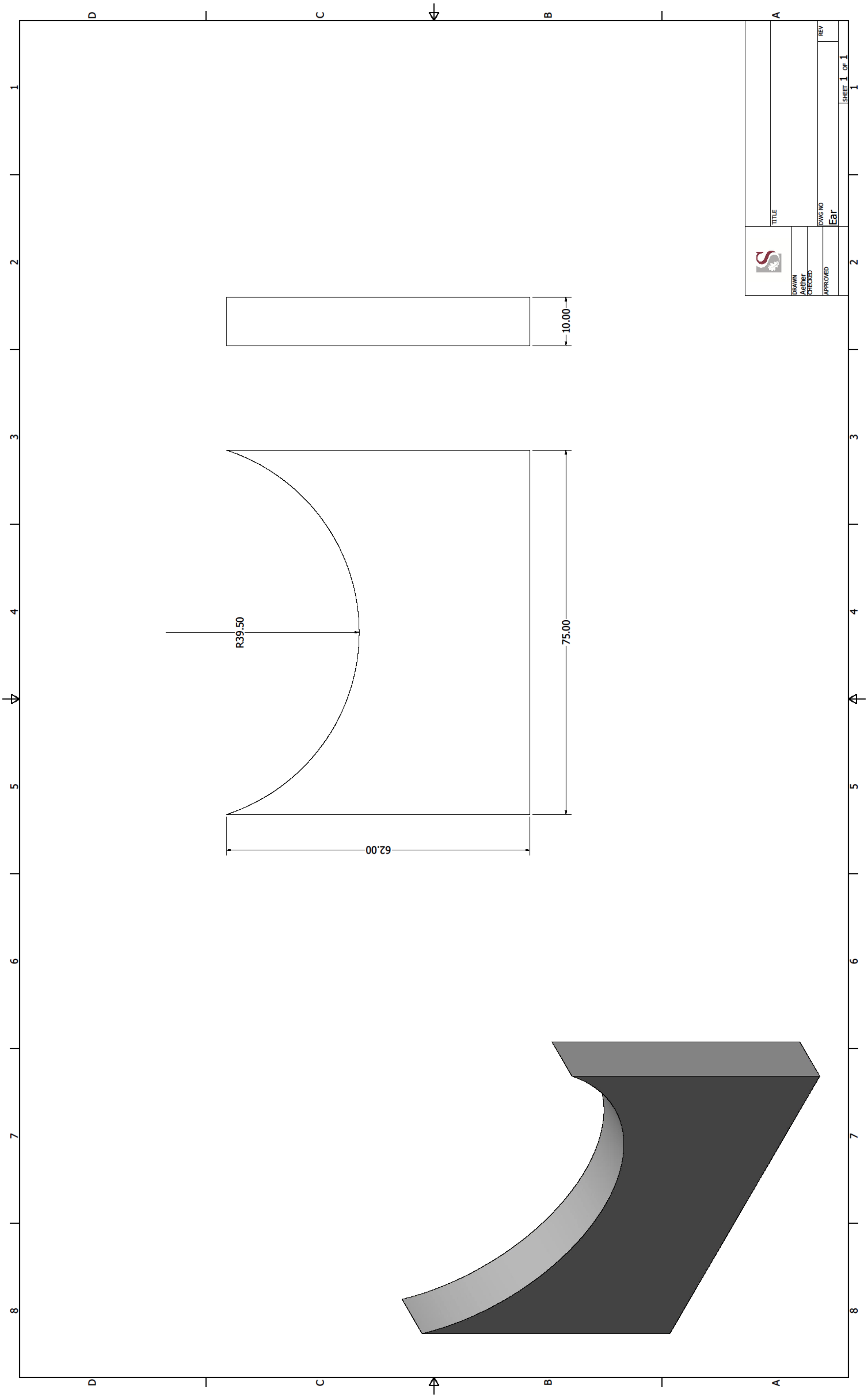

D.5.6.5 Cell Rod

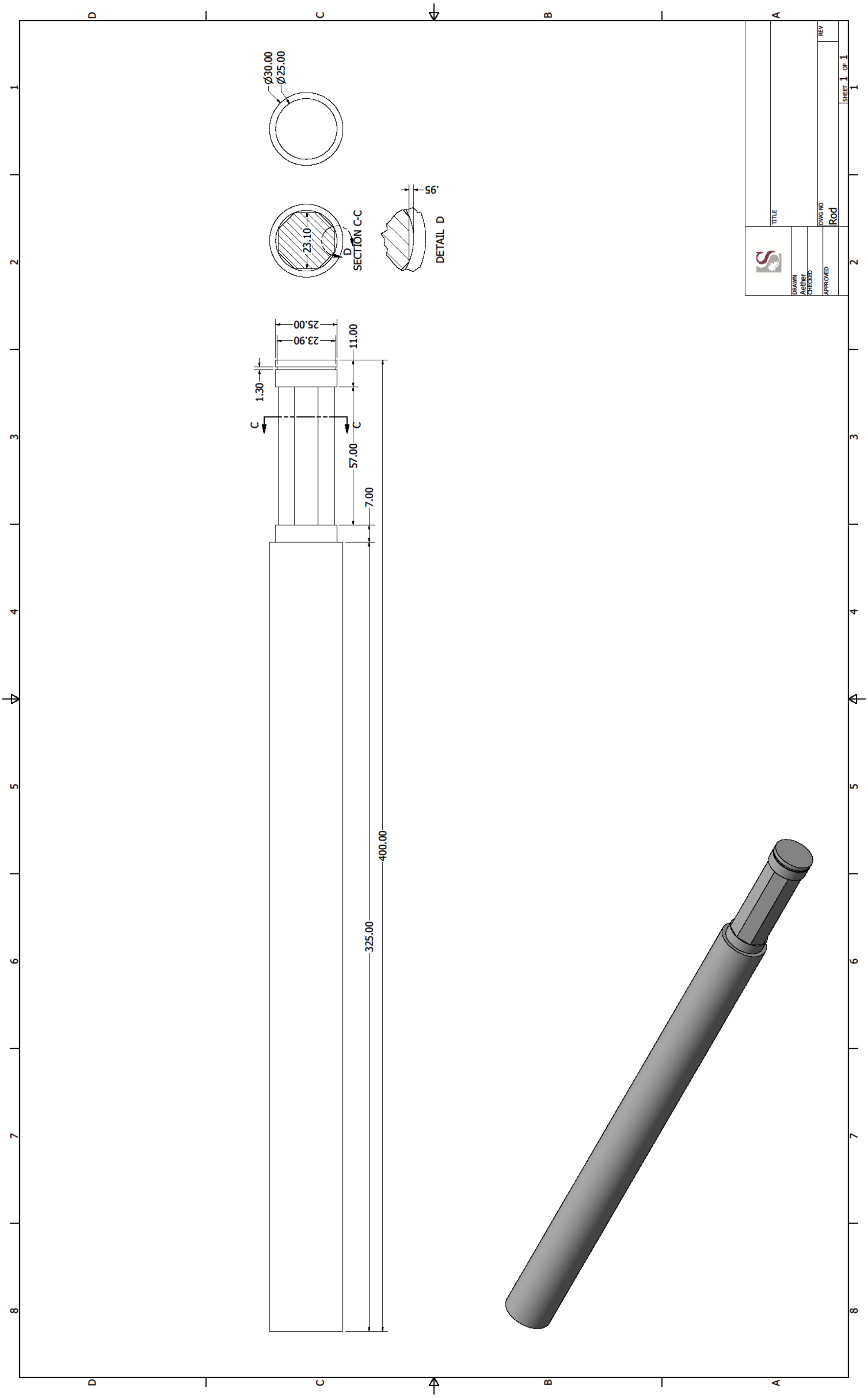

D.5.6.6 Assembled Stand

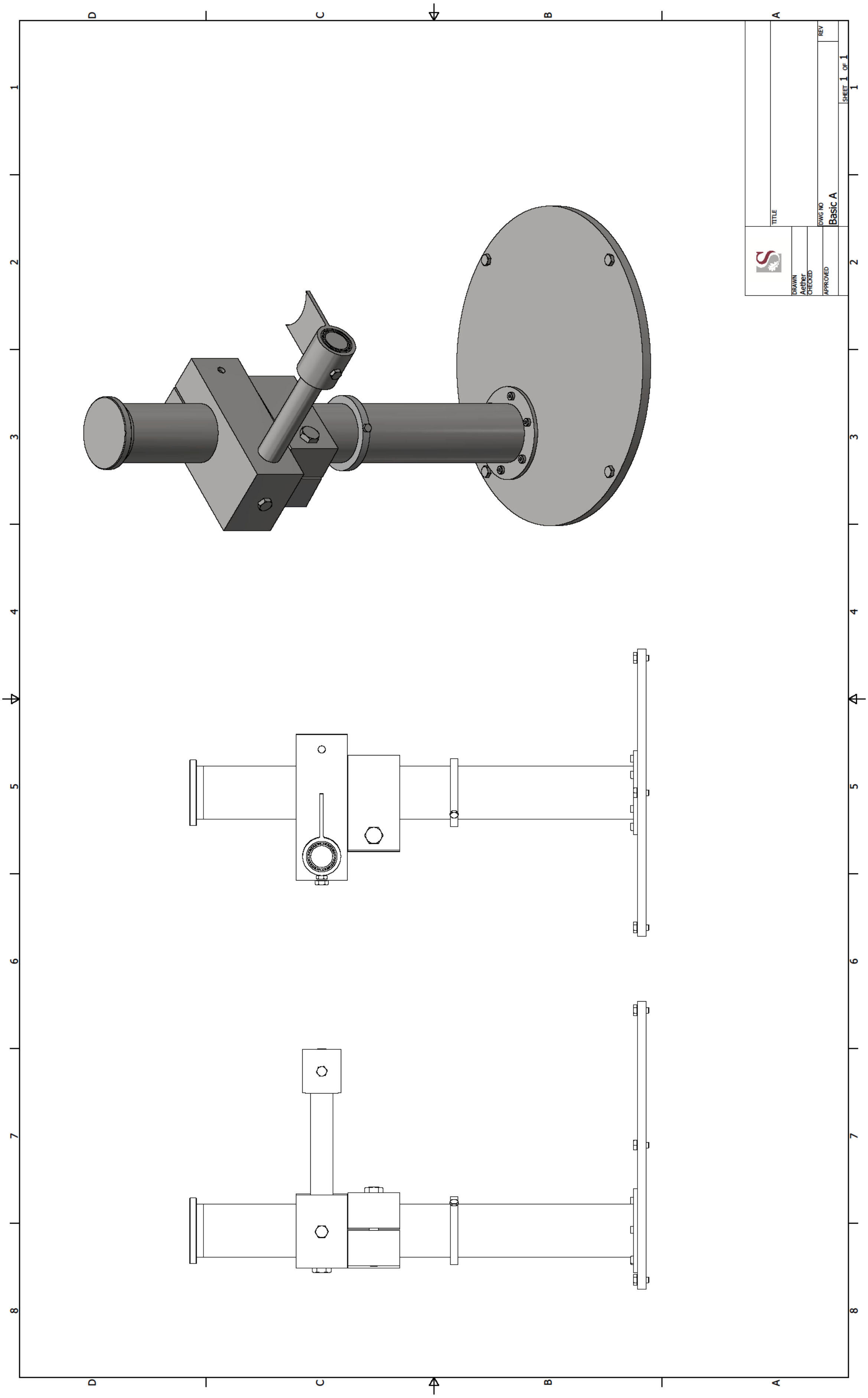

D.5.6.7 Assembled Stand and Cell

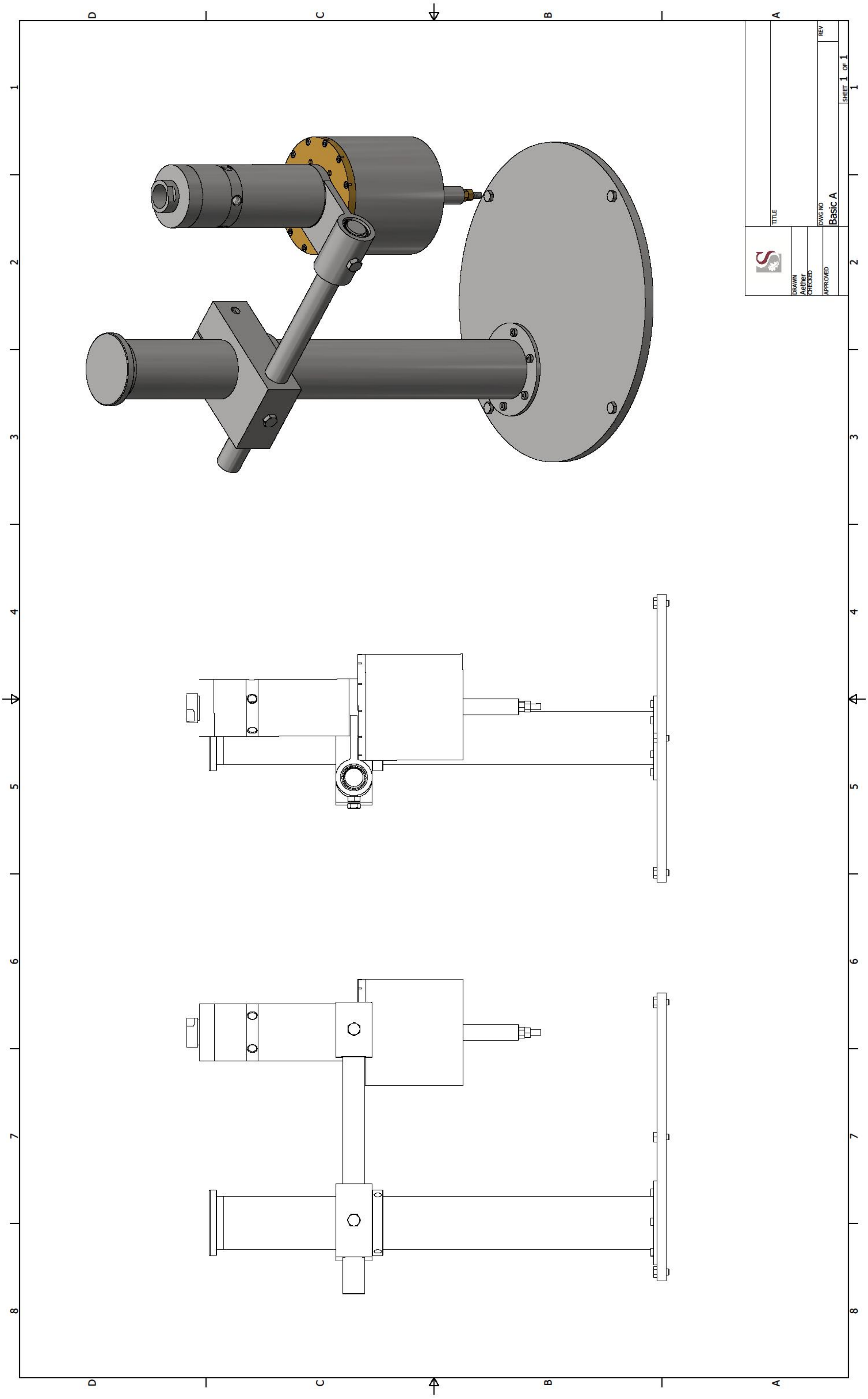

D.5.7 Temperature Control

The high pressure barrel of the cell is kept at thermal equilibrium using a high flow hot water bath. The high pressure barrel of the cell is jacketed, with the liquid in direct contact with the barrel to ensure sufficient heat transfer. As per the SWP in Appendix B.3.4, the cell is checked for thermal equilibrium.

Thermal equilibrium of the cell is measured through two temperature probes (calibration data available D.5.8.1) and is indicated by a stable temperature reading. Typically the cell takes between 30 to 45 minutes to achieve equilibrium. Due to the high mass of the cell and the excellent heating capacity of the bath, the cell shows good thermal stability, even when pressurising or depressurising the contents. Active stirring in the cell is done through a magnetic stirring bar, driven by the setup described in Section D.10, to ensure uniform thermal gradients in the liquid.

Specifications:

Hot Water bath:	Thermo Haake DL3
Heating Duty:	2 kW
Flow Rate:	17 l/min
Temperature accuracy:	± 0.02 K
Water reservoir volume:	~45 l

D.5.8 Measurement and Calibration Data

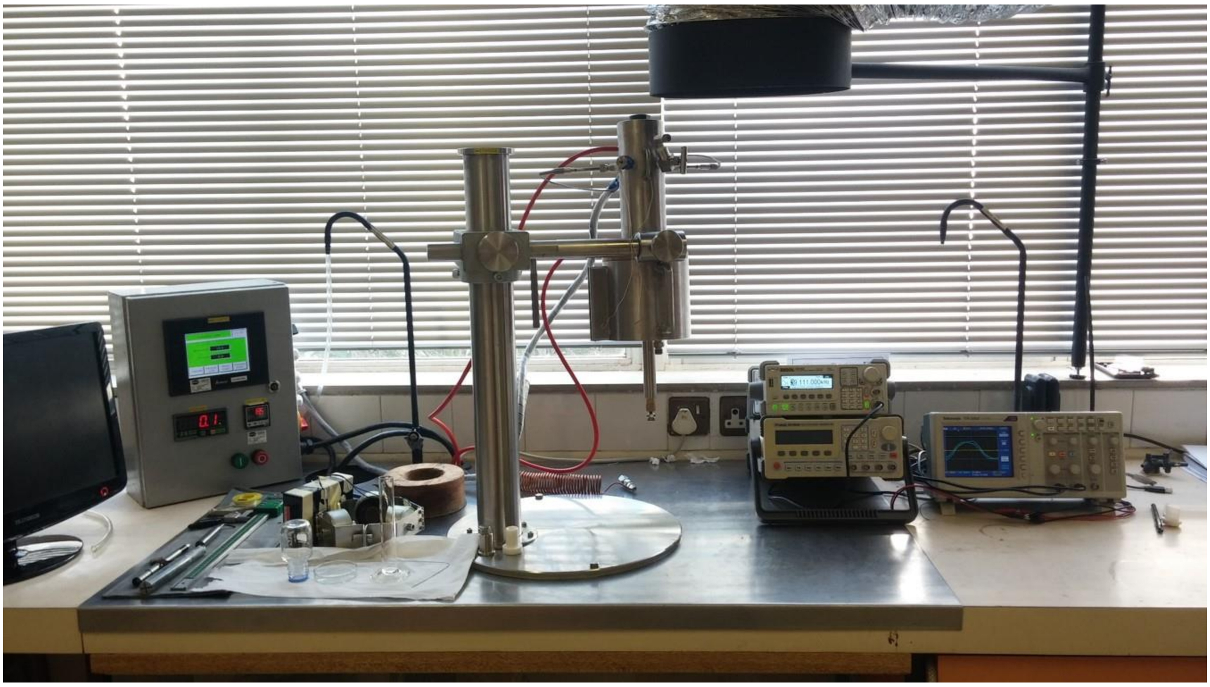

Figure D- 5: Finished high-pressure cell assembly – Note the PLC setup on the left.

Temperature and pressure are logged using a Delta PLC and HMI setup. Temperature is calibrated by a 3rd Party, while pressure is calibrated in-house. The mass loaded into the cells is weighed using two scales, calibrated by a 3rd party. The cell volume is measured using a height gauge, with the volume calibrated using a known mass of CO_2.

Each of the calibrations, with relevant certificates and/or data, is presented in this section.

D.5.8.1. Temperature Calibration 348

  D.5.8.1.1. Temperature Probe Calibration Certificates – Probe 1 349

  D.5.8.1.2. Temperature Probe Calibration Certificates – Probe 2 352

D.5.8.2. Pressure Calibration 355

  D.5.8.2.1. Dead Weight Tester Calibration Certificate 358

D.5.8.3. Mass Calibration 362

D.5.8.4. Volume Calibration 364

D.5.8.5. Crystal Calibration 367

  D.5.8.5.1. Vacuum Calibration – Temperature Dependence 367

  D.5.8.5.2. Electromechanical Constant Determination 368

D.5.8.1 Temperature Calibrations

Temperature is measured using two identical 4-wire PT 100 probes, sourced from WIKA Instruments. Both probes are directly in contact with the fluid medium, with one probe slightly protruding into the cell and the other slightly recessed. The probes are calibrated yearly to a standard uncertainty of <0.2 K by Thermon South Africa (Pty) Ltd., a SANAS and ISO 17011:2004; ISO 9001:2008 accredited temperature metrology laboratory. The Calibration certificates are found in Section D.5.7.1.1 and D.5.7.1.2 below

D.5.8.1.1 Temperature Probe Calibration Certificates – Probe 1 (Display)

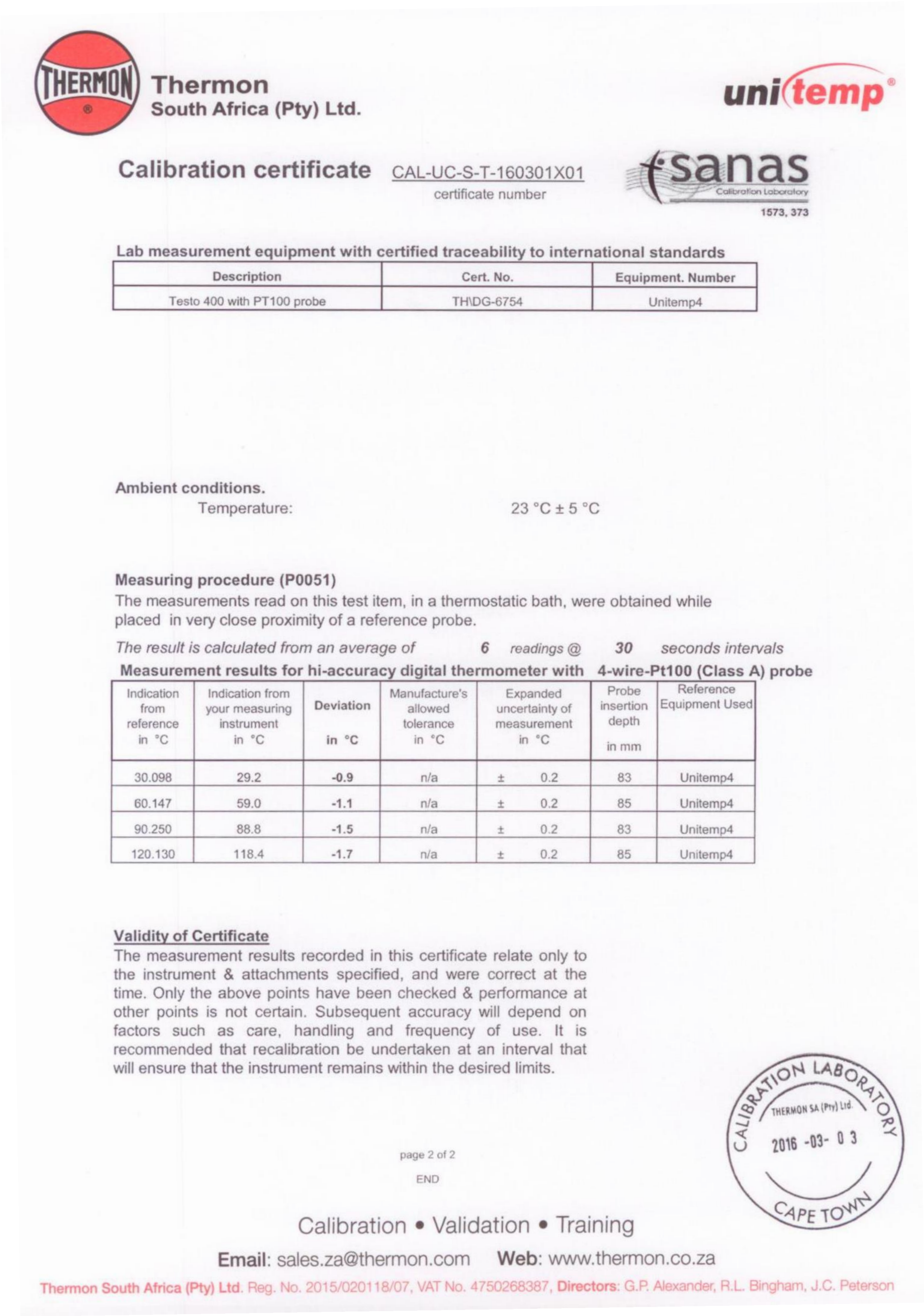

Thermon
South Africa (Pty) Ltd.

unitemp®

Calibration certificate

CAL-UC-S-T-160301X01
certificate number

sanas
Calibration Laboratory
1573, 373

Lab measurement equipment with certified traceability to international standards

Description	Cert. No.	Equipment. Number
Testo 400 with PT100 probe	TH\DG-6754	Unitemp4

Ambient conditions.

Temperature: 23 °C ± 5 °C

Measuring procedure (P0051)

The measurements read on this test item, in a thermostatic bath, were obtained while placed in very close proximity of a reference probe.

The result is calculated from an average of 6 *readings @* 30 *seconds intervals*

Measurement results for hi-accuracy digital thermometer with 4-wire-Pt100 (Class A) probe

Indication from reference in °C	Indication from your measuring instrument in °C	**Deviation in °C**	Manufacture's allowed tolerance in °C	Expanded uncertainty of measurement in °C	Probe insertion depth in mm	Reference Equipment Used
30.098	29.2	**-0.9**	n/a	± 0.2	83	Unitemp4
60.147	59.0	**-1.1**	n/a	± 0.2	85	Unitemp4
90.250	88.8	**-1.5**	n/a	± 0.2	83	Unitemp4
120.130	118.4	**-1.7**	n/a	± 0.2	85	Unitemp4

Validity of Certificate

The measurement results recorded in this certificate relate only to the instrument & attachments specified, and were correct at the time. Only the above points have been checked & performance at other points is not certain. Subsequent accuracy will depend on factors such as care, handling and frequency of use. It is recommended that recalibration be undertaken at an interval that will ensure that the instrument remains within the desired limits.

CALIBRATION LABORATORY
THERMON SA (Pty) Ltd.
2016 -03- 0 3
CAPE TOWN

page 2 of 2

END

Calibration • Validation • Training

Email: sales.za@thermon.com **Web:** www.thermon.co.za

Thermon South Africa (Pty) Ltd. Reg. No. 2015/020118/07, VAT No. 4750268387, **Directors:** G.P. Alexander, R.L. Bingham, J.C. Peterson

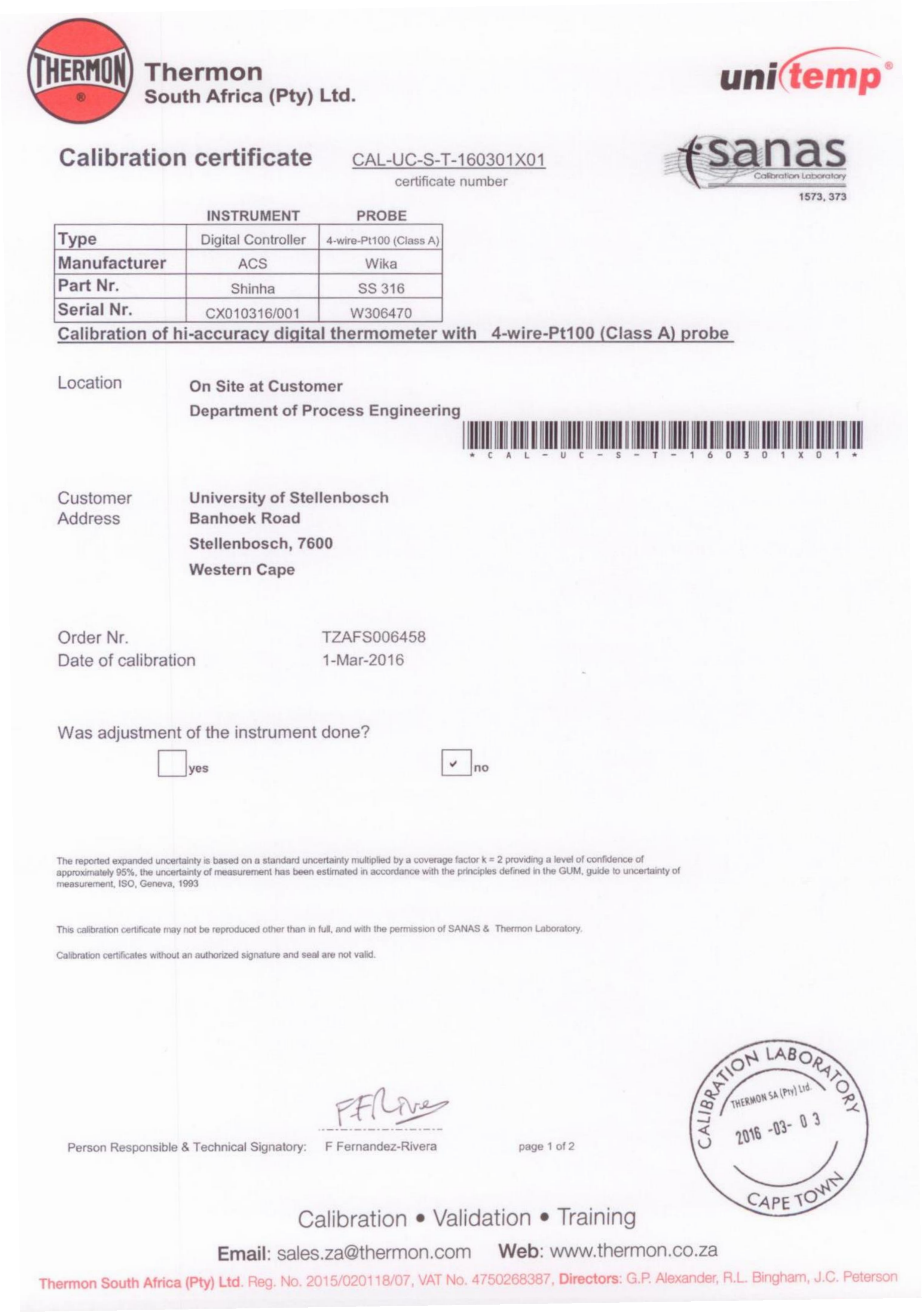

Thermon
South Africa (Pty) Ltd.

unitemp®

sanas
Calibration Laboratory
1573, 373

Calibration certificate

CAL-UC-S-T-160301X01
certificate number

	INSTRUMENT	PROBE
Type	Digital Controller	4-wire-Pt100 (Class A)
Manufacturer	ACS	Wika
Part Nr.	Shinha	SS 316
Serial Nr.	CX010316/001	W306470

Calibration of hi-accuracy digital thermometer with 4-wire-Pt100 (Class A) probe

Location
On Site at Customer
Department of Process Engineering

CAL-UC-S-T-160301X01

Customer Address
University of Stellenbosch
Banhoek Road
Stellenbosch, 7600
Western Cape

Order Nr. TZAFS006458
Date of calibration 1-Mar-2016

Was adjustment of the instrument done?

☐ yes ☑ no

The reported expanded uncertainty is based on a standard uncertainty multiplied by a coverage factor k = 2 providing a level of confidence of approximately 95%, the uncertainty of measurement has been estimated in accordance with the principles defined in the GUM, guide to uncertainty of measurement, ISO, Geneva, 1993

This calibration certificate may not be reproduced other than in full, and with the permission of SANAS & Thermon Laboratory.

Calibration certificates without an authorized signature and seal are not valid.

Person Responsible & Technical Signatory: F Fernandez-Rivera page 1 of 2

CALIBRATION LABORATORY
THERMON SA (Pty) Ltd.
2016 -03- 03
CAPE TOWN

Calibration • Validation • Training

Email: sales.za@thermon.com **Web:** www.thermon.co.za

Thermon South Africa (Pty) Ltd. Reg. No. 2015/020118/07, VAT No. 4750268387, **Directors:** G.P. Alexander, R.L. Bingham, J.C. Peterson

Thermon South Africa (Pty) Ltd. - Cape Lab

Temperature Insertion Probe Calibration Protocol

Dept: Process Engineering

Date:	1-3-2016	Company Name:	University of Stellenbosch
I/O No:	TZAFS006458	Cert.no:	CAL-UGS-T-160301X01
Person Responsible:		Francisco FE	
Ambient Conditions:	21.3 °C	— %RH	
Instrument:	Digital Controller	Probe:	4-wire-Pt100 A (100mm)
PART NUMBER:	ACS	PART NUMBER	SS 316
SERIAL NUMBER:	CX010316/001	SERIAL NUMBER:	W306470
MANUFACTURER:	Shinha	MANUFACTURER:	Wika

FY
2-3-201

AMETHYSTOS

Measuring Point (°C)			Reference value (°C)	Measured value (°C)	Info
30	°C	1	30.085	29.2	
0.1	Resolution	2	30.076	29.1	
	Accuracy	3	30.071	29.1	
4	Reference		30.070	29.2	
24LI	Bath		30.073	29.2	
			30.074	29.1	
60	°C	1	60.125	59.0	
0.1	Resolution	2	60.135	59.0	
	Accuracy	3	60.121	58.9	
4	Reference		60.119	58.9	
24LI	Bath		60.120	58.9	
			60.126	59.0	
90	°C	1	90.219	88.8	
0.1	Resolution	2	90.222	88.7	
	Accuracy	3	90.218	88.8	
4	Reference		90.234	88.8	
24LI	Bath		90.231	88.7	
			90.246	88.7	
120	°C	1	120.107	118.4	
0.1	Resolution	2	120.118	118.4	
	Accuracy	3	120.109	118.4	
4	Reference		120.105	118.4	
24LI	Bath		120.106	118.5	
			120.113	118.4	

Immersion depth (mm)	Temp. (° C)
83	30
85	60
83	90
85	120

D.5.8.1.2 Temperature Probe Calibration Certificates – Probe 2 (PLC)

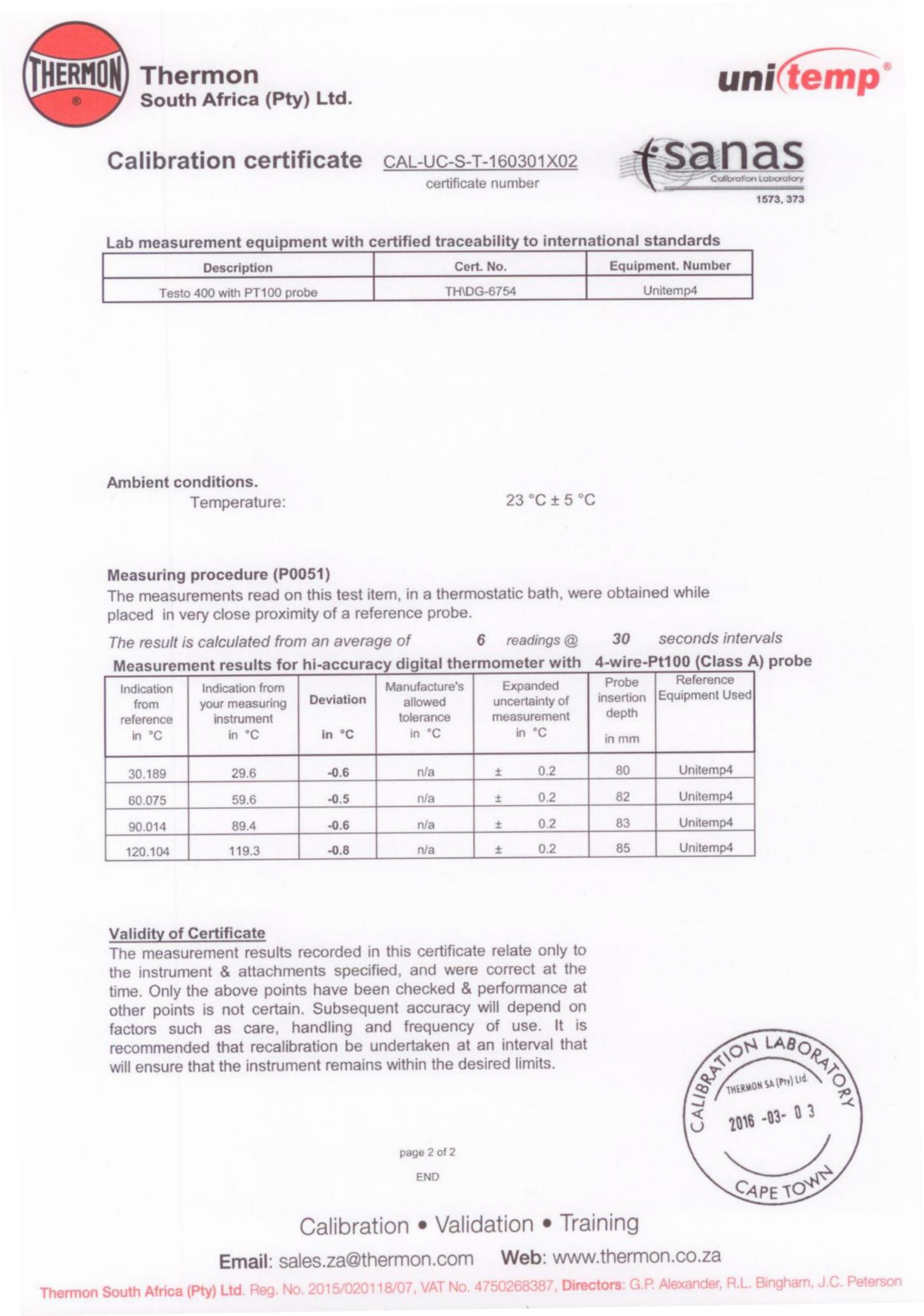

Thermon
South Africa (Pty) Ltd.

unitemp®

Calibration certificate CAL-UC-S-T-160301X02
certificate number

sanas
Calibration Laboratory
1573, 373

Lab measurement equipment with certified traceability to international standards

Description	Cert. No.	Equipment. Number
Testo 400 with PT100 probe	TH\DG-6754	Unitemp4

Ambient conditions.
Temperature: 23 °C ± 5 °C

Measuring procedure (P0051)
The measurements read on this test item, in a thermostatic bath, were obtained while placed in very close proximity of a reference probe.

The result is calculated from an average of ***6*** *readings @* ***30*** *seconds intervals*

Measurement results for hi-accuracy digital thermometer with 4-wire-Pt100 (Class A) probe

Indication from reference in °C	Indication from your measuring instrument in °C	**Deviation in °C**	Manufacture's allowed tolerance in °C	Expanded uncertainty of measurement in °C	Probe insertion depth in mm	Reference Equipment Used
30.189	29.6	**-0.6**	n/a	± 0.2	80	Unitemp4
60.075	59.6	**-0.5**	n/a	± 0.2	82	Unitemp4
90.014	89.4	**-0.6**	n/a	± 0.2	83	Unitemp4
120.104	119.3	**-0.8**	n/a	± 0.2	85	Unitemp4

Validity of Certificate
The measurement results recorded in this certificate relate only to the instrument & attachments specified, and were correct at the time. Only the above points have been checked & performance at other points is not certain. Subsequent accuracy will depend on factors such as care, handling and frequency of use. It is recommended that recalibration be undertaken at an interval that will ensure that the instrument remains within the desired limits.

CALIBRATION LABORATORY
THERMON SA (Pty) Ltd.
2016 -03- 03
CAPE TOWN

page 2 of 2
END

Calibration • Validation • Training

Email: sales.za@thermon.com **Web:** www.thermon.co.za

Thermon South Africa (Pty) Ltd. Reg. No. 2015/020118/07, VAT No. 4750268387, **Directors:** G.P. Alexander, R.L. Bingham, J.C. Peterson

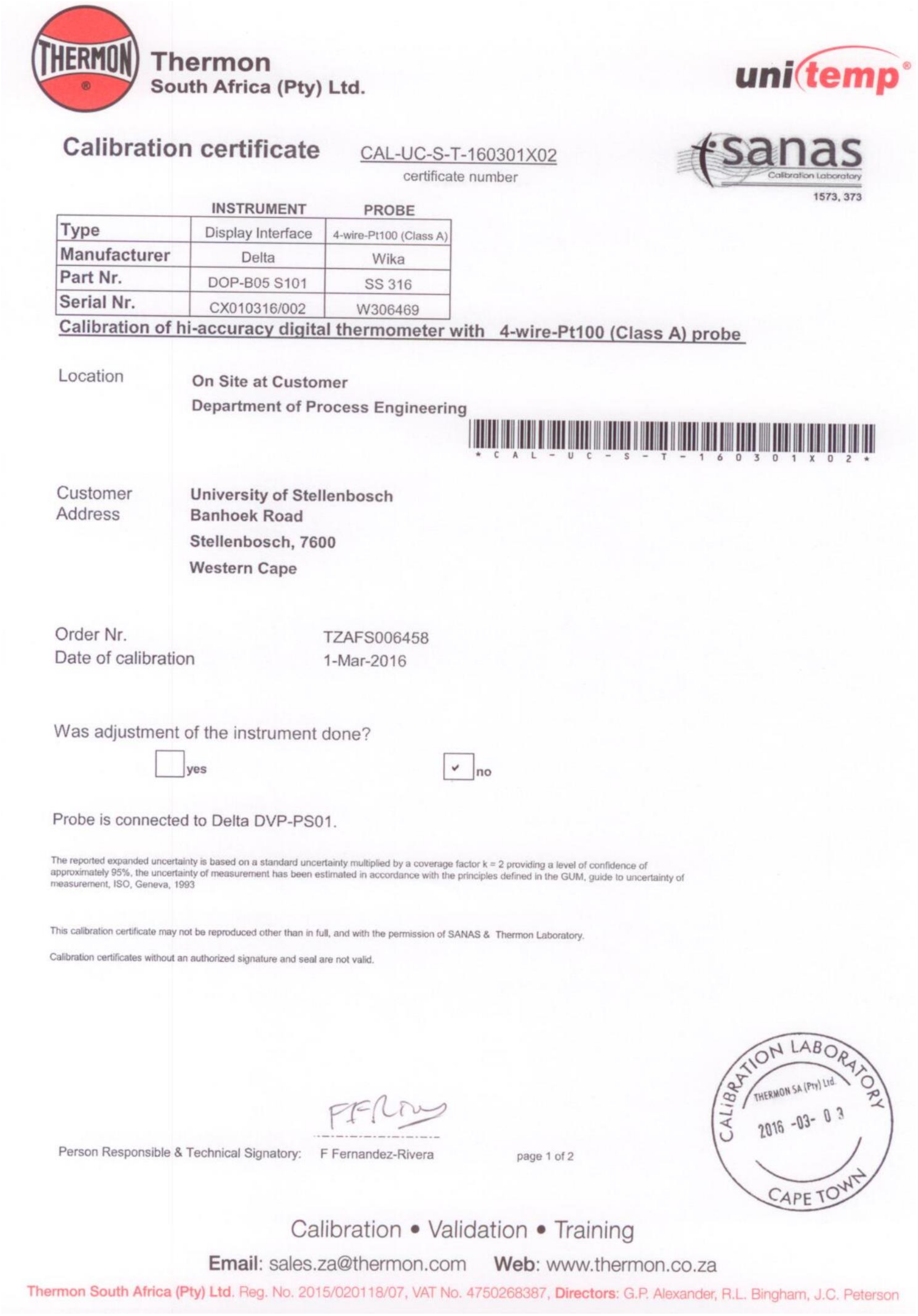

Thermon
South Africa (Pty) Ltd.

unitemp

sanas
Calibration Laboratory
1573, 373

Calibration certificate

CAL-UC-S-T-160301X02
certificate number

	INSTRUMENT	PROBE
Type	Display Interface	4-wire-Pt100 (Class A)
Manufacturer	Delta	Wika
Part Nr.	DOP-B05 S101	SS 316
Serial Nr.	CX010316/002	W306469

Calibration of hi-accuracy digital thermometer with 4-wire-Pt100 (Class A) probe

Location **On Site at Customer**
Department of Process Engineering

CAL-UC-S-T-160301X02

Customer Address
University of Stellenbosch
Banhoek Road
Stellenbosch, 7600
Western Cape

Order Nr. TZAFS006458
Date of calibration 1-Mar-2016

Was adjustment of the instrument done?

☐ yes ☑ no

Probe is connected to Delta DVP-PS01.

The reported expanded uncertainty is based on a standard uncertainty multiplied by a coverage factor k = 2 providing a level of confidence of approximately 95%, the uncertainty of measurement has been estimated in accordance with the principles defined in the GUM, guide to uncertainty of measurement, ISO, Geneva, 1993

This calibration certificate may not be reproduced other than in full, and with the permission of SANAS & Thermon Laboratory.

Calibration certificates without an authorized signature and seal are not valid.

Person Responsible & Technical Signatory: F Fernandez-Rivera page 1 of 2

CALIBRATION LABORATORY
THERMON SA (Pty) Ltd.
2016 -03- 03
CAPE TOWN

Calibration • Validation • Training

Email: sales.za@thermon.com **Web:** www.thermon.co.za

Thermon South Africa (Pty) Ltd. Reg. No. 2015/020118/07, VAT No. 4750268387, **Directors:** G.P. Alexander, R.L. Bingham, J.C. Peterson

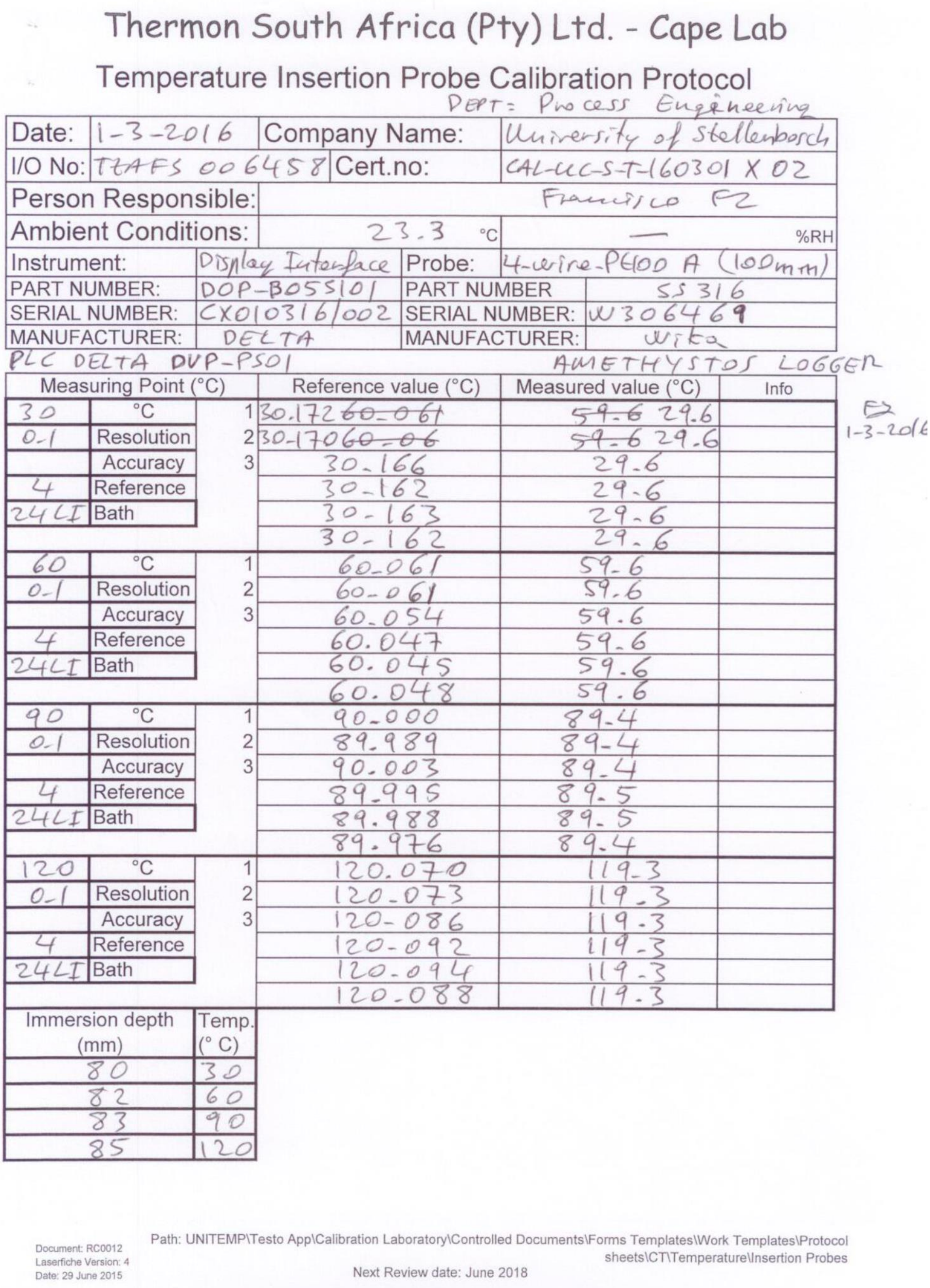

Thermon South Africa (Pty) Ltd. - Cape Lab

Temperature Insertion Probe Calibration Protocol

DEPT= Process Engineering

Date:	1-3-2016	Company Name:	University of Stellenbosch
I/O No:	TZAFS 006458	Cert.no:	CAL-UC-S-T-160301 X 02
Person Responsible:		Francisco FZ	
Ambient Conditions:	23.3 °C	— %RH	
Instrument:	Display Interface	Probe:	4-wire-Pt100 A (100mm)
PART NUMBER:	DOP-B05S101	PART NUMBER	SS 316
SERIAL NUMBER:	CX010316/002	SERIAL NUMBER:	W306469
MANUFACTURER:	DELTA	MANUFACTURER:	Wika

PLC DELTA DVP-PS01

AMETHYSTOS LOGGER

Measuring Point (°C)			Reference value (°C)	Measured value (°C)	Info
30	°C	1	30.172 ~~60.061~~	~~59.6~~ 29.6	
0.1	Resolution	2	30.170 ~~60.06~~	~~59.6~~ 29.6	
	Accuracy	3	30.166	29.6	
4	Reference		30.162	29.6	
24LI	Bath		30.163	29.6	
			30.162	29.6	
60	°C	1	60.061	59.6	
0.1	Resolution	2	60.061	59.6	
	Accuracy	3	60.054	59.6	
4	Reference		60.047	59.6	
24LI	Bath		60.045	59.6	
			60.048	59.6	
90	°C	1	90.000	89.4	
0.1	Resolution	2	89.989	89.4	
	Accuracy	3	90.003	89.4	
4	Reference		89.995	89.5	
24LI	Bath		89.988	89.5	
			89.976	89.4	
120	°C	1	120.070	119.3	
0.1	Resolution	2	120.073	119.3	
	Accuracy	3	120.086	119.3	
4	Reference		120.092	119.3	
24LI	Bath		120.094	119.3	
			120.088	119.3	

FZ
1-3-2016

Immersion depth (mm)	Temp. (° C)
80	30
82	60
83	90
85	120

Document: RC0012
Laserfiche Version: 4
Date: 29 June 2015

Path: UNITEMP\Testo App\Calibration Laboratory\Controlled Documents\Forms Templates\Work Templates\Protocol sheets\CT\Temperature\Insertion Probes

Next Review date: June 2018

D.5.8.2 Pressure Calibration

Pressure is measured using an ONEhalf20 melt pressure transducer, model number: CT6MA-DLX-3.5CB. The pressure sensor is calibrated to a standard uncertainty of 0.02 MPa after each full experimental set, using a Barnett Industrial deadweight tester. The Barnett tester is calibrated to a standard uncertainty smaller than 0.01 MPa by Unique Metrology (Pty) Ltd. [a SANAS (South African National Accreditation System) accredited pressure metrology laboratory]. The deadweight tester pressure calibration is presented in Section D.5.7.2.1. The combined uncertainty is at worst 0.06 MPa of the phase equilibria pressure measurements considering all errors, including repeatability, sensor hysteresis, and human error.

For the sake of brevity, only the last calibration is shown here, with the raw data available in Table D- 1. For each sensor reading, a calibration curve is created. The calibration curve is used during experiments to correct the reading. These curves are always found to be perfectly linear, agreeing with the sensor's specifications. An example of a calibration curve is seen below in Figure D- 6.

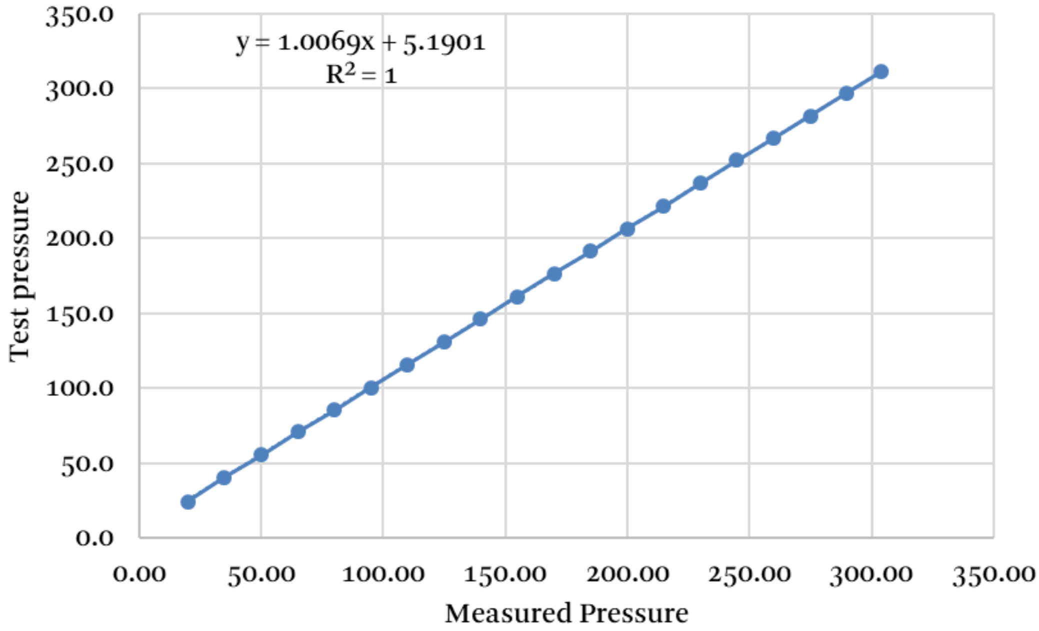

Figure D- 6: Example pressure calibration curve. PLC reading at 40 °C

Table D- 1: Pressure calibration data

	Temperature				Pressure					
Cum. weight	T SetP	T Cont	T PLC	T Avg	Pressure PLC	Pressure Ctrlr	Test Pressure	PCL P Error	Ctrlr P Error	Pressure Rel Error
1	39.8	39.81	40.2	40.00	24.5	24.2	19.99	-4.51	-4.21	-21.82%
2	39.8	39.81	40.3	40.10	40.7	40.3	34.97	-5.73	-5.33	-15.80%
3	39.8	39.81	40.3	40.10	55.8	55.4	49.96	-5.84	-5.44	-11.29%
4	39.8	39.81	40.3	40.10	71.0	70.5	64.95	-6.05	-5.55	-8.94%
5	39.8	39.71	40.3	40.00	85.5	85.4	79.93	-5.57	-5.47	-6.91%
6	39.8	39.81	40.3	40.10	100.5	100.5	94.91	-5.59	-5.59	-5.88%
7	39.8	39.81	40.3	40.10	115.7	115.7	109.90	-5.80	-5.80	-5.28%
8	39.8	39.81	40.3	40.10	130.8	130.7	124.88	-5.92	-5.82	-4.70%
9	39.8	39.81	40.3	40.10	146.0	146.1	139.87	-6.13	-6.23	-4.42%
10	39.8	39.81	40.3	40.10	161.2	161.3	154.85	-6.35	-6.45	-4.13%
11	39.8	39.81	40.3	40.10	176.5	176.6	169.83	-6.67	-6.77	-3.95%
12	39.8	39.81	40.3	40.10	191.6	191.7	184.82	-6.78	-6.88	-3.70%
13	39.8	39.81	40.3	40.10	206.5	206.7	199.80	-6.70	-6.90	-3.40%
14	39.8	39.81	40.3	40.10	221.5	221.8	214.79	-6.71	-7.01	-3.20%
15	39.8	39.81	40.3	40.10	236.8	237.1	229.77	-7.03	-7.33	-3.13%
16	39.8	39.81	40.3	40.10	252.0	252.3	244.75	-7.25	-7.55	-3.02%
17	39.8	39.81	40.3	40.10	266.4	267.0	259.73	-6.67	-7.27	-2.68%
18	39.8	39.81	40.3	40.10	281.5	282.2	274.72	-6.78	-7.48	-2.60%
19	39.8	39.81	40.3	40.10	296.7	297.4	289.70	-7.00	-7.70	-2.54%
ALL	39.8	39.81	40.3	40.10	310.8	311.6	303.68	-7.12	-7.92	-2.48%
1	61.3	59.68	60.2	59.94	27.7	27.2	19.99	-7.71	-7.21	-37.33%
2	61.3	59.68	60.2	59.94	42.9	42.6	34.97	-7.93	-7.63	-22.23%
3	61.3	59.68	60.2	59.94	58.0	57.4	49.96	-8.04	-7.44	-15.49%
4	61.3	59.68	60.2	59.94	73.0	72.6	64.95	-8.05	-7.65	-12.09%
5	61.3	59.78	60.3	60.04	87.7	87.4	79.93	-7.77	-7.47	-9.53%
6	61.3	59.78	60.3	60.04	103.0	102.8	94.91	-8.09	-7.89	-8.41%
7	61.3	59.78	60.3	60.04	118.0	117.8	109.90	-8.10	-7.90	-7.28%
8	61.3	59.78	60.3	60.04	129.9	132.8	124.88	-5.02	-7.92	-5.18%
9	61.3	59.78	60.3	60.04	148.1	148.0	139.87	-8.23	-8.13	-5.85%
10	61.3	59.78	60.3	60.04	163.3	163.2	154.85	-8.45	-8.35	-5.42%
11	61.3	59.78	60.3	60.04	178.5	178.5	169.83	-8.67	-8.67	-5.10%
12	61.3	59.78	60.3	60.04	193.6	193.6	184.82	-8.78	-8.78	-4.75%
13	61.3	59.78	60.3	60.04	208.8	208.9	199.80	-9.00	-9.10	-4.53%
14	61.3	59.78	60.3	60.04	224.0	224.1	214.79	-9.21	-9.31	-4.31%
15	61.3	59.78	60.3	60.04	238.9	239.0	229.77	-9.13	-9.23	-4.00%
16	60.8	59.88	60.4	60.14	253.3	253.9	244.75	-8.55	-9.15	-3.62%
17	60.8	59.78	60.3	60.04	267.6	268.5	259.73	-7.87	-8.77	-3.20%
18	60.8	59.78	60.3	60.04	282.8	283.7	274.72	-8.08	-8.98	-3.11%
19	60.8	59.78	60.3	60.04	297.9	298.8	289.70	-8.20	-9.10	-2.99%
ALL	60.8	59.78	60.3	60.04	311.8	312.8	303.68	-8.12	-9.12	-2.84%

Continued on next page...

	Temperature				Pressure					
Cum. weight	T SetP	T Cont	T PLC	T Avg	Pressure PLC	Pressure Ctrlr	Test Pressure	PCL P Error	Ctrlr P Error	Pressure Rel Error
1	82.2	80.77	79.4	80.09	29.4	28.8	19.99	-9.41	-8.81	-45.58%
2	82.2	80.77	79.4	80.09	44.0	43.7	34.97	-9.03	-8.73	-25.38%
3	82.2	80.77	79.3	80.04	59.4	58.7	49.96	-9.44	-8.74	-18.19%
4	82.2	80.77	79.3	80.04	74.6	74.0	64.95	-9.65	-9.05	-14.40%
5	82.2	80.77	79.3	80.04	89.1	88.7	79.93	-9.17	-8.77	-11.22%
6	82.2	80.77	79.3	80.04	104.2	103.9	94.91	-9.29	-8.99	-9.62%
7	82.2	80.77	79.3	80.04	119.4	119.1	109.90	-9.50	-9.20	-8.51%
8	82.2	80.77	79.4	80.09	134.3	134.1	124.88	-9.42	-9.22	-7.46%
9	82.2	80.77	79.4	80.09	149.6	149.5	139.87	-9.73	-9.63	-6.92%
10	82.2	80.77	79.4	80.09	164.6	164.5	154.85	-9.75	-9.65	-6.26%
11	82.1	80.77	79.5	80.14	179.7	179.7	169.83	-9.87	-9.87	-5.81%
12	82	80.87	79.5	80.19	194.7	194.8	184.82	-9.88	-9.98	-5.37%
13	82	80.77	79.5	80.14	209.9	209.9	199.80	-10.10	-10.10	-5.05%
14	82	80.77	79.4	80.09	225.1	225.2	214.79	-10.31	-10.41	-4.83%
15	82	80.77	79.3	80.04	240.4	240.5	229.77	-10.63	-10.73	-4.65%
16	82.2	80.67	79.3	79.99	255.0	255.4	244.75	-10.25	-10.65	-4.27%
17	82.2	80.77	79.4	80.09	270.0	270.4	259.73	-10.27	-10.67	-4.03%
18	82.2	80.77	79.4	80.09	284.9	285.4	274.72	-10.18	-10.68	-3.80%
19	82.2	80.77	79.4	80.09	300.3	300.8	289.70	-10.60	-11.10	-3.75%
ALL	82.2	80.77	79.4	80.09	314.3	315.0	303.68	-10.62	-11.32	-3.61%

D.5.8.2.1 Dead Weight Tester Calibration Certificate

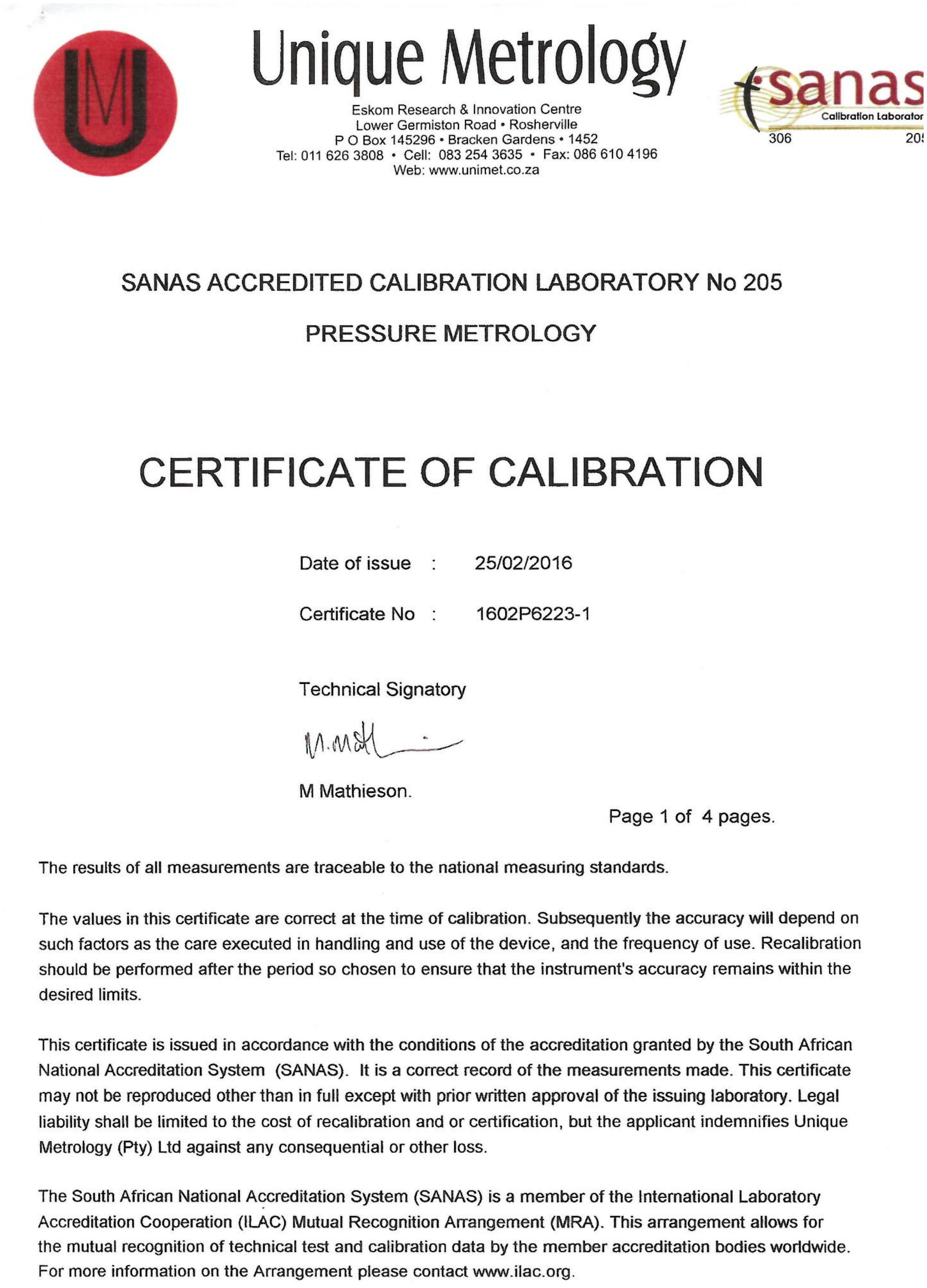

Unique Metrology
Eskom Research & Innovation Centre
Lower Germiston Road • Rosherville
P O Box 145296 • Bracken Gardens • 1452
Tel: 011 626 3808 • Cell: 083 254 3635 • Fax: 086 610 4196
Web: www.unimet.co.za

sanas
Calibration Laborator
306 20

SANAS ACCREDITED CALIBRATION LABORATORY No 205

PRESSURE METROLOGY

CERTIFICATE OF CALIBRATION

Date of issue : 25/02/2016

Certificate No : 1602P6223-1

Technical Signatory

M Mathieson.

Page 1 of 4 pages.

The results of all measurements are traceable to the national measuring standards.

The values in this certificate are correct at the time of calibration. Subsequently the accuracy will depend on such factors as the care executed in handling and use of the device, and the frequency of use. Recalibration should be performed after the period so chosen to ensure that the instrument's accuracy remains within the desired limits.

This certificate is issued in accordance with the conditions of the accreditation granted by the South African National Accreditation System (SANAS). It is a correct record of the measurements made. This certificate may not be reproduced other than in full except with prior written approval of the issuing laboratory. Legal liability shall be limited to the cost of recalibration and or certification, but the applicant indemnifies Unique Metrology (Pty) Ltd against any consequential or other loss.

The South African National Accreditation System (SANAS) is a member of the International Laboratory Accreditation Cooperation (ILAC) Mutual Recognition Arrangement (MRA). This arrangement allows for the mutual recognition of technical test and calibration data by the member accreditation bodies worldwide. For more information on the Arrangement please contact www.ilac.org.

Unique Metrology
Eskom Research & Innovation Centre
Lower Germiston Road • Rosherville
P O Box 145296 • Bracken Gardens • 1452
Tel: 011 626 3808 • Cell: 083 254 3635 • Fax: 086 610 4196
Web: www.unimet.co.za

sanas
Calibration Laboratory
306 205

CERTIFICATE OF CALIBRATION

Page 2 of 4 pages.

Certificate Number	:	1602P6223-1		
Calibration of a	:	Pressure Balance		
Manufacturer & Type	:	Barnetts		
Serial Number	:	3692/74		
Calibrated for	:	Stellenbosch University, Stellenbosch.		
Procedure Number	:	53-131		
Date of Calibration	:	25/02/2016		
Date of Issue	:	25/02/2016		
Laboratory Environment	:	20.3 °C		
Reference Standards	:	205-S-06	Budenberg 280D	S/N 27702
	:	205-S-07	Budenberg Mass Set	S/N 205-S-07
	:	205-S-10	Mass Set	S/N 1406-01
	:	205-S-11	Mass Set	S/N 1406-02

1. Procedure

The values of the pressure balance ring weights and of the weight of the piston assembly were determined by comparison against calibrated standard mass pieces.

The piston-cylinder assembly was balanced against a calibrated standard piston-cylinder assembly at several pressures within the normal working range. The effective area was determined and corrected to 20 °C assuming an increase in area of 22 ppm/°C rise in temperature.

2. Results

2.1 Weights

See next page for weight values.

Calibrated by : A Mathieson

Technical Signatory

Unique Metrology
Eskom Research & Innovation Centre
Lower Germiston Road • Rosherville
P O Box 145296 • Bracken Gardens • 1452
Tel: 011 626 3808 • Cell: 083 254 3635 • Fax: 086 610 4196
Web: www.unimet.co.za

sanas Calibration Laboratory
306 205

CERTIFICATE OF CALIBRATION

Page 3 of 4 pages.

Certificate Number : 1602P6223-1
Calibration of a : Pressure Balance
Manufacturer & Type : Barnetts

2.1 Weights (cont)

Component marked		Nominal Value (kg)	Value measured (kg)	Uncertainty of measurement (g)	Error %
150 kPa	1	1.23371	1.23389	0.07	0.015
150 kPa	2	1.23371	1.23391	0.07	0.016
150 kPa	3	1.23371	1.23394	0.07	0.019
150 kPa	4	1.23371	1.23388	0.07	0.014
150 kPa	5	1.23371	1.23386	0.07	0.012
150 kPa	6	1.23371	1.23393	0.07	0.018
150 kPa	7	1.23371	1.23383	0.07	0.010
150 kPa	8	1.23371	1.23392	0.07	0.017
150 kPa	9	1.23371	1.23385	0.07	0.011
150 kPa	10	1.23371	1.23392	0.07	0.017
150 kPa	11	1.23371	1.23389	0.07	0.015
150 kPa	12	1.23371	1.23395	0.07	0.019
150 kPa	13	1.23371	1.23392	0.07	0.017
150 kPa	14	1.23371	1.23391	0.07	0.016
150 kPa	15	1.23371	1.23388	0.07	0.014
150 kPa	16	1.23371	1.23384	0.07	0.010
150 kPa	17	1.23371	1.23388	0.07	0.014
150 kPa	18	1.23371	1.23388	0.07	0.014
150 kPa	19	1.23371	1.23386	0.07	0.012
50 kPa	1	0.411237	0.411342	0.024	0.026
50 kPa	2	0.411237	0.411383	0.024	0.036
10 kPa	1	0.082247	0.082282	0.006	0.042
10 kPa	2	0.082247	0.082286	0.006	0.047
10 kPa	3	0.082247	0.082275	0.006	0.034
10 kPa	4	0.082247	0.082278	0.006	0.037
Piston Assy		Unknown	0.411942	0.022	

M.Math

Technical Signatory

Calibrated by : A Mathieson

Unique Metrology
Eskom Research & Innovation Centre
Lower Germiston Road • Rosherville
P O Box 145296 • Bracken Gardens • 1452
Tel: 011 626 3808 • Cell: 083 254 3635 • Fax: 086 610 4196
Web: www.unimet.co.za

sanas
Calibration Laboratory
306 205

CERTIFICATE OF CALIBRATION

Certificate Number	:	1602P6223-1	Page 4 of 4 pages
Calibration of a	:	Pressure Balance	
Manufacturer & Type	:	Barnetts	

2.2 Piston-cylinder assembly

The effective area of the high-pressure piston-cylinder assembly was found to be expressible as

where
$A = A0(1 + ßP)$
$A0 = 8.0641 \pm 0.0070\ \text{mm}^2$
$ß = 3.92\text{E-}6 \pm 2.5\text{E-}6\ /\text{MPa}$
P is the pressure in MPa.
The nominal value is 8.0645 mm^2.

3. Accuracy of pressure measurement.

When the pressure balance is used with the weight set supplied and after making suitable corrections for gravity, temperature and air buoyancy the total error in pressure measurement (ie the deviation from the nominal value) does not exceed 0.04% above 2 MPa.

4. Notes

The reference level for the pressure measurements was taken to be the base of the piston's cylinder.
The oil used for the calibration was a mineral oil of nominal density 870 kg/cm^3.
The buoyancy volume was found to be negligible.

5. Uncertainty of Calibration

The reported uncertainty is based on a standard uncertainty multiplied by a coverage factor of k=2, which unless specifically stated otherwise, provides a confidence level of 95%, in accordance with the Guide to the expression of Uncertainty in Measurement, first edition, 1993.

6. Comments.

The weight set was marked with the serial number 3692/74.

Calibrated by : A Mathieson

Technical Signatory

D.5.8.3 Mass Calibration

Two scales were used during the experiments. The mass of the synthetic mixture loaded into the cell was weighed to within 0.0001 g for liquid samples and to within 0.001 g for the gas. The calibration certificates for both scales are found below.

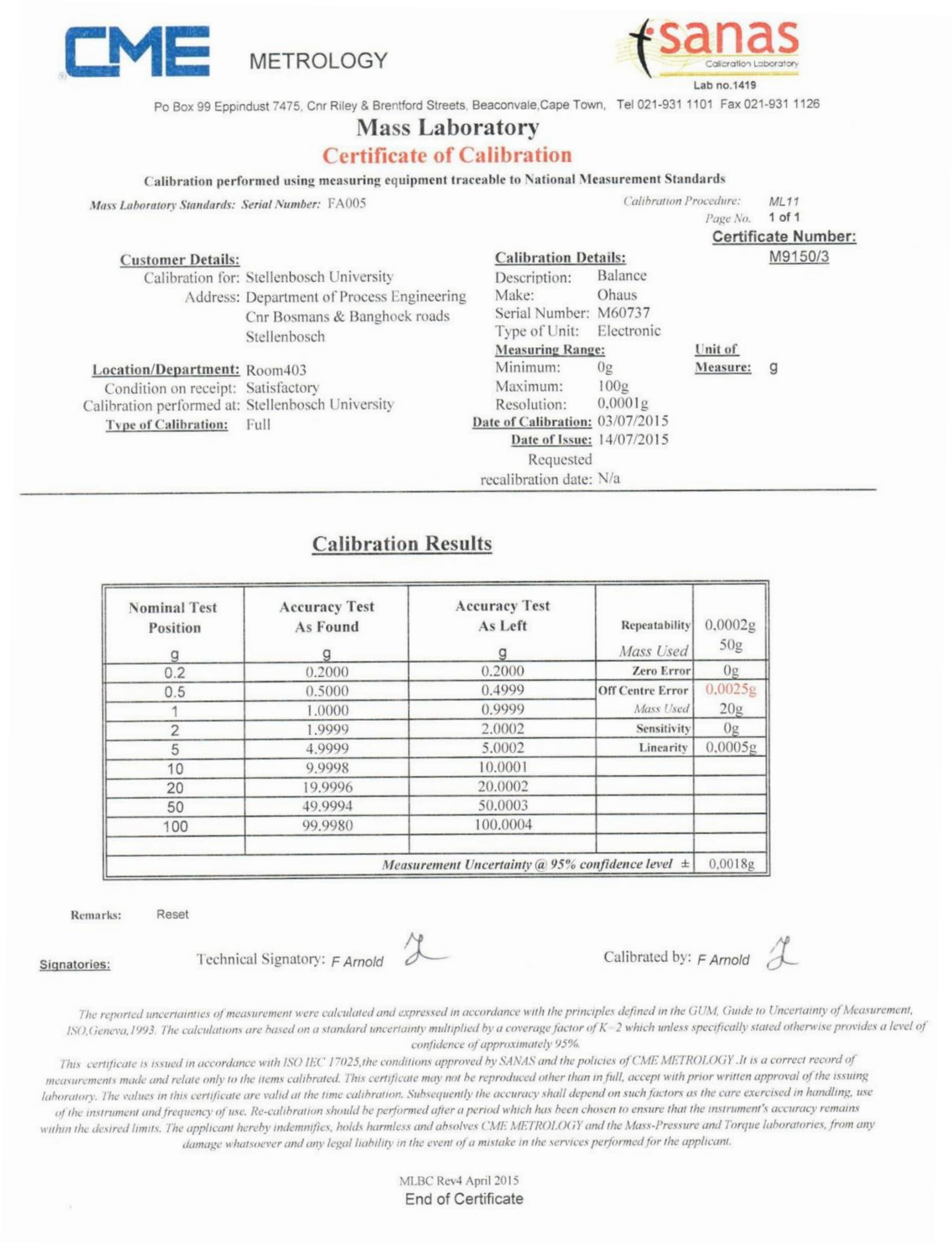

CME METROLOGY

sanas Calibration Laboratory
Lab no.1419

Po Box 99 Eppindust 7475, Cnr Riley & Brentford Streets, Beaconvale,Cape Town, Tel 021-931 1101 Fax 021-931 1126

Mass Laboratory

Certificate of Calibration

Calibration performed using measuring equipment traceable to National Measurement Standards

Mass Laboratory Standards: Serial Number: FA005

Calibration Procedure: ML11
Page No. 1 of 1

Certificate Number:
M9150/3

Customer Details:
Calibration for: Stellenbosch University
Address: Department of Process Engineering
Cnr Bosmans & Banghoek roads
Stellenbosch

Location/Department: Room403
Condition on receipt: Satisfactory
Calibration performed at: Stellenbosch University
Type of Calibration: Full

Calibration Details:
Description: Balance
Make: Ohaus
Serial Number: M60737
Type of Unit: Electronic
Measuring Range:
Minimum: 0g
Maximum: 100g
Resolution: 0,0001g
Unit of Measure: g
Date of Calibration: 03/07/2015
Date of Issue: 14/07/2015
Requested recalibration date: N/a

Calibration Results

Nominal Test Position g	Accuracy Test As Found g	Accuracy Test As Left g	Repeatability *Mass Used*	0,0002g 50g
0.2	0.2000	0.2000	Zero Error	0g
0.5	0.5000	0.4999	Off Centre Error	0,0025g
1	1.0000	0.9999	*Mass Used*	20g
2	1.9999	2.0002	Sensitivity	0g
5	4.9999	5.0002	Linearity	0,0005g
10	9.9998	10.0001		
20	19.9996	20.0002		
50	49.9994	50.0003		
100	99.9980	100.0004		
			Measurement Uncertainty @ 95% confidence level ±	0,0018g

Remarks: Reset

Signatories: Technical Signatory: *F Arnold* Calibrated by: *F Arnold*

The reported uncertainties of measurement were calculated and expressed in accordance with the principles defined in the GUM, Guide to Uncertainty of Measurement, ISO,Geneva,1993. The calculations are based on a standard uncertainty multiplied by a coverage factor of K=2 which unless specifically stated otherwise provides a level of confidence of approximately 95%.

This certificate is issued in accordance with ISO IEC 17025,the conditions approved by SANAS and the policies of CME METROLOGY .It is a correct record of measurements made and relate only to the items calibrated. This certificate may not be reproduced other than in full, accept with prior written approval of the issuing laboratory. The values in this certificate are valid at the time calibration. Subsequently the accuracy shall depend on such factors as the care exercised in handling, use of the instrument and frequency of use. Re-calibration should be performed after a period which has been chosen to ensure that the instrument's accuracy remains within the desired limits. The applicant hereby indemnifies, holds harmless and absolves CME METROLOGY and the Mass-Pressure and Torque laboratories, from any damage whatsoever and any legal liability in the event of a mistake in the services performed for the applicant.

MLBC Rev4 April 2015
End of Certificate

CME METROLOGY

sanas Calibration Laboratory
Lab no.1419

Po Box 99 Eppindust 7475, Cnr Riley & Brentford Streets, Beaconvale,Cape Town, Tel 021-931 1101 Fax 021-931 1126

Mass Laboratory

Certificate of Calibration

Calibration performed using measuring equipment traceable to National Measurement Standards

Mass Laboratory Standards: Serial Number: FA005,FA001,CN001

Calibration Procedure: ML11
Page No. 1 of 1

Certificate Number: M9786/1

Customer Details:

Calibration for: Stellenbosch University
Address: Department of Process Engineering
Cnr Bosmans & Banghoek roads
Stellenbosch

Condition on receipt: Satisfactory
Calibration performed at: Department of Process Engineering
Location/Department: Room301
Temperature(°C): 18-25
Type of Calibration: Full

Calibration Details:

Description: Balance
Make: Precisa
Serial Number: 2805807
Type of Unit: Electronic

Measuring Range:

Minimum: 0g
Maximum: 4000g
Resolution: 0.01g

Unit of Measure: g

Date received: 13/11/2015
Date of Calibration: 04/12/2015
Date of Issue: 08/12/2015
Requested recalibration date: December-16

Calibration Results

Nominal Test Position g	Accuracy Test As Found g	Accuracy Test As Left g	**Repeatability** *Mass Used*	0.01g 2000g
20	20.00	20.00	**Zero Error**	0g
50	50.00	50.00	**Off Centre Error**	0.04g
100	100.00	100.00	*Mass Used*	1000g
200	200.00	200.00	**Sensitivity**	0g
300	300.00	300.00	**Linearity**	0.05g
500	500.00	500.00		
1000	999.99	999.99		
1500	1500.00	1500.00		
2000	1999.99	1999.99		
3000	3000.02	3000.02		
4000	4000.05	4000.05		
			Measurement Uncertainty @ 95% confidence level ±	0.04g

Remarks: Off Centre error taken starting in lefthand corner at the back of pan.

Signatories: Technical Signatory: F Arnold Calibrated by: F Arnold

The reported uncertainties of measurement were calculated and expressed in accordance with the principles defined in the GUM, Guide to Uncertainty of Measurement, ISO,Geneva,1993. The calculations are based on a standard uncertainty multiplied by a coverage factor of K-2 which unless specifically stated otherwise provides a level of confidence of approximately 95%.

This certificate is issued in accordance with ISO IEC 17025,the conditions approved by SANAS and the policies of CME METROLOGY . The accuracy of the equipment used during calibration is traceable to the National Measuring Standards as maintained in the Republic of South Africa or International Measuring Standards. It is a correct record of measurements made and relate only to the items calibrated. This certificate may not be reproduced other than in full, accept with prior written approval of the issuing laboratory. The values in this certificate are valid at the time calibration. Subsequently the accuracy shall depend on such factors as the care exercised in handling, use of the instrument and frequency of use. Re-calibration should be performed after a period which has been chosen to ensure that the instrument's accuracy remains within the desired limits. The applicant hereby indemnifies, holds harmless and absolves CME METROLOGY and the Mass-Pressure and Torque laboratories, from any damage whatsoever and any legal liability in the event of a mistake in the services performed for the applicant.

MLBC Rev5 September 2015
End of Certificate

D.5.8.4 Volume Calibration

Volume Stability:

Additionally, the volume calibration determines the total available volume – including any dead volumes, with all equipment set up as for an actual experiment. By evacuating the chamber with a vacuum pump and calibrating with a gaseous phase, it is ensured that no inclusions of other phases or exclusions through surface tension or capillary flow problems (potential problems with a liquid calibration) occur.

Thermal expansion for stainless steel 316 is <16 x 10-6 /K at the temperatures investigated implies a change in the nanometer range. Such a small change can be considered negligible for the volume investigated.

Concerning the measurement of the piston position, the piston head and central shaft is one single piece of stainless steel, with the LVDT (linear variable differential transformer) measuring at the end of the shaft. Therefore, the measurement of the piston position relates directly to the position of the piston head and face, effectively negating the effect of gasket deformation. Additionally, the piston gasket (thick, compressed Teflon ring) is pre-deformed into position by tightening the piston before operation, as described in the full operating procedures in Appendix B. Hysteresis, which can be attributed to gasket deformation, thermal expansion, physical linkage-, or sensor lag, was noticed in the piston displacement measurement during calibration. The effect of hysteresis was included in the uncertainty in volume.

Dead Volume

The dead volumes are minimized during design with Teflon/PEEK inserts. There are three sources of potential dead volume:

1) Solvent loading valve: Dead volume was minimised through custom Teflon inserts, as stated on Page 63. The entry port is filled with Teflon with a needle used to keep the aperture open (otherwise Teflon creeps to fill the hole.)
2) The electrical connection. A combination of soft Teflon and hard PEEK inserts were used to eliminate dead volume.
3) Pressure and temperature gauges: The pressure gauge is sealed at the interior of the cell using a collapsible aluminium washer. Temperature gauges are made tight fit to eliminate dead volume and sealed on the stem through a compression seal. 4) The sight

glass – was made with enough tolerance around the glass up to the seal to ensure that mixing is possible.

Method:

The cell volume was calibrated using pure CO_2. First, a known mass of CO_2 was loaded into the cell. The mass was chosen to ensure operation in the area where the fluid is in a single, supercritical phase, and the fluid density is variable. This density variability allows the whole cell volume/range to be measured with a single mass loading.

The temperature was kept constant while the applied nitrogen pressure is varied in order to effect measurable density changes. After allowing for sufficient time (with the piston no longer moving after a 5 min interval), the piston position was noted using the height gauge. The cell pressure was then adjusted and allowed to reach a new equilibrium. The procedure was repeated until the piston reached its maximum stroke. The pressure was then slowly decreased, and the cell tested for any sign of hysteresis. No significant hysteresis was noted.

Using the NIST approved EOS by Span and Wagner [*J. Phys. Chem. Ref. Data, 25* (1996) 1509-1596] to predict the density at the indicated pressure and temperature, the density at a given pressure and temperature was calculated. An estimated cell volume was calculated using the calculated density and the known loaded mass. The volume values are plotted against piston position below in Figure D- 7. It is seen that the values show excellent agreement and linearity is achieved with an $R^2 = 0.999$. The raw data for the calibration is seen in Table D- 2.

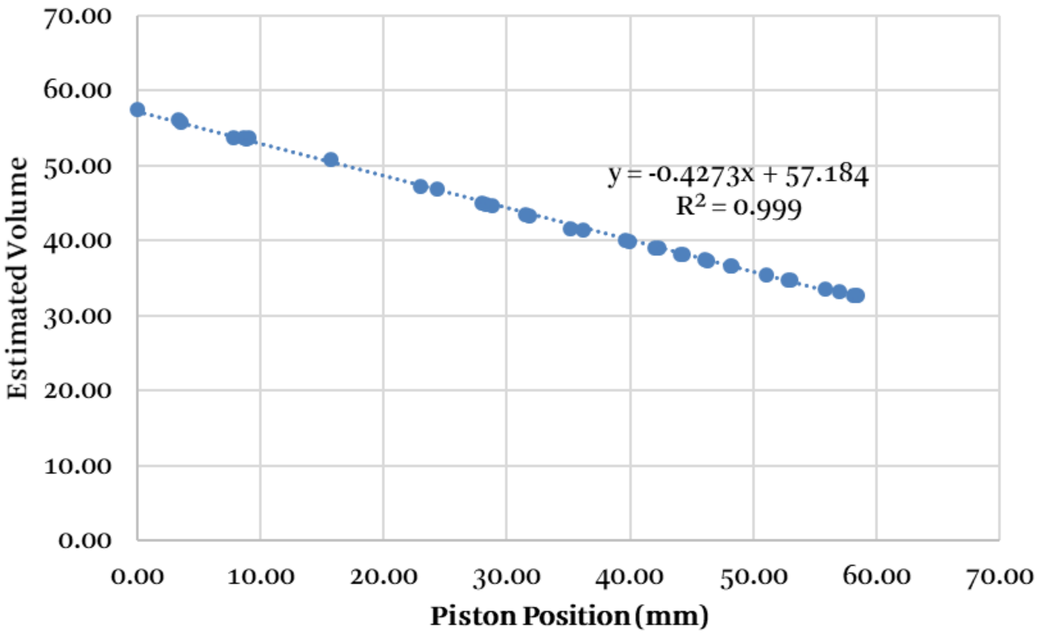

Figure D- 7: Volume Calibration Linearity

Table D- 2: Volume Calibration Data.

Mass Solvent (g)	30.12	11-Apr-16	Pressure ATM (bar)	1.014
Temperature	**Corrected Pressure**	**Piston Position**	**Calculated Density**	**Estimated Volume**
˚C	**bar (abs)**	**mm**	**g/ml**	**ml**
40.05	90.7	0.00	0.52374	57.51
40.05	91.4	3.34	0.53780	56.00
40.05	91.5	3.60	0.53968	55.81
40.05	92.6	7.87	0.56012	53.77
40.05	92.7	8.68	0.56166	53.62
40.05	92.8	8.83	0.56317	53.48
40.05	92.8	9.02	0.56166	53.62
40.05	325.7	58.36	0.92355	32.61
40.05	326.1	58.40	0.92375	32.60
40.05	320.3	58.18	0.92091	32.70
40.05	297.2	57.02	0.90871	33.14
40.05	277.2	55.90	0.89726	33.57
40.05	232.9	53.00	0.86778	34.71
40.05	232.0	52.86	0.86710	34.73
40.05	210.5	51.07	0.84986	35.44
40.05	183.6	48.23	0.82421	36.54
40.05	183.2	48.18	0.82378	36.56
40.05	168.2	46.25	0.80669	37.34
40.05	167.4	46.08	0.80557	37.39
40.05	155.7	44.30	0.78993	38.13
40.05	155.0	44.11	0.78892	38.18
40.05	145.0	42.36	0.77355	38.93
40.05	144.7	42.00	0.77288	38.97
40.05	134.4	39.90	0.75402	39.94
40.05	133.9	39.62	0.75301	40.00
40.05	122.5	36.20	0.72685	41.44
40.05	121.5	35.18	0.72419	41.59
40.05	112.2	31.82	0.69561	43.30
40.05	111.7	31.57	0.69341	43.43
40.05	107.1	28.82	0.67459	44.65
40.05	106.6	28.33	0.67229	44.80
40.05	106.0	28.04	0.66946	44.99
40.05	101.1	24.30	0.64292	46.85
40.05	100.5	23.04	0.63831	47.18
40.05	95.2	15.70	0.59282	50.80

D.5.8.5 Crystal Calibration

D.5.8.5.1 Vacuum Calibration – Temperature Dependence

The vacuum resonance, density and geometry of the crystal are effectively independent of pressure in the range investigated in this work. Temperature, however, has a noticeable effect. Temperature dependency means the setup needs to be calibrated for different temperatures. This calibration is achieved by measuring the vacuum resonance at each of the experimental temperatures.

The crystal and crystal cage were first thoroughly cleaned to remove any residuals using a series of solvents (Water, Methanol, Xylene and Isopropanol). No physical cleaning was used, as this could damage the sensitive wire leads and gold electrodes. The crystal was then left in a vacuum chamber overnight to ensure it is perfectly dry.

After ensuring the crystal is clean and dry, it was then loaded into the cell. The cell was brought up to operating temperature while being open to the atmosphere. After allowing for sufficient time for the cell to reach thermal equilibrium (+1h), a vacuum was then pulled around the crystal. The crystal was only turned on for the amount of time needed to determine a resonance curve, as potentially the crystal can fractionally heat up from the current flowing through it. This effect can become significant if the crystal is kept running in a vacuum, with no heat dissipation possible.

After measuring the crystal resonance in a vacuum, the vacuum on the cell was broken and the atmosphere allowed to return. The temperature was adjusted if needed, and the cell was again allowed to reach thermal equilibrium under atmospheric conditions. Reintroducing the air while reaching thermal equilibrium ensures the crystal is at the same temperature as the surrounding cell. The experiment was then repeated. Each resonance was determined using at least three repetitions, and individual repetitions were found to agree within 0.1 Hz. The calibration was performed before and after experimentation, with no change in crystal resonance observed. Measured vacuum resonances are seen in Table D- 3.

Table D- 3 Determined vacuum resonance, f_0, (measured at temperature, under vacuum).

Temperature (K)	Vacuum Resonance (Hz)
313.15	39136.62
323.15	39136.98
333.15	39137.80
343.15	39137.86
353.15	39137.92

D.5.8.5.2 Electromechanical Constant Determination

When the crystal is placed in a fluid medium and excited, the generated transverse waves propagate into the fluid in the form of an ultrasonic wave. The ultrasonic wave is damped logarithmically in the fluid, with the vibrations effectively extinguished only a few micrometres away from the surface. This physical damping affects the electrical response of the crystal, as per the converse piezoelectric effect, changing the crystal impedance and, hence, the loaded resonance, f_{res}. The degree of damping is directly related to the product of the dynamic viscosity and density of the fluid, and is expressed as:

$$f_o - f_{res} = k \cdot (\pi \cdot f_{res} \cdot \eta \cdot \rho_f)^{1/2}$$

where η (Pa.s) is the dynamic viscosity, ρ_f (kg/m^3) the fluid density and k (m^2/kg) the electromechanical constant.

In the case of the equipment presented, k was calculated by placing the crystal in a liquid of known viscosity for each experimental temperature. For this, n-Dodecane at atmospheric conditions was used. The crystal resonance was then measured a minimum of three times at each temperature, with excellent agreement between measurements found.

The actual fluid density was then calculated using a semi-empirical equation derived by Caudwell, Trusler, Vesovic and Wakeham, The Viscosity [*Int. J. Thermophys. 25* (2004) 1339–1352] and then. The density was then used, along with the measured resonance, to calculate the electromechanical constant.

k was found to be temperature-dependent, in agreement with literature. Determined k vales are found below in Table D- 4.

Table D- 4 Determined constants k determined using n-Dodecane at atmospheric conditions.

Temperature (K)	Viscosity (mPa.s)	Calculated (kg/m^3)	Constant K (m^2/kg)
313.15	1.0610	739.1676	0.11839
323.15	0.91601	732.1626	0.12249
333.15	0.80022	725.0992	0.12290
343.15	0.70612	717.9797	0.12972
353.15	0.62843	710.8063	0.13204

D.5.9 HD Camera Setup

Figure D- 8: Camera equipment from left to right: Camera Unit, Endoscope, Light Source

The optical measurements are done with the assistance of a Medical Endoscope HD camera assembly. The assembly provides a wide angle of view down the narrow aperture of the cell, as well as magnifying the contents. This wide viewing angle, with magnification, eases the detection of the phase transitions.

Specifications:

Camera:	Stryker HD 1188
Scope	SN KG 110660
Light Source:	Olympus CLV-U40
Display:	Telefunken TLCD-19JA

D.5.10 Magnetic Stirrer

The cell is stirred with a magnetic stirring bar. The bar is driven using an assembly of three electromagnets with a custom driver circuit. The setup allows variable stirring of the cell in any orientation. During operation, the cell is positioned in an upright position. Firstly, this positioning avoids gravitational effects on the crystal, and secondly, encourages the settling of any denser phase towards the bottom of the cell where the stirrer can best mix it. The stirrer is also kept from bumping into the delicate crystal assembly while stirring in this position.

The stirrer assembly is powered using an old 400 W computer power supply, repurposed to the task.

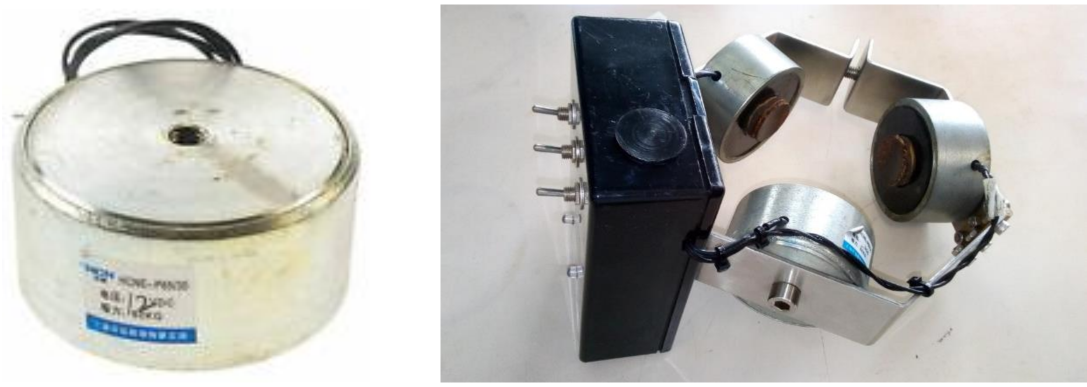

Figure D- 9: Electromagnet and Magnet Stirrer Assembly and control unit.

Specifications:

Solenoid electromagnet x 3	
Diameter:	65 mm
Voltage:	12V
Lift strength:	80 kg

D.5.10.1. Magnet Holder Components 371
D.5.10.2. Magnet Holder 3D Representation 372

D.5.10.1 Magnet Holder Components

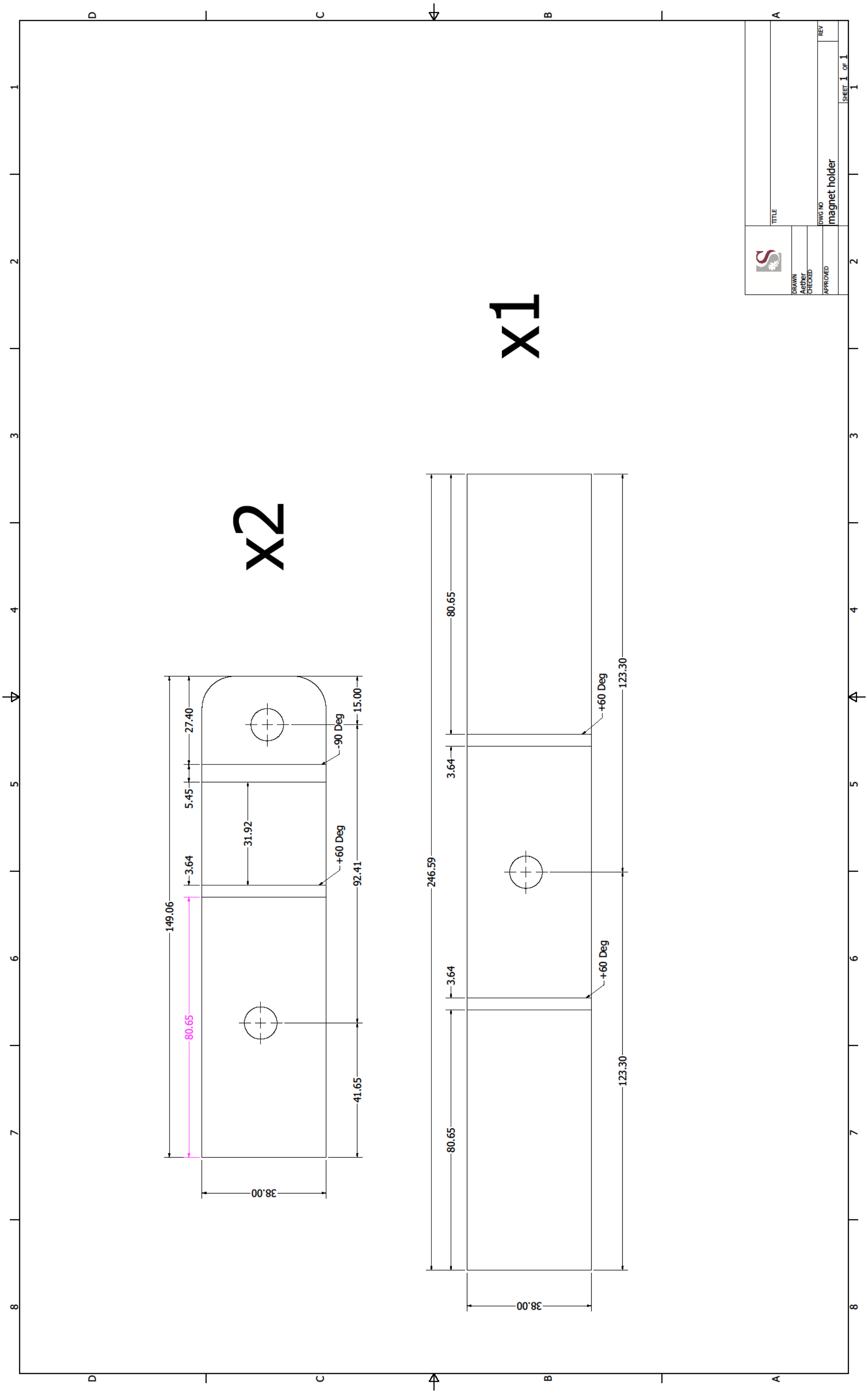

D.5.10.2 Magnet Holder 3D Representation

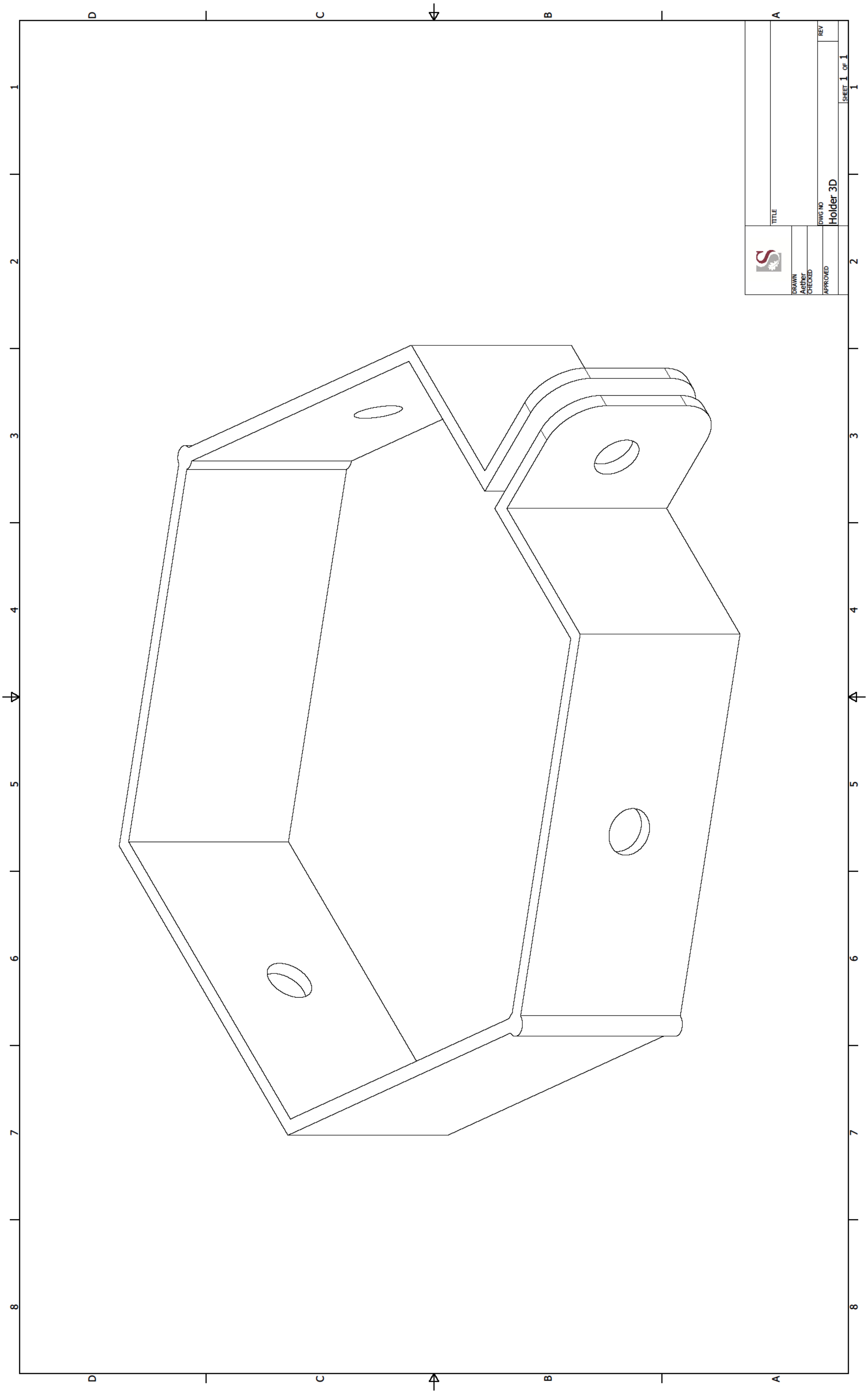

D.5.10.3 Controller Details and Code

The electromagnets are controlled using a custom driver circuit, switchable between three different stirring speeds. The circuit was designed and coded with the assistance of Anton Kramer, a fellow engineering student.

Specifications:

Microcontroller:	dsPIC30F4012 (28pin configuration)
Assembly Voltage:	12 V DC
Software	MPLab, PicKit3

Microcontroller code:

```
/*
 * File:   main.c
 * Author: Anton
 *
 * Created on October 19, 2015, 9:20 PM
 */

#include <stdio.h>

#include <stdlib.h>


// DSPIC30F4012 Configuration Bit Settings

// 'C' source line config statements

#include <p30Fxxxx.h>

int FOSC __attribute__((space(prog), address(0xF80000))) = 0xC301;
//_FOSC(
//    FRC_PLL4 &         // Primary Oscillator Mode (FRC w/ PLL 4x)
//    PRI &              // Oscillator Source (Primary Oscillator)
//    CSW_FSCM_OFF       // Clock Switching and Monitor (Sw Disabled, Mon Disabled)

//);
int FWDT __attribute__((space(prog), address(0xF80002))) = 0x3F;
//_FWDT(
//    WDTPSB_16 &        // WDT Prescaler B (1:16)
//    WDTPSA_512 &       // WDT Prescaler A (1:512)
//    WDT_OFF            // Watchdog Timer (Disabled)
//);
int FBORPOR __attribute__((space(prog), address(0xF80004))) = 0x7A3;
//_FBORPOR(
//    PWRT_64 &          // POR Timer Value (64ms)
//    BORV27 &           // Brown Out Voltage (2.7V)
//    PBOR_ON &          // PBOR Enable (Enabled)
//    PWMxL_ACT_HI &     // Low-side PWM Output Polarity (Active High)
//    PWMxH_ACT_HI &     // High-side PWM Output Polarity (Active High)
//    RST_IOPIN &        // PWM Output Pin Reset (Control with PORT/TRIS regs)
//    MCLR_DIS           // Master Clear Enable (Disabled)
//);
int FGS __attribute__((space(prog), address(0xF8000A))) = 0x7;
//_FGS(
//    GWRP_OFF &         // General Code Segment Write Protect (Disabled)
```

```
//    CODE_PROT_OFF       // General Segment Code Protection (Disabled)
//);
int FICD __attribute__((space(prog), address(0xF8000C))) = 0xC003;
//_FICD(
//    ICS_PGD             // Comm Channel Select (Use PGC/EMUC and PGD/EMUD)
//);

void delay(void);

const unsigned int sinus[] = {0x0,0xD,0x19,0x26,0x32,0x3F,0x4B,0x58,0x64,0x71,0x7E,
0x8A,0x97,0xA3,0xB0,0xBC,0xC9,0xD5,0xE2,0xEF,0xFB,0x108,0x114,0x121,0x12D,0x13A,0x1
46,0x153,0x15F,0x16C,0x178,0x185,0x192,0x19E,0x1AB,0x1B7,0x1C4,0x1D0,0x1DD,0x1E9,0x
1F6,0x202,0x20F,0x21B,0x228,0x234,0x241,0x24D,0x25A,0x266,0x273,0x27F,0x28C,0x298,0
x2A5,0x2B1,0x2BE,0x2CA,0x2D7,0x2E3,0x2EF,0x2FC,0x308,0x315,0x321,0x32E,0x33A,0x347,
0x353,0x35F,0x36C,0x378,0x385,0x391,0x39E,0x3AA,0x3B6,0x3C3,0x3CF,0x3DC,0x3E8,0x3F4
,0x401,0x40D,0x419,0x426,0x432,0x43F,0x44B,0x457,0x464,0x470,0x47C,0x489,0x495,0x4A
1,0x4AD,0x4BA,0x4C6,0x4D2,0x4DF,0x4EB,0x4F7,0x503,0x510,0x51C,0x528,0x534,0x541,0x5
4D,0x559,0x565,0x572,0x57E,0x58A,0x596,0x5A2,0x5AF,0x5BB,0x5C7,0x5D3,0x5DF,0x5EB,0x
5F8,0x604,0x610,0x61C,0x628,0x634,0x640,0x64C,0x659,0x665,0x671,0x67D,0x689,0x695,0
x6A1,0x6AD,0x6B9,0x6C5,0x6D1,0x6DD,0x6E9,0x6F5,0x701,0x70D,0x719,0x725,0x731,0x73D,
0x749,0x755,0x761,0x76D,0x778,0x784,0x790,0x79C,0x7A8,0x7B4,0x7C0,0x7CC,0x7D7,0x7E3
,0x7EF,0x7FB,0x807,0x812,0x81E,0x82A,0x836,0x842,0x84D,0x859,0x865,0x870,0x87C,0x88
8,0x894,0x89F,0x8AB,0x8B7,0x8C2,0x8CE,0x8DA,0x8E5,0x8F1,0x8FC,0x908,0x914,0x91F,0x9
2B,0x936,0x942,0x94D,0x959,0x964,0x970,0x97B,0x987,0x992,0x99E,0x9A9,0x9B5,0x9C0,0x
9CB,0x9D7,0x9E2,0x9EE,0x9F9,0xA04,0xA10,0xA1B,0xA26,0xA32,0xA3D,0xA48,0xA54,0xA5F,0
xA6A,0xA75,0xA81,0xA8C,0xA97,0xAA2,0xAAD,0xAB8,0xAC4,0xACF,0xADA,0xAE5,0xAF0,0xAFB,
0xB06,0xB11,0xB1C,0xB28,0xB33,0xB3E,0xB49,0xB54,0xB5F,0xB6A,0xB75,0xB7F,0xB8A,0xB95
,0xBA0,0xBAB,0xBB6,0xBC1,0xBCC,0xBD7,0xBE1,0xBEC,0xBF7,0xC02,0xC0D,0xC17,0xC22,0xC2
D,0xC38,0xC42,0xC4D,0xC58,0xC62,0xC6D,0xC78,0xC82,0xC8D,0xC97,0xCA2,0xCAD,0xCB7,0xC
C2,0xCCC,0xCD7,0xCE1,0xCEC,0xCF6,0xD01,0xD0B,0xD15,0xD20,0xD2A,0xD35,0xD3F,0xD49,0x
D54,0xD5E,0xD68,0xD73,0xD7D,0xD87,0xD91,0xD9C,0xDA6,0xDB0,0xDBA,0xDC4,0xDCF,0xDD9,0
xDE3,0xDED,0xDF7,0xE01,0xE0B,0xE15,0xE1F,0xE29,0xE33,0xE3D,0xE47,0xE51,0xE5B,0xE65,
0xE6F,0xE79,0xE83,0xE8C,0xE96,0xEA0,0xEAA,0xEB4,0xEBD,0xEC7,0xED1,0xEDB,0xEE4,0xEEE
,0xEF8,0xF01,0xF0B,0xF15,0xF1E,0xF28,0xF31,0xF3B,0xF44,0xF4E,0xF57,0xF61,0xF6A,0xF7
4,0xF7D,0xF87,0xF90,0xF99,0xFA3,0xFAC,0xFB5,0xFBF,0xFC8,0xFD1,0xFDB,0xFE4,0xFED,0xF
F6,0xFFF,0x1009,0x1012,0x101B,0x1024,0x102D,0x1036,0x103F,0x1048,0x1051,0x105A,0x10
63,0x106C,0x1075,0x107E,0x1087,0x1090,0x1099,0x10A2,0x10AA,0x10B3,0x10BC,0x10C5,0x1
0CE,0x10D6,0x10DF,0x10E8,0x10F0,0x10F9,0x1102,0x110A,0x1113,0x111B,0x1124,0x112D,0x
1135,0x113E,0x1146,0x114F,0x1157,0x115F,0x1168,0x1170,0x1179,0x1181,0x1189,0x1192,0
x119A,0x11A2,0x11AA,0x11B3,0x11BB,0x11C3,0x11CB,0x11D3,0x11DC,0x11E4,0x11EC,0x11F4,
0x11FC,0x1204,0x120C,0x1214,0x121C,0x1224,0x122C,0x1234,0x123C,0x1244,0x124B,0x1253
,0x125B,0x1263,0x126B,0x1272,0x127A,0x1282,0x1289,0x1291,0x1299,0x12A0,0x12A8,0x12B
0,0x12B7,0x12BF,0x12C6,0x12CE,0x12D5,0x12DD,0x12E4,0x12EB,0x12F3,0x12FA,0x1302,0x13
09,0x1310,0x1318,0x131F,0x1326,0x132D,0x1334,0x133C,0x1343,0x134A,0x1351,0x1358,0x1
35F,0x1366,0x136D,0x1374,0x137B,0x1382,0x1389,0x1390,0x1397,0x139E,0x13A5,0x13AB,0x
13B2,0x13B9,0x13C0,0x13C7,0x13CD,0x13D4,0x13DB,0x13E1,0x13E8,0x13EF,0x13F5,0x13FC,0
x1402,0x1409,0x140F,0x1416,0x141C,0x1423,0x1429,0x142F,0x1436,0x143C,0x1442,0x1449,
0x144F,0x1455,0x145B,0x1462,0x1468,0x146E,0x1474,0x147A,0x1480,0x1486,0x148C,0x1492
,0x1498,0x149E,0x14A4,0x14AA,0x14B0,0x14B6,0x14BC,0x14C2,0x14C7,0x14CD,0x14D3,0x14D
9,0x14DE,0x14E4,0x14EA,0x14EF,0x14F5,0x14FB,0x1500,0x1506,0x150B,0x1511,0x1516,0x15
1C,0x1521,0x1527,0x152C,0x1531,0x1537,0x153C,0x1541,0x1547,0x154C,0x1551,0x1556,0x1
55B,0x1560,0x1566,0x156B,0x1570,0x1575,0x157A,0x157F,0x1584,0x1589,0x158E,0x1593,0x
1597,0x159C,0x15A1,0x15A6,0x15AB,0x15B0,0x15B4,0x15B9,0x15BE,0x15C2,0x15C7,0x15CC,0
x15D0,0x15D5,0x15D9,0x15DE,0x15E2,0x15E7,0x15EB,0x15F0,0x15F4,0x15F8,0x15FD,0x1601,
0x1605,0x160A,0x160E,0x1612,0x1616,0x161A,0x161E,0x1623,0x1627,0x162B,0x162F,0x1633
,0x1637,0x163B,0x163F,0x1643,0x1647,0x164A,0x164E,0x1652,0x1656,0x165A,0x165D,0x166
1,0x1665,0x1668,0x166C,0x1670,0x1673,0x1677,0x167A,0x167E,0x1681,0x1685,0x1688,0x16
8C,0x168F,0x1692,0x1696,0x1699,0x169C,0x16A0,0x16A3,0x16A6,0x16A9,0x16AC,0x16B0,0x1
6B3,0x16B6,0x16B9,0x16BC,0x16BF,0x16C2,0x16C5,0x16C8,0x16CB,0x16CE,0x16D0,0x16D3,0x
16D6,0x16D9,0x16DC,0x16DE,0x16E1,0x16E4,0x16E6,0x16E9,0x16EC,0x16EE,0x16F1,0x16F3,0
x16F6,0x16F8,0x16FB,0x16FD,0x16FF,0x1702,0x1704,0x1706,0x1709,0x170B,0x170D,0x170F,
0x1712,0x1714,0x1716,0x1718,0x171A,0x171C,0x171E,0x1720,0x1722,0x1724,0x1726,0x1728
,0x172A,0x172C,0x172D,0x172F,0x1731,0x1733,0x1735,0x1736,0x1738,0x173A,0x173B,0x173
D,0x173E,0x1740,0x1741,0x1743,0x1744,0x1746,0x1747,0x1748,0x174A,0x174B,0x174C,0x17
4E,0x174F,0x1750,0x1751,0x1753,0x1754,0x1755,0x1756,0x1757,0x1758,0x1759,0x175A,0x1
75B,0x175C,0x175D,0x175E,0x175F,0x175F,0x1760,0x1761,0x1762,0x1762,0x1763,0x1764,0x
```

```
1764,0x1765,0x1766,0x1766,0x1767,0x1767,0x1768,0x1768,0x1769,0x1769,0x1769,0x176A,0
x176A,0x176A,0x176B,0x176B,0x176B,0x176B,0x176C,0x176C,0x176C,0x176C,0x176C,0x176C
};

int main(int argc, char ** argv) {

  unsigned int counterA = 0;
  unsigned int counterB = 500;
  unsigned int counterC = 1000;
  int directionA = 0;
  int directionB = 1;
  int directionC = 1;

  int target_speed = 15; // 20 = 1000opm, 15 = 750opm, 10 = 500opm, 1 = 50opm
  int speed = 1;

  unsigned int micro405 = 0;

  TRISBbits.TRISB0 = 1;
  TRISBbits.TRISB1 = 1; // speed pins
  TRISBbits.TRISB2 = 1;

  ADPCFGbits.PCFG0 = 1;
  ADPCFGbits.PCFG1 = 1; // B0 - B2 as digital
  ADPCFGbits.PCFG2 = 1;

  CNPU1bits.CN2PUE = 1;
  CNPU1bits.CN3PUE = 1; // enable pull-ups on B0 - B2
  CNPU1bits.CN4PUE = 1;

  TRISEbits.TRISE1 = 0;
  TRISEbits.TRISE3 = 0; // PWM high pins as outputs
  TRISEbits.TRISE5 = 0;

  TRISFbits.TRISF2 = 0; // PWM1 direction outputs
  TRISFbits.TRISF3 = 0;

  TRISEbits.TRISE8 = 0; // PWM2 direction outputs
  TRISDbits.TRISD0 = 0;

  TRISDbits.TRISD1 = 0; // PWM3 direction outputs
  TRISCbits.TRISC15 = 0;

  PTCONbits.PTCKPS1 = 0; // set prescaler to 1:1
  PTCONbits.PTCKPS0 = 0;

  PTCONbits.PTMOD1 = 0;
  PTCONbits.PTMOD0 = 0;
        PTPER = 0xBB7; // f_PWM = 20kHz
        PDC1 = 0x2ED; //0x375 //0x2ED //0x176C
        PDC2 = 0xBB3;
        PDC3 = 0x5DB;
        PWMCON1bits.PEN1H = 1;
        PWMCON1bits.PEN2H = 1;
        PWMCON1bits.PEN3H = 1;
        PTCONbits.PTEN = 1; // enable PWM time base

        //PORTDbits.RD0 = 1;
        //LATDbits.LATD0 = 1;
        //PORTDbits.RD1 = 1;

        IFS2bits.PWMIF = 0;
        PORTFbits.RF3 = 1; // PMOS A2 off
        LATFbits.LATF3 = 1;
        PORTFbits.RF2 = 0; // PMOS A1 on
        LATFbits.LATF2 = 0;
```

```
        while (1) {
          if (IFS2bits.PWMIF == 1) // 405us has passed
          {
            IFS2bits.PWMIF = 0;

            if (micro405++ > 1236) //0.5s
            {
              micro405 = 0;

              if (speed < target_speed) {
                speed++;
              }
              if (speed > target_speed) {
                speed--;
              }
            }

            // PWM A
            if (counterA == 0) {
              if (directionA == 0) {
                PORTFbits.RF2 = 0; // PMOS A1 on
                LATFbits.LATF2 = 0;
              } else {
                PORTFbits.RF3 = 0; // PMOS A2 on
                LATFbits.LATF3 = 0;
              }
            }
            if (counterA <= 749) {
              PDC1 = sinus[counterA];
            } else {
              PDC1 = sinus[1498 - counterA];
            }
            counterA += speed;
            if (counterA > 1498) {
              counterA = 0;
              if (directionA == 0) {
                PORTFbits.RF2 = 1; // PMOS A1 off
                LATFbits.LATF2 = 1;
                directionA = 1;
              } else {
                PORTFbits.RF3 = 1; // PMOS A2 off
                LATFbits.LATF3 = 1;
                directionA = 0;
              }
            }

            // PWM B
            if (counterB == 0) {
              if (directionB == 0) {
                PORTEbits.RE8 = 0; // PMOS B1 on
                LATEbits.LATE8 = 0;
              } else {
                PORTDbits.RD0 = 0; // PMOS B2 on
                LATDbits.LATD0 = 0;
              }
            }
            if (counterB <= 749) {
              PDC2 = sinus[counterB];
            } else {
              PDC2 = sinus[1498 - counterB];
            }
            counterB += speed;
            if (counterB > 1498) {
              counterB = 0;
              if (directionB == 0) {
                PORTEbits.RE8 = 1; // PMOS B1 off
```

```
          LATEbits.LATE8 = 1;
          directionB = 1;
        } else {
          PORTDbits.RD0 = 1; // PMOS B2 off
          LATDbits.LATD0 = 1;
          directionB = 0;
        }
      }

      // PWM C
      if (counterC == 0) {
        if (directionC == 0) {
          PORTDbits.RD1 = 0; // PMOS C1 on
          LATDbits.LATD1 = 0;
        } else {
          PORTCbits.RC15 = 0; // PMOS C2 on
          LATCbits.LATC15 = 0;
        }
      }
      if (counterC <= 749) {
        PDC3 = sinus[counterC];
      } else {
        PDC3 = sinus[1498 - counterC];
      }
      counterC += speed;
      if (counterC > 1498) {
        counterC = 0;
        if (directionC == 0) {
          PORTDbits.RD1 = 1; // PMOS C1 off
          LATDbits.LATD1 = 1;
          directionC = 1;
        } else {
          PORTCbits.RC15 = 1; // PMOS C2 off
          LATCbits.LATC15 = 1;
          directionC = 0;
        }
      }

      // Update speed
      if ((PORTBbits.RB1 == 0) && (PORTBbits.RB0 == 0)) {
        target_speed = 20;
      } else if ((PORTBbits.RB1 == 0) && (PORTBbits.RB0 == 1)) {
        target_speed = 15;
      } else if ((PORTBbits.RB1 == 1) && (PORTBbits.RB0 == 0)) {
        target_speed = 10;
      } else if ((PORTBbits.RB1 == 1) && (PORTBbits.RB0 == 1)) {
        target_speed = 5; //250rpm?
      }
    }
  }

  return (EXIT_SUCCESS);
}

void delay(void) {
  unsigned int count;
  unsigned int count2;
  for (count = 0; count <= 30000; count++) {
    for (count2 = 0; count2 <= 100; count2++) {

    }
  }
}
```

D.5.11 Viscosity Measurement Equipment and Method

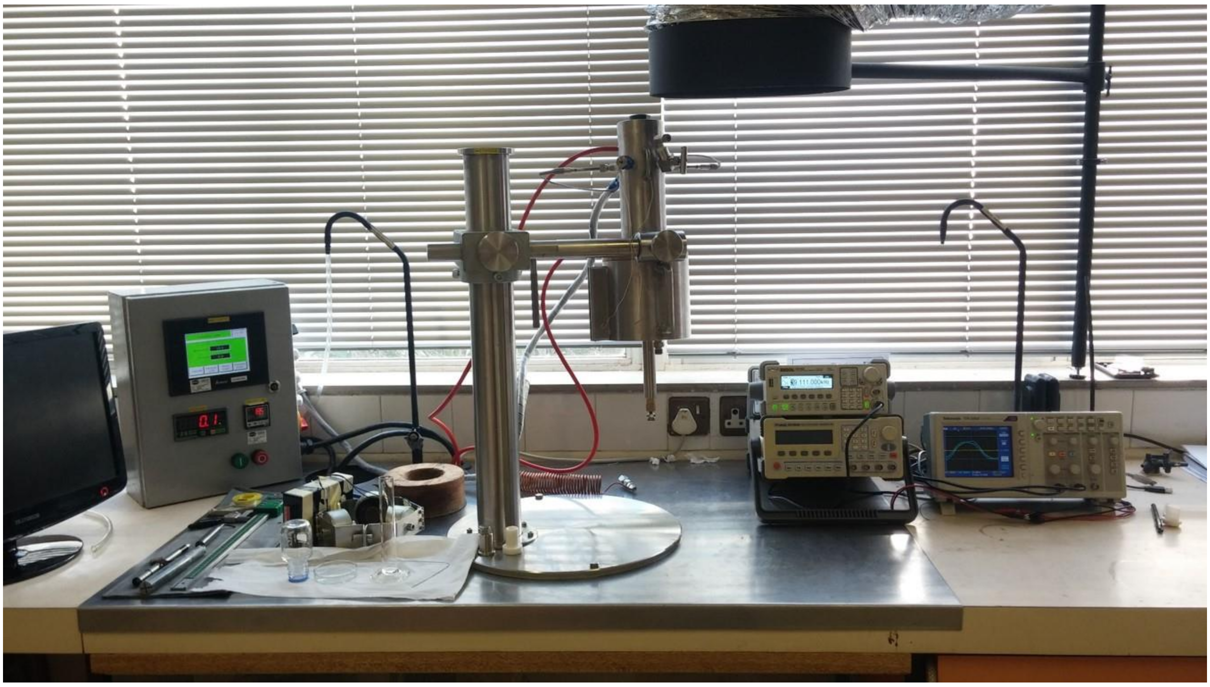

Figure D- 5: Finished high-pressure cell assembly – Note the Signal generator and Oscilloscope on the right.

The crystal is excited by an AC signal, generated by a RIGOL DG1022 signal generator, to a standard uncertainty of 1 µHz, ± 100 ppm of the signal per year. A Tektronix TDS2002 oscilloscope, with a sampling rate of 1.0 GS/s and accurate within ± 5 mV (± 3 % of the selected vertical range), is used to measure the response of the crystal. Combined uncertainties for the measurement of the dynamic viscosity value are calculated to be lower than 0.01 times the measured mPa.s value, considering the equipment uncertainty, variability between repeated measurements and deviation from known values.

The signal generator and Oscilloscope are controlled using two USB connections to a laptop computer. The computer runs custom software programmed in python. The software handles both the changes in voltage and frequency, as well as the measurement of the frequency, voltage peak and phase shift.

Requirements:

Python v 3.5.1.
OpenChoice TekVISA v4.1.0

D.5.11.1 Software Screenshots and Instructions

The software runs in a Windows environment, using the Python 3.5.1 framework and TekVisa. After the program is opened, the software will prompt the user to ensure the Oscilloscope and Frequency Generator is connected. Ensure both pieces of equipment are turned on and connected, with the Oscilloscope connected first. The prompt for the Oscilloscope are seen below Figure D- 10.

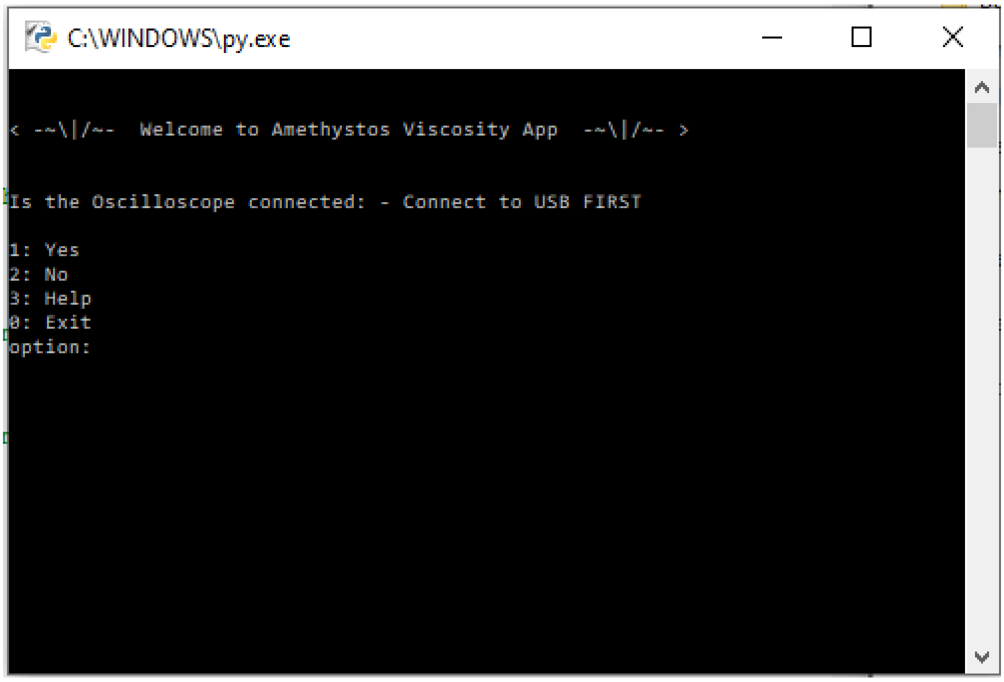

```
< -~\|/~-  Welcome to Amethystos Viscosity App  -~\|/~- >


Is the Oscilloscope connected: - Connect to USB FIRST

1: Yes
2: No
3: Help
0: Exit
option:
```

Figure D- 10: Software welcome screen.

The software primes the Oscilloscope and Signal Generator with the default values:

start_freq = 39100
end_freq = 39200
increment = 5
timeleng = 1
Volt = 3

The user can then select the method of the frequency sweep. The selection is made by either defining a frequency start, stop and step (increment), or a midpoint, span and step (increment). The start-stop method is useful to determine the rough location of the resonance first, after which the midpoint-span method can be used to measure the frequencies around the resonance point. The frequency selection screen is seen in Figure D- 11

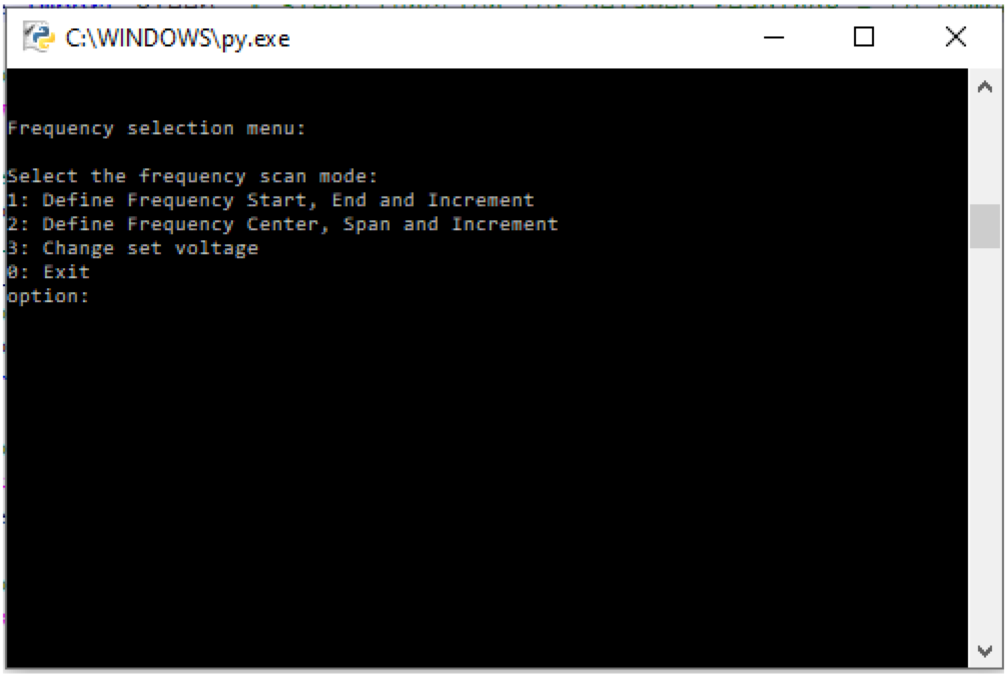

```
Frequency selection menu:

Select the frequency scan mode:
1: Define Frequency Start, End and Increment
2: Define Frequency Center, Span and Increment
3: Change set voltage
0: Exit
option:
```

Figure D- 11: Frequency method selection menu.

After the method is selected, the software gives an estimated runtime in seconds. The user can either start testing, change the parameters, change the filename, or exit the programme. The pre-test options are seen in Figure D- 12.

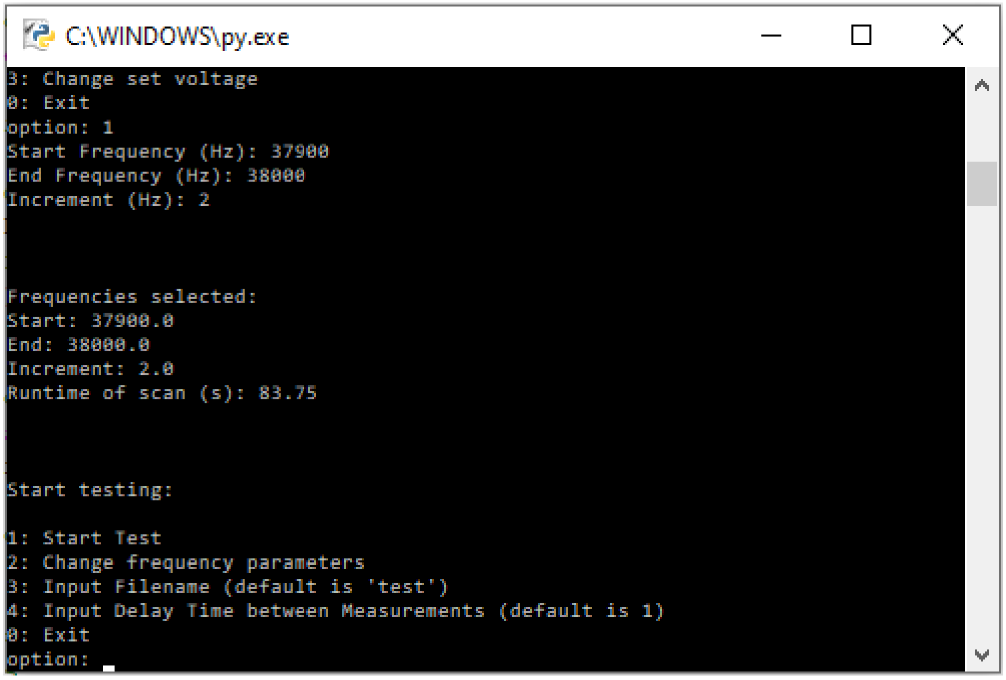

```
3: Change set voltage
0: Exit
option: 1
Start Frequency (Hz): 37900
End Frequency (Hz): 38000
Increment (Hz): 2



Frequencies selected:
Start: 37900.0
End: 38000.0
Increment: 2.0
Runtime of scan (s): 83.75



Start testing:

1: Start Test
2: Change frequency parameters
3: Input Filename (default is 'test')
4: Input Delay Time between Measurements (default is 1)
0: Exit
option: _
```

Figure D- 12: Programme ready for experimental measurement.

D.5.11.2 Software Python Code

The following Python code was used during experiments:

```python
import pyvisa  # Equipment Interface library
import time  # Import time/date info
from time import sleep  # Sleep function for delayed readings - to compensate for oscilloscope delay


# Function for writing to a text file:
def txt_write(FILENAME, DATA, MODE):

    # Open file:
    f = open(FILENAME, MODE)
    # Write data to file:
    f.write(DATA + "\n")
    # Close file:
    f.close()
    return ()


# Function for sending Frequency to the Sig-Gen
def freqtrans(freq):
    siggen.write("FREQ " + str(freq))


# Function for setting Frequency parameters for the Sig-Gen
def freqset():

    m = -1  # Initialize m counter - menu counter
    #defaults
    start_freq = 39100
    end_freq = 39200
    increment = 5
    timeleng = 1

    while m != 0:

        # Menu Text
        print("\n\n")
        print("Frequency selection menu: \n")
        print("Select the frequency scan mode:")
        print("1: Define Frequency Start, End and Increment")
        print("2: Define Frequency Center, Span and Increment")
        print("3: Change set voltage")
        print("0: Exit")

        # Menu Input
        try:
            m = int(input("option: "))
        except:
            print("\n Invalid input - try again")

    # m validity check
        if m > 3 or m < -1:
            print("\n Invalid input - try again")

        # Menu opt 1
        if m == 1:

            start_freq = float(input("Start Frequency (Hz): "))
            end_freq = float(input("End Frequency (Hz): "))
            increment = float(input("Increment (Hz): "))
```

```

            timeleng = ((end_freq - start_freq) / increment
                        ) * 1.675  # constant to reflect true processing time.

            print("\n\n")
            print("Frequencies selected:")
            print("Start:", start_freq)
            print("End:", end_freq)
            print("Increment:", increment)
            print("Runtime of scan (s):", timeleng)

            break

        # Menu opt 2
        if m == 2:

            midpoint = float(input("Frequency midpoint (Hz): "))
            span = float(input("Frequency Span (Hz): "))
            increment = float(input("Increment (Hz): "))

            start_freq = (midpoint - (span / 2))
            end_freq = (midpoint + (span / 2))

            float(timeleng=((end_freq - start_freq) / increment)
                  ) * 1.675  # constant to reflect true processing time.

            print("\n\n")
            print("Frequencies selected:")
            print("Start:", start_freq)
            print("End:", end_freq)
            print("Increment:", increment)
            print("Runtime of scan (s):", timeleng)
            print("                  in seconds with default of 1s per point")

            break

        # Menu opt 3
        if m == 3:

            volt = str(input("Volt - a.k.a. amplitude (V): "))

            siggen.write("VOLT " + volt)

            print("\n\n")
            print("Voltage selected:", volt)

        # Hidden Menu opt 123 - skip
        if m == 123:
            break

        # Menu opt 0
        if m == 0:
            return ()

        m = -1  # Reset m
    return (start_freq, end_freq, increment, timeleng)


# Function retreiving scope parameters
def scopepar():
    scope.write("MEASU?")
    par = scope.read()
    return par


# Fuction to set default scope parameters
```

```
    def scopeset():
        sleep(.01)
        scope.write("MEASU:MEAS1:SOU CH1")
        sleep(.01)
        scope.write("MEASU:MEAS1:TYP FREQ")
        sleep(.01)
        scope.write("MEASU:MEAS2:SOU CH1")
        sleep(.01)
        scope.write("MEASU:MEAS2:TYP PK2")
        sleep(.01)
        scope.write("MEASU:MEAS3:SOU CH2")
        sleep(.01)
        scope.write("MEASU:MEAS3:TYP FREQ")
        sleep(.01)
        scope.write("MEASU:MEAS4:SOU CH2")
        sleep(.01)
        scope.write("MEASU:MEAS4:TYP PK2")
        sleep(.01)
        scope.write("MEASU:MEAS5:SOU CH1")
        sleep(.01)
        scope.write("MEASU:MEAS5:TYP PHA")
        sleep(.01)
        scope.write("MEASU:MEAS5:SOURCE1 CH1")
        sleep(.01)
        scope.write("MEASU:MEAS5:SOURCE2 CH2")
        sleep(0.1)
        scope.write("HOR:DEL:SEC 0.000005")

        return ()


    # Function for reading values from the Scope
    def measure_scope(out=True):

        scope.write("MEASU:MEAS1:VAL?")
        m1 = float(scope.read())
        scope.write("MEASU:MEAS2:VAL?")
        m2 = float(scope.read())
        scope.write("MEASU:MEAS3:VAL?")
        m3 = float(scope.read())
        scope.write("MEASU:MEAS4:VAL?")
        m4 = float(scope.read())
        scope.write("MEASU:MEAS5:VAL?")
        m5 = float(scope.read())

        meas = str(m1) + "," + str(m2) + "," + str(m3) + "," + str(m4) + "," + str(
            m5)

        if out == True:
            print(meas)

        return meas


    # Main Function
    def main():

        m = -1  # Initialize m counter - menu counter

        # Welcome
        print("\n\n< -~\|/~-  Welcome to Amethystos Viscosity App  -~\|/~- >")

        ### MENU 1 - Confirm oscilloscope connected and ready

        while m != 0:

```

```
        # Menu text
        print("\n")
        print("Is the Oscilloscope connected: - Connect to USB FIRST \n")
        print("1: Yes")
        print("2: No")
        print("3: Help")
        print("0: Exit")

        # Menu Input
        try:
            m = int(input("option: "))
        except:
            print("\n Invalid input - try again")

        # m validity check
        if m > 4 or m < -1:
            print("\n Invalid input - try again")

        # Menu opt 1
        if m == 1:
            print("\n")
            print("Scope initialization")
            rm = pyvisa.ResourceManager()
            visaDeviceTuple = rm.list_resources()
            visaDeviceList = rm.list_resources_info()
            print(visaDeviceTuple)
            print(visaDeviceList)

            global scope
            scope = rm.get_instrument(visaDeviceTuple[1])
            scope.write("*IDN?")
            print(scope.read())

            # Set Measurement channels

            scopeset()

            print(scopepar())

            break

        # Menu opt 2
        if m == 2:
            print("\n")
            print("Please connect scope and try again")
            m = -1

        # Menu opt 3
        if m == 3:
            print("\n\n")
            print("HELP:")
            print("\n")
            print(
                "Go read the manual - and why are you using my equipment in the first place?!"
            )
            print("I'm watching you O.o")
            print(
                "Sigh - be sure TEKVisa is installed and that the scope is connected FIRST."
            )
            m = -1

        # Hidden Menu opt 123 - skip
        if m == 123:
            break
```

```

            # Menu opt 0
            if m == 0:
                return ()

            m = -1  # Reset m

        ### MENU 2 - Confirm Signal Generator is connected and ready

        while m != 0:

            # Menu text
            print("\n\n")
            print("Is the Signal Generator connected: - Connect to USB SECOND \n")
            print("1: Yes")
            print("2: No")
            print("3: Help")
            print("0: Exit")

            # Menu Input
            try:
                m = int(input("option: "))
            except:
                print("\n Invalid input - try again")

            # m validity check
            if m > 4 or m < -1:
                print("\n Invalid input - try again")

            # Menu opt 1
            if m == 1:
                print("\n\n")
                print("Sig-Gen initialization")
                rm = pyvisa.ResourceManager()
                visaDeviceTuple = rm.list_resources()
                visaDeviceList = rm.list_resources_info()
                print(visaDeviceTuple)
                print(visaDeviceList)

                global siggen
                siggen = rm.get_instrument(visaDeviceTuple[0])
                sleep(0.01)
                siggen.write("*IDN?")  #Can give trouble
                sleep(0.01)
                print(siggen.read())
                siggen.write(
                    "APPL:SIN 39000,4.0,0")  #Applies defaults and turns on siggen
                sleep(0.01)
                siggen.write("OUTP ON")
                print(
                    "\nSignal Generator Initialized and set to defaults (39kHz, 1V)"
                )

                break

            # Menu opt 2
            if m == 2:
                print("\n\n")
                print("Please connect Sig-Gen and try again")
                m = -1

            # Menu opt 3
            if m == 3:
                print("\n\n")
                print("HELP:")
                print("\n")
```

```
            print(
                "You seriously expect comprehensive help from a python script?"
            )
            print("Are you even a real postgrad?")
            m = -1

        # Hidden Menu opt 123 - skip
        if m == 123:
            break

        # Menu opt 0
        if m == 0:
            return ()

        m = -1  # Reset m

    ### MENU 3 - Select frequency scan mode

    start_freq, end_freq, increment, timeleng = freqset()

    slp = 1  # Initialize sleep counter
    filename = str("test.csv")  #Default filename

    ### MENU 4 - Run Scan

    while m != 0:

        # Menu Text
        print("\n\n")
        print("Start testing:\n")
        # print("NB!")
        # print("Make sure that scope is set to measure and the correct values are selected")
        # print("Make sure that the scope ranges values are correct")
        print("1: Start Test")
        print("2: Change frequency parameters")
        print("3: Input Filename (default is 'test')")
        print("4: Input Delay Time between Measurements (default is 1)")
        print("0: Exit")

        # Menu Input
        try:
            m = int(input("option: "))
        except:
            print("\n Invalid input - try again")

        # m validity check
        if m > 5 or m < -1:
            print("\n Invalid input - try again")

        # Menu opt 1
        if m == 1:

            #Write time and scope measurement parameters to file

            localtime = time.asctime(time.localtime(time.time()))
            futuretime = time.asctime(time.localtime(time.time() + timeleng))
            print("Local current time :", localtime)
            print("\n")
            print("Run end time :", futuretime)
            print("\n")
            txt_write(filename, localtime, 'a')

            params = scopepar()
            txt_write(filename, params, 'a')

```

```
            # Set and sweep frequency
            freq = start_freq
            while freq <= end_freq:
                freqtrans(freq)  #Set Sig-Gen Frequency
                sleep(slp)  #Set delay
                measurements = measure_scope(out=True)  #Fetch measurements
                print(freq)
                txt_write(filename,
                          str(freq) + "," + measurements,
                          'a')  #Write measurements to file
                freq = freq + increment  #Freqency Step

        # Menu opt 2
        if m == 2:

            start_freq, end_freq, increment, timeleng = freqset()

        # Menu opt 3
        if m == 3:

            filename = str(input("Input Filename: "))
            filename = filename + ".csv"

            print("\n\n")
            print("Filename selected:", filename)

        # Menu opt 4
        if m == 4:

            slp = float(input("Input Delay (s): "))

            timeleng = timeleng * slp

            print("\n\n")
            print("Delay selected:", slp)
            print("Runtime of scan (s):", timeleng)

        # Hidden Menu opt 123 - skip
        if m == 123:
            break

        # Menu opt 0
        if m == 0:
            return ()

        m = -1  # Reset m


########################################################################
# Start of code:
if __name__ == "__main__":
    # Call main function:
    main()
    # Exit confirmation:
    input("\nTest done, press enter to quit")
    #pass
```

Appendix E: Pilot Plant Supplementary discussions

This section presents supplementary data to the operation of the Supercritical pilot plant.

E.1 Steady state determination 390
E.2 Liquid hold-up measurement 391

E.1 Steady state determination

Steady-state establishment is demonstrated in the preceding Master's study [Franken, H.H., *Establishment of a Supercritical Pilot Plant and the Hydrodynamics of Supercritical Countercurrent Columns*; Masters Dissertation, Stellenbosch University, Department of Process Engineering, 2014], but can be briefly summarised as follows.

During an experimental run, the column is first operated with only supercritical CO2 at the desired gas flow rate. Time was allowed until the pressure drop over the column stabilized. Equilibrium is determined by monitoring the pressure drop over the column and the liquid solvent mass flow rate. Equilibrium is assumed as soon as both values stop fluctuating for an extended period (~10 minutes). This can take up to an hour.

For all runs at the same solvent flow rate with the column only operating with the supercritical fluid, the value of the pressure drop was found to be the same. The measured value was also aligned with the dry pressure drop. If any difference was observed, the lines to the DP cell were purged.

The liquid feed pump is then turned on at a chosen liquid rate and time is again allowed for the system to stabilize at a stable pressure drop (or to flood). An example of an equilibrium curve can be found below in Figure E-1.

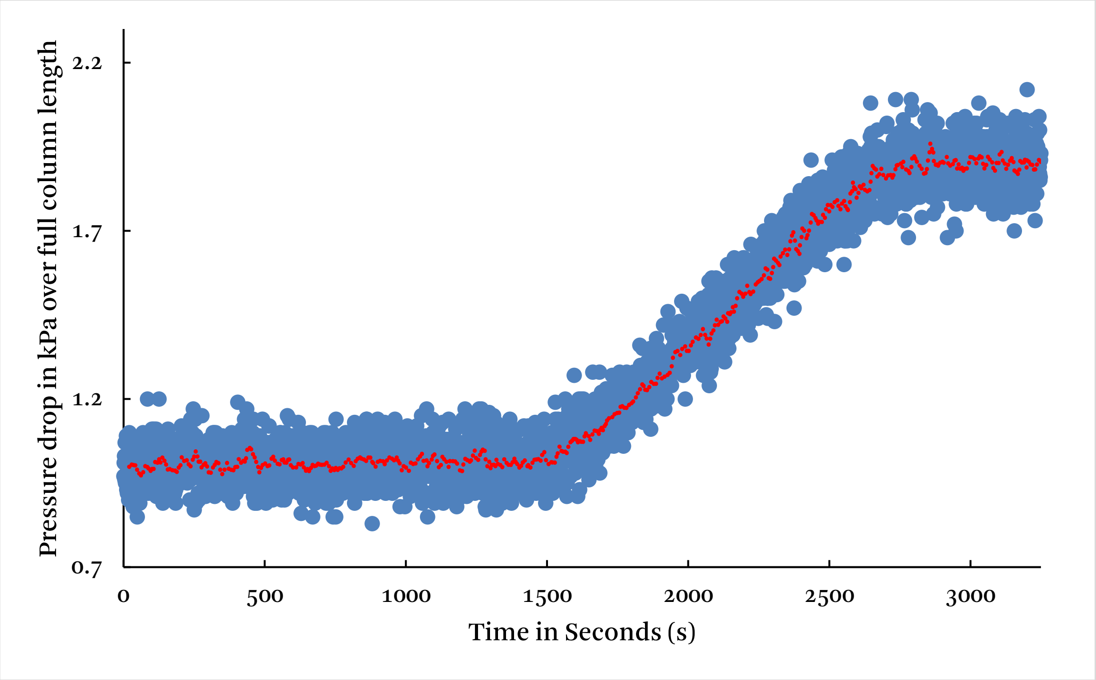

Figure E-1: an example of the measured pressure drop during an experimental run.

As the data shows some instability in momentary readings, an average of the steady state values is taken to determine the pressure drop reading. Fluctuations are taken into account when stating the accuracy of the values.

E.2 Liquid hold-up measurement

Liquid hold-up measurement is demonstrated in the preceding Master's study [Franken, H.H., *Establishment of a Supercritical Pilot Plant and the Hydrodynamics of Supercritical Countercurrent Columns*; Masters Dissertation, Stellenbosch University, Department of Process Engineering, 2014].

During the preceding study the bottoms were decanted batch wise, but it was found that this disturbs the equilibrium in the column. Figure E- 2below illustrates how decanting the bottoms disturbed the process.

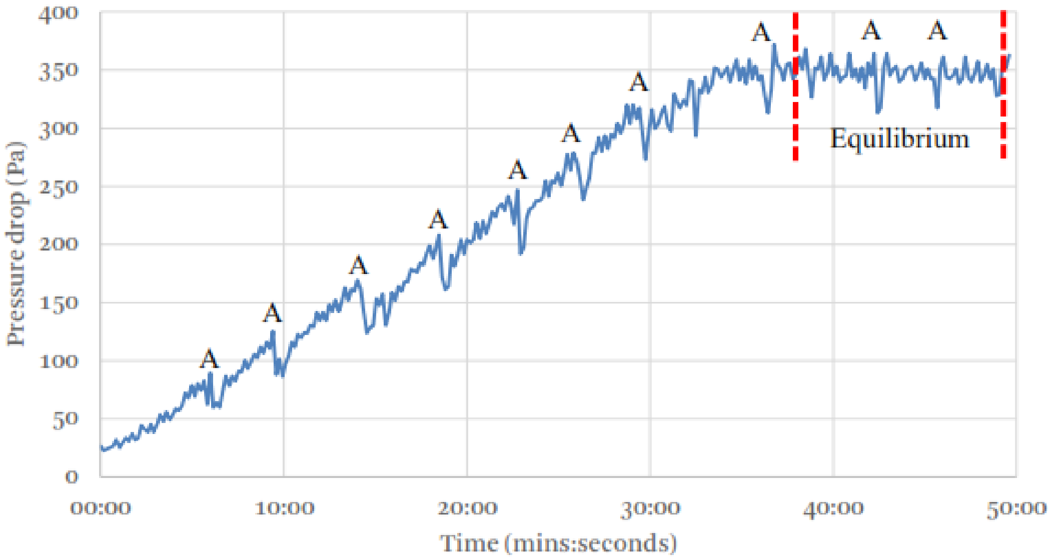

Figure E- 2: The disturbance of hydrodynamics through the intermittent decanting of the column bottoms. Decant events are indicated by the letter A in the figure. Reproduced from the preceding Masters study [Franken, H.H., *Establishment of a Supercritical Pilot Plant and the Hydrodynamics of Supercritical Countercurrent Columns*; Masters Dissertation, Stellenbosch University, Department of Process Engineering, 2014].

To remedy this a bottoms tank was connected to the column to allow smooth, uninterrupted collection of the column bottoms, eliminating the need for decanting during operation. To ensure an 'airlock' doesn't form in the flow to the tank the tank was connected directly to the bottom of the column, with a capilliary connection from the top side of the tank to the column just below where the packing starts.

When shutting down the column to determine the hold-up. the connection to the tank was immediately closed. This served to separate the column bottoms and the hold-up. The collected bottoms were then decanted while the hold-up was allowed to drain in the column. After the bottoms are fully drained, the connection to the tank is re-opened and the hold-up allowed to drain and decanted. The bottoms are drained intermittendly, until no liquid further exits the column for 10 minutes. During the hold-up removal the column is kept at operating pressure and temperature to ensure accurate measurement.

NOTE: The hold-up and bottoms are calculated from the drained mass. The solubility of CO2 at atmospheric conditions is typically minute as the CO2 flashes off. To determine if a significant amount of CO2 remains in the bottoms, samples from different conditions should be weighed, then degassed in a vacuum. After degassing the samples are weighed again to determine if a significant amount of CO2 remained in the samples. The mass of the liquid in the column is projected using the binary phase properties measured in the prior high pressure cell experiments.

Appendix F: Pilot Plant Experimental Data Tables

This section contains the data gathered during the pilot plant experiments.

Table E- 1: Dry pressure drop data measured at 313.15 K, including the calculated and measured friction factor and pressure drop per unit length.

Superficial Supercritical Fluid Flow Rate	Reynolds number, Re_G	Calculated Column Friction Factor	Measured Column Friction Factor	Calculated Pressure Drop per Unit Length	Measured Pressure Drop per Unit Length
mm/s	-	-	-	Pa/m	Pa/m
7.53	55.5	12.4	13.1	88.0	93.3
7.79	57.4	12.1	10.5	92.1	80.0
7.79	57.4	12.1	10.5	92.1	80.0
8.42	62.0	11.5	11.3	102	100
8.44	62.1	11.5	12.0	103	107
8.47	62.3	11.5	12.6	103	113
8.83	65.0	11.2	12.3	109	120
8.89	65.5	11.1	12.1	110	120
9.02	66.4	11.0	9.82	112	100
9.40	69.2	10.7	9.64	119	107
9.42	69.4	10.7	10.8	119	120
9.47	69.7	10.7	10.1	120	113
9.84	72.5	10.4	10.4	127	127
9.87	72.6	10.4	10.4	127	127
9.90	72.9	10.4	10.9	128	133
10.4	76.3	10.1	10.4	136	140
10.5	77.3	10.1	11.1	139	153
10.6	77.9	10.0	9.51	140	133
10.7	78.9	9.92	9.72	143	140
11.2	82.4	9.68	10.2	152	160
11.4	84.0	9.57	8.59	156	140
11.4	84.2	9.56	8.96	156	147
11.5	84.5	9.54	8.90	157	147
11.7	85.9	9.45	9.77	161	167
11.7	86.1	9.44	9.72	162	167
11.7	86.3	9.43	8.52	162	147
11.9	87.6	9.35	8.27	166	147
11.9	87.8	9.34	8.24	166	147

Continued on next page

Table E- 1 continued

Superficial Supercritical Fluid Flow Rate mm/s	**Reynolds number, Re_G** -	**Calculated Column Friction Factor** -	**Measured Column Friction Factor** -	**Calculated Pressure Drop per Unit Length** Pa/m	**Measured Pressure Drop per Unit Length** Pa/m
12.0	88.7	9.28	8.80	169	160
12.1	88.9	9.27	8.75	169	160
12.1	89.3	9.25	8.33	170	153
12.2	89.9	9.22	8.93	172	167
12.3	90.9	9.16	9.78	175	187
12.4	91.0	9.15	9.76	175	187
12.5	92.0	9.10	8.86	178	173
12.5	92.4	9.08	9.14	179	180
12.6	92.7	9.06	9.40	180	187
12.6	92.8	9.06	9.71	180	193
12.9	95.0	8.94	9.26	187	193
12.9	95.1	8.94	9.26	187	193
13.2	97.3	8.83	8.85	193	193
13.3	97.6	8.81	8.79	194	193
13.5	99.1	8.74	8.22	198	187
13.5	99.3	8.73	8.78	199	200
13.6	100	8.71	8.39	201	193
13.8	102	8.61	8.62	207	207
13.9	102	8.61	9.16	207	220
14.0	103	8.55	8.64	211	213
14.1	104	8.52	7.72	213	193
14.2	104	8.50	8.20	214	207
14.2	105	8.50	8.72	215	220
14.4	106	8.44	7.72	219	200

Table E- 2: Pilot plant experimental results for the system PDMS 100 cSt + CO_2

Average Column Temperature	Superficial Supercritical Fluid Flow Rate (avg)	Superficial Liquid Flow Rate	Saturated Supercritical Fluid Viscosity	Saturated Supercritical Fluid Density	Saturated Liquid Viscosity	Saturated Liquid Density	Mass Fraction Liquid in Overheads	Dynamic Liquid Hold-up	Pressure Drop per Unit Length	Operable
K	mm/s	mm/s	mPa.s	kg/m³	Pa.s	kg/m³	g/g	m³/m³	Pa/m	-
332.45	12.7	0.309	0.0428	569.4	2.85	870.1	0.0032	0.061	380	Y
332.65		0.496	0.0426	567.1	2.87	870.0	0.0029	0.069	433	Y
334.05		0.637	0.0412	551.1	2.99	869.5	0.0049	0.138	667	Y
332.45		0.635	0.0428	569.4	2.85	870.1	0.0048	0.169	747	Y
331.15		0.991	0.0441	584.4	2.75	870.5	0.0055	0.288	1287	Y
333.05		0.976	0.0422	562.5	2.90	869.9	0.0066	0.275	1647	Y
333.85		1.38	0.0414	553.4	2.97	869.6	0.0069	0.490	2127	Y
331.65		1.62	0.0436	578.6	2.79	870.3	0.0306	0.529	2233	N
333.05	15.7	0.359	0.0422	562.5	2.90	869.9	0.0045	0.059	187	Y
332.95		0.514	0.0423	563.7	2.90	869.9	0.0045	0.078	293	Y
333.45		0.734	0.0418	557.9	2.94	869.7	0.0047	0.162	747	Y
330.75		0.819	0.0445	588.9	2.71	870.6	0.0102	0.366	1727	N
330.75		0.882	0.0445	588.9	2.71	870.6	0.0155	0.373	1700	N
330.55		1.08	0.0448	591.2	2.70	870.7	0.0195	0.373	1687	N
332.05		1.21	0.0432	574.0	2.82	870.2	0.0211	0.371	1873	N
333.15		1.18	0.0421	561.4	2.91	869.8	0.0243	0.418	2147	N
332.25		1.27	0.0430	571.7	2.84	870.1	0.0292	0.374	1987	N
333.35	18.5	0.389	0.0419	559.1	2.93	869.8	0.0043	0.115	327	Y
334.45		0.568	0.0408	546.5	3.02	869.4	0.0035	0.157	687	Y
330.65		0.741	0.0447	590.1	2.70	870.6	0.0074	0.354	1740	N
331.55		0.897	0.0437	579.8	2.78	870.3	0.0108	0.346	1700	N

Continued on next page

Table E- 2 continued.

331.75	18.5	1.08	0.0435	577.5	2.80	870.3	0.0126	0.331	1780	N
333.65		1.23	0.0416	555.6	2.96	869.7	0.0146	0.310	1480	N
333.05		1.25	0.0422	562.5	2.90	869.9	0.0250	0.346	1287	N
332.75	21.3	0.381	0.0425	566.0	2.88	870.0	0.0044	0.115	620	Y
332.85		0.385	0.0424	564.8	2.89	869.9	0.0037	0.109	500	Y
332.35		0.551	0.0429	570.6	2.85	870.1	0.0075	0.200	767	N
332.35		0.716	0.0429	570.6	2.85	870.1	0.0112	0.212	800	N
333.15		0.896	0.0421	561.4	2.91	869.8	0.0110	0.214	820	N
333.35		0.910	0.0419	559.1	2.93	869.8	0.0121	0.204	853	N
332.25		1.04	0.0430	571.7	2.84	870.1	0.0108	0.274	847	N
332.55		1.06	0.0427	568.3	2.86	870.0	0.0130	0.252	867	N
332.05		1.26	0.0432	574.0	2.82	870.2	0.0185	0.279	800	N
329.55	12.7	0.372	0.0458	602.7	2.61	871.0	0.0047	0.115	373	Y
327.65		0.572	0.0480	624.0	2.45	871.6	0.0057	0.136	540	Y
327.65		0.711	0.0480	624.0	2.45	871.6	0.0059	0.247	807	Y
327.45		0.902	0.0482	626.3	2.44	871.7	0.0175	0.373	680	N
328.15	15.7	0.278	0.0474	618.5	2.50	871.4	0.0015	0.117	Err	Y
328.15		0.363	0.0474	618.5	2.50	871.4	0.0016	0.119	Err	Y
327.95		0.326	0.0476	620.7	2.48	871.5	0.0028	0.109	540	Y
327.75		0.472	0.0478	622.9	2.46	871.6	0.0019	0.177	700	Y
328.05		0.605	0.0475	619.6	2.49	871.5	0.0041	0.196	673	Y
326.95		0.905	0.0487	631.8	2.39	871.8	0.0278	0.294	727	N
328.35	18.5	0.162	0.0472	616.2	2.51	871.4	0.0014	0.058	233	Y
328.35		0.311	0.0472	616.2	2.51	871.4	0.0022	0.085	340	Y
328.25		0.329	0.0473	617.3	2.50	871.4	0.0028	0.080	340	Y

Continued on next page

Table E- 2 continued.

327.55	18.5	0.741	0.0481	625.1	2.45	871.6	0.0222	0.183	600	N
326.95		0.724	0.0487	631.8	2.39	871.8	0.0184	0.195	460	N
329.45	21.3	0.399	0.0459	603.8	2.60	871.0	0.0064	0.157	693	Y
326.55		0.392	0.0492	636.2	2.36	872.0	0.0063	0.160	673	Y
327.45		0.568	0.0482	626.3	2.44	871.7	0.0175	0.134	633	N
323.45	12.7	0.188	0.0528	669.1	2.10	873.0	0.0074	0.055	180	Y
323.45		0.379	0.0528	669.1	2.10	873.0	0.0119	0.105	267	N
323.65		0.384	0.0526	667.0	2.12	872.9	0.0122	0.082	293	N
323.45		0.396	0.0528	669.1	2.10	873.0	0.0131	0.123	287	N

Table E- 3: Pilot plant experimental results for the system PDMS 200 cSt + CO_2

Average Column Temperature	Avg Superficial Supercritical Fluid Flow Rate	Superficial Liquid Flow Rate	Saturated Supercritical Fluid Viscosity	Saturated Supercritical Fluid Density	Saturated Liquid Viscosity	Saturated Liquid Density	Mass Fraction Liquid in Overheads	Dynamic Liquid Hold-up	Pressure Drop per Unit Length	Operable
K	mm/s	mm/s	mPa.s	kg/m^3	Pa.s	kg/m^3	g/g	m^3/m^3	Pa/m	-
333.15	12.7	0.257	0.0421	561.4	4.44	863.9	0.0043	0.145	580	Y
332.65		0.251	0.0426	567.1	4.39	864.4	0.0040	0.152	580	Y
332.65		0.375	0.0426	567.1	4.39	864.4	0.0048	0.177	647	Y
333.05		0.473	0.0422	562.5	4.43	864.0	0.0113	0.214	780	N
332.65		0.540	0.0426	567.1	4.39	864.4	0.0142	0.204	607	N
333.15		0.646	0.0421	561.4	4.44	863.9	0.0272	0.204	707	N
333.05	15.7	0.14	0.0422	562.5	4.43	864.0	0.0031	0.077	340	Y
332.95		0.27	0.0423	563.7	4.42	864.1	0.0033	0.126	513	Y

Continued on next page

Table E- 3 continued.

333.05	15.7	0.357	0.0422	562.5	4.43	864.0	0.0089	0.172	767	N
332.95		0.376	0.0423	563.7	4.42	864.1	0.0078	0.188	700	N
332.65		0.429	0.0426	567.1	4.39	864.4	0.0095	0.176	633	N
332.95		0.619	0.0423	563.7	4.42	864.1	0.0148	0.194	607	N
333.35	18.5	0.117	0.0419	559.1	4.46	863.6	0.0029	0.053	420	Y
333.15		0.33	0.0421	561.4	4.44	863.9	0.0038	0.152	627	Y
333.15		0.47	0.0421	561.4	4.44	863.9	0.0121	0.191	840	N
333.05		0.49	0.0422	562.5	4.43	864.0	0.0122	0.179	940	N
332.85		0.68	0.0424	564.8	4.41	864.2	0.0152	0.191	687	N
333.45	21.3	0.104	0.0418	557.9	4.48	863.5	0.0018	0.052	387	Y
332.45		0.228	0.0428	569.4	4.36	864.6	0.0026	0.115	547	Y
332.95		0.35	0.0423	563.7	4.42	864.1	0.0040	0.174	693	Y
333.05		0.48	0.0422	562.5	4.43	864.0	0.0064	0.187	707	Y
332.35		0.632	0.0429	570.6	4.35	864.7	0.0186	0.202	600	N
328.05	12.7	0.104	0.0475	619.6	3.87	869.4	0.0035	0.054	173	Y
327.85		0.228	0.0477	621.8	3.85	869.6	0.0057	0.106	327	Y
327.95		0.370	0.0476	620.7	3.86	869.5	0.0079	0.178	760	Y
328.35		0.47	0.0472	616.2	3.91	869.1	0.0215	0.165	487	N
328.25	15.7	0.12	0.0473	617.3	3.89	869.2	0.0038	0.060	307	Y
327.75		0.20	0.0478	622.9	3.84	869.8	0.0036	0.124	567	Y
328.05		0.345	0.0475	619.6	3.87	869.4	0.0060	0.160	887	Y
327.75		0.478	0.0478	622.9	3.84	869.8	0.0077	0.179	713	Y
328.15		0.621	0.0474	618.5	3.88	869.3	0.0362	0.157	480	N
327.65	18.5	0.120	0.0480	624.0	3.83	869.9	0.0035	0.094	327	Y
327.95		0.222	0.0476	620.7	3.86	869.5	0.0047	0.122	593	Y
328.15		0.359	0.0474	618.5	3.88	869.3	0.0078	0.148	880	Y

Continued on next page

Table E- 3 continued.

328.15	18.5	0.461	0.0474	618.5	3.88	869.3	0.0224	0.109	307	N
327.65	21.3	0.115	0.0480	624.0	3.83	869.9	0.0035	0.082	260	Y
328.25		0.240	0.0473	617.3	3.89	869.2	0.0042	0.108	613	Y
328.45		0.397	0.0471	615.1	3.92	869.0	0.0156	0.116	333	N
324.15	12.7	0.096	0.0520	661.8	3.44	873.7	0.0052	0.042	187	Y
323.55		0.235	0.0527	668.1	3.37	874.3	0.0082	0.114	153	N

"The start and finish of things was always dangerous"

Wintersmith – Terry Pratchett